WIND

and its effects on (Canterbury) forests

A thesis presented for the Degree of Doctor of Philosophy in Mechanical Engineering in the University of Canterbury

by

A. J. G. PAPESCH

B.E.(Hons), C.Eng., M.I.Mech.E., M.R.Ae.S.

Department of Mechanical Engineering,
University of Canterbury,
Christchurch,
New Zealand.

February 1984

Who has seen the wind?
Neither I nor you:
But when the leaves hang, trembling
The wind is passing thro'.

Who has seen the wind?
Neither you nor I:
But when the trees bow down their heads
The wind is passing by.

. . . . . Christina G. Rossetti

ABSTRACT

The importance of man-made coniferous forests to the New Zealand economy makes the protection of this renewable resource essential. Forests on the Canterbury Plains are subject to high winds and are susceptible to internal wind damage when they are thinned, particularly near forest fronts. This has prompted research on wind and its effects on flat Canterbury-type forests. Tree response is studied in relation to wind changes at forest borders.

A brief review of open country boundary layers establishes a reference wind structure upwind of forests. Changes in wind structure occur as infinite length forests are thinned. The responses of trees within conifer-type forests and of agricultural crops are compared.

A study is then made of the forest leading edge. The wind structure is further modified by the abrupt change process, by the density of the roughness and by the response of the individual trees. So that tree response can be studied analytically in such a modified wind structure, simple and complex mathematical equations are formulated using a modified form of Solari's along-wind response calculations.

Two full scale and two model experiments contribute to the assessment of the modified wind structure and the tree response from the leading edge inwards.

After making a number of comparisons, both model and full scale, of mean wind speed profiles, mean turbulent intensity profiles, spectra, and tree response both by calculation and by photography, there is enough correspondence in results to state that premature wind damage to forests will occur just in from forest leading edges unless optimum spacing is used. Both model tests indicate that this spacing is about 1/3 of mean tree-top height. It is also evident that the wind spectra above tall flexible crops have more energy than is normal in the inertial region, especially near the leading edge. They have steeper gradients than that given by the Kolmogorov Laws. Also, these spectra sometimes possess two or more peaks probably resulting from frequency shifts in wind turbulence from the interaction of discrete vortices and turbulence generated by shear distortion coupling with the waving motion of the tree tops, causing coherent tree sway or 'Honami'.

LIST OF CONTENTS

CHAPTER PAGE

CHAPTER PAGE

CHAPTER PAGE

APPENDICES PAGE

LIST OF FIGURES

LIST OF TABLES

LIST OF PHOTOGRAPHS

LIST OF SYMBOLS

A_x	Cross-sectional area of the crown.
A_z	Frontal area of the crown.
A	Fluctuating along-wind tree-top deflection.
A_B	Area of power spectrum curve for background response.
A_r	Plan surface area of tree (or model) crown.
A_R	Area of power spectrum curve for resonant response.
A_T	Total along-wind r.m.s. tree-top deflection.
A_t	Plan surface area of ground.
a	A constant.
a_e	A constant.
B	Tree excitation due to background turbulence.
$C_{D_{\ell_o}}$	Form drag coefficient at the forest front (x = 0).
C_{Df}	Fluctuating form drag or reduced drag coefficient.
C_{D_2}	Form drag coefficient.
C_{D_T}	Profile drag coefficient.
C_f	Shear stress coefficient. (Ap. II).
C_{f_T}	Shear or Reynold's stress coefficient down to transition.
C_{f_ℓ}	Shear or Reynold's stress coefficient in inner layer.
C_{f_O}	Shear or Reynold's stress coefficient referenced to upstream winds at 10 m height.
C.P.	Centre of pressure as a ratio of total tree height.
C_z	Crown width at height z.
C_{z_0}''	Crown width at height ($\bar{U}_z = 0$)
D	Mean alongwind tree-top deflection.
D_B	Breast height diameter (cm).
d	Zero plane displacement of inner layer. (Ap. II).
d_c	Distance constant.
d_o	Zero plane displacement at stagnant air layer.

E Modulus of elasticity.

F_w Wind force.

F_T Tree force.

F_1 Background total admittance. (Ap. II.)

F_2 Resonant aerodynamic admittance.

$\hat{f}$ Non-dimensional wind frequency, $\frac{n\ {}^{x}L_u}{\bar{U}_z}$

f_n Wave number, $\frac{2\pi n}{\bar{U}_z}$.

$G(f)$ Correlation function for aerodynamic admittance.

g Gravitational constant.

H Tree height.

H_m Mean tree-top height (model).

H_p Mean tree-top height (full scale).

$H_{z_o''}$ Crown height subject to mean wind pressures measured to minimum mean velocity measured.

I_1, I_2, I_3 Integrals in alongwind response calculation (Ch.3, Ap.I.).

I_{σ_u} Alongwind turbulence intensity, $\frac{\sigma_u}{\bar{U}_z}$

$|J_{y(n)}|^2$ Horizontal transverse joint acceptance function (Ch.3, Ap.I.).

$|J_{z(n)}|^2$ Vertical transverse joint acceptance function (Ch.3, Ap.I.).

K_{10} Shear stress coefficient, $\frac{C_{f_o}}{2}$

K_T, K_1, K_2 Terms in alongwind response calculation (Ch. 3).

k_a Von Karman's constant, (0.41).

k_s Tree stiffness.

L Monin-Obukhov length. (Ap. II.)

ℓ_z A mixing length.

${}^{x}L_u$ Length scale of turbulence in x-direction.

${}^{x}L_{u_m}$ Length scale of turbulence in x-direction above a model forest.

M_R Magnification factor.

M_T Above ground generalised tree mass.

m	Subscript means model.
m_u	Number of hill heights.
M	Natural logarithm of z'_o/z_o.
N_f	Correlation function for reduced drag (Ap.I.).
n	Wind frequency.
n_m, n_p	Wind frequency (model and full scale).
n_o	Tree natural fundamental frequency.
n_{pk_w}	Wind frequency at peak of power spectrum.
$\hat{n}$	Non-dimensional wind frequency, $\frac{nz}{\bar{U}_z}$.
n_{pk}	Non-dimensional frequency at peak turbulence.
$\overset{*}{n}$	Non-dimensional wind frequency, $\frac{nH}{\bar{U}_{*_\ell}}$.
P	Height above ground to lowest tree crown branch, (pruned height).
p	Subscript means 'full scale' (prototype).
pk	Subscript means 'peak'.
R	Tree excitation due to resonant turbulence.
Re No.	Reynolds Number.
Ri_f	Flux Richardson's Number. (Ap.II)
Ri_g	Gradient Richardson's Number.
S	Mean tree spacing.
$Sk_{u'}$	Skew in a turbulent velocity distribution.
$S(n)_u$	Power spectral density of the horizontal turbulent wind component.
$S_{(u)}$	Speed-up factor.
T	Duration of sample.
t	Time.
t_c	Time constant.
$\bar{U}_z$	Mean wind velocity at height z.
$\bar{U}_H$	Mean wind velocity at mean tree-top height.
$\hat{\bar{U}}_z$	Non-dimensional mean wind velocity at height z.
$\bar{U}_{*_\ell}$	Friction velocity at local height z. (Ap. II).

$\bar{U}_{*prof.}$ Friction velocity at transition z_T. (Logarithmic profile)

$\bar{U}_{R_z}$ Total resultant mean wind velocity at height z.

$\bar{U}_o$ Mean wind velocity upstream at reference height 10 m.

u' Alongwind turbulent wind velocity component. (Ap. II)

$\bar{V}_z$ Mean wind velocity at height z $\perp$ to $\bar{U}_z$.

v' Transverse turbulent wind velocity component.

$\bar{W}_z$ Vertical mean wind velocity (+ve downwards).

w' Vertical turbulent wind velocity component.

X Horizontal distance to ½ hill height.

x, y, z } System of rectangular cartesian co-ordinates with x-axis defined in the alongwind direction.

x_t Generalised tree stem displacement.

z Height above ground.

z_i Height above ground to the limits of the internal boundary layer.

$\hat{z}$ Non-dimensionalised height above ground $\left(\frac{z}{H}\right)$.

z_T Height above ground to the mean wind profile point of inflexion. (This is the same as aerodynamic crop height, h.)

z_g Height of the surface layer.

z_o Aerodynamic roughness height of open country terrain. (Ap.II)

z'_o Aerodynamic roughness height of a forest measured at transition.

z''_o Aerodynamic roughness height of a forest within the inner layer.

z'_{o_m} Aerodynamic roughness height of an infinitely long model roughness.

α Mean velocity profile power law exponent.

α' A constant.

δ Boundary layer thickness.

e Dissipation rate or eddy viscosity (Ap. II).

ε Means 'between'.

$^{o}\theta_S$ Resultant wind vertical angle.

λ_e Roughness parameters for high roughness.

Δ Smallest dimension of a structure.

ν Kinematic viscosity.

ν_o Average number of zero crossings in unit time.

ζ Damping ratio.

$\frac{\pi}{4\zeta}$ Mechanical admittance at resonant tree frequencies.

ρ Air density.

σ_u Standard deviation of horizontal turbulent wind component.

τ_z Shear or Reynolds stress at height z. (Ap.II.)

τ_{z_o} Constant shear or Reynolds stress in the inner layer.

χ_m Integral value of vertical shear stress.

$|\chi|^2$ Aerodynamic admittance x $\left(\frac{C_{D_f}}{C_{D_\ell}}\right)^2$ (Ap. II.)

ϕ_e Non-dimensional dissipation energy.

ϕ_m Non-dimensional shear stress ratio above transition.

ϕ_R Phase angle for a 2nd order oscillation.

^oT Wind direction compared with true North.

CHAPTER 1

INTRODUCTION

1.1 AIM OF THESIS

Windthrow is a major and persistent problem in forest management. Despite research and experimentation, particularly during this century, no absolute method of protecting forests from wind damage has been found satisfactory, for during severe storms (such as the one experienced in Canterbury in 1975) wind damage has continued to occur on a vast scale.

The aim of this thesis is to provide a study of the nature of wind and its associated forces on mature forests and on individual trees within forests. In particular an attempt will be made to show that a change in canopy structure of a forest as it is thinned alters the distribution of mean wind and turbulence, causing variations in wind/tree interaction and therefore wind damage to the forest from the leading edge inwards. It is important to measure variations in the wind/tree interaction as a function of thinning density or spacing, since these may be altered by managers beyond the normally accepted limits indicated by the site exposure level.

1.2 A BRIEF HISTORY OF WIND PROTECTION

Although forests have been important to man as a source of timber since the earliest times[1], forest management proper (that is, regulated use for continuity) does not seem to have been practised, at least in Western cultures, until after the Middle Ages.

Windthrow, as a problem of forest management, was first recognised in Germany. In 1565 an ordinance prescribed the retention of parts of the stand to protect the shallow-rooting spruce seedtrees which were left in an attempt to secure reproduction after the felling of the mature stand. This evolved first into a system of leaving parcels standing on all four sides, then later into the strip system.[2]

---

1. It is known that the Romans practised silviculture to some extent on both natural forests and artificial plantations.

2. Fernow, B. E. (1909), p.54.

In the first half of the 18th century it was recognised that wind danger was reduced by making fellings progress from east to west. The idea of a regular, properly-located felling series was first put forward by von Langen (1845) in the Harz mountains. He also emphasised the importance of maintaining a wind mantle on exposed situations.[1]

Berlepsch (1760) recommended cutting in echelons so that long strips were avoided and fellings were distributed more evenly. It was also Berlepsch who provided the first good statement on thinning theory (1761). He advised taking out suppressed trees, leaving sound poles clear of the lower and middle branches (pruning). In the same period Zanthier recommended two thinnings for conifers for rotations of over 50 years.[2]

Hartig (1764 - 1837) and Cotta (1763 - 1844) are recognised as "the fathers of modern forestry". In 1808 Hartig published his eight "General Rules". These, coinciding closely with the teaching of Cotta, were formulated for the benefit of uninformed underforesters to make the change from the unregulated selection forest that was generally practised to intensive management.[3]

It was not until the second half of the nineteenth century that experimental stations in forest management were set up, the first being nine stations in Saxony for collecting forest meteorological data. This marked the beginning of modern systematic research. The traditional approach, based on observation techniques using carefully documented field material,was used to produce statistical analysis of storm damage in forests to establish scientific propositions from which useful methods of wind protection have been devised. However an understanding of the fundamental mechanics of wind damage makes possible the provision of more effective protection.

---

1. Fernow, ibid. p.55.
2. Fernow, ibid. p.63
3. Fernow, ibid. p.9. These rules were valid only for beech forests and their application to forests in general had unfortunate consequences for pine forests in particular, since the forest canopies were very different.

In his thesis "Storm Damage in New England Forests" (1946), D. M. Smith documents some wind protection methods.

1. Mixed stands are more wind resistant than pure stands. Bergmann (1904) believed that mixing conifers and hardwoods was the best and simplest way to gain wind resistance.

2. In most situations uneven-aged stands are more wind-resistant to severe damage than even-aged stands. "....the greater frictional surface offered by an uneven-aged stand results in a greater lowering of velocities as the wind progresses over an extensive stand".[1]

3. Thinning practice differs between American and European foresters. The European foresters appear to have no doubts that early and frequent thinnings greatly increase wind firmness. On the other hand, most American foresters believe that thinning is an important cause of windthrow.

4. The Wagner felling series is chiefly applied to even-aged stands. Essentially it is a system of clear-cutting in strips, so that the clear-cutting progresses into the direction of dangerous winds. The objectives are to avoid exposure to wind of the cut edges of the stand and to provide a uniform and gradual upward slope, away from the wind, of the top surface of the new stand.[2]

5. Decreased rotation times reduce the risk of windthrow, especially on exposed sites (Fisher, 1907).[3]

6. Stand borders should be thinned but not pruned and attempts made to advance growth in the understorey, especially on the edges of the stand (Fisher, 1907).[4]

---

1. D. M. Smith, ibid. p.138.

2. D. M. Smith, p.144. Here is one area where a clear answer to the forester has not been available. "Hess (1900) mentioned that trees recently exposed by thinnings and regeneration cuttings suffer severely from windthrow but their root systems soon enlarge and improve wind resistance."

3. Ibid. p.149.

4. Ibid. p.149. Thinning of borders is not practised widely in New Zealand but border protection methods, natural or artificial, have been used extensively in Australia and New Zealand.

1.3 DEFINITION OF THE RESEARCH PROBLEM

1.3.1 Previous research on wind behaviour over forests

The science of forestry had little input from the physicist or the engineer prior to the 1970's. Yet Heyer (1799 - 1856), more than a century earlier, had emphasised the necessity of basing forest management on exact scientific enquiry, instead of empiricism alone.[1]

D. M. Smith (1946) states "Baker (1915) and Smith and Westknecht (1915), as a result of studies on windfall in the Pacific Northwest, indicated that tall, dominant trees, with dense, well-formed crowns are most susceptible to windfall.....".[2] Cajander (1934) found that trees of largest crown area had the greatest tendency to fall in directions other than the predominant wind direction of the storm causing the damage.[3] This must imply that the trees are swaying and releasing stored energy opposite to the mean wind direction.

Morosov (1928) states that forest vegetation reduces windspeeds through the conversion of energy into heat by friction and motion of vibrating vegetation. He found that turbulence and gustiness were at a maximum in a narrow zone inside and outside the stand border and that his measurements did not approach a state of near calm until a distance of about 100 m in from the edge was reached.[4] This proposition was supported by Jacobs, (1936).

D. M. Smith (1944) also gives an account of research by West and East European, British and American scientists from 1900 - 1946 and of the research he records, the most relevant to this thesis is the study of gusts. He emphasised that gusts are the elements of wind which cause most blowdown[5] and breakage. Discussing suggestions made by Schmauss (1920) and Conrad (1946) that these gusts become particularly dangerous when their frequencies are near the natural frequency of oscillation of the tree, Smith states, "Their theory was that the tree has less resistance to a wind which is oscillating in velocity at nearly the same frequency as the tree oscillates, because the tree does not damp its vibration by

---

1. Fernow, op. cit., p.95.
2. D. M. Smith (1946), p.133.
3. Ibid., p.134.
4. Ibid., p.117.
5. In this thesis, windthrow encompasses both blowdown (uprooting) and stem breakage.

swaying to windward during strong gusts. .....less force is necessary to swing the crown of the tree beyond its allowable amplitude and thus bend the stem or supporting roots past the elastic limit of the wood."[1]

Fritsche (1933) and Woelfle (1939a) recognised the fact that turbulent air flowing over forest borders caused internal windthrow, although their interpretation of the behaviour of the wind in causing this windthrow indicates a lack of understanding of the aerodynamics involved. They described a form of windthrow which started inside the stand and worked outward, leaving only the border trees. Smith comments, "This phenomenon was frequently noticed in New England following the 1938 hurricane."[2] This theory was expressed more than thirty-five years ago, yet it appears that no attempts were made to either prove or disprove it.

One of the most quoted, yet erroneous, conceptions on blowdown is well illustrated in an article by Roper (1975) where he states, "If a gale strikes an unbrashed plantation, it is like hitting a solid wall, and as soon as the better-rooted trees on the outside go, the inner trees fall like nine-pins. Clean boles of trees will cause eddies in the wind and stop it doing any damage." On the contrary, there is enough evidence to show that it is the trees behind the front that blow down first as a result of eddies, allowing the wind forces to decrease on the front trees (see photographs 1 - 16). In the latter, blowdown results from the high mean wind speeds, while breakage is the result of high turbulence in the wind. Either case can be dominant.

Wendelken (1966) investigated the storm damage of 1964 at Eyrewell Forest in the Canterbury Plains. He observed that in each of the four gales which struck the forests in March, 1964, damage started from zones inside relatively undamaged stands or from pockets of damage inside forest stands. "Direction of tree fall was more confused, with some crossing of stems, but the overall pattern of windfall remained orderly." Peak gusts in this storm ranged between 64 mph (28 m/s) and 69 mph (30 m/s), with an hourly average of 42 mph (18 m/s), destroying over 7,200 acres (2,919 ha) of forest (see 4.4.1).

---

1. D. M. Smith, Ibid., p.131.
2. Op. cit., p.121.

Cremer et al (1977) investigated the 1974 windthrow in Radiata pine plantations near Canberra, Australia. From their studies, they conclude that there is ample evidence to show that stands do fail behind the front before edge trees blow down. Their Figure 3 on page 285 shows trees lying in all directions behind the front. Evidence that this phenomenon is widespread and occurs in other forests is described by Somerville (1978) and shown by photographs (1 - 11) and by the ground plot study at Burnham Forest. This may be due to 'Honami'[1] (Finnigan, 1979).

After consulting the writer, Somerville (1978) carried out a systematic survey of wind damage profiles for Eyrewell and Balmoral Forests from the forest front to the internal forest. He found that, although a high percentage of the front trees were left standing, there was extensive damage just behind the forest front. The damage then reduced, but beyond 10 H^2 it again increased at a less severe level.

Surface roughness is also adjusted by topographical changes which increase the risk of windthrow. Undulations in terrain create more turbulence and increase the risk of breakage rather than blowdown in forests on the lee side of hills. In addition, the ratio of breakage to blowdown for trees on the lee side of individual hills within the rough terrain is greater than that for trees in the lee of the total hill system. Similarly, the ratio of blowdown to breakage for trees on the windward slopes of individual hills within the rough terrain is higher than for trees on the windward side of the total hill system (O. P. Cramer and Lynott, 1961; Cremer, 1965; Cremer et al 1977).

Full scale experiments on plant canopies by F. B. Smith (1961), Fraser (1962b), Raymer (1962), Landsberg and Thom (1971), Hoag et al (1971) and, more recently, by White et al (1975), Hutchinson et al (1979), Finnigan (1979), Maitani (1979), Holbo et al (1980), Mayer (1981) and Johnson et al (1982), support the proposition that both rapid distortion of the wind over forest leading edges, and tree sway, together influence forest wind instability.

Some research workers who applied engineering principles to develop a model for the wind interaction with the forest were Woelfle (1936), Hirata (1951), Inoue (1955), Fraser (1962b), Hutte (1968), Kawatani and Meroney (1968), Landsberg and James (1971) and Finnigan and Mulhearn (1978b).

---

1. See Appendix II.
2. See Symbols List.

Woelfle (1939a) conducted some very interesting wind tunnel experiments to determine the frictional resistance of different types of stand contours. The model forests were composed of spruce twigs attached upright to fixed bases.[1] The writer recognises these model tests as the first real attempt to quantify wind drag on stand borders.

An excellent treatise on the mechanics of stem breakage and blow-down has been published by Hirata (1951), while Fraser, and Kawatani and Meroney, made positive attempts to measure the resistive bending moment of model trees as the canopy roughness was changed. However, their models were unable to oscillate. The more recent full scale experiments on plant canopies take account of wind-induced waving by individual elements. In particular, Finnigan and Mulhearn arrive at a mathematical model to accommodate element sway induced by both background and resonant wind turbulence (defined by Davenport, 1967) which are normally considered as separate components in wind-induced motion of engineering structures.

1.3.2 Results of previous research

The research outlined above has provided the forest manager with some practical methods for assessing forest stability. These are:-

(a) Zones of susceptibility - used in Britain, particularly in Scotland and the Border area. Information compiled from storm damage has been used to map these zones, which are divided into four categories of risk, the risk increasing with altitude.[2]

(b) Critical height - the height of forests at which windthrow on a large scale occurs at the expected maximum wind velocity for that forested area, is now a common criterion for planning crop rotations. The critical height decreases with increased susceptibility.

(c) Tatter flags - developed in Scotland for the purpose of assessing site suitability. Wind velocity and flag tear are correlated empirically in an aeronautical tunnel. Flags are then placed randomly in the open at various potential forest sites (including damaged forests) and left for periods of up to eighteen months, after which flag damage is measured.

---

1. D. M. Smith, Op. cit., p.120.

2. Booth et al (1967).

(d) Assessment of surface boundary layer wind profiles and near-ground turbulence - the wind profile over forests, extending from above tree-top height to ground, was apparently first measured by Geiger and Amman in 1931.[1] Their profiles demonstrated that the maximum retardation of the wind occurs in the top portion of the crowns and they suggested that this is also the region where swaying tops favour the formation of eddies. More documentation of profiles for forests, wheat, corn, maize, suburban areas, open grassland and oceans now exists and will be discussed later.

In these profile studies little attention is paid to the subject of crop and tree dynamics. Yet much evidence existed to suggest risk of wind damage from tree sway generated by turbulent winds associated with the high stress variations occurring near forest fronts (Finnigan, Somerville 1978).

(e) Tree pulling - methods of tree pulling have been developed by Fraser (1962a), Mayhead and Booth (pers. comm., 1972) and Papesch (unpublished). Some useful relationships between soil and tree types are recorded and measurements of resistive bending moment of conifers are compared to provide relationships that assess crop stability.

(f) Wind tunnel modelling. Model forests with canopies constructed from scaled wire gauze, plastic trees, nails, pegs and other roughness types are placed in wind tunnels. Dimensional adjustments to the roughness, spacing and model forest shape are made while monitoring wind characteristics over the canopy. (None of the model tests mentioned allowed for turbulence changes due to model tree swaying motion).

(g) Photography. Because high winds devastate the forest it is necessary to learn from wind damage patterns before evidence is lost. Usually high level aerial photographs are used to analyse patterns of wind damage, but low level aerial photographs can show more clearly the mechanics of wind/tree interaction. For example, low level aerial photographs (Appendix III, 1-11) taken after damaging storms in Canterbury, show that

---

1. D. M. Smith.

stem breakage and blowdown exist in more or less equal amounts in all forms of topographic variations and soil types, with, perhaps, slightly more breakage near a forest border or over hills.

In photographs 7 and 8 (Appendix III) the atypical occurrence of bands of blowdown and stem breakage on the same soil type which occurred in the Selwyn Plantation Board Burnham Forest is a significant indication that tree sway is a dominant mode of instability in high velocity north-west winds. When scaled up from the photographs, the width of the blow-down bands is close to 80 m. Normally the gusts are randomly disposed, giving random but equal amounts of stem breakage and blowdown. On this occasion two large gusts close together (see anemometer records of 1.8.75)[1] traversing the forest in this area provided excessive sway consistent with the type of damage shown. The first gust would have caused tree sway to develop in phase perpendicular to the wind direction. Another severe gust, (reaching 91 Kts (45 m/s) then traversed the forest reaching the trees swaying perpendicular to the wind in phase with each other. Since the periodicity of the trees was measured as 7 seconds at Burnham (5 samples), the blowdown bands should have the same width as a ¼ of a wave-length of the in-phase trees, be $\frac{91 \times 7}{2 \times 4}$ metres ≃ 80 metres wide[2], and be smaller in width than the breakage bands, if tree sway contributes to blowdown and breakage. This appears to be the case. The blowdown bands are near 80 m wide and the breakage bands at least twice this width.

Tree sway may therefore be a dominant factor in wind damage to forests. This dynamic movement must be added algebraically to the mean deflection of the stem instead of regarding the latter as the only cause of windthrow. If the deflections add to increase the bending moment at the tree base, blowdown may result. On the other hand, if they add to give a point of inflection up the deflection curve of the stem, this may reduce the bending moment at the base and move the point of maximum bending stress anywhere up the stem; the result may be stem breakage. This can occur into the wind or with the wind, depending on the tree's final movement as it sways (Photographs 7 and 8). A study of wind mean velocities and the spectra of the turbulence from the leading edge of forests rearwards is therefore necessary (Ch. 6 and Finnigan 1978a).

---

1. Christchurch Airport, New Zealand. (Figure 7.1).
2. Photographs 7 and 8 (App.III).

The methods listed above must take into account variations of species, nursery management, soils, roots, drainage, tree crown and stem shape, topography, climate and planting techniques, all of which will modify forest wind resistance. At the same time, topography, turbulent wind, tree form, canopy roughness, energy absorption in the branches and stems, and soils, all interact to produce a situation of complexity when studying forest stability. It is apparent that there is still a need to understand the wind and tree behaviour at forest leading edges and just in from the leading edge as thinning (and pruning) changes the canopy roughness.

1.3.3 Application of previous research in New Zealand

Wind protection methods currently practised in New Zealand are well documented (Wendelken, 1966 and Jackson 1974). Prior to 1968 research on the mechanics of wind damage appears to have been minimal, but some protection methods were in use throughout the country. The Canterbury Plains forests of Eyrewell, Ashley, Balmoral and Selwyn Plantations have provided very flat terrain for assessing wind behaviour. This may be applied to other terrain, with adjustments made to the protection measures to allow for differences in soils and topography.

The last decade has brought wind research into prominence in various fields such as wind energy, pasture growth, building design, vehicle aerodynamics and airport wind shear, as well as wind effects on forests and shelterbelts. Wind is, in fact, becoming an important part of engineering research in New Zealand, to the benefit of forestry science[1].

1.3.4 Thesis research on wind behaviour over forests

Surface roughness exerts a profound influence on the wind passing over the surface. In particular, changes in surface roughness in forests produced by different spacing and thinning practices are likely to cause interactive shifts in the turbulence spectra of winds, with consequent changes in the momentum transfer process. The precise nature of these changes is only partly understood but appears to be very significant in determining wind damage

---

1. Berg (1978). Workshop on Canterbury forests.

through aeromechanical exchanges between the stand and the wind. Early research by the British Forestry Commission at Kielder Forest (Northumberland) between 1966-1972 detected changes in wind structure in the transition from open terrain to an unthinned spruce block and a thinned block within the forest. Unfortunately, instrument sensitivity was too low to measure the more critical changes in wind properties under these surface roughness conditions.

Since 1972 rapid advances have been made in understanding the behaviour of wind over rough surfaces. The development of microprocessors is allowing analysis of wind data on field experiment sites. Parallel to the increase in wind record analysis techniques, wind tunnel facilities now provide measurements of turbulence and spectra in output form and with the increase in capacity of microcomputers the analysis of results from wind tunnel studies now allows experimental testing times in the wind tunnel to be considerably reduced.

1.3.5 Some theoretical considerations

Measurements of the velocity and turbulence intensity profiles of the natural wind in neutral, stable and unstable temperature conditions, over smooth and rough terrain, around ridges and isolated hills, over escarpments and over various forests, continue to add to the knowledge of wind behaviour. Standard texts, notably the Engineering Sciences Data Unit's[1] Volumes, now provide some valuable reference material allowing research in wind tunnels and over open country to be studied concurrently with the assurance of accurate wind assessment by comparison with various standards.

Many natural and man-made physical systems oscillate when displaced by natural wind forces. Generally, a system possessing mass and elasticity can vibrate if displaced from its equilibrium position. Trees within a forest are no exception to this principle when made to oscillate in response to gust loading in the natural wind.

There are several common aerodynamic mechanisms which cause oscillations in elastic systems free to vibrate in the wind, which may or may not initiate closed loop aeroelastic instabilities causing destructive amplitudes. (Honami waves caused by the interaction of larger gusts and the turbulence generated at canopy height can be added to the list).

---

1. Subsequently referred to as ESDU.

The natural wind is turbulent; the wind speed varies continuously, and the amplitude and frequency of the fluctuations vary randomly. This periodic motion, having a non-sinusoidal or complex shape, can be represented by a Fourier series consisting of a constant term, equal to the mean value (mean wind speed) and by a number of sinusoidal terms of different frequencies and phases with in-phase (resonant) and out-of-phase (background) components. Thus, if we assume that the tree is equivalent to a linear springmass system and is subjected to a mean wind force coupled to a periodic but non-harmonic (non-sinusoidal) force imposed by wind turbulence, the resulting motions will consist of a mean deflection and an oscillatory motion. These motions are the sum of the individual motions due to each component of turbulent wind, expressed as a Fourier series split into all the various harmonics. The distribution of the turbulent wind components of force versus wind frequency provides a diagram, or spectrum of wind forces, as does the study of the motion of the tree resulting from this wind. The ratio of the output motion of the tree to the input motion of the wind, termed the transfer function, (or compliance), can be compared for differing canopy roughnesses (Holbo, 1980)

The motion of plantation trees in the wind is usually damped motion, and the oscillatory motion resulting is usually stable, with the restoring forces due to stem elasticity overcoming the applied forces due to the natural wind. The influence of damping in a system is often expressed as the ratio of the actual damping to the critical damping, the latter being a measure of damping which just allows a system to oscillate. The presence of damping increases the periodic time of the oscillating tree, and this loss of energy within each cycle is proportional to the square of the amplitude, to the frequency, and to the amount of damping in the system.

Previously, it was mentioned that the wind can cause instabilities in structures. Differing physical mechanisms cause different instabilities because of the method of interaction of aerodynamic wind forces and elastic structural forces. A stable oscillation results when the elastic forces predominate, and the system is described as having negative feedback. Generally, systems with large negative feedback are stable; unstable systems result from systems which have positive feedback where the mechanical and aerodynamic damping cannot negate the forces being imposed on the structures.

It is suggested that a rough forest canopy disturbs the natural wind to such an extent that:-

(a) the turbulence in the wind is increased, and

(b) there is a shift in wind frequencies to a higher order of magnitude, such that the aerodynamic wind forces may predominate over the elastic tree forces even though damping is increased, particularly near the forest leading edge. Large resonant tree oscillations may result which cause either windthrow or stem breakage depending on the phase relation between the wind and tree motions.. Inside the forest, the variation in tree density may adjust the ratio of resonant to background turbulence causing tree oscillations.

The analysis of the wind data to determine these proportions involves determination of the variations in the square of the amplitudes of all the different wind fluctuations. This necessitates summations using Fourier series methods. It is termed "spectral density" because all wind frequencies are analysed in small band widths and grouped together to form a distribution of wind forces (not wind power but a force power distribution). The spectra distribution is therefore the magnitude of the dynamic pressure in all the wind components in small band widths of wind frequencies. The distribution, besides altering with temperature, terrain roughness, instrument response and mean velocity trends, may also alter with forest geometry and tree geometry. This would cause positive feedback aero-elastic instabilities to develop as thinning treatments changed the roughness of the forest canopy.

However, since the wind is random, the wind spectrum must first be multiplied by an aerodynamic admittance term which describes how the wind gusts strike the crown. The aerodynamic admittance terms reflect the decreased ability of very small gusts (with a length scale much smaller than the tree crown size) in the dissipative region of the spectrum to move the trees. The hump in the response spectrum from the mechanical admittance $(\frac{\pi}{4\zeta})$ is centred slightly below the tree natural frequency (Annand, 1966). The resonant hump is usually well to the right of the broad peak in the wind spectrum where most of the wind kinetic energy exists. However when the wind moves up over the leading edge of the forest its spectrum peak is nearer tree response spectra (Ch.6).

1.3.6 The research problem

The problem therefore, is to measure the wind properties over the canopy structure of a forest (model and full scale) as thinning density is changed and relate this to wind damage both at the leading edge of a forest and internally within a forest.

The problem is classified by studying the wind parameters in three zones, as illustrated in Fig. 1.1 below:

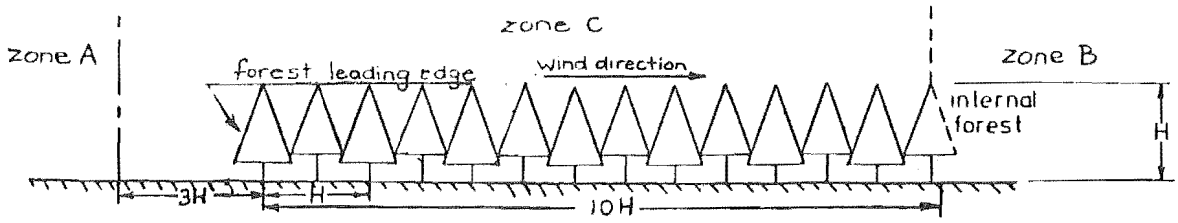

ZONE A	ZONE C	ZONE B
Low roughness	Changing roughness (i) abrupt height change (ii) roughness density change	High roughness
Rural boundary-layer	Non-uniform boundary layer	Urban type layer
Power law mean velocity profile	S-shaped mean velocity profile with three separate logarithmic parts	Logarithmic profile displaced in the z direction
Constant shear stress in x & z directions	Variation in shear stress in the x & z directions	Constant shear stress in the x & z directions
Constant pressure in x & z directions	Variable pressure gradient in the x & z directions	Constant pressures in x & z directions
No acceleration	Deceleration, acceleration, deceleration.	No acceleration
Turbulence Spectra defined as ESDU model	Turbulence Spectra non-gaussian and skewed.	Turbulence Spectra defined as ESDU model.

FIGURE 1.1: Zones of study

Chapter 2 covers zone A, Chapter 3 zone B, and Chapter 4 describes zone C.

The solution of the problem will, it is hoped, propose a method of reducing forest wind damage.

1.4 LIMITS OF STUDY

The scope of the study dictates the size and nature of the experiments designed to measure the effects of aeromechanical interaction within a conifer forest; that is, a crop composed of trees with a conically shaped crown and an elastic stem.

1.4.1 Experimental objectives

The main objectives are:-

1. To measure the total (3-dimensional) turbulent velocity of wind passing over a stand which is treated by a series of thinnings to progressively increase canopy roughness.
2. To calculate and measure the approximate dynamic response of trees within the stand following increases in thinning intensity.
3. To compare and integrate the full scale data(derived from 1. and 2. above)with the wind and tree deflection data derived from scale model studies in boundary layer wind tunnels.
4. To compare the results of these studies with other research results and to make recommendations on spacing/respacing/ thinning for sites subject to high windthrow risk.

1.4.2 Experimental scope

The thesis investigates the wind damage problem defined in 1.3.6 by measuring wind characteristics for neutral stability conditions, model and full scale:-

(i) over the leading edge of a forest (mean height 'H')[1] representing an abrupt change of roughness and,

(ii) behind the leading edge of a forest, by analysing the adjacent air layer at tree-top level and its aerodynamic features such as:-

- mean wind speed profiles from measurements of wind at four values of z for z_o', d, $\bar{U}_*$ as a function of x;
- turbulence intensity or variance as a function of x, z, z_o' and $\bar{U}_*$;
- Reynolds stress measurements ($\overline{u'w'} \rightarrow (\bar{U}_*^2)$) at z = H compared with the logarithmic profile stress measurements just above the canopy, (ϕ_m);
- turbulence spectra curve-shape changes from the leading edge inwards at two heights (model) and at one position for x (full scale) as roughness density varies;

---

1. See Symbols list.

- tree sway by calculation and photographic measurement (model) at $z = H$, and accelerometers (full scale) at $z = 0.7\ H$, as a function of x.

The thesis also assesses any significant changes in the characteristics of wind and tree behaviour noted in the results; in particular:-

(i) changes in mean wind speed and turbulence intensity profile characteristics with references to upstream conditions as a function of x;

(ii) changes in surface shear and stress and aerodynamic roughness due to a step change in mean roughness height (H) and roughness density (tree space to height ratio $(\frac{S}{H})$), as a function of x and z;

(iii) changes in spectral characteristics as a result of (i) and (ii) above and their effects on tree motion (mean deflection (D) and amplitude (A)) as a function of x and z.

(iv) changes in wind damage as a result of (iii).

1.4.3 Experimental work

The main experiments comprise two full scale studies and two model/wind tunnel studies.

(a) The first full scale experiment was set up at Kielder, England, by the Forestry Commission in 1968, to measure wind conditions over a Sitka spruce stand. The stand was thinned and records of wind conditions were compared to assess structural changes in the wind as a result of thinning. The results were inconclusive due to major faults with the experimental measuring equipment: the Munro Cup anemometers, although suitable for establishing the boundary layer mean wind profile shape over the forest leading edge, were not designed to respond to the high gust frequencies associated with the turbulent nature of the wind. Secondly, the thinning at 20% in one of the experimental plots did not provide enough change in canopy architecture to allow trends in the data to be established for variation in thinning density. The experiment did, however, produce mean wind velocity profiles and roughness variations (z_o') over the leading edge of a typical spruce forest.

(b) The first model forest experiment, using a planetary boundary wind tunnel, was conducted at Canterbury University in 1975. The major fault with this wind tunnel study was that the model size was too large in

relation to the size of the wind tunnel. (However, the sizes of the model trees were designed to allow the model to oscillate in the wind in a realistic way.) Instrumentation used to measure the turbulence was also inadequate. At the time of the experiment, spectra could not be measured in the wind tunnel.

(c) The second field experiment was set up in 1982 by the writer and the British Forestry Commission, Northern Research Station, Roslin, Scotland, in a Sitka spruce stand at Rivox, near Moffat. This experiment will conclude in July 1984 after at least three thinning treatments to the stand. This field study uses two separate masts carrying wind and temperature sensors. One mast, which had previously been erected on the site, holds an upstream reference Gill UVW anemometer array, and the other mast with 4 Gill UVW anemometers holds arrays from just within the canopy to 12 metres above the canopy. In addition, four vane-type very sensitive wind triad sensors were fixed to the mast tower within the canopy for selected time periods, giving detailed information on within-canopy turbulence and thus augmenting the information being recorded simultaneously by Gill propeller anemometers above. Accelerometers and scratch gauges were attached to selected trees to monitor crop motion.

The assessment of crop height and spacing in four plots and several transects within the compartment gives information on the gross stand architecture. Nil-wind tree sway tests in the stand were undertaken to assess the natural frequency distribution of trees.

(d) The second model forest study was carried out by the writer in the Osney Laboratories, Oxford University, in May 1982. Wind-tunnel selection was based on the suitability, cost and availability of facilities capable of printing mean wind and turbulence intensity profiles and suitable spectra over the model forest. This was a repeat of the wind tunnel experiment undertaken in New Zealand using the same model tree design scaled for stiffness and mean crown shape from full scale measurements and arranged in a sequence of square and staggered patterns with increasing spacing. The model forest had a height and frequency distribution which was the mean of a normal Yield Class 20 Sitka spruce stand in Scotland, and of two stands in Whakawerawera forests in New Zealand.

1.4.4 Allied experiments

In addition to the experiments listed in 1.4.3, the writer:-

1. collaborated with Dr. D. Ford of ITE[1] and Dr. M. P. Coutts FC on the mathematical modelling of the windthrow process;
2. measured the resistive bending moments by tree-pulling on sites at Eyrewell forest at different tree-spacings near the edge and internally;
3. measured the drag coefficient and the centre of pressure of a forest leading edge at Burnham Forest;
4. measured the occurrence of wind damage that had occurred over a period of 20 years at Burnham Forest;
5. measured the damping ratio of trees in a forest stand at Burnham Forest (Loo, 1975).
6. measured the sway properties of trees at Rivox, Eyrewell and Burnham.

As well, contributions to windthrow studies are being made by other researchers who are investigating:-

- root movement due to wind;
- diffusion rates of spraying in Sitka spruce crops (Cranfield, England);
- the shape of the tree crown, stem and branches and weight distribution (Institute of Terrestrial Ecology, Scotland);
- the relation between root strength and soil mechanical strength (M. P. Coutts);
- the shape of a tree stem when deflected by applied point loads compared with the tree stem shape that develops in the wind (Aberdeen University);
- the response of Gill UVW sensing instrumentation compared with the sensitive vane-type Lowne anemometers developed at Cranfield.

---

1 ITE refers to the Institute of Terrestrial Ecology.

1.5 CHAPTER SUMMARY

Improved understanding of the influence of canopy configuration on momentum transfer has important practical implications affecting stand management in high windthrow hazard classes.

The aim of this thesis is to study wind behaviour over forests, emphasising the importance of the abrupt changes in roughness which occur at forest leading edges, and the gradual changes in roughness which result from thinning. The brief history of wind protection practices shows how systematic wind protection has developed. This indicates that crop roughness changes make a significant contribution to wind damage patterns in from the leading edge of a forest, thus defining the problem to be researched. The limits of the study are stated, so that the appropriate wind properties above the crop can be analysed by specific experiments designed to measure the varying wind forces over conifer forests and consequent tree swaying motion.

CHAPTER 2

THE SURFACE WIND BOUNDARY LAYER OVER OPEN COUNTRY

In this chapter a study is made of Zone A, (see Fig. 1.1).

2.1 DEFINITION OF THE RURAL SURFACE BOUNDARY LAYER

The planetary boundary layer is a region of air movement existing in the lowest part of the broadscale air movements of the atmosphere, which has 75% of its mass below 10 km and 50% below 5.7 km. The air currents result from the differences in heating by solar radiation of the earth's surface in high and low latitudes. This produces horizontal density differences, and the resulting pressure gradient in the atmosphere, together with the earth's rotation, produces the wind system present in the free atmosphere.

The lowest 10% of the planetary boundary layer is called the surface boundary layer and is about 100 m thick. The properties of the air in the surface boundary layer are related to the properties of the surface by vertical exchange of momentum through mixing by turbulence. The properties of the surface layer over land vary with vertical temperature distribution.

In the surface boundary layer the Coriolis force may be disregarded when compared with the effects of the surface so that wind direction changes with height can generally be disregarded. Within the surface layer it is generally accepted that there are two regions with differing properties; an outer layer above the surface roughness in which there is little vertical variation of shear stress or wind direction, and an inner layer (an interfacial layer) that forms within the depth of any surface roughness with a linear change in stress (normally assumed constant with height under equilibrium conditions). The remainder of the atmospheric boundary layer (the original layer and any developing Ekman layer) has no direct influence on the flow. When assessing wind loads, turbulence variations in these two layers are taken as the prime scaling factor

where the eddies interlock and form feedback processes with the related surface as exchange of mass and energy take place. These exchange processes can be grouped by describing a horizontal time spectrum of wind which was first presented by Van der Hoven. Fluctuations in winds of less than one hour are contributions to turbulence, while fluctuations over longer periods produce trends of the hourly mean wind speed. Measurements of the mean wind variations with height provide the mean wind profiles, while turbulence changes near the ground, treated statistically, provide horizontal and vertical turbulence intensity profiles and frequency distributions (or spectra) of the turbulence, (Figure 2.1 and 2.2; 2.3.1).

2.2 MEAN WIND CHARACTERISTICS

To obtain a model of the mean wind characteristics in the surface boundary layer, the following assumptions enable a compromise between simplicity and validity:-

- the mean wind velocity is assumed to be large enough, so that its changes with height are the same as in a neutrally stable surface layer;
- Taylor's Hypothesis, or the assumption of frozen flow, is valid over the entire gust spectrum range of interest;
- the gross features of the terrain of open country and forest are assumed to be uniform, so that a roughness parameter represents the surface adequately;
- the flow is stationary for 15 minute periods, each of which is as long as the record length used to obtain steady mean velocity values;
- the flow is assumed to be homogeneous and in equilibrium with the surface in any horizontal plane.

The surface mean velocity profile is defined by:

$$\frac{1}{T}\int_0^T U_z\,dt \equiv \bar{U}_z \equiv \frac{\bar{U}_*}{k_a}\int_0^{z_i}\frac{1}{z}\,dz \equiv z^{\alpha}$$

where z_i is the height of the surface layer.

2.2.1 The mean wind velocity profile

In the equilibrium surface boundary layer, the Prandtl logarithmic law for the mean velocity in a neutral atmosphere is commonly accepted. Here, the assumptions made are that :—

- viscous stress is negligible;
- mixing length is proportional to height ($\ell_z = k_a z$);
- shearing stress is constant and equal to the surface stress τ_o

where $$\sqrt{\frac{\tau_o}{\rho}} = \bar{U}_* = k_a z \frac{\partial \bar{U}}{\partial z} .$$

Also, if $\bar{U} = 0$ at $z = z_o$ where, in the open country, $z_o \ll z$,

$$\frac{\bar{U}}{\bar{U}_*} = \frac{1}{k_a} \ln \left(\frac{z}{z_o} \right) ,$$

while, for the same condition with high z_o ,

$$\frac{\bar{U}}{\bar{U}_*} = \frac{1}{k_a} \ln \left(\frac{z + z_o}{z_o} \right) .$$

k_a is the von Karman constant (0.41) and z_o is a roughness length, normally $\simeq 0.03$ m for open country and $\simeq 1.0$ m over forests. z_o is about 1/30 times the average dimension of a typical roughness particle. In practice, both z_o and $\bar{U}_*$ are determined from measurements of at least two values of $\bar{U}$ and z.

In the surface layer in non-neutral conditions,

$$\frac{\bar{U}}{\bar{U}_*} = \frac{1}{k_a} \left[\ln \left(\frac{z + z_o}{z_o} \right) - \psi \left(\frac{z}{L} \right) \right]$$

where L is a temperature-dependent scaling length (or Monin-Obukhov length).

Above the surface layer, Coriolis forces increase, surface roughness effects decrease, and the logarithmic law begins to depart from empirical data. In the planetary layer as a whole, the power law can be used to define the wind profile:-

$$\bar{U}/\bar{U}_1 = (z/z_1)^{\alpha}$$

where α is an index which changes with roughness.

The logarithmic law and the power law are linked by the relation

$$\alpha = \frac{1}{\ln \frac{z+z_o}{z_o}} \qquad \text{(Panofsky 1970)},$$

since $z_o << z$ it is often neglected in rural conditions.

Davenport (1967) summarises the available evidence for the mean velocity profile for heights 150 m to 300 m above the ground. The range of values of the velocity profile index α for different surfaces is summarised below:-

TABLE 2.1: Variations of Power Law Index, (after Davenport).

Type of Surface	Index, α	K_{10}
Cities	0.25 - 0.45	0.050
Treed & rough country	0.17 - 0.35	
Open level country	0.14 - 0.20	0.005
Open water	0.10 - 0.11	

There is a general increase in α with an increase of roughness and it is about 0.22 in the open country surface layer upstream of high surface roughness. The power law is of only limited use since high aerodynamic roughness (z_o') and changes in roughness $\left(\frac{z_o'}{z_o}\right)$ shape the velocity profile above high roughness. The power law also enables an estimate of the mean wind velocity at geostrophic height to be made at the top of the surface layer. Theoretically, this represents the maximum wind speed (geostrophic wind) which is often needed when estimating peak wind loads on buildings and other structures within the open country surface boundary layer. The power law is therefore the appropriate model to use when calculating the wind forces on tall structures placed in the rural boundary layer; Davenport uses this approach. On the other hand, the logarithmic law applied either in the rural open country surface boundary or over high roughness such as forests, provides a reference for assessing the wind loads on structures placed in such high roughness zones. The logarithmic law is used by Solari (1982), Simui (1980) and others for wind profile estimates and will also be used in this thesis to represent mean velocity profiles in equilibrium with the surface.

2.2.2 The resultant mean wind direction

In the surface boundary layer the direction of the resultant mean wind velocity in the horizontal plane is required to calculate wind loads on structures.

The existence of shear stresses and Coriolis forces (due to centripetal forces at different earth latitudes) produce mean wind deflections away from the isobars in the direction of the lowest mean pressures, providing rotations anticlockwise with increasing height in the Southern Hemisphere. These deflections produce spiralling wind directions called 'Ekman' spirals, in the vertical direction.

Very close to the ground, within the inner layer and below the mean height of the roughness geometry under consideration, resultant wind speed direction veers because of the net effect of the static pressure distribution at the ground and the surface stress distribution immediately above the stagnant air adjacent to the ground. Between this region and the rest of the inner and outer layers near the mean roughness height, wind direction is considered constant with height up to approximately 200 metres. As pointed out earlier, this is essential since, as changes in wind direction occur, they can be related to roughness variation, terrain slope changes, or the influence of major obstructions within the layers under neutral stabilities upstream of the areas under consideration.

2.2.3 Mean wind speed errors

Mean wind properties are never perfectly stationary. Mean wind speed averages over different periods of 15-minute blocks may increase in any one hour period. The variances ($\bar{u}'^2$ $\bar{v}'^2$) of velocity fluctuations (u', v') over the same 15-minute periods may also tend to increase, and cross-correlation functions which measure gust size may not tend to zero. A slowly changing mean wind direction over the one hour may result in upwind fetches of varying surface roughness, which will again influence the turbulence distribution or spectra. This gives a large scatter in the measurements of turbulence data and any model used is a mean of a large number of measurements. Also, because of the lack of detailed and accurate measurements of winds at high speeds for different terrain roughnesses, applications of models to represent wind conditions in, say, a wind tunnel are often suspect. However the data that are available particularly for the horizontal wind velocity components ($\bar{U} + u'$, and

$\bar{V}$ + v') provide models which are now generally accepted and presented in detail in E.S.D.U. data sheets. Most models available cover the open country surface boundary layer characteristics, but in more recent research, information accrues for wind characteristics over complex terrain such as forests (see Chapter 3).

2.3 TURBULENT WIND CHARACTERISTICS

Because of its turbulent nature, the wind speed varies continuously and the amplitude and frequency of the fluctuations vary randomly. Turbulence can only be generated as a result of a shearing velocity gradient in a viscous fluid; such shear flows occur adjacent to any solid boundary and also in the boundaries between streams flowing at different velocities. Once generated, the turbulent motion dissipates its kinetic energy by viscous action, extracting energy from the shear flow in order to maintain balance. In the absence of a shear flow or any other inducement, such as a change of roughness height or spacing, a change of terrain, temperature gradients, or roughness movement, mechanical turbulence is inertially transferred from larger anisotropic (or stretched) eddies to smaller, high frequency eddies which eventually disappear in momentum and heat sinks. The term 'size' is used to quantify the diameter of the rotating eddy masses, or parcels of fluid, which provide turbulence. The 'intensity' of turbulence is the ratio of the rms fluctuating velocity ($\sqrt{u'^2}$, or σ_u) to the mean flow velocity at any instant in one direction. It is proportional to the angular velocities of the eddies. Eddies of equal size produce different intensities of turbulence, depending on their speed of rotation. The kinetic energy in large eddies is much greater than in small eddies for a given turbulence intensity.

Investigation of turbulent flow by solving the general equations of momentum, energy and continuity would be ideal; but because of the complex nature of the turbulence this is not possible.

Assumptions are made so that the flow is made up of a mean 'steady' motion upon which are algebraically superimposed fluctuating velocity components.

Representing the total wind velocity by the mean wind velocity $\bar{U}$ (see 2.2) and a fluctuating wind component u',

$$U = \bar{U} + u'$$

The average value of u'^2 at any point is

$$\overline{u'^2} \equiv \sigma_u^2 \equiv \frac{1}{T} \int_o^T u'^2 \, dt \equiv \int_o^\infty S(n)_u \, dn \quad ,$$

where T is an averaging time of at least 15 minutes fixed by the Van der Hoven Spectrum (Fig. 2.1).

u'^2 is the variance and σ_u is the standard deviation of the total turbulence, or r.ms amplitude, of the fluctuating components of the wind (u', v') along and across the instantaneous wind paths. The averaging technique used here for turbulence estimates becomes suspect over high roughness where accelerations and pressure changes occur, but as yet it has not been replaced by a higher order solution to the turbulent flow equations because of the number of unknowns generated in high order solutions.

Standard deviations of the wind components are useful for estimating peak gusts if the distributions of wind components are approximately gaussian, as in strong winds. The 3 second peak gust is normally

$$U_{max} = \bar{U} + 3\sigma_u$$

or three standard deviations away from the mean wind speed.

Panofsky pointed out that $\sigma_u / \bar{U}$ is equal to α, the index in the power law for strong winds. The equations show that the turbulence intensities in strong winds increase with increasing roughness length and decreasing height.

Peak dynamic loads on structures in the surface rural boundary layer can be obtained from the logarithmic mean wind profile by assuming that the peak gust is made up of the mean wind speed and another component which is $3\sigma_u$ so that

$$\ddot{U}_{peak} = \bar{U}\left[1 + \frac{3\sigma_u}{\ln \left| \frac{z+z_o}{z_o} \right|}\right]$$

The gust factor[1] is defined as the ratio of the average of the peak wind speeds occurring in one hour divided by the mean wind speed for the same interval of time.

Davis et al (1968) showed that the gust factor increases with decreasing mean wind speed, increases with decreasing height, and has no obvious relationship to the temperature lapse rate. They showed that at wind speeds above 20 m/s the gust factor can be assumed to be independent of wind speed and temperature.

In brief, the turbulent wind characteristics are that :—

- the motions are unpredictable in detail;
- the fluctuations are three dimensional;
- properties of the fluid are efficiently mixed throughout the fluid;
- energy must be supplied to maintain the turbulence.

2.3.1 The turbulent wind velocity profile

To obtain a model for the turbulent wind velocity profile in the rural surface boundary layer, the following assumptions are made:-

- that atmospheric turbulence in equilibrium has a 'normal' or gaussian distribution. In practice, atmospheric turbulence contains regions of non-gaussian distribution, often skewed in either direction, especially near the surface of high roughness and at abrupt changes in roughness.
- viscosity exerts negligible influence so that a laminar sublayer does not exist, nor do viscous stresses exist;
- a stress associated with eddy size (Reynolds Stress), provides a constant of proportionality known as eddy viscosity. (The determination of this constant is a major obstacle in the solution of the surface boundary layer equations);

---

1 Canterbury Meteorological records showed an average gust factor of 1.41 for 10 different periods of high north-west winds, and an average gust factor of 1.38 for four periods of high south-west winds. The highest mean wind speeds of 30 m/s recorded on 1.8.75, gave a value of 1.40.

- turbulent transfer in the equilibrium rural surface boundary layer is based on first-order closure methods, and some second-order terms for turbulence over high roughness are added, using the 'mixing-length theory' developed by Prandtl and von Karman;

- processes in the surface layer are considered to occur at constant pressure, since fluctuations in temperature of a few degrees celsius in the last 10 m do not generate large enough pressure fluctuations at the surface;

- momentum transfer takes place in the absence of buoyancy forces, when temperature varies with height at the adiabatic lapse rate (neutral stability);

- under steady conditions the mean velocity at a vertical reference position (ℓ_m) does not change, so the deficits and excesses of momentum of the various eddies add up to zero in the average, i.e.

$$0 = \bar{U}_z + \ell_m \frac{\partial \bar{U}_z}{\partial z};$$

- $\ell_m \frac{\partial \bar{U}}{\partial z}$ is the downward vertical momentum flux or kinetic energy and is related to the stress by introducing Prandtl's mixing-length concept, $\ell_m \propto z$, and the stress is related to mean velocity profile by

$$\left(\frac{\tau}{\rho}\right)^{1/2}_{z=0} \equiv \bar{U}_* = k_a \frac{\partial \bar{U}_z}{\partial z}$$

where $\bar{U}_*$ represents the friction velocity and the constant of proportionality k_a is known as von Karman's constant. The friction velocity is introduced as a shorthand notation of $(\tau/\rho)^{1/2}_{z=0}$ and as a convenient scaling velocity. Integration of the shear stress at height z provides a link between the mean velocity, the turbulence and the roughness at a height z, i.e.

$$\bar{U}_z = \frac{\bar{U}_*}{k_a} \ln \frac{z}{z_o} \quad ;$$

- an increase in stability from isothermal or inversion conditions will damp out low frequency large scale turbulence, while a decrease in stability such as on sunny days generates low frequency turbulence;

- changes in atmospheric instabilities produce little distortion of the velocity profile at windspeeds above 17 m/s and, in the inertial subrange, little distortion of the turbulence spectra even for high roughness conditions.

By averaging many wind speed values over rural surface boundary layers the following models for all three components of wind turbulence up to a height of 20 m have been derived. Teunissen (1970) gives:

$$\sigma_u : \sigma_v : \sigma_w : \bar{U}_* = 2.5 : 2.0 : 1.3 : 1 .$$

Counihan (1975) suggests:

$$\sigma_u : \sigma_v : \sigma_w : \bar{U}_* = 2.5 : 1.875 : 1.25 : 1 , \text{ and}$$

$$\sigma_u : \sigma_v : \sigma_w = 1 : 0.73 : 0.46 .$$

More than 20 m above the surface the logarithmic profile provides the relationships

$$I_{\sigma_u} = \frac{\sigma_u}{\bar{U}} = \frac{1.0}{\ell n \frac{z}{z_o}} ,$$

$$I_{\sigma_v} = \frac{\sigma_v}{\bar{U}} = \frac{0.76}{\ell n \frac{z}{z_o}} ,$$

and $$I_{\sigma_w} = \frac{\sigma_w}{\bar{U}} = \frac{0.5}{\ell n \frac{z}{z_o}} .$$

These equations indicate that σ_u, or $\sqrt{\bar{u}'^2}$, does not vary with height above 20 m. ESDU standards provide a more accurate estimate of the average turbulence intensity variation with height for different roughness conditions and suggest

$$I_{\sigma_u} = \frac{\sigma_u}{\bar{U}_z} \quad \frac{1}{\ln (z/z_o)} \left[0.867 + 0.556 \log_{10} z - 0.246 (\log_{10} z)^2\right] \lambda ,$$

up to 300 m.

where $\lambda = 0.76/z_o^{0.07}$ for $z_o > 0.02$ m. and $\lambda = 0.76$ for $z_o \geq 1$ m.

and z = height above the effective surface.

Two more models for turbulence in the rural surface layer are

$\sigma_u = C\bar{U}_*$ Lumley and Panofsky.

$\sigma_u = Cz^{-.07}$ (neutral air) Fichtl & McVehil.

$\sigma_u = Cz^{-0.315}$ (unstable air) Fichtl & McVehil.

Often the turbulence must be related to the mean velocity at a reference height, say 10 metres.

Harris (1970) gives values $\frac{\sigma_u}{\bar{U}_{10}}$ for the three broad categories of site :—

Open country	$\frac{\sigma_u}{\bar{U}_{10}} = 0.18$
Woodland, suburbs	$\frac{\sigma_u}{\bar{U}_{10}} = 0.32$
High roughness	$\frac{\sigma_u}{\bar{U}_{10}} = 0.58$

In many experiments, as in this work, all velocities can be related to an upstream reference condition at 10 metres. The last result is not very meaningful as z = 10 m is below the height of the roughness elements in forests.

Distribution of turbulence intensity with height is reproduced in Figure 2.2 (over) taken from Walshe (1972). The graph shows a model often used in assessing wind turbulence intensities on structures. At heights above 200 m $\frac{\sigma_u}{\bar{U}}$ is almost a constant value of 0.12.

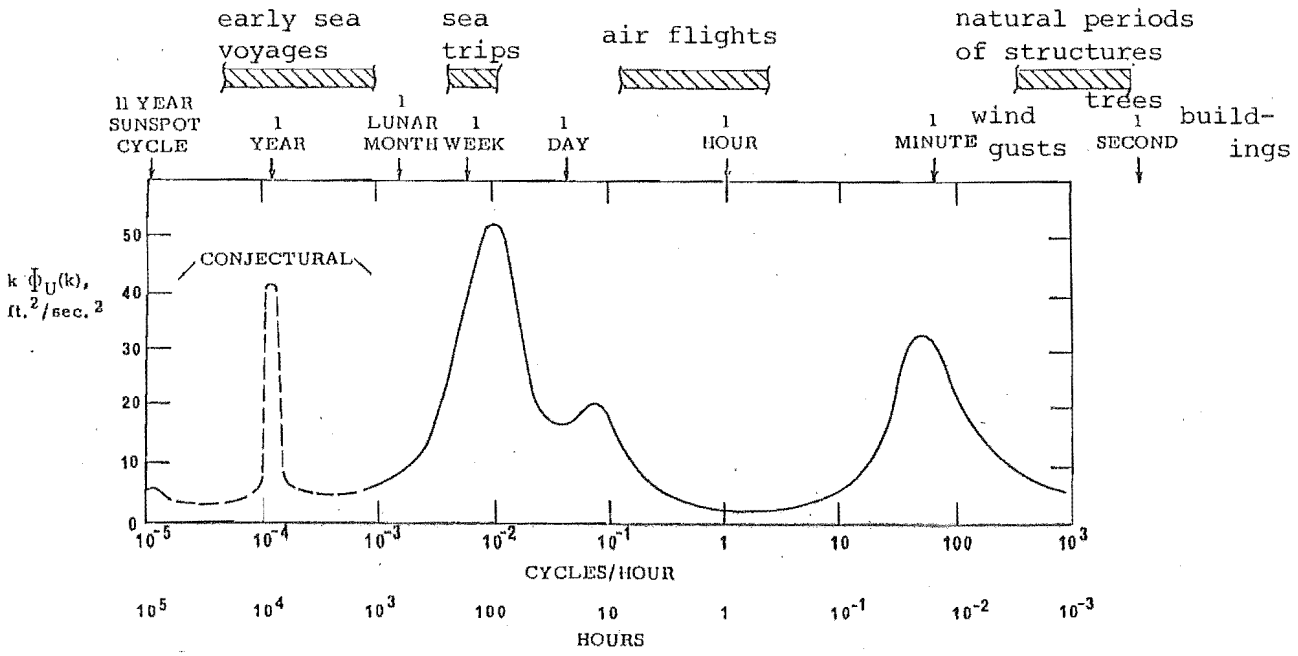

FIGURE 2.1 Van der Hoven Spectrum, (Brookhaven; after Teunissen)

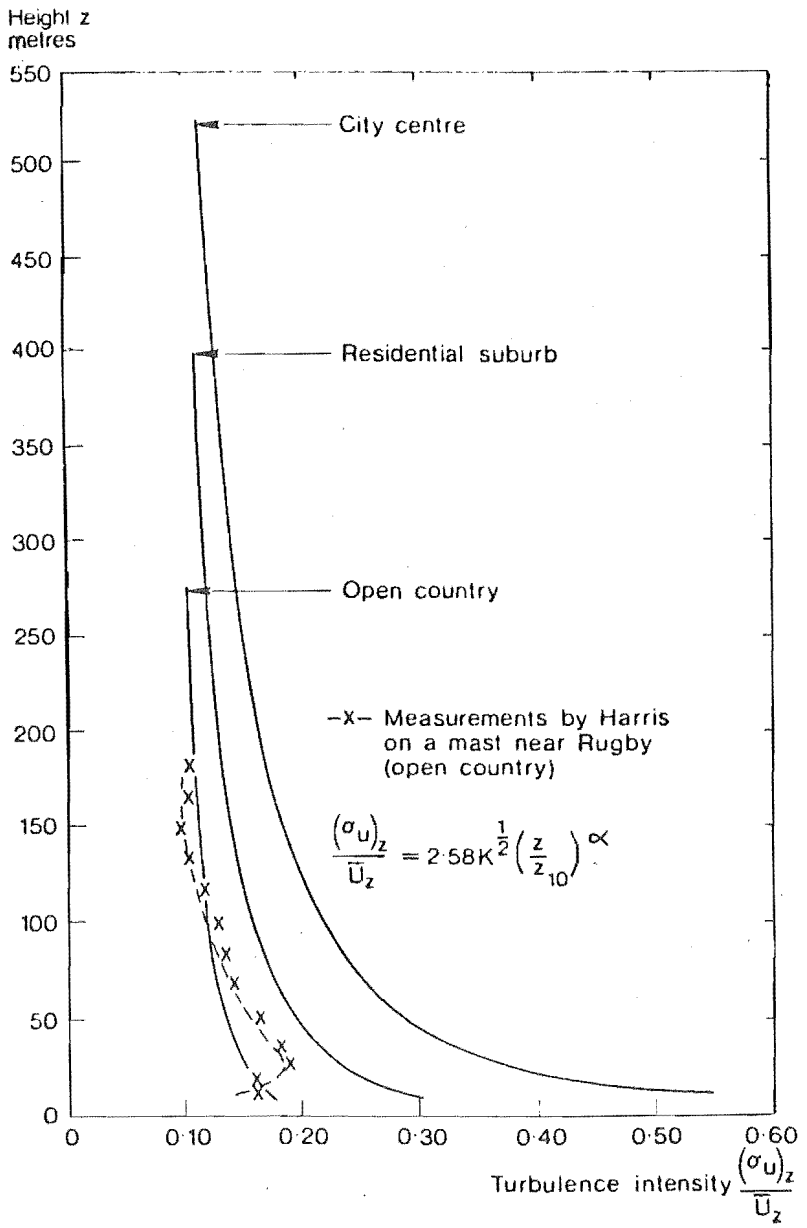

FIGURE 2.2 Turbulence intensity profiles (after Walshe)

2.3.2 Length scales of turbulence

Length scales of turbulence, a measure of the average eddy size of all the gust components, are often used to assess wind loads on structures, since 'average' eddy sizes of the same order of magnitude as the dimensions of the structure will affect the movement of the structure.

However, since distribution of the kinetic energy of these eddies is considered the appropriate method of obtaining wind loads, length scales of turbulence are not discussed in any detail here. The 'average' length scale can be found from the 'peak' (often difficult to assess) in the power spectral density curves of the turbulence data, or by using an inverse Fourier transform of the kinetic energy density of the turbulence.

The length scales are a function of height, thermal stability and surface conditions. For very high Reynolds numbers in the surface layer the length scales of turbulence are little affected by changes in wind speed in neutral stability conditions but are significantly adjusted by changes in surface roughness conditions.

In the case of homogeneous, isotropic turbulence (non-layered and equal properties in 3 dimensions), the length scales in the three directions are related by:

$$ {}_{x}L_{u} = 2\,{}_{y}L_{u} = 2\,{}_{z}L_{u} $$

However, this is also approximately true for non-isotropic conditions, but nevertheless still invalid for representing eddy sizes over abrupt changes in roughness where there is significant horizontal 'stretching' of the turbulence.

Teunissen's (1970) summary shows that ${}_{x}L_{u}$ is considerably greater than the other scales in stable air; but in an unstable atmosphere ${}_{x}L_{v}$, ${}_{x}L_{u}$, ${}_{x}L_{u}$, ${}_{x}L_{u}$ are all equal but tend to be larger than in a stable atmosphere.

When length scales of turbulence are required for modelling purposes, the peak of each power spectrum at its specific location in the horizontal direction can be used where:

$$ {}_{x}L_{u} = 0.146\,\frac{\bar{U}_{z}}{n} \quad \text{(ESDU)} \quad . $$

The peak is not always clearly defined so it is difficult to obtain good estimates of ${}_{x}L_{u}$. Also the peak normally occurs in the low frequency end of the spectrum, where the data is not reliable.

Another definition of the length scale is that given by Walshe (1972) where, at the peak of $n\,S(n)$,

$$ {}_{x}L_{u} = \frac{\bar{U}_{z}}{n_{max}.\,2\pi} \quad , $$

where n_{max} = the frequency at $S(n)_{max}$.

Length scales found from the raw data can have instrument errors, averaging errors, and trends in the data which lead to inaccurate estimates. Also, because of the large separations in the frequency at the low

end of the turbulence spectra, the integrated area under the cross product curve of the u', w', components produces an inaccurate length scale. The use of a specific averaging time, say 15 minutes, can lead to large changes in the correlation of u' and w' and hence the value of the $_xL_u$. These problems are not specific to length scale estimates but can be a source of concern when analysing spectra (Ch. 6).

$_xL_u$ is also used as a length-scaling parameter from full scale to model sizes for tree and forest dimensions. The ESDU standard used is

$$_xL_u = 25z^{0.35}/z_o^{0.063} ,$$

for $z_o > 0.02$ m, in the rural surface boundary layer.

Above the surface boundary layer

$$_xL_u = 4.2\ z^{0.73} \qquad \text{(Teunissen 1970)}.$$

2.4 THE DERIVED PARAMETERS FROM THE MEAN WIND VELOCITY PROFILES

2.4.1 The aerodynamic roughness (z_o)

The logarithmic mean wind profile was defined earlier as

$$\bar{U}_z = \frac{\bar{U}*}{k_a} \ln \frac{z + z_o}{z_o}$$

where, $\bar{U} = 0$ at $z = z_o$. z_o is an 'aerodynamic' model of any actual physical roughness of variable structural shape and size with the same effect on the wind profile above the roughness variations. Panofsky (1970) suggests that: "z_o represents the eddy size at $z = z_o$. If the ground is smooth, z_o is zero, and momentum has to be transferred to the surface by molecular action. Over rough terrain, momentum is transferred by differential pressure on the upwind and downwind sides of the roughness elements. z_o ranges from 0.1 mm over the sea or ice to 1 mm over undisturbed grass land to 100 mm over pasture to 1 m or more over cities, forests and hills. Accurate values of z_o can only be determined from measured wind profiles". If the wind speed is measured at 2 or more heights, U_* and z_o can be determined for equilibrium conditions.

A plot of $\bar{U}$ vs $\log_e z$ has a slope of $k_a/\bar{U}_*$ and an intercept of z_o. Since $k_a = 0.41$, $\bar{U}_*$ and z_o can be derived from the mean wind velocity profiles.

The equation is adequate provided the roughness elements are not too large or winds too strong. The effect of surface conditions is not completely represented by the roughness length, since z_o is a measure only of the small scale features of the surface and does not account for large sudden changes in z that occur over hills or at the leading edges of forests. A displacement of the surface layer at the ground takes place which modifies the logarithmic law, (see Chapter 3). Also contributions to turbulent kinetic energy from convective energy in unstable air can alter z_o. However over rough terrain, most of the turbulence is of mechanical origin, especially in the high frequency components of the wind that adjust the mean wind profiles as well as the turbulence spectra.

It was shown earlier that the turbulence intensity I_{σ_u} is related to z_o provided the shear stress is constant and values of z_o are less than 0.10 m, as in the rural surface boundary in equilibrium conditions. As the roughness increases, adjustments to any model equation representing the turbulence intensity profile must be made, (Counihan, Fig. 2.3).

(a)

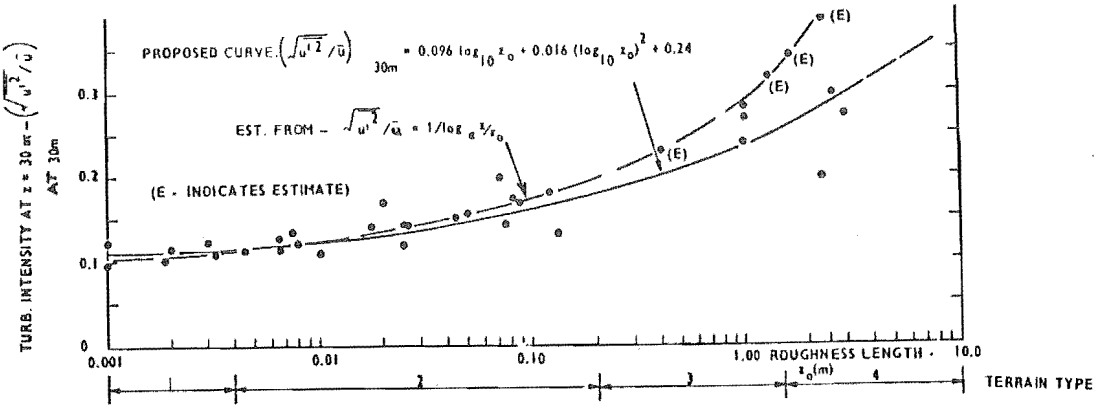

(b)

TERRAIN TYPE / QUANTITY	1 SMOOTH ICE - MUD - SNOW - SEA	2 MODERATELY ROUGH SHORT GRASS + GRASS - CROPS - RURAL	3 ROUGH RURAL + WOODS - WOODS - SUBURBS	4 VERY ROUGH URBAN (forests)
z_o, cm	0.001 - 0.04 - 0.1 - 2.0	0.1 - 3 ~ 7 - 20	100 - - 150	100 - 300 - 400
$\overline{u'w'}/\hat{U}_o^2$	0.0004 - 0.006 - 0.001	0.0014 - 0.0020 - 0.0040	-	-
$1/\alpha$	0.09 - 0.11 - 0.12	0.13 - 0.143 - 0.16	0.20 - 0.23	0.25 - 0.40
$\left(\sqrt{u'^2}/\bar{u}\right)_{0 \le z(m) \le 30}$	0.10 - 0.12	0.13 - 0.20	- 0.20 -	0.30 - 0.48

FIGURE 2.3 (a) & (b) Turbulence intensity and roughness categories over terrain (after Counihan).

2.4.2 Reynolds stresses, friction velocity and friction coefficients

The Reynolds stresses resulting from averaging techniques of the fluctuating wind components in 3 directions are shearing stresses which can be three orders of magnitude larger than the shear stresses which arise from the direct action of viscosity, the difference increasing with the scale of the turbulence. In the turbulent surface boundary layer the shearing actions are made independent of the fluid viscosity.

The laminar sub-layer (frequently quoted in controlled environments) and the task of modelling for Reynolds number similarity, are largely irrelevant in the turbulent boundary layer flow of the atmospheric surface winds.

The Reynolds stresses $\rho\overline{u'v'}$ and $\rho\overline{v'w'}$ are assumed equal to zero throughout the planetary layer. In the surface layer, the $\rho\overline{u'w'}$ Reynolds stress, determined by the variance ratios, is assumed constant,

$$\overline{u'w'}/u'w' = -0.31 \qquad \text{(Teunissen 1970)} .$$

$-\rho\overline{u'w'}$ represents the downward flux of x-momentum through unit area per unit time. But momentum/time is force, hence $-\rho\overline{u'w'}$ has the dimensions of force per unit area, represented by a stress on a horizontal area in the x-direction.

Near the ground where the stresses rise because of accelerations, roughness variations and stability changes, these stresses (Reynolds stresses) become significant.

Now $-\rho\overline{u'w'} = \tau = \tau_o = \rho\bar{U}_*^2$, as defined earlier, and a shear stress coefficient (C_f) can be defined as a ratio of this shear stress to the normal pressure at any location. At reference height (say 10 metres) in the open rural boundary layers

$$C_{f_o} = \frac{\rho\bar{U}_*^2}{\frac{1}{2}\rho\bar{U}_0^2} = 2K_{10} .$$

The table below shows the magnitude of the coefficient, K_{10}, as roughness increases.

TABLE 2.2 Values of the surface drag coefficient at a height of 10 m

(after Counihan)

Ground Roughness Condition	K_{10}
Rough open water	.001 - .002
Open grassland	.003 - .005
Woodland, forests, suburbs	.015 - .030
Urban centres	.030 - .050

Notice how the tangential stresses over the urban type roughness are still only 5% of the normal dynamic pressures produced by the same mean wind velocity at 10 m above datum (cf. Table 4.1).

The ESDU standard for the stress assumes $\bar{U}_z = \frac{\bar{U}_*}{k_a} \cdot \ln \frac{z}{z_o}$, and σ_u is proportional to $\bar{U}_*$ and the roughness z_o in the surface boundary layer. This produces a function for the horizontal stress in equilibrium conditions, as

$$\tau_u = \left[0.867 + 0.556 \log_{10} z + 0.246(\log_{10} z)^2\right] . \lambda$$

where $\lambda = 1.0$ for $z_o \leq 0.02$ m

or, $\lambda = 0.76/z_o^{0.07}$ for $0.02\text{m} < z_o \leq 1.0$ m

or, $\lambda = 0.76$ for $z_o \geq 1.0$ m (i.e. forests)

The local Reynolds stress $-\rho\overline{u'w'}$ in a neutrally stable boundary layer near the surface is equivalent to the profile Reynolds stress $\rho\bar{U}_*^2$, since the stress is assumed constant.

Counihan (1975) proposed that the ratio of this component of Reynolds stresses to the normal pressure at 10 metres above ground in a rural boundary layer can be represented by:-

$$\frac{\overline{u'w'}}{\bar{U}^2_{.0}} = 2\, C_{f_o} = 2.75 \times 10^{-3} + 6 \times 10^{-4} \log_{10} z_o$$

which applies for all rural mean wind profiles in neutral equilibrium between 20 m and 45 m height.

The above relationships do not apply when the temperature lapse rate in the surface layer is non-adiabatic.

2.4.3 The role of Richardson's Number (Ri) or the Monin-Obukhov length (L)

Richardson's Number is a dimensionless quantity which represents the ratio of buoyant energy input into turbulence to the energy input by shear of the mean flow. Two extreme conditions exist in the surface layer: if the buoyancy is positive and provides all the turbulence, it is called *free convection* and Ri is very large and negative; if the buoyancy is large and negative, Ri is large and positive, turbulence is suppressed, and vertical mixing is almost non-existent. So a positive critical Richardson number ($Ri_c \simeq 0.25$) exists above which turbulence is suppressed and below which turbulence is generated.

The Richardson's Number as defined is a flux Richardson's Number (Ri_f) since it measures the rate of exchange of turbulence between the convective and mechanical forms of energy. For practical reasons the ratio is normally defined as a gradient Richardson's Number (Ri_g) (which is proportional to the flux Richardson's Number (Ri_f)) by the relation:

$$Ri_g = \frac{g}{\bar{T}} \frac{\partial \theta}{\partial z} \Big/ \left(\frac{\partial \bar{U}_z}{\partial z}\right)^2 .$$

In strong mean winds, gradient Richardson's Number (Ri_g) in the surface layer is nearly always below 0.25 and turbulence is present from convective transfer. Even in very light winds of about 1 m/s little turbulence exists unless the total temperature change is above $-2.1^{\circ}C/km$, which is extremely large, (Panofsky pers comm.).

The Richardson's Number is important for several reasons:-

- it shows the relative magnitudes of convective turbulence and mechanical turbulence;
- when modelling the atmosphere in wind tunnel tests, which require accurate modelling of the low frequency eddies in the spectra of the boundary layer (e.g. diffusion, shelter), the boundary layer must have the correct Richardson's Number;
- distortion of the mean wind velocity profile by the convective term requires adjustment of the shear stress.

By defining a non-dimensional wind shear

$$\phi_m = \frac{k_a}{\bar{U}_*} \cdot \frac{\partial \bar{U}_z}{\partial z} = f.(Ri_f),$$

(which by observation is unity for purely mechanical turbulence), and a

length (L) independent of z but proportional to a height at which convection and turbulence are in equilibrium with each other,

$$\phi_m \times Ri_f = \frac{z}{L} \quad ,$$

so that the integral of ϕ_m from z = 0 to z = L, called χ_m, provides a measure of the stress adjustment. Tables of this adjustment have been prepared by Businger (1970).

A table of χ_m^{-1} versus $\bar{U}_{*prof}$ (Garratt 1978(b) and results by Bache and Unsworth, show changes in the values of χ_m for changes in stability and mean velocity profile shape: χ_m appears constant with $\bar{U}_{*prof}$.

Panofsky (pers. comm.) gives

$$\frac{z}{L} = Ri_g \qquad (\text{if } Ri_g < 0)$$

and,

$$\frac{z}{L} = \frac{R_{ig}}{1-5\ Ri_g} \qquad (\text{if } Ri_g > 0).$$

In this study the behaviour of the turbulence in the high frequency end of the spectrum of turbulence is important, so the dissipation rate of spectral fluctuations of the turbulent velocity components is required. Here, the variance at any frequency, n_1, is,

$$S(n_1) = ae^{\frac{2}{3}} n_1^{-\frac{5}{3}}$$

where 'e' is the rate of turbulence dissipation which can be replaced by a normalised form for dissipation rate,

$$\phi_e = e. \frac{k_a}{\bar{U}_*^3} = \frac{k_a}{\bar{U}_*} \frac{\partial \bar{U}_z}{\partial z} \quad ,$$

which is the ratio of the slopes of the wind profiles. The slope is constant for neutral equilibrium conditions so $\phi_e = \phi_m = 1$ in those conditions.

The difference between ϕ_m and ϕ_e at two heights is the stress adjustment

$$\phi_m - \phi_e = \frac{z}{L} \quad .$$

Panofsky suggests that a better approximation is

$$\phi_e = \left[1 + 2.5 \left(\frac{z}{L}\right)^{0.6}\right]^{3/2} \quad .$$

2.5 THE SPECTRA OF TURBULENCE IN THE RURAL SURFACE BOUNDARY LAYER

Often when assessing wind loads on structures a distribution of the rms amplitudes of the turbulent components of the wind is required over the full range of frequencies, since structures receiving the loads will respond to frequencies close to their own natural frequency far more readily than to gust frequencies in the wind away from resonance.

Hence a distribution of the variances and the full range of turbulence frequencies is required. The distribution of the velocity fluctuations is:-

$$\sigma_u^2 = \int_0^\infty \left(\frac{\sigma_{u_{\Delta n}}^2}{\Delta n} \right)_u . \, dn \quad ,$$

where $\sigma_{u_{\Delta n}}^2$ is the mean square value of the fluctuations within a band-width Δn at a centre frequency n_c. The quantity $\sigma_{u_{\Delta n}}^2 / \Delta n$ is known as the power spectral density and is denoted by $S(n)_{n=n_c}$

i.e.
$$\sigma_u^2 = \int_0^\infty S(n)_u \, dn \quad ,$$

$$\sigma_u^2 = \int_0^\infty nS(n)_u \, d(\ln) \quad .$$

Thus a distribution of the individual variances with time is obtained showing the distribution of the "frequencies" of the "eddy sizes". This distribution is a transform of the space domain of the auto-correlation functions which depict the "scale", or magnitude, of the eddy sizes.

Generally these spectra of large samples of wind data possess frequency band-widths which are treated statistically independent of other band-widths and, for linear processes, the output dynamic response of a structure can be obtained by multiplying the input wind energy at that frequency by a response function (Davenport, 1967 ; Solari, 1982).

Because of the error in assuming the flow is 'frozen' at low frequencies (Taylor's Hypothesis), errors in the spectra can be significant. These errors are summarised below:-

- low frequency spectral densities increase with increasing convection or instability in the atmosphere;

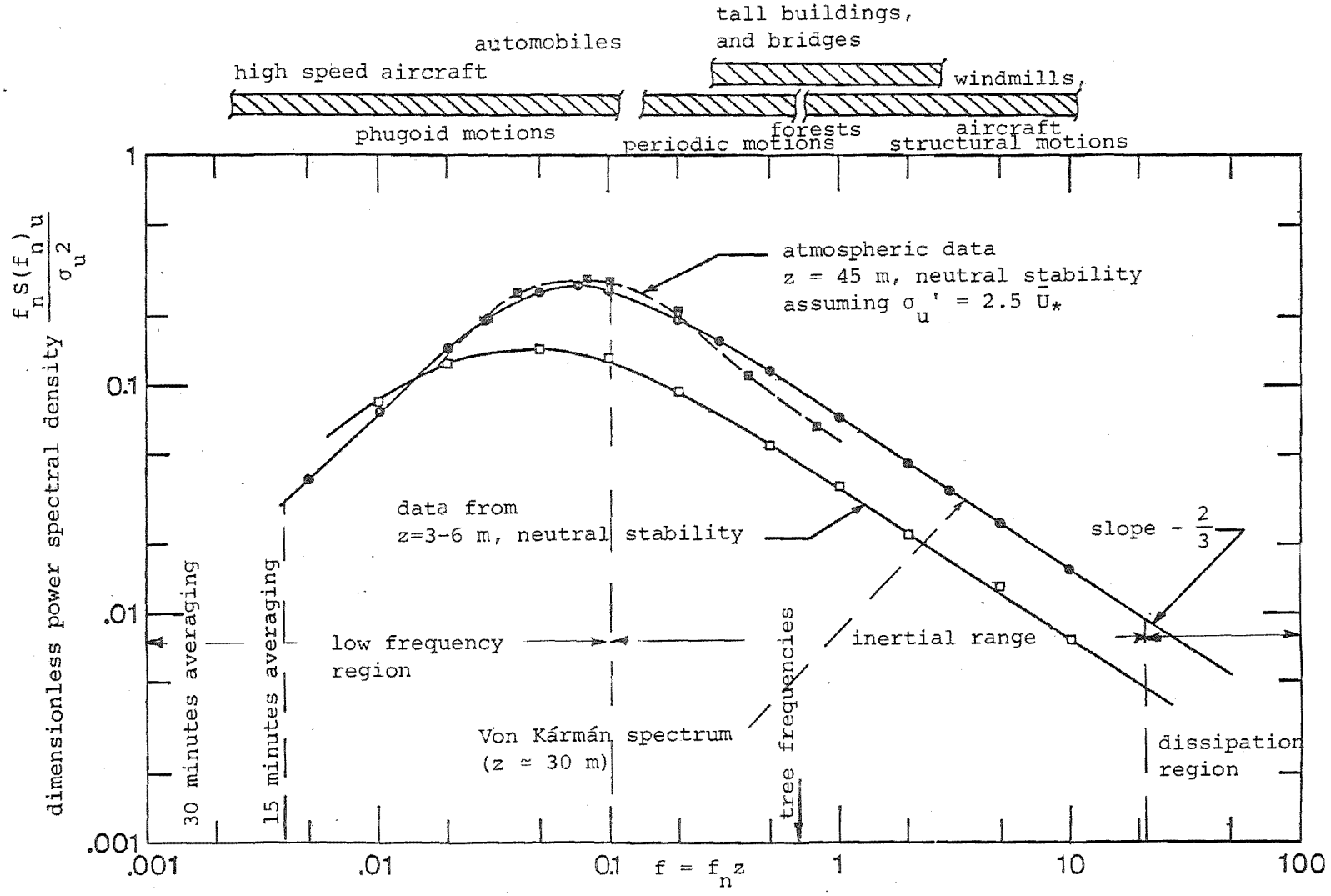

FIGURE 2.4 Longitudinal component power spectra in the surface layer (after Teunissen)

- the total turbulence, and hence the area of the spectral distribution, nSn versus ln(n), increases with increasing mean wind speed, with increasing roughness and with increasing depth of the surface layer;
- other mechanical and convective momentum and/or heat sources and sinks contribute to the distortion of the spectra, such as mean wind accelerations over large obstacles, pressure changes at the earth's surface and, very specifically, the movements of structures immersed in that layer being studied.

All spectra are divided into three components: the low frequency range containing most of the kinetic energy; the inertial higher frequency range; and, at the highest frequencies, the dissipation range or Kolmorgorov region. The inertial range transfers energy from the low frequency range to be dissipated as heat in the high frequency dissipation region. In the inertial range the turbulence is more isotropic than in the low frequency region and very little energy normally enters this region directly from the atmosphere. However, structural motions occur at frequencies within the inertial range and can act as a momentum source to distort the spectra (Finnigan, 1979). A spectral curve of the normal shape with the variance calculated as a function of wave number, f_n, is given in Fig. 2.4.

In the inertial range the spectral density in each direction depends on the dissipation rate 'ε' and the frequency, so that a simple equation can be made to fit the spectral distribution in this region. This is particularly relevant to the method used in this thesis to assess the response of trees to the wind turbulence. A method of assessing the deflections, proposed by Solari (1982) and based on previous work by Davenport (1967), Velozzi and Cohen (1968), and Simui (1980), is used to assess the tree response, (Chapter 6).

In an open country surface layer wavelengths less than 1 m, or frequencies above 10 Hz, are not present in the spectrum in the dissipation range; the variance is dependent on the molecular coefficients as well as ε.

It is therefore implied that stability effects do not significantly adjust the shape of the spectral distribution in the inertial range, but that it is affected by accelerations over abrupt changes in

height 'z', or by aero-mechanical interaction between the forest roughness and the wind.

Højstrup (1981) proposed that the spectrum was made up of two parts where

$$S(n)_u = S(n)_{lower} + S(n)_{upper}$$

where $S(n)_{lower}$ depends on n and $\frac{z}{L}$, while $S(n)_{upper}$ depends only on n in normal conditions

with $$\frac{\hat{n}S(n)_u}{\bar{U}_{*\ell}^2} = \frac{\hat{n}.S(n)_{lower}}{\bar{U}_{*\ell}^2} + \frac{\hat{n}.S(n)_{upper}}{\bar{U}_{*\ell}^2} ,$$

$$= \frac{0.5\ \hat{n}_i}{1 + 2.2\ \hat{n}_i^{5/3}} \left(\frac{z_i}{-L}\right)^{2/3} + \frac{105\ \hat{n}}{(1 + 33\ \hat{n})^{5/3}} ,$$

where $\hat{n} = \frac{nz}{\bar{U}_z}$.

As pointed out by Højstrup, close to the surface a very slight change in $\frac{z}{L}$ from zero to -0.003 may cause a large change in the magnitude of the variance at these low frequency regions. Such conditions are generally regarded as "neutral" since this effect on structural dynamic response is slight. One engineering model for the total spectra is the von Karman shape

$$\frac{n\ S(n)_u}{\sigma u^2} = \frac{4\hat{f}}{(1 + 70.8\ \hat{f}^2)^{5/6}} ,$$

where n is the frequency at variance Sn and $\hat{f}$ is the non-dimensional value $\frac{nxL_u}{\bar{U}}$. This spectrum is too narrow for most atmospheric spectra and the slope in the inertial range is not great enough; the slope should be $-\frac{2}{3}$ when $\ln(n).S(n)_u$ is plotted against $\ln(n)$. The curve has a peak, or maximum, and $n\ S(n)_{max}$ is 0.5 in neutral air and becomes smaller in unstable conditions.

A more general form of the above spectrum which applies to the whole spectrum is given by Panofsky as:-

$$nS(n)_u = \frac{ak_a^{4/3}\bar{U}_z^{8/3}\phi_e^{2/3}(f_n z)^{-2/3}}{\left[\ell n \frac{z}{z_o} - \psi_m\right]^2} .$$

Under neutral conditions (strong winds) this equation simplifies to

$$nS(n)_u = \frac{ak_a^{4/3} \cdot U_z^{8/3} \cdot (f_n z)^{-2/3}}{\ell n^2 \frac{z}{z_o}}$$

so that $S(n)_u$ decreases with increase in height by $\left(\ell n \cdot \frac{z}{z_o}\right)^2 \cdot z^{\frac{2}{3}}$ and increases with $\bar{U}_z^{\frac{8}{3}}$. With increased convection $S(n)_u$ increases as ϕ_e and χ_m both slowly increase. On very sunny days e is independent of height and Sn does not change in the inertial range. This is of practical significance when assessing the wind loads on forests since temperature distributions just above the crop in the inertial region can be ignored.

Panofsky uses;

$$\frac{nS(n)_u}{\bar{U}_{*\ell}^2} = \phi_e^{2/3} \cdot k_a^{-2/3} \cdot \left(\frac{f_n z}{U_z}\right)^{-2/3}$$

and, when ϕ_e is transferred (Högström et al (1983), Ch. 3), in the inertial region at least, the shape of the spectral distribution depends only on 'n' and not stability; so,

$$\frac{nS(n)_u}{\bar{U}_{*\ell}^2 \cdot \phi_e^{\frac{2}{3}}} = a.k_a^{-\frac{2}{3}}.n^{-\frac{2}{3}} \simeq 0.27.n^{-\frac{2}{3}}$$

is a good representation of the spectra shape where a is 0.15 and k_a is 0.41.

Kaimal et. al. (1976) provide some field data of spectra (see Chapter 3) which are regarded as the best source from which to make spectra comparisons; while Davenport obtained some spectral curve equations from which the assessment of wind loads on structures in the open country boundary layer is often made. The wind loads on structures within high roughness cannot use simple velocity profiles often assumed for tall structures in open country.

2.6 CHAPTER SUMMARY

This chapter describes the wind structure in Zone A upwind of a forest leading edge before it is affected in any way by the edge. Some of the conditions described apply equally to flow over infinitely long forest fetches discussed in Chapter 3.

CHAPTER 3

WIND CHARACTERISTICS OVER FORESTS AWAY FROM THE INFLUENCE OF THE FOREST LEADING EDGE

In this chapter a study is made of Zone B (see Fig. 1.1, P.14).

When considering wind characteristics over an infinitely long forest, the vital parameter is the aerodynamic roughness. This is controlled by planting systems, thinning practices within these systems and, as a consequence, the architecture of the canopy which may be either homogeneous or heterogeneous. Knowledge of the aerodynamic roughness allows the wind type to be studied with greater accuracy.

3.1 AERODYNAMIC ROUGHNESS OF FORESTS

3.1.1 Planting systems

Planting systems[1] in man-made forests come into the following four categories which may be found either singly or in various combinations.

(a) Even-aged stands are each of a single age and species, grown in large blocks and forming a quilted pattern.

(b) Mixed species stands are usually even-aged and consist of a mixture of conifers and hardwoods. Canopy roughness increases with age because the trees grow at different rates, producing increased turbulence.

(c) Uneven-aged stands occur when an understorey of young trees is established beneath the canopy of a maturing stand.

(d) The strip system consists of a forest with small strips of even-aged trees at right-angles to the wind.

3.1.2 Scale of roughness

As a result of management procedures using these planting systems, three distinct forms of forest canopy roughness emerge:-

(a) large-scale roughness, which results from terrain changes, forest clearings, roads, fire-breaks, farms and forest leading edges, and so on;

(b) medium-scale roughness, which results from variations in terrain slope and different types of planting systems;

---

1. For further reading, see Foresty Handbook 1977. Ed. C. Chavasse.

(c) small-scale roughness, which results from thinning and pruning treatments within even-aged stands. The controlling parameter is the mean space to height ratio $\frac{S}{H}$ [1].

Current research indicates that wind damage can be either reduced or increased, depending on the canopy roughness, and that small scale roughness can be controlled by stocking density ($\frac{S}{H}$). This implies that the essential factor is a controlled, rather than an arbitrary, thinning programme (Faber, 1975).

Small scale roughness variations are classed as changes to a homogeneous surface of high roughness, whereas the large scale and, to a lesser degree, the medium scale classes of roughness are regarded as heterogeneous surfaces.

3.1.3 Roughness type; homogeneous or heterogeneous

Faber (1975), discussing the stability of stands, makes a valuable distinction between two roughness types:-

homogeneous surfaces with
- optimum roughness of the forest stand;
- optimum roughness between forest stands;

heterogeneous surfaces with
- optimum stability of the forest stand;
- optimum stability of trees within the stand.

A system of forest management in which the aim is the optimum stability of each tree is more flexible than one which aims at optimum aerodynamic stability of the whole forest. It therefore follows that a management system adopting a heterogeneous system (strip) is more flexible than one using a homogeneous system (even-aged stands).

3.1.4 Thinning practices

The first good statement on the theory of thinning was made by Berlepsch, 1761 (Fernow, 1909). Since then, there have been many significant developments.

D. M. Smith (1946) revealed a contrast in attitude towards thinning between European and American foresters. The Europeans believed that early and frequent thinning greatly increased wind firmness, while the

---

1. The inverse of stems/ha is proportional to S.

Americans believed that thinning was an important cause of windthrow. (These apparently contradictory ideas are both correct if the age of the forests and time between thinning are considered as well).

The infinitely long forest has two physical properties which are considered essential to change wind characteristics. Firstly, the forest is extremely rough when compared with other surfaces; this alters with stocking density which produces a very turbulent flow above the canopy especially during the day. Secondly, the forest canopy is not solid but is a moving porous surface where the trees do not all touch their neighbours and where there are sometimes large, cross-sectional gaps (or discontinuities). Stands where stocking densities are high offer minimal aerodynamic disturbance to the wind; the canopy is aerodynamically quite smooth. However, timber quality is low and any break in the canopy due to factors such as logging, roads, natural mortality and disease, will leave the stand susceptible to wind damage.

Thinning, pruning and strip planting schemes in the monospecies forest increase the flexibility[1] of management but decrease forest stability. Other factors that alter roughness, such as soils, moisture and topography are essentially out of the manager's control.

As a stand grows, the mean tree-top height of the forest increases. Mean spacing between trees increases at each thinning (Table 3.1).

3.1.5 Definition of canopy architecture

Bull and Reynolds (1968) state that it is justifiable to characterise the relative turbulence of wind passing over differently managed land and even of different silvicultural treatments. The more aerodynamically rough the surface, the more turbulent the airflow and the faster are the momentum transfer processes.

Immediately after thinning the forest canopy has greater roughness so that, for a given wind velocity over the canopy, the possibility of windthrow increases.

The heterogeneous nature of a forest front will generate extra wind turbulence which adds to windthrow in forests (see Ch. 4). Furthermore, the swaying properties of the canopy and the strong gusts are more damaging than the time-length of the storm. Thus the architecture of the canopy and its swaying properties must be included in any studies of wind damage (Palmer 1968).

---

1. Flexibility refers to such operations as ease of logging, spraying, planting and tending.

TABLE 3.1 Actual thinning practices - Canterbury forests (pers comm. N.Z. Forest Service)

	PLAINS (EYREWELL)				FOOTHILLS (ASHLEY - WORST CASE)			
	BEFORE TENDING		AFTER TENDING		BEFORE TENDING		AFTER TENDING	
AGE (YRS)	$\frac{S}{H}$[1]	$\frac{P}{H}$[1]	$\frac{S}{H}$	$\frac{P}{H}$	$\frac{S}{H}$	$\frac{P}{H}$	$\frac{S}{H}$	$\frac{P}{H}$
6					$\frac{3.65}{6.4} = 0.57$	0	$\frac{4.17}{6.4} = 0.65$	$\frac{2.2}{6.4} = 0.39$
6½	$\frac{2.6}{6.8} = 0.38$	0	$\frac{2.6}{6.8} = 0.38$	$\frac{2.5}{6.8} = 0.37$				
7					$\frac{4.17}{7.6} = 0.55$	$\frac{2.2}{7.6} = 0.29$	$\frac{4.17}{7.6} = 0.55$	$\frac{2.2}{7.6} = 0.29$
7½	$\frac{2.6}{7.7} = 0.34$	$\frac{2.5}{7.7} = 0.32$	$\frac{3.18}{7.7} = 0.41$	$\frac{2.5}{7.7} = 0.32$				
8½	$\frac{3.18}{9.9} = 0.32$	$\frac{2.5}{9.9} = 0.25$	$\frac{3.18}{9.9} = 0.32$	$\frac{4.5}{9.9} = 0.45$	$\frac{4.17}{9.7} = 0.43$	$\frac{2.2}{9.7} = 0.23$	$\frac{4.17}{9.7} = 0.43$	$\frac{4.3}{9.7} = 0.44$
10½	$\frac{3.18}{11.5} = 0.28$	$\frac{4.5}{11.5} = 0.39$	$\frac{5.55}{11.5} = 0.48$	$\frac{6}{11.5} = 0.52$	$\frac{4.17}{12.5} = 0.36$	$\frac{4.3}{12.5} = 0.41$	$\frac{6.03}{12.5} = 0.52$	$\frac{6}{12.5} = 0.52$
13½	$\frac{5.55}{14.7} = 0.38$	$\frac{6}{14.7} = 0.41$	$\frac{5.55}{14.7} = 0.38$	$\frac{6}{14.7} = 0.41$	$\frac{6.03}{16.5} = 0.37$	$\frac{6}{16.5} = 0.36$	$\frac{6.03}{16.5} = 0.37$	$\frac{6.0}{16.5} = 0.36$
PROJECTED 17			$\frac{5.55}{18.1} = 0.31$	$\frac{6}{18.1} = 0.33$			$\frac{6.03}{21.2} = 0.28$	$\frac{6.0}{21.2} = 0.28$
22			$\frac{5.55}{23.1} = 0.24$	$\frac{6}{23.1} = 0.26$			$\frac{6.03}{28.0} = 0.22$	$\frac{6.0}{28.0} = 0.21$
28			$\frac{5.55}{27.0} = 0.21$	$\frac{6}{27.0} = 0.22$			$\frac{6.03}{36.2} = 0.17$	$\frac{6.0}{36.2} = 0.17$
32			$\frac{5.55}{28.6} = 0.19$	$\frac{6}{28.6} = 0.21$			$\frac{6.03}{41.8} = 0.14$	$\frac{6.0}{41.8} = 0.14$

1. For definitions of H, S and P, see Symbols List.

If wind variations over infinitely long forests are to be assessed, roughness away from the leading edge must be:-

(a) homogeneous, so that individual trees are of the same mean top height in the horizontal plane and at a common spacing;

(b) in equilibrium with the flow, particularly in the inner layer, so that there are no additions of energy except from waving of the trees;

(c) of a common canopy architecture which makes changes to tree type, soils, terrain slopes, moisture, elevation, or any management treatment of equal importance;

(d) of the same

mean height,	H
spacing,	S
variance of height,	σH
aerodynamic roughness,	z'_o
zero plane displacement	d
form drag coefficient	C_{D_ℓ}
natural frequency	n_o

mass, M; stiffness, k_s; damping ratio, ζ,

(e) of a fetch at least 10 H long.

The mean tree-top height of a homogeneous forest is H. The tree spacing (S) is found from the number of stems/ha.

In the outer layer the large scale eddies arise from convectional flow, from upstream terrain, or from forest borders (see Ch. 4). The aerodynamic roughness (z'_o) quantifies the canopy architecture and its porosity over a homogeneous roughness. z''_o quantifies the surface roughness in the inner layer over heterogeneous surfaces such as forest borders.

3.2 PREVIOUS RESEARCH ON MEAN AND TURBULENT WIND PROFILE SHAPES DEVELOPED OVER HIGH ROUGHNESS INCLUDING FORESTS

Full scale research over various terrain types has been made by Davenport (1967), Counihan (1970), Kaimal (1972) and Teunissen (1980). Their work and other major contributions have been used to keep ESDU data sheets updated.

Wind profiles in full scale forests have been studied by Reifsnyder (1955), Oliphant (1964), Valendik (1964), Shinn (1969), Turin and Shen (1969), Bergen (1971), Martin (1971), Oliver (1971), Smith et al (1972), Landsberg and Powell (1973), Hicks (1973), Peterson, (1975), Raynor et al, (1976), Garratt (1978a & b), Sadeh and Fox (1982), Cremer et al (1982), Ming et al (1983) and others.

Wind profiles in smaller crops have been studied by Uchijima and Wright (1964, corn), Preston (1969, orchard), Baines (1972, wheat), Legg (1975, wheat), Legg and Long (1975, wheat), Bill et al (1976, maize), Bache and Unsworth (1977, cotton), Finnigan and Mulhearn (1978, wheat), and Maitani (1979, rush and wheat).

Wind profiles in model forests have been studied by Jacobs (1936), Hirata (1951), Fraser (1962), Plate and Quraishi (1965), Meroney (1968), Hsi and Nath (1970), Sadeh et al (1971), Thom (1971) and Johnson et al (1982).

Other studies of wind profiles over artificial roughness have been made by Landsberg and James (1971), Cionco (1972), Seginer (1972), Gartshore (1973), Wooding (1973), Counihan (1975), Faber (1975), White et al (1975), Finnigan and Mulhearn (1978), Knight and MacDonald (1979), Johnson et al (1982), and Cionco (1983).

Comparisons of many of these profiles have been made by Cionco (1978) and are used in this thesis (Figs 3.2; 3.3).

Theoretical models of wind effects over roughness density changes by Silbert (1970), Landsberg and James (1971), Munro and Oke (1973), Lo (1977), Faber (1975), and Shaw and Pereira (1982) have supplemented the model and full scale experiments.

Shinn (1969) summarised the mean wind and turbulence characteristics in and above a particular forest in South Carolina. The mean wind vector

had two notable features: a nearly constant speed in the lower two-thirds of the canopy and a turning of the wind direction with height in the same layer. All three components of turbulence intensity were larger below the canopy, especially the longitudinal component. Energy dissipation was nearly constant with height. The turbulence intensity profile just above the canopy fell rapidly from 75% to 30%; it remained constant at 75% from H to 2/3 H, then increased again to 120% at 1/3 H. The lateral component of the turbulence intensity was nearly constant at 40% from ground level through H to 2 H. The vertical component of turbulence was distributed in a similar way to the lateral component, with the average value falling from 35% at 2/3 H to zero at ground level. It decreased again from 35% at 2/3 H to 20% at 2 H (cf Fig. 7.3; 4.4.3).

Martin (1971) studied turbulence profiles in tall canopies and suggested that the ratio of the wind speed in the trunk space to the wind speed above the canopy is a measure of the magnitude of turbulent transfer through the canopy. The ratio relates to the forest's physical properties; it is maximum at noon and reduces to 75% of the maximum at night.

Maitani (1978) studied the mechanism of downward flux of turbulent kinetic energy in the surface layer just above plant canopies. He concluded that:-

(a) the intensities of turbulence u', v', w' are very high and gradually decrease with increasing $\frac{z}{H}$;

(b) the spectra of u'^2, v'^2, w'^2 are non-gaussian with appreciable skewness and flatness higher than 3;

(c) the u' component has positive skewness and the w' component has negative skewness;

(d) the skewness is at maximum just above the canopy height and decreases with increasing $\frac{z}{H}$;

(e) the height dependency of u' in the field is similar to that obtained by Seginer (1972) in wind tunnel experiments;

(f) the skewness, flatness and high variance are closely related to the downward transport of turbulent kinetic energy and hence $\bar{U}_*$;

(g) the non-gaussian and skewed nature occurs because the level of downward flux of kinetic turbulent energy is much greater than the upward flux. The net flux expresses x-momentum transport change in the $\frac{z}{H}$ direction (Reynolds stress divergence) from equilibrium.

Panofsky (pers. comm. 1983) suggests that the non-gaussian and skewed nature can be modelled by equivalent gaussian distributions with differing variances σ_u^2, so that, if local levels of turbulence intensity are measured in the vertical direction, the spectra of turbulence intensity can still be modelled using the Von Karman constant, k_a, and $\bar{U}_{*_\ell}$ related by a mixing length. Garratt (1978) uses a mixing length, as above, to establish a link between the aerodynamic canopy height (which is above mean tree-top height) and the displacement thickness.

Högström et al (1983) suggest that the skewness of u' can depict the extremes of the gusts by using the relation:-

$$Sk_{u'} = \frac{\overline{u'^3}}{(\overline{u'^2})^{\frac{3}{2}}} = \frac{\overline{u'^3}}{\sigma_u^{\frac{3}{2}}}$$

and that the value of $Sk_{u'}$ is strongly influenced by the canopy architecture.

Turbulence at canopy height results from three factors: the first, indicated by previous research, is the increase in canopy turbulence up to the transition region which depends on z_o" or tree spacing; the second is the generation of turbulence by the waving motion of the trees; the third is the turbulence arriving from the transition region above, where high shear flows are produced by terrain changes or other large disturbances upstream.

3.2.1 The structure of the wind above homogeneous forest canopies in equilibrium

At the base of the inner layer (Fig. 3.1) the airflow is essentially a drift with low mean wind speeds (<1 m/s) and very high turbulence levels. The maximum shear contour of the wind profile produced over the mean tree-top height forms the boundary between the inner and outer layers. Turbulence intensities are high and slowly decrease as the eddies penetrate into the canopy towards the stagnant air. Leaf area distribution in the canopy has no special significance, but canopy shape and porosity are significant since eddies are of the same order of magnitude at the exposed crowns of the trees. The transition height is to the point of inflexion in the mean wind profile which is a further 0.3 H above the mean tree-top height, H.

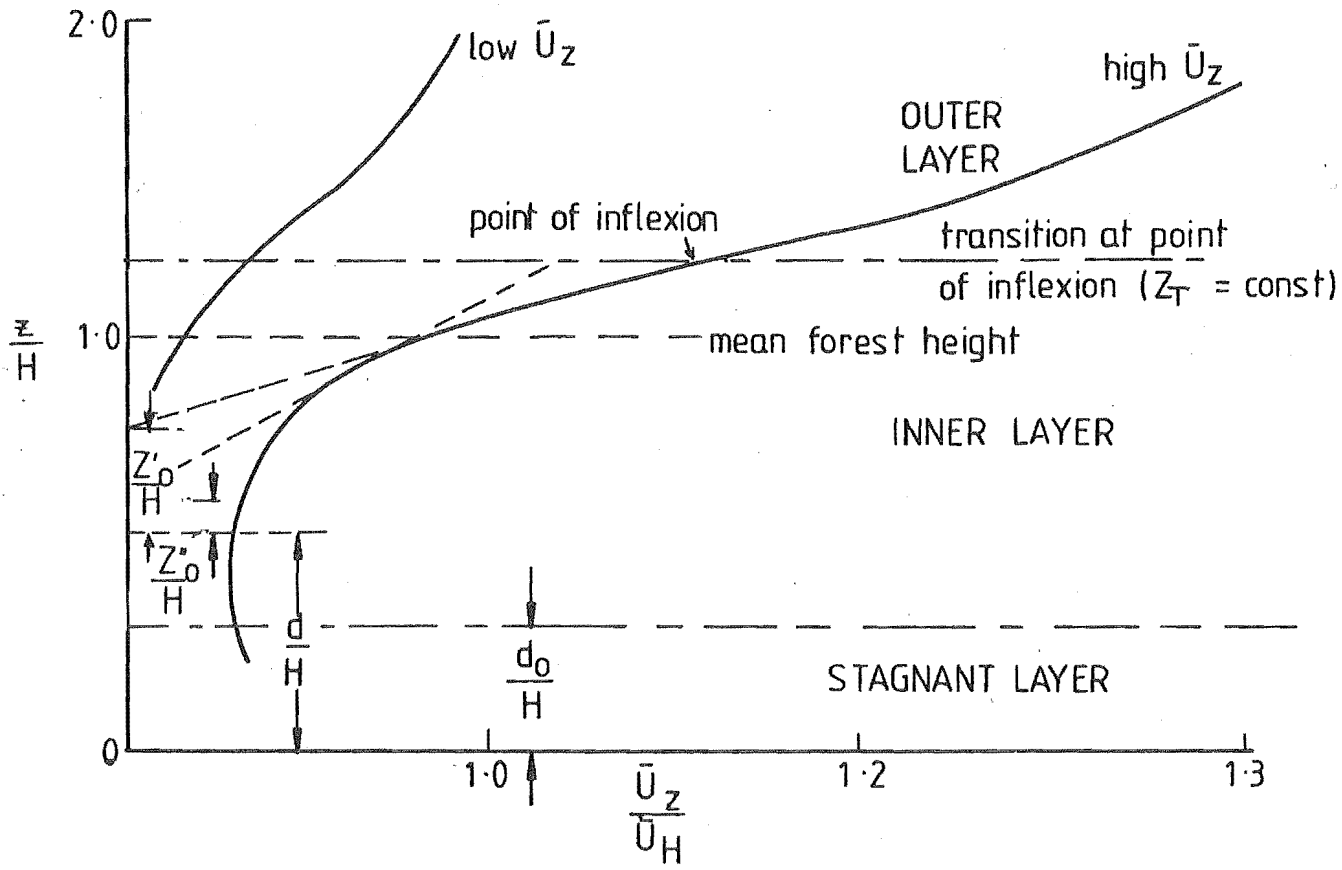

FIGURE 3.1 Mean wind profile over a forest canopy

Valendik (1964) established that the wind forces in the understorey of a forest are entirely lost and that equilibrium is reached 200 m in from the forest front. The decay rate is logarithmic and

$$\bar{U}_{internal} = \bar{U}_{external} \cdot e^{-a.x} ,$$

where a = 0.023 for a spruce forest.

Static pressures in the understorey and trunks up to a certain height, known as zero-plane displacement, d, form a static pressure field over the forest floor (stagnant layer).

Cionco (1978; Fig.3.2) relates canopy density, element flexibility, and mean wind speed profiles in tall crops, both model and full scale. His graphs represent simple canopies (rigid or very flexible elements) and complex canopies (elements with small flexibility). Note the difference in wind speed profile shapes.

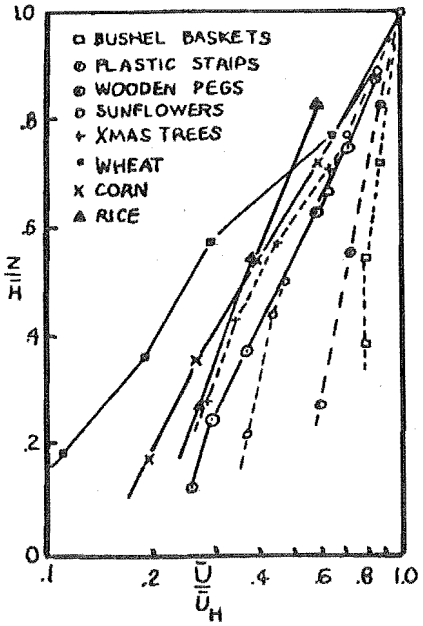

FIGURE 3.2 Wind Profiles - Simple Canopies (After Cionco)

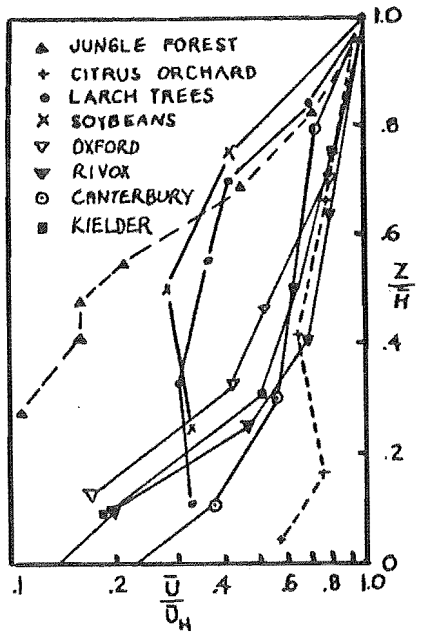

FIGURE 3.3 Wind Profiles - Complex Canopies (after Cionco) with model and full scale profiles

Garratt (1978), when estimating the changing stress at tree top height, observes that ϕ_m and ϕ_e (see Ch. 2) are significantly below unity when the logarithmic law is observed. He notes that if $z_o' > 1$ m, then no logarithmic section exists in the mean wind profile above the crop, and other non-dimensional parameters characterize the surface besides aerodynamic roughness (see Ch. 4).

3.3 THE IDEALISED MEAN WIND VELOCITY PROFILE SHAPE

An ideal canopy architecture could be postulated as having:-

(a) a uniform vertical leaf area distribution.

(b) a uniform vertical distribution of the drag coefficient of the canopy elements;

(c) a drag coefficient that is independent of the local Reynolds number;

with the following wind properties of a forest canopy of infinite length;-

(a) a mixing length that is constant with height except near the ground;

(b) a turbulence intensity that is constant with height;

(c) a windspeed that has two logarithmic curves as a function of height, with the flow continuous through the interface of the inner and outer layers (Cionco, 1978).

Note that these wind properties are modified at, and just in from, the leading edge (see Ch. 4).

Using the accepted logarithmic law, the inner layer of the velocity profile will start at a zero-plane displacement (d) above the ground which represents a vertical displacement of the momentum sink by the physical nature of the trees. Also, the profile within the crown will have a logarithmic slope $\left(\frac{\bar{U}*_{\ell}}{k_a}\right)$ and intercept z_o'' while the outer layer starts at the point of inflection with a slope $\left(\frac{\bar{U}*_{prof}}{k_a}\right)$ and an intercept z_o'. (By definition here $k_a = 0.41$ is assumed constant). The momentum source for the lower layer is a distance (d_o) from the ground and below the normal value of $d \simeq 0.75\ H$ (Thom 1972). Thus for neutral strong wind conditions:-

$$\bar{U}_z = \frac{\bar{U}*_{\ell}}{k_a} \ln\left(\frac{z-(d_o-z_o'')}{z_o''}\right) \quad \ldots\ \text{(inner layer)}$$

and, $$\bar{U}_z = \frac{\bar{U}*_{prof}}{k_a} \ln\left(\frac{z-(d-z_o')}{z_o'}\right) \quad \ldots\ \text{(outer layer)}.$$

In equilibrium $\bar{U}*_{prof} = \bar{U}*_{\ell}$, $z_o' = z_o''$, and internally within the forest, $\bar{U}_z$ is a function of $d + z_o'$ at any height z.

If any instability is present then the mean wind profile is adjusted so that,

$$\bar{U}_z = \frac{\bar{U}*_{prof}}{k_a} \ln\left(\frac{z-(d-z_o')}{z_o'} \pm \frac{\alpha'(z-(d-z_o'))}{L}\right)$$

where L is the Monin-Obukhov Length, and α' is a Monin-Obukhov coefficient which is unity for neutral conditions.

3.4 THE TURBULENT WIND VELOCITY PROFILE SHAPE

The turbulent velocity profile alters with roughness. Over forests the turbulence intensity can reach 75 - 80% (Turin and Shen, 1969; Sadeh et al, 1971). The turbulent wind velocity profile over terrain with high

roughness (z_o > 1 m) is represented by the same relation that is given in Ch. 2 for smooth terrain except that the parameter in the equation (λ) is adjusted for high values of z_o.

Vegetation interacts with the turbulent flow above the canopy, producing sources and sinks of momentum and heat which modify the above-canopy turbulence. The non-uniform distribution of sources and sinks differs from the constant heat and momentum flux rates that exist in the open country surface layer discussed in Ch. 2. (Mayer, 1981; Holbo et al, 1980). Comparisons of turbulence intensities over model and full scale forests are made in Chapter 7 (Figs 7.3; 7.4).

3.5 OTHER FEATURES OF WINDS AT TREE-TOP HEIGHT

Wind profiles above a forest canopy in neutral conditions, where $Ri_g \in (-0.05, 0.10)$, follow a pure log form. Outside this stability range a log-linear profile can be fitted.

In an equilibrium state the turbulence intensity varies with stability of the air and with height above the canopy; the 'decay parameter' (e) decreases with increasing height and decreases with increasing wind speed up to 20 m/s for $Ri_g \in (0.1, 0.3)$. There is no decay in unstable air up to 20 m/s. Above 20 m/s turbulence intensity is 20% and can be assumed to be independent of wind speed and temperature at least down to 3 H above the canopy; it then increases with decreasing height (Oliver, 1971). In the case of forests, turbulence intensity is proportional to $(z-d)^{-\frac{1}{2}}$ just above the canopy (Inoue, 1952).

Differences in canopy temperature, humidity and carbon dioxide content do not appear to affect z_o' ; hence the vertical wind profiles are unaffected (Bowen ratio is constant).

Ri_g has little influence on the turbulence in the higher frequency end of the spectrum (see Ch. 2) where the effects of the turbulent winds are related to z_o'' and tree waving. Energy dissipation near the canopy is essentially constant with altitude in unstable air, but decreases as $\frac{1}{z}$ in neutral air (see Ch. 4).

For very large roughness $\frac{\sigma_u}{\bar{U}_z}$ is independent of $\frac{z}{L}$ (Högström et al, 1983) (Fig. 3.4).

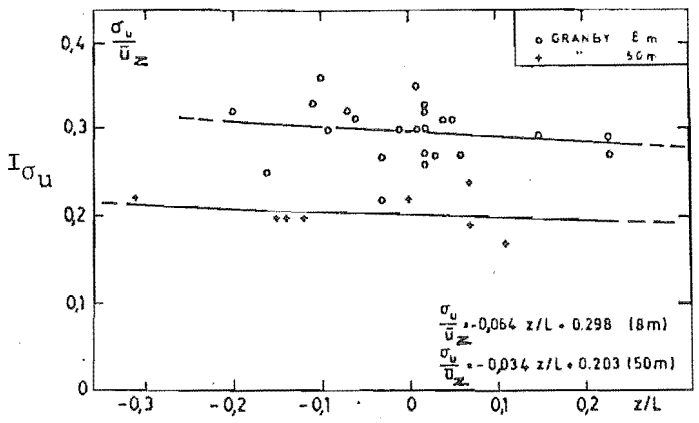

FIGURE 3.4 Turbulence intensity of longitudinal wind component versus stability (after Högström et al)

Up to 150 m height, Ri_g changes sign at 50 m from negative to positive values, even though the buoyancy force is upwards. $\frac{z}{L}$ does not change sign and is therefore used more to modify shear stress relationships.

3.6 RELATIONSHIPS BETWEEN TREE SPACING AND AERODYNAMIC ROUGHNESS

In a study of a vineyard crop array, Hicks (1973) tested the crop on two occasions, three months apart, during which the leaf density increased and the crop grew from 0.9 m to 1.4 m. Roughness lengths were approximately 13% of the crop height in each case $\frac{z'_o}{H} = 0.13$.

Young apple trees placed in a large wind tunnel, with the leaf density altered between runs by thinning, gave drag from interference 50% higher before thinning than the resistance of unsheltered leaves (Landsberg and Powell, 1973).

Now, since

$$U_z = \frac{U_{*\ell}}{k_a} \ln.\left(\frac{z-(d-z'_o)}{z'_o}\right),$$

therefore,

$$\mathbb{I}\sigma_{u_z} = \frac{\sigma_u}{\bar{U}_z} = \frac{k_a \sigma_u}{\bar{U}_{*\ell}.\ln.\left(\frac{z-(d-z'_o)}{z'_o}.\right)}$$

If k_a, $\bar{U}_{*\ell}$ and σ_u can be measured at any height z, it is possible to show dependence of the turbulence intensity ($\mathbb{I}\sigma_{u_z}$) on z'_o with height change (z) for any particular value of z'_o and d (see Ch. 2).

A formula from the work of Koloseus and Davidian relating to the friction velocity, and comparing shear stress with thinning (Wooding et al, 1973) is:-

$$\frac{\bar{U}_z}{\bar{U}_{*\ell}} = B \ln \left(\frac{\delta}{k_a} \cdot \frac{\lambda_e}{k_a}\right)$$

where $\lambda_e = S$ = equivalent spacing,

B = constant = 2.44,

$$\frac{\bar{U}}{\bar{U}_{*\ell}} \cdot \frac{\delta^*}{\delta} = 3.83 ,$$

with $\delta^* \equiv d$,

$\delta \equiv H$,

and $k_a = 0.41$ = Von Karman's constant.

Wooding et al, Gartshore, Knight and Macdonald have all suggested that this relationship is consistent with findings by other investigators, but Gartshore implies that it is also suitable where the boundary layer is not fully developed in the streamwise direction.

Meroney (1968) studied the flow over a canopy with high roughness elements made of pegs 180 mm high and 48 mm in diameter arranged in four patterns, $\frac{S}{H}$ varying between 0.2 and 0.564. The friction velocity and the stocking or roughness density affected the flow field. (In this investigation instrumentation errors have been found. See Ch. 7).

Counihan (1971) modelled canopy roughness and established the variation of the roughness length as a function of both fetch and roughness density (the degree of thinning) by the relations:-

$$\frac{z'_o}{H} = 8.2 \frac{H}{x} + 1.08 \frac{A_r}{A_t} - 0.08 \qquad \text{(for short fetch)} ,$$

and

$$\frac{z'_o}{H} = 1.08 \frac{A_r}{A_t} - 0.08 \qquad \text{(for large fetch)} ,$$

$$\frac{A_r}{A_t} = 0.25 \quad \text{when} \quad \frac{S}{H} = .30 ,$$

where A_r = plan surface area of the roughness elements

and A_t = total plan surface area.

For $\frac{A_r}{A_t} \varepsilon (0.10, 0.25)$, each roughness element (tree) produces its maximum energy. Secondary flow effects are minimal in the flow regime. $\frac{A_r}{A_t} = 0.25$ is regarded as the ratio common to suburban or urban areas and forests (Counihan 1971).

If stocking density reduces beyond $\frac{A_r}{A_t} = 0.25$ then the risk of generated turbulence from the foliage roughness increases, instead of decreasing, as suggested by Counihan (Fig. 6.38).

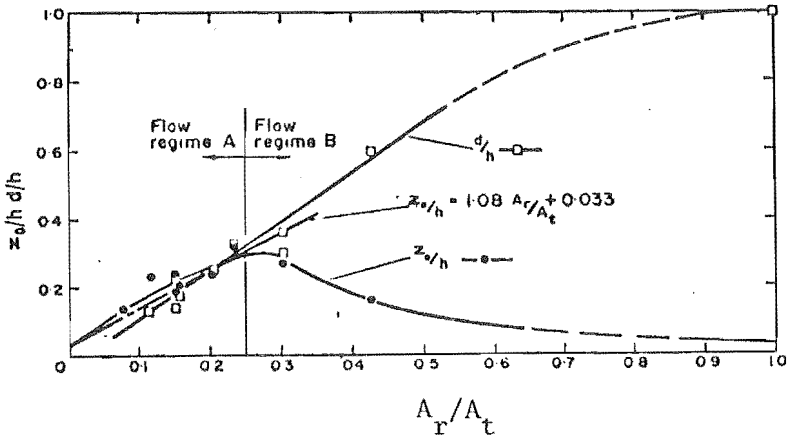

FIGURE 3.5 Variation of mean roughness length and mean zero-plane displacement with roughness element density at constant fetch (+70H) (after Counihan)

When $\frac{z''_o}{H}$ is a maximum, $\frac{A_r}{A_t} = 0.25$ is equivalent to an $\frac{S}{H}$ value of 0.30. The zero-plane displacement increases as element spacing reduces. For spacings beyond $\frac{S}{H} = 0.30$, $\frac{d}{H}$ reduces to $\frac{d}{H} = 0.4$ (Counihan).

Alteration in the wind profile power index increases for increased wind velocity and canopy roughness (see Fig. 3.6).

When the tree crown shape is a side elevation normal to the wind and a plan view, the ratio of the projected crown areas is λ_e.

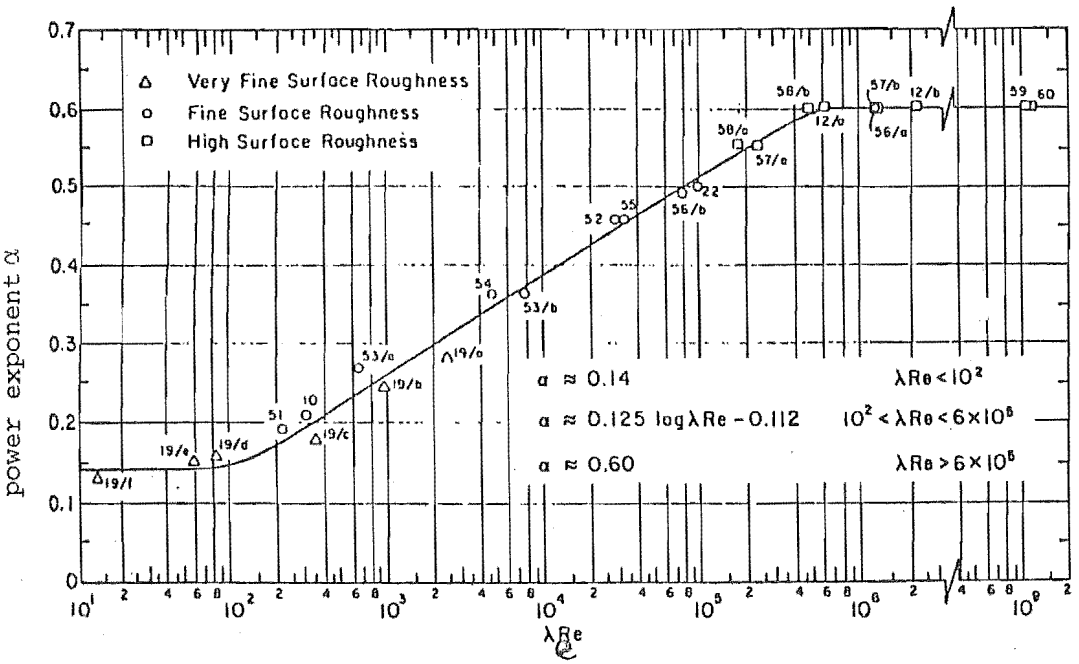

FIGURE 3.6 Variation of the power-index with increasing roughness-wind interaction parameter (from Sadeh and Fox after Wooding)

So, λ_e is related to spacing by

$$\lambda_e \simeq \frac{S}{H\ C_{z_o}''} \simeq \frac{z_o''}{H-d} \quad .$$

C_{z_o}'' is the tree crown diameter at the zero plane displacement (d)
so,

$$\frac{1}{\lambda_e Re} \alpha \frac{S}{H} \quad .$$

Thom (1971) similarly linked canopy architecture to the aerodynamic roughness with $\lambda_e = 0.1$.

3.6.1 Zero-plane displacement and aerodynamic roughness

These parameters are controlled by the structure of the forest canopy architecture. Shaw and Pereira (1983) related the zero-plane displacement and aerodynamic roughness mathematically and constructed Fig. 3.7.

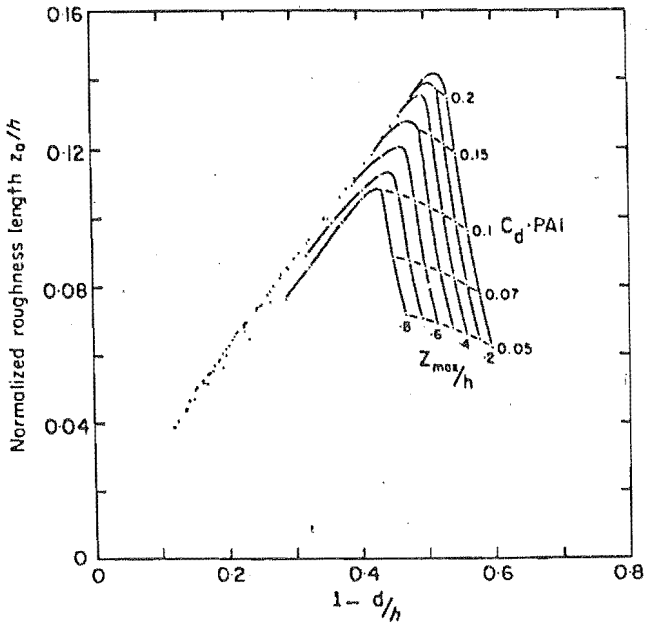

FIGURE 3.7 Plot of roughness length against displacement height (after Shaw and Pereira)

There is a unique relationship between d and z_o'' as roughness density reduces after a maximum value of $\frac{z_o''}{H}$ is reached.

When $\frac{x}{H}$ is large enough, ($z_o''=z_o'$) the aerodynamic roughness is related by:-

$$\ln.z_o' = -1.24 + 1.19\ \ell n.H. \qquad \text{(Hsi and Nath 1970)}$$

A list of $\frac{z_o''}{H}$ and $\frac{d}{H}$ values is presented below in Table 3.2.

TABLE 3.2 $\frac{z'_o}{H}$ and $\frac{d}{H}$ values for tall crops

Research by:	$\frac{z'_o}{H}$	$\frac{d}{H}$	C_P, Cf_o		Type
Tanner et al (1960)	0.13	Cowan 0.64			
Oliphant (1964)	0.11	0.67			full scale
Plate et al (1965)	0.15				model
Kawatani & Merony (1968)	0.32				model
Szeiz (1969)	0.10				model
Lettau (1969)	$0.5 \frac{A_r}{A_t}$				model
Wooding et al (1973)					model
Thom (1971)		0.75			model
(1975)		0.79			full scale
Smith et al (1972)	0.065	0.75	.087		full scale
Kalma & Stanhill (1972)	0.095	0.67			full scale
Hicks (1973)	0.130				full scale
Seginer (1974)	0.14		0.6 H,		model
Hicks (1975)	0.051			8 m spruce	full scale
Legg et al (1975)		0.67			
Kondo et al (1976)	0.31 max		0.6 H,		
Högström et al (1983)					full scale

The average value for $\frac{z'_o}{H}$ is 0.13 and for $\frac{d}{H}$ is 0.71.

Peak values of $\frac{z'_o}{H}$ are quoted by Counihan, Kondo et al, and Shaw and Pereira.

3.6.2 Shear stress and stocking or roughness density

The shear stress coefficient over the inner layer is assumed constant with height at high wind speeds. Thus, in equilibrium, the mean wind speed profiles are the same, with the generation of turbulence constant. The scale of turbulence remains constant with fetch but must be characterised by the roughness and the forest height as well as the movement of the roughness (Martin 1971).

As the surface boundary layer grows downwind of a forest leading edge, equilibrium conditions are reached in the inner layer sooner than in the outer layer and shear stress variations are constant sooner.

Static pressure variations in the stagnant air layer below the inner layer are also constant.

Smith, Carson and Oliver (1972) apply the equations of motion to the wind field in a forest canopy, and balance the shearing stress gradient $\frac{\partial \tau}{\partial z}$ against the form drag of the leaves in the canopy. The horizontal pressure gradient in the more open space beneath will have almost zero pressure gradient, and the shear stress gradient is constant.

Over a cotton crop the aerodynamic features of the upper levels of the canopy can be scaled using $\lambda_e \bar{U}_*$, and (H-d) (both regarded as measures of the stocking density and wind speed).

Mixing length increases with increase in height and its variation may be due to the stiffness characteristics (flexibility) of the stems. $\bar{U}_{*_{prof}}$ above the canopy is plotted against the minimum within-canopy mean wind velocity (Bache and Unsworth, 1977).

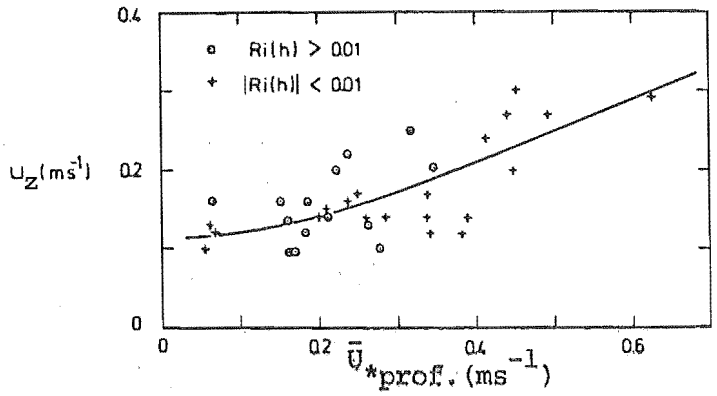

FIGURE 3.8 Variation of the minimum in-canopy mean velocity $\bar{U}_z$, with friction velocity ($\bar{U}_{*prof}$) above the canopy, (after Bache and Unsworth)

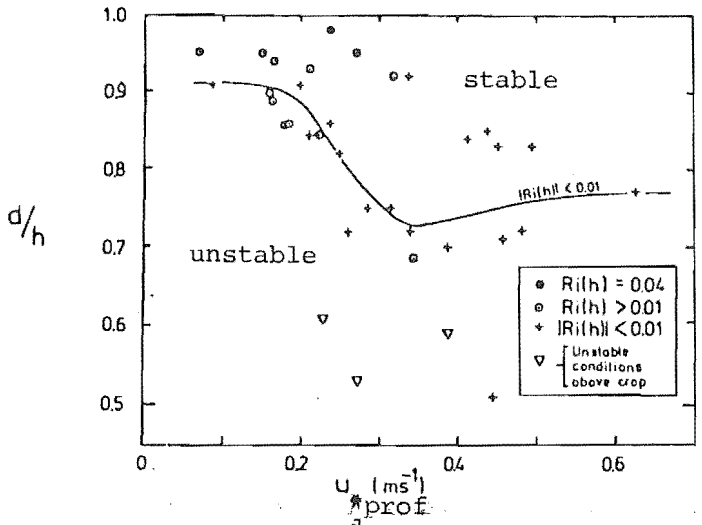

FIGURE 3.9 Variation of $\frac{d}{H}$ with transition friction velocity U_{*prof} (after Bache and Unsworth)

$\bar{U}_*$ and z'_o are influenced by the wind speed over a range of Richardson's numbers measured in full scale experiments (Saugier and Ripley, 1978).

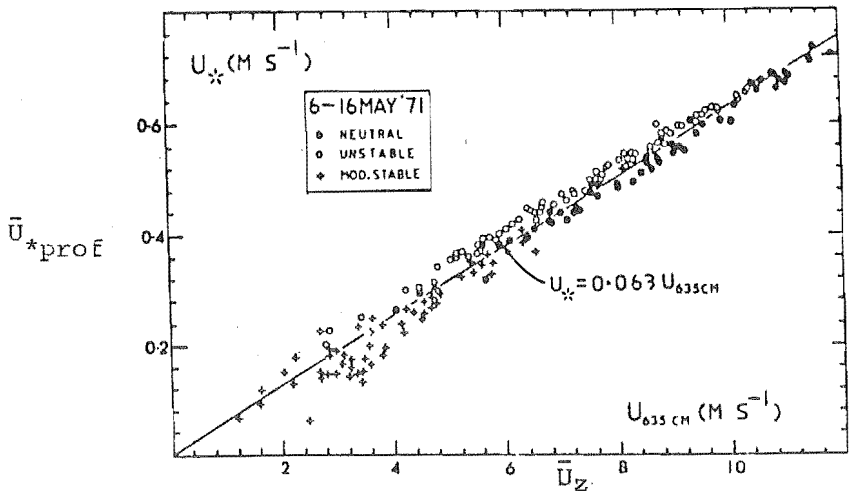

FIGURE 3.10 A relationship between $\bar{U}_{*prof}$ and $\bar{U}_z$ over grassland, (after Saugier and Ripley)

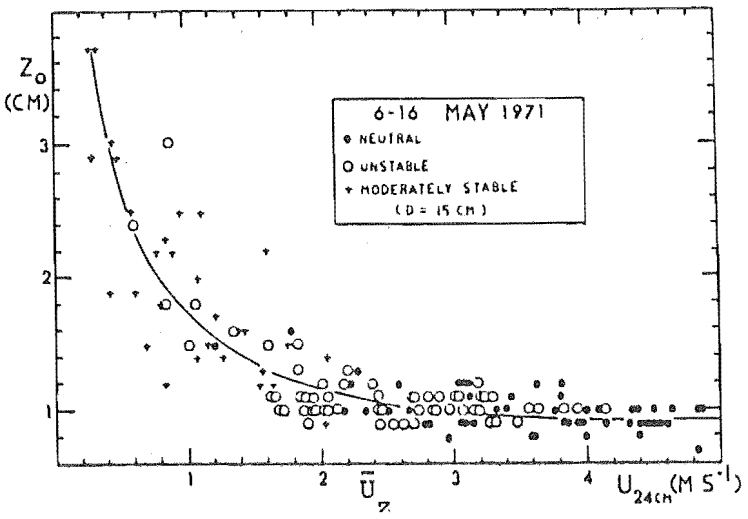

FIGURE 3.11 A relationship between z'_o and $\bar{U}_z$ over grassland, (after Saugier and Ripley)

So, spectra can be compared more exactly using $\bar{U}^2_{*\ell}$ and not σ^2_u or $\bar{U}^2_z$. A horizontal spectrum of wind turbulence non-dimensionalised by $\bar{U}^2_{*\ell}$ compares the ratio of local normal pressures to shear stresses. It is an advantage to have $\bar{U}_{*\ell}$ increasing with $\frac{S}{H}$ at least up to where $\frac{z'_o}{H}$ reaches a maximum.

For complex terrain $\frac{\sigma_u}{\bar{U}_{*\ell}}$ is near 2.5 for a wide range of Richardson's numbers in urban and forest areas (Högström et al, 1983). Mayer (1981) suggests $\frac{\sigma_u}{\bar{U}_{*\ell}}$ is near 2.0 for forests (see Chapter 7). Högström et al's values compare favourably with the values obtained by Kaimal and others over smooth open country surface winds (see Ch. 2).

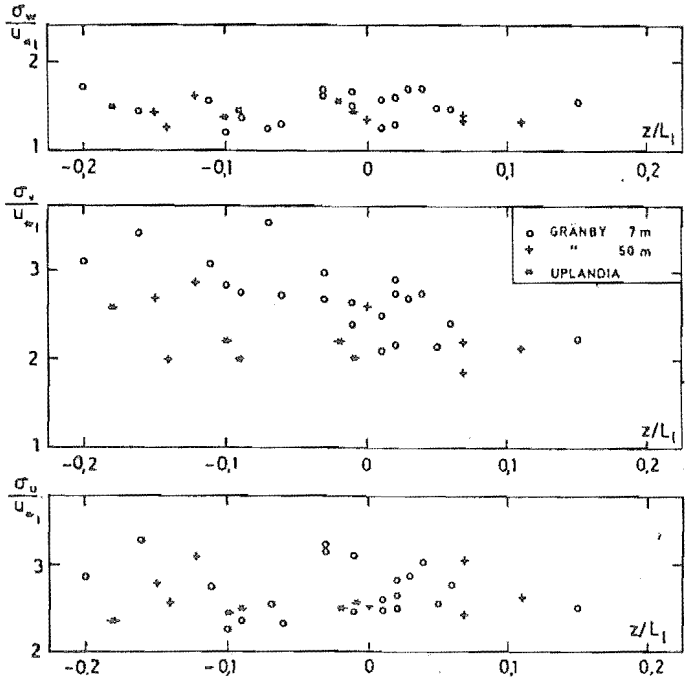

FIGURE 3.12 Values of $\frac{\sigma_u}{\bar{U}_{*\ell}}$, $\frac{\sigma_v}{\bar{U}_{*\ell}}$, $\frac{\sigma_w}{\bar{U}_{*\ell}}$, versus stability (after Högström et al)

These results suggest that σ_u is dependent on $\bar{U}_{*\ell}$ and tree spacing $(\frac{S}{H})$, considerably more than on the effects of convection, (Figs 7.5; 7.6).

3.7 COMPARISONS OF SHEAR STRESS BETWEEN THE INNER LAYER AND THE OUTER LAYER

The slope of the velocity profile at the point of inflexion (transition region) produces $\bar{U}_{*prof}$ and z'_o which identify the flow in the outer layer. Within the crowns, where the wind forces are applied, the slope of the local wind profile (assumed logarithmic) gives $\bar{U}_{*\ell}$ and z''_o for the inner layer up to the transition region.

The shear stress coefficient in the transition region must be multiplied by ϕ_m^2 to obtain the shear stress in the outer layer.

Bill et al (1976) measured the canopy stress over a maize crop. $\overline{u'w'}/\overline{u'w'}_{max}$ was plotted against z(cm). His results (Fig.3.13) showed how ϕ_m varied with z for a mean stand height of 4 m. (See also Rao et al, Ch. 4).

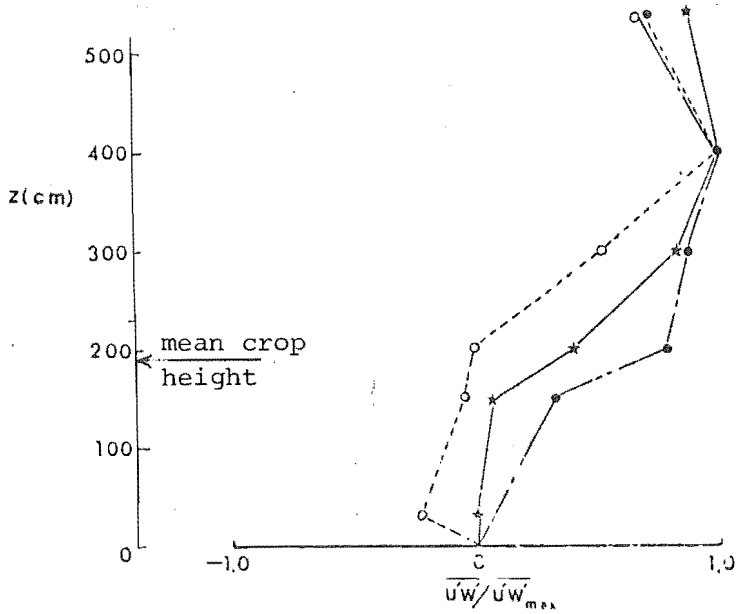

FIGURE 3.13 Normalised Reynolds stress ($\overline{u'w'}/\overline{u'w'}_{max}$) vs elevation (after Bill et al)

ϕ_m can be modified to allow for instabilities in the outer layer. In unstable conditions a good approximation is that

$$R_{i_g} = \frac{z}{L}$$

and

$$\phi_m = (1 - 16\,\frac{z}{L})^{-\frac{1}{4}} \quad ;$$

or the stress can be adjusted directly, if it is known how ϕ_m varies with height, from the integral values of ϕ_m provided by Businger (1970).

ϕ_m is often greater than unity, implying a double kink in the wind profile. ϕ_m values indicate that the differences between open country boundary layers and forest surface boundary layers are considerably reduced in stable conditions. However, most strong winds occur in unstable conditions (Garratt 1978).

3.8 THE WAVING MOTION OF TREES WITHIN FOREST STANDS

3.8.1 Spectra over tall rigid plant canopies

In Chapter 2 it was shown how the spectrum was affected by stability and roughness changes in the open country surface boundary layer.

Over high rigid roughness the shapes of the high frequency part of the spectra are similar and a terrain factor is normally introduced to account for any differences.

Assuming $\sigma_u = 2.5\ \bar{U}_*$, then in neutrally stable surface layers over homogeneous terrain

$$\frac{n\ S_u(n)}{\sigma_u^2} = \frac{66.5\ \hat{f}}{(1+75\ \hat{f})^{5/3}} \qquad \text{(Kaimal et al 1976)}$$

For more complex but still homogeneous terrain, Teunissen modified Kaimal's spectra by introducing a scaling factor,

$$\beta = \frac{\bar{U}_{*\ell}^2}{\sigma_u^2}$$

giving,

$$\frac{n\ S(n)_u}{\sigma_u^2} = \beta\ \frac{\bar{U}_{*\ell}^2}{\sigma_u^2} \cdot \frac{415\ \hat{f}}{(1+75\ \hat{f})^{5/3}} \qquad \text{(Teunissen 1980)}$$

so that,

$$\frac{n\ S_n}{\bar{U}_{*\ell}^2 \cdot \beta} = \frac{105\ \hat{f}}{(0.44+33\ \hat{f})^{5/3}} \quad . \qquad \text{(See Ch. 4)}$$

The E S D U standard is

$$\frac{n\ S_n}{\sigma_u^2} = \frac{4\ \hat{f}}{(1+70.8\ \hat{f}^2)^{5/6}} \quad ,$$

where

$$\hat{f} = \frac{x L_u, n}{\bar{U}_z} \quad .$$

The length scale of the eddies ($_x L_u$) can be found from the measured peak value of the turbulent kinetic energy of the horizontal spectrum.

Teunissen uses Kaimal's measurements of spectra which are regarded as the most accurate shapes of the turbulent wind over homogeneous rough surfaces in neutral conditions. (Sonic anemometers were used). Højstrup (1981) incorporates an addition to the spectra for unstable conditions, using the Monin-Obukov correction at the low frequency end of the spectrum.

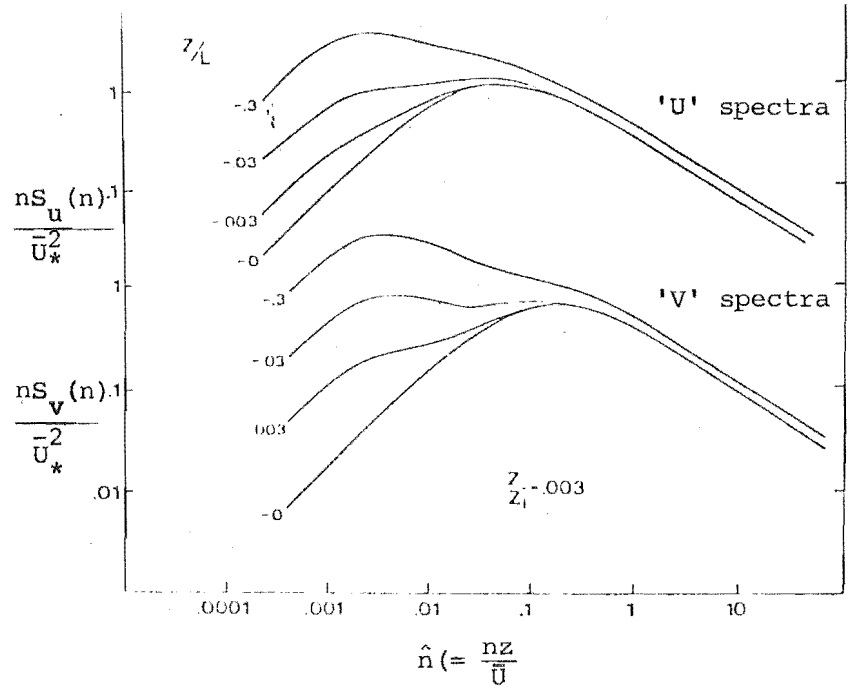

FIGURE 3.14 Longitudinal and lateral velocity spectra plotted for different stabilities at a fixed height (after Højstrup)

Högström et al (1983) modified Højstrup's spectrum shape by adding a further non-dimensional term, ϕ_e, the ratio of the buoyant energy to the dissipative turbulent energy. This improves the spectrum shape at both ends of the curve and gives a more accurate formula for calculating the turbulent energy contributions to structural motion in both homogeneous and heterogeneous terrain (see Ch. 4).

When normalised by $\bar{U}_{*_\ell}$ the spectrum has the shape

$$\frac{nS_u(n)}{\bar{U}_{*_\ell}^2} = \frac{a}{(2\pi k_a)^{2/3}} \cdot \left(\frac{k_a z \phi_e}{\bar{U}_{*_\ell}^2}\right)^{2/3} \left(\frac{nz}{\bar{U}_z}\right)^{-2/3}$$

where $$\phi_e = \frac{k_a z \phi_e}{\bar{U}_{*_\ell}^2} ,$$

$$\hat{n} = \frac{nz}{\bar{U}_z} ,$$

$$k_a = 0.41 ,$$

and $$a = 0.15 ,$$

so

$$\frac{nS_u(n)}{\bar{U}^2_{*\ell} \cdot \phi_e^{2/3}} = \frac{a}{(k_a)^{2/3}} \cdot \hat{n}^{-2/3} = 0.27 . \hat{n}^{-2/3}$$

where, according to Kaimal et al (1976),

$$\phi_e^{2/3} = 1 - 0.5 \left(\frac{z}{L}\right)^{2/3} ; \frac{z}{L} < 0$$

$$= 1 + 2.5 \left(\frac{z}{L}\right)^{3/5} ; \frac{z}{L} > 0.$$

This improves both ends of the spectrum, but more significantly, the top end of the spectrum is almost a unique curve for different types of terrain (see Fig. 3.16).

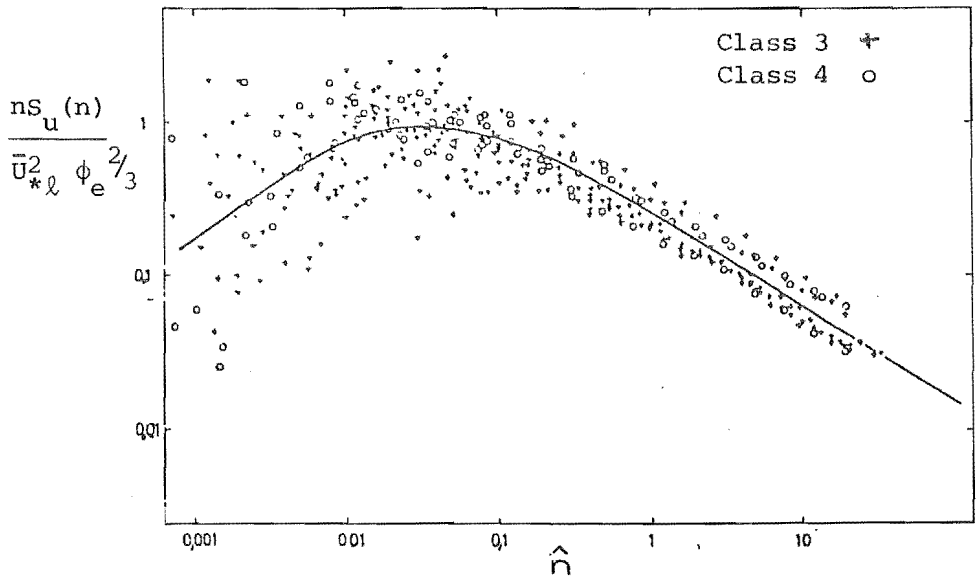

FIGURE 3.15 Normalised spectra of the longitudinal wind component plotted against normalised frequency $n = nz/\bar{U}_z$, Gränby 8; class 3 and 4 refer to 'urban' and 'almost urban' fetch (after Högström et al)

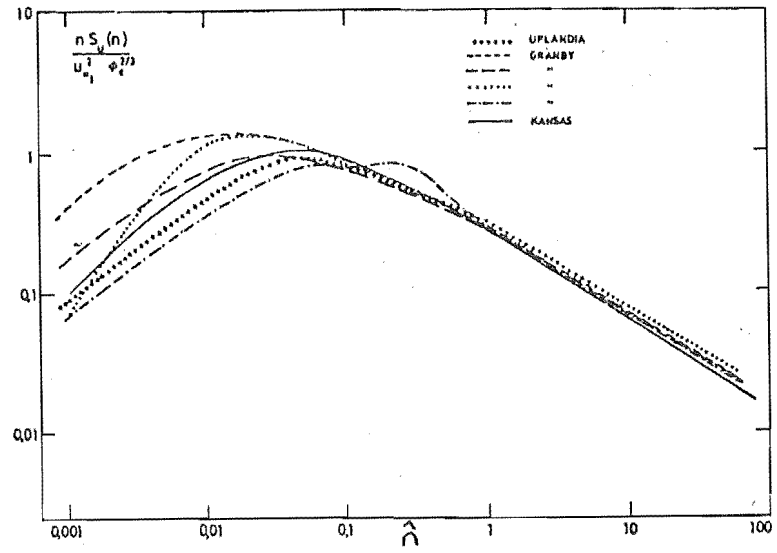

FIGURE 3.16 Comparison of normalised u spectra from the two Gränby levels, from Uplandia and from Kansas. (The dots together with inequality denote 'slightly') (after Högström, et al)

Högström et al show how this non-dimensionalised curve form can be further modified to provide a model for the shapes of spectra at different heights above the roughness under equilibrium conditions.

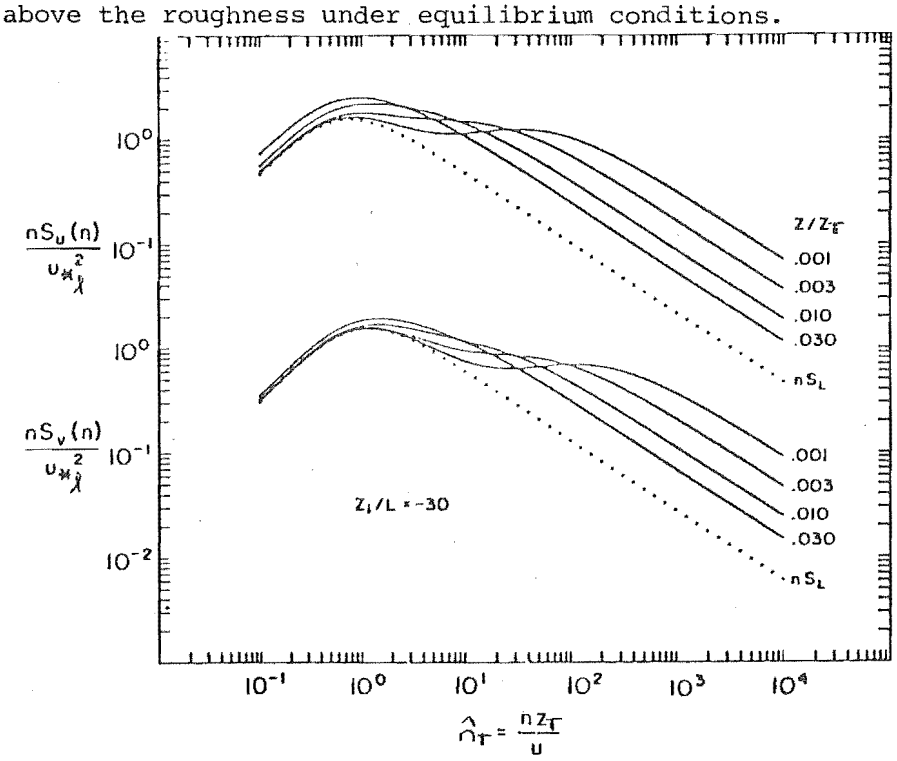

FIGURE 3.17 Model U and V spectra for varying height at fixed $z_T/L = -30$, (after Högström et al)

The spectrum inaccuracies produced by inadequate wind and temperature sensors, by inaccurate recording and analysis, or by poor site location, make it extremely difficult to organise the low frequency end of the spectrum to allow scaling between full scale and model experiments (Chapter 5). In the case of wind-loading analysis of structure, this part of the

spectrum is entirely responsible for background quasi-mean wind forces which increment the mean wind drag forces (see Ch. 4). Changes in thermal stability will contribute to this background load, but do not affect the high frequency end of the spectrum beyond its peak.

Modification of the spectral expression gives

$$\frac{nS(n)}{\bar{U}_{*\ell}^{2}} = a.k_a^{-2/3} . \left(\frac{nz}{\bar{U}_z}\right)^{-2/3}$$

as required for comparisons over high roughness. Since a = 0.15 and k_a = 0.41 below the transition region at z = 1.1 H, $\frac{z_o''}{H}$ = 0.11 and d = 0.70 H (cf Table 3.2).

$$\therefore \quad \bar{U}_{*\ell} = \frac{0.41 \times \bar{U}_z}{\ln.\frac{(1.1 - 0.7 + 0.11)}{0.11}}$$

$$= 0.25\ \bar{U}_z$$

$$\text{hence} \quad \frac{nS(n)}{\bar{U}_{*\ell}^{2}} = 0.64 \left(\frac{nH}{\bar{U}_{*\ell}}\right)^{-2/3} , \qquad (1)$$

In section 3.8.2 following, it is clear that the spectrum shape is drastically altered by the swaying motion of the roughness, but the log-log slopes of spectra are still similar at $\frac{-5}{3}$ or $\frac{-2}{3}$, as indicated in this relationship; (Uchijima and Wright (1964), Finnigan (1979)). Spectra are plotted and compared in Chapter 7 and a modified relationship for swaying crops is developed from equation (1) (Fig. 7.4).

3.8.2 Spectra over tall flexible plant canopies

Uchijima and Wright (1964) studied the plant-air layer of corn and obtained mean and turbulent wind profiles similar to that of a forest canopy. Shearing stress, friction velocity, coefficient of eddy viscosity and mixing length were calculated for various heights. Near the ground, within the corn, the mixing length increased linearly with height. Divergence in momentum flux occurred but comparisons of spectra in the inner air layer up to transition indicated that the ragged nature of the curve within this layer may be due to the waving and fluttering of plant leaves. The spectra had a mean slope of $\frac{-5}{3}$ and a definite frequency shift

from $\hat{n}_{pk}$ of 0.05 well above the canopy to $\hat{n}_{pk} \in (.35, 1.5)$ at the crop height. They concluded that the dissipation of turbulent energy in this part of the spectrum was modified by the waving motion of the plant (see Ch. 7.).

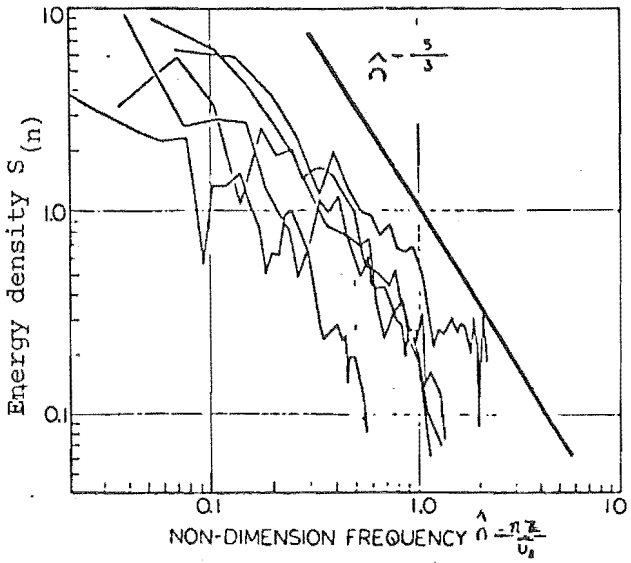

FIGURE 3.18 Energy density of wind velocity fluctuations (after Uchijima and Wright)

Bull and Reynolds (1968) showed that the turbulence produced by a forest canopy made their wind vane tracer frequently hit the vertical and horizontal stops of the recorder. It was possible for them to visualise the distinction in wind structure over the different stations: "In open ground, especially in strong winds, there are large numbers of small, high-frequency eddies. Over the forest the trace has high frequency eddies, (but it also has larger eddies of lower frequency)" presumably produced by the interaction with the roughness element of the corn canopy.

Variations in shear stress due to turbulence exert dynamic shear forces on the canopy top of the internal forest. The turbulence intensity right at the forest border is low (Sadeh et al, 1971). As the flow accelerates, the shear stress increases and the turbulence rises very rapidly. Because of variable amounts of turbulence in each of the three zones, A, B and C (Chapter 1), the response of the trees within each zone will have different amounts of mean and dynamic loading.

Changes in canopy architecture and roughness due to thinning changes are complicated by the flexibility of the elements constituting the roughness (Cionco, 1972).

In a wheat plantation, an increase in either wind speed or plant density enhances the effect of waving wheat upon the wind speed and very high element density gives a decrease of wheat movement fluctuations.

An increase in drag coefficient, or a decrease in the plant mass, magnifies the waving motion of the wheat heads (Finnigan, (1979).

Finnigan concludes that an increase in the aerodynamic damping of individual plants causes large reductions in plant resonance. The aerodynamic admittance terms suppress the higher harmonics at resonance.

The motion of the canopy has been studied using linearised theory with measurements on two aero-elastic wind-tunnel model canopies with different stalk spacings. Despite the difficulties of using hot-wire anemometers in high intensity turbulence, it appears that the large positive skew of u' will reduce errors, especially when Reynolds stresses are high. Pressure fluctuations at ground level exhibit a strong peak at the waving frequency of the stalks.

Below are spectra at two heights: one just above the wheat crop mean height and one well above. Notice the distinct increase in turbulent energy near the natural frequency of the individual wheat stalks in the lower spectrum.

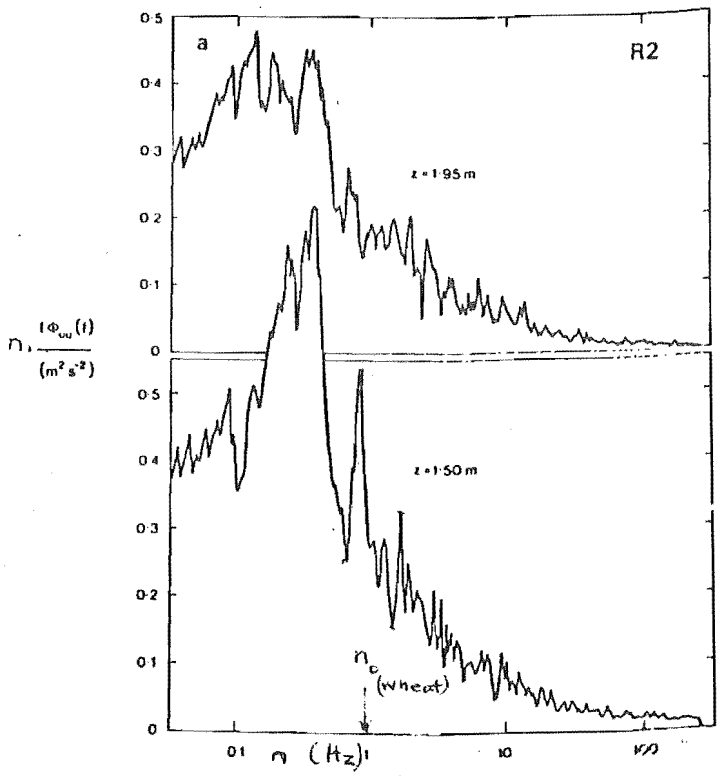

FIGURE 3.19 Power spectra of streamwise velocity fluctuations for R2 (after Finnigan)

Finnigan and Mulhearn (1978) produced two spectra from their mathematical modelling analysis for different canopy densities.

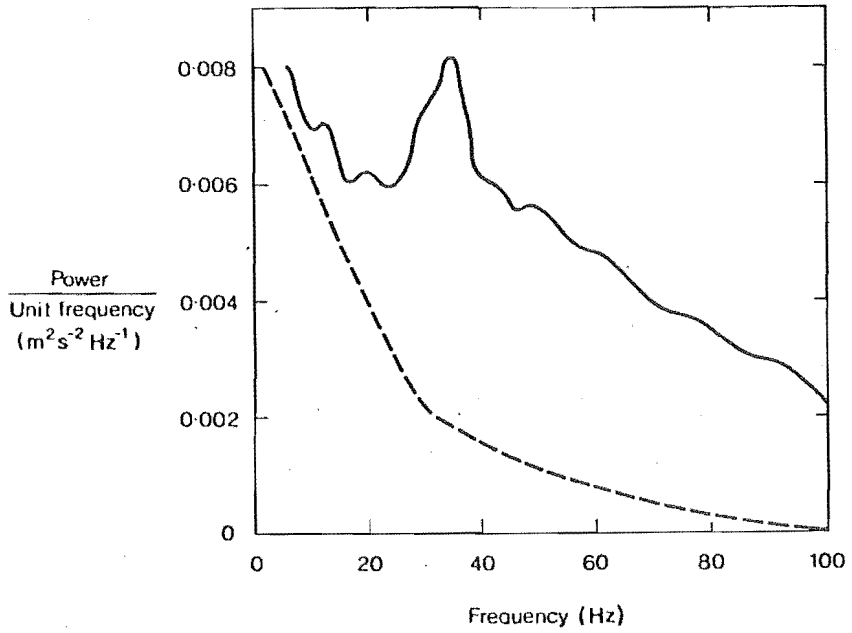

FIGURE 3.20 Power spectra of wind streamwise velocity in two aero-elastic model canopies of different density —— dense; ----sparse (after Finnigan and Mulhearn)

When they made gross assumptions to linearise the equations of motion of their crop, the results showed the spectrum with a hump close to the natural frequency of the individual plants within the crop. The spectrum obtained using the non-linear equations indicated that this model gave slightly more output energy which moved the spectrum upwards. So, predicting response from linearised equations gives stalk displacements which are about 16% below the more realistic non-linear behaviour.

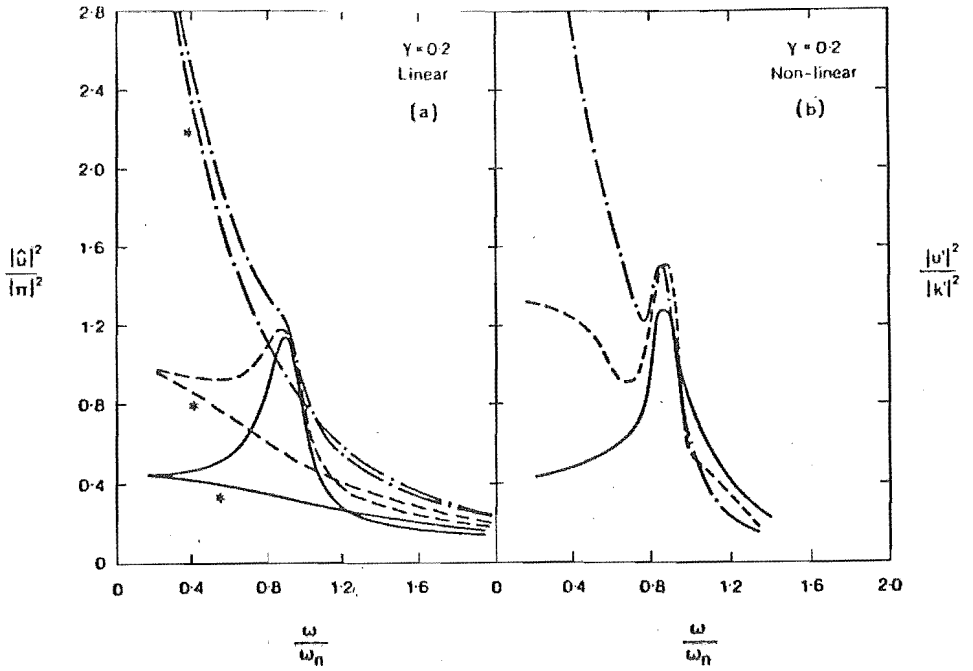

FIGURE 3.21 (a) Results of the linearized response for $\frac{S}{H} \simeq 0.2$; -·-·- $\bar{U}_H$ = 0.25 m/s; --- $\bar{U}_H$ = 0.50 m/s; —— $\bar{U}_H$ = 0.75 m/s; (* = stalks fixed).

(b) Analogue computer solution of the non-linear response for the same values of $\bar{U}_H$ and $\frac{S}{H}$ (after Finnigan and Mulhearn)

Maitani (1978) obtained spectra for wind characteristics over wheat, rush and rice plants that gave very conclusive evidence of turbulent energy concentrating itself near the natural frequency of the wheat stems. As theory predicts, the peak in the distorted spectra is slightly below the natural frequency of the plant (Annand, 1966).

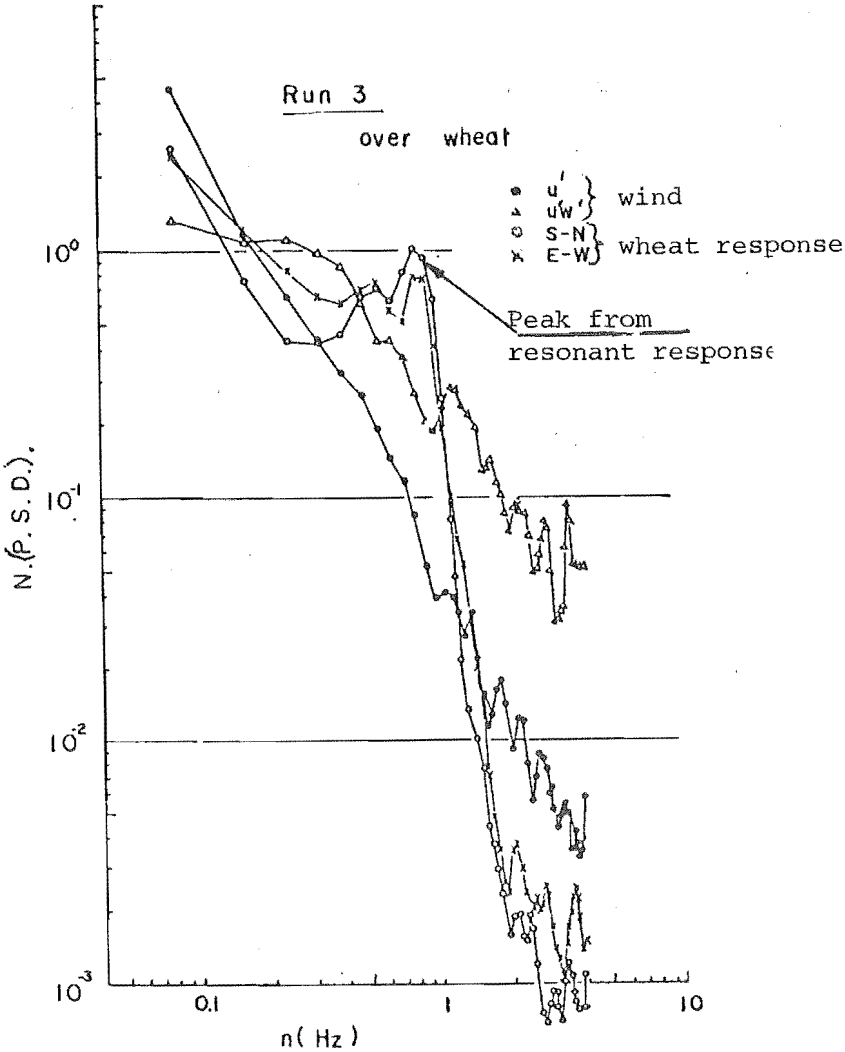

FIGURE 3.22 Normalised spectra of displacements of an ear of wheat, horizontal wind velocity, and instantaneous momentum flux (after Maitani)

The output response of the heads in the wheat-crop experiment exhibited characteristic resonance which indicates that unstable feedback conditions exist (Maitani, 1979).

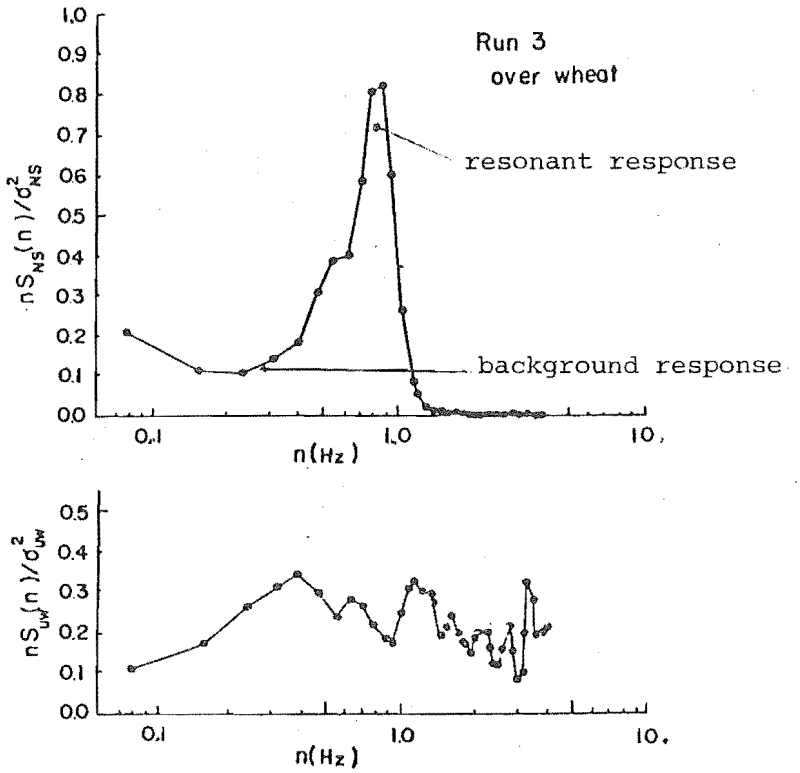

FIGURE 3.23 Normalised power spectra of an ear of wheat and normalised power spectra of instantaneous momentum flux, (after Maitani)

Holbo et al (1980) investigate the aeromechanical behaviour of three Douglas firs in a forest using wind shear force as the input, and tree movement as the output variable. The input and output spectrum produced continued to exhibit coupling between the tree and the wind, and quite clearly, the peaks in the spectrum moved to the right to higher frequencies as mean wind speeds over the forest increased. Maximum tree deflections were 12 - 15 mm at their measurement point in a mean wind speed of 5 m/s at mean crop height.

Recently, Mayer (1981) investigated wind turbulence in spruce forests and shows that the high wind shear caused by the high wind speeds at mean tree-top height cause intense fluctuations in the u',v',w' components of turbulence; $\frac{\sigma_u}{\bar{U}_*} = 2.0$, which shows that the shear forces on a dynamically rough surface must be up by at least 20%, compared with normal high rigid roughness measurements, $(\frac{\sigma_u}{\bar{U}_*} = 2.5)$. Clearly, spectra of wind turbulence in forests should have the same shift to the right and an increase in peak energy depicted earlier in the shorter crops, as spacing between the individual crop elements increase.

3.8.3 Some physical and mechanical properties of trees

Walshe (1972) made a comprehensive study on the subject of structures oscillating in the wind. This study implied that the deflection curve of a tapered cantilever beam was

$$\frac{x_t}{\bar{x}_{t_H}} \varepsilon \left[\left(\frac{z}{H}\right) \quad , \quad \left(\frac{z}{H}\right)^2 \right] \quad .$$

Buffetting of tall structures by high winds causes oscillations of large amplitudes. Two towers near each other interact with different amplitudes

(a) when both towers are free to move,

(b) when the upstream tower is held fixed.

For condition (a), the downstream tower has a significantly greater amplitude than for condition (b). Tower amplitudes rise significantly as spacing increases to more than four tower diameters (Walshe).

In a similar way, internal trees within a forest can respond to turbulent changes differently from trees right at a forest leading edge. A tower held fixed is like a front tree receiving the mean wind force component, and swaying little from turbulence. A few rows in from the front the mean wind speed is reduced and the turbulent wind component increases. Trees near to each other will sway with a different amplitude than trees right at the forest front or trees further in, where turbulent energy is in equilibrium with the surface. From the preceding work it is clear that these changes will amplify as tree spacing increases.

Conifer-type forests such as Sitka spruce or Radiata pine may possess higher aerodynamic admittance than forests with other crown shapes and thus allow the wind forces to be more easily transmitted and cause tree sway.

It was implied earlier that both the mass (M) and the damping ratio (ζ) of a tree contribute to changes in sway motion.

Mayhead (1973a) showed that the stem of a spruce tree is related to its fundamental frequency (n_o) by the relation,

$$\frac{1}{n_o} = 0.86 + 0.74 \frac{H\sqrt{M_T H}}{D_B^2} \quad \text{(from cantilever beam theory)}$$

where n_o = tree natural frequency (Hz)

H = total tree height (m),

D_B = diameter at breast height (cm),

and M_T = total above ground stem mass (kg);

hence if D_B, H, n_o are known, the stem mass can be derived.

Experimental values of the no-wind damping ratio ζ of structures have been available for some time (Davenport, 1967):-

for modern steel structures $\zeta = 0.005 - 0.01$;

for concrete structures $\zeta = 0.01 - 0.02$.

Various tree damping ratios are reproduced below.

TABLE 3.3 Various tree damping ratios

Damping Ratio	Hutchinson et al, 1970	Hoag et al (1971)	Loo (1975)	White et al (1975)
ζ	0.09	0.064-0.075	0.067-0.101	0.065-0.083

The damping ratio appears to lie within the limits of 0.064 and 0.101 and is taken as 0.08. Most trees of 10-15 metres height have frequencies near 0.50 Hz but, in taller Radiata pine trees (over 22 metres high) the writer has measured frequencies as low as 0.2 Hz. The larger, older trees are therefore even more likely to sway and so distort the wind spectra.

3.9 ALONG-WIND RESPONSE OF TREES WITHIN A FOREST

Interaction of aerodynamic wind forces and elastic tree forces cause along-wind and transverse oscillations. A stable oscillation results when the elastic forces predominate, and the system is described as having negative feedback. Generally, systems with large negative feedback are stable; unstable systems result from systems which have positive feedback.

The response of a tall tree within a homogeneous forest stand can be evaluated by treating it as a flexing, spring-mounted cantilever (Mayhead 1973a; White et al, 1975) whose dynamical properties are specified by its natural frequency (n_o) and its damping (ζ). The variance of the output force is the area under the spectrum of the wind after it is multiplied by the compliance factor (Holbo, 1980). This is the square of load magnification factor (M_R, or mechanical admittance) for a one-degree-of-freedom second order oscillating system.

The ratio of the output motion of the tree to the input motion of the wind is termed the compliance factor which is made up of aerodynamical and mechanical admittance terms (Ch. 1).

The analysis of the response can be treated statistically (Davenport, 1967 ; Vellozi and Cohen, 1968 ; Simui, 1980; and Solari, 1982) by dividing the forces into mean components due to the mean wind speeds at the tree tops, and fluctuating forces due to the turbulent wind components. These components undergo dramatic changes at the leading edges of the forest (Chapter 4, Chapter 6). The fluctuating wind forces will have frequency components due to the very large gusts at the low frequency end of the spectrum and very small gusts at the top end of the dissipative region.

Nearer the tree natural frequency there remains a portion of the spectrum which will induce tree sway and promote resonance. The resonance effect (R) and the background effect (B) add together to provide the sway motion or amplitude of swing (A). To this is added the mean deflection (D) to provide the total movement. Measurements of the mean wind speed profile and the turbulent energy distribution in the x-direction are essential if tree swaying motion from the leading edge of a forest inwards is to be assessed.

3.9.1 The simple case - sinusoidal forcing

The simple case of the steady-state-load-response amplitude for a unit sinusoidal gust of forcing frequency (n), can be used to determine the ideal magnitude ratio (M_R) from the leading edge of a forest inwards. With no damping the motion never dies out. The contribution to tree motion directly due to the fundamental frequency in-phase force only, is given by:-

$$M_R = \left[\left[1 - \left(\frac{n_{pk_w}}{n_o}\right)^2\right]^2 + \left[2\zeta\frac{n_{pk_w}}{n_o}\right]^2\right]^{-\frac{1}{2}} \quad \ldots \text{(Annand)}$$

The components of movement are similar in type to B and R without the admittance and spectra effects. There is a phase difference,

$$\phi_R = \tan^{-1}\left(\frac{2\,n_{pk_w}\zeta}{\dfrac{n_o}{n_{pk_w}} - \left(\dfrac{n_{pk_w}}{n_o}\right)^2}\right)$$

between the components of response so that when the components are out-of-phase with each other there is a reduction in the value of M_R. Values of M_R and ϕ_R versus $\frac{x}{H}$ are presented in Chapter 6. When the applied frequency is below the tree natural frequency the resonant amplitude of swing is in the same direction as the turbulent quasi-mean deflection (background effect). However, if the applied frequency is above the tree natural frequency the resonant amplitude opposes the turbulent quasi-mean deflection. This suggests that generation of turbulence above the tree natural frequencies may be beneficial. This is not possible just behind the leading edge but may be the case inwards in the x-direction.

3.9.2 The complex case - random forcing

The procedure used to solve for $\frac{A}{D}$ involves the use of power spectral techniques first applied to tall structures in the rural open country boundary layer by Davenport (1967). The procedure requires a knowledge of the input turbulent wind component spectrum from which the output response of the structure is calculated after determining statistically, the likely aerodynamic admittance and the mechanical admittance terms.

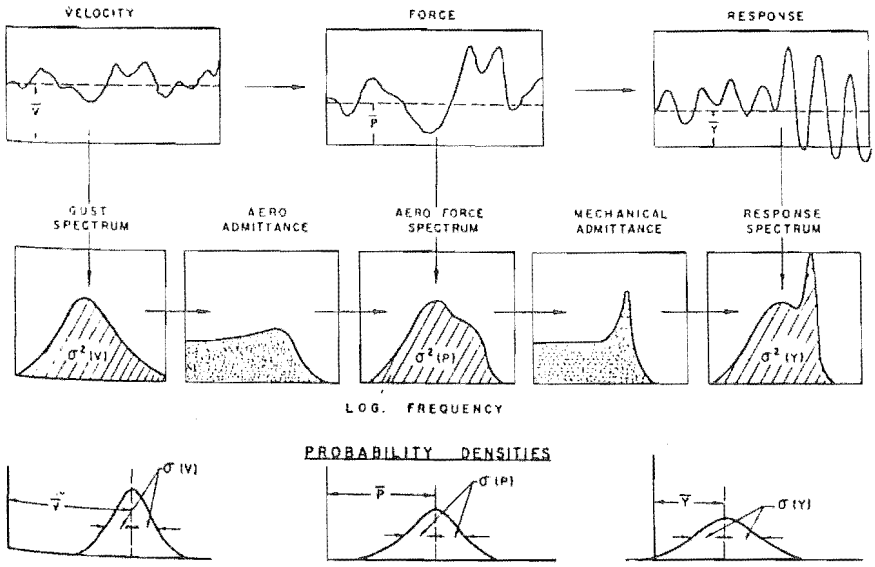

FIGURE 3.24 Elements of the statistical approach to gust loading (after Davenport)

Davenport classifies the effect of the terrain on the mean wind speed profiles using power exponent tables (Ch. 2) and the gust spectrum is represented by a model he obtained from a study of 90 strong-wind spectra from many sources. The computation is relatively simple, since he calculates the weighting given to 'coherence' terms or in-phase and out-of-phase cross-spectral densities for each frequency required to compute the aerodynamic admittance terms, which he calls the joint acceptance functions ($|J_y|^2$, $|J_z|^2$).

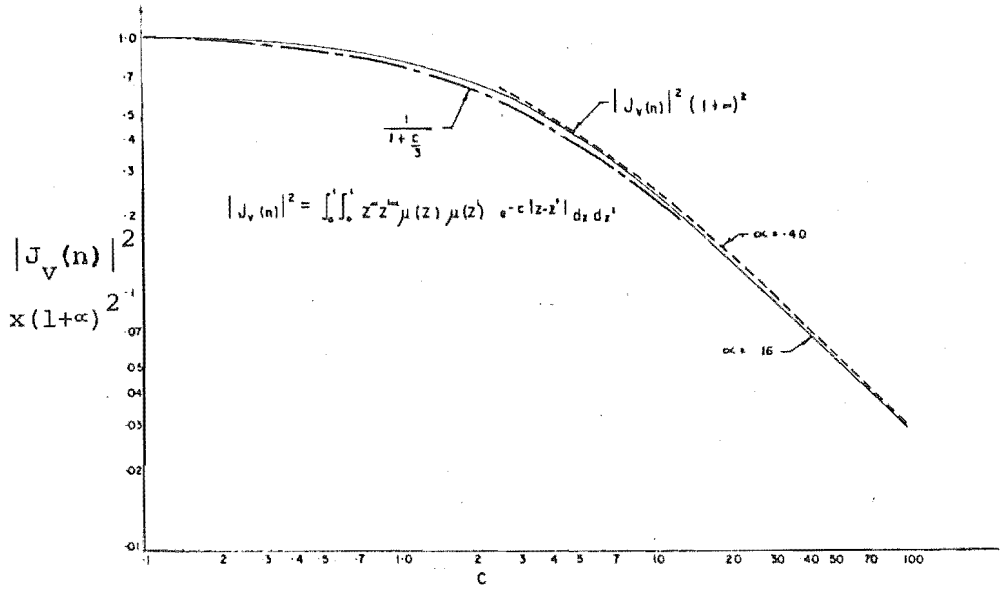

FIGURE 3.25 Vertical joint acceptance function (after Davenport)

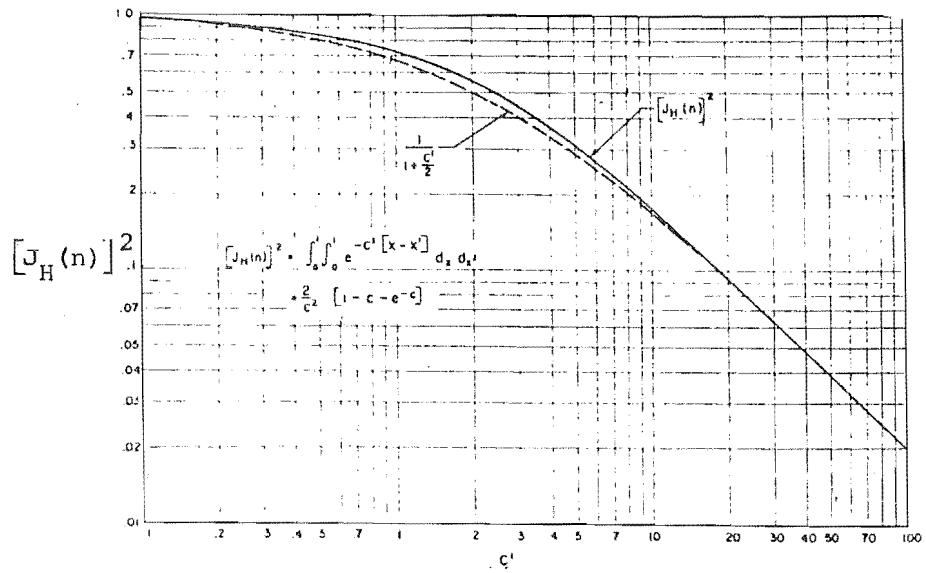

FIGURE 3.26 Horizontal joint acceptance function (after Davenport)

The out-of-phase cross-coupling spectral density components in space and time between the horizontal and vertical turbulent winds are generally neglected in the non-resonant response range (background effect). The resonant components are relatively small scale in the high frequency end of the gust spectrum so that the structure responds to the modes separately and cross-coupling is small. Only the fundamental mode of vibration is normally considered, although it appears that the second mode for tapered structures is often required (Walshe, 1972, Finnigan and Mulhearn).

3.9.3 Wind spectra shapes

Listed below are the various spectral distribution forms recommended when spectra have not been measured. (In the full scale and model forest tests spectra were measured at points of interest; see Ch. 5 and 6).

- Davenport (also Canadian Code)

$$\frac{\hat{n}\, S_{(\hat{n})}}{k_a \bar{U}_H^2} = \frac{4(\hat{n})^2}{(1 + (\hat{n})^2)^{4/3}} \quad ; \qquad \text{open country}$$

- Vellozzi and Cohen

$$\frac{\hat{n}\, S_{(\hat{n})}}{k_a \bar{U}_H^2} = \frac{4(\hat{n})^2}{(1 + \hat{n}^2)^{4/3}} \quad ; \qquad \text{open country}$$

- Simui

the relationship was the same as Davenport's.

- Højstrup

(a) $$\frac{n\, S_{(n)}}{\bar{U}_{*\ell}^2} = \frac{0.5\ \hat{n}}{(1 + 2.2\ \hat{n})^{5/3}} \cdot \left(\frac{z_i}{-L}\right)^{2/3}$$ for very large structures

(b) $$\frac{n\, S_{(n)}}{\bar{U}_{*\ell}^2} = \frac{105\ \hat{n}}{(1 + 33\ \hat{n})^{5/3}}$$ for smaller structures

- Högström et al

$$\frac{n\, S_{(n)}}{\bar{U}_{*\ell}^2 \phi_e^{2/3}} = 0.27 \left(\frac{nz}{\bar{U}_z}\right)^{-2/3}$$ all terrain (unstable conditions)

- Solari

$$\frac{n\, S_{(n)}}{\sigma_u^2} = 1.56 \left(\frac{nz}{\bar{U}_z}\right)^{-2/3}$$ all terrain (neutral)

or $$\frac{n\,S_{(n)}}{\bar{U}_{*\ell}^{2}} = 0.26\,\frac{nz}{\bar{U}_z}^{-2/3}, \qquad \text{all terrain neutral}$$

where $$\hat{n} = \frac{nz}{\bar{U}_z},$$

$$\bar{U}_{*\ell}^{2} = 6\,\sigma_u^{2} \quad \text{(Ch. 2)},$$

and $$z_o\,(\text{Solari}) = z_o' \quad \text{(and not } z_o''),$$

$$\bar{U}_{*\ell}^{2} = 4\,\sigma_u^{2} \quad \text{for forests (Mayer, 1981)}.$$

3.9.3.1 Wind-type assumptions

Wendelken (1966) studied wind records collected for 10 periods of wind damage to Canterbury forests from 1914 to 1964. The writer studied wind records for 1968 and 3. 7.75 to 1. 8. 75. Extensive wind damage to forests by winds appears to begin when mean wind speeds near 20 m/s at 10 m height are maintained for periods of 30 minutes or more, devastating wide areas when they reach 27 m/s.

So, for a wind, it is assumed that:-

(a) The mean wind velocity is steady and unidirectional at 20 m/s at 10 m height in an open country neutrally stable boundary layer with a power law index of 0.22.

(b) Over the forest tree tops and into the canopy the flow is in equilibrium with the surface with a logarithmic profile shape up to the transition region.

(c) Turbulent kinetic energy in the wind affects the swaying motion.

(d) The zero-plane displacement of full scale forests is in 0.70 H and model forests is 0.75 H (note: Rivox result 0.74 H).

3.9.3.2 Terrain, forest and tree type

It is assumed that:-

(a) The upstream terrain has no slope with an aerodynamic roughness of $z_o = 0.03$ m.

(b) The forest canopy architecture is homogeneous (Ch. 3) with a local aerodynamic roughness of z_o'' in the inner layer.

(c) The forest front drag coefficient decreases linearly as spacing of trees increases (Seginer, 1972; see Ch. 4).

(d) At the front the normal wind pressure is experienced by the full crown depth.

(e) Inside the front the normal form drag forces are experienced by the crown depth down to the zero plane displacement $d(\simeq d + z_o'')$.

(f) The tree crown area remains constant and triangular in shape and can sway to and fro, producing a reduced fluctuating form drag coefficient (C_{D_f}).

(g) The damping ratio and mass are constant at mean tree height with the total tree mass concentrated at the centre of pressure of the crown (pointlike structure).

(h) The tree can be treated as a cantilever beam fixed at its base with a modal shape of $(\frac{z}{H})^{1.5}$ (Mayhead; Walshe, 1972).

3.10 THE RESPONSE EQUATIONS FOR RANDOM WIND INPUTS

Following Davenport's approach as extended by Solari (1982), the simple second order equation for the movement of a tree stem swaying as if it were a cantilever beam is:-

$$\frac{\text{Total tree force}}{M_{T_{C.P}}} = \frac{F_T}{M_{T_{C.P}}} = \ddot{x}_t + 2\zeta . w_o . \dot{x}_t + w_o^2 . x_t \qquad (1)$$

where $w_o = 2\pi n_o$ = tree natural frequency (r/s),

ζ = damping ratio,

M_T = tree mass concentrated near the centroid of the crown at the centre of pressure,

x_t = tree stem displacement at height z.

$$\text{Total wind force } F_w = C_{D_\ell} \frac{1}{2} \rho \int_o^H \int_o^{C(d + z_o'')} U_{R_z}^2 |J_y| |J_z| \chi . dy\, dz \qquad (2)$$

where U_{R_z} = total resultant wind speed at height z,

$|J_z|$ = coherence in vertical direction z up the tree crown,

$|J_y|$ = coherence in horizontal direction y across the crown width,

χ = admittance term to account for pressure fluctuations around a swaying tree crown and the mean form or pressure drag coefficient.

At the extremes of the tree sway the $\dot{x}$ term is zero and the maximum tree displacement is A_T which can be split into its mean deflection (D) and amplitude (A) components. Similarly the resultant wind striking the crown can be divided into mean and fluctuating components:-

$$U_{R_z}^2 = (\bar{U}_z + u'_z)^2 = \bar{U}_z^2 + 2\bar{U}_z . u'_z + (u'_z)^2 \quad , \tag{3}$$

so that there are mean drag forces and drag forces associated with the fluctuating winds.

3.10.1 Mean forces and deflections

At a distance z from the ground using (1), (2) and (3),

$$d\bar{F}_w = M_T \, d\bar{x}_{z_t} \, (2\pi n_o)^2 = C_{D_\ell} \frac{1}{2} \rho \, \bar{U}_z^2 \, dydz$$

but,

$$\frac{d\,\bar{x}_{z_t}}{d.\bar{x}_H} = \left(\frac{z}{H}\right)^{1.5} \quad ,$$

and since there are no admittance terms or fluctuating effects,

$$\bar{x}_{H_t} = \frac{C_{D_\ell} \cdot \frac{1}{2} \rho \, \bar{U}_H^2}{M_T (2\pi n_o)^2} \cdot H.C_{z=d} \int_o^H \int_o^{C_{d+z_o''}} \hat{U}^2 \hat{z}^{1.5} C_z \, dy.dz \quad . \tag{4}$$

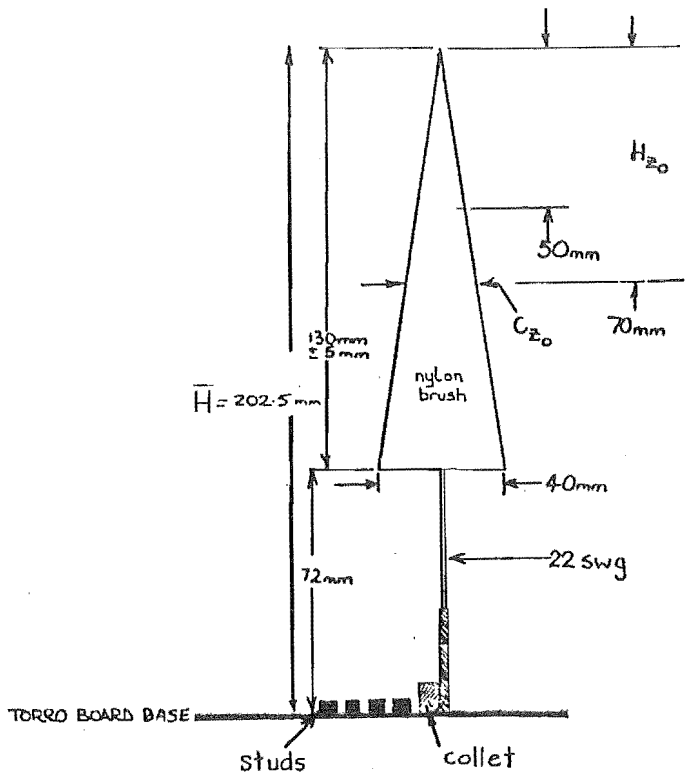

FIGURE 3.27 Model tree dimensions, (also Fig. 6.15)

From Figure 3.27,

$$\frac{C_z}{C_{d+z''_o}} \simeq \frac{C_z}{C_{z=d}} = \frac{H - z}{H-0.05}$$

$$\therefore \quad C_z = C_{z=d} \cdot \frac{H-z}{H-0.05} \quad . \tag{5}$$

From (4) and (5)

$$\bar{x}_{H_t} = \frac{C_{D_\ell} \cdot \frac{1}{2} \rho \bar{U}_H^2}{M_T (2\pi n_o)^2} \cdot H \, C_{(d+z''_o)} \int_o^1 \hat{U}^2 \cdot \hat{z}^{1.5} \cdot \frac{H - z}{H-0.05} \cdot d\hat{z}$$

$$\boxed{D = \bar{x}_{H_t} = \frac{C_{D_\ell} \cdot \frac{1}{2} \rho \bar{U}_H^2 \cdot H \, C_{(d+z''_o)}}{M_T (2\pi n_o)^2} \cdot I_1} \quad . \tag{6}$$

The shape parameters required for solving C_{D_f}, J_z and J_y are found from the tree geometry (6.4.5).

If $z''_o \simeq .05$ H for all Oxford values, then

$$\frac{C_{d+z''_o}}{40} = \frac{202 - (d + z''_o)}{130} \quad ,$$

$$C_{(d+z''_o)} = \frac{40}{130} (200 - (150 + 10)) \quad ,$$

$$C_{(d+z''_o)} = 12.3 \text{ mm} \quad .$$

$$\therefore \quad \frac{C_{z_o}}{H} = \frac{12.3}{200} = 0.06$$

and also, $$\frac{H_{z_o}}{H} = \frac{40}{200} = 0.2 \quad .$$

Since these ratios are less than 0.5, the structure (tree) can be considered 'pointlike'. The coefficient terms in the J_z and J_y functions can be assumed constant and so solutions are easier (Solari).

3.10.2 Fluctuating forces and amplitudes

The fluctuating force components and amplitudes are treated in a similar way, except that there are two parts of the kinetic energy, $\bar{U}u'$ and u'^2, and there are the admittance terms, aerodynamic and mechanical, to consider. Normally the component u'^2 is omitted, but since turbulence levels are high over forests (up to 75% of the mean wind component), they contribute to about 12% of the total wind force. The fluctuating winds produce an amplitude

$$A = x'_{H_f} = \frac{C_{D_\ell} \cdot \frac{1}{2} \rho \bar{U}_H^2 . H \, C_{z=d} \cdot f \left[B, R, \ldots\ldots\right]}{M_T (2\pi n_o)^2} \qquad (7)$$

from (6) and (7)

$$\frac{A}{D} = \sqrt{\frac{\left[B, R, \ldots\ldots\right]}{I_1}} \cdot \qquad (8)$$

3.10.2.1 Background effect 'B'

The coherence terms are Jy_B and Jz_B and the mechanical admittance is unity. The aerodynamic drag coefficient C_{D_ℓ} is unaffected, since eddies encompass total canopy area covering very little pressure fluctuation around the crowns.

3.10.2.2 Resonant effect 'R'

The coherence terms are much smaller and are Jy_R and Jz_R; the mechanical admittance is $\frac{\pi}{4\zeta}$ and the aerodynamic drag coefficient is reduced from C_{D_ℓ} to C_{D_f} because of the pressure fluctuations around the tree crown.

3.10.3 Total along-wind rms tree-top deflection

If the bracket in equation (8) is squared so that the component kinetic energy terms in the wind can be separated, we obtain

$$f.\left[B,R,..\right]^2 = \left[\frac{2}{\bar{U}_H} \cdot \int_o^1 \int_o^\infty \frac{\hat{}}{U_z} u' . \hat{z}^{1.5} . \hat{C}_z d\hat{z}\, dn + \int_o^1 \int_o^\infty u'^2 . \frac{\hat{z}^{1.5} . \hat{C}_z d\hat{z}}{\bar{U}_H^2}\, dn \right]^2 . \chi^2 .$$

where χ^2 is the admittance terms or compliance so that the background effect in the expansion is,

$$B = \left[\frac{4}{\bar{U}_H^2} \sigma_u^2 \, I_2^2 \, A_B \left| J_{z_B} \right|^2 \left| J_{y_B} \right|^2 . 1 + \frac{\sigma_u^4}{\bar{U}^4} \, I_3^2 \, A_B^2 \left| J_{z_B} \right|^2 \left| J_{y_B} \right|^2 . 1^2 + 2\sqrt{B_1 B_2} \right] ,$$

and the resonant effect is

$$R = \left[\frac{4}{\bar{U}_H^2} \sigma_u^2 \, I_2^2 \, A_R \, \chi^2 \left| J_{z_R} \right|^2 \left| J_{y_R} \right|^2 . \frac{\pi}{4\zeta} + \frac{\sigma_u^4}{\bar{U}_H^4} \, I_3^2 \, A_R^2 \left| J_{z_R} \right|^2 \left| J_{y_R} \right|^2 . \frac{\pi}{4\zeta} + 2\sqrt{R_1 R_2} \right] ,$$

where (a) B_1, R_1 are the first group of terms in the bracket (the B and R terms of Solari),

(b) B_2, R_2 are the second group of terms in the bracket,

(c) σ_u^2 = variance of wind ,

(d) $A_R = \int_{n_o - \Delta n_o}^{n_o + \Delta n_o} n_o . \frac{S(n_o)}{\sigma_u^2} d(\ln.(n_o))$ = area of spectrum about the centre frequency of the tree natural frequency, n_o,

(e) $A_B = \int_o^\infty n . \frac{S(n)}{\sigma_u^2} . d(\ln.(n)) - A_R$

and $A_B + A_R$ = unity, the total area under the power spectral density curve,

and (f) I_1, I_2, I_3, are integrals of the near wind profile characterising the wind force and where it acts up the crown;

$$I_1 = \int_o^1 \frac{\hat{U}_z^2}{} . (\hat{z})^{1.5} . \frac{H - z}{H - d} \, d\hat{z} ,$$

$$I_2 = \int_o^1 \bar{U}_z . (\hat{z})^{1.5} . \frac{H - z}{H - d} \, d\hat{z} ,$$

$$I_3 = \int_o^1 (\hat{z})^{1.5} . \frac{H - z}{H - d} . d\hat{z} ,$$

which can be found by numerical analysis,

and $\chi = \frac{C_{D_f}}{C_{D_\ell}}$ (from Solari),

$$\text{So } B = \frac{\sigma_u^2}{\bar{U}_H^2} A_B . \left| J_{z_B} \right|^2 . \left| J_{y_B} \right|^2 . \left[4 \, I_2^2 + 2\sqrt{4 I_2^2 . \frac{\sigma_u^2}{\bar{U}_H^2} A_B . I_3^2} + \frac{\sigma_u^2}{\bar{U}_H^2} . A_B . I_3^2 \right]$$

$$\text{or } B = K_1 . F_1 . \left[4 \, I_2^2 + 4\sqrt{I_2^2 \, I_3^2 \, K_1} + K_1 \, I_3^2 \right] \quad \ldots\ldots \text{(a)}$$

Similarly,

$$R = K_2 \cdot F_2 \left[4\ I_2^2 + 4\sqrt{I_2^2 \cdot I_3^2 \cdot K_2} + K_2 \cdot I_3^2 \right] \quad , \qquad (10)$$

where $K_1 = \frac{\sigma_u^2}{\bar{U}_H^2} \cdot A_B$,

$$K_2 = \frac{\pi}{4\zeta} \cdot \frac{\sigma_u^2}{\bar{U}_H^2} \cdot A_R \quad ,$$

$$F_1 = \left| J_{z_B} \right|^2 \cdot \left| J_{y_B} \right|^2 \quad ,$$

$$F_2 = \left(\frac{C_{D_f}}{C_{D_\ell}} \right)^2 \cdot \left| J_{z_R} \right|^2 \cdot \left| J_{y_R} \right|^2 \quad .$$

3.10.4 Conclusions to Along-wind Response Derivations

These equations can solve for $\frac{A}{D}$ r.m.s full scale and model (see Chapters 6 and 7) from measured mean velocity profiles and spectra.

A closed-form solution, assuming mean velocity profiles shapes and spectra over high roughness (Ch. 3), can also be used (Solari, 1982).

Both methods use Davenport's joint probability distribution curves to obtain the aerodynamic admittance terms. Graphical methods by (Simui, 1980) can be used but are inaccurate, while Davenport's, and Vellozzi and Cohen's methods, apply to structures sited in open country, and to a lesser extent, urban boundary layers using exponential mean velocity profiles (Ch. 2). Simui produces a useful algorithm for the solution of along-wind response of structures; the graphical method still requires extension by numerical extrapolation of curves to cover cases of structures in thick boundary layers.

The relationships given in this thesis are derived from an extension of Solari's method: his method assumes mean wind profile and turbulent energy spectrum shapes. A sample calculation of along-wind response of model trees within model forests with a changing roughness density is reproduced in Appendix I. Resonant background and mean components of model tree-top swaying motion are compared by this method and by photographic methods which produces 'averages' of the total tree response.

3.11 SUMMARY OF THE AERODYNAMIC PROPERTIES OVER AN INFINITELY LONG FOREST

(a) There is stratified flow consisting of:-

(i) an outer layer well above the tree tops;

(ii) a transition region where shear stresses are at a maximum;

(iii) an inner layer where the shear stress is constant and the velocity profile is logarithmic;

(iv) a stagnant cushion of air beneath the inner layer.

(b) The 'infinite' forest starts at about 5 tree heights in from the forest border. The shearing stress at the canopy top remains constant in the x-direction, (Oliphant, Cionco 1981).

(c) The Reynolds Number of the vegetation must be above 1×10^4 for the shearing stresses to be constant.

(d) For the inner forest $d = 0.70\ H$ and $z_o'' = 0.11\ H$. (3.2, 5.10.4).

(e) The mean wind speed at tree top height in the infinite forest is 65% of the upstream wind in inversion conditions and is even less, 55%, in lapse conditions (6.8.2).

(f) The boundary layer growth is a function of spacing which adds to the shear stresses and turbulence levels above and within a forest canopy.

(g) The main factors affecting aerodynamic roughness are tree size and spacing which change as thinning and pruning practices change.

(h) The aerodynamic roughness varies linearly as $\frac{A_r}{A_t}$ changes, and for a limited range of $0.1 \leq \frac{A_r}{A_t} \leq 0.25$ the aerodynamic roughness can be found for various thinning regimes in the inner forest.

(i) Inner layer growth continues well into a forest, but the region of mixing alters with $\frac{A_r}{A_t}$ and equilibrium is probably closest to the front for forests without thinning.

(j) The forest canopy is an extremely rough moving surface which interacts with the wind, altering the turbulence and the tree response (7.1).

(k) Each tree within the forest contributes to the production of turbulent energy with a scale similar to the roughness. The shed vortices so formed add a frequency bandwidth to the oncoming spectrum of frequencies in the surface boundary layer and adjust the spectra (7.2.4).

(l) Fluctuating wind forces on the trees within the stand can be assessed using the high frequency end of spectra (6.10.2).

CHAPTER 4

WIND CHARACTERISTICS OVER FOREST BORDERS AND OTHER ABRUPT CHANGES IN ROUGHNESS

This chapter describes the surface layer wind changes that occur in Zone C (see Chapter 1).

4.1 NON-EQUILIBRIUM CONDITIONS OVER A FOREST LEADING EDGE

The wind, passing from open country and over the leading edge of the forest, will have its approach wind vector altered by the canopy. As the wind approaches the leading edge it will decelerate, then immediately, on passing over the leading edge, it will accelerate so that the magnitude and direction of the mean and turbulent velocity components are drastically altered (see Ch. 6, $\bar{W}_z$ measurements). Consequently, the normal pressures and shear stress variations resulting from these velocity changes will be redistributed unequally and act very differently on trees that are at the front of the forest, and on trees that are in the first few rows behind the front (Walshe). The normal pressures are highest right at the front, while the shear stresses are highest just in from the front.

At some distance downstream from the leading edge the wind stresses will reach equilibrium at the forest surface. This equilibrium condition extends down to the stagnant air layer below the canopy, and later, above the inner layer to the outer layer. All the layers exhibit constant velocity variations with height, even though the outer layer grows in thickness (Wood, 1978). (Fig. 4.1.)

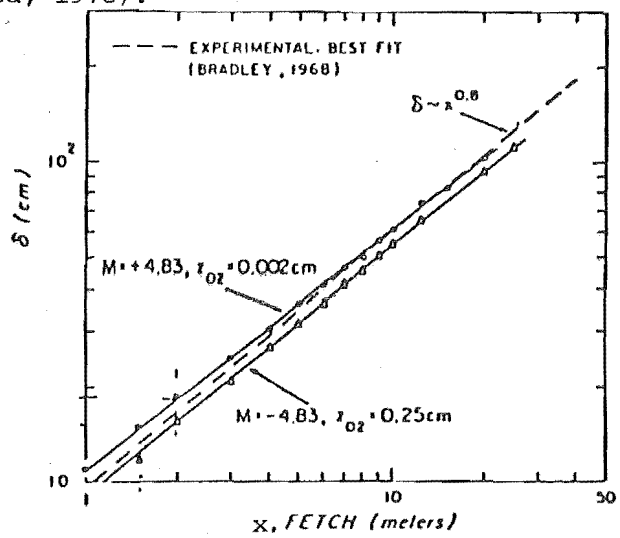

FIGURE 4.1 Growth of IBL thickness with fetch (after Wood).

Upstream, the open country boundary layer roughness (z_o) is low (0.03 m). At the interface of the outer layer with the upstream surface layer the velocity variations change rapidly with height, producing a kink in the mean wind profiles. In this region the wind variations are changed by the geometry of the leading edge with its higher surface roughness (z_o') and change in height (d) displacing the wind vectors vertically ($\bar{W}_z > 0$) and increasing the turbulent mixing.

Coming down from the outer layer the average eddy size becomes non-linear with height. The departure from linearity is greatest in the transition region and the highest shear stress occurs there. The transition region separates the total wind changes in the outer layer, (including previous upstream influences) from the inner layer wind changes produced by the tree tops alone.

Below the transition region mixing gradually returns to equilibrium, since now eddy sizes are controlled by the canopy aerodynamic roughness itself (z_o''). Since eddy sizes are far smaller and energy dissipation more rapid, equilibrium between the inner layer and the thin transition region will be reached downwind from the leading edge much earlier than equilibrium between the transition region and the surface layer above the outer layer. It is evident that the shear stress distribution along the transition region will result in rapidly increased turbulence just in from the leading edge which then slowly decays inwards to where equilibrium exists.

Honami waves with frequencies much higher than the average gust frequencies can arise in this region, especially at wider tree spacings. The interaction of the waving motion of the plants and the travelling waves can result in a Doppler shift so that the spectra over the waving crops exhibit 'peaks' due to the combined effect of the travelling waves and the individual plant natural frequencies (Finnigan).

4.2 DISTRIBUTION OF WIND DAMAGE TO FORESTS FROM THE LEADING EDGE INWARDS

Hütte (1968b) recognised that topographical changes influence the distribution of wind damage to forests. He observed that storm damage is more frequent where turbulence and mean winds both increase together. Stands were damaged more on middle windward slopes, immediately behind the crest of a line of hills, on the terraces of lee slopes, and on steep

To p.94

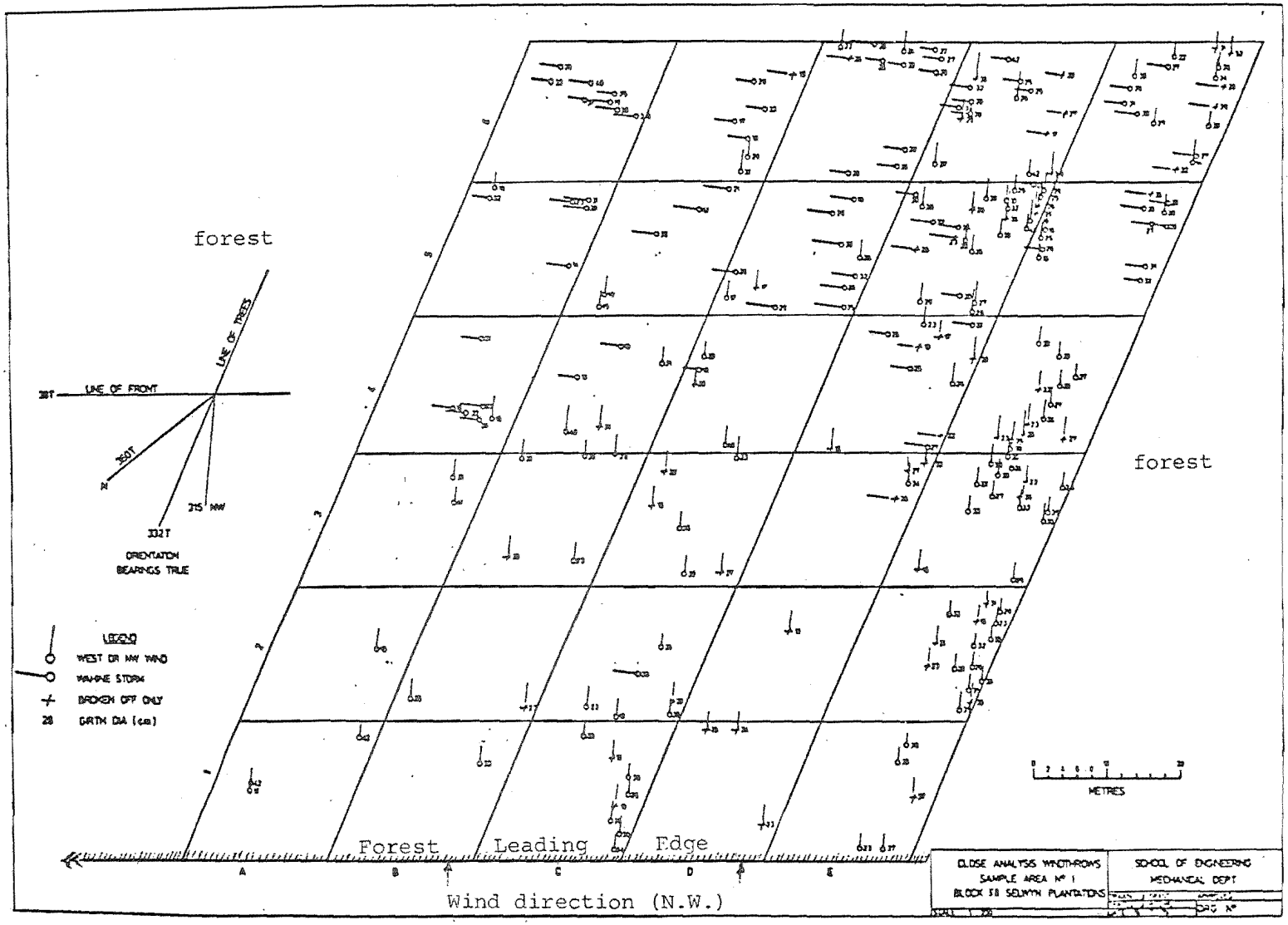

FIGURE 4.2 Edge windthrow history - Smith's Block, Burnham, Canterbury.

mountain slopes at their junction with lower lee slopes. He noticed that storm damage rarely arose through the acceleration alone of a wind in a valley.

Bull and Reynolds (1968) recognised that the leading edges of forests generate extra turbulence in addition to any upstream effect or thinning density change. There is repeated evidence to show that additional zones of high windthrow occur just behind the leading edge in recently-thinned forests (Ch. 1 and Appendix III). Often the front remains upright while rows immediately behind the front sustain extreme damage. The damage first reduces as the wind moves further inwards from the forest border, then rises again, but to less extreme levels (Cremer et al, 1977; Somerville, 1978; Appendix III).

The aerodynamic influences caused by the abrupt changes in the wind that occur at the forest front are further complicated by the waving motion of the trees and travelling waves, or Honami (Inoue, 1955) which appear to contribute to the turbulent wind energy spectra already existing (see Ch. 3). The net effect of this complication on the turbulence is to produce levels of wind damage from the leading edge inwards as described above. Figure 4.2 depicts the location of trees blown over in a mature stand of Radiata pine over a period of 15 years. Concentrations of storm damage are away from the leading edge.

4.3 SOME PREVIOUS RESEARCH ON THE ABRUPT CHANGE PROCESS

Theoretical studies of boundary layer growth following a change in surface roughness associated with a step change of mean height have been reviewed by Panchev and Donev (1971). Since then, extension of the theoretical studies have been made by Landesberg and James (1971), Landesberg and Thom (1971), Narasimha and Sreenivasan (1973), Rao et al (1974), Jackson and Hunt (1975), Mulhearn (1977), Wood (1978), Højstrup (1981), Shaw and Pereira (1982), and Panofsky et al (1982).

Modelling experiments on forests relating to leading edge conditions, all using non-waving roughness, have been undertaken by Hirata (1951a & b), Fraser (1962(a). 1962(b) Walsh and Fraser (1963), Plate and Quraishi (1965) Meroney (1968), and Hsi and Nath (1970). Other wind tunnel modelling work on the abrupt change process includes Raine (1974), Lo (1977), Mulhearn (1978), Jensen and Peterson (1978), Bowen (1979), Knight and Macdonald (1979), Pearse et al (1981) and Antonia and Luxton (1971).

There have been fewer full scale experiments studying the abrupt change of a forest leading edge. The most important are those by Reifsnyder (1955), Oliphant (1964), Shinn (1969), Raynor et al (1976), Garratt (1978 a&b), and Högström et al (1983), all of whom were concerned with diffusion processes resulting from high turbulence. Other researchers who have studied the abrupt change processes other than at forest leading edges are Panofsky and Townsend (1964), Freeston (1974), Bradley (1968, 1980), Bergen (1971), Peterson (1975), Bowen (1979), Hunt (1980), Højstrup (1981), Pearse et al (1981), Panofsky et al (1982) and Stevenson and Neal (1983).

The main theoretical attempts to assess the wind characteristics of abrupt changes are:-

Elliot's Method (Miyake);
Panofsky - Townsend's Method;
Bradshaw's Method;
Peterson's Method;
Rao et al's Method;
Wood's Method;
Panofsky et al's Method.

The basic assumptions are that:-

- the air is incompressible;
- the flow can be assumed steady in the inner layer (Taylor's Hypothesis);
- the air is neutrally stable;
- roughness heights are small compared with the abrupt change in height;
- the flow is two-dimensional and at right angles to the abrupt change.

The Elliot Method assumes local equilibrium everywhere, with a sharp discontinuity in shear stress at the leading edge. (A modified form of Elliot's simple method may be the most appropriate: Bradley, 1980).

The Panofsky-Townsend Method assumes local equilibrium with a gradual change in shear stress from the leading edge inwards. This means that above the canopy, in the transition region where rapid shear stress changes occur, a simple logarithmic law cannot be assumed.

Panofsky and Townsend's method agrees with Elliot's provided the fetch is not too small. Measurable accelerations occur in their outer layer for long distances ($\frac{z_o''}{H} \times 10^5$), yet their profiles are determined by the inner layer which reaches equilibrium much sooner.

The Bradshaw Method solves the equations allowing for the same shear stress changes horizontally and a constant vertical shear stress in the inner layer up to the transition region. This is much the same as the Panofsky-Townsend Method but separates the flow into 3 parts, the inner, the outer layer and the upstream surface layer. Equilibrium conditions are reached considerable distances in from the leading edge. This method shows that equilibrium can be reached much sooner if the normal boundary layer equations are applied to the growth of the interface between the surface layer and the outer layer over the new roughness. This appears to be a better approximation where high shear stress changes occur at the abrupt change.

Jackson and Hunt (1975) use the linear perturbation method to solve the boundary layer equations applying to flow over low hills. They considered the pressure gradient up sloping hills to be as important as the acceleration terms. In their adaptation they applied local equilibrium to the boundary layer at the surface right up to the maximum hill height. Their solution has some relevance for more sudden increases in height (Bowen, 1979; Panofsky et al, 1982).

The Peterson Method allows for an abrupt change in height by assuming that upstream, the large scale pressure gradients are in equilibrium with the friction forces, with no acceleration. Downstream of the abrupt change Peterson assumed that the acceleration was proportional to the sum of the local pressure gradient and friction forces which produce shear stress distributions proportional to turbulent energy changes from the discontinuity inwards. Mean pressure changes between the three areas were neglected. He did not need to assume a mixing length or any other momentum coefficient at the discontinuity. In Peterson's model, the variation in turbulence occurred in the transition region.

Rao et al's Method (1974) produced a stress distribution similar in shape to that predicted by Peterson. To his model they added third order acceleration terms to their initial equations, again making no assumptions about mixing length or its distribution. They solved the equations by knowing the shape of the mean wind profile at the leading edge.

Wood (1978) modified Rao et al's Method by neglecting mean stress variations. Both Wood's and Rao et al's Methods assume that the vertical stress change in the inner layer is constant up to the transition region (that is, in 'equilibrium'). Wood showed that his and Rao et al's methods agreed with the modelling tests by Bradley (1980). (Wood suggests that his model is preferable.)

Bowen (1979) conducted model and full scale experiments on flow over hills and showed that Jackson and Hunt's approach had reasonable validity for steep hills. It was suggested by Bowen that this may be because of the upstream stagnation vortex in front of steep hills.

Panofsky et al's Method (1982) follows on from Bowen's. It allows for the acceleration of the wind over the leading edge of the abrupt change in height. This provides an added component to the shear stress at the abrupt change due to the speed-up factor (Jackson and Hunt, Bowen (1979), Bradley (1980), and §4.4).

Kawatani and Meroney (1968) and Counihan (1971) conducted wind tunnel tests and measured flow over high roughness elements. They showed that, in the change from smooth to rough conditions, the non-equilibrium conditions generated a turbulence variation at the surface proportional to the shear stresses; the roughness element density changes were responsible for alteration of the turbulence levels. It appears from these model tests that z_o' became constant once equilibrium was attained, but varied in the non-equilibrium Zone C. In the inner layer it appears that the roughness characteristics can still be measured by the tree-top height mean velocity profile intercept z_o'', with the mean wind velocity 'local' profile slope giving the friction velocity $U_{*\ell}$.

Seginer (1972) used a method similar to that of Rao et al to assess the drag distribution behind a porous abrupt change in height. In this thesis Seginer's method is used to assess the drag coefficient distribution along a forest surface from the leading edge inwards to the equilibrium point.

Controversy surrounds theoretical models used to calculate the distance from the leading edge to where equilibrium is regained. The earlier perturbation theories predict a large distance to equilibrium, whereas the theories of Peterson, Rao et al and Wood predict a shorter distance. Bradley (1980) concludes that equilibrium between the inner

and outer layers is reached at about 200 H in from the leading edge, while Elliot's simple theory suggests that equilibrium exists 20 H in from the leading edge. It is important to distinguish between equilibrium return in the outer layer (for diffusion processes) and equilibrium return in the inner layer (for wind-loading purposes). Over forests, the added input to the small-scale turbulence by travelling waves interacting with the wind frequencies due to tree-top movement must help the early return to equilibrium. Reifsnyder (1955) measured wind profiles at leading edges and he concluded that equilibrium conditions were reached in the inner layer about 7 H in from the leading edge. He noted that wind reductions in the crowns were about 60% lower than upstream values (6.8.2; Fig. 6.25).

Oliphant (1964) conducted a full scale experiment on boundary layer growth from forest leading edges. The aerodynamic properties of the forest are consistent with current values; that is, $\frac{d}{H} \simeq 0.67$ and $\frac{z''_o}{H} \simeq 0.11$. The diagram shows how his experimental results give a return to equilibrium at about 5 H in from the leading edge which is about the same as Reifsnyder's values and which is much sooner than predictions.

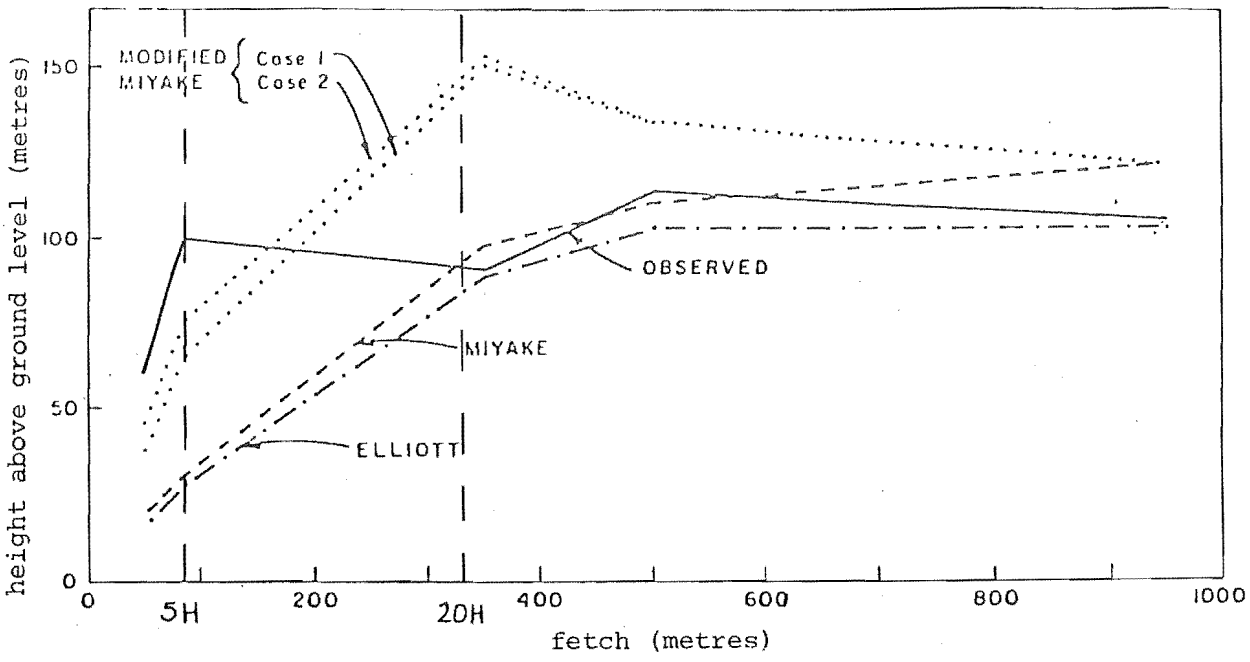

FIGURE 4.3 Observed and predicted height of the outer boundary layer (after Oliphant).

4.4 WIND ACCELERATION OVER HILLS AND OVER FOREST LEADING EDGES

Speed-up over smooth hills has been studied by Jackson and Hunt (1975). They note that as the air passes over the hill the constant velocity lines converge. The air accelerates to its highest velocity at the maximum hill height. This speed-up is almost constant with height in the inner layer and a logarithmic vertical wind profile exists. Accordingly, friction velocity and shear stress grow as a function of hill shape. Prior to the speed-up, the air slows down. The pressure first rises, then falls as the flow accelerates, and then begins to rise again after the wind passes over the hill top. Full scale tests by Bowen (1979), Neal (1979), Bradley (1980), Panofsky et al (1982) and Carruthers and Choularton (1982) adopt Jackson and Hunt's methods for estimating shear stress and turbulence changes over hills using speed-up factors. Most research indicates that if the change in height is abrupt, analysis of the flow is complicated because of large three-dimensional changes in the wind velocities and the development of leading edge and trailing edge vortex formations and separations. Most vortex formations in these types of flow result from rapid changes in vertical shear stress distributions.

Jackson and Hunt suggest that, under most conditions, the speed-up factor

$$S_{(U)} = \frac{\Delta \bar{U}_{max}}{\bar{U}_o} = \frac{m_u}{\frac{x}{H}}$$

which suggests that $S_{(U)}$ is unity when $m = 2 = \frac{x}{H}$ and the wind speed at the crest is $2\ \bar{U}_o$.

In addition, Bowen et al (1981) studied flow over escarpments and showed that for a right-angled escarpment, 9.5 m high, the flow soon adjusts to a near-equilibrium state at + 4 H. They use Jackson and Hunt's approach to compare the measured profiles with predicted shapes (see Fig. 4.4).

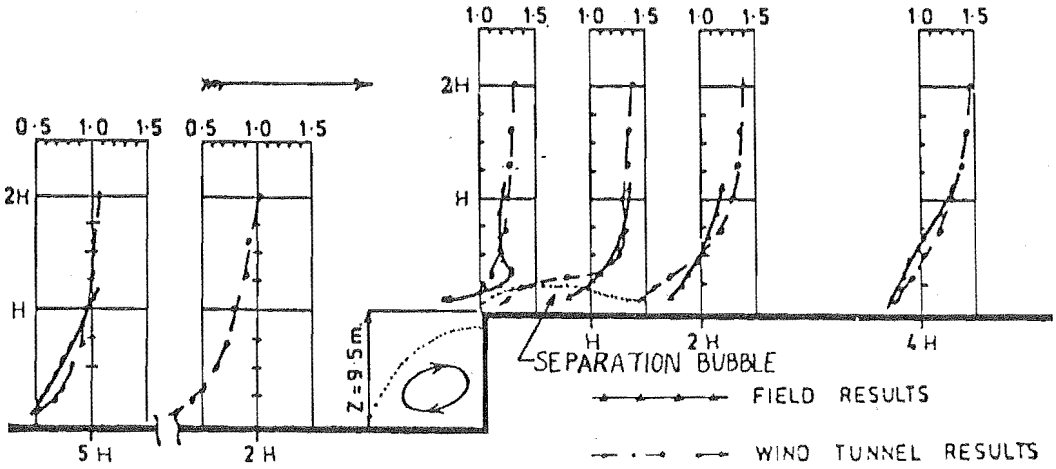

FIGURE 4.4 Flow over an abrupt change of height (after Bowen et al)

It appears, then, that similarities exist between the flows over hills to the crest and flows over the leading edge of a forest, up to the location of the maximum velocity point. The diagrams below suggest a possible relationship between the two (Fig. 4.5(a)-(c)).

Note that Jackson and Hunt's proposal for flow over hills shows a convergence in the flow at hill-top height, whereas the forest has a convergence 3 H in from the leading edge (see Ch. 6). A similar pattern, although less realistic, exists in the constrained flow case of a sudden contraction in a pipe, with a vena contracta occurring past the contraction, providing similar mean flow patterns and similar high turbulence (Massey, 1971).

4.4.1 Speed-up factor ($S_{(U)}$) relationships

Jackson and Hunt (1975) use the boundary layer momentum and continuity equations, applying the classical perturbation methods to develop equations for changes in velocity up hills with low slopes. Upstream, conditions are considered to be steady and in equilibrium (Zone A), and they revert to equilibrium (Zone B) after the wind passes over the hill.

It is obvious that near the leading edge large values of $\bar{W}_z$ and w' will exist. The vertical components of turbulence (w') with strong positive skewness, and the horizontal components (u') with strong negative skewness, correlate to provide the Reynolds stress changes over the hill (or forest) up to $\frac{x}{H} = 3$. The pressure gradient rises and the change in

To p.102

(a) Jackson and Hunt;

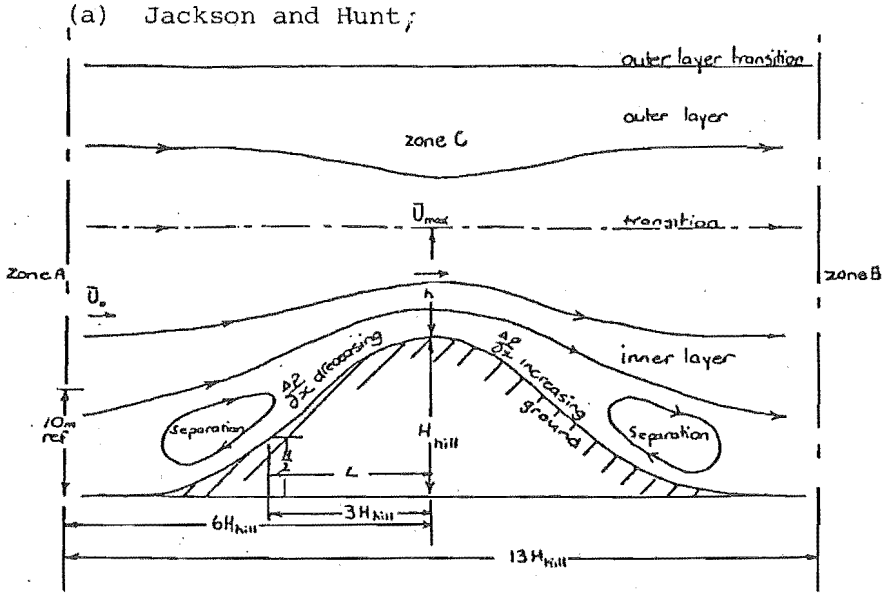

(b) Lo;

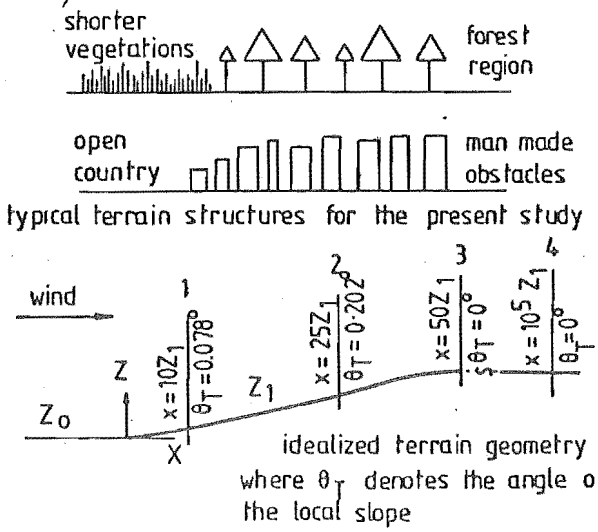

(c) Thesis model;

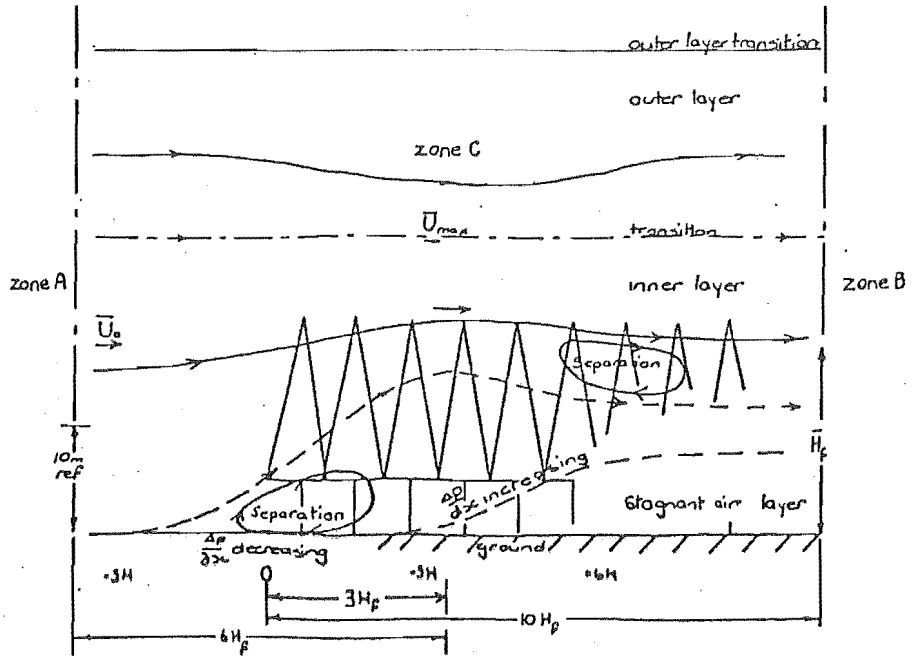

FIGURE 4.5(a)-(c): Suggested patterns of flow over a hill and a forest leading edge

pressure is, to some extent, balanced by the reduction in shear stress beyond $\frac{x}{H} = 3$.

Up to the crest of the hill, Jackson and Hunt show that if $\bar{U} = \bar{U}_o(\Delta z) + \Delta u$, $\bar{W}_z = (H/X_1) f'(x/X) \left[\bar{U}_o(\Delta z) + \Delta u\right] + \Delta w$, are the mean horizontal and vertical velocity components, then

$$\bar{U}_o(\Delta z) \frac{\partial \Delta u}{\partial x} + \Delta w \frac{\partial \bar{U}_o(\Delta z)}{\partial \Delta z} = -\frac{1}{\rho} \frac{\partial \Delta p}{\partial x} + \frac{1}{\rho} \frac{\partial \Delta \tau_{xz}}{\partial \Delta z} \quad ,$$

$$\bar{U}_o(\Delta z) \; \partial \Delta w / \partial x = -\frac{1}{\rho} \frac{\partial \Delta p}{\partial \Delta z} + \frac{1}{\rho} \frac{\partial \Delta \tau_{zz}}{\partial \Delta z} \quad ,$$

$$\frac{\partial \Delta u}{\partial x} + \frac{\partial \Delta w}{\partial \Delta z} = 0 \quad ,$$

and the perturbation pressure gradient $\partial \Delta p / \partial x$ is as important as the acceleration terms $(\bar{U}_o \partial \Delta u / \partial x)$.

After the crest of the hill, where the maximum velocity is reached, the turbulence near the surface is assumed to be in local equilibrium. The terms containing Δw in the above equations can therefore be neglected and the horizontal pressure gradient opposes the shear stress distribution as the flow decelerates. This latter condition applies vertically up to the transition region where $\bar{U}_{max}$ occurs, which is some distance above the crest of the hill (approximately half a hill height). From the hill crest therefore:

$$\bar{U}_o(\Delta z) \frac{\partial \Delta u}{\partial x} = -\frac{1}{\rho} \frac{\partial \Delta p}{\partial x} + \frac{1}{\rho} \frac{\partial \Delta \tau_{xz}}{\partial (\Delta z)} \qquad (2)$$

and since for the transition region (Chapter 4):-

$$\bar{U}_o + \Delta u_z = \bar{U}_z \quad ,$$

$$\text{so,} \quad \bar{U}_o(z) \frac{\partial \Delta u}{\partial x} = (\bar{U}_z - \Delta u_z)(\Delta z) \cdot \frac{\partial (\bar{U}_z - \bar{U}_o)}{\partial x} \quad .$$

$$\text{but,} \quad \frac{\partial \bar{U}_o}{\partial x} \simeq 0 \quad \text{once} \quad \frac{x}{H} > 3$$

$$\text{therefore,} \quad \bar{U}_o(z) \frac{\partial \Delta u}{\partial x} = \frac{\partial \left(\frac{\bar{U}_z}{2}\right)^2}{\partial x}$$

and equation (2) becomes

$$\frac{\partial(\bar{U}_z)^2}{\partial x} = -\frac{1}{\rho}\frac{\partial \Delta p}{\partial x} + \frac{1}{\rho}\frac{\partial \Delta \tau_{xz}}{\partial(\Delta z)} \quad , \qquad (3)$$

which may also be applied to the forces governing the flow of the wind over the tree tops of the forest after + 3 H (4.7).

By noting that Rao et al account for the fact that pressure changes and shear adjust the deceleration of the flow over the tree tops, equation (3) can solve for the pressure gradient term if the friction velocity from the velocity profiles at tree-top height and the change in velocities in the x-direction are calculated.

Up to the hillcrest Panofsky et al (1982) show that the change in velocity (from Jackson and Hunt) is

$$S_{(u)} = \frac{\Delta u}{\bar{U}_o} = \frac{Z_t}{X}\frac{\ln(X/z_o)}{\{\ln(\delta/z_o)\}^2}\ln(z/z_o) \quad ,$$

where X = distance to ½ hill height,

z_o = upstream roughness,

S = thickness of upwind boundary layer

z_T = height to transition above the hill top

z = .75 H for the case of a forest edge, = d.

Panofsky et al also suggest an equation for the inner layer based on Jackson and Hunt's method. It adds the speed-up velocity at the leading edge to the non-equilibrium mean wind profile which occurs over the roughness change just in from the leading edge.

Since, $\bar{U}_z = \bar{U}_o + \Delta\bar{U}$,

where $\bar{U}_z$ is the velocity at a height z above the hill and $\bar{U}_o$ is the upwind velocity at the same relative height above the level ground,

$$U_z = \frac{\bar{U}_{*p}}{k_a}\left[1 + \frac{h}{X}\left(\frac{\ln(X/z_o)}{\ln(\delta/z_o)}\right)^2\right]\ln(z/z_o) .$$

In the lower layers then, logarithmic profile probably exists, but the friction velocity is altered relative to hill slope,

$$\bar{U}_{*prof.} + \Delta\bar{U}_{*prof.} = \frac{k_a(\bar{U}_z)\left[1 + \Delta\bar{U}\right]}{\log\frac{z}{z_o}}$$

where $\Delta\bar{U}_{*_{prof.}}$ is added to the $\bar{U}_{*_{prof}}$ in the transition region when assessing shear stress values just behind the leading edge of the forest (or just past the hill crest).

4.4.2 The velocity profile shape

At the inner layer region, where equilibrium exists, the velocity profile shape can be used to determine the shear stress distribution along the tree-tops.

The wind profile shape has three sections separated by two kinks. Below the lower kink a section exists where the flow adjusts to the combined effects of surface roughness and the pressure field, then an intermediate steep section exists in the transition region: finally there is a section above the upper kink where the flow is not influenced by surface conditions. The stress variation above the transition region can be found from the slope of the velocity profile in the steep section to where $\phi_m = 1$ at the top of the outer layer (Peterson, 1969). (Fig.4.6.)

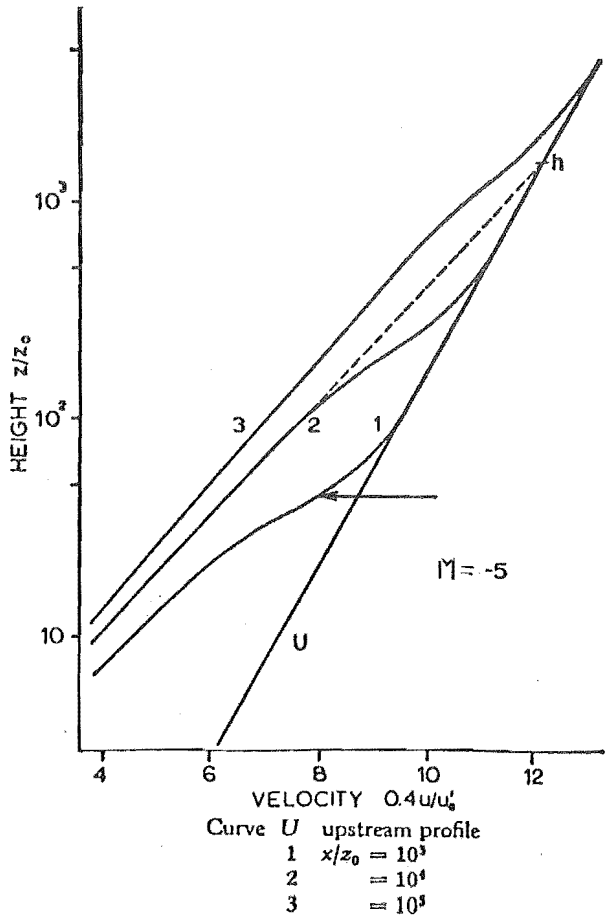

Curve U upstream profile
1 $x/z_0 = 10^3$
2 $= 10^4$
3 $= 10^5$

h is the height of the interface for $x/z_0 = 10^4$.

$z_o = 0.03$ m, $x = 300$ m, $h = z_i = 300$ m, $\frac{x}{H} \simeq 20$

FIGURE 4.6 Velocity profiles for smooth to rough terrain change, M = -5. (after Peterson).

Below the transition region, the slope $\frac{\partial \bar{U}_z}{\partial z}$ gives a value of aerodynamic roughness, z_o'', characteristic of the physical and geometrical nature of the surface and of the eddies (related to turbulent wake generation around individual roughness elements) directly responsible for the drag on the surface (Högström et al, 1983).

Högström et al suggest that $z_o'' \simeq z_o'$ at equilibrium and that $\frac{k_a \bar{U}_z}{\bar{U}_{*\ell}}$ is greater by an amount $\Delta\chi_m$ (defined in Ch. 2).

Bradley (1980) points out that Klemp and Lilly (1978), when considering small shear stress changes, take the average wind velocity in each layer as a good approximation to the flow. This produces a very simple, stepped, wind profile shape.

Panofsky (pers. comm.)shows how the effect of the vertical motion up to and beyond an abrupt change combined with the canopy roughness can provide a stress estimate, assuming that the profile shapes above and below the interface are almost logarithmic.

These predictions of profile shapes can be used to give a mathematical shape to model and full scale mean wind profile shapes, and produce a mathematical relationship for the stress distribution at the point of inflexion of the measured wind profile, using the modified friction velocity $\bar{U}_{*_{prof}} + \Delta\bar{U}_{*_{Prof}}$ due to speed-up (Lo, 1977).

4.4.3 Turbulent velocity changes

Sadeh et al (1971) investigated the mean velocity profile and the longitudinal turbulence intensity variations, inside and above high roughness, by using model forests positioned in an atmospheric wind tunnel. Their results give divided zones of transition and fully developed flow regions with a short adjustment at the downstream end of the forest. The transition zone has a strong effect on the flow characteristics within and above the layer of roughness. The influence of the roughness zone affects both the velocity and the turbulence to more than 3 times the model height.

Upwind turbulence is distorted in the same manner as the mean winds and so $\bar{W} \alpha w'$. This is called the rapid distortion theory (Narasimha and Sreenivasan,1973; Bearman,1972; Townsend, 1976).

In Sadeh et al's study the minimum velocity occurs within the canopy at 0.3 H. The strongest growth rate (of 30%) of the outer layer occurs at the leading edge. Once equilibrium is reached well away from x=z=0, the boundary layer growth rate reduces to 10%. The canopy causes the development of an inner layer extending to 1½ H, while an outer layer extends upwards from 1½ H. Within the transition layer the friction velocity changes rapidly at the leading edge and increases by more than 6 times over a distance of 10 H rearward in the positive x-direction. The friction velocity then decreases gradually and becomes constant in the fully-developed region of flow, indicating a constant shear stress or drag over the forest canopy. At the leading edge they found that the turbulence intensity is as high as 90%. At the canopy top, where the velocity increases with height, the turbulence intensity reduces to 60% - 65% and above this it gradually attenuates to about 10% at 2.33 H. Within the fully developed flow region the same trends are evident, with a maximum turbulence intensity of 80% to 90% inside the canopy down to 0.83 H. Turbulence amplification is observed over the leading edge above the canopy. The important aspect of these results is the strong dependence of turbulence on the canopy architecture. The roughness affects the turbulence up to ½H above tree height and the flow is highly turbulent (Fig. 7.3; Shinn, 3.2).

Kawatani and Meroney (1968) quote Inoue (1952), who, with field tests, established relations for turbulence intensity variation with height. He found that the turbulence intensity is proportional to $(z-d)^{-\frac{1}{2}}$ for regions in the outer layer and is independent of height within the canopy. There exists conflict of opinion about the lower layer properties (within the canopy) as Uchijima and Wright (1964) suggest that the turbulence intensity decreases gradually downwards from the canopy top.

Hunt (1972) summarises research on the mean and turbulent velocity distributions in flows around bluff bodies. He concludes that the absolute value of r m s turbulence remains approximately constant near the front of a building (forest front) even when the mean velocity changes significantly: the relative turbulent velocities can be found from the local mean velocities. Also, he states that if the length scale of the body is less than the length scale of turbulence, then the turbulence intensity generated is less than unity; but if the length scale of the bluff body is larger than the length scale of the turbulence, then the turbulence intensity is greater than unity.

Bearman (1972) also studied flow around bluff bodies. He states that two shear layers, free to interact, are basically unstable and roll up to form a staggered array of discrete vortices - an entrainment process. An examination of the wake behind a porous flat plate up to a porosity of 30% - 40% shows that the peak in the spectrum spreads itself over a broader band of frequencies (also Raine, 1974). The condition described by Bearman will be similar at the transition region above a forest border. Firstly, turbulence levels will be high because of the physical dimensions of the forest. Secondly, at the transition region and in high shear near the leading edge (+ 3 H), significant increments to turbulence intensity will occur (Finnigan).

In the inner layer, where turbulence intensity is considered to be in equilibrium,

$$\frac{\Delta\sigma_u^2}{\sigma_{u_o}^2} = \frac{\Delta\sigma_w^2}{\sigma_{w_o}^2} = \Delta C_{f_\ell} = \frac{4H}{X}$$

for low sloping hills; all the turbulent wind components are distorted equally.

In the outer region, σ_u^2 decreases as σ_w^2 increases and the change is related to the speed-up factor ($S_{(u)}$)

$$- \frac{\Delta\sigma_u^2}{\sigma_{u_o}^2} = \frac{\Delta\sigma_w^2}{\sigma_{w_o}^2} = \frac{\Delta u}{\bar{U}_o} = S_{(u)} \quad .$$

Bradley (1980) indicates that the turbulence profiles reach an unchanged form at a distance of approximately 20 H in from the leading edge, and at the same time as the mean velocity profiles reach equilibrium. These Reynolds stress variations are not of the form encountered in a zero pressure-gradient condition which occurs further along in the x-direction; Bradley suggests that the turbulent winds are in equilibrium within the transition region and are not so in the outer layer well above.

4.5 SHEAR STRESS VARIATION IN THE x-DIRECTION IN THE INNER LAYER

When the open country winds flow over a sudden change of terrain there are large changes in shear stress within the inner layer. Well above this, in the outer region, the changes in stress are negligible and the flow behaves as if it were inviscid shear flow. The flow condition is similar to turbulent boundary layer flow adjacent to a wall with zero pressure gradient, and the small perturbations theory can be used to solve the boundary layer equations. The solution gives a decreasing shear stress from a maximum at z_T (the height to the transition layer) to zero at the outer layer, about 300 m up above the ground (ESDU).

Below z_T it is not possible to neglect the accelerations of the flow in the x- and z- directions, or the pressure gradient and accompanying shear stress variations in the x-direction. The drag coefficient can be calculated for each station (see Chapter 6) provided the leading edge drag coefficient is known (see Fig. 4.14).

Although the methods of Rao et al and Wood are suitable within the inner layer near the forest leading edge, right at the front (where horizontal and vertical shear stresses undergo rapid changes) a modified form of the Elliot (Miyake) Method fits observed data more accurately (Oliphant and Bradley).[1]

In the outer layer the mixing length is not constant (the growth rate of eddies is not linear) and the ratio $\frac{\ell_z}{k_a}$ is needed to obtain vertical stress variations (Figs 4.7; 4.8; 4.0).

To p.110

---

1. Experiments measuring shear stress due to wind changes over hills in the Outer Hebrides (Scotland) are being undertaken at the time of writing; these may show that Panofsky et al's Method is the most appropriate.

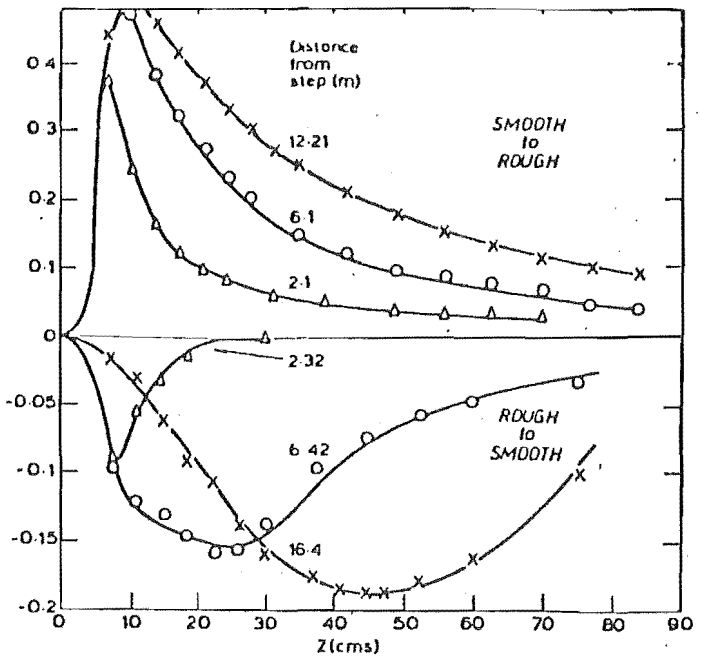

$\frac{\ell_z - k_a z}{k_a z}$

Wood (1978)

FIGURE 4.7 Distribution of eddy characteristics within the internal layer (after Wood).

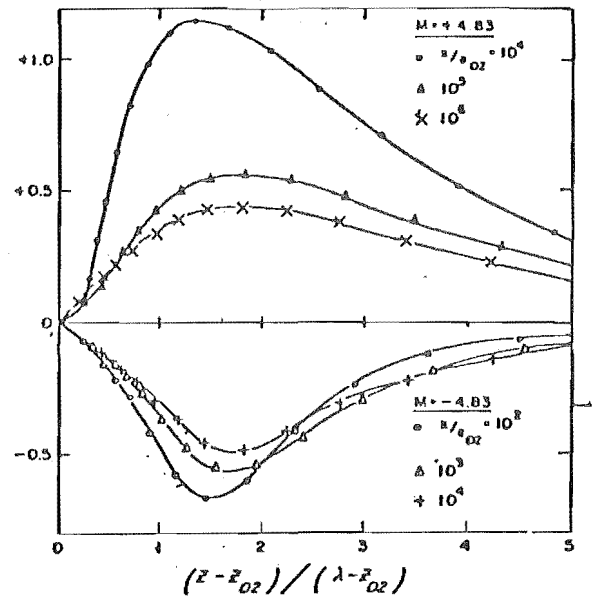

$\frac{\ell_z}{k_a z} - 1$

Rao (1974)

FIGURE 4.8 Variation of the dissipation length scale ℓ_z in the IBL (after Rao et al).

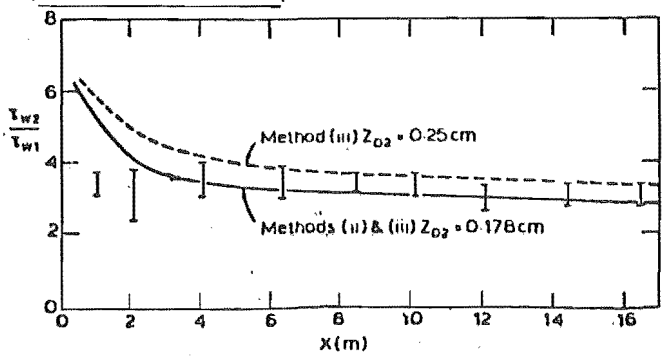

(a) Stress distribution with x. Wood & Rao compared with Bradley.

FIGURE 4.9 Stress distribution from the leading edge of a change of roughness (after Wood).

The value of ϕ_m can be as low as 0.15, and even when the ratio $\frac{\ell_z}{k_a}$ is known, the numerical solution of the quantity in the x-direction demands x-intervals which are excessive. Hence peak stress levels go unnoticed (Wood). Lower down in the inner layer, where flow conditions are more gradual, the horizontal stress distribution $\frac{\ell_z}{k_a}$ is constant up to the transition region.

Hsi and Nath (1970) investigated the variation of shear stress for one specific spacing (one model tree for 360 mm^2 of wind tunnel floor area) with an average canopy height of 165 mm and a fetch of 11.06 m. They adjusted the approaching turbulent velocity profile to the $\frac{1}{7}$ th power law distribution and measured the shear stress by direct measurement of the local drag forces over the forest, (Also, Walshe and Fraser, 1963; Meroney, 1968).

C_{f_ℓ} values at 2 H were 0.2 and reached a constant value of 0.015 for large fetches over a brush canopy. Their profiles correlate well with other tests. The shear stress value at 2 H was about 10 times that of the upstream value with increased eddy size in the x-direction and rapid reduction in eddy size down into the tree crowns. Reynolds stress changes are rapid enough in the inner layer to use $\bar{U}_{*_\ell} = k_a z(\frac{\partial \bar{U}_z}{\partial z})$, because neither velocity nor shear stress have had the chance to adjust in the short horizontal directions under investigation.

The distance in from the leading edge, where equilibrium may not be assumed constant, is about 3 H and is given by the turbulent energy divided by the rate of turbulent energy produced from the shear stress variation, i.e.

$$x = \frac{\frac{1}{2}\overline{u'^2} \cdot \bar{U}_z}{\bar{U}_\ell^{*2} \cdot \frac{\partial \bar{U}_z}{\partial z}} \quad \text{(Panofsky et al)}$$

Right at the front it appears that the only acceptable way of dealing with high Reynolds stresses arising from the high accelerations is by measuring spectra in the x-, y- and z-directions using highly sensitive, but robust, sensors.

4.6 SPECTRA VARIATIONS OVER AN ABRUPT CHANGE IN HEIGHT

Eddies which contribute to the spectral distributions of wind just above ground level are distorted and reduced in size by the very nature of the roughness itself. All types of eddy formations occur in such a complex flow region. They can be subdivided as follows:-

convectional eddies - caused by convection due to vertical temperature changes;

wave eddies - formed where two masses of air, moving with different velocities, meet;

frictional eddies - formed when masses of air flow over rough surfaces and are easily-produced in unstable air;

splashing eddies - formed where an air mass strikes an obstacle, for example a forest border, and is broken up into smaller moving masses.

If, in each of these groups, an eddy size dominates over other sizes, then the turbulent wind spectrum will alter its shape, and the peak will occur where most eddies of a similar size are grouped. Roughness element spacing and breaks in land or forest contours will produce spectral peak density shifts and even flatten the spectrum because of the wide-band nature of the turbulence sizes and frequencies (Finnigan). The turbulent wind components are greatly distorted and most spectra have a considerable amount of their energy at the low frequency end. This low frequency energy will persist after traversing large blocks of forest or after negotiating abrupt height changes. The spectrum possesses 'memory' or a consistent distribution, resulting from changes in upstream terrain or temperature gradients. Both Højstrup (1981) and Panofsky et al (1982) assess the nature of these complex spectra which possess high values of u', v' and w'. They suggest that spectra have the following characteristics:-

(a) wavelengths which are very short in relation to the fetch over the new terrain: some wavelengths readily possess equilibrium with the new surfaces;

(b) wavelengths which are long compared with the size of the fetch, having spectral densities remaining unchanged over flat horizontal terrain;

(c) a peak for u' components which moves to lower frequencies if the flow is uphill, and to higher frequencies if the flow is downhill (slopes at Rivox $\pm 5^{o}$);

(d) vertical components with a consistent level of peak energy; these spectra contain less low frequency energy and rapidly reach equilibrium with the local terrain features[1];

(e) increases in energy levels at higher frequencies because they adjust rapidly to abrupt increases in roughness;

(f) high levels of turbulence at low frequencies because of large scale terrain changes and upstream hills and any accompanying temperature gradient changes;

(g) effects from the influence of the inertial region from small scale roughness undulations due to changes to the canopy surface geometry or to interaction of the wind with flexible surface geometry;

(h) skew, and high frequency energy levels which vary from the outer layer, through transition, to the inner layer.

Højstrup suggests that, as big eddies preserve their identity, the local scaling concept has general validity for spectra measured over transitions from smooth to rough surfaces.

When comparing spectra from different tests and sites it is normal to non-dimensionalise the turbulence by dividing it by $(\bar{U}_{*\ell})^2$ from the local slope of the mean velocity profile, rather than by $(\bar{U}_{*})^2_{prof}$ taken from the slope of the profile at the point of inflexion in the transition region. Normally the ratio of the slopes when squared (ϕ_m^2) is used and the frequency is non-dimensionalised by using $\frac{nH}{\bar{U}_z}$ or (even better) $\frac{nH}{\bar{U}_{*\ell}}$ (see Ch. 7). In the majority of cases the regions of the spectra which can be compared are in the high-frequency end up to a cut-off frequency where the anemometers will not respond to the high frequency eddies flowing over their blade surfaces. (Sonic anemometers are an exception because they have a much higher frequency cut-off).

---

1. This may account for the terrain modelling at Bristol University, for assessing forest damage, being so successful.

In this range,

$$S_{(n)_{upper}} = \alpha_1 e^{2/3} f_n^{-\frac{5}{3}} \qquad \text{(Højstrup)}$$

where α_1 is the one-dimensional Kolmogorov constant, e is the dissipation rate and f_n the wave number.

If $\alpha_1 = 0.50$ $k_a = 0.41$ and $f_n = \frac{2\pi n}{\bar{U}_z}$ so that Taylor's Hypothesis can still apply,

then $$S_{(n)_{upper}} = \frac{0.136\ e^{\frac{2}{3}}}{f_n^{\ 3}}$$

provided that there is no additional mechanical turbulence generated in the region (see Ch. 7). Within the tree canopy and near any smooth ground, larger length scales of turbulence are damped down and elongated in the horizontal direction.

In the canopy (or near the ground) the spectral shape can be split up into two parts (2.5):-

$$nS_{(n)} = n\left[S_{(n)_{lower}} + S_{(n)_{upper}}\right]$$

$$= \alpha_1\left[e^{\frac{2}{3}}_{lower} + e^{\frac{2}{3}}_{upper}\right].f_n^{-\frac{2}{3}} \quad .$$

If ϕ_ε is the non-dimensionalised dissipation coefficient and mixing is in equilibrium,

$$\phi_\varepsilon^{2/3} = \left[\frac{k_a z.e_{lower}}{\bar{U}^3_{*\ell}}\right]^{2/3} + \left[\frac{k_a z.e_{upper}}{\bar{U}^3_{*\ell}}\right]^{2/3}$$

$$= 1 + \left[\frac{k_a z.e_{lower}}{\bar{U}^3_{*\ell}}\right]^{\frac{2}{3}} ,$$

since at the upper end equilibrium gives $\phi_{\varepsilon_{upper}} = 1$.

Kaimal (1976) observed that, at the surface, the ratio of dissipation rate to buoyant energy produced is constant at approximately 0.65. This can be shown using the equation above.

Højstrup therefore suggests that it is convenient to split up the spectrum into two forms over complex terrain:-

$$\frac{n\,S_{(n)_{lower}}}{\bar{U}_{*\ell}^{2}} = \frac{0.5\,f_n}{1 + 2.2\,f_n^{5/3}} \cdot \left(\frac{z_T}{-L}\right)^{2/3} \qquad (1)$$

and,

$$\frac{n\,S_{(n)_{upper}}}{\bar{U}_{*\ell}^{2}} = \frac{105\,f_n}{(1 + 33\,f_n)^{5/3}} \qquad (2)$$

where z_T is the height to the transition layer just above the inner layer.

Högström et al (1983), after measuring $\sigma_u : \sigma_v : \sigma_w : \bar{U}_* = 2.5 : 2.2 : 1.3 : 1$, concluded that equation 2 can be written as:-

$$\frac{nS_{(n)}}{\bar{U}_{*\ell}^{2}} = \frac{4.59.\hat{f}/fm}{(1 + 1.57\,\hat{f}/fm)^{5/3}}$$

where fm = 0.53.

If the spectrum is being measured in the inner layer below the transition region, they suggest that the logarithmic law can be used provided the zero-plane displacement and the roughness z_o'' are used, and not z_o' based on the slope of the velocity profile at the transition region above.

Högström et al suggest that these z_o'' values can be from 0.5 to 3.0 m, depending on the type of roughness. Above the transition region the variation of $\bar{U}_{*\ell}$ with height measured by ϕ_m changes must be considered (Rao et al, Wood), but with z_o values relevant to upwind conditions at the leading edge. In the case of a continuous forest this would be z_o': (z_o is normally about $\frac{1}{100}$ of z_o').

$\frac{\bar{U}_{*_\ell}}{\bar{U}z}$ in the x-direction away from the leading edge decays at a rate $e^{-a_\ell x}$ where $a_\ell = 6.3 \times 10^{-3}$ (Högström et al). (Oliphant, 1964 shows that a modified form of Elliot's theory is also suitable here).

When data is analysed from a spectrum:-

(a) the instruments must be able to respond to wind frequencies of major interest (have a small distance constant);

(b) enough samples of different spectra from one general direction must be collected;

(c) runs must be long enough to avoid mean velocity and turbulent velocity statistical errors such as trends and aliasing by choosing the correct sampling frequency (see App. II);

(d) the length scales of the turbulence must be greater than the distance constants of the sensors (see Ch. 5).

So over forests, and especially at leading edges where high mixing and feedback processes with the trees occur, high frequency eddies dominate. Conditions allow the use of a logarithmic mixing law in the inner layer, provided the instruments have a range of turbulent wind frequency response of interest for wind-loading studies.

Högström et al suggest that scaling in such quasi-equilibrium layers is valid, and that comparisons between full scale and model tests can be made in the inner region of the forest canopy, provided appropriate precautions in recording are taken (5.3).

In the transition region spectra are complicated and skewed in either direction (6.8.1). It is thought that the transition region, turbulent energy rising from the tree-tops in the inner layer, and turbulent energy descending from high wind shear in the outer layer, reach a balance, producing a non-skewed, gaussian distribution of turbulence. (There is little likelihood of separation zones developing where the larger accelerations are occurring, even though turbulence levels can be very high).

Honami, or coherent crop waving, can interact with turbulence generated by the waving plants and cause a frequency shift. These wind frequencies result in spectra exhibiting frequency shifts with steeper and larger concentrations of turbulence at crop height. The spectra contain turbulence levels up to three times the normal levels, are skewed and show at least two peaks. (This is observed in some of the Oxford model forest spectra.)

4.7 ESTIMATION OF THE FORM DRAG COEFFICIENT VARIATION FROM THE LEADING EDGE INWARDS

4.7.1 Previous work

Information on the drag of discs, flat plates and porous flat plates suggests that the drag of a forest front is distinctly different from the drag of individual trees.

Most textbooks on aerodynamic drag put drag coefficients between 1.0 and 2.0 for circular discs and low aspect ratio flat plates at right angles to the wind (Arie and Rouse, 1956; Hoerner, 1965, ESDU, 1974).

As the aspect ratio of a rectangular flat plate increases, so does the drag coefficient, rising up to C_{D_T} values of 2.0. The shape of the leading edge geometry dramatically affects C_{D_T} so that any curvature or porosity rapidly reduces the drag coefficient. In turbulent flows the drag coefficient is reasonably constant for fixed geometry bluff bodies as Reynolds number increases beyond 5×10^5, and can be as low as 0.01 for thin aerofoil shapes. For automobiles of average aerodynamic design C_{D_T} values are about 0.35.

The first recorded full scale drag tests on conifers in open country were made by Sauer et al (1951).

Hirata (1951) first investigated the drag coefficient and the centre of pressure of a model conifer forest. He found that C_{D_T} at the forest front increased with speed, staying between 0.5 and 1.0. He attributed the rise in C_{D_T} to model crown deformation increasing blockage at the border. The centre of pressure was constant for the crown with a value of $\frac{1}{3}$ for various velocities. He related this value to the centroid of the cross-section of the crown shape: an increase in crown height, with the crown diameter constant, made the centre of pressure move higher.

Fraser (1962b) developed single tree (conifer) drag relationships from data obtained from tests in the uniform-wind, large (7.32 m) tunnel at Farnborough, using trees 7 m tall. Blockage was not severe (as suggested by Johnson, 1982) since the working section is exposed within a large hangar.

In 1972, while on study leave with the Forestry Commission, the writer helped Mayhead (1973b) to adjust some of Raymer's (1962) tree drag coefficients and to produce more consistent results. C_{D_T} values

were found to lie between 0.7 and 0.35 for single conifers, and to reduce as the uniform wind speeds increased with the crown deformation.

Wardlaw et al (1974) quoted C_{D_T} values for individual structural towers between 0.4 and 0.6 (similar to Raymer's values for individual trees) and found that drag coefficient increases as aerodynamic interference between the towers increases, giving C_{D_T} values of between 0.8 and 1.2. Seginer's work (1972) on windbreak drag shows that, as porosity of the windbreak increases from 0% to 60%, the C_{D_T} value falls from a band between 0.8 and 1.6 to a band between 0.25 and 0.45; this confirms the work of Hirata and Wardlaw et al. B.R.S. Digest 119 gives $C_{D_T} = 1.2$ for buildings with aspect ratios greater than 4.

Thom (1971) made measurements in a wind tunnel of the drag on elements of a simply structured artificial crop (a bed of nails) and of the wind profiles above and within this crop. His analysis demonstrated that:-

(a) the drag on an element in the array was different from the drag on the individual elements, but a relationship could be found between the two if the wind profile of the array was measured;

(b) the zero-plane displacement, d, of an aerodynamically rough surface can be identified with the level of action of the drag on its elements so that $d = 0.76\ H$ and $z'_o = 0.36\ (H - d)$;

(c) values of eddy viscosity, a measure of the turbulence, are almost constant in the height range (the inner layer range);

(d) Von Karman's constant (k_a) is 0.40 ± 0.03 (for the inner layer only);

(e) the drag on the surface of the canopy is 3.5 times greater than the drag on individual elements.

Khalsa and Businger (1977) provide corrections for drag coefficient values for obstructions in stable atmospheres, while Shaw and Pereira (1982) give some numerical models for z'_o and d (see Ch. 3) with spacing from which $\bar{U}_{*\ell}$ values and drag coefficients can be calculated.

From the leading edge inwards, the shear stress distribution changes with four spacings of model roughness (Hsi and Nath, 1970). Similar changes in stress, using a uniform windspeed tunnel with low turbulence, have been obtained. 'Humps' were noticed at about + 2 H in from the leading edge of a model forest test, on the latter shear stress distribution curves (Fig.4.10).

(Walshe and Fraser, 1963; Meroney, 1968; Counihan, 1972). All these tests were done with rigid roughness elements which had no sway motion.

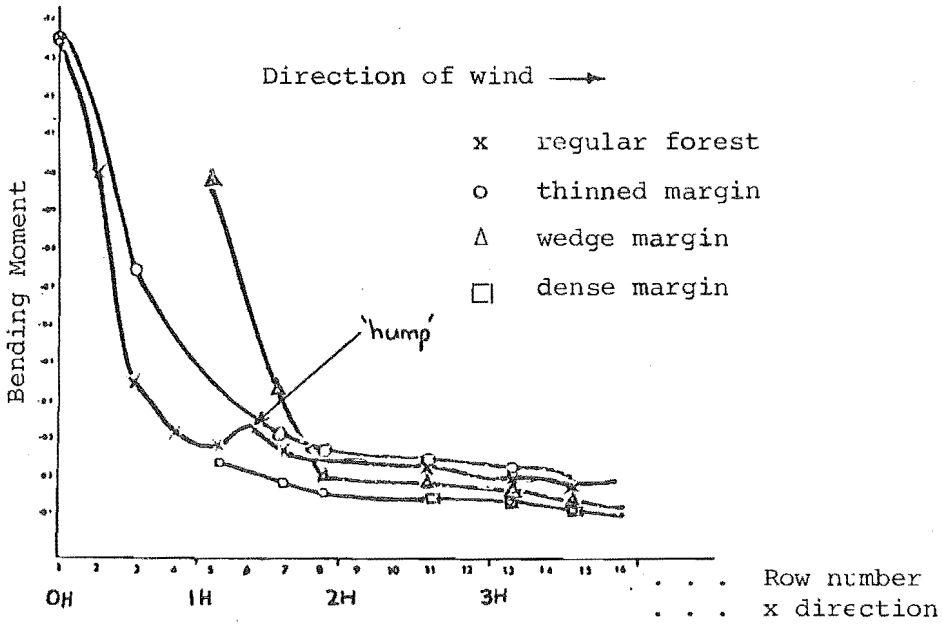

FIGURE 4.10 The distribution of forces over a model forest with different windward margins (after Walshe and Fraser).

The drag coefficient of single dwarf trees with dense crowns, tested in a uniform-wind velocity wind tunnel, gave C_{D_T} values of 1.05 at 20 m/s, which compare well with Mayhead's results (Johnson, 1982 ; Fig.4.11.) These results, when converted to above critical Reynold's Numbers (>1 x 10^4) for single trees reduce to a C_{D_T} of about 0.4 at 20 m/s, which compares well with wind tunnel tests on 6 m trees (Raymer).

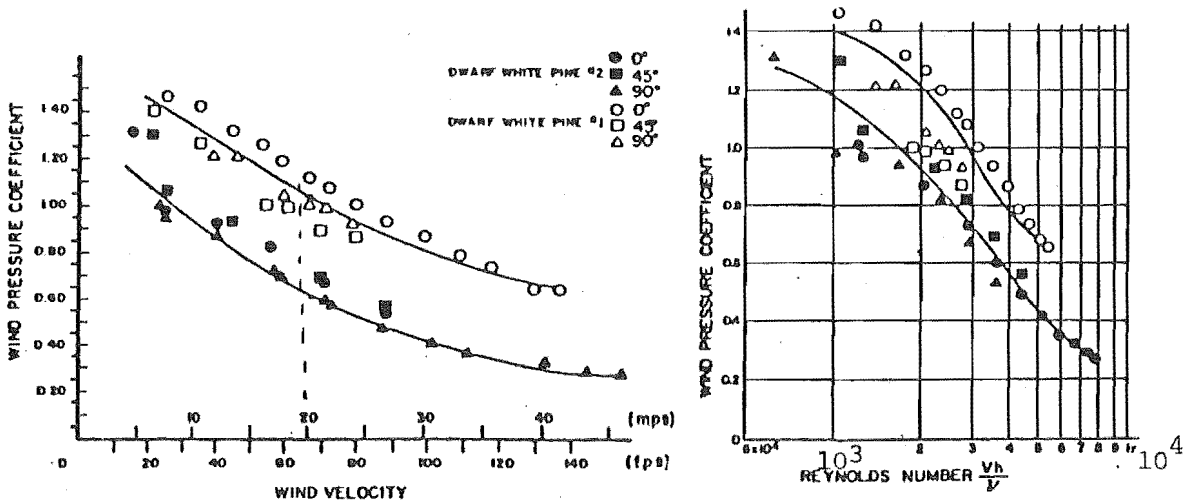

FIGURE 4.11 White pine form drag coefficients (after Johnson et al)

The friction velocity calculated from the drag force suddenly increased near the leading edge of roughness, because the stagnation pressure exerted on the front of the roughness contributed to the increase of drag force in this region; reduction of stagnation pressure by increasing the tree spacing at the leading edge will reduce the stresses there.

The writer measured the drag coefficient and centre of pressure of a full scale forest front (Papesch, 1977; see Figs 4.12; 4.13).

The average value of C_{D_T} for the 75 different sets of readings (from 15 different trees) was 1.22 ± 0.42. This compares favourably with values given by Hirata, Seginer, B.R.S. Digest and Wardlaw et al; but, as expected, is significantly higher than Raymer's and Johnson's results of drag coefficients for individual trees.

The average value of the centre of pressure for the 75 different sets of readings was 0.397 H ± 0.051 H. This is consistent with Hirata's and Johnson's work.

These details were used to assess the form drag and friction coefficient (C_{D_ℓ}, C_{f_ℓ}) from the profile drag coefficient C_{D_T}.

4.7.2 Calculation of form drag coefficients

From Newton's Law, inertia forces = viscous forces + pressure forces. In equilibrium the static pressure reduces, maintaining the flow momentum against the surface friction. Before the flow accelerates up the leading edge of the forest the static pressure rises, then rapidly falls, until maximum shear stresses are reached at the maximum speed-up point (+ 3 H). After this, pressures gradually rise as the flow decelerates towards the equilibrium region (+ 10 H) where the pressure gradient and the new shear stresses are once again in balance back at Zone B (Chapter 3).

Seginer obtained values of C_{D_ℓ} (cf Fig. 4.15) by:—

(a) calculation of the acceleration term $\rho(\bar{u}_1^2 - \bar{u}_2^2)$;

(b) measuring Reynolds stresses;

(c) estimating the stress change $(\tau_1 - \tau_2)$;

(d) and estimating the effect of the static pressure change at the ground level $(P_1 - P_2)$.

To p.121

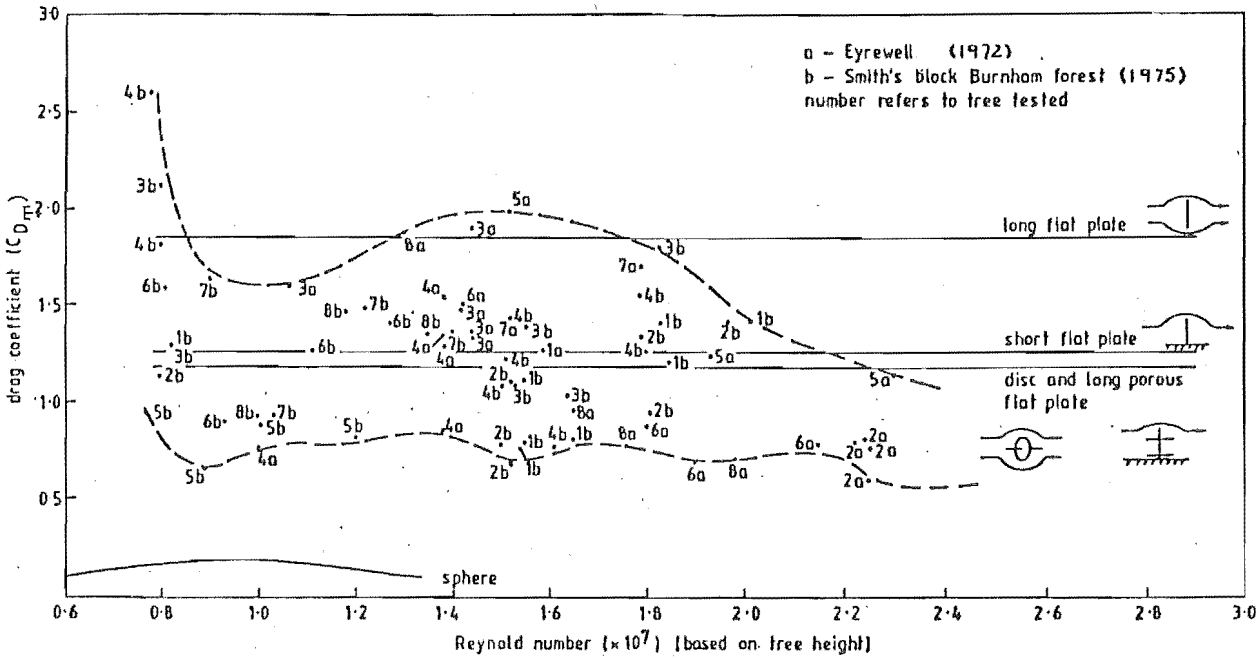

FIGURE 4.12 The drag coefficient of a forest front ($\frac{S}{H} \simeq 0.15$) Burnham, Canterbury.

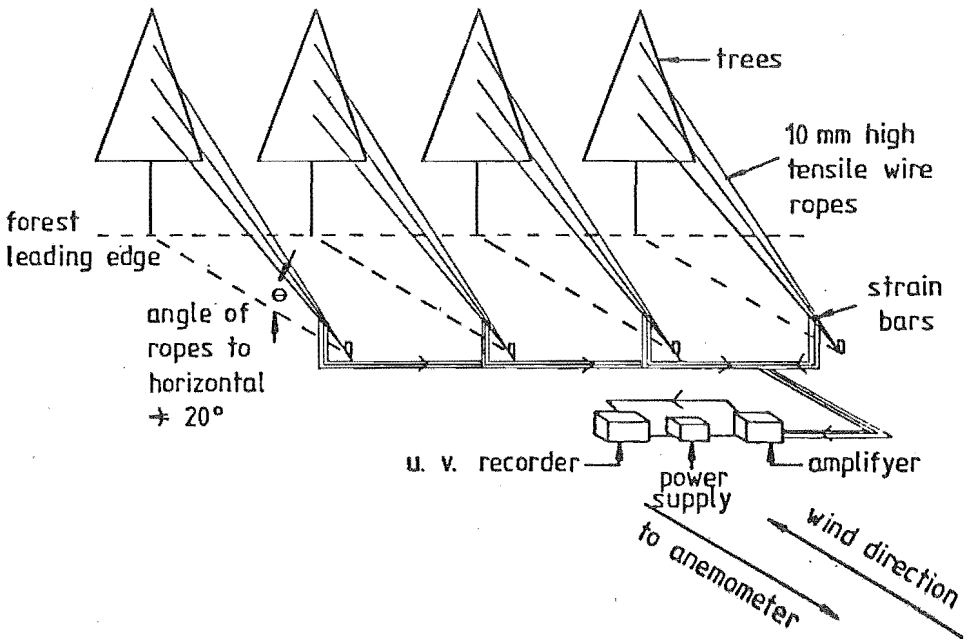

FIGURE 4.13 Test site wind force measurement system.

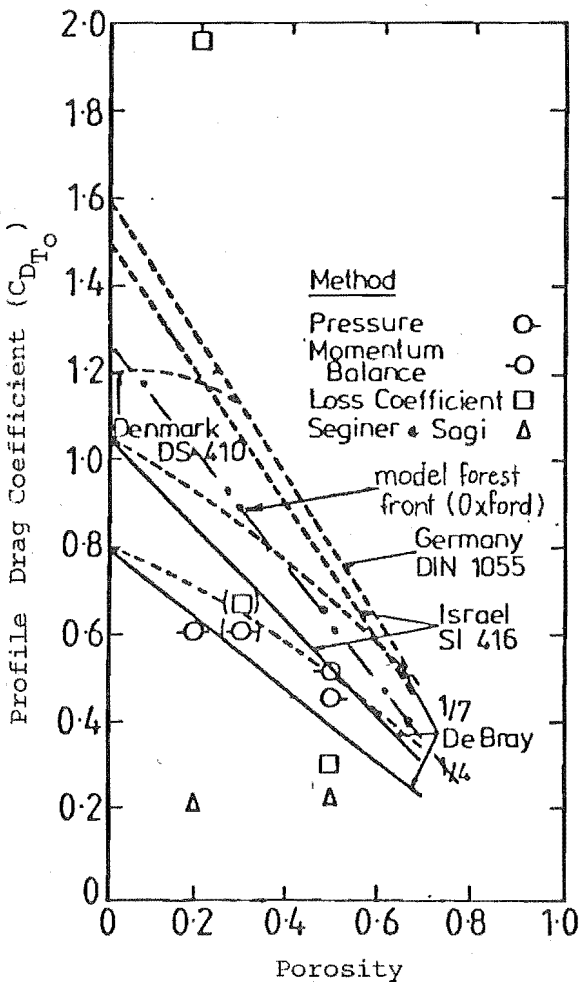

FIGURE 4.14 Drag coefficient changes with porosity (after Seginer)

A drag coefficient of 1.22 (for $\frac{S}{H}$ of 0.17) at a forest front, and of 0.35 for a single tree, were superimposed on Seginer's work (Fig.4.14) which gave drag coefficients for the leading edge of model forests tested at different spacings (Table 4.1).

Since the form drag ($C_{D\ell_o}$) at the forest front is required, the relation

$$C_{D_{T_o}} \; A_z = C_{D\ell_o} \; A_{z_o} + C_{f\ell_o} \; A_{y_o} \quad \text{is used.}$$

$C_{f\ell_o}$ is the local shear stress coefficient taken from the mean velocity profile slope at the crown. A_{z_o} is the total area of crown subject to wind forces. A_{y_o} is the cross-sectional area of the crown where the shear stress acts at 0.4 H, the centre of pressure.

All coefficients were referenced to the upstream wind conditions at -3 H and 10 m full scale from the ground.

TABLE 4.1 Model forest leading edge profile and form drag coefficients

Pattern	$\frac{S}{H}$	$C_{D_{T_o}}$	$C_{D_{\ell_o}}$
P	0.17	1.22	1.20
$\bar{U}^*$	0.20	1.17	1.15
Q	0.24	1.11	1.10
R	0.28	1.04	1.03
S	0.32	0.98	.97
T	0.34	0.95	.94
V	0.38	0.88	.87
W	0.47	0.74	.74
X	0.51	0.67	.67
Y	0.59	0.54	.54
Z	0.61	0.51	.50

After the flow has passed the leading edge at + 3 H, the equation (cf 4.4.1)

$$\frac{\partial\left(\frac{\bar{P}}{\frac{\bar{U}_z}{2}}\right)}{\partial x} = -\frac{\partial P}{\rho dx} + \frac{1}{\rho}\cdot\frac{\partial T'}{\partial z}$$

can be used, since equilibrium is assumed at crown height.

By dividing by $\frac{1}{2}\rho\bar{U}_o^2$, the dynamic head upstream at -3 H, we obtain

$$\left(\frac{\bar{U}_{z_{x_2}}}{\bar{U}_o}\right)^2 \pm \left(\frac{\bar{U}_{z_{x_1}}}{\bar{U}_o}\right)^2 = 2\left(\left(\frac{\Delta x}{\Delta z}\right)\cdot\Delta Cf_{\ell_{x_2x_1}} \pm \Delta C_{D_{\ell_{x2,x1}}}\right)$$

from which the variation of form drag coefficient from the leading edge inwards is calculated (see Figs 4.16; 4.17).

Fig.4.15 shows how the form drag varies behind a fence when different terms of the above equations are neglected (Seginer).

To p.125

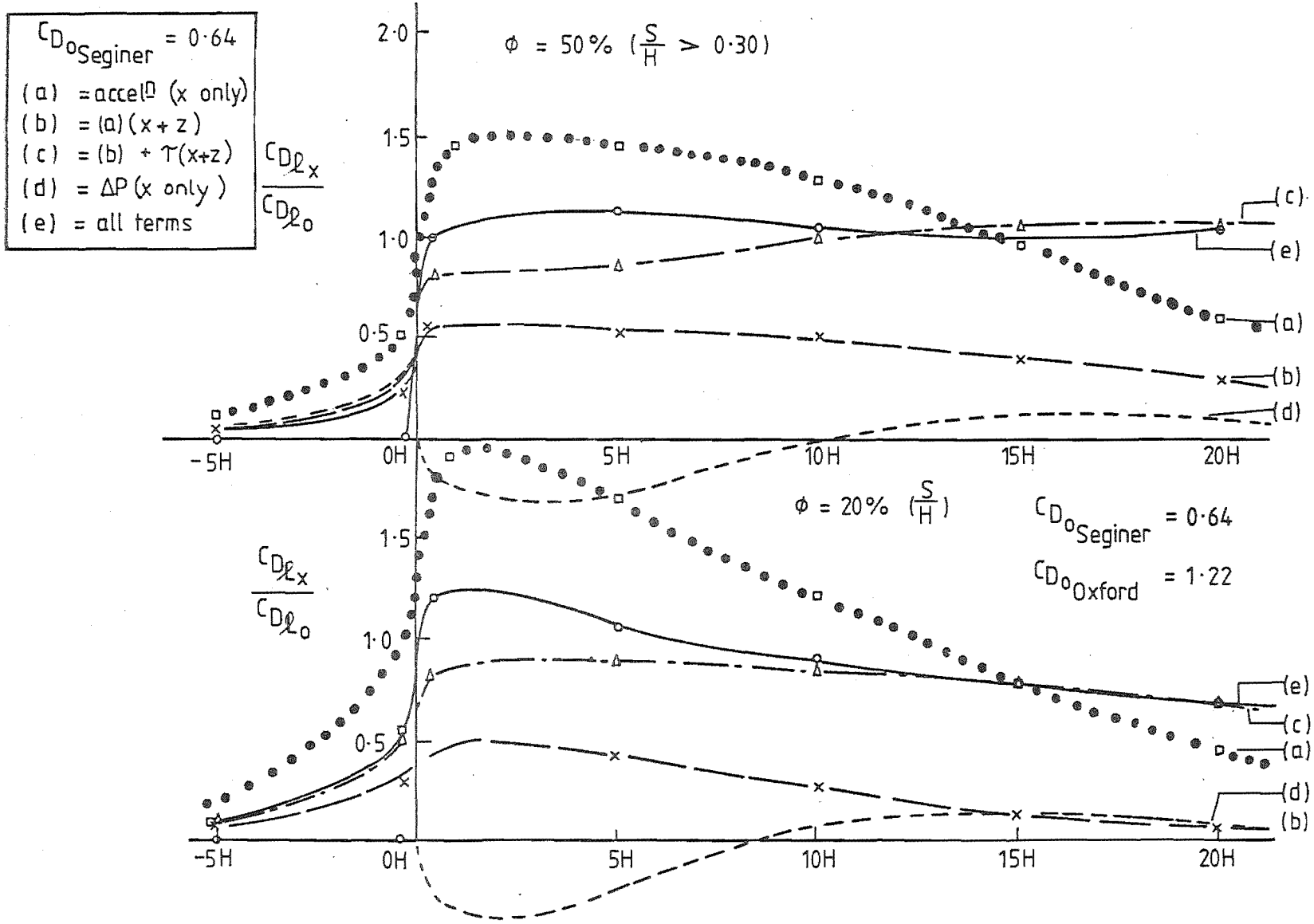

FIGURE 4.15 Form drag coefficient variations with fetch (after Seginer)

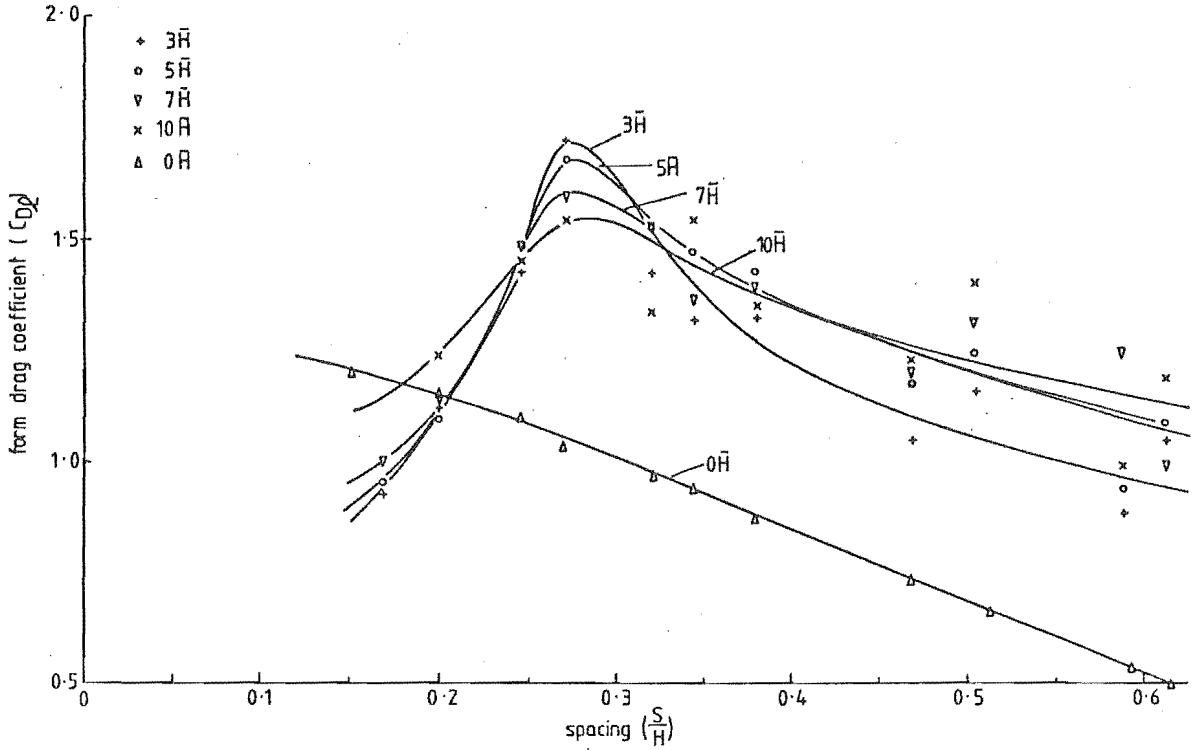

FIGURE 4.16 Oxford model forest form drag coefficient variations with fetch and spacing.

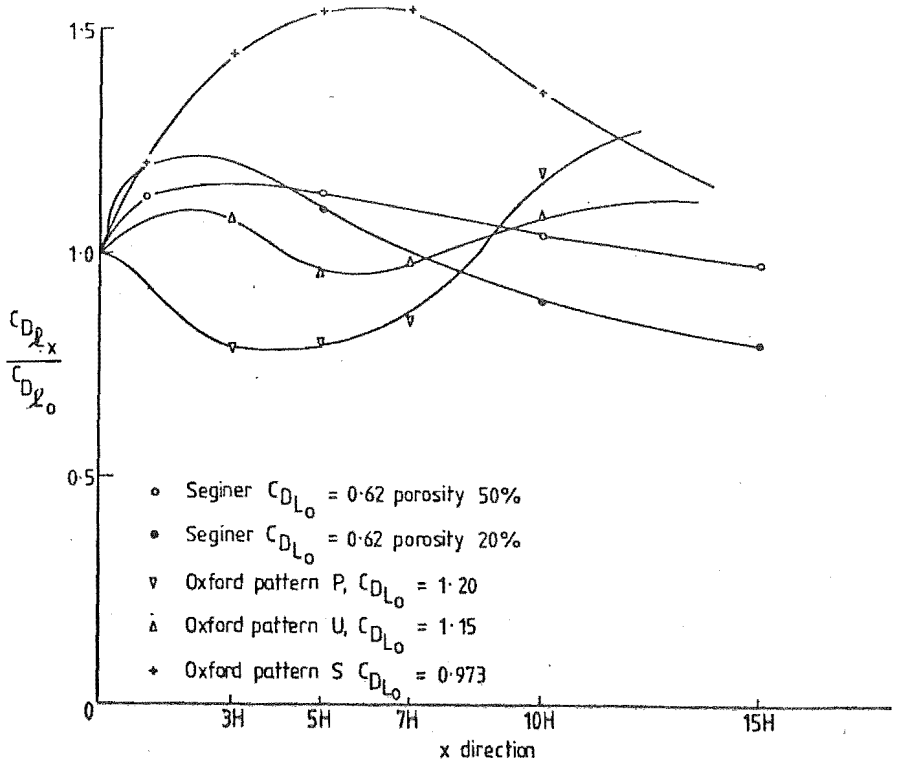

FIGURE 4.17 Form drag coefficient comparisons (Seginer, fence; Oxford model forest).

4.8 SUMMARY OF AERODYNAMIC PROPERTIES OF A FOREST FRONT

(a) The average wind profile over smooth terrain upstream from the forest border is given by $z \propto U^{0.14-0.22}$ (2.2.1 ; 5.5.1)

(b) The average wind profile just upstream of the front border is almost uniform with height.

(c) The average wind speed profile in the inner layer is logarithmic in front of the forest leading edge.

(d) In the inner layer, from $\frac{2}{3}$ H to about 1.5 H, there is little vertical variation of shear stress or wind direction.

(e) The process of turbulent energy production by the forest elements continues further downstream than theory predicts.

(f) There is an increase in turbulence intensity in the accelerating flows, due to the roughness itself as a momentum source rather than to the change in zero-plane displacement (generates high $\bar{U}_z$).

(g) Friction velocity $(\bar{U}_*)_{prof}$ and roughness length (z'_o) cannot be regarded as similarity parameters, but vary with time and space.

(h) The form drag coefficient at the forest edge is about 1.22 and is independent of Reynolds Number, but depends on spacing of the trees.

(i) The border area of the forest has an aerodynamic roughness controlled by the fetch, tree spacing, tree pruning and tree height.

(j) Because the trees sway more at the border, the aerodynamic roughness changes are not gradual but fluctuate and Honami waves adjust the spectra.

(k) The centre of pressure of the forest border is at the centroid of the cross-sectional area of the exposed front (Hirata; Johnson).

(l) Maximum shear stresses over a forest leading edge occur 0.3 H above mean tree-top height at the point of inflexion of the mean wind velocity profile (Fig. 6.25).

(m) Maximum shear stresses over a forest leading edge occur not at the front, but in from the front ε(3 H, 5 H) (Table 4.1; Fig. 6.25).

CHAPTER 5

FULL SCALE FOREST STUDIES

5.1 SOME PREVIOUS WORK ON FULL SCALE FORESTS

Recent full scale field experiments measuring above-canopy and within-canopy turbulence in forests have been made by Raynor et al (1976), Garratt (1978), Holbo et al (1980), Mayer (1981) and Sadeh and Fox (1982). None of these studies manipulated the forest canopy architecture to any extent. Holbo et al measured wind and tree sway motion spectra at tree-top level (28 m) in a Douglas fir stand ($\frac{S}{H} = 0.21$). Mayer notes that the relationships between tree response and wind turbulence must be investigated in model and full scale studies in greater detail.

Numerous papers in forestry relate thinning and wind turbulence. (cf Batzr, 1960; Boe, 1965; Cremer, 1975; Cremer et al, 1977; Somerville, 1978, Cremer et al 1982). A theoretical study by Faber (3.1.3) emphasises the importance of canopy structure modification to control the stability of forests in high winds. The following full scale and model experiments help to increase the understanding of wind/forest interaction.

5.2 EXPERIMENTAL OBJECTIVES

The scope of the full scale experiments is much narrower than in the model studies because of limitations imposed by data, site, cost, instrumentation, time and complexity. Consequently, full scale experimental matching of the model forest findings is limited.

In the Kielder experiment, mean wind speed profiles at the leading edge and further into the forest are compared with upstream mean wind profiles. Transverse effects are neglected.

In the Rivox experiment mean and turbulent wind speeds away from the leading edge (>10H) are measured in each dimension for the unthinned and first thinning stages of the experiment. Within this narrower study comparisons are made with the model forests (Ch. 6) where possible to meet the objectives. Data from the initial spacing and first adjustment to thinning density at Rivox indicate that changes in wind spectra and tree

response are minimal at close spacings.

5.2.1 The Kielder experiment

This experiment, begun by A. I. Fraser of the British Forestry Commission, concluded in 1971 without any analysis of data.[1] Thinning changes were minor and the experiment failed to produce adequate turbulence data. The mean wind speed profiles and the resulting local shear stress coefficients measured by the Munro anemometors are, however, significant because there are few other reliable data available at forest leading edges.

5.2.2 The Rivox experiment

The cost of establishing an experiment comparable to that at Kielder, but with modern equipment capable of responding sensitively to wind gusts as well as having long-term serviceability in the harsh climate, is prohibitive. Therefore the Rivox experiment was limited to one objective: to assess tree response to the wind structure within a medium fetch forest as it is adjusted by thinning. The mean and turbulent wind velocity profile and turbulence spectra for the initial spacing and first thinning are used to test the validity of the model forest experiments at the same close spacings.

5.3 FULL SCALE EXPERIMENTAL LIMITATIONS

5.3.1 Experimental sites

The ideal forest site for wind studies should:-

(a) be flat, both within the forest and around it, so that it is wind stable;

(b) be free from upstream topographical obstacles and shelterbelts, and have uniform soils, age and tree quality;

(c) have a well defined leading edge;

(d) be accessible upwind and internally for the installation and maintenance of equipment to produce results, and be near the research station headquarters;

(e) have on-site accommodation, power supply and all necessary back-up facilities.

---

1 The writer analysed the Kielder data at Alice Holt Research Station, Surrey, in 1972-73.

5.3.2 Terrain homogeneity

The general terrain at the site should be homogeneous and have no slope. For equilibrium, the homogeneity should extend 20 tree heights upwind. Any hills upstream affecting the approach flow will add low frequency components to the wind spectra and cause changes in flow direction (3.9.3). Upstream influences on the wind structure can be quantified if the wind structure is measured at one, or preferably two, locations each 20 tree heights distant along-wind.

5.3.3 Meteorological considerations

For general condition see 3.9.3 and 4.4. Some specific requirements are:

(a) the proximity of at least two weather stations with full weather reporting facilities (Lowther Hill and Eskdalemuir);

(b) a prevailing wind direction which is sufficiently consistent for the collection of useful wind data.

5.3.4 Wind speeds and directions

The mean wind speeds should have components ($\bar{U} + u'$, $\bar{V} + v'$) which do not change magnitudes and directions more than 10% during data collection periods. Changes in mean winds with larger and smaller values of turbulent components will cause variations in σ_u^2 reducing spectrum heights and flattening spectrum peaks (ESDU 1974).

At least eight different sets of data in strong winds (> 8 m/s above transition) and from a common direction must be collected at two, and preferably at more, data points. One of these points should be at least 2 tree heights above the ground and, to establish the lower logarithmic profile, the other data points should be in the inner layer. Weather conditions should be overcast and as close as possible to neutral stability conditions.

5.3.5 Tower interference

Provided anemometers are mounted on booms at least three mast diameters upstream from the leading edge of the mast, the accuracy of the wind speeds and directions is between ± 5% within a 130° arc and ± 10% for a 360° arc (Gill et al 1967). (In both field experiments all anemometer booms were 7 mast diameters long, except the bottom U.V.W array at Rivox which was 1.5 m away from the front of the 'Hiway' lattice tower top supporting the F.C.[1] mast).

1. F.C. refers to "Forestry Commission".

5.3.6 Wind sensors

There are conflicting requirements for wind sensors used for long periods of data collection when measuring strong wind speeds in the field. They must be sufficiently robust to withstand all weathers, especially hail impact and freezing temperatures, yet sensitive enough to record accurately turbulent wind fluctuations. Calibrated Munro Cup anemometers are suited to some of these conditions. They record mean winds accurately over long periods in all weathers, but overestimate average gusts by 10% or more.

Gill polystyrene propeller anemometers are a primary sensor with propeller revolutions linear with wind speed over a range of gust frequencies (0.01 Hz-2.0 Hz). For high frequency eddies, neglecting frictional torque, propellers act as a first order system with a time constant (t_c) given by

$$t_c = \frac{d_c}{\bar{U}_z}$$

where d_c is the distance constant.

The smaller the distance constant the more rapidly the instrument responds to wind speed changes. The sensor does not respond to wind frequencies in the atmosphere beyond twice the half-power point of the response time. The upper limit before aliasing (n_{max}) is given by

$$n_{max} = \frac{\bar{U}_z}{\pi d_c}$$

(a) The upper limits for four-bladed polystyrene Gill propellers in 10 m/s winds are 3.21 Hz for a diameter of 190 mm and 3.9 Hz for a diameter of 230 mm. They measure gust wave lengths (rms length scales) with accuracy down to 12 m (Gill, 1975).

(b) The 190 mm diameter propellers have a starting speed of 1.0 m/s and can withstand mean winds of 30 m/s; the 230 mm diameter propellers have a starting speed of 0.5 m/s and can withstand mean winds of 20 m/s.

(c) Gill anemometer wind data must be corrected for cosine-response by monitoring the U and V components of wind speeds continuously. The cosine correction, $\frac{\text{cosine smaller signal}}{\text{cosine larger signal}}$ for all wind component angles is available (Horst, 1973b). The correction for the $\bar{W}$

component is constant for approach angles less than 10^{o} above and below its axis of rotation. The accuracy of Gill anemometer response begins to reduce above 0.3 Hz.

Lowne sensors have light weight mica vanes and were developed by the Cranfield Institute of Technology for small period runs. They withstand wind speeds up to 10 m/s and, with distance constants down to 0.25 m and almost perfect cosine response, they are very suitable for in-canopy turbulence studies. They respond to wind frequencies up to 10.0 Hz.

5.3.7 Other anemometers

Three component drag anemometers, of spherical and flat plate design have been tested and found superior to Gill anemometers at 4.5 m height; they have better response, fewer moving parts, and no friction or momentum errors. They require calibration and cross-coupling corrections. Aliasing errors occur with the Gill anemometer beyond 2 Hz and with the drag anemometer beyond 5 Hz (Appendix II). Both types produce wind data close to that produced by sonic anemometers up to these frequencies (Redford et al 1981).

When Gill anemometers are corrected for cosine response their signal output comes within 80% of the drag anemometer signal from 0.4 Hz to 6 Hz (Redford et al, 1981).

Hot wire anemometers are used in small scale experiments (6.7.3). Sonic anemometers are ideal but U,V,W arrays are very costly (> $100,000).

5.3.8 Sampling and averaging

Medium response wind sensors such as propellor anemometers can average instantaneous wind fluctuations over very short intervals (O(3s)). The power spectrum of the turbulence will not contain the very low and very high wind frequencies, therefore the spectrum is truncated at the low frequency end due to sample time length, and at the high frequency end because of instrument response. The wind variance is therefore smaller than the true value, and non-dimensionalised spectra will have peaks above their true height. For Gill anemometers the half-power point of 1.6 Hz suggests that data collected continuously can be sampled as the tapes are digitised at a rate of 5 Hz without undue aliasing. The data can also be corrected statistically for sampling errors and smoothed (Hann-smoothed).

5.3.9 Trends in data

Trends in mean wind speed and turbulence levels can cause distortions in the true shape of spectra. Spectra obtained from wind data collected by Gill anemometers can be corrected for both mean wind speed trends and for wind turbulent energy distortions. The need for long periods of data capture to increase sampling accuracy conflicts with the need to keep wind collecting periods short to reduce trend errors. Normally, the minimum sampling period acceptable is eight minutes (Doran and Powell, 1982). Minimum sampling frequency at the high frequency end of the wind spectrum is 1.875 Hz, while at the low frequency end the Gill readings are unreliable below 0.01 Hz (Flay, 1979).

By assuming a gaussian fluctuation in the atmospheric signal, the spectral estimates have a normal distribution. The degree of freedom depends on the number of data and frequency points required for calculation of the spectrum. The gaussian assumption, although used, is not accurate for boundary layer winds.

E.S D U standards suggest that errors increase with increasing surface roughness and that turbulence intensity errors greater than ± 15% can exist in all wind data collected near the ground.

5.4 FULL SCALE FOREST EXPERIMENT AT KIELDER, REDESDALE FOREST, NORTH-EAST ENGLAND

This field study was conducted on a crop of Sitka spruce, planted in 1939. The raw data were collected by the British Forestry Commission on computer tape. In 1972, the information on these tapes was processed by the writer to obtain some aerodynamic properties of this forest.

5.4.1 Aims and objectives

The aims of the Kielder study were to determine:-

(a) the changes in boundary layer shape as the wind passed from the open country, over a forest leading edge inwards;

(b) the effects of thinning and crop structure on the mean wind speeds.

5.4.2 The experiment site

The principal requirements for this site were that it should:-

(a) be large enough for typical airflow conditions to be established over the forest leading edge and inwards;

(b) be downwind of smooth rolling country with a straight line

To p.133

interface between the forests and the open country;

(c) have a uniform tree crop, homogeneous canopy.

(d) be in an area where wind damage to crops is prevalent;

(e) have easy access for equipment servicing, and data collecting.

An 8-hectare area was selected for the test. It was situated on the south-west margin of a forest block of approximately 400 hectares which extended 2 km north-east from the site of the experiment. The whole area, about 300 m above sea level, was relatively flat, with ground sloping away to north-east and south-west. A minor dip across the centre of the site, where tree growth was slightly poorer, divided the area into two sections. The terrain fell away gradually downwind of the prevailing south-west wind, so that the external mast (Mast No. 1) was sited on ground slightly below the general level of the terrain where the plots were situated (Fig. 5.1).

To the south-west, the highest ground between the site and the sea on the west coast was approximately 370 m.

The tree crop was very uniform. The average height of the dominant trees around each mast was measured (Table 5.1).

TABLE 5.1 Tree heights at mast locations (Kielder)

Mast Number	Average Tree Height (m)	
	May 1967	February 1971
2	11.1	12.8
3	12.3	15.4
4	11.1	13.1
5	12.2	14.5

The figures in the right-hand column were used in analyses of data for the period June 1970 to February 1971.

A section of the area, the southeast block, was thinned in August 1969. Between 19% and 20% of the crop was removed. With knowledge of the number of stems per hectare before thinning (452.2 st/ha) and after (364.4 st/ha), $\frac{S}{H} \in (0.31, 0.43)$ was found. The soil was a moderately shallow intergrade, common to the Border region. With this soil the crop was therefore anticipated to be wind-stable for the duration of the experiment.

(a)

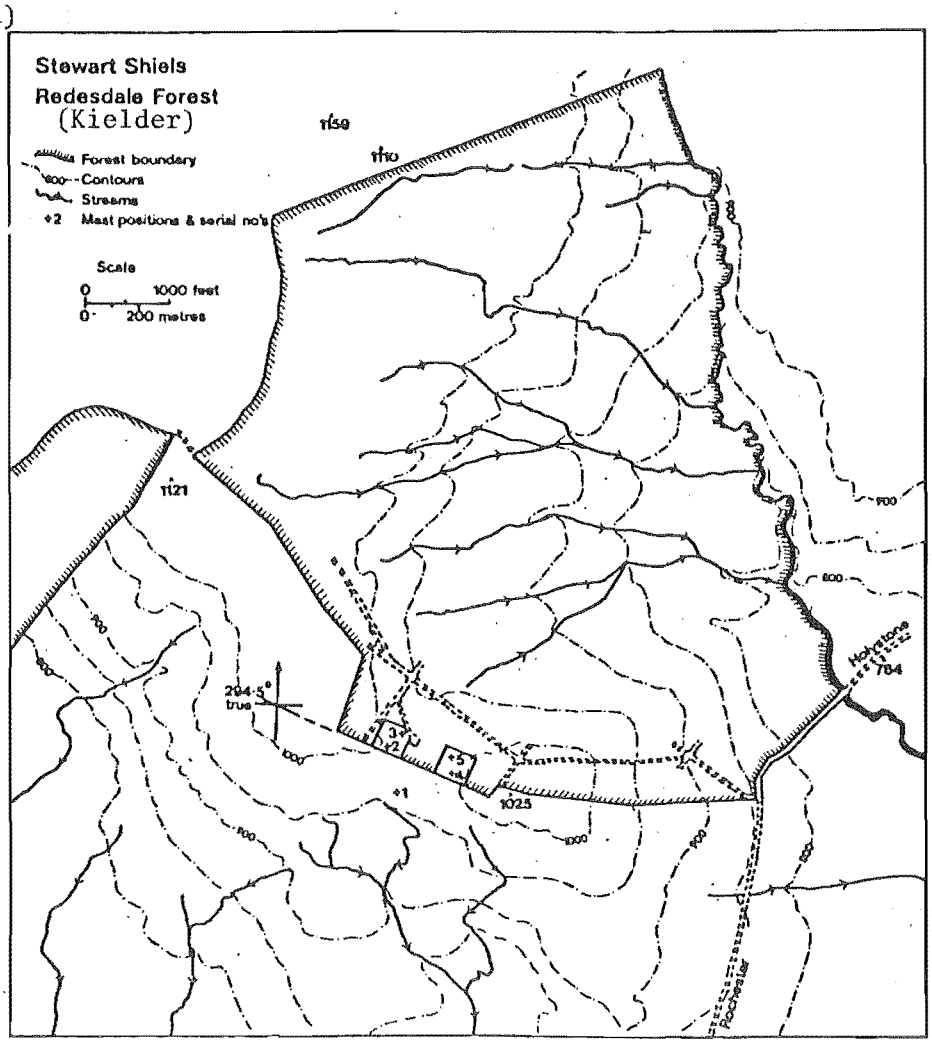

(b)

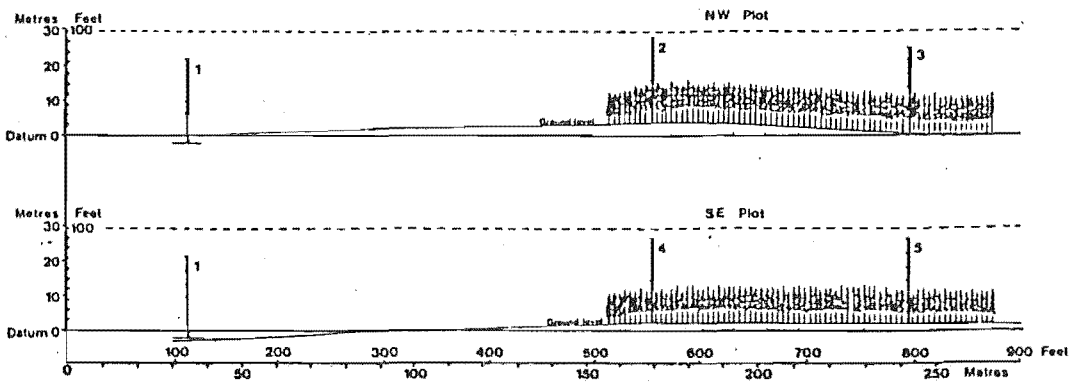

FIGURES 5.1(a) & (b): The Kielder experimental site and mast locations.

5.4.3 Wind direction in the Redesdale area

For the data collected in 1970 and 1971, the direction of the wind was measured and recorded by a Westinghouse data logger. For data collected between 1st October 1967 and 18th March 1968, erratic performance of instruments made the record of wind direction unreliable. In an attempt to estimate the missing data, records from anemographs close to Kielder (at Spadeadam, Eskdalemuir, and Acklington) were examined. It was found for the period in late 1970 and early 1971 that, when the three stations each recorded a similar wind direction over a minimum period of two hours, the wind direction at Redesdale was also similar.

A linear regression equation between the mean direction of the three anemograph stations had a coefficient of 0.9921 and a constant of 1.52. These values did not differ significantly from the expected slope of 1.0 and constant of 0. Therefore figures for the mean of the wind directions from the three stations were accepted without modification as a valid estimate for each corresponding period at Redesdale.

5.4.4 Site layout and mast locations

Five tubular steel masts were erected as a framework on which to mount the wind measuring instruments. Their positions are shown in plan in Fig. 5.1(a) and in projected profile in Fig. 5.1(b).

On each mast, five anemometers were mounted at different heights (Table 5.2; Photograph 12).

TABLE 5.2 Anemometer heights at mast locations (Kielder)

Period 1967	ANEMOMETER HEIGHT	
	All Masts	
	10 m; 13 m; 17 m; 21 m; 25 m	
1.1.70 - 6.10.70	Mast 1	Masts 2, 3, 4 and 5
	9.7 m; 12.4 m; 15.5 m; 19.7 m; 24.7 m;	12.5 m; 15.2 m; 18.5 m; 22.5 m; 28 m
6.10.70 onwards	Mast 1	Masts 2, 3, 4 and 5
	10 m; 12.9 m; 16.7 m; 21.6 m; 28 m	12.5 m; 15.2 m; 18.5 m; 22.5 m; 28 m

PHOTOGRAPH 12
Munro cup anemometers on an inside mast at Kielder

The anemometers were numbered from 1 to 25. Anemometer 1 was at the bottom of Mast No. 1, Anemometer 5 at the top of Mast 1, Anemometer 6 at the bottom of Mast 2, Anemometer 10 at the top of Mast 2 and so on.

5.4.5 Instrumentation and recording equipment

The anemometers used for this experiment were meteorological Mark IV Munro cup generators producing an AC output with voltage amplitude proportional to the wind velocity. Changes in frequency were used as the data source, since the length of line to the data logger from the mast position did not then affect the signal. A pulse-counting frequency meter was used to convert the frequency output to digital output suitable for the data logger.[1]

The Westinghouse 50-channel automatic data-logger accepted and recorded the output from the instruments. The scan rate for the anemometers was 5 channels per second. Thus, when on continuous scan, the interval between successive records from any given channel was 10 seconds.

---

1. A full description is given by Fraser (1968).

Where necessary, instruments were zeroed using trimming potentiometers to eliminate the effect of power losses over long line lengths.

In addition to being able to scan continuously, the logger could be set up to scan the 50 channels either at 15 or 60 minute intervals.

5.4.6 Data capture and analysis procedure

Raw data collected in any unbroken period on a particular day, whether from continuous or regular periodic scanning, were recorded on 5-hole paper tape in digital form. The speed of the punch was the factor limiting the rate of acceptance of data and hence the scan rate. The data tapes were run through a computer programme which first checked that each item of data had a permissible number of digits, then edited the data into a format acceptable for analysis on the ICL Sirius computer at the Forest Research Station, Alice Holt, Farnham, Surrey.

The data used are those sets of wind speeds (sets 1, 2, 3 and 4) measured by the anemometer array, logged and selected according to wind direction and the reliability of data. Temperature data were not used because of the high wind speeds selected. Many more data tapes were collected than were used for computation and analysis. The grounds for rejection of all or parts of data tapes were:-

(a) malfunction of data-punch;

(b) unwanted wind directions;

(c) insufficient high velocities.

The velocity range used was 6 - 19 m/s. The wind velocities occurring within each of seven classes were added to give an estimate of the sample size of each velocity class.

The periods of the tests were from 1.10.67 to 18.3.68 and from 3.2.70 to 9.2.71. Table 5.3 gives details of the tapes used for the determination of mean velocity profiles.

TABLE 5.3 Mean wind velocity profile data sets (Kielder)

(THINNED PERIOD) Set 1/SSE $45^{o} \pm 20^{o}$ to front	(THINNED PERIOD) Set 2/SSW $90^{o} \pm 20^{o}$ to front	(THINNED PERIOD) Set 3/SSW $90^{o} \pm 20^{o}$ to front	(PRE-THINNED PERIOD) Set 4/SSW $90^{o} \pm 20^{o}$ to front
Period Covered 3.2.70 to 10.7.70	3.2.70 to 10.7.70	27.10.70 to 8.1.71	3.9.67 to 18.11.67
Velocity Range	For all sets, 5 m/s to 18 m/s distributed evenly over velocity range		
Approx. No. of Scans 119 from 17 tapes	200 from 15 tapes	96 from 5 tapes	169 from 6 tapes
Mast Heights Front Mast 25 m Others 29 m	Front mast 25 m Others 29 m	All masts 29 m	All masts 25 m

5.5 RESULTS OF THE KIELDER EXPERIMENT

5.5.1 Mean wind profiles

The characteristics of the wind at the edge of a forest and the effect of thinning on those characteristics were examined. The profiles for winds normal to the forest front were obtained for each mast from tapes scanned at 15-minute intervals over the velocity range 6 - 19 m/s. These data are summarised in Table 5.4 and shown in graphical form in Fig. 5.2(a) - (c) and Fig. 5.3. From the mean velocity profiles the three parameters d, z_o'' and $\bar{U}*_{\ell}$ can be found (3.4.2)

Zero plane displacements varied considerably and when used to estimate friction velocity $\bar{U}*$ and C_{f_o} (the surface stress coefficient), produced higher surface stress coefficients for the masts further from the forest edge than for those near the edge; a result which is obviously incorrect. (An alternative method of calculation using a computer programme by S. M. Robinson, 1962, was used but gave similar results.).

Finally, a value of d = 0.75 H was selected on which to base calculations for the aerodynamic properties of the forest (5.10.4).

Values for U_1, U_2, z_1, z_2 and so on were read from the wind profiles (Fig. 5.2). The results are given in Table 5.5.

There is close agreement between the profiles at each pair of masts; the correlation coefficient for profiles between Masts 2 and 4 and also between Masts 3 and 5 was 0.998. The velocity profile for the external mast (Mast 1) obeyed the power law. The power exponent of 0.22 is above the open country surface boundary layer index normally used (Table 2.1). Mast height differences, topographical variations in the moorland lying to the south-west of the site, terrain slope upwards towards the forest front, and the thick tussock covering the upwind ground surface, may account for some of the difference. Convective turbulence could account for the rest.

5.5.2 Surface shear stress coefficients

From these profiles surface stress coefficients are calculated and are presented in Table 5.5. These values are compared with Rivox full scale and the model forest results in Table 5.12.

The Kielder surface stress coefficients agree with the results quoted by Harris (1972) and Davenport (1968) (between 0.015 and 0.030 for woodland, forests and suburbs, and between 0.030 and 0.050 for urban centres; Ch. 2). The mean surface stress near the front at Masts 2 and 4, is at least twice as high as these values. This may be attributed to the acceleration of the air mass flow over the front at these points (ϕ 4.1). The rear surface stress coefficients suggest that the mean air flow has almost reached equilibrium after travelling 7 tree heights in from the front, across the thinned plot. However, the markedly less consistent but much higher values at Masts 2 and 4 indicate that, over the leading edge of the forest, the airflow is not in equilibrium where high shear exists in the transition region (Fig. 4.5).

The roughness change showed no significant trends between the thinned and unthinned stands. z_o' was at 0.10 H for 16 sets of results; this agrees with results by Thom (1971) of 0.10 H, and the value of 0.095 H of Kalma and Stanhill (1972) and others (Table 3.2).

There were two major faults with the Kielder experiment: the Munro Cup anemometers, although suitable for establishing the mean wind profile shape over the forest were not designed to respond to the high gust frequencies associated with the turbulent nature of the wind. Secondly, the thinning at 20% in one of the experimental plots did not provide enough change in canopy architecture to allow any trends in the mean data to be established for variation in thinning density.

To p.143

TABLE 5.4: Mean wind velocity profile data (Kielder)

Mast No	Anemometer No.	Set 1, 45° to forest edge (SSE)					Set 2, 90° forest edge (SSW)					Set 3, 90° to forest edge (SSW)					Set 4, 90° to forest edge (SSW)				
		Tree Ht (metres) Averaged	z	$\frac{z}{z_5}$	U metres/ sec	$\frac{U}{U5}$	Tree Ht (metres) Averaged	z	$\frac{z}{z_5}$	U metres/ sec	$\frac{U}{U5}$	Tree Ht (metres) Average	z	$\frac{z}{z_5}$	U metres/ sec	$\frac{U}{U5}$	Tree Ht (metres) Averaged	z	$\frac{z}{z_5}$	U metres/ sec	$\frac{U}{U5}$
1	1	-	9.7	.39	8.5	.82	-	9.7	.39	8.8	0.83	-	10.0	.36	7.6	0.79	-	10.0	..40	10.2	0.86
	2	-	12.4	..50	8.7	.83	-	12.4	.50	9.8	0.86	-	12.9	.46	7.8	0.81	-	13.0	.52	10.3	0.87
	3	-	15.5	.63	9.2	.89	-	15.5	.63	9.5	0.88	-	16.7	.60	8.5	0.88	-	17.0	.68	11.0	0.93
	4	-	19.7	.80	9.7	.93	-	19.7	.80	10.5	0.98	-	21.6	.77	8.9	0.92	-	21.0	.84	11.7	0.99
	5	-	24.7	1.00	10.4	1.00	-	24.7	1.00	10.7	1.00	-	28.0	1.00	9.7	1.00	-	25.0	1.00	11.9	1.00
				$\frac{Z}{H}$					$\frac{Z}{H}$					$\frac{Z}{H}$					$\frac{Z}{H}$		
2	6	12.7	(12.5	.98	1.8	.25	12.7	(12.5	.98	4.0	0.44	12.7	(12.5	.98	4.6	0.43	11.15	(10.0	0.90	2.5	0.14
	7		(15.2	1.20	7.9	.78		(15.2	1.20	10.1	0.96		(15.2	1.20	7.2	0.78		(13.0	1.17	11.0	0.84
	8		(18.5	1.46	9.1	.90		(18.5	1.46	10.0	0.96		(18.5	1.46	8.3	0.90		(17.0	1.53	11.5	0.87
	9		(22.5	1.77	9.7	.96		(22.5	1.77	10.6	1.02		(22.5	1.77	8.9	0.96		(21.0	1.89	12.6	0.96
	10		(28.0	2.21	10.1	1.00		(28.0	2.21	10.4	1.00		(28.0	2.21	9.2	1.00		(25.0	2.25	13.2	1.00
3	11	15.4	(12.5	.81	1.5	.17	15.4	(12.5	0.81	0.0	0.00	15.4	(12.5	0.81	1.5	0.18	12.35	(10.0	0.81	0.0	0.00
	12		(15.2	.99	4.3	.50		(15.2	0.99	1.6	0.17		(15.2	0.99	4.1	0.50		(13.0	1.05	2.4	0.28
	13		(18.5	1.19	5.1	.59		(18.5	1.19	3.3	0.34		(18.5	1.19	4.8	0.58		(17.0	1.38	5.7	0.52
	14		(22.5	1.46	6.8	.79		(22.5	1.46	6.5	0.66		(22.5	1.46	6.3	0.76		(21.0	1.70	8.6	0.78
	15		(28.0	1.82	8.6	1.00		(28.0	1.82	9.8	1.00		(28.0	1.82	8.3	1.00		(25.0	2.03	11.0	1.00
4	16	13.1	(12.5	.95	3.2	.36	13.1	(12.5	0.95	5.8	0.61	13.1	(12.5	0.95	4.0	0.48	11.15	(10.0	0.90	0.7	0.05
	17		(15.2	1.16	7.0	.79		(15.2	1.16	8.9	0.93		(15.2	1.16	6.8	0.81		(13.0	1.17	11.0	0.82
	18		(18.5	1.41	8.1	.91		(18.5	1.41	9.7	1.08		(18.5	1.41	7.7	0.92		(17.0	1.53	12.3	0.92
	19		(22.5	1.72	9.1	1.02		(22.5	1.72	10.5	1.10		(22.5	1.72	8.7	1.03		(21.0	1.89	12.8	0.96
	20		(28.0	2.14	8.9	1.00		(28.0	2.14	9.6	1.00		(28.0	2.14	8.4	1.00		(25.0	2.25	13.4	1.00
5	21	14.5	(12.5	.86	2.8	.24	14.5	(12.5	0.86	0.7	0.05	14.5	(12.5	0.86	2.8	0.25	12.35	(10.0	0.81	0.6	0.04
	22		(15.2	1.05	5.1	.44		(15.2	1.05	3.0	0.22		(15.2	1.05	5.0	0.45		(13.0	1.05	3.7	0.30
	23		(18.5	1.28	6.7	.57		(18.5	1.28	5.5	0.40		(18.5	1.28	6.5	0.58		(17.0	1.38	7.2	0.57
	224		(22.5	1.55	8.2	.71		(22.5	1.55	7.9	0.58		(22.5	1.55	8.0	0.71		(21.0	1.70	10.0	0.80
	25		(28.0	1.93	11.6	1.00		(28.0	1.93	13.7	1.00		(28.0	1.93	11.2	1.00		(25.0	2.03	12.5	1.00

U = Velocity at a particular anemometer
U5 = Velocity of top anemometer on same mast

z = Height of observation
z_5 = " " observation at top of Mast 1
H = Average tree height around the particular mast

(a)

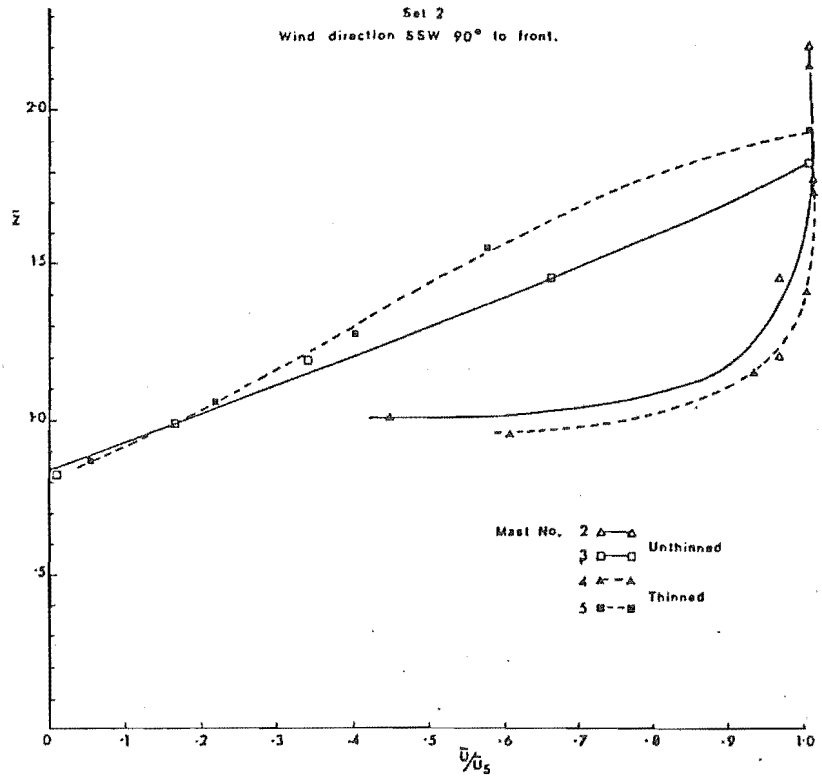

FIGURE 5.2(a): Mean wind velocity profiles (Kielder).

(b)

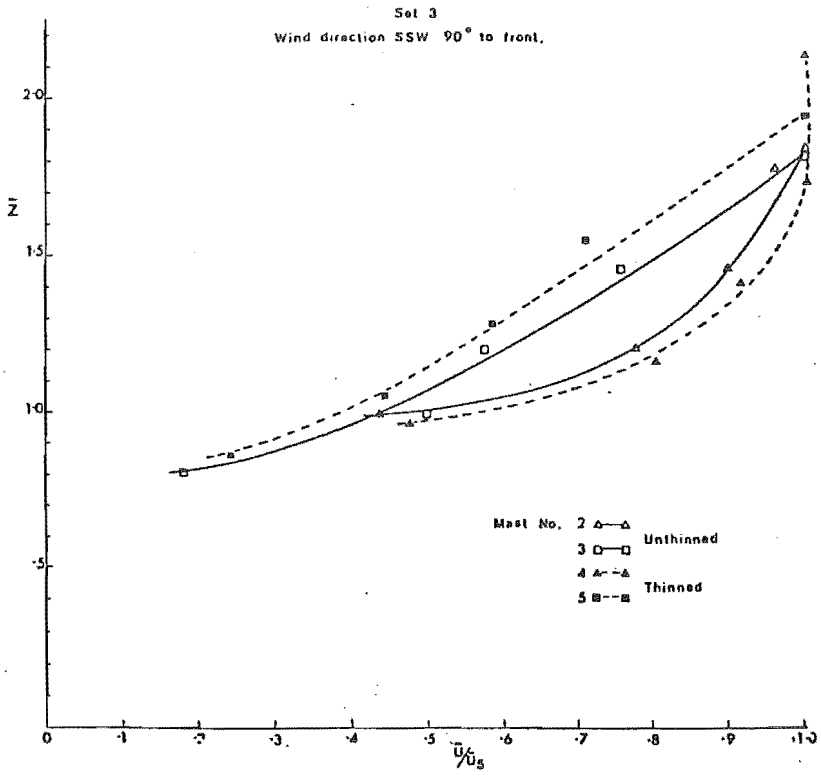

FIGURE 5.2(b): Mean wind velocity profiles (Kielder).

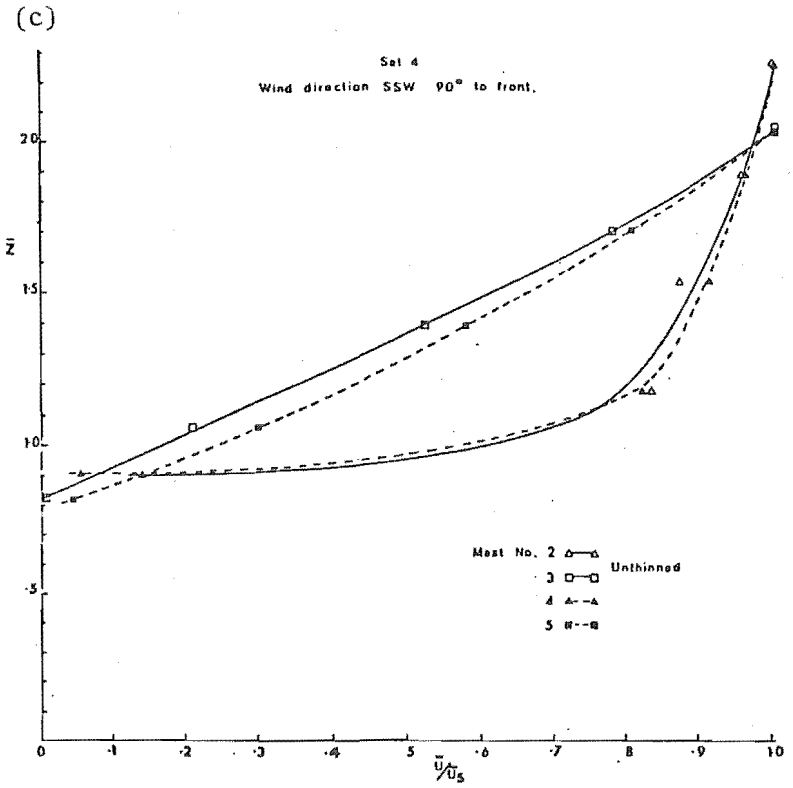

FIGURE 5.2(c): Mean wind velocity profiles (Kielder).

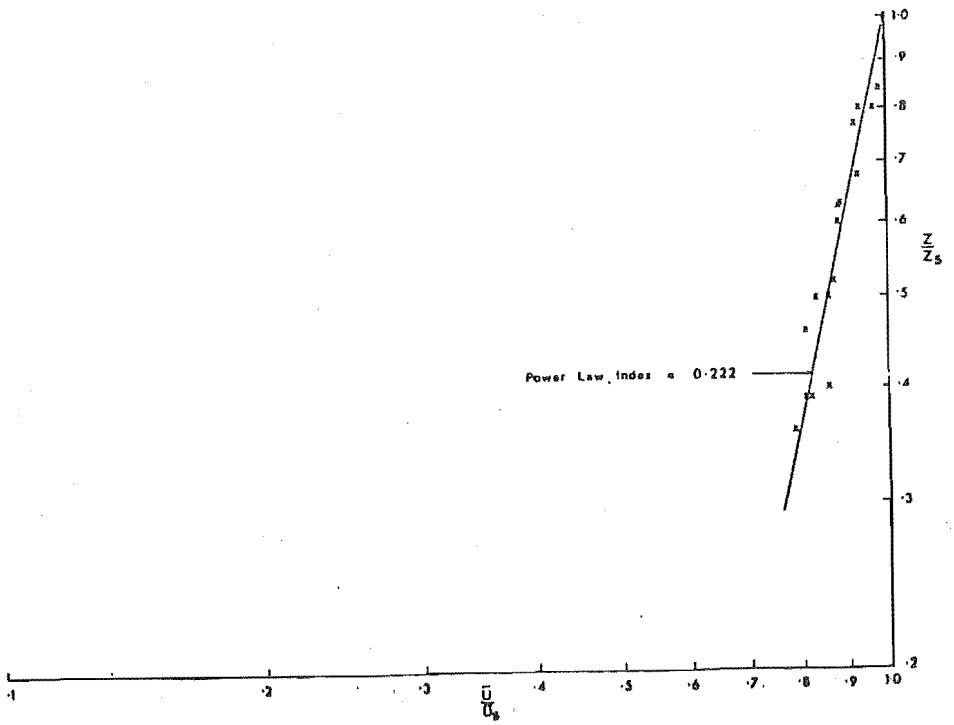

FIGURE 5.3: Mean wind velocity profiles, upwind (Kielder).

TABLE 5.5: Aerodynamic parameters calculated from mean wind velocity profiles.

Set No.	Mast No.	$\frac{U_1}{U_5}$	$\frac{U_2}{U_5}$	z_1	z_2	d	U_5	Friction Velocity $U^*_{profile}$	Roughness Height $\frac{z_o''}{H}$	Shear Stress $\tau_{profile}$	Surface Stress Coefficient C_{f_o}
	2	0.25	0.77	0.98	1.20	0.75	10.10	3.32	0.172	13.47	0.215
	3	0.25	0.57	0.85	1.25	0.75	8.61	0.70	0.028	0.60	0.013
1	4	0.35	0.75	0.90	1.13	0.75	8.89	1.57	0.066	3.02	0.062
(45°)	5	0.37	0.73	1.00	1.50	0.75	11.63	1.56	0.080	2.99	0.036
	2	0.45	0.92	1.00	1.25	0.75	10.44	2.93	0.130	10.55	0.158
	3	0.17	0.70	1.00	1.50	0.75	9.83	1.94	0.174	4.63	0.078
2	4	0.55	0.96	0.95	1.25	0.75	9.60	1.78	0.059	3.89	0.069
(90°)	5	0.17	0.54	1.00	1.50	0.75	13.67	1.86	0.148	4.25	0.037
	2	0.48	0.80	1.00	1.23	0.75	9.25	1.86	0.094	4.24	0.081
	3	0.41	0.82	1.00	1.50	0.75	8.28	1.27	0.082	1.97	0.047
3	4	0.50	0.80	0.97	1.17	0.75	8.42	1.57	0.073	3.03	0.070
(90°)	5	0.38	0.80	1.00	1.61	0.75	11.19	1.54	0.080	2.91	0.038
	2	0.20	0.80	0.90	1.20	0.75	13.18	2.95	0.104	10.67	0.100
	3	0.17	0.80	1.00	1.72	0.75	10.99	2.07	0.171	5.24	0.071
4	4	0.10	0.80	0.90	1.16	0.75	13.38	3.82	0.130	17.88	0.163
(90°)	5	0.24	0.80	1.00	1.68	0.75	12.47	2.16	0.140	5.72	0.060

5.5.3 Summary

This experiment at Kielder has established the mean wind profile shapes and surface stress coefficients existing at the front of a forest stand for winds normal to the forest edge. Equilibrium appears to exist near 7 H in from the leading edge.

5.6 FULL SCALE FOREST TESTS AT RIVOX

5.6.1 Experiment objectives

This experiment tests the hypothesis that thinning changes to forests influences eddy size and distribution to such an extent that the peak in the turbulent energy spectrum of the wind shifts towards the natural periodicity of the trees. This shift in the energy spectrum causing more tree sway, may cause premature wind damage, especially just in from forest leading edges.

The experiment compares wind and tree response results from the initial spacing and first thinning at Rivox with model forest results at the same spacings (Ch. 7).

5.6.2 The experimental site

A suitable experimental site was found at Rivox, Moffatt, S.W. Scotland (5.3.1). This had been established by the Institute of Terrestrial Ecology (ITE) on Forestry Commission land. It had short term field accommodation, and two generators, supplying stable 24 V. DC and 240 V. AC power. On site, were two masts already carrying automatic weather station systems (the ITE mast and the Strathclyde University mast with tower).

For accurate wind turbulence and spectra studies the wind sector was restricted to between WSW and SSW (Fig. 5.4), (Fig. 5.8).

The canopy was more uneven than normal with reduced growth areas in patches within the compartment allocated for research studies and the crop was a little immature for thinning. With these site limitations it was decided to confine the study to wind structure and tree response measurements on one mast, leeward of the ITE mast, aligned to winds of restricted direction between WSW and SSW (Fig. 5.4, Photograph 13). (Extension of the experiment to monitor winds from all compass bearings is possible at Rivox but would require a much greater expenditure on instrumentation and extra masts.).

With only 9 months in which to set up and calibrate the experiments and because finance was limited, decisions were made to purchase five arrays of UVW Gill anemometers and to use items of data logging equipment which were already Forestry Commission property. This involved some modification to the initial experimental site arrangement but was still considered sufficient to fulfil the experiment objectives. Collaboration with ITE[1], and with The Cranfield Institute of Technology added to the experimental data output.

Tree growth between wind measurement periods may affect spectral comparisons. The data will, however, be from typical spruce forest under normal forest management, except that the forest will be selectively thinned to reduce the risk of having the site destroyed by windthrow before data can be collected.

5.6.2.1 Site layout

The experimental site is in Compartment 513a at Rivox, part of Moffat Forest in the South Scotland Conservancy. The total area of the compartment is 10.0 ha and it is stocked with Sitka spruce planted in 1962 at close spacing. In May 1982 total average tree-top height was 9.11 m and the General Yield Class (see App.II) was 14 although in some places, particularly near the Institute of Terrestrial Ecology (ITE) and the Forestry Commission (FC) masts, the mean height was 10.10 m and Yield Class was as high as 20.

Site elevation is 360 m and is very exposed with a windthrow hazard class rating of Class 5 (Booth 1977). The soil is a peaty gley and, prior to afforestation, the site was classified as Molinia blanket bog. General topography provides a slight slope towards the south, with Haningshaw Hill, upstream and to the WNW of the site 1.0 km away, at an elevation of 469 m.

The layout of the site is shown in Photograph 13 and Fig. 5.4. The latter was used to find the best wind sector and terrain slopes for the site. The ITE mast is 214 m upwind of the FC mast. Winds from the WSW (250°T) run parallel with a line joining these two towers.

Upwind of the ITE mast there is 0° slope for 260 metres. The ground then rises at a slope of 1.9° for the next 90 metres. From the ITE mast the ground slopes down at 4.6° for the first 37 metres towards the FC mast, then is at 0° for the next 59 metres and finally slopes down again at 2.9° for the last 119 metres. The ITE mast carries a UVW Gill anemometer array

1. The Gill UVW array on the ITE mast was purchased by the Institute of Terrestial Ecology.

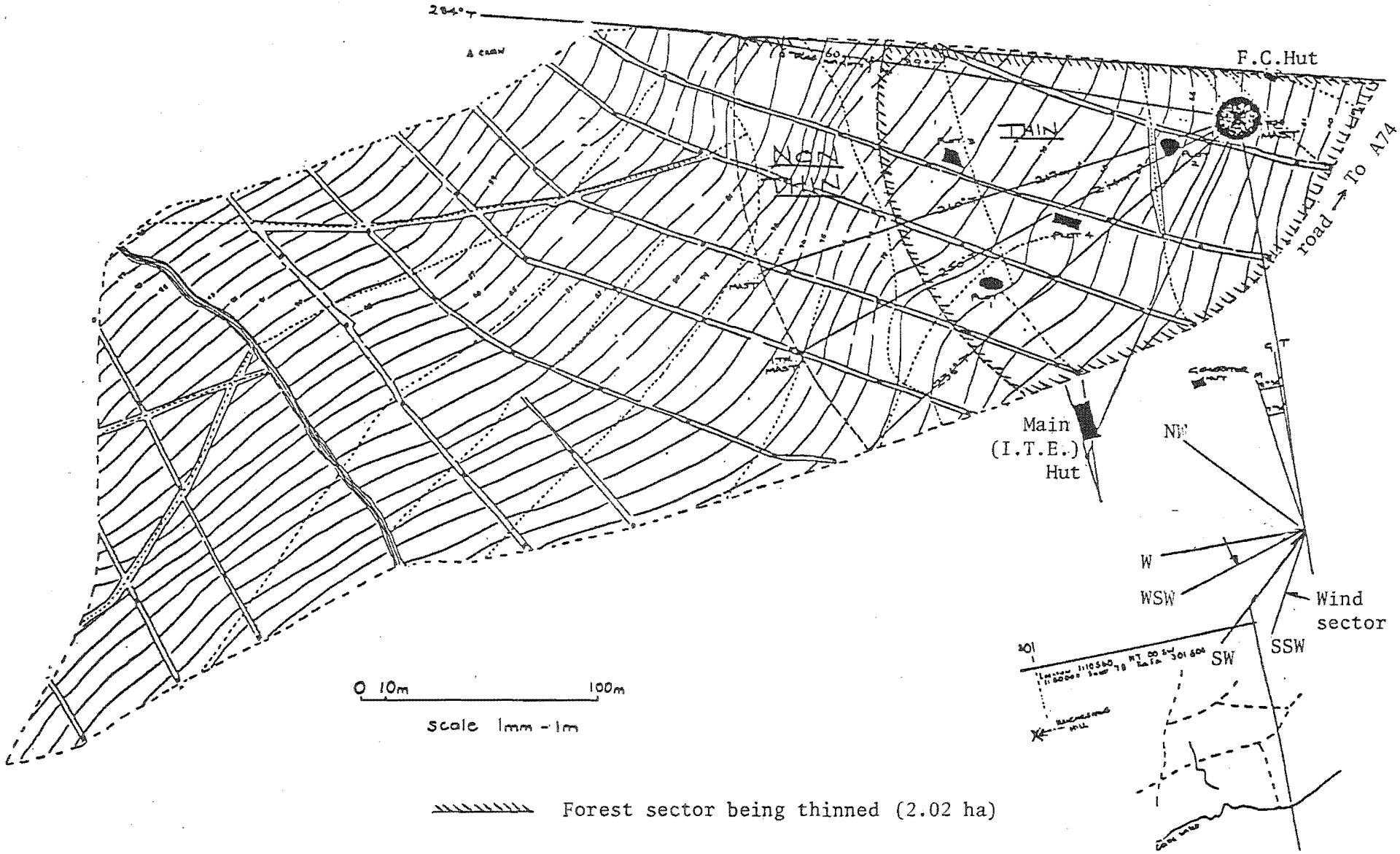

FIGURE 5.4: Site plan of full scale thinning experiment (Rivox)

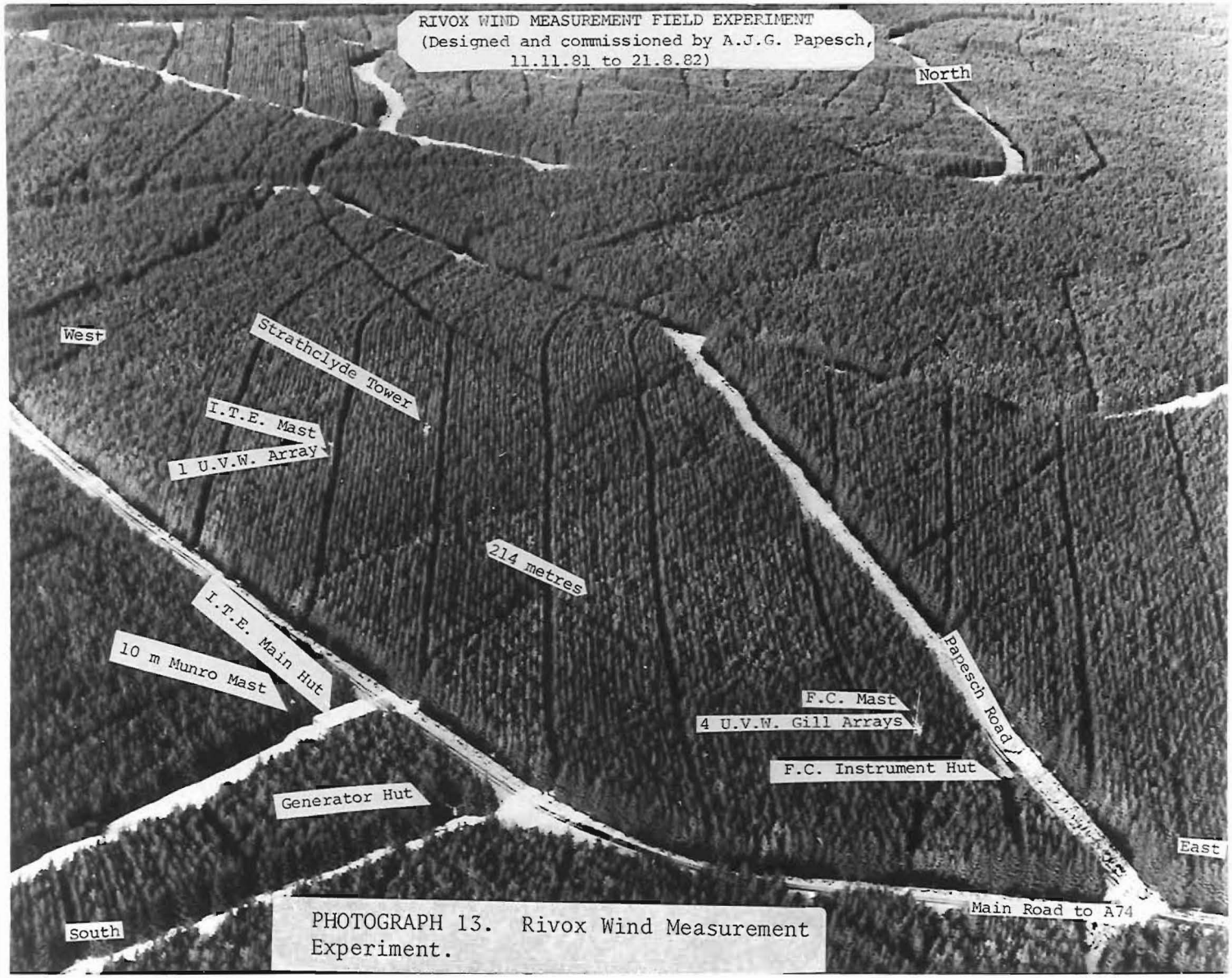

PHOTOGRAPH 13. Rivox Wind Measurement Experiment.

at 13.6 m height.[1] This Gill array is positioned so that the bisector of the 'U' and 'V' Gill anemometers is at 247°T. At the top of the ITE mast there is an automatic weather station.

Ground slopes need to be found for the upper and lower limits of the wind vectors acceptable for subsequent wind analysis in the test sector. At the upper limit of the test sector (260°T), the ground slopes down at 5.7° for the first 60 metres and down at 4.8° for the last 155 metres before reaching the FC mast. At the lower limit of the test sector (236°T) the fall is 2.7° for the first 70 metres, 0° for the next 43 metres, and 2.1° for the last 110 metres.

5.6.2.2 Forestry commission tower and mast

The FC tower and mast were previously used in the Kielder experiment. The tower and mast dimensions and guy locations are shown in Fig. 5.7. The anemometer heights and designations are for the unthinned period to 31/10/83.

The mast holding the Gill anemometers was in position by March 1982. The Gills and the Geostore were tested in April 1982 and some modifications to the AM/FM converters (designed by R. Jones of IGS) were necessary. Wind data were first recorded on 27th April 1982. On 4th May 1982 there was a hail storm. The mast was lowered and the system adjusted to enable direct servicing of the Gills on the mast.

A 10 metre mast, carrying a Munro Cup anemometer vane and a Vector recording vane positioned just above the canopy, was erected at the Main Hut but has since been moved near to the FC mast. Mean wind direction and speed can be continuously monitored and recorded to ensure that winds over the main instrument masts are from the right sector.

The zone to be thinned commences 60 metres downwind from the ITE mast because the forest stand around the upstream masts is in use for other experiments (Fig. 5.4).

5.6.3 Wind direction in the Moffat (Rivox) area

The meteorological stations closest to Rivox are Eskdalemuir and Lowther Hill. Lowther Hill is a very exposed site with the wind sensors 27 m above ground. Table 5.6 shows the winds above 8.5 m/s between 230°T and 310°T

1. From the wind results (Table 5.11) it appears that the array has been positioned higher up the mast since 3/9/83.

To p.150

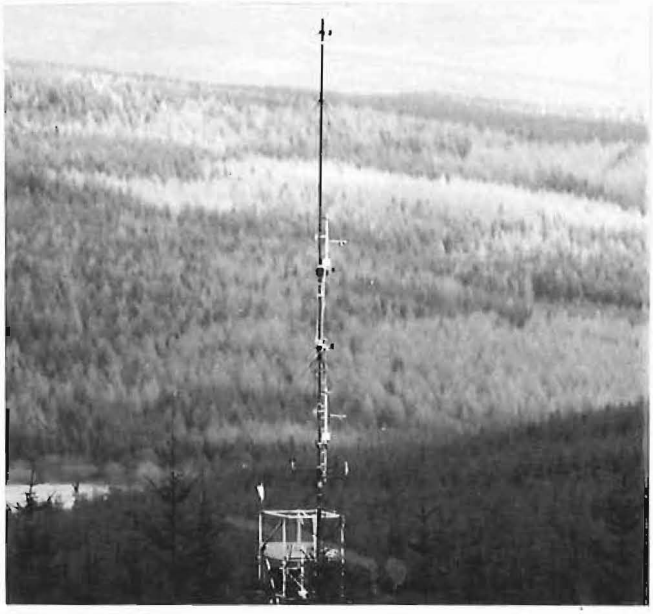

Photograph 1

The Forestry Commission (FC) mast 214m downwind from the I.T.E. reference mast.

Photograph 2

A view towards the I.T.E. upstream mast on the left.

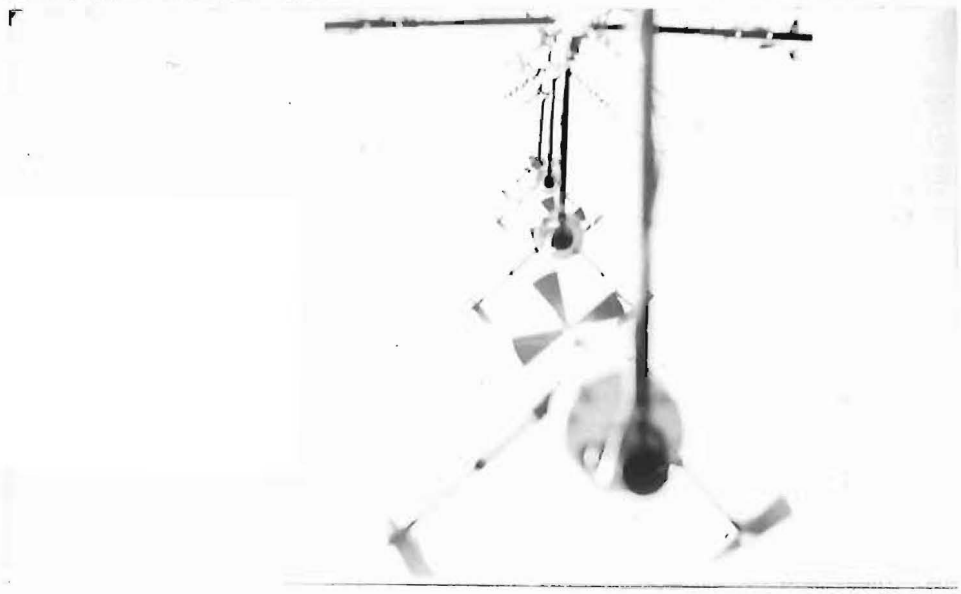

Photograph 3

Four U.V.W. Gill anemometer arrays in action up the FC mast.

FIGURE : 5.5 Rivox, Scotland: Thinning Experiment Site and Gill Arrays.

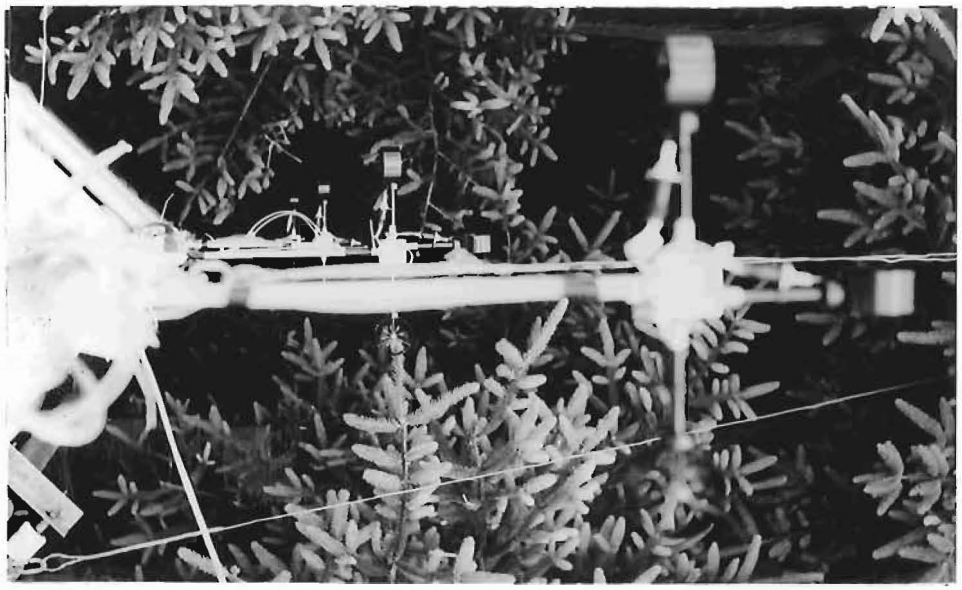

Photograph 1

Four U,V,W, Lowne anemometer arrays positioned below mean tree top height.

Photograph 2

Bottom $U_1V_1W_1$ Gill anemometer array on a 1.5m boom 11.3m above ground.

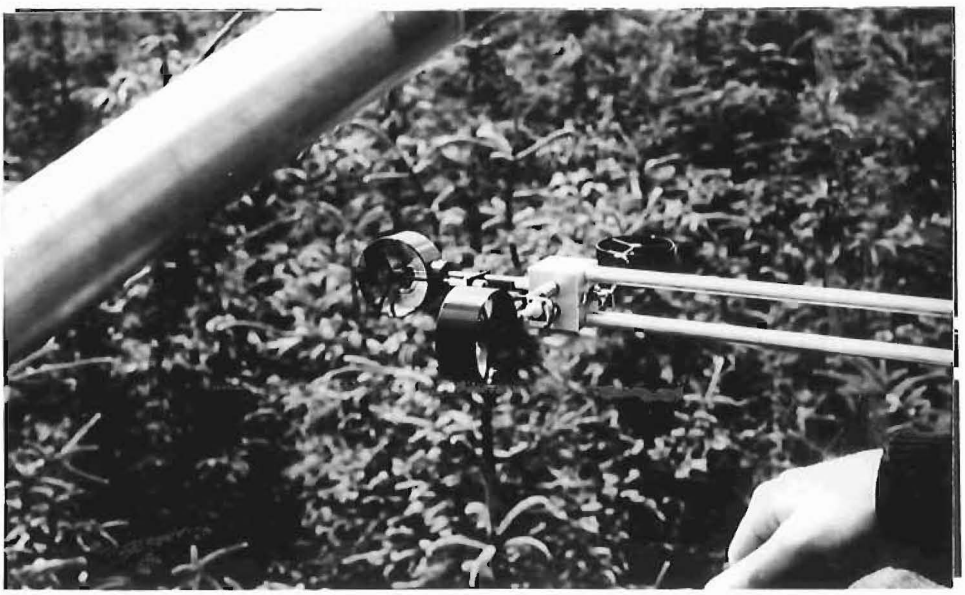

Photograph 3

Top $U_1V_1W_1$ Lowne anemometer array mounted on tower at 11.3m and at 45° to the Gill arrays.

FIGURE 5.6: Rivox; Field Experiment Anemometer Arrangement.

at these two stations. The two wind vectors were at the initial limits set for wind direction over the site at Rivox. Between these two bearings the winds with a mean direction of 250°T (WSW) at the site should occur for about a third of the time and half of the winds in this sector range above 10 m/s. Half of the winds above 8.5 m/s should lie between 8.5 m/s and 10.5 m/s. Winds above 17 m/s are uncommon in the area. (Table 5.6.)

TABLE 5.6: Average wind history at Eskdalemuir and Lowther Hill meteorological stations.

TIME OF YEAR	WINDSPEED % OF TOTAL ABOVE 8.5 m/s ½ WINDS OF THIS BETWEEN (17-21 Kts)	WIND DIRECTION % OF TOTAL BETWEEN 230°T-310°T	WIND DIRECTION % OF TOTAL BETWEEN 230°T-310°T ABOVE 8.5mm/s
WHOLE YEAR	31.9%	26.2%	12.5%
JANUARY	43.1%	30.4%	21.6%
FEBRUARY	33.2%	19.8%	10.0%
MARCH	35.4%	21.0%	10.1%
APRIL	28.6%	23.9%	11.1%
MAY	25.5%	20.0%	7.1%
JUNE	24.3%	25.6%	8.2%
JULY	23.9%	34.0%	13.1%
AUGUST	19.7%	20.0%	6.4%
SEPTEMBER	35.0%	31.1%	15.5%
OCTOBER	36.4%	23.9%	11.9%
NOVEMBER	38.4%	33.8%	14.5%
DECEMBER	40.3%	29.4%	17.5%
TOTAL	32.% ⅓ WINDS	26.1% ¼ DIRECTION	12.25% ½ ABOVE 10 m/s

To p.152

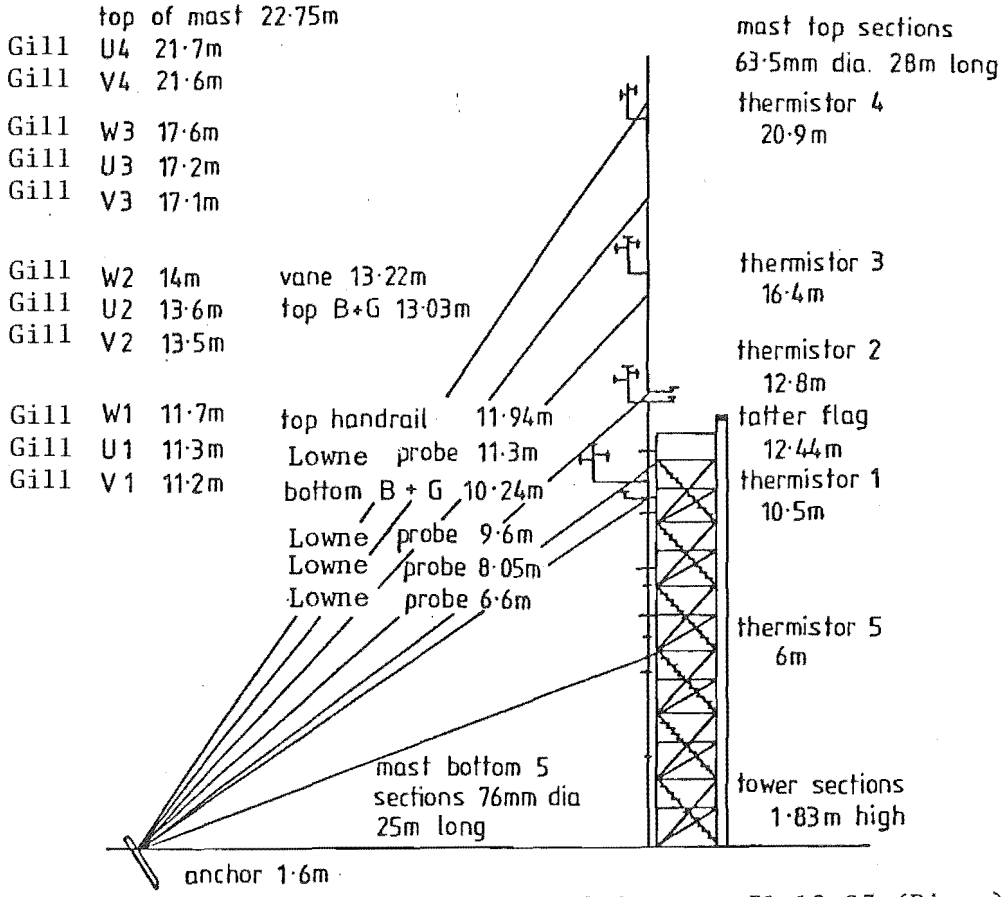

FIGURE 5.7: F.C. mast and anemometer positions to 31.10.83 (Rivox)

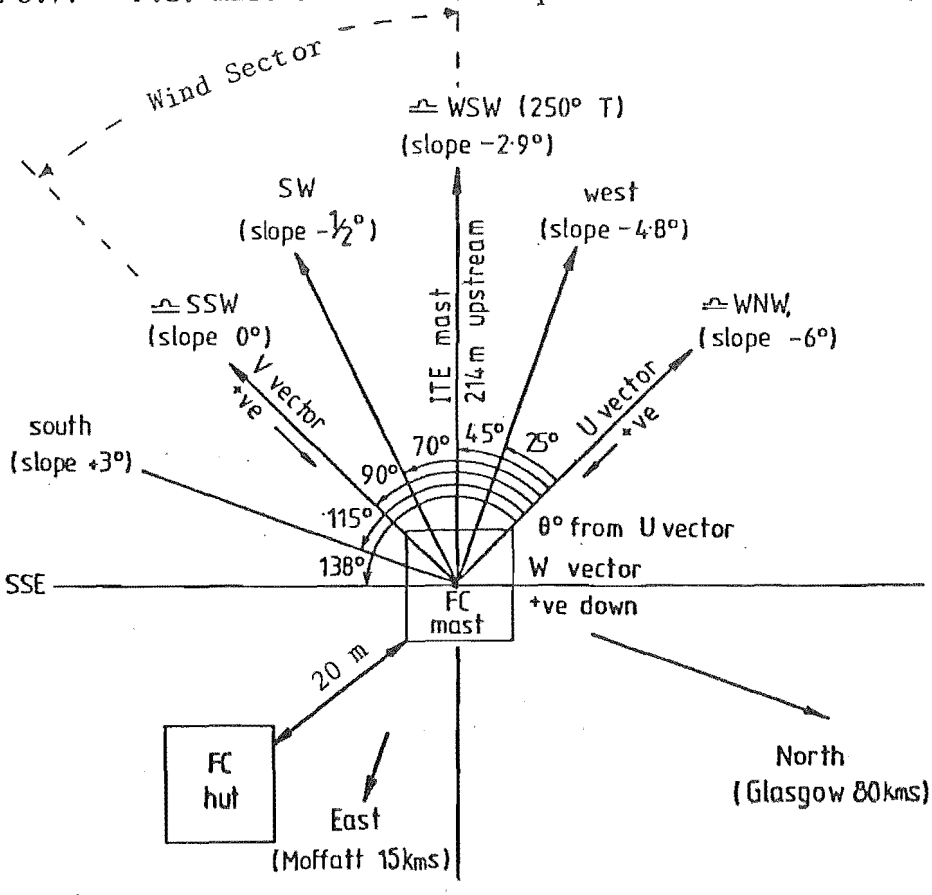

FIGURE 5.8: Anemometer (°θ) and compass (°T) directions and terrain slopes towards F.C. mast.

5.6.4 Plot characteristics in the thinned sector

Five separate plots within the thinned sector were measured to obtain tree heights, diameters, mean spacing and tree natural frequencies, needed for later analysis. These plots are located on the Site Plan (Fig. 5.4) as dark shaded areas. The radius of the plot around the FC mast is 10 metres and includes over 100 trees. Several transects within the compartment will allow assessment of the gross stand architecture at a future date.

Histograms of the height and diameter of all the trees in all five plots were obtained and the standard deviation provided the model forest height distribution. The mean height for the whole sector was 9.11 m and the mean spacing was found from the 2.02 ha block containing 6380 trees.

The mean spacing to mean height ratio $(\frac{S}{H})$ was 0.176 for the unthinned plot and $\frac{S}{H} = 0.186$ for the first thinning.

A graph of sway period was plotted against $\frac{H^2}{D_B}$ to show the distribution of tree period within the sector. The average natural frequency of the spruce trees within the FC plot was 0.522 Hz with a mean height of 10.10 m (27/5/82).

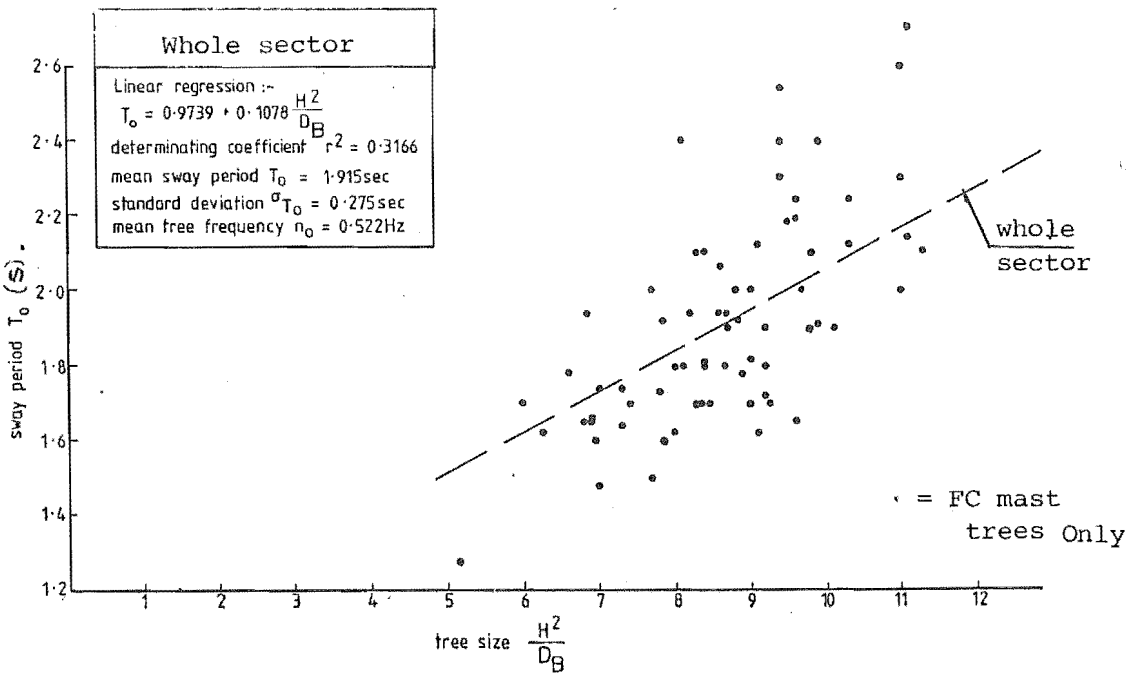

FIGURE 5.9: Distribution of the natural frequency of 100 trees around F.C. mast compared to the total sample from the whole test sector.

5.7 INSTRUMENTATION AT THE FC MAST, RIVOX

5.7.1 Gill propeller anemometers

These are the primary wind sensors (Fig. 5.10). 12 anemometers on the main (FC) mast are deployed as 4 orthogonal arrays in a vertical sequence rising from within the canopy to 12 metres above the canopy (Fig. 5.7). A fifth triad is located above the canopy at 13.6 m on a separate reference ITE mast 214 m upstream. Output signals and voltages are directly proportional to wind speed, and all Gill anemometer signals are recorded as analogue FM signals on a multi track Racal Geostore tape logger, via voltage/frequency converter units, (Fig. 5.13).

The 4 UVW Gill arrays are mounted on booms with the top 3 booms 0.8 metres away from a 76 mm diameter mast. The bottom UVW array is mounted on a boom which is 1.5 metres forward of the top module of the tower and is stayed by ropes to prevent boom movement. This is necessary to ensure minimum interference to the wind turbulence at the Gill propellers (5.3.5). The mast carries ladder sections which allow anemometers to be serviced *in situ*.

Thermistor probes of the thermo-couple type are fitted to the boom and are carefully located so that air, which is pumped through each anemometer arm by a 24 Volt AC motor/fan unit, ventilates the temperature probes. The temperature probes initially used were inadequate. Differential thermistor probes have not been fitted as yet. Wind runs, therefore, are taken on cloudy, windy days when atmospheric stability is assumed at neutral conditions (Panofsky, pers. comm.).

The Gill voltage outputs are transmitted along cables to the instrument hut positioned 20 m from the FC mast. The anemometer output signals are conditioned by specially designed AM/FM converters, with low pass filtering and drift compensation. Input signals to the converters are low pass filtered to remove any high frequency noise produced on the signal by the miniature AC generators in the Gill anemometers. Each channel is calibrated separately and checked again at the end of every data run. The voltage outputs of the Gills and their converted equivalent frequencies are linear within the range ± 800 mV for the U,V, anemometers, and within the range ± 200 mV for the W component Gills (Table 5.8).

To p.155

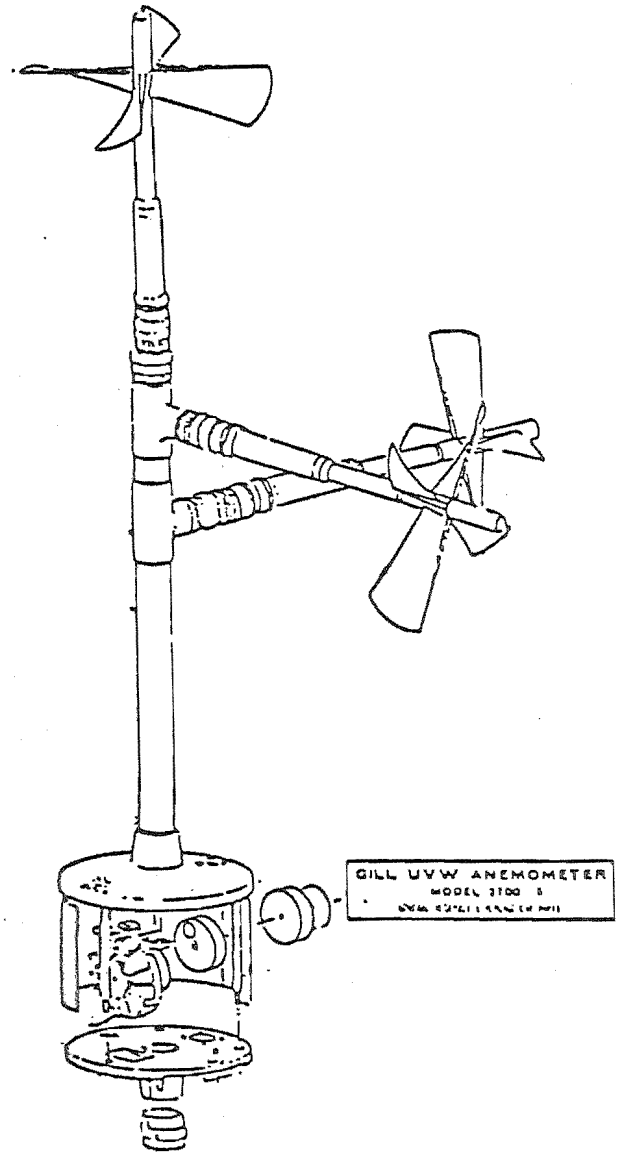

FIGURE 5.10; Gill U.V.W. Anemometer Array.

TABLE 5.7: Anemometer positions on F.C.mast to 31.10.83.

Triad Number	Instrument Type	Component	Height (m)
	Lowne	u,v,w	6.60
	Lowne	u,v,w	8.05
	Lowne	u,v,w	9.60
	Lowne	u,v,w	11.30
1	Gill	u	11.30
		v	11.20
		w	11.70
2	Gill	u	13.60
		v	13.50
		w	14.00
3	Gill	u	17.20
		v	17.10
		w	17.60
4	Gill	u	21.70
		v	21.60
		w	22.75

TABLE 5.8 Linear operating range of Gill anemometers

	Input Signal (mV)	Frequency Output (Hz)	R.P.M.
(a) Horizontal (U,V) Gills	0	676	0
	+800	946	+2880
	-800	406	-2880
(b) Vertical (W) Gills	0	676	0
	+200	946	+720
	-200	406	-720

Above these limits there is a progressive deterioration in linearity up to the anemometer structural limits (6000 rpm).

To convert Gill output signals from digitised data to metres per second: the U and V Gill anemometers have a conversion factor of 0.0050 m/s/RPM and

1 digit on the computer = 21.955 RPM

= 21.955 x .005 m/s

= 0.1098 m/s .

The W Gill anemometers have a conversion factor of 0.00510 m/s/RPM and

1 digit on the computer = 5.489 RPM

= 5.489 x .0051 m/s

= 0.0279 m/s .

The main limitations of Gill sensors have been discussed (§5.3.5 and 5.3.6).

5.7.2 The Lowne wind vane sensors

Four sets of vane type Lowne wind sensors (Fig. 5.6) were fixed to the mast tower within the canopy, for three periods. These instruments gave detailed information on within-canopy turbulence and checked the performance of the Gill propeller anemometers.

These sensitive wind vane sensors are a modified version of Lowne handheld wind vane sensors and have a distance constant of 0.25 m. The mechanical gearing has been removed and the hub holding the vane has been

boxed out and fitted with a micro-electronic chopper system. The output signal is fed by cable down the hub support arm then, via the triad support arm, down the mast to the signal processor and conditioner, and then multiplexed onto a Racal 4 channel recorder (or Floppy Disc store via a microprocessor).

The Lowne sensors have an excellent cosine response even though the vanes are shrouded by a hoop at least 30 mm in width (Schaeffer J. pers. comm.). They can withstand mean wind speeds of up to 10 m/s. The sensors are therefore suited to in-canopy turbulence studies whereas the Gills are more suited to above-canopy turbulence measurements where higher mean speeds prevail. The Lowne anemometers were used in position and coupled with accelerometer readings during June 1982, October 1982 and March 1983. Their presence allowed in-field calibration and operational checks on the Gill anemometers.

5.7.3 The Brookes and Gatehouse (B&G) cup anemometers, and the Vector wind vane and logger.

The B & G 159 Cup anemometers and a Vector wind vane are positioned on support arms 0.62 m to the left and right of the main mast (Fig. 5.7). The anemometers provide 2 pulses per revolution and these pulses are logged onto the wind-logger system storing data in "bins" set with a calibration constant of 0.42. A vertical cumulative display of all information on each channel is readily available and mean wind distributions can be read directly, stored on a tape recorder, or linked to a microcomputor. The instruments act as a background check during Gill windspeed measurements at the FC mast.

5.7.4 Tree response measurements

Four accelerometers were positioned as orthogonal pairs, in X and Y orientations on 2 trees adjacent to the main instrument mast. Two Bell and Howell units, and 2 Pioden units were used (Fig. 5.26). These sensors produce very small but precise voltage changes in response to tree accelerations. Typical accelerations generated by the action of wind on trees at the mid-crown mounting position (7.5 m) range between 0 to 0.25 g. The Bell and Howell units produce ± 7.5 mv/g and the Pioden accelerometers ±1.75 mv/g when powered by a bridge voltage of 6.25 volts. Normal output from accelerometers in strong wind conditions is under ± 2 mV, and so differential amplification to the accelerometer signals is required for DC recording. The Bell and Howell accelerometer signals are amplified (gain 670) and the Pioden control signals are amplified by 3000 to produce voltage levels suitable for DC tape recording or input to the multiplexing process.

Since the tree motion is a random variable, the signals generated by the accelerometers are described in the frequency domain by their power spectral density which gives a measure of the mean square value of the acceleration signals in a given frequency band width

$$\text{i.e.} \quad PSD = \frac{(\text{Volts})^2}{\text{Hz}} = \frac{(\text{w})}{\text{Hz}}$$

To analyse the accelerometer spectral records for tree response, inverse Fourier transforms are used. The complex spectrum F(w) is divided by $(-w^2)$ to obtain the tree deflections. As well, scratch gauges are mounted on the same tree stems near the accelerometers, and at ground level root movement sensors using modified Casella thermographs act as ancillary background checks during calibration and recording from the accelerometers.

5.7.5 Instrument digitising errors

When the Gill and Lowne anemometers were used together, their output signals were digitised directly by multiplexing 15 channels on to a magnetic tape. A discrete representation of continuous signals (from the multiplexed signals) produces a noise source on the tape, depending on the resolution per bit of the digitised signals. For the instruments used, error levels corresponding to the resolutions are:-

Instrument	Resolution/bit	error
Gill (U, V)	1.8×10^{-1} m/s	2.6×10^{-3} m^2/s^2
Gill (W)	5.6×10^{-2} m/s	2.6×10^{-4} m^2/s^2
Lowne	2.4×10^{-1} m/s	4.7×10^{-3} m^2/s^2
Accelerometers	9.8×10^{-3} g	7.9×10^{-6} g^2

5.8 RECORDING AND PROCESSING SYSTEMS

5.8.1 The main recording system

From the FM convertors signals are passed to a Racal geostore 14 channel tape recorder. This has 11 data channels available for analogue FM recording. An accurate Vela time code is recorded simultaneously onto the 12th data channel, and the 2 remaining tape tracks are used for flutter compensation.

The Vela time code clock is set to GMT before commencing recording. Preliminary checks of all 11 input signals passing into the geostore are made using the ancillary field test unit. This unit monitors the record head signals (Fig. 5.11) and gives a clear audio check that the FM signal is being presented at the tape heads for recording. Normally data logging runs involve one hour sequences of Gill data.

5.8.2 The main processing system

The geostore tapes containing raw field data analogue FM signals are processed initially at the Institute of Geological Sciences. Field tapes are replayed on a Racal Store 14 tape deck which demodulates the FM signals and decodes the Vela time pulse train to enable accurate identification of data sequences held on tape. The demodulated signal is distributed through a pinboard matrix to an analogue filter bank and then split to an analogue ink jet printer which displays all 14 channels from the data tape. The demodulated signal is digitised on a PDP mini-computer, and the digital data recorded on magnetic tape or floppy discs for input to mainframe ICL 2988 computer for subsequent analysis. During this process several points of detail must be noted:

(a) The speed gain is 40; this is the ratio of the replay speed on Store 14 to the record speed on geostore.

(b) Filter Bank Settings: the demodulated analogue data signals are preconditioned in a bank of Kemo dual filters from 0.1 Hz to 10 kHz. These filters give the option of filtering any channel for high pass, low pass or to any band pass within that range. For the anemometer signals recorded on the geostore, double low pass filtering is used to remove any high frequency aberrations beyond the response capability of the wind sensors.

Once the sampling rate is selected and the speed up factor calculated, filtering is made at one-third of the sampling rate. Therefore at 10 Hz sampling rate, filtering at 3.3 Hz low pass is appropriate. With this aim the filter cut-off level is multiplied by the speed gain to give the filter setting on the Kemo Bank of 132 Hz.

(c) Sampling Rate: the filtered analogue-signal is sampled at a rate commensurate with the response sensitivity of the anemometer. This is 10 Hz, and the sampling rate fed to the digitising programme and the filter settings is adjusted to correspond.

(d) Ink Jet Printer: this produces a permanent analogue record of the demodulated/filtered data. Variable speed controls on the paper drive allow expansion of the time base to examine response characteristics of the anemometers, and the Vela time pulse channel checks the start point for digitising the wind data.

(e) Gain Settings: the gain settings define the window width (digital scale length) to be used: computer digits can be converted to wind speeds (see 5.7.1).

(f) Digital Data: normal data runs comprise half hour blocks of data digitised at 10 Hz from 12 channels (10 x 60 x 30 x 12 = 216,000 values). Each digital data file is held temporarily and then reformatted to card image for subsequent input to the EMAS Edinburgh computer. Smaller digital data files can be held on floppy disc and read directly into the FC process from IGS. Digital data can be replayed to check with the original analogue output from the geostore (Table 5.9). Special arrangements are necessary to input the large data files to the EMAS computer.

5.8.3 Apple II data logger multiplexer recording system

The data logger/multiplexer enables the output from the 15 Gill anemometers and 4 accelerometers to be interfaced to an Apple II micro-computer, whilst simultaneously providing 12 anemometer outputs and 6 accelerometer monitor outputs for input to the geostore. The system is comprised of two units, a junction box and a multiplexer. The junction box provides the interconnection between the various transducers and the multiplexer unit. Each triad is wired into a single connector. The 21 data lines are then fed to the multiplexer unit or to a set of 4 output sockets, for connection to the geostore. The accelerometer sockets are supplied with a voltage-regulated stabilised voltage (6.2 volts), which is fed to the transducers and used to drive the accelerometer bridges. High input impedance differential amplifiers allow the various inputs to the Apple computer to reach the required d.c. levels. A gain of X5 is used for the Gill U and V channels and a gain of X20 is used for the W channels.

Normal outputs from the differential amplifiers, are fed to a 25 channel multiplexer. This unit, operating at 250 Hz, sequentially interrogates each channel, beginning with the anemometers, followed by the accelero-

To p.161

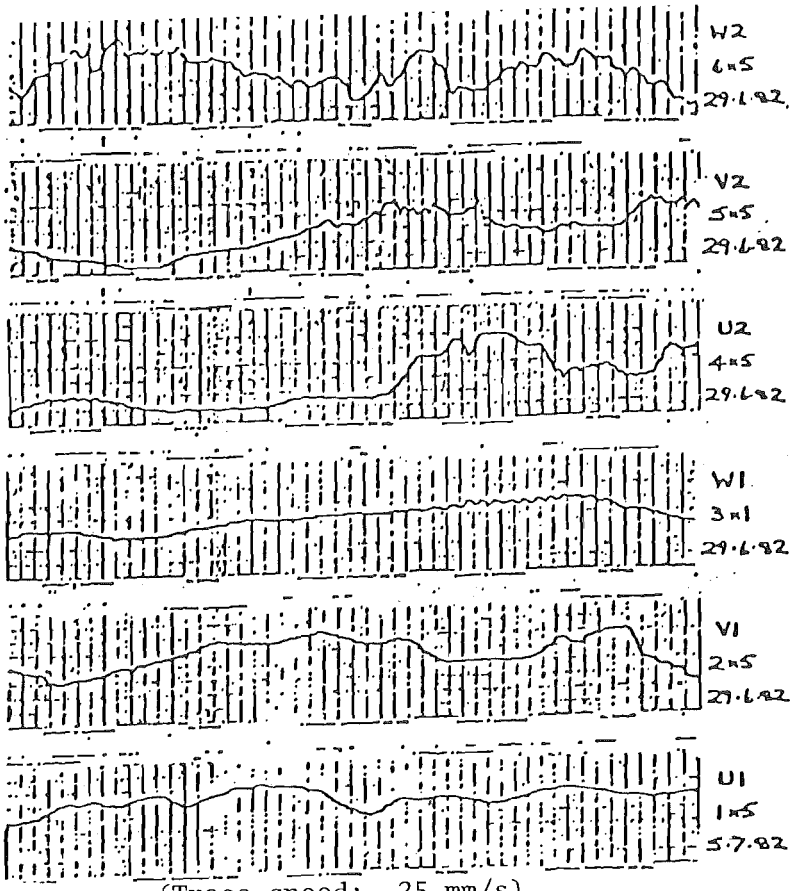

(Trace speed: 25 mm/s)

FIGURE 5.11: Gill anemometer calibration trace at Geostore sensor head (Tape FC3/D).

TABLE 5.9: Digital read-out from part of Tape FC3/D (25.5.82).

Pulsed Time	U_1	V_1	W_1	U_2	V_2	W_2	U_3	V_3	W_3	U_4	V_4
-954	-118	39	-199	-110	55	-268	-298	72	-331	-258	54
-984	-116	31	-186	-98	54	-284	-310	-4	-333	-264	61
-984	-118	28	-189	-110	54	-285	-326	-7	-333	-260	60
-987	-120	27	-182	-103	65	-293	-325	22	-349	-265	74
863	-119	31	-176	-118	65	-298	-317	6	-350	-253	82
841	-123	34	-206	-114	48	-310	-316	-12	-353	-256	92
939	-157	23	-210	-114	55	-317	-334	6	-359	-262	98
911	-129	23	-197	-136	60	-319	-334	5	-362	-274	98
911	-105	27	-200	-125	68	-318	-326	-2	-366	-292	106
917	-111	23	-194	-134	82	-329	-320	21	-376	-292	114
923	-101	29	-173	-129	90	-325	-335	38	-394	-304	122
927	-101	26	-165	-118	104	-289	-346	113	-410	-299	123
926	-96	26	-157	-129	119	-287	-336	124	-404	-306	124
934	-102	26	-144	-108	120	-305	-329	95	-392	-326	131
919	-101	23	-140	-92	122	-310	-330	53	-411	-326	130
923	-113	19	-128	-87	112	-304	-341	72	-445	-330	127
930	-129	22	-122	-78	117	-318	-334	44	-461	-336	138
-880	-134	28	-106	-86	126	-325	-310	34	-445	-318	150
-897	-92	30	-91	-82	145	-313	-301	61	-458	-317	154
-921	-96	25	-97	-95	159	-283	-304	88	-454	-331	152
-894	-113	27	-94	-106	156	-268	-318	24	-422	-324	156
-1003	-120	22	-85	-110	140	-245	-298	-16	-392	-326	146
-982	-124	17	-86	-137	139	-240	-288	17	-378	-334	140

meters and finally 4 unspecified data channels, at a data sampling rate of 10 Hz per channel.

The sampling rate may be derived internally from the system clock, (or from the geostore clock). Synchronisation signals are used to inform the computer when data are available and when the beginning of each 10 Hz block occurs. These are used as interrupts within the data collection programme.

The two optional data channels are connected to the common rail, which allows the Apple computer to check that no offset is present in the system as a whole. The unit operates from ± 12 volts DC nominal and has been designed for use in the field powered by two 12 volt car batteries when the main generators are turned off.

5.8.4 Apple II signal processing

The raw data are processed by an Apple II micro-computer which:-

(a) demultiplexes the data using interrupt control of the computer by the synchronisation channel;

(b) converts the analogue data to digital form using a 12 bit A/D converter with 35 microsecond conversion time;

(c) scales the converted data to 8 bit words;

(d) stores the converted Gill and accelerometer data, with the digital Lowne data if required, in the computer memory;

(e) dumps the data from computer memory to floppy disc for permanent storage after 30.25 Kbytes of computer memory has been filled;

(f) checks for errors in the data sequence and print error codes on the monitor;

(g) continues the processing of the data sequence until the disc has been filled.

The discs provided can store 124 Kbytes of memory, thus requiring four complete data transfers to utilise its full storage capacity.

The real time available on the disc depends on the number of data channels stored and the sampling rate. As an example, 16 channels of data storage at a 10 Hz sampling rate gives about 12 minutes of real time per disc. A data transfer takes about 7 seconds and causes a loss of integrity of the

data sequence. For the above example, there is in total a 4% loss of data during the transfers to disc.

5.8.5 Summary of recording systems and costs of equipment at Rivox

Fig. 5.12 shows photographs of some instrumentation. Fig. 5.13 represents a schematic diagram of the main instrumentation and recorder systems adopted. Fig. 5.14 shows the Apple II field recording system set-up. The data logging system has been developed for inputs from the wind sensors and accelerometers to two different recording systems. It is important, therefore, to synchronise the recordings when wind data is collected. Spectral densities of the wind along with acceleration time runs can then be accurately compared for each thinning treatment.

The total value of equipment at the FC mast, including the Lowne anemometers and recording, is estimated to be near £35,000.

5.9 DATA ANALYSIS

5.9.1 The geostore system

After digitising, raw data files are held in EMAS and are analysed in the following way.

(a) Conversion of digital values to wind speed by the application of separate conversion factors for U,V and W data respectively. These factors include allowances for differences in propeller size and in the FM conversion units.

(b) Data correction for non-cosine responses carried out by iterative calculation comparing raw data sequences (W), and data ratios (U, V) against tabulated correction factors, Corrected U,V wind speed data are then combined to give a resultant horizontal wind speed vector (Horst).

(c) Mean and standard deviations of the wind fluctuations are calculated for each U, V and W channel over the full 1 hr data file, and also for ¼ hr blocks.

(d) Mean velocity profiles and turbulence intensity profiles are then calculated and presented in graphic form. (Mean velocity profiles are now available for the unthinned forest (Fig. 5.19(a), (b)) and the first thinning (Fig. 5.20(a), (b)).

To p.165

Photograph 1

Racal 14 channel recorder for 11 Gill channels.

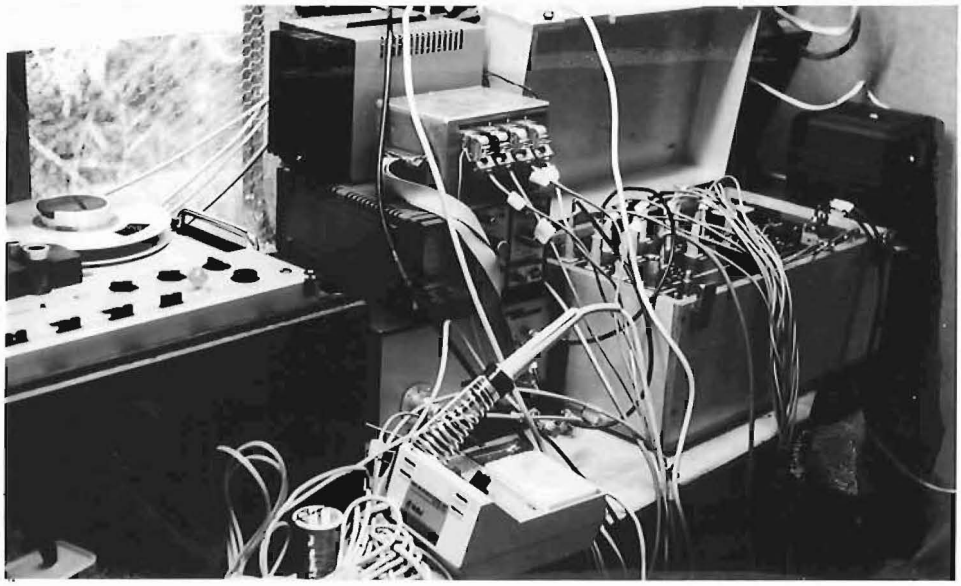

Photograph 2

Racal recorder junction box multiplexer and calibration unit.

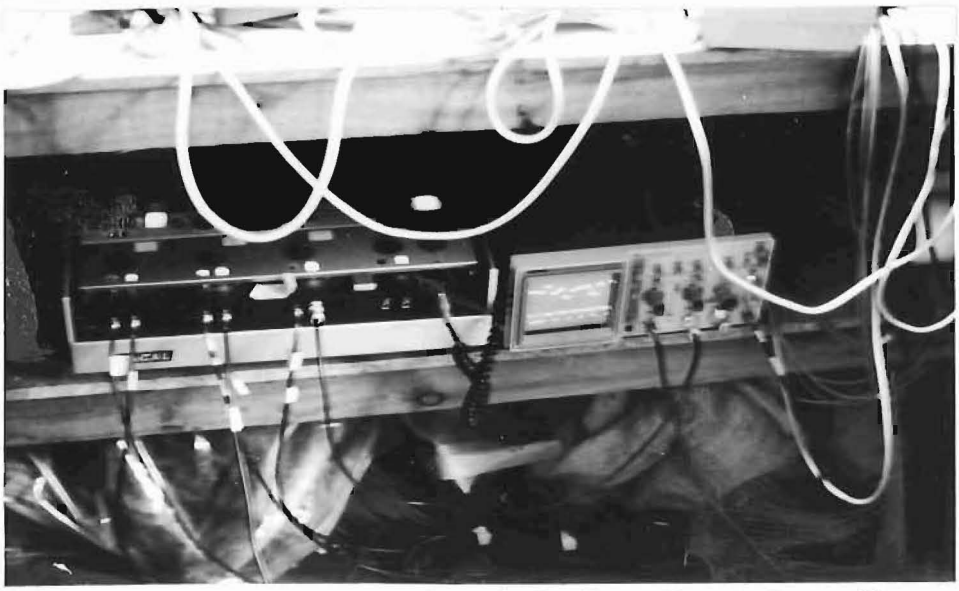

Photograph 3

Gill and Lowne output checks on oscilloscope before multiplexing to recorder.

FIGURE : 5.12 Some of the Field Experiment Recording Equipment.

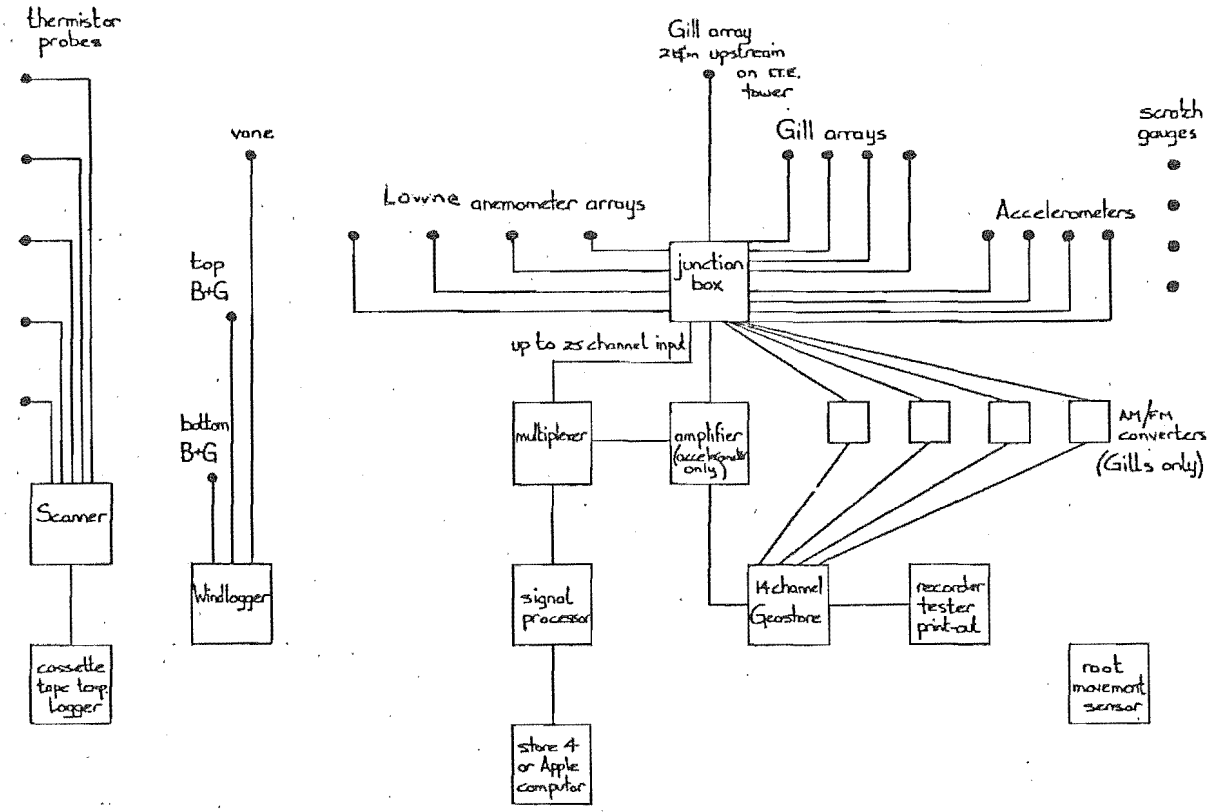

FIGURE 5.13: Complete instrumentation layout.

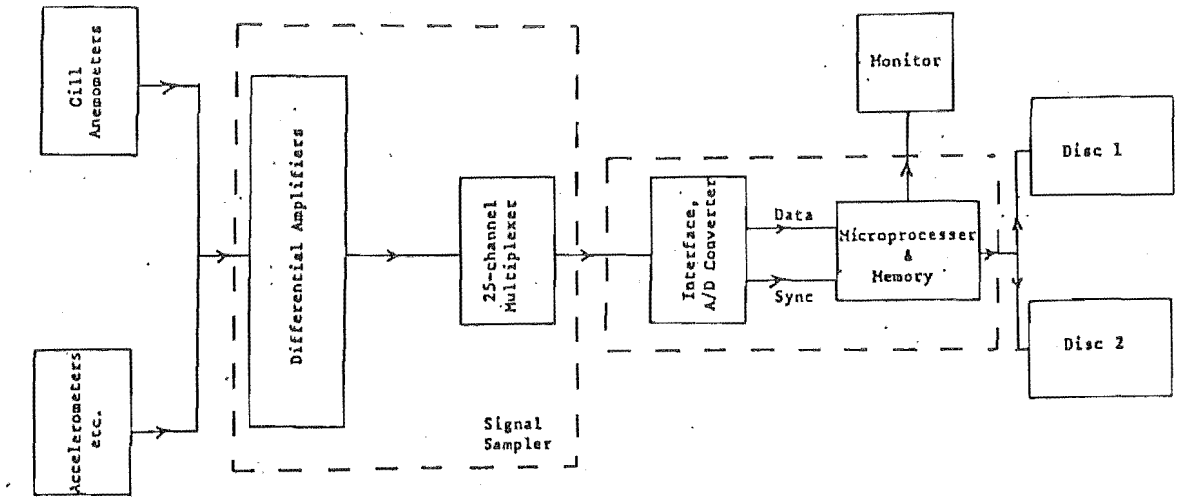

FIGURE 5.14: Apple II data logging system.

(e) Power spectra will be calculated for each sequence of corrected wind speed data, and power spectra printouts will be produced. These spectra have yet to be analysed to determine the nature and extent of spectral frequency shifts between thinnings.

(f) Local Reynolds stresses $\overline{-\rho\ w'\ u'}$ and $\overline{-\rho\ w'\ v'}$ will be available at each height. As the thinning stages are completed in the field experiment, wind frequency alterations from changes in canopy roughness will be calculated and recorded for each thinning density.

5.9.2 The Apple II computer system

After signal conditioning and multiplexing on to the Apple II computer, the stream of data goes to microprocessor memory for intermediate storage before being dumped to disc store. This permits continuous recording of data, with periodic interrupts during transfer from microprocessor memory to disc store. Each disc holds approximately 10 minutes of data derived from 5, 2-minute blocks of uninterrupted data, and with twin disc drive facility it is possible to replace full discs with blanks alternating between disc drives, to obtain long duration recording. The system also has the facility to display recorded data and carry out preliminary analysis of data. A machine language programme recalls the data from the disc to the computer memory for analysis, the position of the data on the disc and the amount recalled being controlled by the operator.

Compiled basic programmes were used for the analysis of the wind structure.

(a) Mean component and resultant velocity profiles are produced after cosine response corrections. The turbulent intensity profiles are calculated from the component results. The results of 8-minute averages from Runs 5 (10. 7.82), 9 (12. 7.82) and 11 (11.11.82) are presented in Figs 5.15 - 5.18.

(b) Spectra are produced using the Cosine Transform method. This enables an estimate of an integral scale to be made, which can be useful in identifying a characteristic time scale for the fluctuations.

The spectra presented are plotted as normalised energy density (Figs 5.21 - 5.24). They are deduced for durations in the range of 3 - 6 mins. (This duration time will be increased to 15 minutes when the main frame computer is used).

5.10 DISCUSSION OF RESULTS

5.10.1 Component mean wind velocity profiles

Fig. 5.15 shows the velocity component profiles for Run 5 table data. The wind has a major v component indicating a wind direction of 205°T, SSW (see Table 5.10).

The Lowne readings are about 10% higher than the Gill measurements. This could be due to the proximity of the Lowne anemometers to the Hiway tower where some speed-up could occur. However, the reliability and accuracy of the mean windspeed components recorded by the Gill and Lowne triads is acceptable.

5.10.2 Component turbulence intensity profiles

Figures 5.16 and 5.18 are the along-wind (x), across-wind (y), and vertical (z) turbulence intensities for Runs 5 and 9. The magnitudes of I_{σ_u}, I_{σ_v} and I_{σ_w} increase downwards to the forest canopy.

Other component turbulence intensity profiles can be found using the data sets presented in Table 5.10. These are the components I_{σ_u}, I_{σ_v}, I_{σ_w} or $\frac{u'}{\bar{U}}$, $\frac{v'}{\bar{V}}$ and $\frac{w'}{\bar{W}}$. Average values of $\frac{u'}{\bar{U}_1}$, and $\frac{v'}{\bar{V}_1}$ in the unthinned forest are 52% (10 data sets) and after the first thinning, are 55% (16 data sets). The average value of $\frac{w'}{\bar{W}}$ before thinning was 38% (5 data sets). After the first thinning $\frac{w'}{\bar{W}}$ increases to 44% (8 data sets). There is a small increase in turbulence intensity levels at tree-top height at the first thinning stage but this result is not yet significant: $\frac{S}{H}$ has only increased from 0.176 to 0.186.

In Figure 5.15 unity standard deviation bars compare the relative response of the Gill and Lowne anemometers to turbulent winds. The Lowne on average responds 40% more to the high turbulence in the canopy than the Gill anemometers do. This is because the Lowne anemometers have a distance constant which is ½ the value of the UV Gill anemometers.

To p.176

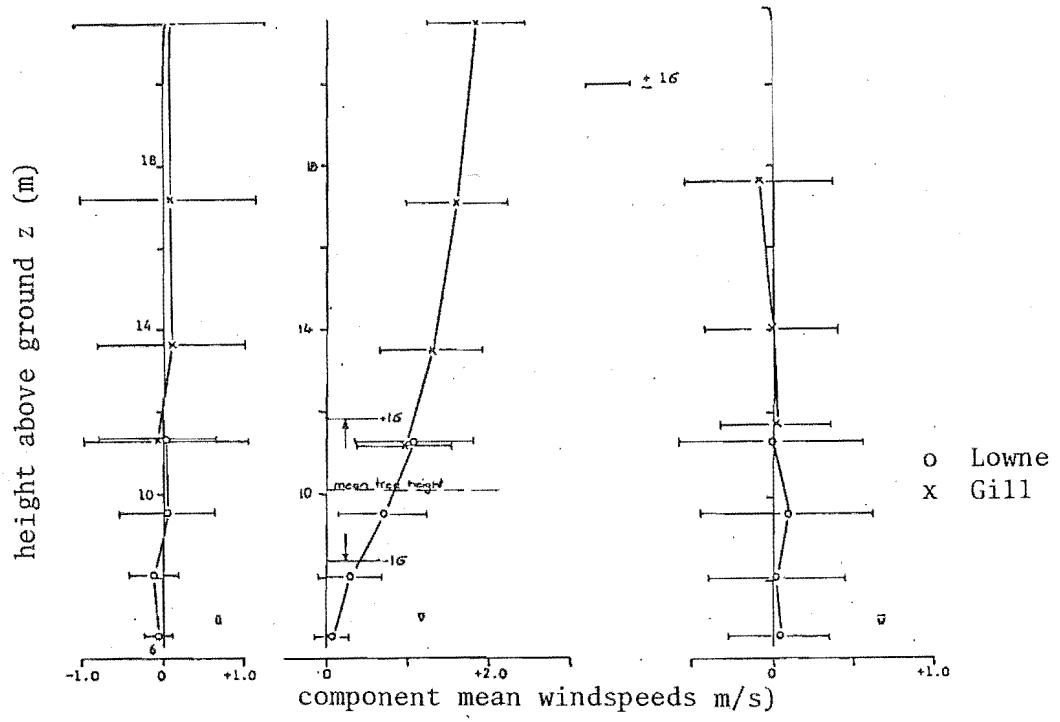

FIGURE 5.15: Calibration mean wind speed component profiles (Run 5)

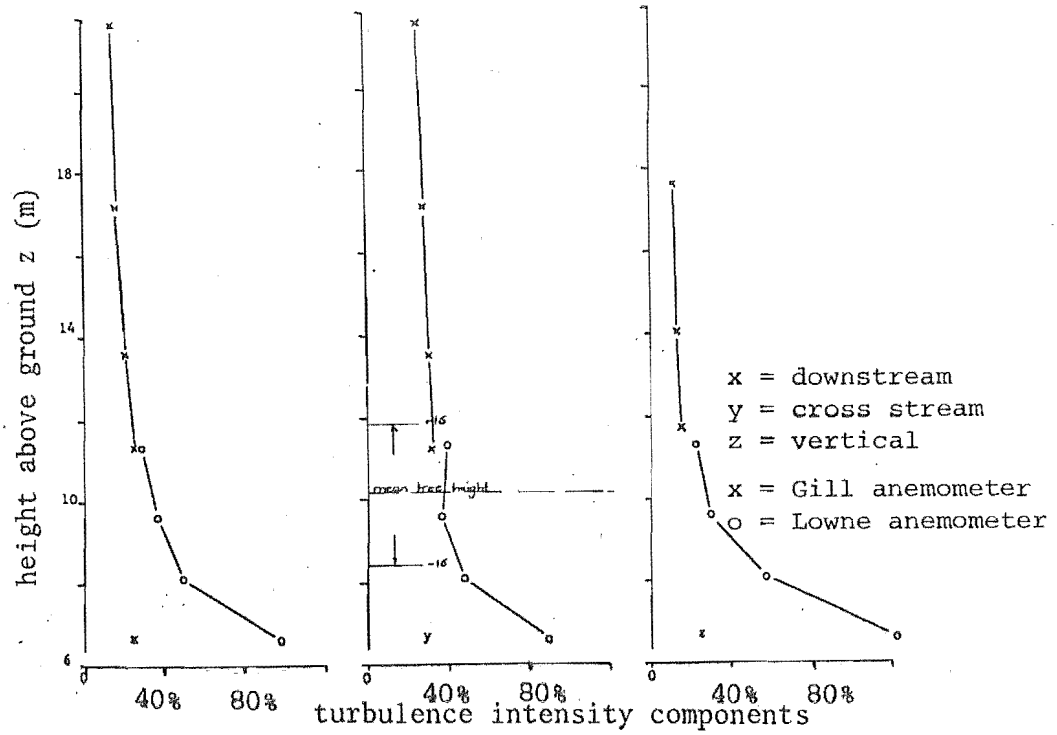

FIGURE 5.16: Calibration turbulence intensity component profiles (Run 5).

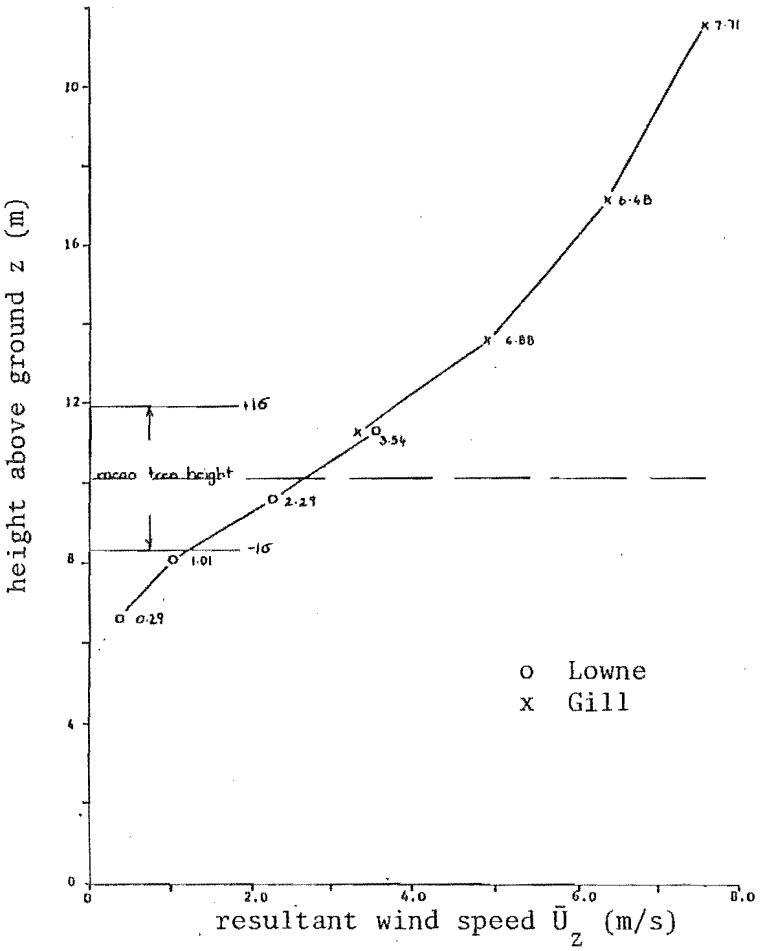

FIGURE 5.17: Calibration resultant mean wind speed profile (Run 9)

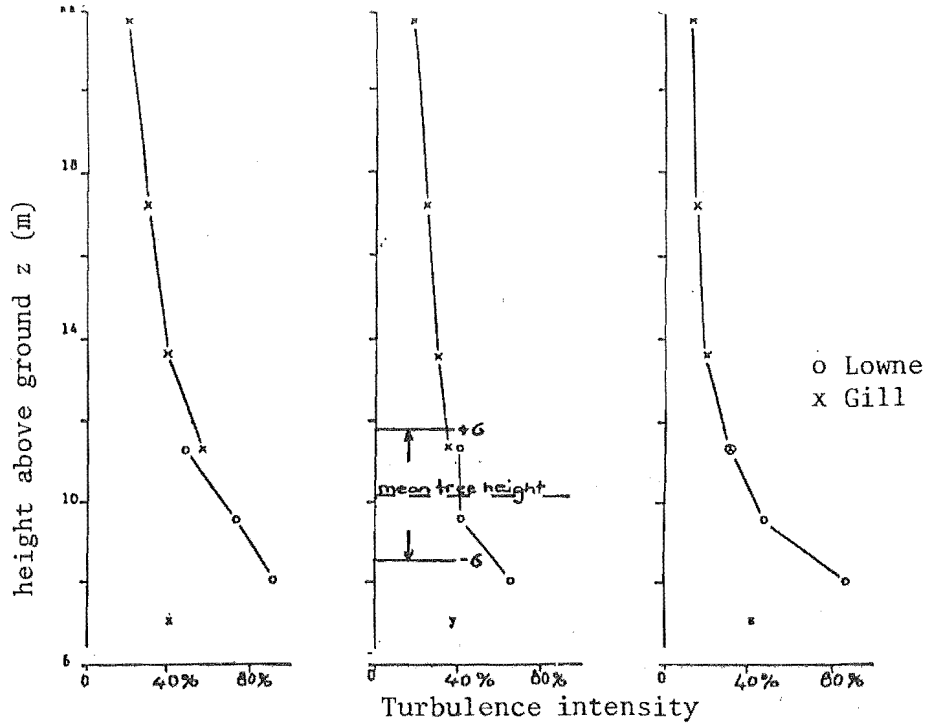

FIGURE 5.18: Calibration turbulence intensity component profiles(Run 9)

(a)

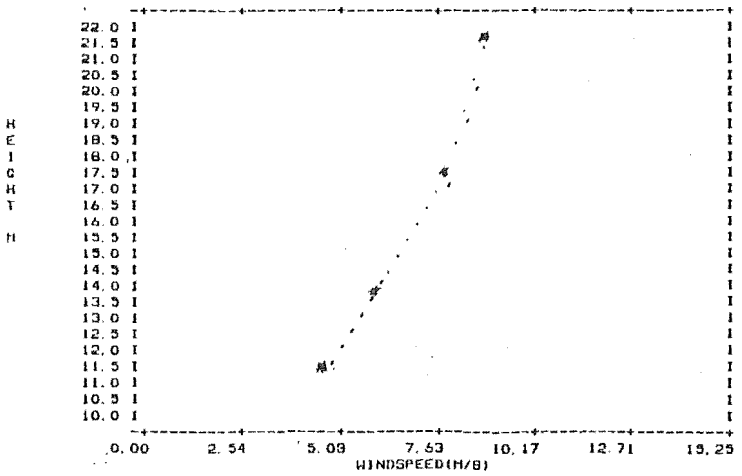

*** PARAMETER ESTIMATES ***

	ESTIMATE	S.E.
D	6.41613	3.24016
USTAR	4.05616	
USTARLNZ	-1.97369	

	DF	SS	MS
RESIDUAL	1	0.059785	0.059785

*** FITTED VALUES AND RESIDUALS ***

UNIT	OBSERVED	FITTED	RESIDUAL
1	4.4600	4.4174	0.0426
2	5.8500	5.9961	-0.1461
3	7.0300	7.6532	0.1768
4	9.0000	9.0733	-0.0733

20 1.63

FIGURE 5.19(a): Resultant mean wind speed profile - unthinned, 2.9.83.

(b)

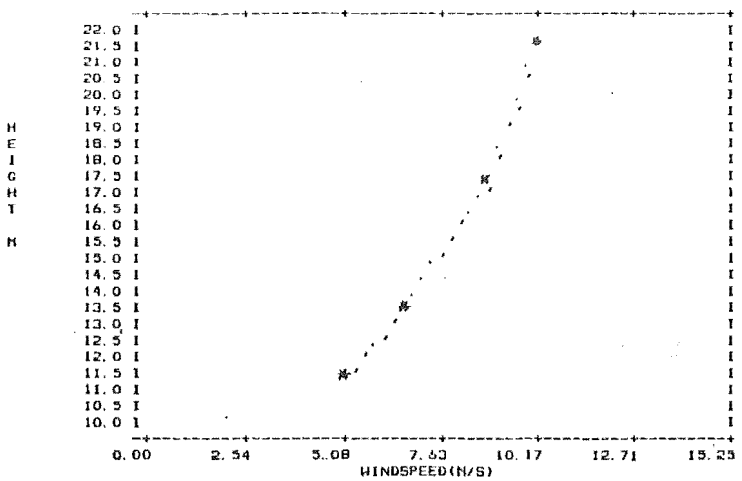

*** PARAMETER ESTIMATES ***

	ESTIMATE	S.E.
D	6.28395	3.14138
USTAR	4.64941	
USTARLNZ	-2.45669	

	DF	SS	MS
RESIDUAL	1	0.063792	0.063792

*** FITTED VALUES AND RESIDUALS ***

UNIT	OBSERVED	FITTED	RESIDUAL
1	5.0300	4.9846	0.0454
2	6.6000	6.7541	-0.1541
3	8.0100	8.6251	0.1849
4	10.1600	10.2362	-0.0762

20 1.70

FIGURE 5.19(b): Resultant mean wind speed profiles - unthinned, 2.9.83.

(a)

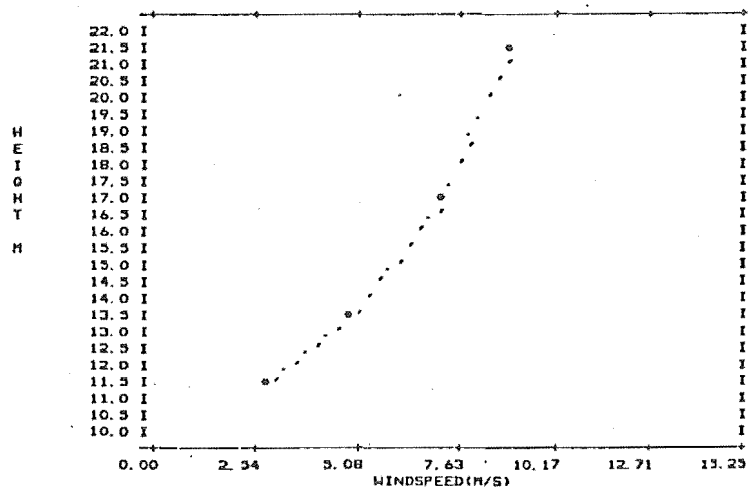

*** PARAMETER ESTIMATES ***

	ESTIMATE	S.E.
D	8.10149	0.62539
USTAR	4.46567	
USTARLNZ	-2.39639	

	DF	SS	MS
RESIDUAL	1	0.008236	0.008236

*** FITTED VALUES AND RESIDUALS ***

UNIT	OBSERVED	FITTED	RESIDUAL
1	2.8300	2.8136	0.0164
2	4.7200	4.7731	-0.0531
3	7.1800	7.1144	0.0656
4	8.9300	8.9590	-0.0290

Z0	1.79
USTAR	1.83
D	8.10

FIGURE 5.20(a): Resultant mean wind speed profiles - first thinning, 27.12.83.

(b)

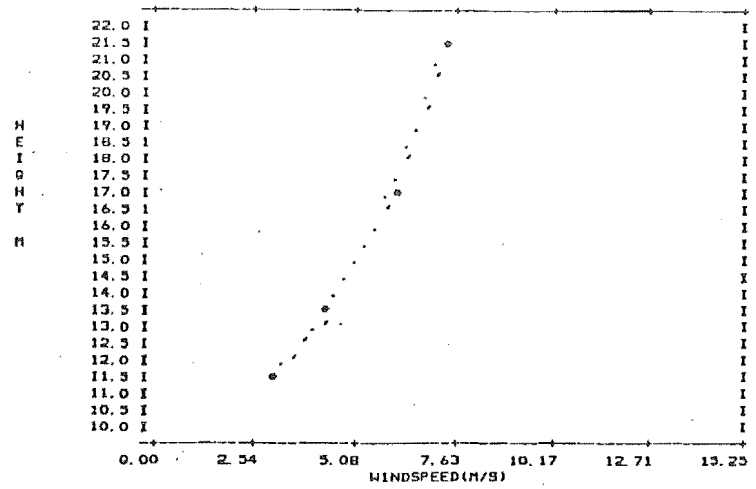

*** PARAMETER ESTIMATES ***

	ESTIMATE	S.E.
D	7.68712	0.25361
USTAR	3.33904	
USTARLNZ	-1.38928	

	DF	SS	MS
RESIDUAL	1	0.000476	0.000476

*** FITTED VALUES AND RESIDUALS ***

UNIT	OBSERVED	FITTED	RESIDUAL
1	3.0400	3.0444	-0.0044
2	4.3900	4.3767	0.0133
3	6.0100	6.0254	-0.0154
4	7.3600	7.3534	0.0065

Z0	1.32
USTAR	1.37
D	7.69

FIGURE 5.20(b): Resultant mean wind speed profiles - first thinning, 27.12.83.

TABLE 5.10(a): Mean and turbulent wind components in the x direction (I.T.E.) and the z direction, (up F.C. Mast).

$\frac{S}{H}$ = 0.176; $\frac{d}{H}$ = 0.70 ; Unthinned Forest

Anemometer Heights	Velocity Components	Run 5 10.7.82	Run 9 4.20 pm 12.7.82	Wind 3 (1 hr)	Wind 4 (1 hr)	Wind 5 (1 hr)	Wind 8A 10.8.83	Wind 8C 10.8.83	BT 8 10.5.83
L = Lowne G = Gill	$\bar{U}_1$	-0.10	(L +0.60 G -0.26	0.86	2.14	0.15	3.50	4.22	3.18
z_1 = 11.25 m; z_1-d = 4.17 m; $\frac{z}{H}$ = 1.1.	u_1'	0.60	(L 0.21 G -0.15	1.02	1.57	1.41	2.42	2.72	1.22
	$\bar{V}_1$	0.92	(L 3.44 G 3.62	2.29	2.35	3.62	3.36	3.69	4.95 ?
	v_1'	0.73	(L 1.46 G 1.45	1.21	1.52	2.10	2.09	2.42	1.45
	$\bar{W}_1$	0.01	(L 0.40 G -	-	-	-	-	-	-0.09
	w_1'	0.35	-	-	-	-	-	-	0.05
z_2 = 13.55 m; z_2-d = 6.47 m; $\frac{z}{H}$ = 1.35	$\bar{U}_2$		0.15	1.88	3.80	0.49	5.73	6.79	3.35
	u_2'		0.06	1.14	1.84	1.62	2.86	3.12	1.69
	$\bar{V}_2$		4.88	3.13	3.47	4.95	5.30	5.24	7.36 ?
	v_2'		1.56	1.45	2.07	2.35	2.50	2.91	1.18
	$\bar{W}_2$		0.25	0.28	0.27	0.04	0.52	0.58	0.57
	w_2'		-	0.72	1.09	1.07	1.64	1.87	0.04
z_3 = 17.15 m; z_3-d =10.07 m; $\frac{z}{H}$ = 1.7	$\bar{U}_3$		0.50				7.53	9.17	3.92
	u_3'		0.16				3.14	3.39	1.47
	$\bar{V}_3$		6.46				6.74	7.47	8.34
	v_3'		1.68	AN3 and AN4 ?	AN3 and AN4 ?	AN3 and AN4 ?	3.14	3.35	1.27
	$\bar{W}_3$		0.45				0.37	0.44	0.61
	w_3'		-				1.76	2.01	1.11
z_4 = 21.7 m; z_4-d = 14.57 m; $\frac{z}{H}$ = 2.14	$\bar{U}_4$		0.85	Data Reversed Between	Data Reversed between	Data Reversed between	8.00	9.84	3.86
	u_4'		0.19				3.08	3.24	1.34
	$\bar{V}_4$		7.66				Est. 6.91	8.06	18.42 ?
	v_4'		1.53				-	-	-
	$\bar{W}_4$								
	w_4'								

TABLE 5.10(b): Mean and turbulent wind components in the x direction (I.T.E.) and the z direction, (up F.C. Mast).

$\frac{S}{H}$ = 0.176; Unthinned forest

Anemometer Heights	Velocity Components	BT 11 2.9.83	BT 7 10.5.83	A 2 2.9.83	BT 14*	BT 15* 4.9.83	A 3 3.9.83
z_1 = 11.25 m; z_1-d = 4.17 m; $\frac{z}{H}$ = 1.1.	$\bar{U}_1$	2.35	2.45	2.64	2.59	1.68	2.55
	u_1'	1.49	1.43	1.82	2.09	1.57	1.65
	$\bar{V}_1$	1.20	2.69	0.12	3.58	2.53	0.47
	v_1'	1.44	1.71	1.37	2.24	1.91	1.17
	$\bar{W}_1$	-0.36	-0.09	0.29	0.32	-0.009	0.53
	w_1'	0.79	0.05	1.24	1.61	1.38	1.19
z_2 = 13.55 m; z_2-d = 6.47 m; $\frac{z}{H}$ = 1.35	$\bar{U}_2$	3.48	2.32	4.15	4.35	2.74	4.72
	u_2'	1.78	1.69	2.19	2.42	2.21	2.32
	$\bar{V}_2$	1.96	5.93	-0.23	5.57	3.93	0.06
	v_2'	1.60	1.65	1.57	2.84	2.34	1.33
	$\bar{W}_2$	-0.44	0.57	0.36	0.53	0.21	0.47
	w_2'	0.81	0.02	1.33	1.85	1.42	1.17
z_3 = 17.15 m; z_3-d =10.07 m; $\frac{z}{H}$ = 1.7	$\bar{U}_3$	4.55	3.06	5.98	5.89	4.24	6.57
	u_3'	1.91	1.63	2.28	2.75	2.38	2.27
	$\bar{V}_3$	2.32	7.35	-0.22	8.03	5.71	0.92
	v_3'	1.80	1.53	1.85	3.08	2.71	1.65
	$\bar{W}_3$	-0.89	-0.22	0.52	0.21	0.03	0.45
	w_3'	0.38	1.16	1.42	1.82	1.43	1.15
z_4 = 21.7 m; z_4-d = 14.57 m; $\frac{z}{H}$ = 2.14	$\bar{U}_4$	5.02	2.90	7.22	6.92	5.29	7.13
	u_4'	1.96	1.18	2.28	2.48	2.09	1.90
	$\bar{V}_4$	2.70	18.34?	-0.04	9.96	8.04	0.11
	v_4'	1.61		1.91	3.05	2.27	1.56
	$\bar{W}_4$			0.75	0.77	0.40	0.72
	w_4'			1.58	1.87	1.46	1.30
z_{ITE} = 13.55 m; z_{ITE}-d = 6.47; $\frac{z}{H}$ = 1.34	$\bar{U}_{ITE}$			3.72	3.71	3.15	4.71
	u_{ITE}'			2.34	2.32	2.01	2.20
	$\bar{V}_{ITE}$			0.62	7.20	7.11	0.53
	v_{ITE}'			1.59	3.01	2.86	1.55
	$\bar{W}_{ITE}$			-0.10	0.44	0.36	-0.38
	w_{ITE}'			1.11	1.55	1.41	1.25

TABLE 5.10(c): Mean and turbulent wind components in the x direction (I.T.E.) and the z direction, (up F.C. Mast).

$\frac{S}{H}$ = 0.187 : First thinning at Rivox

Anemometer Heights	Velocity Components	21 27.12.83	22 27.12.83	23 27.12.83	BT 770 X 3 31.12.83	X 4 31.12.83	X 5 31.12.83	SW Gale 31.12.83
z_1 = 11.46 m; $\frac{z}{H}$ = 1.06	$\bar{U}_1$	1.77	1.83	1.94	2.05	2.62	3.77	3.40
	u_1'	1.44	1.68	1.59	1.93	1.84	2.79	2.68
	$\bar{V}_1$	2.47	2.15	2.51	3.09	2.53	3.23	3.53
	v_1'	1.56	1.39	1.81	2.15	1.89	2.34	2.49
	$\bar{W}_1$	0.36	-0.02	0.13	0.04	0.31	0.45	0.31
	w_1'	1.22	1.43	1.39	1.54	1.77	2.26	2.19
z_2 = 13.31 m; $\frac{z}{H}$ = 1.23	$\bar{U}_2$	2.99	2.87	3.00	3.53	4.71	6.37	5.64
	u_2'	1.75	2.31	2.32	2.39	2.50	3.77	3.49
	$\bar{V}_2$	3.22	3.75	3.68	4.67	3.77	4.39	4.91
	v_2'	1.95	1.85	2.15	2.51	2.23	2.89	3.04
	$\bar{W}_2$	0.36	0.19	0.26	0.32	0.35	0.49	0.37
	w_2'	1.28	1.61	1.43	1.83	1.71	2.28	2.27
z_3 = 16.90 m; $\frac{z}{H}$ = 1.56	$\bar{U}_3$	3.73	4.12	3.95	4.99	6.41	5.77	7.59*
	u_3'	1.93	2.17	2.38	2.43	2.76	3.71	3.16†
	$\bar{V}_3$	4.71	5.88	5.49	7.32	6.25	7.72	4.91*
	v_3'	1.90	2.21	2.43	2.83	2.84	2.83	3.04†
	$\bar{W}_3$	0.10	0.04	0.06	0.11	0.08	0.23	0.37
	w_3'	1.28	1.57	1.44	1.77	1.75	2.29	2.27
z_4 = 21.40m; $\frac{z}{H}$ = 1.98	$\bar{U}_4$	4.14	4.79	4.45	5.62	7.20	9.28	8.03
	u_4'	1.83	1.86	2.00	2.26	2.31	2.88	3.07
	$\bar{V}_4$	6.08	7.54	7.17	9.51	7.68	9.47	9.78
	v_4'	1.94	2.36	2.22	2.69	2.64	3.39	3.50
	$\bar{W}_4$	0.45	0.27	0.23	0.41	0.48	0.65	0.76
	w_4'	1.38	1.42	1.53	1.81	1.84	2.36	2.03
z_{ITE} = ?	$\bar{U}_{ITE}$	2.66	2.24	2.58	2.41	4.47	6.40	4.46
	u_{ITE}'	1.70	1.47	1.66	1.68	2.39	3.07	2.47
	$\bar{V}_{ITE}$	5.69	5.80	6.48	7.58	6.71	8.22	8.25
	v_{ITE}'	1.94	2.31	2.76	2.89	2.72	3.14	3.17
	$\bar{W}_{ITE}$	0.01	0.30	0.22	0.46	0.20	0.03	0.26
	w_{ITE}'	1.22	1.19	1.23	1.34	1.40	1.86	1.62

*& * appear to be reversed
†& † appear to be reversed

TABLE 5.11(a): Resultant wind speeds, directions and derived parameters: Rivox unthinned.

$\frac{S}{H}$ = 0 176; $\frac{d}{H}$ = 0.70 (assumed). († = Figures 5.15 - 5.20)

Anemometer Heights	Wind Parameters	Run 5 † 10.7.83	Wind 3 (1 Hr)	Wind 4 (1 Hr)	Wind 5 (1 Hr)	Wind 8A 10.8.83	Wind 8C 10.8.83	BT 11 2.9.83	A2 2.9.83	A3 3.9.83	BT † 14 4.9.83	BT † 15 4.9.83
(L = Lowne) (G = Gill)	$\bar{U}_{R_1}$ (m/s)	(L = 1.04 (G = 0.93	2.45	3.18	3.62	4.85	5.61	2.64	2.64	2.59	4.42	3.04
z_1 = 11.25 m	u_{R_1}' (m/s)	(L = 0.75 (G = 0.57	1.59	2.18	2.53	3.19	3.64	2.07	2.28	-	3.06	-
z_1-d = 4.17 m	$(u'/\bar{U})_{R_1}$ %	(L = 71 (G = 61	65	69	70	66	65	78?	86	78	69	76
$\frac{z}{H}$ = 1.10	°T	(L = 205 (G = 199	219	240	196	240	254	233?	292	285	241	245
	$°\theta_s$	---	--	--	--	--	--	-8°?	--	-11°?	-4°	0°
z_2 = 13.55 m	$\bar{U}_{R_2}$ (m/s)	1.31	3.65	5.15	4.97	7.81	8.58	3.99	4.16	4.72	7.07	4.79
z_2-d = 6.47 m	u_{R_2}' (m/s)	0.67	1.84	2.75	2.86	3.80	4.27	2.30	2.69	2.67	3.73	3.22
$\frac{z}{H}$ = 1.35	$(u'/\bar{U})_{R_2}$ %	51	50	53	58	49	49	60	65	57	53	67
	°T	206	229	246	204	245	250	266	294	292	243	240
	$°\theta_s$	--	-4½°	-3°	-½°	-4°	-4°	-6°	--	-5½°	-4°	-2½°
z_3 = 17.15 m	$\bar{U}_{R_3}$ (m/s)	1.60				10.11	11.85	5.11	5.98	6.63	9.96	7.11
z_3-d = 10.07 m	u_{R_3}' (m/s)	0.66				4.44	4.77	2.62	2.94	2.81	4.13	3.61
$\frac{z}{H}$ = 1.70	$(u'/\bar{U})_{R_3}$ %	41				44	40	51	49	42	41	51
	°T	205				246	249	268	--	287	241	239
	$°\theta_s$	--	AN_3 and AN_4 reversed?	AN_3 and AN_4 reversed?	AN_3 and AN_4 reversed?	-2°	-2°	-7°	--	0°	-1°	0°
z_4 = 21.7 m	$\bar{U}_{R_4}$ (m/s)	1.86						5.70	7.22	7.13	12.13	9.62
z_4-d = 14.57 m	u_{R_4}' (m/s)	0.65						2.54	2.97	2.46	3.93	3.09
$\frac{z}{H}$ = 2.15	$(u'/\bar{U})_{R_4}$ %	35				AN_4 u/s.	AN_4 u/s.	45	41	34	32	32
	°T	205						267	295	186?	240	228
	$°\theta_s$	--						--	--	-6°	-3½°	-2½°
z_{ITE} = 13.55 m ?	$\bar{U}_{R_{ITE}}$ (m/s)					10.47	10.39	--	3.77	4.74	8.10	7.78
z_{ITE}-d = 4.17 m	$u_{R_{ITE}}$ (m/s)	AN_{ITE}	not fitted			4.28	4.33	--	2.75	2.64	3.79	3.50
$\frac{z}{H}$ = 1.35	$u'/\bar{U}_{R_{ITE}}$ %					41	42	--	74?	57	47	45
	°T					248	247	--	286	--	243	240
	$°\theta_s$					--	--	--	--	--	-3°	-2½°
Derived Parameters	z_o' (m)	0.73	1.70	2.00	1.20	1.65	1.70	1.40	2.14	1.95	2.00	2.25
	z_o'/H	0.07	0.17	0.20	0.12	0.16	0.17	0.14	0.21	0.19	0.20	0.22
	$\bar{U}_*$prof(m/s)	0.25	1.14	1.84	1.43	2.28	2.72	1.04	1.48	1.54	2.52	1.93
	C_{f_H}	0.26	1.09	1.98	0.56	0.96	1.13	0.57	--	--	--	--
	d (m)	--	--	--	--	--	--	--	--	--	--	--
	d/H	0.70	0.70	0.70	0.70	0.70	0.70	0.70	0.70	0.70	0.70	0.70
	Wind sector	SSW	SW	WSW	SSW	WSW	WSW	WSW	WNW	WNW	WSW	WSW

TABLE 5.11(b): Resultant wind speeds, directions and derived parameters: Rivox thinned.

$\frac{S}{H}$ = 0.187. († = Figures 5.15 - 5.20)

Anemometer Heights	Wind Parameters	Run 21 † X1 27.12.83	Run 22 X2 27.12.83	Run 23† X3 27.12.83	BT770 † X3 27.12.83	Run 25 31.12.83	Run 26 Gale 31.12.83	Run 27 Gale 31.12.83	Averages
z_1 = 11.46 m; z_1-d_{av} = 3.88 m; $\frac{z}{H}$ = 1.06	$\bar{U}_{R_1}$ (m/s)	3.04	2.83	3.17	3.71	3.64	4.96	4.91	I_{σ_u} 71.2% ± 5% (17 sets)
	u_{R_1}' (m/s)	2.12	-	2.41	2.89	2.64	3.64	3.67	
	$(u'/\bar{U})_{R_1}$ %	70	77	76	78	72	73	75	74.4% (7 sets)
	°T	241	245	243	239	251	254	249	
	$^\circ\theta_s$	-7°	0°	-2½°	-½°	-5°	-5°	-3½°	
z_2 = 13.31 m; z_2-d_{av} = 5.73 m; $\frac{z}{H}$ = 1.23	$\bar{U}_{R_2}$ (m/s)	4.39	4.72	4.75	5.85	6.06	7.74	7.48	I_{σ_u} 58.6% ± 7% (18 sets
	u_{R_2}' (m/s)	2.62	2.96	3.16	3.47	3.35	4.75	4.63	
	$(u'/\bar{U})_{R_2}$ %	60	62	67	59	55	61	62	60.90% (7 sets)
	°T	248	242	244	242	256	259	254	
	$^\circ\theta_s$	-4½°	-2½°	-3°	-3°	-3½°	-3½°	-3°	
z_3 = 16.9 m; z_4-d_{av} = 9.32 m; $\frac{z}{H}$ = 1.56	$\bar{U}_{R_3}$ (m/s)	6.01	7.18	6.76	8.86	8.95	11.68	10.95	I_{σ_u} 44.3% ± 4% (22 sets)
	u_{R_3}' (m/s)	2.71	3.10	3.40	3.73	3.96	4.67	5.07	
	$(u'/\bar{U})_{R_3}$ %	45	43	50	42	44	40	46	44.3% (7 sets)
	°T	243	240	240	239	251	242	238	
	$^\circ\theta_s$	-1°	-½°	-½°	-1°	-½°	-1°	-2°	
z_4 = 21.4 m; z_4-d_{av} = 13.82 m; $\frac{z}{H}$ = 1.98	$\bar{U}_{R_4}$ (m/s)	7.36	8.93	8.43	11.05	10.53	13.26	12.65	I_{σ_u} 34% ± 2% (11 sets)
	u_{R_4}' (m/s)	2.67	3.00	2.99	3.51	3.51	4.45	4.66	
	$(u'/\bar{U})_{R_4}$ %	36	34	35	32	33	34	37	34.4% (7 sets)
	°T	223	222	230	230	243	244	229	
	$^\circ\theta_s$	-3½°	-2°	-1½°	-2°	-2½°	-3°	-3½°	
z_{ITE} = ?; $z_{ITE}-d$ = ?; $\frac{z}{H}$ = ?	$\bar{U}_{R_{ITE}}$ (m/s)	6.28	6.22	6.97	7.95	8.06	10.42	9.38	
	$u_{R_{ITE}}$ (m/s)	2.58	2.74	3.22	3.34	3.62	4.39	5.05	
	$u'/\bar{U}_{R_{ITE}}$ %	41	44	46	42	45	42	54	
	°T	230	226	227	223	239	243	233	
	$^\circ\theta_s$	0°	-3°	-2°	-3½°	-1½°	0°	-1½°	
Derived Parameters	z_o' (m)	1.52	1.79	3.37?	1.97	0.79	0.71	0.99	1.63(21 sets)
	z_o'/H	0.14	0.17	0.31?	0.18	0.07	0.07	0.09	0.15 (22 sets)
	$\bar{U}_*$ prof(m/s)	1.37	1.83	2.24	2.34	1.60	1.96	2.35	
	C_{f_H}	0.56	1.45	1.33	1.62	-	0.98	1.19	1.05 (10 sets)
	d (m)	7.69	8.10	5.48?	7.70	9.47	9.26	9.49	
	d/H	0.71	0.75	0.51?	0.71	0.87	0.88	0.74	0.74 (10 sets)
	Wind sector	WSW	WSW	WSW	WSW	WSW	WSW	WSW	

5.10.3 Resultant mean wind speed profiles

Some resultant mean wind speed profiles calculated from the component mean windspeeds are presented in Figs 5.17 and 5.19 for the unthinned stage and in Fig. 5.20 for the first thinning. A complete summary of the resultant wind vectors is given in Table 5.11 and all except two are from the SW - SSW sector.

The azimuth angle of the resultant horizontal vector and the mean vertical velocity vector (+ve downwards), reflect the contour slope of the topography and forest cover. The altitude angles do correlate with the surface topography slopes (Fig. 5.8). The two NW profiles reflect the effects of the upstream topography, especially Hangingshaw Hill (469 m) (Fig. 5.4).

Equilibrium conditions appear to exist from the ITE mast for 214 m to the FC mast. Turbulence intensity levels "at $\frac{z}{H} = 1.7$" are much the same. There is some difference in mean wind speeds, possibly because the anemometer array at the ITE mast has been shifted upwards.[1]

5.10.4 Rivox aerodynamic roughness, zero-plane displacement, and friction velocities

From the resultant mean wind speed profiles z_o' , d and $\bar{U}_*$ values were obtained:-

(a) graphically, using the log-linear relationship for neutral atmospheres (Ch. 3), assuming d = 0.70 H;

(b) by computer plotting, using the same relationship but obtaining the best fits to the logarithmic wind profiles for all three parameters, z_o' , d and $\bar{U}_*$.

The mean values of z_o' for the unthinned forest and the first thinning are much the same. The mean value of z_o' for 21 sets of data was 1.63 m or $\frac{z_o'}{H}$ is 0.15. This compares favourably with $\frac{z_o'}{H} \simeq 0.11$ obtained in Chapter 3.

From 10 sets of data the mean value of $\frac{d}{H}$ was 0.74. This is in agreement with values found by Thom and by Smith and Oliver, but is slightly higher than the average of 0.71 found in other research (Table 3.2, Chapter 3). Kondo, Counihan and Shaw and Pereira showed that $\frac{d}{H}$ varied with z_o'. At the close spacings tested ($\frac{S}{H} = 0.176$ and 0.186), $\frac{d}{H}$ values should be above the average. This is the case.

---

1. Forestry Commission yet to verify.

From 21 sets of resultant mean windspeed profiles, the log-linear relationship for neutral stability produces a mean friction velocity of 1.63 m/s. There is a considerable spread of values (0.25 to 2.72). $\bar{U}_*$ is related to mean wind speed (Bache & Unsworth). However, Högström suggests $\frac{\sigma_{u_R}}{\bar{U}_*}$ is almost independent of windspeed and temperature at 2.5, while both Mayer and Holbo suggest that for forests $\frac{\sigma_{u_R}}{\bar{U}_*}$ is near 2.0. $\frac{\sigma_{u_R}}{\bar{U}_*}$ from 14 sets of data at tree-top level is $\frac{2.71}{1.63} = 1.66$; at $\frac{z}{H} = 2.14$, the logarithmic mean wind profile is still observed, and $\frac{\sigma_{u_R}}{\bar{U}_*}$ for 12 sets of data is $\frac{3.32}{1.63} = 2.03$. This agrees with the result obtained by Mayer (1981). Actual values of the resultant turbulent windspeed, σ_{u_R}, do not decay significantly with height; 3.32 m/s to 2.71 m/s is only a 16% reduction from $\frac{z}{H} = 2.14$ to $\frac{z}{H} = 1.1$. A common assumption is that turbulent velocities are constant with height change. This appears to be the case for these measurements at Rivox with the trees closely spaced ($\frac{S}{H} \simeq 0.18$) but may not be true for the next two thinnings since z_o' should increase (Fig. 3.5) and σ_{u_R} with it.

5.10.5 Aerodynamic roughess of Rivox and Kielder compared

Comparisons of z_o' at Kielder (6H) with z_o' at Rivox (> 20 H) are given in Table 5.12.

The mean value of $\frac{z_o'}{H}$ for Kielder is 0.10 where $\frac{S}{H}$ is 0.38, and the mean value for Rivox is 0.15 where $\frac{S}{H}$ is 0.18. This suggests that equilibrium is reached much sooner than some research work indicates (Fig. 4.1).

5.10.6 Rivox turbulent energy spectra

Spectra produced from the Apple II process are presented in Figures 5.21 - 5.24. (Spectra curves from the main frame EMAS computer are not yet available). For the unthinned and first thinning forest surfaces, spectra are compared with other spectra over full scale and model forests and with other crops able to sway in the wind (Figs 7.3; 7.4).

The spectra are derived from 350 seconds of data and therefore the variance of these spectra will be above normal and reduce the normalised levels of $\frac{S_n}{u^2}$ to below those commonly accepted. However the normalised kinetic energy levels in the inertial range are the same along-wind, across-wind and vertically, which means that the analysis method and instruments are functioning correctly. (Note: spectra shapes at the lower frequency end of the spectra do not coincide). The slopes of the log-log spectra plots of energy density versus wind frequency are close to $-\frac{5}{3}$ as predicted by Kolmogrov and measured by Uchijima and Wright, Maitani, and Finnigan. There are no humps of

To p.181

TABLE 5.12: Kielder and Rivox: Aerodynamic roughness and shear stress coefficients compared.

Kielder: $\frac{S}{H} \approx 0.38$; $\frac{z_o'}{H} = 0.10$; $\alpha = 0.22$; $z_o = 0.2$ m

Run	Set 1	Set 2	Set 3	Set 4	Set 1	Set 2	Set 3	Set 4
$\bar{U}_o$(m/s) (-9H)	8.55	8.90	7.45	9.65	8.55	8.90	7.45	9.65
$\bar{U}_{*p} = \bar{U}_{*p}$(m/s) (1H)	← Mast 2 → 3.32	2.93	1.86	2.95	← Mast 4 → 1.57	1.78	1.57	3.82
$\frac{z_o'}{H}$ (1H)	0.17	0.13	0.09	0.10	0.03	0.17	0.08	0.17
C_{f_o} (1H)	0.302	0.217	0.125	0.187	0.061	0.080	0.089	0.313
$\bar{U}_{*p}$ (m/s) (6H)	← Mast 3 → 0.70	1.94	1.27	2.07	← Mast 5 → 1.56	1.86	1.54	2.16
$\frac{z_o'}{H}$ (6H)	0.07	0.06	0.07	0.13	0.08	0.15	0.08	0.14
C_{f_o} (6H)	0.013	0.095	0.058	0.092	0.067	0.087	0.085	0.100

Rivox: $\frac{S}{H} = 0.176$; $\frac{z_o'}{H} = 0.16$; $\frac{d}{H} = 0.70$. $\frac{\bar{U}_H}{\bar{U}_o} = 0.30$. (Oxford)

$\frac{S}{H} = 0.186$; $\frac{z_o'}{H} = 0.15$; $\frac{d}{H} = 0.074$. $\frac{\bar{U}_H}{\bar{U}_o} = 0.30$. (Oxford)

Run	9	← 2 Arrays → Wind 3	Wind 4	Wind 5	Wind 8 A.A.	Wind 8 C.A.	21	22	23	BT 770	26	27
$\bar{U}_z$(m/s)	4.88	3.65	5.15	4.97	7.81	8.58	4.90	5.40	5.30	6.75	8.90	8.40
$\bar{U}_H$(m/s)	2.71	1.55	1.85	2.70	3.30	3.60	2.65	2.60	2.80	2.60	2.80	3.05
Sampling Rate	10	20	20	20	10	10	10	10	10	10	10	10
Sampling Time	480	4000	4000	4000	4000	4000	4000	350	350	350	350	350
Wind Direction	S	SSW	SW	SSW	SW	SW	SSW	SSW	SSW	SSW	SW	SW
$\bar{U}_{*p}$	1.34	1.14	1.84	1.43	2.28	2.70	1.37	1.83	2.24	2.34	1.96	1.91
$\bar{U}_{*H}$	0.93	1.14	1.84	1.43	2.28	2.70	1.37	1.69	2.24	2.34	1.96	1.91
$\frac{z_o'}{H}$	0.15	0.17	0.20	0.12	0.16	0.17	0.14	0.17	0.31	0.18	0.07	0.08
$\frac{z_o''}{H}$	0.09	0.17	0.20	0.12	0.16	0.17	0.14	0.15	0.31	0.18	0.07	0.08
C_{f_p}	0.15	0.20	0.26	0.17	0.17	0.20	0.16	0.23	0.36	0.24	0.10	0.10
C_{f_H}	0.24	1.09	1.98	0.56	0.96	1.13	0.53	0.85	1.28	1.62	0.98	0.78
C_{f_o}(est.)	0.02	0.10	0.18	0.05	0.09	0.10	0.05	0.08	0.12	0.15	0.09	0.07

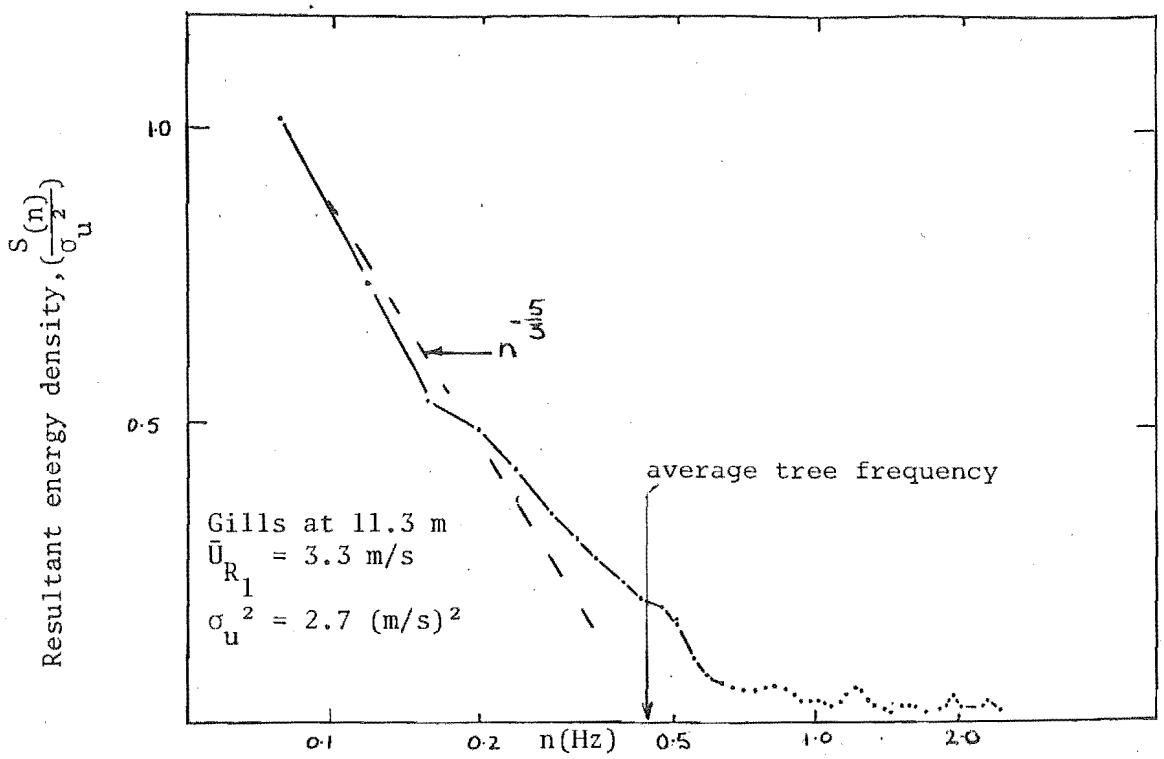

FIGURE 5.21: Energy density distribution at 11.3 m (Run 9, 12.7.82).

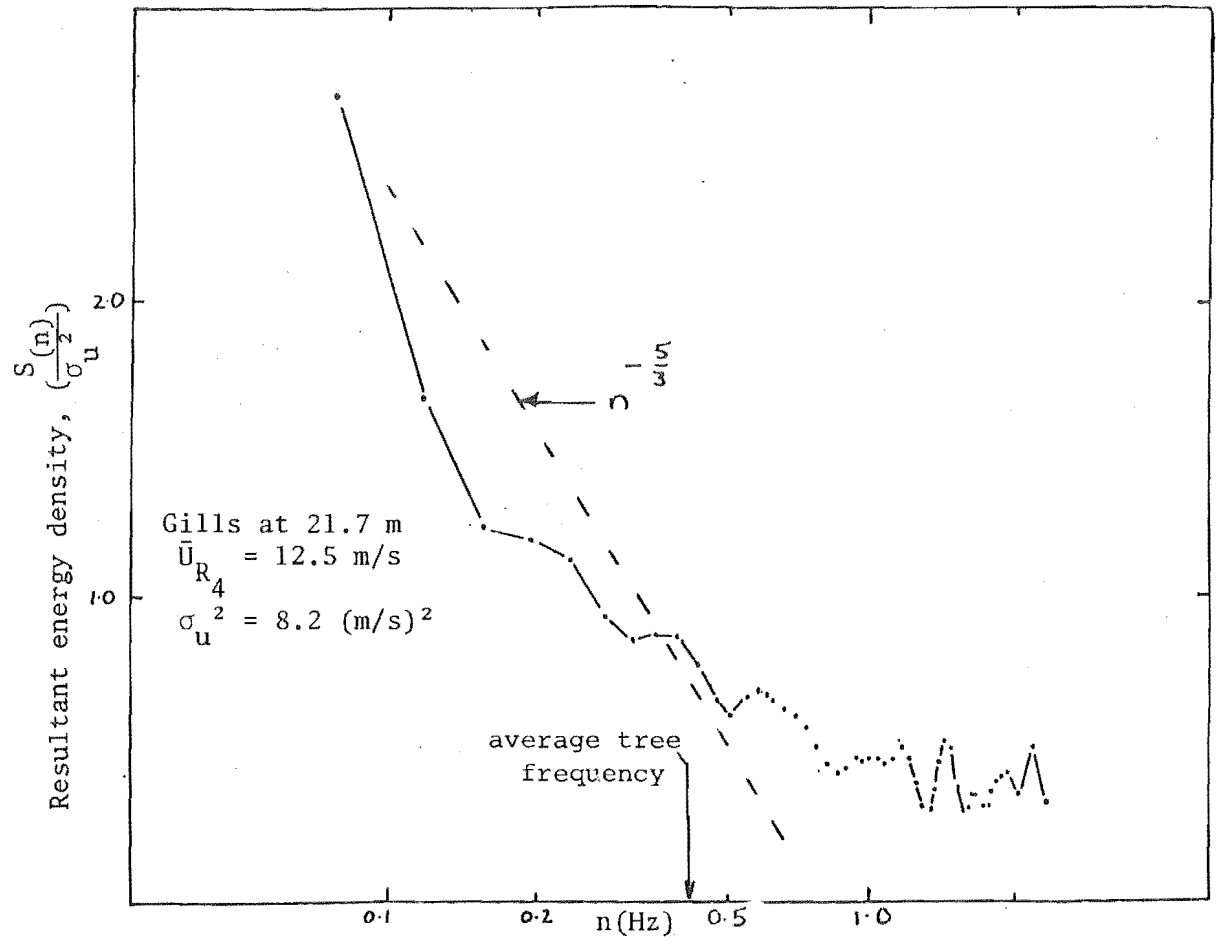

FIGURE 5.22: Energy density distribution at 21.7 m (Run 11, 11.11.82).

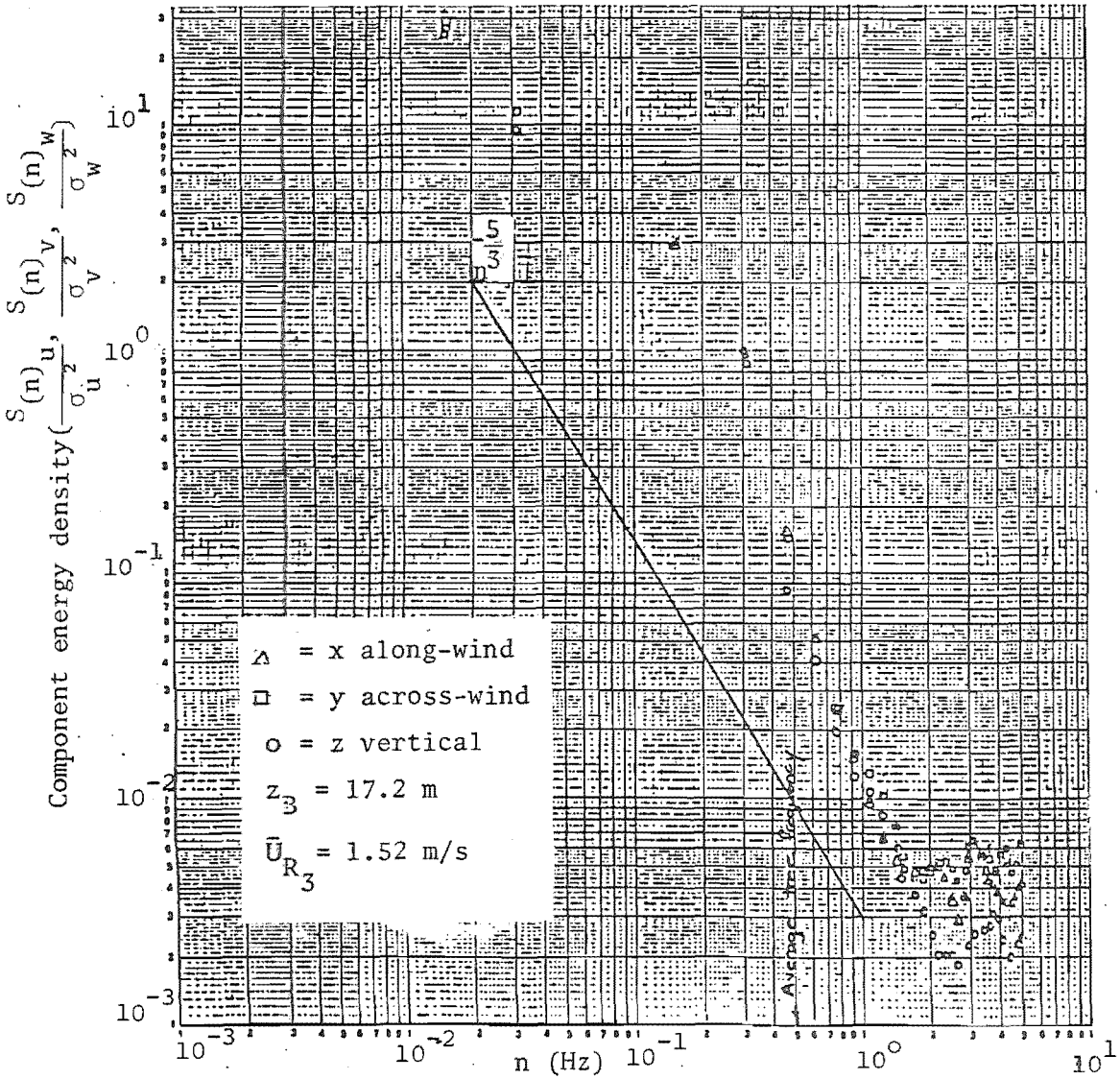

FIGURE 5.23: Turbulent wind component energy spectra
(Run 5, 10.7.82)

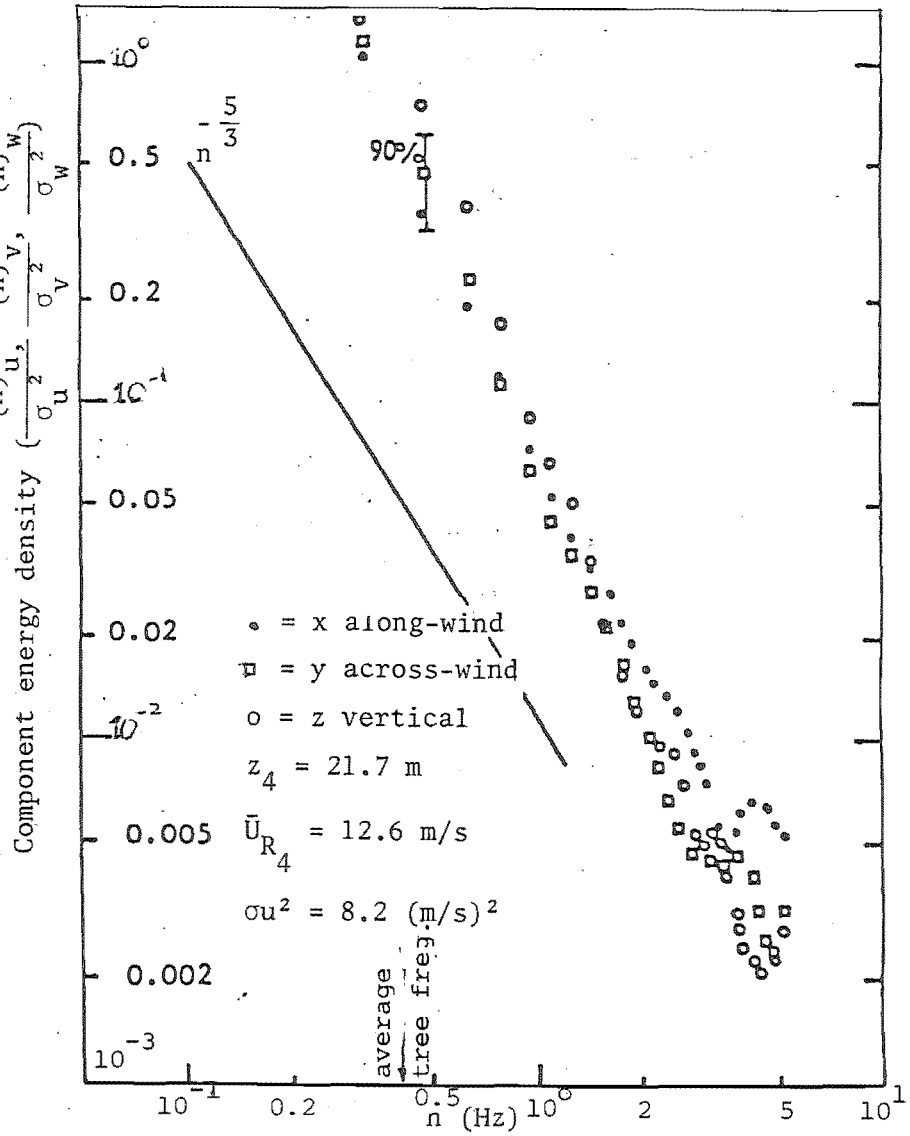

FIGURE 5.24: Turbulent wind component energy spectra
(Run 11, 11.11.82)

any significance in the measured spectra near the natural tree frequencies. This suggests that, at these close spacings, tree response does not materially affect the wind structure flowing over a homogeneous dense forest canopy (3.6).

5.11 TREE RESPONSE MEASUREMENTS AT RIVOX

At the time of writing, tree acceleration spectra were not available from the main frame computer. The Apple II processsing, however, provides these spectra with limited sampling times of near 400 seconds. Resultant acceleration energy spectra are given for a strong wind case before the first thinning (Figs 5.25, 5.27, 5.28). After the first thinning a component acceleration spectra is given in Fig. 5.29.

In strong wind conditions (5 m/s at near tree-top height) the frequencies at the peak in the acceleration energy spectra are the same as the natural frequencies of the trees measured during tree-sway tests (Fig. 5.9).

TABLE 5.13 Natural frequency of spruce in strong winds and nc winds compared

Tree No.	Acceleration	Run 11 11.11.82	Run 17 (Snow) 11.11.82	BT 778 31.12.83	No-wind (sway tests 7.6.82)
93	B & H (No.2)	0.56	0.39		0.52
81	Pioden (No.4) (711)	0.45	0.29	0.42	0.42

The tree frequencies in Run 17 were reduced by as much as 30% because of snow loading. This shifted the tree frequency down to nearer the higher turbulent wind energy levels; but the resonant accelerations of the tree stems were lower than normal, presumably because of increased tree total mass. Once again, close spacings of the trees appear to inhibit tree movement. Also, crown contact at close spacings appears to reduce tree response (cf. Pattern P. - Oxford model forest, Ch. 6). Inspection of Fig. 5.29 shows acceleration peaks at 0.42 Hz, the fundamental frequency. There is another less defined peak at 1.1 Hz. Holbo et al also noted that the wind excites 28 m Douglas firs to move at their no-wind natural frequency, while Finnigan noted that a second peak often occurred in his wheat movement spectra plots.

To p.184

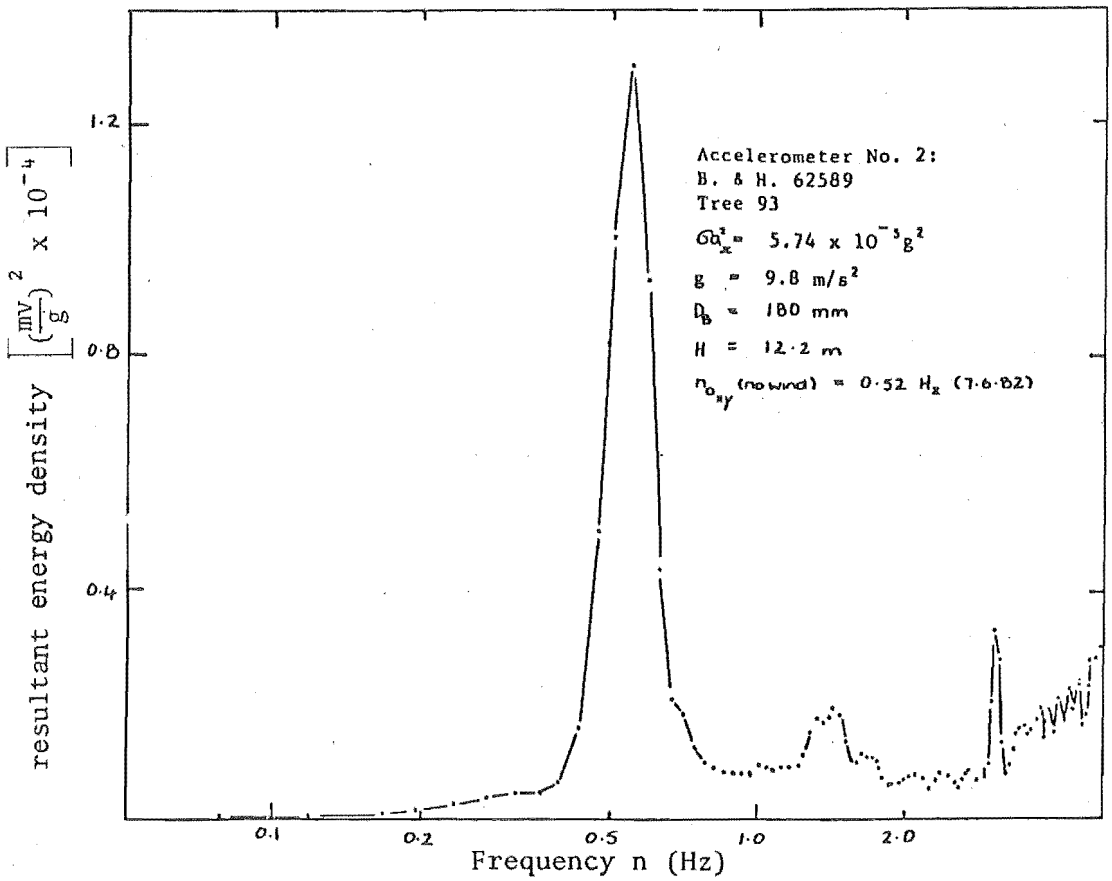

FIGURE 5.25: Accelerometer energy density spectrum for tree 93 (Run 11 ; 11.11.82).

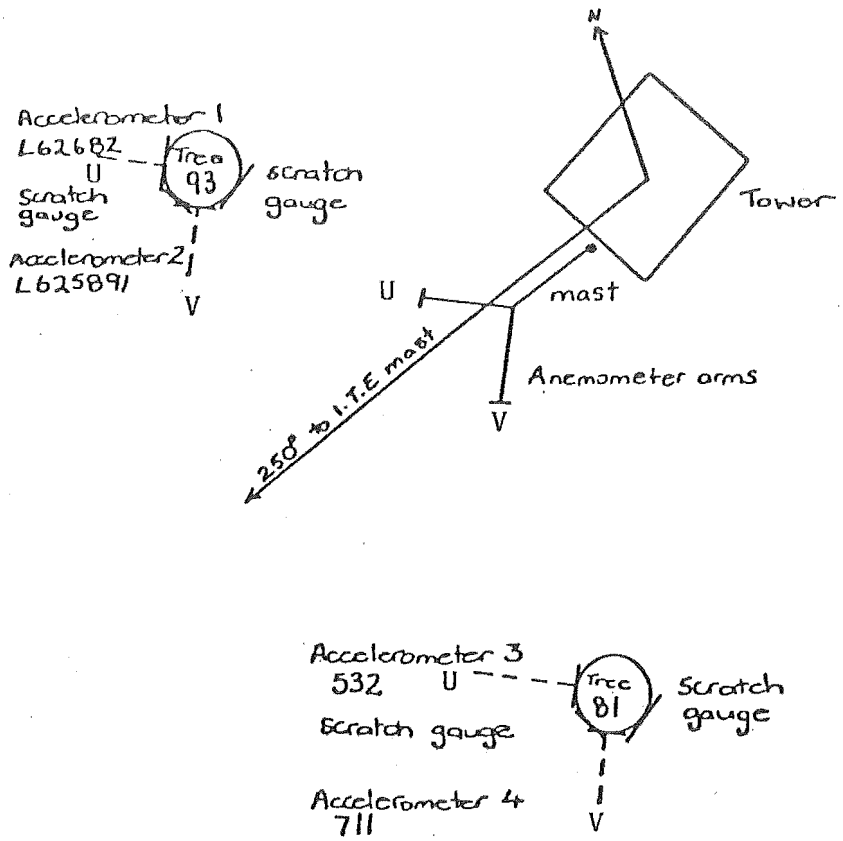

FIGURE 5.26: Accelerometer and scratch gauge locations on trees 81 and 93 upwind of F.C.mast.

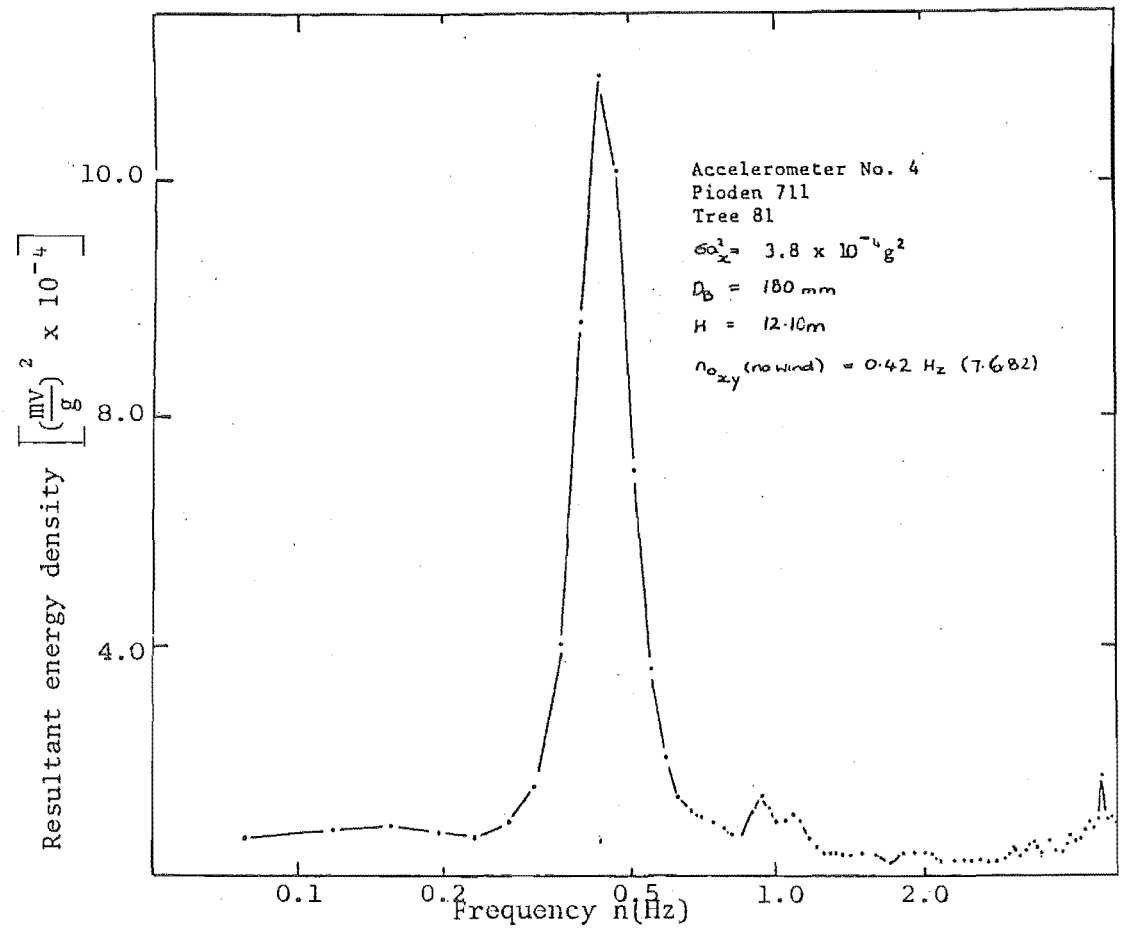

FIGURE 5.27: Accelerometer energy density spectrum for tree 81 (Run 11 ; 11.11.82).

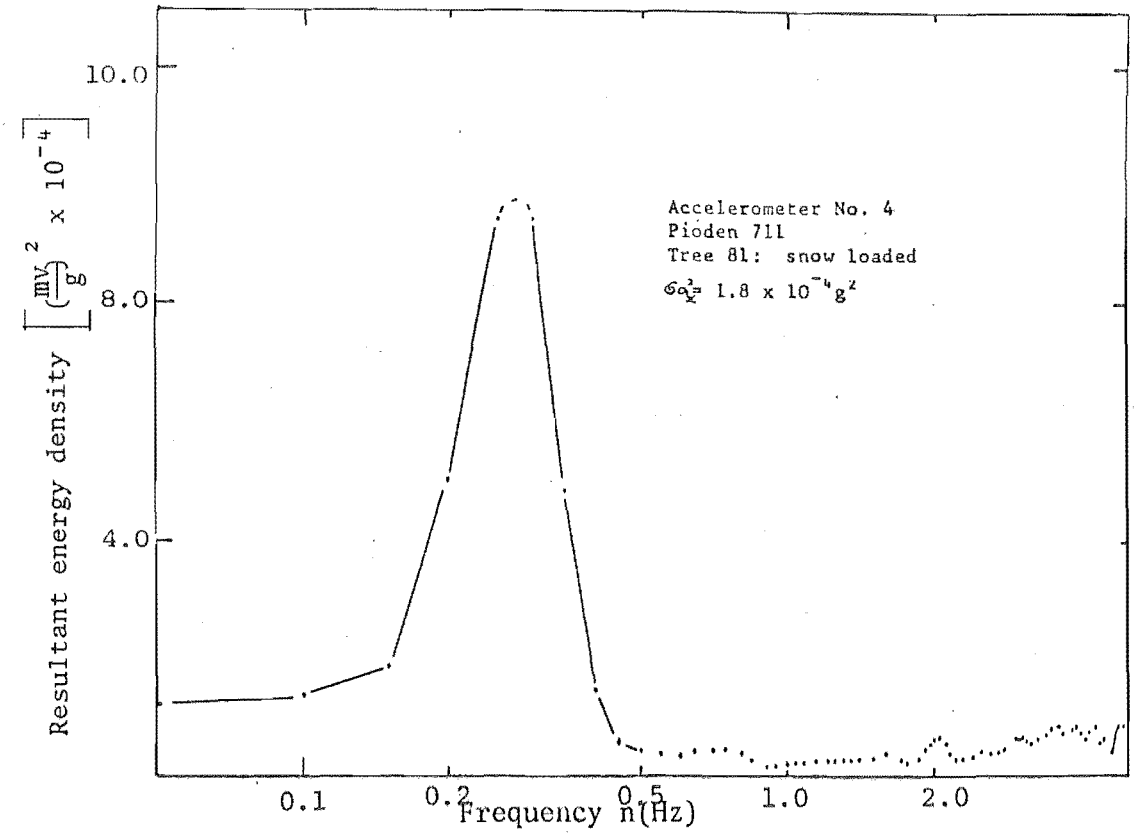

FIGURE 5.28: Accelerometer energy density spectrum for tree 81 (snow laden) (Run 11 ; 11.11.82).

A comparison of component wind speeds and corresponding acceleration levels for Runs 11 (11/11/82) and BT 778 (31/12/83) appear to be significant (Figs 5.27, 5.29). Both spectra are for Tree 81 which has grown from 12.10 m to an estimated 12.97 m.

If tree stem displacement to wind speed is proportional (see 3.10) as proposed by Maitani (Fig. 7.6) then,

$$\frac{x_{t_{(\text{Run 11})}} \times \bar{V}_{1_{(\text{BT 778})}}}{x_{t_{(\text{BT 778})}} \times \bar{V}_{1_{(\text{Run 11})}}} = 1.$$

In fact,

$$\frac{1.96 \times 3.54}{2.84 \times 2.26} = 1.08, \text{ which is close to unity.}$$

The Apple II computer produced an integral length scale for BT 778 of 0.36 m for stem sway motion at 7.5 m stem height in the V direction.

So,

$$\frac{A}{H}(R) = 0.029 \times \frac{2.6}{2.72} \qquad (6.10.2)$$

$$= \underline{0.028}$$

But,

$$\frac{A}{H}_{rms\,(7.5\text{ m})} = \frac{0.36}{2}\text{ m} \qquad \text{(Fig. 5.29)}$$

or,

$$\frac{A_{rms_{top}}}{A_{rms_{(7.5\text{ m})}}} = \left(\frac{12.97}{7.5}\right)^{1.5} \qquad (3.9.3.2)$$

$$\therefore \quad A_{rms_{top}} = (0.18 \times 2.27)\text{ m}$$

$$\therefore \quad \frac{A}{H}_{rms} = \frac{0.41}{12.97}$$

$$= \underline{0.032} \quad .$$

To p.186

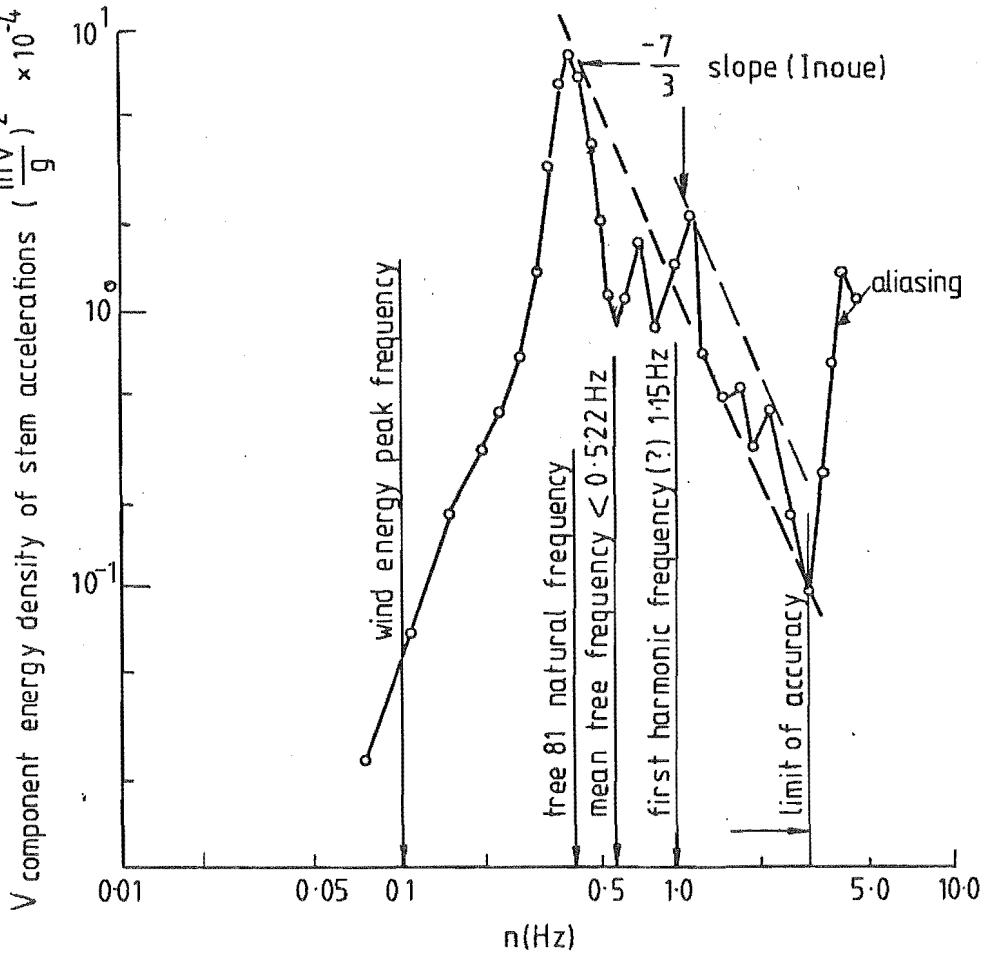

		Tree 81 11.11.82	Tree 81 31.12.83			
WIND(m/s)	°T	265	244			
	$\bar{U}_{R_4}$	12.50	12.65			
	$\bar{U}_{R_1}$	—	4.91			
	$\bar{V}_1$	≈2.26	3.54			
	σ_{V_1}	—	2.49			
FOREST	H(m)	10.11	10.83			
	S/H	0.176	0.186			
	z_o' (m)	1.63	1.63			
	d/H		0.74			
	$\bar{U}_{*\ell}$ (m/s)	—	1.91			
TREE	H(m)	12.10	12.97			
	n_o Hz	0.42	0.42			
	D_B(mm)	180	200			
	Accel. Ht (m)	7.5	7.5			
	Accel. Dir(°T)	205	205			
ACCELEROMETER RESULTS	Type	Pioden 711	Pioden 711			
	S.Rate	10Hz	10Hz			
	S.Time	200 s	200 s			
	$\sigma_{a_x}^2$ (g^2)	3.8×10^{-4}	7.47×10^{-3}			
	g.max (V.dir)	—	0.24			
	A_{rms}x2	—	0.36			
	A_{rms}/H	—	0.038			

FIGURE 5.29: Accelerometer energy density spectrum and results for tree 81 (BT 778, 31.12.83).

The maximum acceleration/g is obtained from the variance. For Run BT 778 this was $74.7 \times 10^{-4}/g^2$ and so,

$$g_{max} = \sqrt{74.7 \times 10^{-4} \times 8.093} = 0.24$$

The spectra slope of Fig. 5.29 is about $-\frac{7}{3}$. This was predicted by Inoue, and was measured by Uchijima and Wright, Maitani, and Finnigan for smaller crops (mean height 1 m) (Fig. 5.30 ; vertical axis should be $\frac{S(n)}{\sigma_u^2}$.

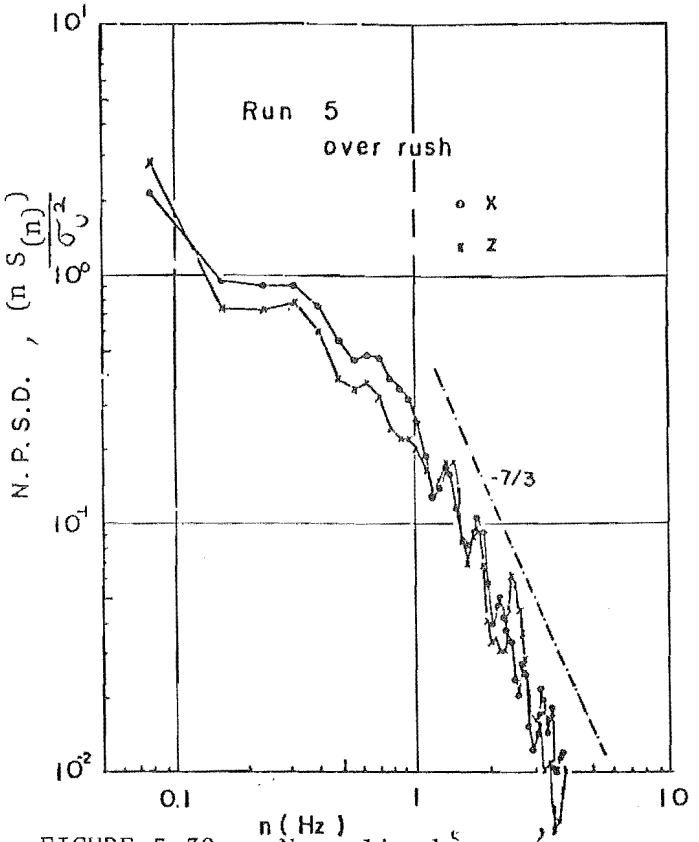

FIGURE 5.30: Normalised power spectra of displacement of a rush plant along the mean wind (x), in the vertical direction (z). (After Maitani.)

The data necessary for calculating tree response by the simple and complex methods have been included on Fig. 5.29 (see also Appendix I). At the close spacings under investigation, tree response is mainly due to background turbulence.

5.12 CHAPTER SUMMARY

At the time of writing, the experiment at Rivox is beginning to provide valuable field data which appear to be compatible with the wind tunnel results and other research work. From these data the following conclusions can be made.

(a) Mean wind speed profiles are similar to those of the Kielder Experiment at 6 H (Fig. 7.2).

(b) Turbulence intensity profiles just above the canopy are reasonably consistent with the ESDU and model forest profiles, except that the fullscale turbulence intensity profile is displaced vertically upwards. This could arise since the Rivox forest has not been pruned and displacement heights may be higher than if the forest understorey is pruned (Fig. 7.3).

(c) Turbulence intensities in all three orthogonal directions have not materially altered at the close spacings now being tested.

(d) Peak turbulent wind energy migration to higher frequencies (possibly because of frequency shift effects between wind gust and turbulence generated by tree sway) is just observed at the close spacings now being tested at Rivox. Frequency shifts should be noticed at spacings beyond $\frac{S}{H} = 0.3$ (Fig. 7.5).

(e) The wind structure above forests appears to obey the Kolmogorov Laws and one tree response spectra obeys the predictions of Inoue at the close spacings tested at Rivox.

(f) The Apple II process acts as an initial check on wind data validity before it is processed by the main frame computer when longer sampling times will improve wind and accelerometer spectra.

It appears that:-

(a) the experiment will consolidate values of $\frac{z'_o}{H}$ and $\frac{d}{H}$ for close-spaced forests (Table 3.5);

(b) as stocking density is reduced, tree dynamic response is proportional to mean windspeed (Fig. 7.7);

(c) the experiment will be able to detect changes in tree responses as tree spacing is increased.

CHAPTER 6

MODEL FOREST EXPERIMENTS

6.1 BACKGROUND AND REVIEW

When a full scale forest is represented by a model forest, the wind and other important variables which govern the tests are controlled. Idealisations can be made to the model tree design, the forest geometry and the nature of the surface boundary layer flow, including the extent of the closed volume to be studied.

It is essential to reproduce in the wind tunnel the full scale local surface boundary layer changes in mean velocity distributions, turbulence intensities, shear stress distributions and power spectral density distributions of the longitudinal, lateral and vertical wind structure. This requires sophisticated simulation techniques, and assumes that the correct information is available for the simulations of the wind and of full scale forests. This information has been covered in Chapters 2, 3 and 4.

Modelling the upstream open country surface boundary layer is the main prerequisite for simulating the flow conditions over model forests; additional information is covered in ESDU standards.

Boundary layer wind tunnels with the correctly modelled wind have been used for testing model forest behaviour previously (3.2). Attempts to model canopy flow were undertaken by Wilson and Shaw (1977), and more recently by Newell and Sheng (1980), using second order closure approaches (Sadeh et al, 1981).

All model forest tests have used model trees that were either rigid, or too flexible, to respond dynamically to fluctuating wind forces. More recently, work by Maitani, Finnigan, Finnigan and Mulhearn, Holbo, and Mayer make it clear that the model tree design must respond to wind fluctuations. Finnigan modelled a wheat field in a wind tunnel using flexible models to simulate some fullscale measurements of wheat and rush-top response in the natural wind. Finnigan and Mulhearn have mathematically modelled the response of waving crops in the wind (Fig.3.20). Mayer makes the point that model forests must take into account the dynamic component

of tree-top movement if the problem of wind damage to forests is to be investigated. A full scale response test by Holbo on selected Douglas firs confirms these views.

The two experiments described in this chapter (see 1.4.3) supplement previous model forest and smaller crop wind tunnel tests. In addition, the effects of crop dynamics on the wind structure is studied at and near the leading edge of the model forest where non-equilibrium wind forces exist. Numerous published papers in forestry science, and also measurements made by the writer, suggest that wind damage to forests propagates rearwards from zones of high wind/tree aero-elastic movement just behind the forest leading edge (see. 4.2).

It is suggested that, just in from the forest front, changes to the wind spectra produce excessive tree sway. These changes increase the aero-elastic movement of the tree stems beyond the stable limits of the stems and soil[1], (Fraser, 1962a; Fraser and Gardiner, 1967). In addition, as crop spacing increases, the wind spectra are displaced to higher frequencies as a result of the interaction of two wind disturbances: the accelerating flow over the forest leading edge, and the wake vortex disturbances at the tree crowns. This displacement in wind frequencies is a frequency shift (Finnigan) and can cause large tree-top sway motion at tree natural frequencies (White et al, Holbo. et al.)

6.2 EXPERIMENTAL OBJECTIVES

The effect of model roughness variation on the flow field suggests the best array for spacing trees (Kawatani and Meroney, 1968). Furthermore, the critical region is in the area just behind the leading edges of forests and just above the tree crowns, where rapid shear stress changes generate turbulence and adjust the spectra at each location (zone C, see 1.3.6).

Model forests with flexible stems were tested in two separate boundary layer wind tunnels. The first experiment was conducted in a small tunnel at Canterbury University in 1975 (6.5.1). The second, duplicating the model forest of the Canterbury test, took place in a larger tunnel

---

1 Bending moments have been obtained for *Pinus radiata* in field tests at Eyrewell, Canterbury, (unpublished).

at Osney Laboraties, Oxford, in 1982 (6.7.1), using hot-wire sensors (6.7.3) to measure the along-wind mean and turbulent wind characteristics.

In each of these experiments 11 different spacings were tested:-

(a) to measure the mean and turbulent wind velocity profiles to obtain z_o', z_o'', $\bar{U}_*$ and σ_u^2 variations;

(b) to measure the turbulence velocity component spectrum changes at tree-top height;

(c) to measure the ratio of average amplitude (A) and mean deflection (D) of the model trees by photography;

(d) to calculate the r.m.s. ratio $\frac{A}{D}$;

(e) to compare the two model experiments for total tree-top response for various thinning densities;

(f) to compare model and full scale wind structure and tree response.

6.3 WIND TUNNEL SELECTION

6.3.1 Canterbury

The University of Canterbury wind tunnel was designed and commissioned in 1974 (Raine). It was the only suitable facility available.

The major experimental faults were:-

(a) scaling of the wind was limited to $\frac{1}{300}$, whereas model tree response required a scale of $\frac{1}{75}$ to record correct dynamic response (6.4.1).

(b) a system of Pitot-tubes connected by tubing to Betz manometers can produce long time constants and can also under-estimate or over-estimate the turbulent wind components (Gumley, pers. comm., 1982). (Hot-wire equipment was not available at that time.)

(c) the small cross-section of the wind tunnel caused 12% blockage which possibly produced some unacceptable along-wind pressure gradients as well as interference at the wall/forest interface;

(d) spectra were not measured;

(e) the proportions of model tree dynamic response to mean deflections, measured by cine film analysis (6.4.8), were inconclusive.

6.3.2 Oxford

The wind tunnel at Osney Laboratories, Oxford University, was the most suitable of the 12 tunnels considered for the experiment in terms of size, ancilliary facilities, availability and cost. It had hot-wire anemometry linked to a computer able to print out mean wind and turbulence intensity profiles as well as spectra (6.7.1). The main limitations of the Oxford model forest experiment were:-

(a) time and cost factors meant that some traverses had to be omitted;

(b) mechanical breakdown of the cine camera and problems with film exposure limited tree response measurements by photography;

(c) mechanical and electrical breakdown of the x-y probes limited measurements of local Reynolds stresses.

Nevertheless, the facility would be suitable for any future model forest retest.

6.4 MODEL TREE AND MODEL FOREST DESIGN

6.4.1 Modelling laws

In the laboratory, the averaging of wind speed fluctuations for each individual measurement produces results which can be repeated. However, in the atmosphere, it is very difficult and extremely costly to obtain enough data runs of similar wind stability to produce accurate wind records. Mean wind speeds at specific meteorological stations at 10 metres reference are repeated on only a few occasions over a number of years (see 5.6.3).

Generally, modelling for wind-loading purposes is accomplished by using a wind tunnel which is large enough to develop an open country wind profile with zero pressure gradient in a neutral atmosphere. (A modified temperature gradient is required for diffusion experiments).

To establish a representative modelling test of the natural wind and its effect on any obstruction, certain modelling rules must be observed. Raine (1974) discussed in detail the modelling of the natural boundary layer and choice of geometric scale $\left(\frac{H_m}{H_p}\right)$, by which the roughness scale $\left(\frac{z_{o_m}}{z_{o_p}}\right)$ can be defined. In the case of a model forest this roughness scale can be related to stocking density (3.6).

The following similarity parameters must be observed for both the wind and the model design when wind loads on model forests are compared with those on full scale forests (Raine, 1974).

$\frac{\bar{U}_z}{z_o}$ mean flow upstream;

$\frac{\sqrt{\overline{u'^2}}}{\bar{U}_z}$ the turbulence intensity upstream;

$\frac{L_u}{z_o}$ a ratio of the length scales of the turbulent and mean flow upstream;

$\frac{\sqrt{\overline{u'^2}}.L_u}{\nu}$ a Reynolds number based on the r.m.s. velocity fluctuations, length scale of turbulence, and the molecular viscosity;

$\frac{\sqrt{\overline{u'^2}}.z_o}{e}$ a Reynolds number based on the r.m.s. fluctuations, length scale of mean flow, and the eddy viscosity (kinematic viscosity);

$\frac{n_o H}{\bar{U}_z}$, or $\frac{n_o L_u}{\bar{U}_z}$ a non-dimensional frequency;

$\frac{\rho \bar{U}_z^2}{E}$ Cauchy Number along-wind (Strouhal Number relates across-wind response and is neglected in this experiment) (Davenport, Solari).

The last two parameters are related (Davenport et al, 1975), so that frequency similarity can suffice.

For fully-aerodynamically rough surfaces, molecular viscosity can be ignored; that is $\frac{\sqrt{\overline{u'^2}}.L_u}{\nu}$ is redundant provided $\frac{\bar{U}_* z_o}{\nu}$ upstream is greater than 2.5[1] (Raine 1974).

---

1 In these tests $\nu \simeq 10^{-5}$; $z_{o_m} = \frac{0.03 \text{ m}}{75}$; and $\bar{U}_* > 0.1$, so $\frac{\bar{U}_* z_o}{\nu} > 4$.

6.4.2 Forest scaling - full scale to model

For boundary layer similarity over the model forest itself, 'inner layer equilibrium' is also required (4.1).

Rao et al's approach fits Bradley's abrupt-change model experimental results, provided that the inner layer transition height at the leading edge is greater than $\frac{z_T}{H}$ of 0.3.[1]

Similarity of flows right at the model forest leading edge (from 0 H to 3 H) is in doubt where highly accelerated flows exist. The mathematical model suggested by Lo (1977) may fit the case of a forest front (Fig. 4.5).

Full scale forests begin to suffer extensive wind damage when mean windspeeds reach 20 m/s and mean tree-top height reaches 15 m (3.9.3).

So, for equivalent wind forces over the model forest, scaling at $\frac{1}{75}$:—

(a) gives a mean model tree height of

$$\frac{H_m}{H_p} = \frac{z_{o_m}}{z_{o_p}} = \frac{xL_{u_m}}{xL_{u_p}} = \frac{1}{75}$$

and a model forest mean tree-top height, H_m, of 200 mm;

(b) for heathland upwind the full scale z_o' is 0.03 m and, because $z_o' = 0.11$ H and d = 0.70 H for forests[2] (Table 3.2)

$$xL_{u_p} = \frac{25(z-d)^{0.35}}{z_o^{0.063}} \qquad \text{(ESDU 74031 A.16)}$$

$$= \frac{25 \times (10-0)^{0.35}}{0.03^{0.063}}$$

$$\simeq 70 \text{ m.} \qquad \text{(at 10 m reference)}$$

---

1 In the Oxford model forest tests the transition height was near 1.3 H (see Fig. 6.26).

2. In the model forest tests d was chosen as 0.75 H which conforms with Smith and Oliver Thetford tests and with Rivox full scale results (Table 5.14).

$$\text{Also,} \quad xL_{u_{p'}} = \frac{25 \times (15-10.5)^{0.35}}{(0.11 \times 15)^{0.063}}$$

$$\text{or,} \quad xL_{u_{p'}} = \frac{25 \times 1.69}{1.03}$$

$$\simeq 41 \text{ m} \quad \text{at tree top height.}$$

$$\text{so,} \quad xL_{u_{m'}} = 0.55 \text{ m} \quad \text{for the model forest.}$$

Both these conditions establish the model tree and model wind length scales.

6.4.3 Model tree natural frequency - full scale to model

Spectral similarity exists between the real wind and the Oxford University wind tunnel scaled wind (6.7.1). Upstream, wind tunnel reference mean wind speed is set at 6 m/s.

Measurements of tree natural frequencies for 15 m spruce are near 0.40 Hz (Mayhead; 1973(a)) and for *Pinus radiata*, 0.25 Hz (Papesch, 1977).

For wind damage studies over model forests, along-wind tree-response similarity requires

$$\frac{n_{o_p} H_p}{\bar{U}_{z_p}} = \frac{n_{o_m} H_m}{\bar{U}_{z_m}}$$

$$\text{so} \quad n_{o_m} \simeq \frac{0.4 \times 75 \times 6}{20} \text{ Hz}$$

$$= 9.0 \text{ Hz}.$$

6.4.4 Modelled wind spectrum peak frequencies

From ESDU (1974)

$$\frac{xL_{u_p} \cdot n_{pk_p}}{\bar{U}_{z_p}} = \frac{xL_{u_m} \cdot n_{pk_m}}{\bar{U}_{z_m}} = 0.146.$$

Upstream of the model forest leading edge the required spectrum peak frequency is

$$n_{pk_m} = \frac{0.146 \times 6}{0.93}$$

$$= \underline{0.94 \text{ Hz}} .$$

(Similarly n_{pk_p} = 0.04 Hz).

Over the rear of the model forest, where equilibrium conditions are considered to exist, the required spectrum peak frequency

$$n_{pk_m} = \frac{0.146 \times 6}{0.55}$$

$$= \underline{1.59 \text{ Hz}}.$$

(Similarly, n_{pk_p}, = 0.07 Hz).

So, as the wind passes over the increased roughness of the model forest there is a shift in the wind frequencies of 0.65 Hz to higher frequencies. These change the wind energy spectrum and will induce greater tree-top swaying motion.

6.4.5 Model tree design

Modelling a tree is difficult. For these experiments, attempts were made to represent full scale tree stiffness and to taper the tree stem. Araldite, which is very suitable for modelling stem stiffness, was rejected because of high labour costs. Instead, each stem was made from two 20 s.w.g. galvanised wire lengths twisted together, so that model tree frequency was reduced to 9 Hz and model height maintained at 200 mm. The stiffness was therefore constant with height.

Crown shape was based on full scale measurements of the crowns of *Pinus radiata* and Sitka spruce growing in a typical forest. The height up to the crown base was made close to the actual full scale pruning heights of $\frac{1}{3}$ H (Table 3.1).

In total, 3000 model trees were manufactured, including extra models made at Bristol, U.K., to complement the number transported to Oxford from Canterbury University.

In earlier attempts to model trees within a forest, none duplicated the dynamic response that exists in full scale trees. Thom used nails, Kawatani and Meroney used wooden pegs, Walshe and Fraser used thick brass

stems and wire gauze, and Meroney used plastic stems and tree crowns (3.2). Finnigan, however, used flexible roughness. He modelled wheat by small stalks, but the stiffness was lower and produced deflections which would be excessive in tree modelling.

The dimensions of the 'average' model used at Canterbury and Oxford are given in Figure 6.15. When the model trees had been manufactured the damping ratio was checked by measuring the settling time of $5/\zeta\omega_o$ for model tree-top response to a step input. The damping ratio came close to 0.08 (Table 3.3), for an average n_o of 8.9 Hz.

6.4.6 Model forest height and frequency distribution

The distribution of tree height within the model forest was found by comparing Sitka spruce stands and two different stands of *Pinus radiata*.

2500 model trees were sorted so that the height variation fitted a normal distribution curve. The average height was 202.8 mm, with extremes of 155 mm and 250 mm, and a standard deviation of ± 20.2 mm (0.1 H). Standard deviations of total crop height appeared to vary considerably from crop to crop and the value of 0.10 H is a mean of several standard deviation values.

The distribution of model tree frequencies was measured once the height distribution was known. The individual frequencies of all model trees were measured for both Canterbury and Oxford tests. The mean model tree frequency (n_o) for the Canterbury tests was 8.6 Hz, and for the Oxford tests, 8.9 Hz. The model tree height range of 150 mm to 255 mm produced extremes of frequency from 5.3 Hz to 18.2 Hz.

6.4.7 Model forest spacings and fetch

In a full scale forest, spacing of trees varies depending on the management practices used in each forest. Comparisons of thinning practices in forests of *Pinus radiata* on the Canterbury Plains with spruce in Scotland, show that spacing between trees can vary from just above 1.5 m to in excess of 6 m. For a maturing forest, the average spacing is 3 - 4 m.

Model forest spacings conformed to the real case for the closest spacings, but were deliberately made greater for the widest spacings. Spacing density was measured using the ratio of the horizontal distance between model tree stems (S) and the mean model tree-top height (H). $\frac{S}{H}$ values changed from 0.17 to 0.61 for the 11 different patterns. Spring-

loaded brass collets attached the trees to Torro board studs to allow spacings to be altered after a pattern was tested. The distance between each Torro board stud was 9 mm. Trees were arranged in square and staggered arrays. The closest spacing tested (45 mm), requiring 2,500 trees, was for Pattern P (Table 6.5). The widest spacings required 252 model trees.

Model forest fetch and width were controlled by features of wind tunnel design such as floor space, traversing equipment limitations and the need to change spacing patterns quickly between runs. Plan dimensions of 1.5 m wide by 2.5 m long for both simulations gave sufficient model forest width to avoid 3-dimensional edge effects, and sufficient fetch to ensure wind force equilibrium is reached (4.1).

For the Oxford tests, side boards were placed alongside the model to give a zero plane displacement of 0.6 H with a ramp input leading edge to reduce edge interference (Fig. 6.16; Fig. 6.18).

6.4.8 Measurement of model tree swaying motion by photography

The movement of the model trees in each of the patterns tested was monitored at row positions ½H, 1H, 3H, 5H, 7H and 10H in from the leading edge. The trees in these rows were coloured and colour-tipped to allow row and tree-tip identification during film analysis. The movement of each tree tip was assessed by fixing a coded 100 mm x 25 mm matt black strip of metal on a brass stem clipped to the Torro board base behind each tree. A short burst of filming was made before each wind tunnel run to establish the no-wind position. Tree movement in each row was then filmed with the wind tunnel set at the required reference speed. At the end of each run, a further short burst of film provided a check on the no-wind tree-tip position. In nearly all cases the tree stems remained firm on the Torro board.

Each frame from the developed film was successively projected on to a screen. When a model tree reached its maximum swing fore and aft, the movement was measured on the calibrated screen. The mean position of the maximum swings could then be estimated and the mean deflection (D) and amplitude (A) measured. Exposure levels were not good for the Oxford tests and the Bolex camera needed frequent adjustments.

6.5 CANTERBURY MODEL FOREST TESTS

6.5.1 Tunnel and wind calibrations

The tests were conducted in the University of Canterbury natural boundary layer wind tunnel, before it was redesigned and the tunnel fans were shifted from near the tunnel inlet to downstream of the working section. (Fig. 6.1 shows the present wind tunnel configuration)

The wind tunnel is of the open circuit type which produces a rural boundary layer using a combination of naturally-grown and artificially-developed turbulence and mean wind profile shapes. Surface roughness elements upstream of the working area maintained the generation of turbulence set up by a grid just downstream of the contra-rotating variable-pitch fans. This configuration allowed a reasonably short upstream boundary layer growth region to develop and established the correct upstream model wind profile for the open country surface boundary layer. The section of the tunnel in which the boundary layer was developed was just over 12 m long, with a constant cross-section of 1.22 m by 1.22 m which allowed for a maximum reference wind velocity of 20 m/s at 600 mm from the floor.

The model forest was located at the rear of the 12 m-long working section (Photograph 14). The maximum along-wind model forest fetch was 11.55 H.

Tunnel reference, pressure, temperature and ambient temperature were recorded for the pattern tests.

6.5.2 Tunnel and instrument limitations

Blockage (6.3.1) expressed as a percentage of the tunnel cross-sectional area is limited, since the upstream velocity profile can be changed and produce a pressure gradient along the model forest. Figures for the maximum value of blockage vary from 5% (Raine) to 7.5% (Pope and Harper, 1966). Blockage for this experiment, using a model height of 202.8 mm and a zero plane displacement of 0.75 H, was 12.25%. Even so, the upstream velocity profiles in this experiment were reasonably consistent with the no-blockage condition (Fig. 6.2).

To p.202

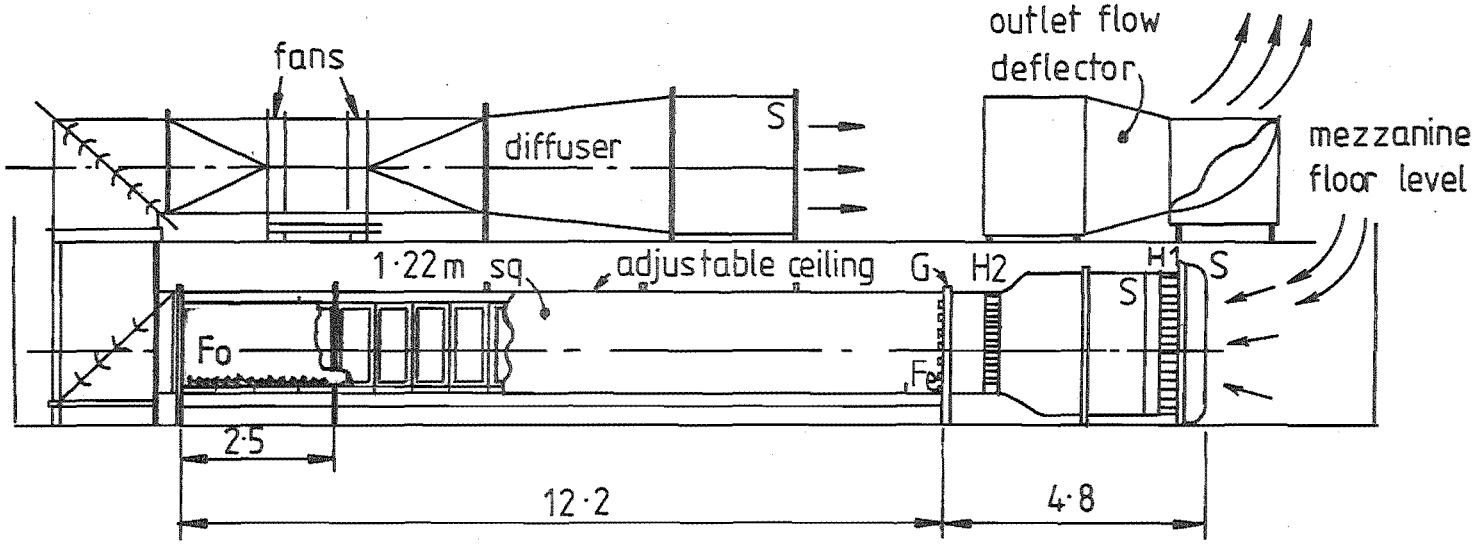

Fo forest
Fe fence
1:2·5 entrance contraction
S screens

H1 honeycomb 6cm D. × 25cm
H2 honeycomb 1cm D × 7·5cm
G grid 2cm × 2cm bars

dimensions in metres

FIGURE 6.1: Boundary layer wind tunnel - modified (University of Canterbury)

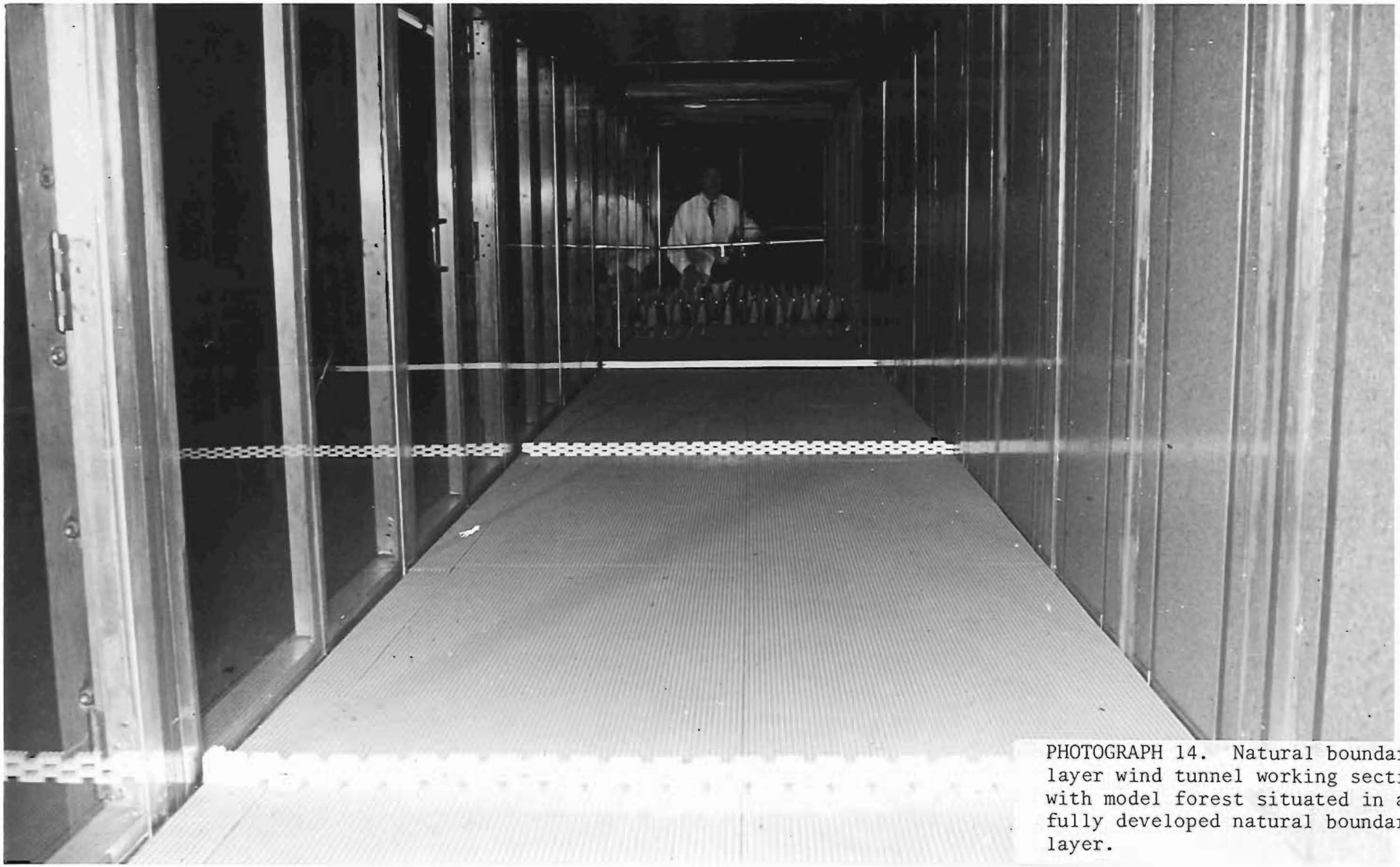

PHOTOGRAPH 14. Natural boundary layer wind tunnel working section with model forest situated in a fully developed natural boundary layer.

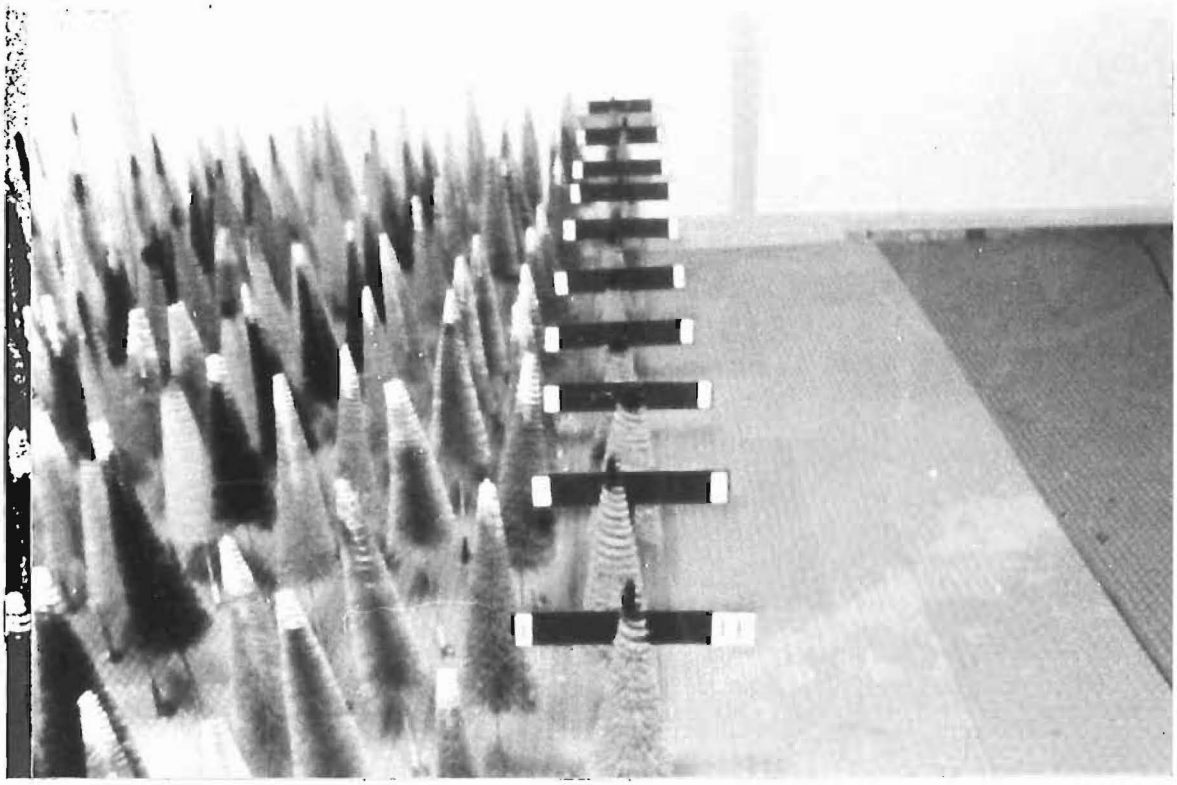

PHOTOGRAPH 15. Model Forest (Pattern F). No wind condition. Markers are 100 mm wide.

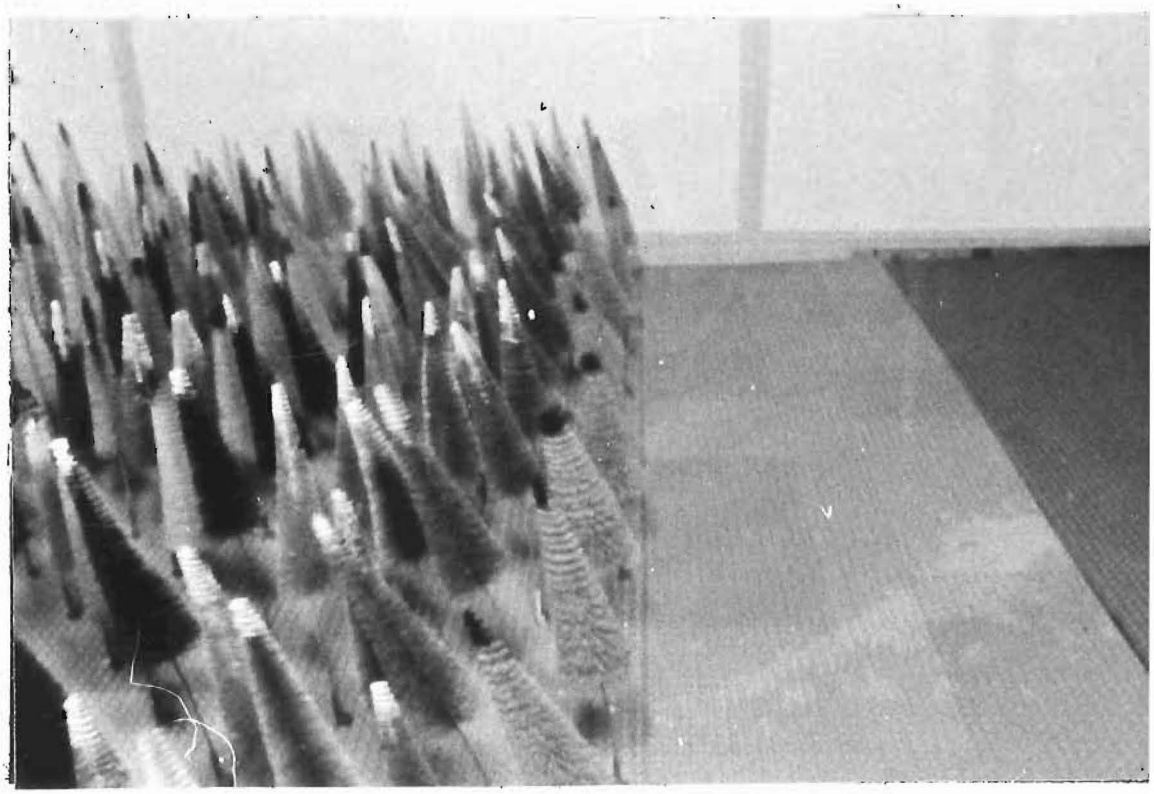

PHOTOGRAPH 16. Model Forest (Pattern F). Maximum wind condition.

6.5.3 Canterbury model forest

1500 model trees were used. $\frac{S}{H}$ values did not extend down to the Oxford experimental spacings. The mis-match of model-to-prototype height ratio of $\frac{1}{75}$ to the wind scaling ratio of $\frac{1}{300}$ was barely acceptable (6.3.1). (Raine suggests $\frac{1}{100}$ scale as a maximum so that the model trees would have a full scale equivalent height of 20 m).

Forest model patterns were given a letter prefix A-J. The following spacing arrays were obtained:-

TABLE 6.1 Model forest spacing patterns (Canterbury)

Pattern Designation	Pattern Shape	Spacing (mm)	$\frac{S}{H}$
A	Square	48	0.24
B	Staggered	55	0.27
C	Square	65	0.32
D	Staggered	67.5	0.33
E	Square	80	0.39
F	Staggered	78.5	0.39
G	Square	96	0.48
H	Staggered	101.5	0.50
I	Square	120	0.59
J	Staggered	124.5	0.62

Velocity profiles were measured for the patterns B, C, E, F and I, using a remotely-controlled Pitot-static tube which could be traversed horizontally and vertically during each run. Traverses were taken just upstream of the forest front, towards the middle of the model forest, and at the rear of the forest.

For photographic analysis, three regions were investigated:-

0H - 3H (the forest front. Photographs 15, 16),
3H - 7H (the middle of the forest),
7H -11H+ (the rear of the forest).

The division at 7H was made to give some idea of the extent of the non-equilibrium zone C.

A 16 mm Bolex movie camera was calibrated so that 3 m of 16 mm colour film gave an average of 62.24 frames per second, with an accuracy of 2.3%. The number of frames per row averaged 350.

6.6 RESULTS OF CANTERBURY MODEL FOREST EXPERIMENT

6.6.1 Mean wind velocity profiles

The power index, α, for the approaching wind (Table 6.7) varies from 0.166 to 0.24, with an average of 0.19 for the traverses taken upstream of the forest front. The average value of 0.19 compares favourably with the value found for the Kielder Forest study where $\alpha = 0.22$ (Fig. 5.3).

Once the wind traverses the front, the mean wind profiles show dramatic changes in shape.

(a) In the horizontal direction equilibrium does not appear to return to the flow until near 7H.

(b) In the vertical direction from within the crown, equilibrium does not return until measurements reach 3 tree-heights above the canopy (Fig. 6.2(a)-(c)).

Mean windspeed profile parameters z_o', d, $\bar{U}_{*_{prof.}}$ and $\bar{U}_{*_{\ell}}$ measure this changing shape for the two dimensions studied. These parameters are compared with the equivalent quantities measured in the Oxford model forest simulation (Table 6.7). These measurements extend the range of the mean wind profile investigation well down into the forest. It is apparent from an inspection of Figure 6.2 that the air below is almost stagnant at 10H in both Patterns B and C. This is surprising, considering the open nature of the model forest 'understorey'. These mean wind speed profiles were measured with pitot tubes (Gumley, pers. comm.), whereas the Oxford model study used delicate hot-wire probes. (Hot-wires cannot reach down to the stagnant air cushion because of possible structural damage from model tree sway motion).

6.6.2 Mean static displacement versus spacing

Model tree mean deflections (D) by photographic analysis are given in Table 6.2 and are plotted in Figs. 6.3(a)-(c) and 6.4(a)-(c).

As spacings increase from $\frac{S}{H}$ of 0.24 to 0.62, D increases 'linearly' with spacing beyond $\frac{S}{H}$ of 0.35. Except for right at the front, $\frac{D}{H}$ increases with $\frac{S}{H}$ at similar rates and magnitudes for the x-positions tested in from

To p. 210

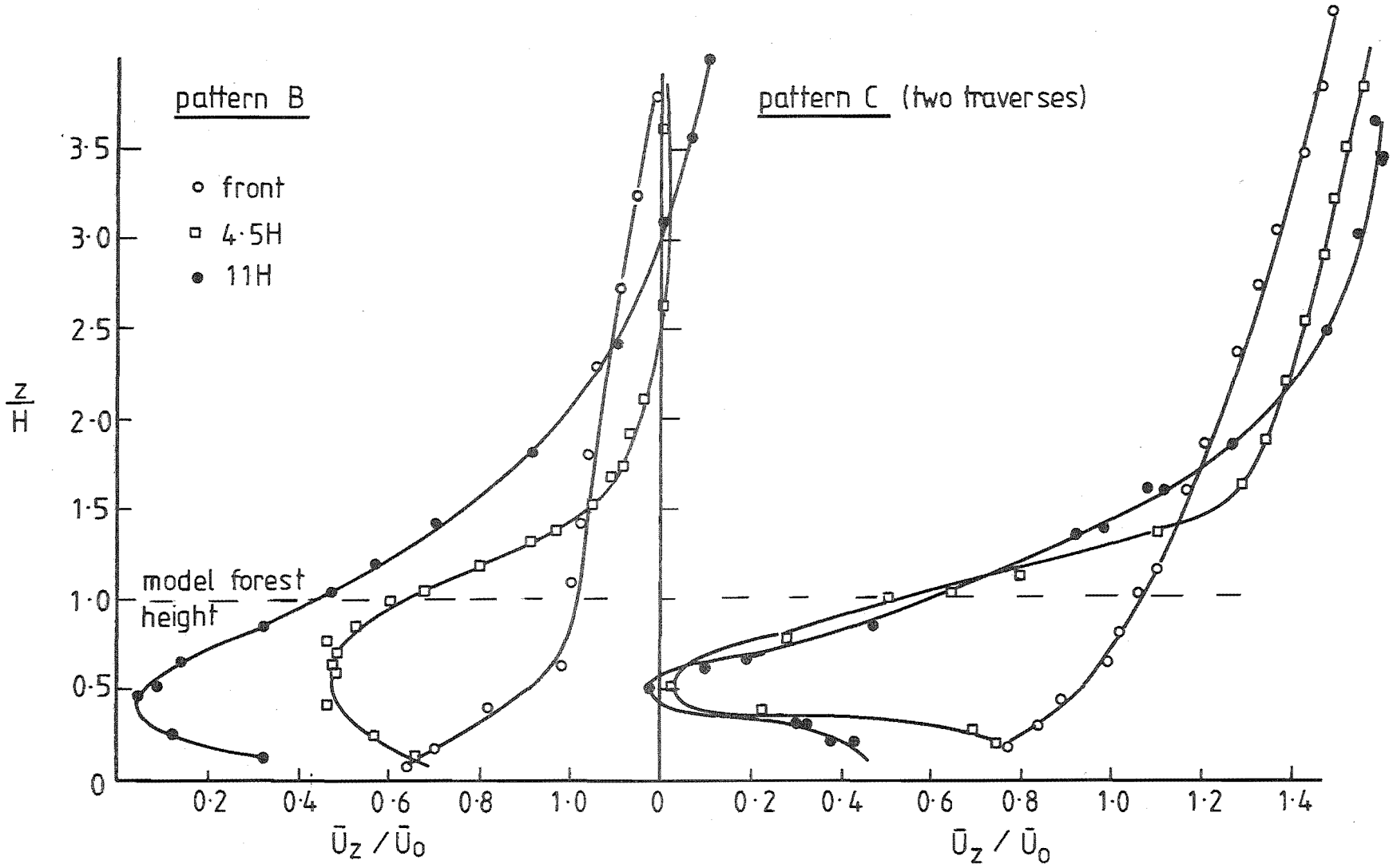

FIGURE 6.2(a): Mean wind velocity profiles from model tests, (Pattern B & C).

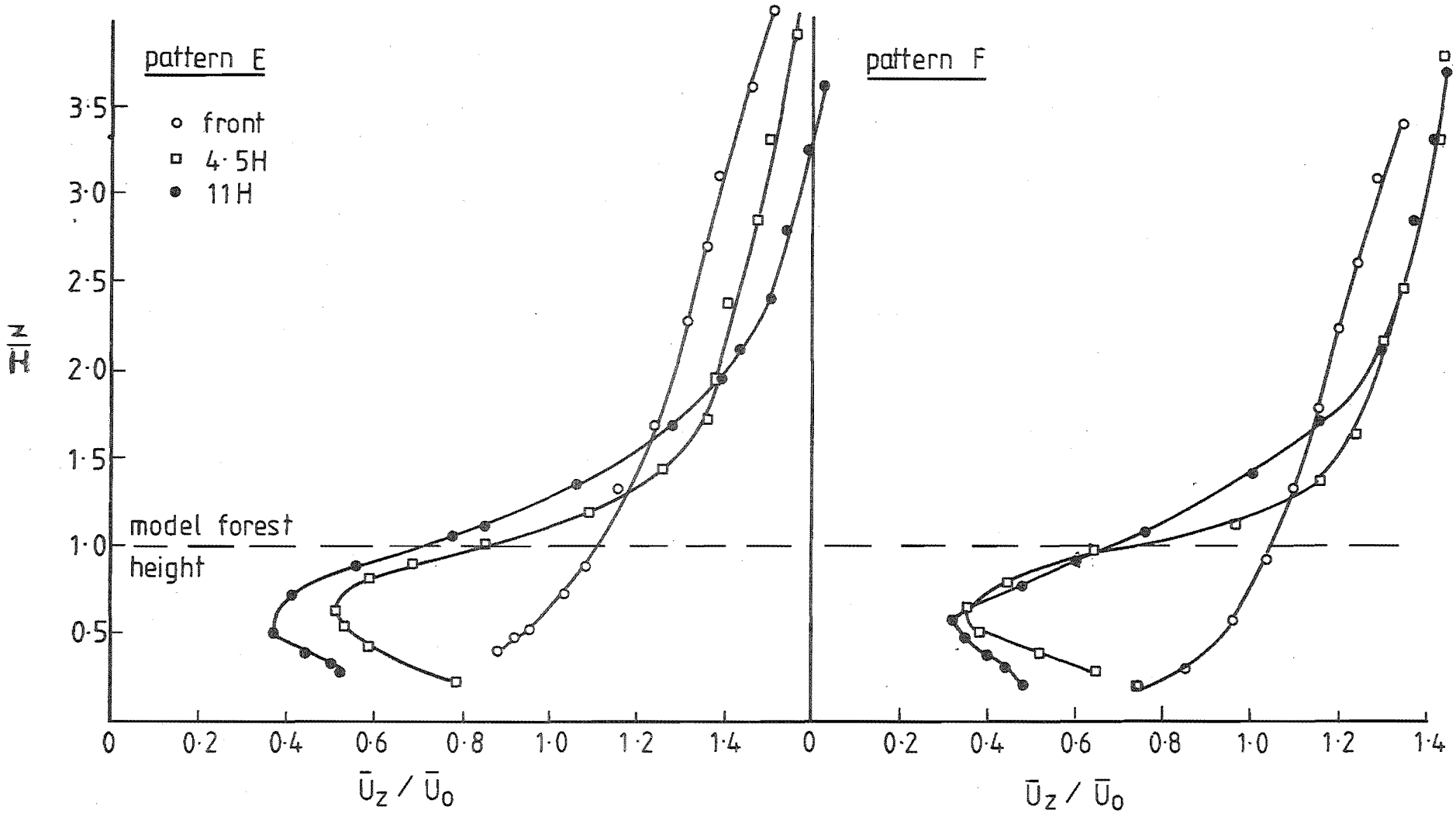

FIGURE 6.2(b): Mean wind velocity profiles from model tests (Pattern E & F).

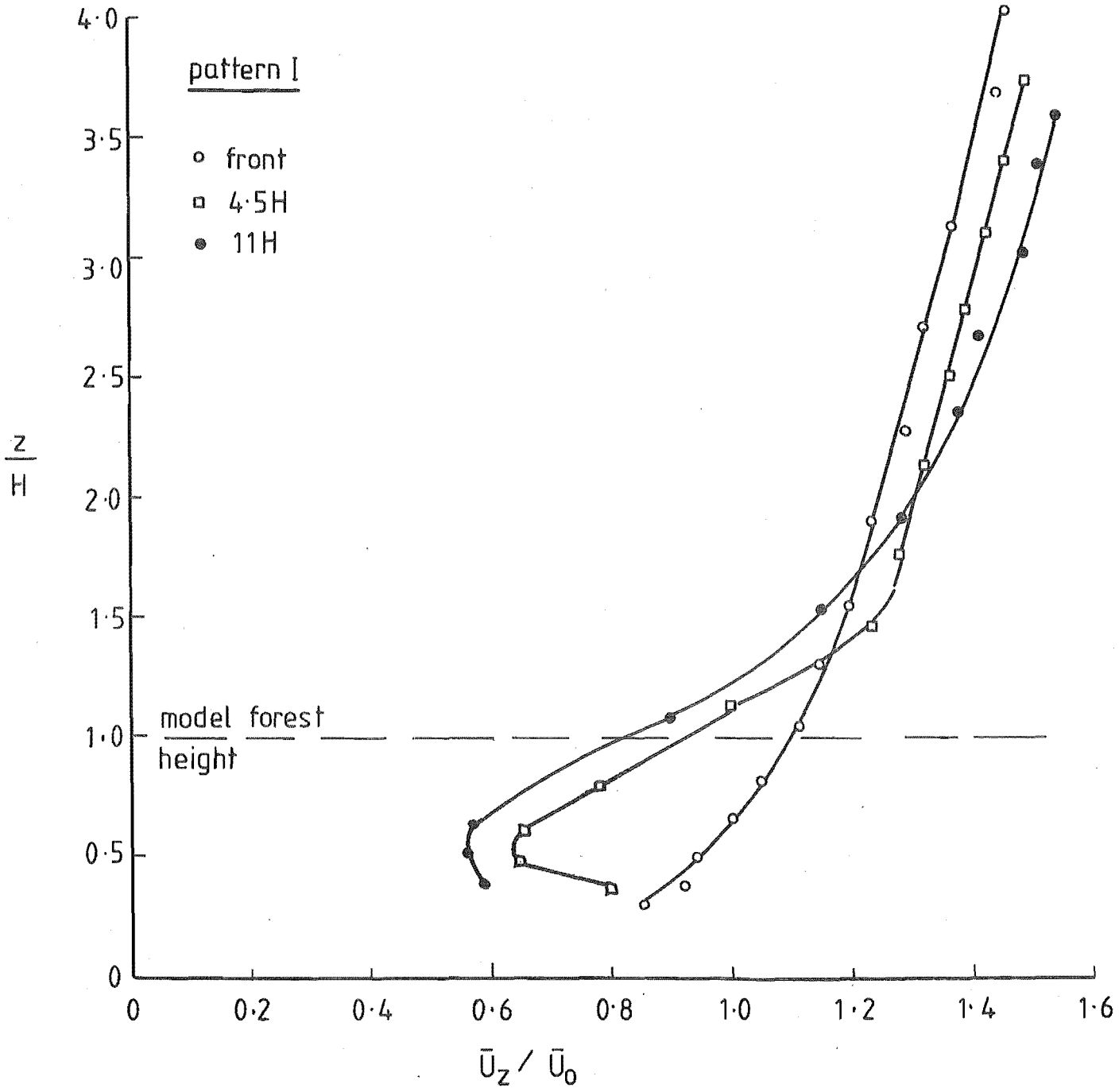

FIGURE 6.2(c): Mean wind velocity profiles from model tests (Pattern I).

TABLE 6.2: Mean deflection (D) and $(\frac{A}{D})$ by photography (Canterbury).

PATTERN DESIGNATION	A	B	C	D	E	F	G	H	I	J
D maximum/ D average	3.396	3.533	3.222	3.797	3.016	2.985	2.500	2.242	2.302	2.130
D front/ D average	2.212	2.311	2.111	2.610	1.311	1.911	1.381	1.537	1.365	1.500
D maximum D front	1.538	1.529	1.526	1.455	2.300	1.562	1.810	1.459	1.687	1.420
D middle/ D average	0.396	0.422	0.610	0.441	0.852	0.706	0.774	0.747	0.896	1.020
D rear/ D average	0.623	0.556	0.578	0.559	0.705	0.588	0.631	0.716	0.802	0.833
$\frac{D}{H}$ average	0.053 (16)	0.045 (28)	0.045 (22)	0.059 (17)	0.061 (19)	0.068 (26)	0.084 (14)	0.095	0.096	0.108
1 Std Devn for $\frac{D}{H}$ average	0.048	0.038	0.036	0.061	0.038	0.044	0.044	0.049	0.042	0.042
$\frac{D}{H}$ maximum	0.180	0.159	0.145	0.224	0.184	0.203	0.210	0.213	0.221	0.230
Row position for $\frac{D}{H}$ maximum	1	1	1	2	1	2	1	2	1	2
$\frac{D}{H}$ (OH-3H)	0.117	0.104	0.095	0.154	0.080	0.130	0.116	0.146	0.131	0.162 (5)
1 Std Devn for $\frac{D}{H}$ (OH-3H)	0.045	0.040	0.036	0.057	0.064	0.048	0.052	0.053	0.061	0.061
$\frac{D}{H}$ (3H-7H)	0.021 (6)	0.019	0.025 (7)	0.026	0.052	0.048 (8)	0.065 (5)	0.071	0.086 (7)	0.111
1 Std Devn for $\frac{D}{H}$ (3H-7H)	0.007	0.009	0.009	0.021	0.007	0.015	0.004	0.039	0.014	0.019
$\frac{D}{H}$ (7H-11H+)	0.033 (5)	0.025	0.026 (7)	0.033	0.043	0.040	0.053 (3)	0.068 (6)	0.077	0.090
1 Std levn for $\frac{D}{H}$ (7H-11H+)	0.019	0.008	0.006	0.012	0.006	0.008	0.014	0.016	0.019	0.022
A average/ D average	1.604	2.111	2.156	1.729	2.262	1.706	1.595	1.411	1.542	1.407
A maximum/ D maximum	0.794	1.415	1.600	0.830	1.223	0.793	0.924	1.019	0.955	1.017
$\frac{A}{D}$ (OH-3H)	1.143	1.519	1.695	1.069	2.100	2.342	1.431	1.130	1.153	1.042
$\frac{A}{D}$ (3H-7H)	2.229	2.226	2.440	2.423	2.192	1.854	1.785	1.408	1.733	1.360
$\frac{A}{D}$ (7H-11H+)	2.697	4.120	3.231	2.970	3.000	2.800	2.132	2.000	1.857	1.622

(a) 3 - 7H

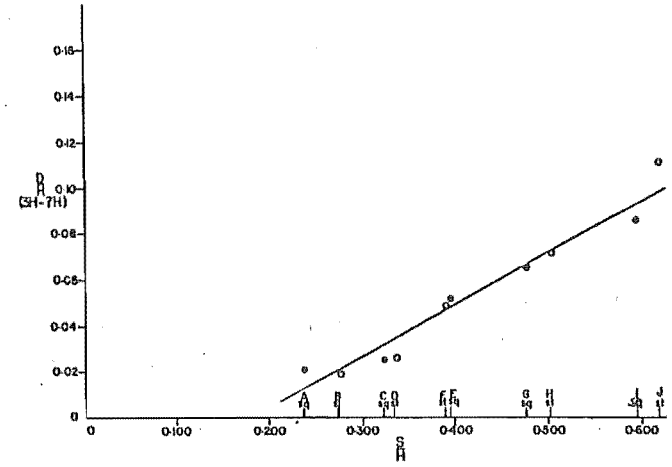

(b) 7 - 11H

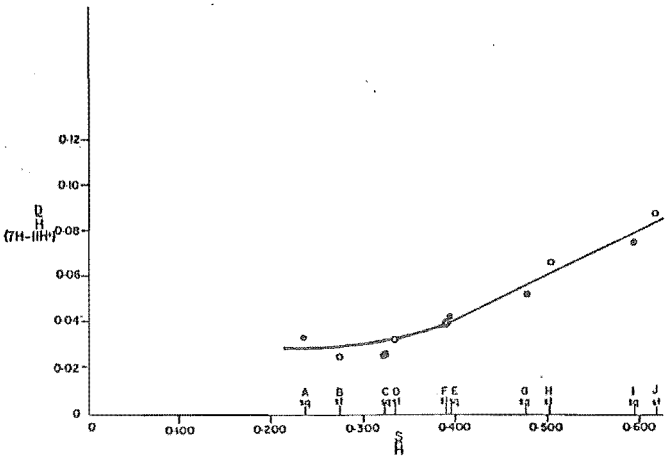

(c) 0 - 11H

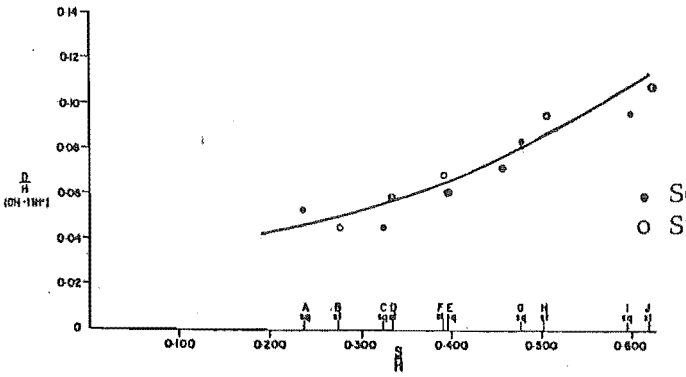

• Square array
o Staggered array

FIGURES 6.3(a) - (c): Mean deflection v spacing density, (Canterbury).

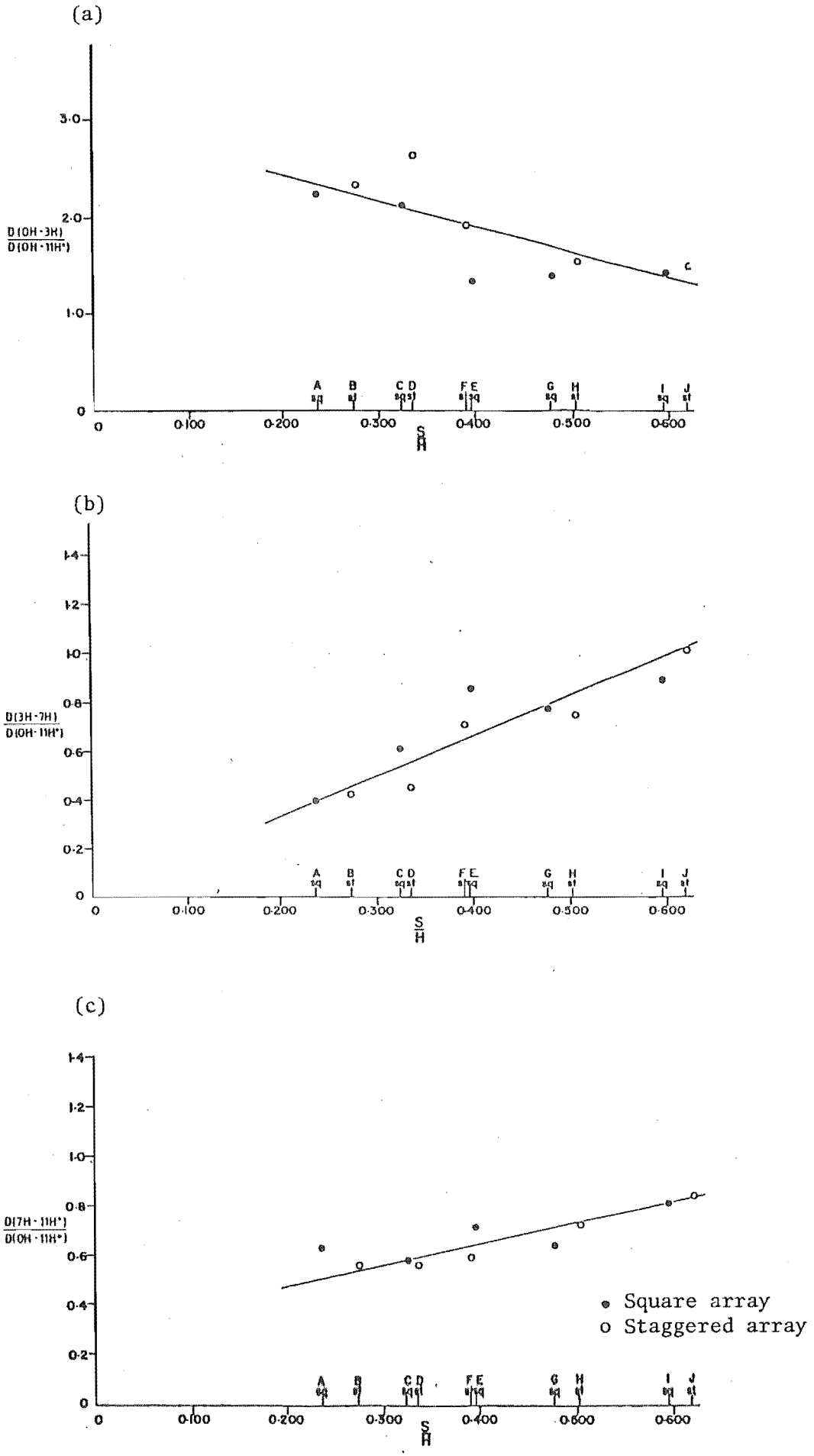

FIGURES 6.4(a) - (c): Mean deflection ratio v spacing density by photography.

the leading edge. Earlier (3.10) it was evident that $\frac{D}{H}$ increases proportionally as $\frac{S}{H}$ and $\left(\frac{\bar{U}_H}{\bar{U}_o}\right)^2$ respectively increase. So, after $\frac{S}{H}$ reaches 0.35, it appears that $\frac{D}{H}$ is a function of $\frac{S}{H}$ and $\left(\frac{\bar{U}_H}{\bar{U}_o}\right)^2$.

Square and staggered patterns showed no significant differences. Notice how D falls to zero as the model trees become very close. In the Oxford wind tunnel tests the model tree crowns in Pattern P actually touch, and separation zones may exist (6.8.1).

6.6.3 Mean of large amplitudes versus spacing

Model tree amplitudes obtained by photographic analysis are given in Table 6.3 and are plotted in Figures 6.5(a)-(d) and 6.6.

As spacings increase from $\frac{S}{H}$ of 0.24 to 0.62, A increases 'linearly' from the closest spacing. Once again, except for right at the front $\frac{A}{H}$ increases with $\frac{S}{H}$, but at different rates and different magnitudes for the same x-positions. Here it is evident that $\frac{A}{H}$ increases as $\frac{S}{H}$, $\frac{x}{H}$ and $\frac{\bar{U}_H}{\bar{U}_o}$ respectively increase (see 3.10; 7.25). So, it appears that $\frac{A}{H}$ is a function of $\frac{x}{H}$, $\frac{S}{H}$ and $\frac{\bar{U}_H}{\bar{U}_o}$.

Square and staggered patterns showed no significant differences. Generally, the contributions to model tree-top deflections from sway components are much larger than contributions from the mean deflection components (Fig. 6.7).

6.6.4 Ratio of $\frac{A}{D}$ versus spacing

The ratio of $\frac{A}{D}$ with spacing and x-position are given in Table 6.2 and Figure 6.7(a)-(c). The relative magnitudes are compared for various spacing densities. Notice the increase in $\frac{A}{D}$ along-wind as spacing density is reduced. These figures must be interpreted correctly. $\frac{A}{H}$ is much higher than $\frac{D}{H}$ near the forest leading edge, while $\frac{A}{H}$ and $\frac{D}{H}$ are similar in magnitude, but are smaller from 7H onwards, as equilibrium conditions return to the tree-top wind structure within the inner layer.

To compare total deflections, the magnitudes of $\frac{A+D}{H}$ indicate that model tree-top deflections are diminishing towards 10H. These reductions are more rapid for closer spacings up to $\frac{S}{H}$ of 0.35 than for spacings beyond (Fig. 6.8(a)-(c)).

To p.216

TABLE 6.3: Amplitude measurements (A) by photography.

PATTERN DESIGNATION	A	B	C	D	E	F	G	H	I	J
A maximum/ A average	1.682	2.368	2.392	1.806	1.630	1.388	1.448	1.619	1.426	1.539
A front/ A average	1.576	1.663	1.660	1.613	1.217	1.263	1.239	1.231	1.021	1.111
A maximum/ A front	1.067	1.424	1.441	1.120	1.339	1.059	1.169	1.315	1.397	1.385
A middle/ A average	0.551	0.445	0.629	0.618	0.833	0.767	0.866	0.746	1.006	0.993
A rear/ A average	1.042	1.084	0.866	0.960	0.935	0.966	0.843	1.015	0.966	0.961
$\frac{A}{H}$ average	0.085 (16)	0.095 (28)	0.097 (22)	0.102 (17)	0.138 (19)	0.116 (26)	0.134 (14)	0.134	0.148	0.152
1 Std Devn for $\frac{A}{H}$ average	0.035	0.048	0.046	0.044	0.031	0.035	0.032	0.039	0.024	0.028
$\frac{A}{H}$ maximum	0.143	0.225	0.232	0.186	0.225	0.161	0.194	0.217	0.211	0.234
Row position for $\frac{A}{H}$ maximum	1	4	2	2	2	1	1	1	4	2
$\frac{A}{H}$ (OH-3H)	0.134	0.158	0.161	0.166 (4)	0.168	0.152	0.166	0.165	0.151	0.169
1 Std Devn for $\frac{A}{H}$ (OH-3H)	0.008	0.049	0.033	0.021	0.035	0.025	0.018	0.027	0.034	0.037
$\frac{A}{H}$ (3H-7H)	0.047	0.042	0.061 (7)	0.063	0.115 (5)	0.089	0.116	0.100 (6)	0.149 (7)	0.151 (10)
1 Std Devn for $\frac{A}{H}$ (3H-7H)	0.010	0.009	0.014	0.012	0.010	0.030	0.025	0.033	0.017	0.018
$\frac{A}{H}$ (7H-11H+)	0.089 (5)	0.103 (9)	0.084	0.098	0.129 (5)	0.112	0.113 (5)	0.136	0.143 (8)	0.146 (11)
1 Std Devn for $\frac{A}{H}$ (7H-11H+)	0.014	0.020	0.008	0.014	0.020	0.024	0.020	0.036	0.024	0.029

(a) 0 - 3H

$\frac{A}{H}$

(OH-3H)

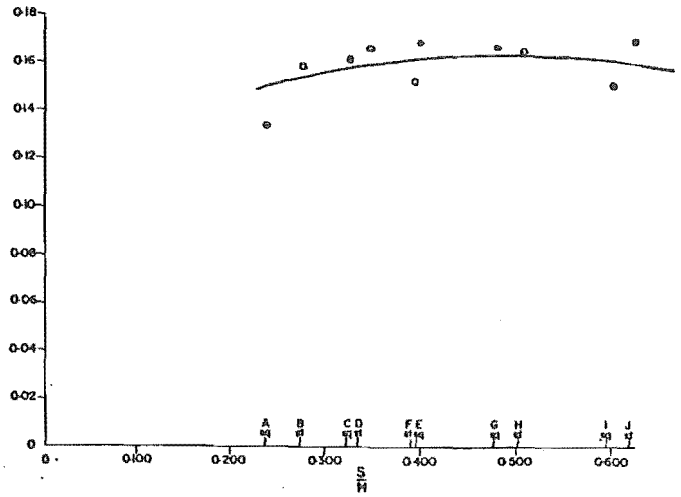

(b) 3 - 7H

$\frac{A}{H}$

(3H-7H)

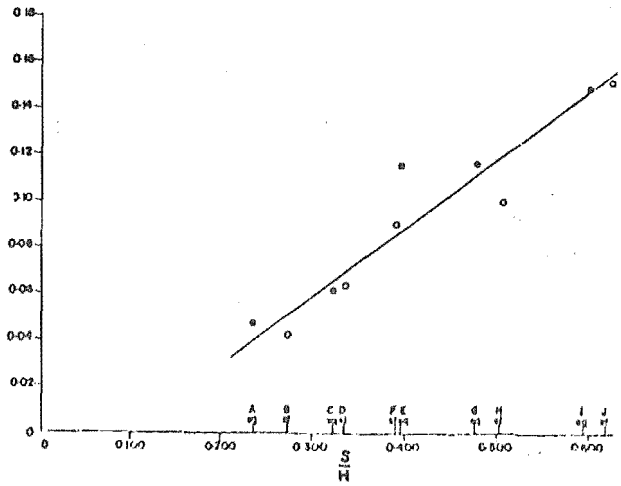

(b) 7 - 11H

$\frac{A}{H}$

(7H-11H+)

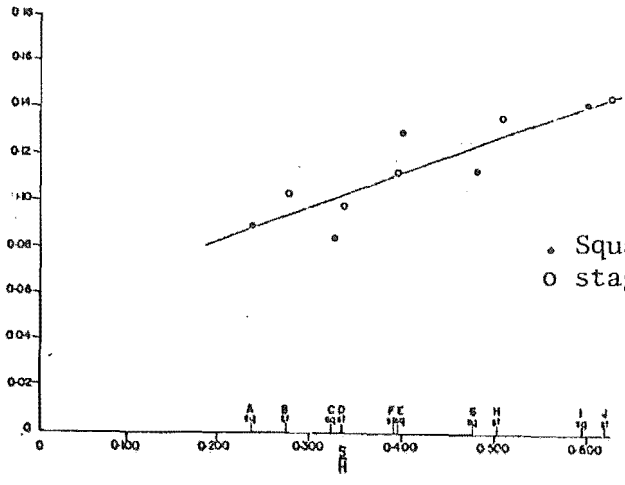

FIGURES 6.5(a) - (c): Amplitude v spacing density.

(d) 0 - 11H

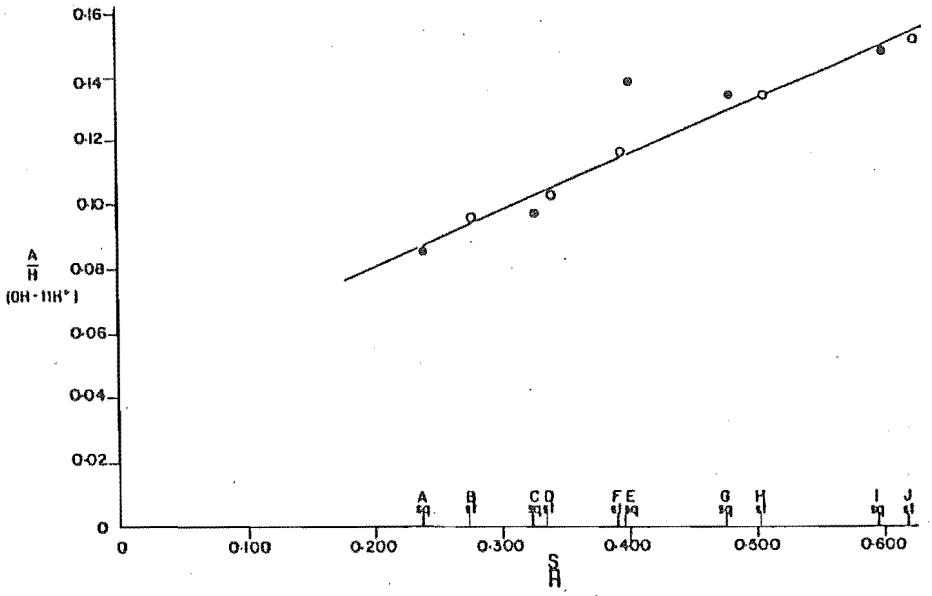

FIGURE 6.5(d): Amplitude v spacing density.

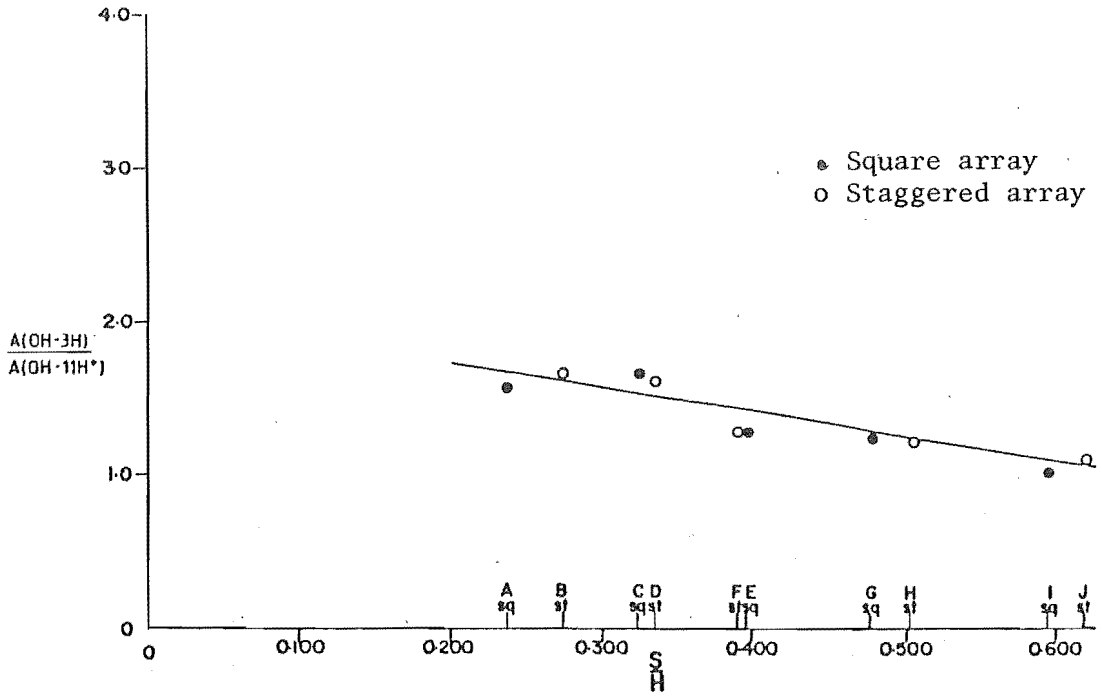

FIGURE 6.6: Amplitude ratio v spacing density.

(a) 0 - 3H

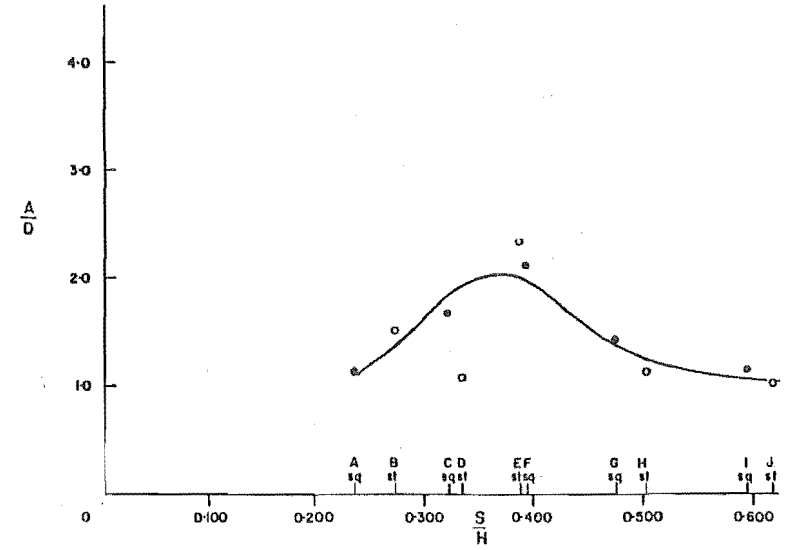

(b) 3 - 7H

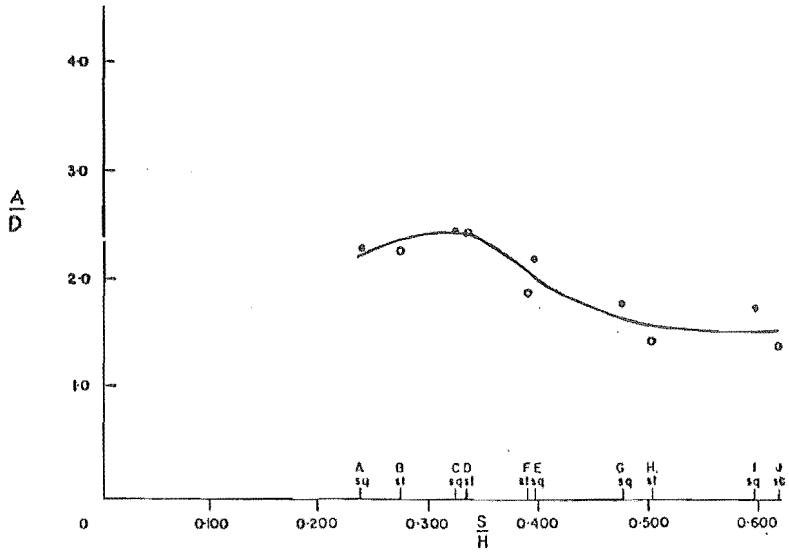

(c) 7 - 11H

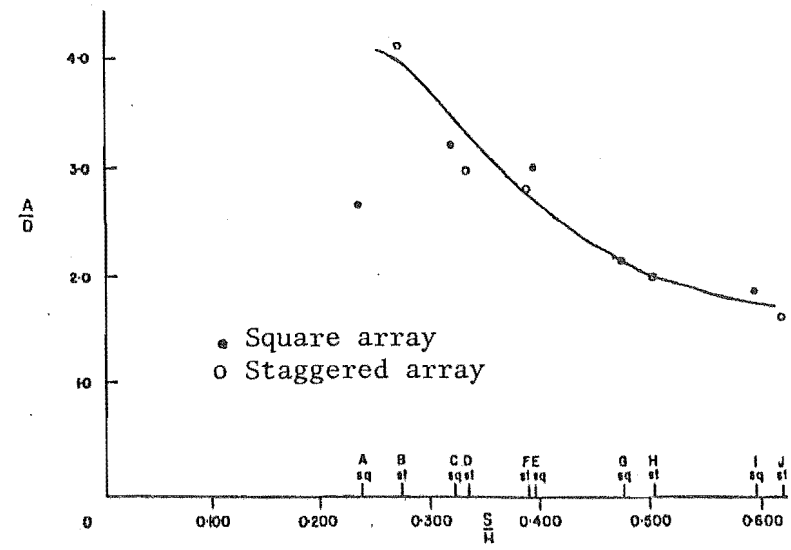

FIGURES 6.7 (a) - (c): $\frac{\text{Amplitude}}{\text{Mean deflection}}$ v spacing density, Canterbury.

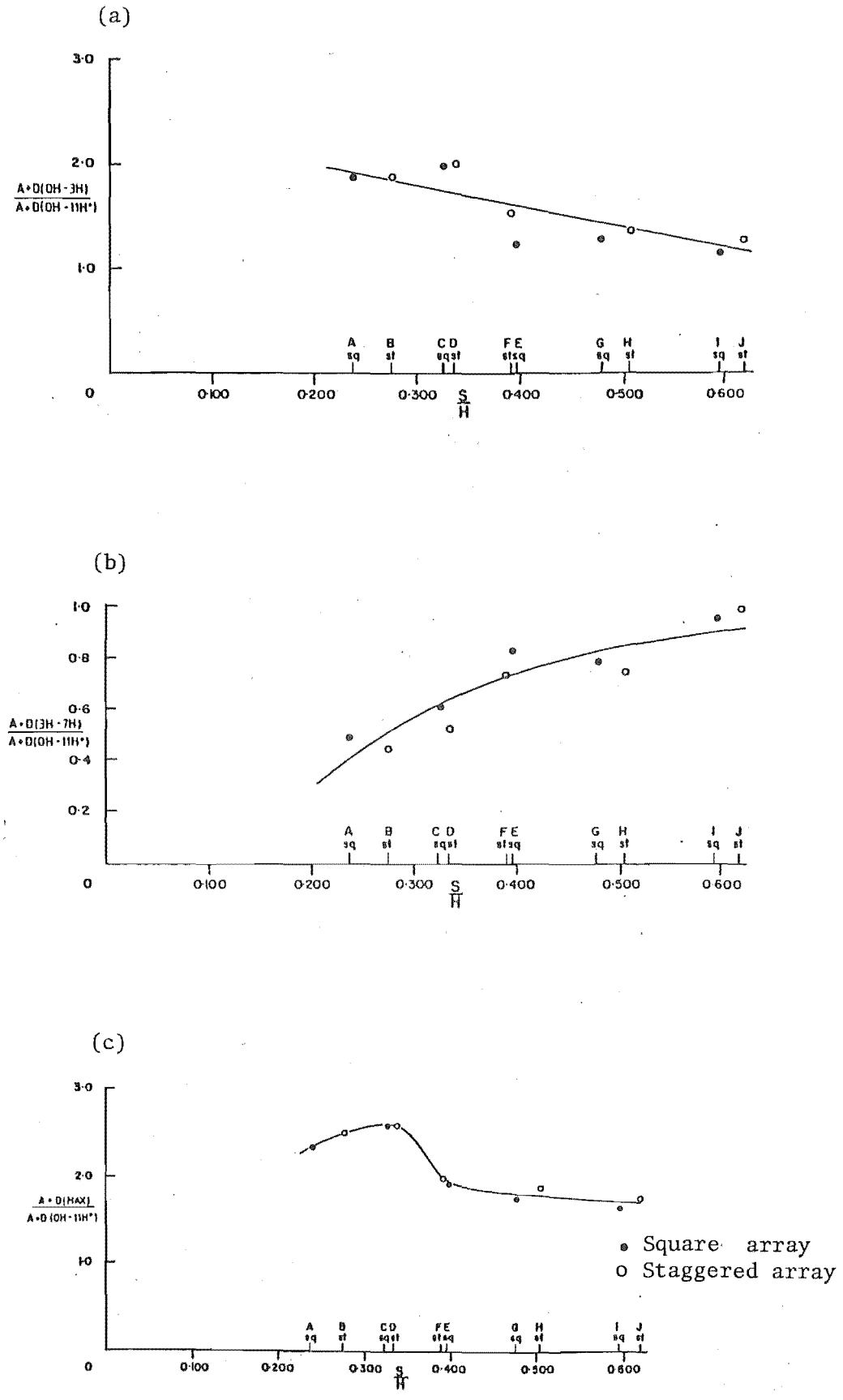

FIGURES 6.8(a) - (c): Total model tree top movement distribution with spacing density.

6.6.5 Summary

This model study gave:-

(a) the shape of the mean velocity profiles near a forest leading edge (6.10.1; Fig. 7.2);

(b) an estimate of the extent of non-zero horizontal pressure gradients along-wind;

(c) an estimate of tree-top swaying motion for different spacings at different x-positions in from the model forest leading edge using motion photography;

(d) some values of the aerodynamic roughness and shear stress coefficients from the mean wind profiles (Table 6.7).

These interpretations were used to design the test procedure in the Oxford model forest study.

6.7 OXFORD MODEL FOREST TESTS

6.7.1 Tunnel and wind calibrations

The tunnel at Osney Laboratories, Oxford University, was commissioned in 1974. It is an open-circuit tunnel with a contraction ratio of 2.8 leading to a 14 m-long, 4 m-wide, 2 m-high working section. The flow divides after the working section and flows through two diffusers where it is drawn out to atmosphere by a pair of Woods variable-pitch 16-bladed axial flow fans. (Fig.6.9). There are two fan speeds, 296 r.p.m. and 594 r.p.m., and the pitch of the fan blades can be adjusted either together or separately to provide, without grids, a range of windspeeds from 0 - 30 m/s. Grid location and upstream roughness of the model reduce the maximum tunnel wind speed to about 7 m/s at 10 m full scale equivalent height. The grid and artificial roughness, for $\frac{1}{75}$ scale, was developed by S. Gumley (1980) and modified in April 1982 for a contract requiring slightly greater roughness (0.07 m) than that used in this experiment (0.03 m). Some minor modifications gave mean wind and turbulence intensity profiles (Fig. 6.10 and 6.11) and spectra (Fig. 6.12) close to the ESDU standard. The Oxford wind tunnel spectra gives a slightly higher energy level in the inertial region of the spectrum, but is still better than other similar wind tunnels of this type (Fig. 6.13). In any case the ESDU spectra standard curve under-estimates in the inertial region (Neal, 1979).

To p.220

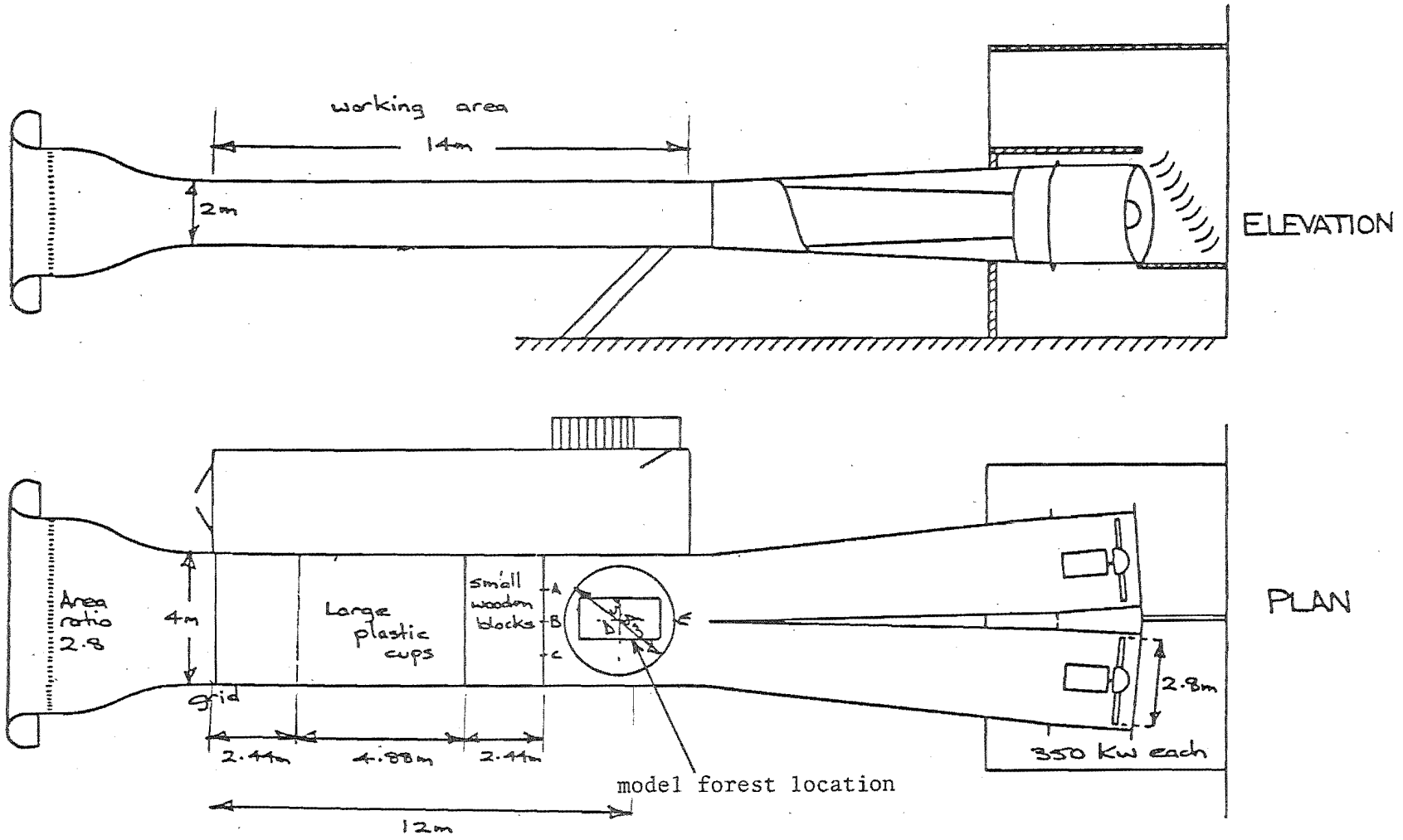

FIGURE 6.9: Boundary layer wind tunnel, University of Oxford.

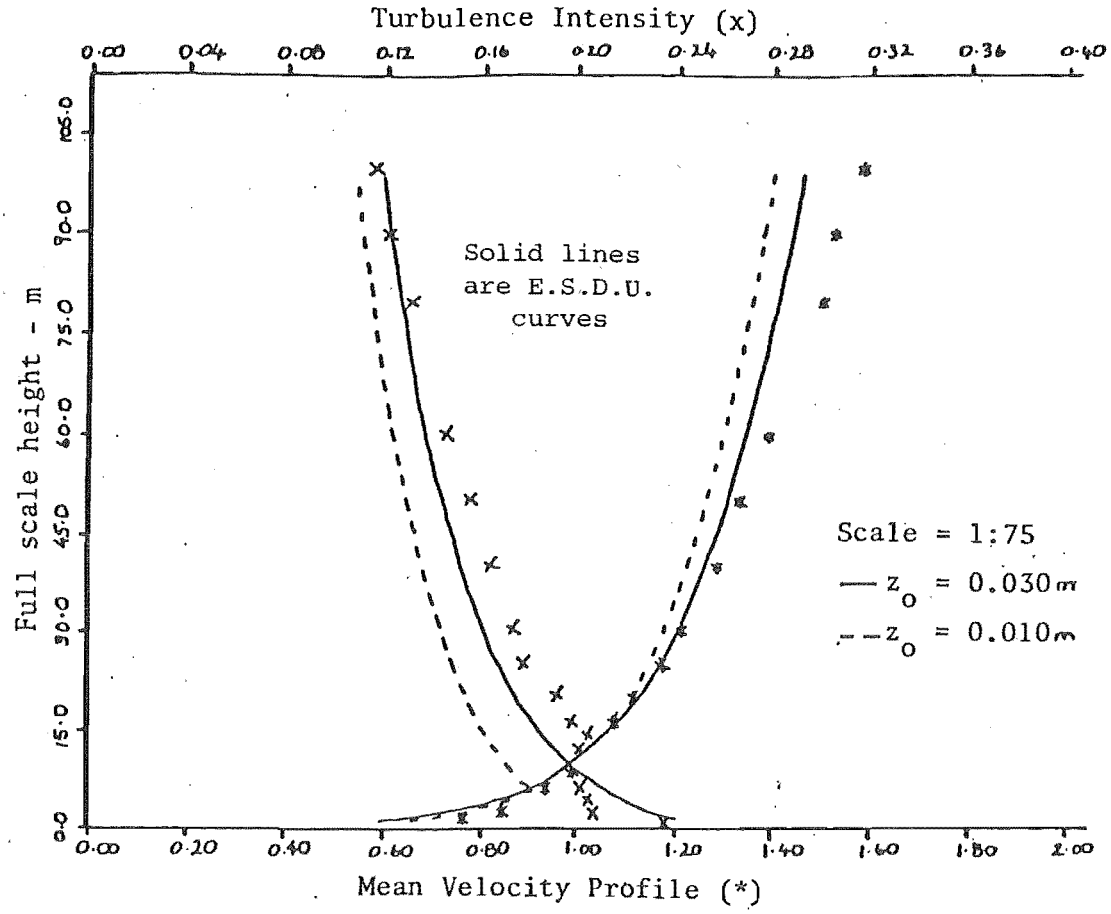

FIGURE 6.10: Velocity and Turbulence Intensity Profiles for 1:75 scale Simulation (Oxford).

DATA FILE FOR001
****

19-APR-82 16:44
UPSTREAM REF POINT
-2.5H, 1:75 SIMULATION
AS USED BY S.J.G.
SET VELOCITY 6 M/SEC

SAMPLING INTERVAL MILLISECS	SAMPLING DURATION SECONDS	TUNNEL HEIGHT METRES	VELOCITY METRES/SEC	TURBULENCE INTENSITY	DEVIATION METRES/SEC
10.0	58.570	0.133	3.356	0.302	1.015
10.0	57.580	0.070	2.499	0.400	1.000
10.0	57.340	0.080	2.657	0.391	1.038
10.0	62.490	0.090	2.876	0.361	1.038
10.0	56.530	0.110	3.220	0.316	1.016
10.0	57.720	0.133	3.385	0.309	1.046
10.0	58.090	0.150	3.599	0.290	1.044
10.0	64.420	0.200	3.940	0.265	1.044
10.0	58.540	0.250	4.291	0.234	1.002
10.0	54.130	0.300	4.446	0.219	0.972
10.0	42.430	0.350	4.665	0.195	0.910
10.0	52.320	0.420	4.725	0.199	0.940
10.0	56.440	0.133	3.527	0.293	1.034

FIGURE 6.11: Calibration run for 1:75 scale simulation.

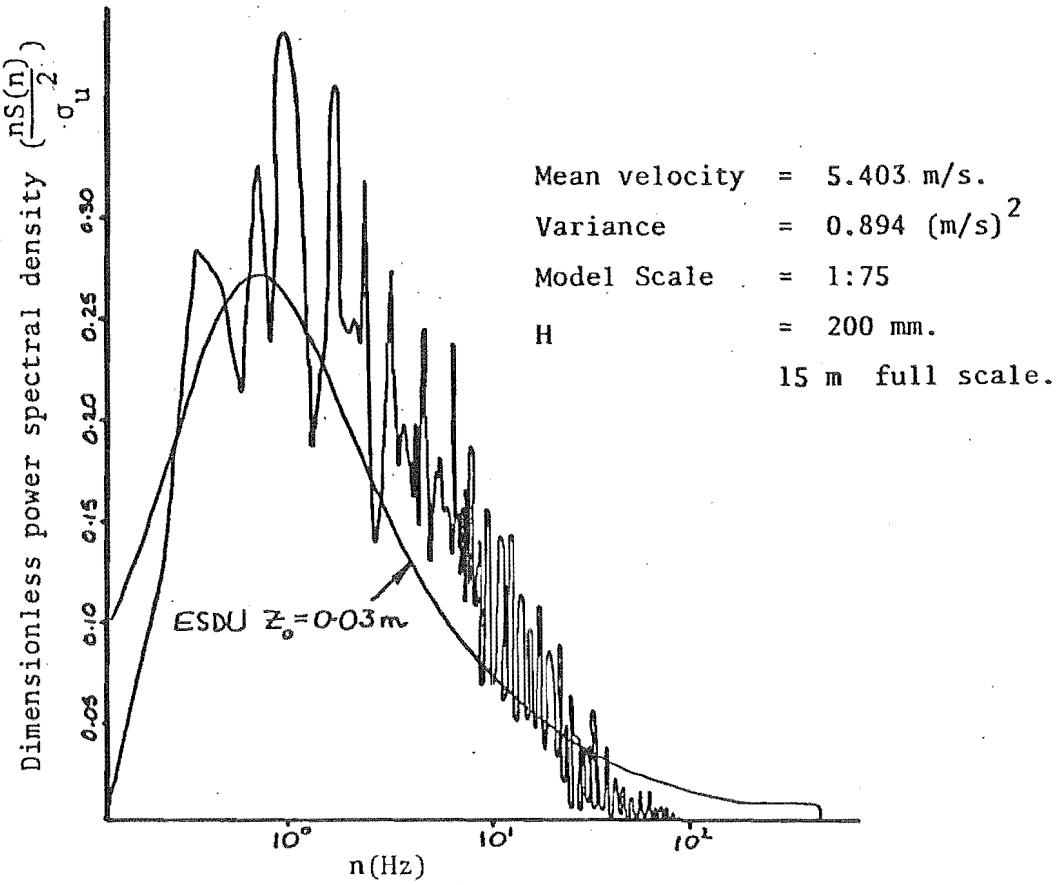

FIGURE 6.12: Power spectrum upstream for 1:75 scale simulation (Oxford)

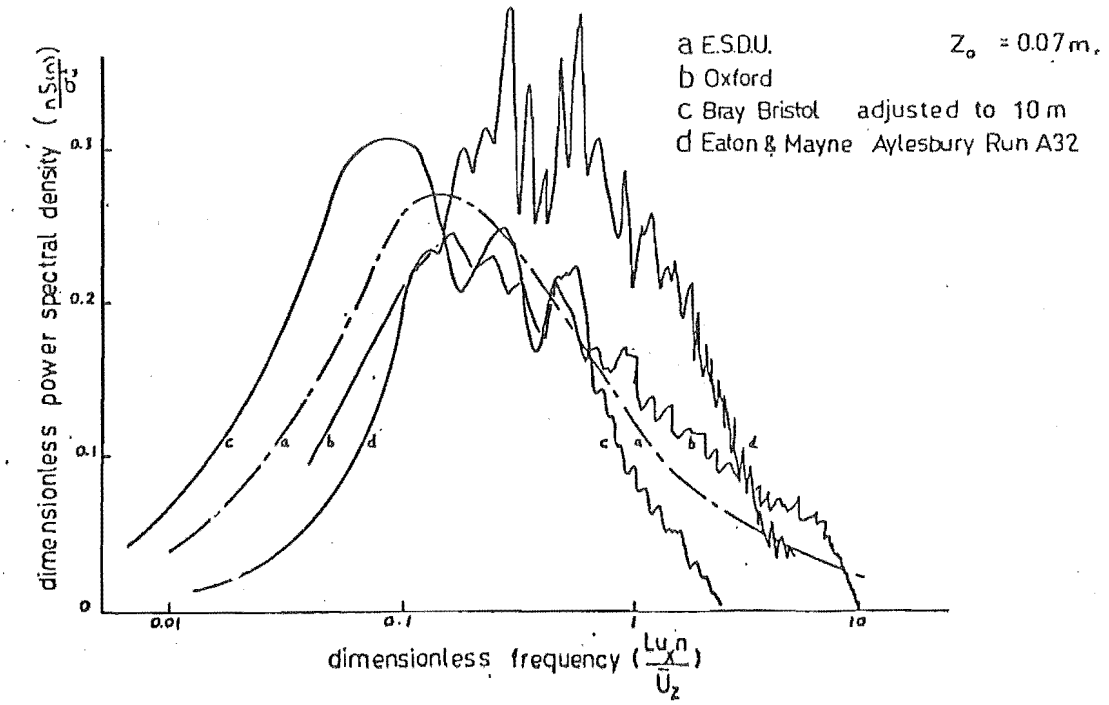

FIGURE 6.13: Power spectrum (Oxford) compared with other simulations.

At the scale of $\frac{1}{75}$, the 2 m height of the working section permits simulation of the wind structure up to a full scale height of 150 m. This is below the full scale requirement of 300 m, which is a common limitation in all atmospheric wind simulations. It is acceptable for wind loading model tests. Because this wind tunnel height is larger than that of most tunnels of this type, cross-section area blockage is below 3% (6.3).

The reference velocity of 6 m/s (6.4.2) 133 mm upstream at -3H from the forest front was maintained within practical limits for the duration of the experiment. After a series of calibration checks at several locations (Fig. 6.14), the vertical grid 11 m upstream and the upstream roughness were slightly adjusted, so that profiles and spectra were close to ESDU standards at -3H from the forest leading edge. At the end of the experiment, checks were made with side boards and no forest, and again with no side boards and no forest, to verify the uniformity of profiles and spectra.

Wind structure homogeneity without the model forest was acceptable (Table 6.4). The mean wind speed profiles varied by ± 4% across the tunnel at -3H, and along-wind, the variation was much the same. Turbulence intensity varied by similar amounts, and spectra were consistent with ESDU standards, with a slight improvement towards the rear of the model forest.

TABLE 6.4 Calibration traverses: model forest and side boards removed

Sampling Interval (millisecs)	Sampling Duration (Seconds)	Traverse Position z = 0.18 m	Mean Velocity (m/s)		Turbulence Intensity		Standard Deviation (m/s)	
			Run (1)	(2)	Run (1)	(2)	Run (1)	(2)
10.0	99.550	-3H centre 'A',	6.506	6.571	0.178	0.171	1.155	1.127
10.0	83.780	-3H LHS 'B',	6.821	6.826	0.164	0.174	1.116	1.189
10.0	93.480	-3H RHS 'C',	6.983	6.977	0.196	0.180	1.366	1.255
10.0	55.110	-1H centre 'D',	6.479	-	0.167	-	1.080	-
10.0	61.770	+1H centre 'E',	6.638	6.758	0.168	0.165	1.117	1.114
10.0	59.350	3H centre 'F',	6.646	6.727	0.155	0.158	1.027	1.073
10.0	52.410	5H centre 'G',	6.668	6.896	0.145	0.147	0.965	1.009
10.0	58.150	7H centre 'H',	6.786	6.910	0.146	0.142	0.992	0.979
10.0	57.420	10H centre 'I',	6.838	6.683	0.135	0.147	0.926	0.985
10.0	66.240	-3H centre 'A',	6.593	6.419	0.165	0.174	1.091	1.117
10.0	61.780	-3H centre 'A',	6.439	6.415	0.175	0.179	1.125	1.150
10.0	62.740	-3H centre 'A',	6.657	-	0.169	-	1.127	-
10.0	70.120	-3H centre 'A',	6.506	-	0.177	-	1.154	-

To p. 222

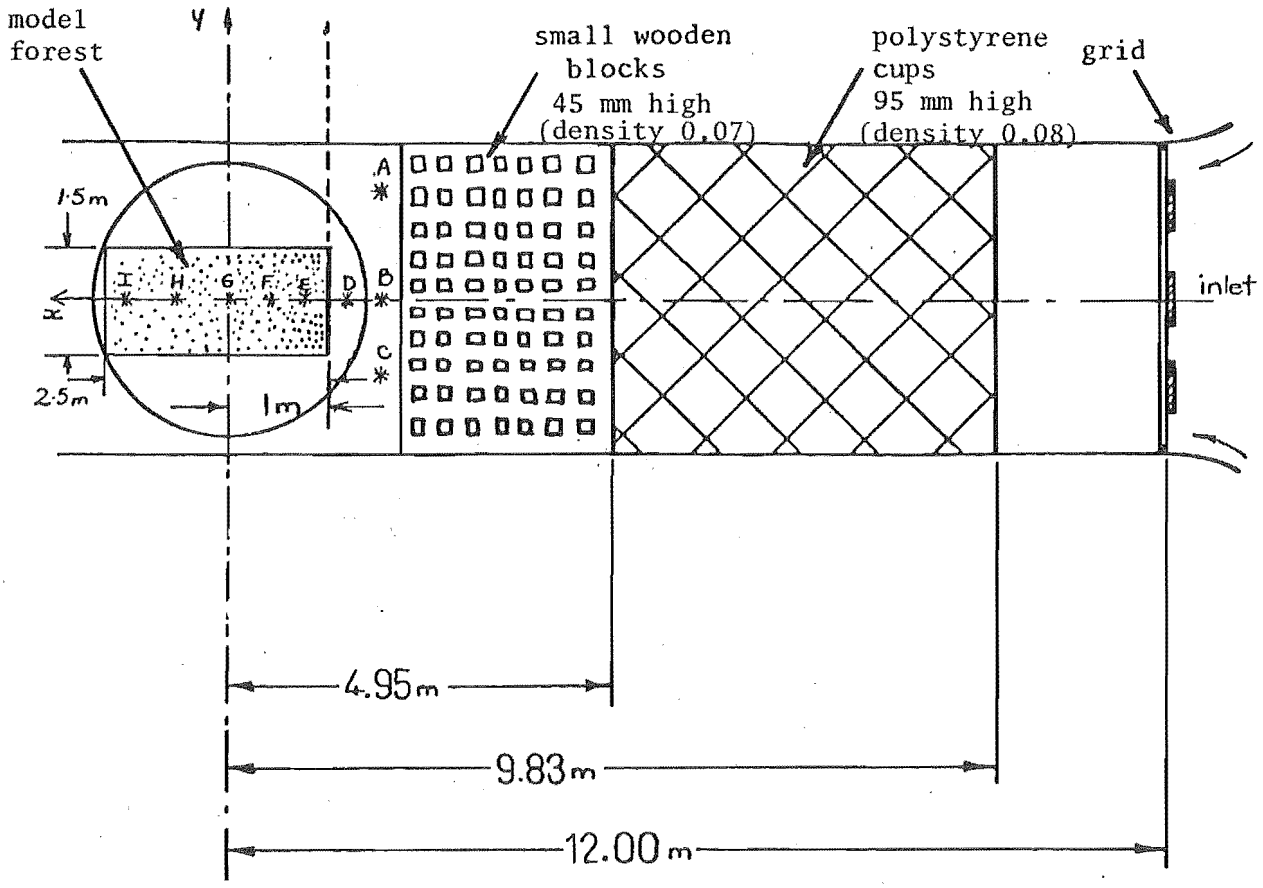

FIGURE 6.14: Plan of Simulation Devices for 1:75 Scale, z_o = 0.03 m.

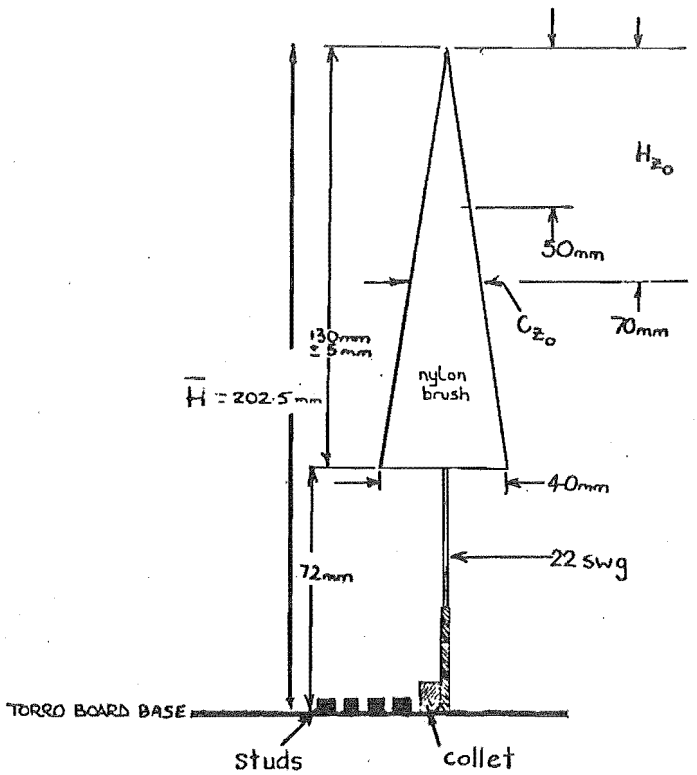

FIGURE 6.15: Diagram of model tree dimensions (also Figure 3.27)

6.7.2 Instrumentation and data processing

For velocity measurements, Disa K series hot-wire anemometers were mounted on a remotely-controlled arm which was fitted to a tripod and located at the grid position required. The arm could traverse a vertical range of 0.35 m from a set position of 0.17 m.

After being calibrated (Fig. 6.17), the output from the hot-wire anemometers is conditioned via dual-channel Kemo switchable filters to a DC amplifier to adjust the level of the output signals. These are then fed to the analogue-digital converter which is situated close to its PDP 11/10 computer. A data-reducing programme produces numerical results from a 100 point probability density distribution (Fig. 6.19) and returns them to a teleprinter in the tunnel control cabin as each run proceeds. Machine-graph plotting of mean wind profiles and turbulence intensity profiles, and of power spectra curves between 1 Hz and 200 Hz, is routine.

In a typical spectrum, 112 separate blocks of data, each containing 512 instantaneous velocity readings, are taken at intervals of 10 ms. The analogue filter settings required a frequency range from near 0.2 Hz to 200 Hz to eliminate the mean value and avoid high frequency aliasing problems (Appendix II).

Each channel was sampled at 100 Hz for periods of about 30 seconds. This was sufficient for probability density distributions which were monitored on a television screen to check for voltage distortions. These distortions indicate the occurrence of separated flow and may be either out of the frequency range for the A.D.C., or negative (Fig. 6.19(a)-(c)).

From the first and second moments of these distributions, the mean velocity and turbulence intensity profiles were computed and then printed. For spectra, a standard Fast Fourier Transform programme was used: when applied to each data block it gave a set of real and imaginary Fourier coefficients. These were then combined to yield the ordinates for a power-spectral density curve. For the final spectrum for each case, the results from the 112 blocks were averaged.

The data reduction programmes produce numerical results in real time and return them to a teleprinter in the tunnel control cabin as each run progresses. Graph plotting was slower and was done later, at the end of a run.

A Hewlett-Packard Correlator from the University of Bristol had been used to verify the programmes and processing systems of the PDP 11/10 computer during previous calibration runs.

6.7.3 Hot-wire anemometer limitations

There are two sources of error when the elements of the hot wires measure turbulence intensity.

(a) As turbulence intensity increases over the hot wires of these anemometers, the resultant cooling velocity for the wires, $\bar{V}_c$, normal to the u' or v' components is,

$$\bar{V}_c \simeq U\left[1 + \frac{1}{2}\left(\frac{\overline{v'}}{U}\right)^2\right] \quad , \text{ (reduced binomial expansion)}$$

(b) The result for variance is;

$$\overline{V^2} - (\bar{V})^2 \simeq U^2\left[\left(\frac{\overline{u'}}{U}\right)^2 - \frac{1}{4}\left[\left(\frac{\overline{v'}}{U}\right)^2\right]^2\right) \quad .$$

i.e. $$\frac{\overline{V^2}}{U^2} - \left(\frac{\bar{V}}{U}\right)^2 \simeq \left(\left(\frac{\overline{u'}}{U}\right)^2 - \frac{1}{4}\left[\left(\frac{\overline{v'}}{U}\right)^2\right]^2\right)$$

Nakagawa and Nezu (1977) showed that downsweep-burst cycles occur as a feature of turbulent flows over rough surfaces as well as over smooth: the dominant momentum transfer mechanism is the downsweep, or gust (u' positive, w' negative), rather than the burst (Finnigan). Finnigan considers that the hot-wire rectification errors are reduced if, instead of being distributed normally, u' fluctuations are positively skewed at times of large contributions to $\overline{u'w'}$, or shear . He shows that, over his wheat canopy, there is large positive skew (sk_u') up from 2½ to 14 times the skew due to rectification effects over gaussian distributions. Therefore, hot-wire errors reduce considerably, especially at times of higher than normal turbulence momentum mixing. Normally, measurements of turbulent velocities for spectra will under-estimate turbulent energies by 6.25%. In any case, ESDU standards state that standard

spectra are a composite of experimental results with differences of up to 30%.

Hot-wire probes should be used with caution for measuring turbulence intensity beyond 50%. If, however, instantaneous flow should reverse because of separated flow, the readings from hot-wires are invalid; they cannot distinguish between positive and negative velocities. The distribution of positive, zero and negative wind velocities can be seen on the screen monitor. In this experiment, the model forest leading edge has enough porosity, and causes sufficient flow acceleration, to prevent large scale separation zones. (In the Canterbury model forest tests, flow visualisation was used to check for the presence of separated zones.)

Crossed-wire x-y probes were used to measure Reynolds stresses at tree-top height. They are subject to even higher reading errors than x-probes. Continual mechanical and electrical malfunction of these sensors produced errors because of run stoppages and false computer printouts (6.3.2). The serviceability of the probes and the print-outs was validated because, in equilibrium conditions, the mean velocity of the vertical wind speed, $\bar{w}$, is close to zero (cf Tables 6.8 and 6.9).

Oxford model forest spectra data were not Hann-smoothed because the smoothing process can damp down any peaks which may occur in any spectrum (Wood, pers. comm.)

6.7.4 Oxford model forest

The model trees and pattern arrangements used in these tests were given a letter prefix, P-Z (Table 6.5). Altogether, 11 patterns were tested in square and staggered arrangements (Fig. 6.16).

To take advantage of the recessed turntable on the tunnel floor, the trees were assembled on Torro boards glued to two galvanised steel sheets. When they were mounted in the tunnel, the ground surface became flush with the tunnel floor, and the forest could be removed quickly for overnight pattern changes. For each pattern, measurements of windspeeds were made, analysed immediately and stored.

Spectra were taken at 180 mm and 220 mm to represent the spectra just above and just below the average model forest height (202.5 mm). During the tests some profiles and spectra were taken upstream as an added check on the uniformity of tests over the duration of the experiment.

To p.226

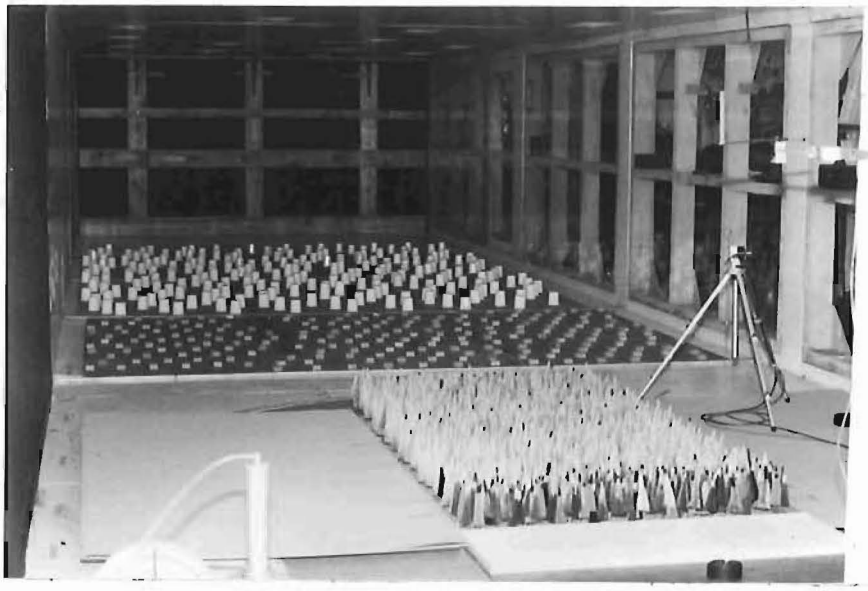

Photograph

Oxford University Osney B/L Wind Tunnel (4m x 2.5m). Grid and roughness for 1/75 scale; z_o = 0.03 m.

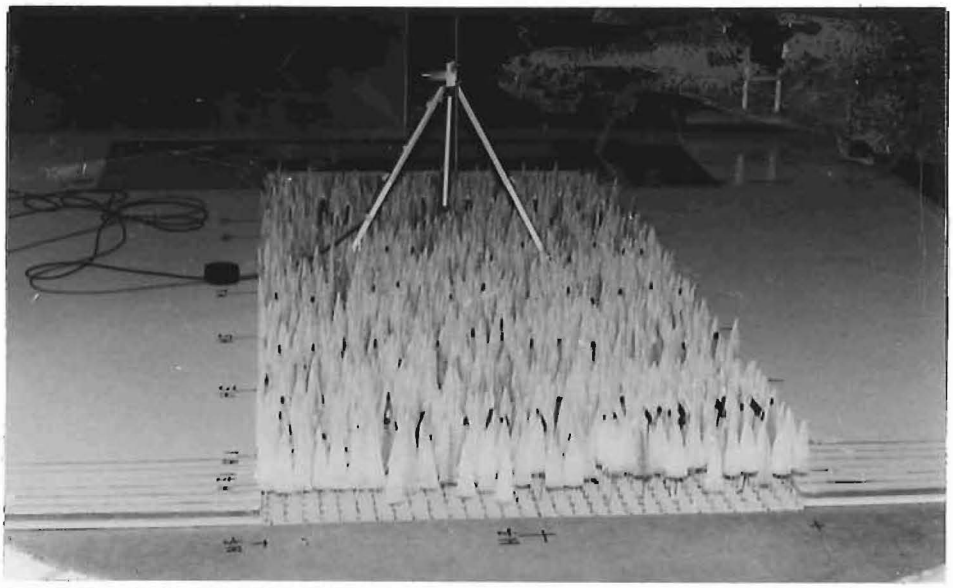

Photograph

Model forest (1.5m x 2.5m). Side boards slope to 0.6$\bar{H}$.

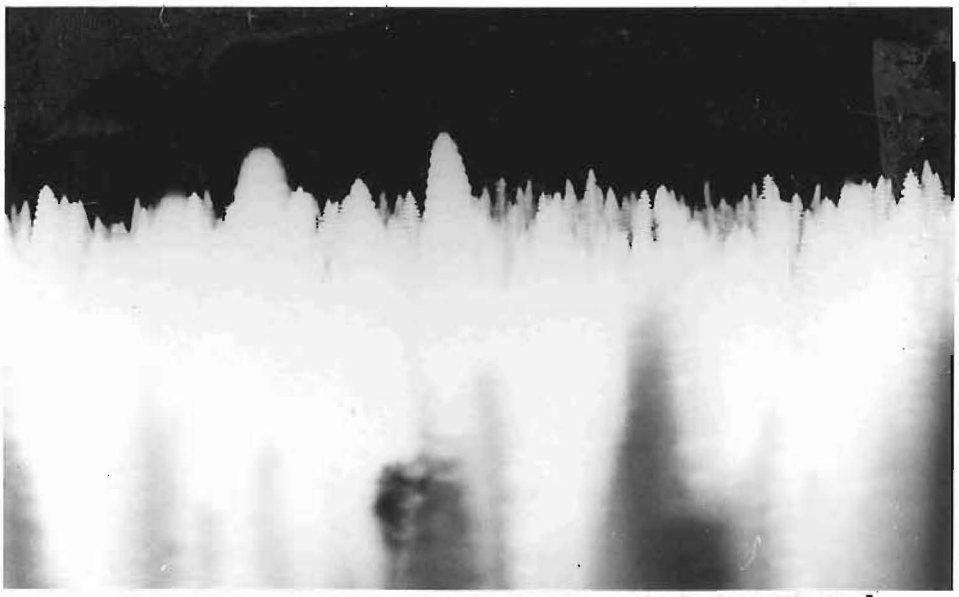

Photograph

Model forest roughness at $\frac{S}{\bar{H}}$ = 0.18 distributed as for sitka spruce and Radiata pine.

FIGURE 6.16 : Oxford University; Wind Tunnel and Model Forest.

TABLE 6.5 Model forest spacing patterns (Oxford)

Pattern Designation	Pattern Shape	Spacing (mm)	$\frac{S}{H}$
P	Staggered	34.5	0.17
U*	Square	40	0.20
Q	Square	48	0.24
R	Staggered	57	0.28
S	Square	64.5	0.32
T	Staggered	68.5	0.34
V	Staggered	79.5	0.39
W	Square	96	0.47
X	Staggered	101.5	0.51
Y	Square	120	0.59
Z	Staggered	124.5	0.61

At the same time 16 mm movie films were taken of tree movement at ½ H, 1 H, 3 H, 5 H, 7 H and 10 H to assess the dynamic response of model trees to recorded wind conditions (Fig. 6.18).

6.8 OXFORD MODEL FOREST RESULTS

The experiment lasted 14 days; 2 days for initial wind tunnel calibration, 11 days for testing the 11 patterns, and one day for concluding calibrations.

A complete file of the wind tunnel data and results is held on computer file at Osney Laboratory, and the original print-outs of all wind records are held by the Forestry Commission.

6.8.1 Separation checks

Vertical traverses of the wind structure were carried out over Pattern S to define the turbulence structure from 133 mm to 520 mm height above the floor (2½ tree heights above the crop). Large scale flow reversals were not evident (Fig. 6.19), but local areas of separation must occur (Fig. 6.26(a)-(k)). Velocity distributions were continually monitored during each run; in regions of likely separation, flow distributions always gave positive mean velocity averages, even at very high variances.

To p.232

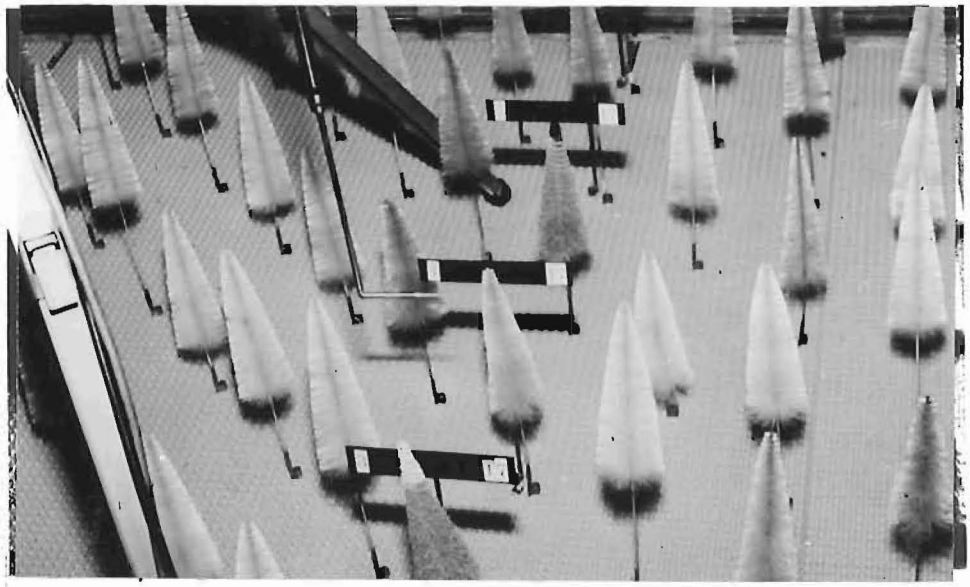

Photograph

Tree identification and x-probe in a wide spaced model forest.

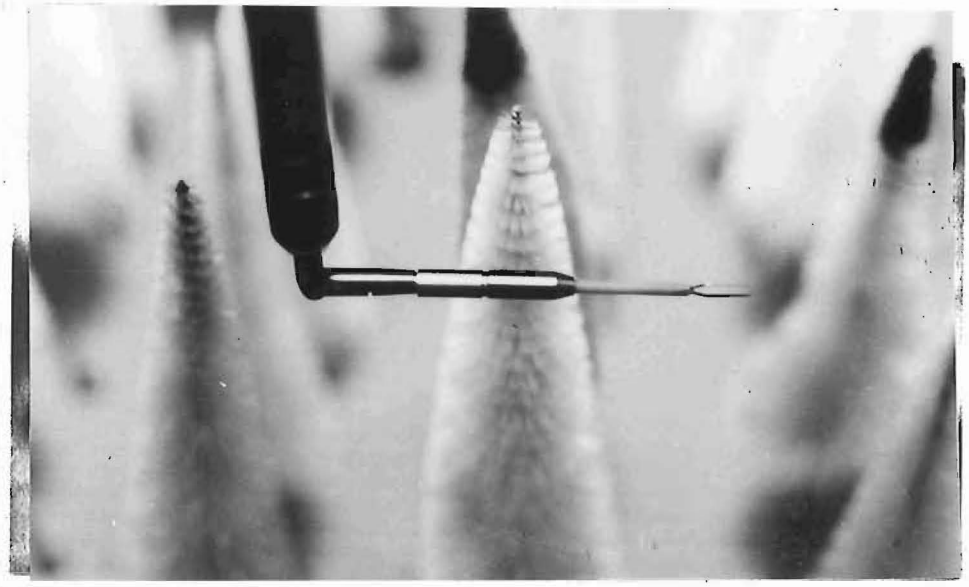

Photograph

Close-up of x-probe located centrally among adjacent tree crowns.

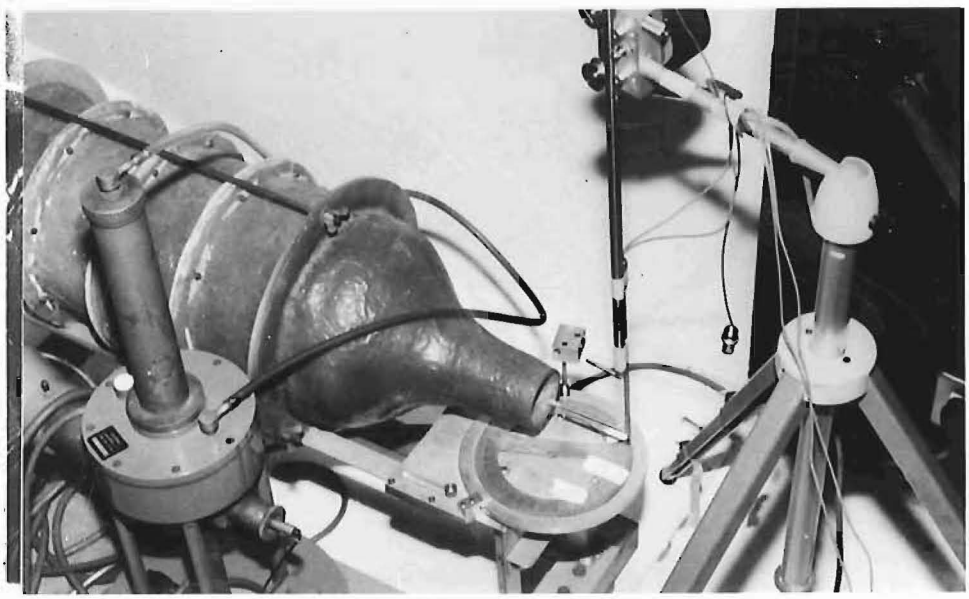

Photograph

Calibration of x-y probe before stress measurements on Pattern S canopy.

FIGURE 6.17: Model Forest; Wind Sensors and Referencing Equipment.

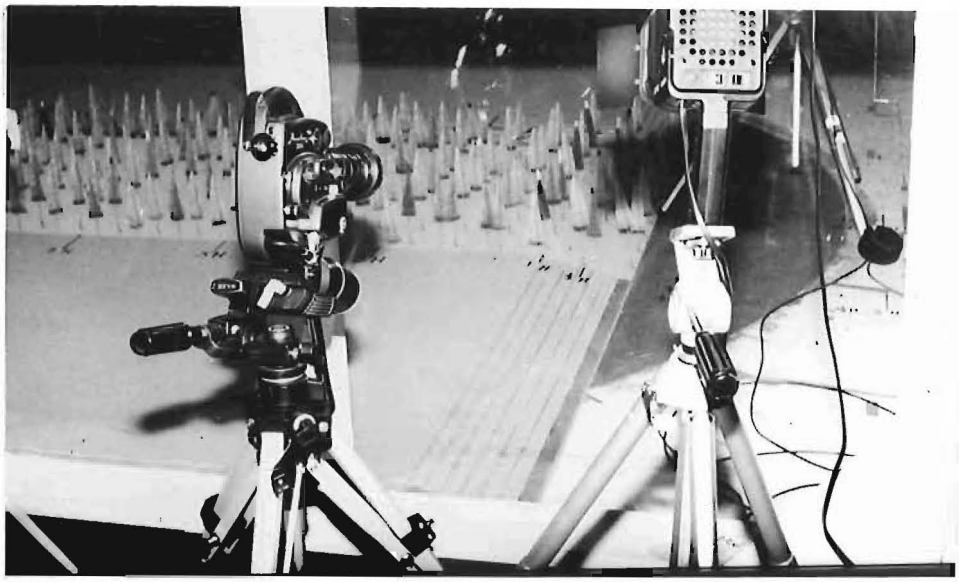

Photograph 1

Bolex 16mm motion camera used for filming tree movement at traverse x-position.

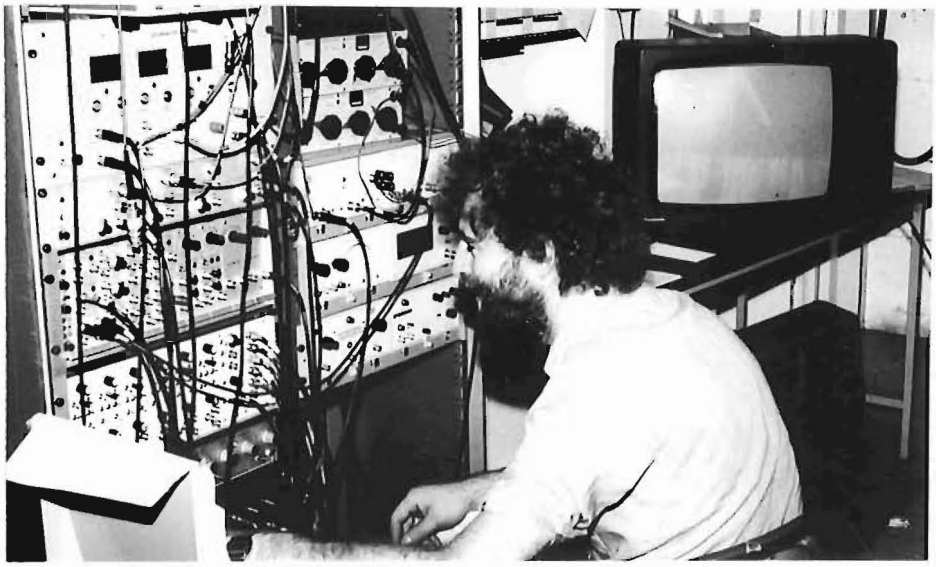

Photograph 2

Control and monitoring equipment; Disa amplifier inputs and analysing x and x-y probe channels. Keyboard and TV monitoring screen.

Photograph 3

x-y graph plotter; produces mean velocity and turbulence intensity profiles, and spectra of wind at each x,y,z position.

FIGURE : 6.18 Model Forest; Wind and Tree Movement Recording and Analysing.

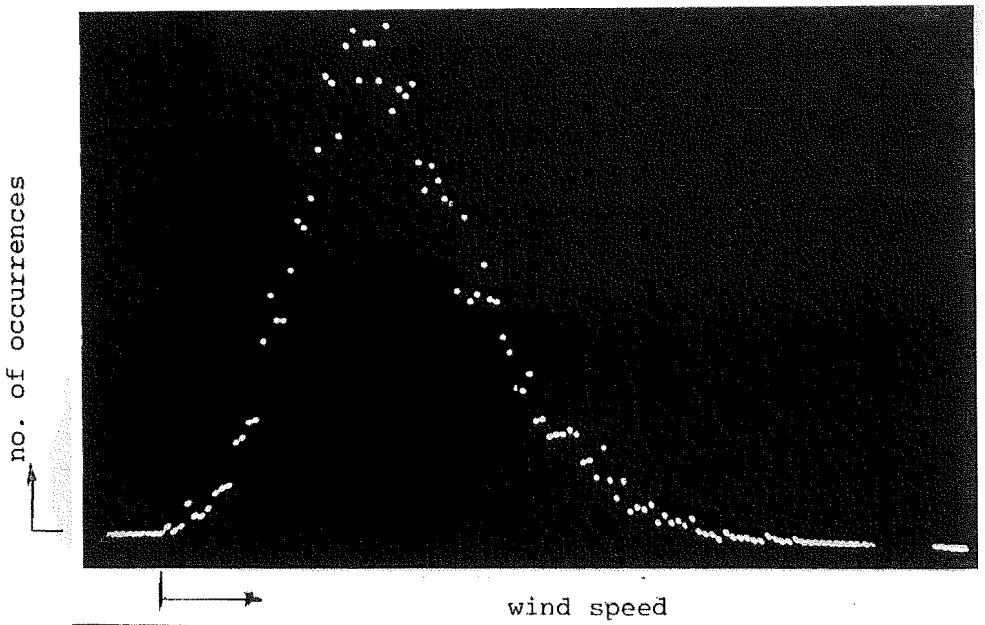

Photograph

Pattern S

x = +5H,

$\frac{S}{H}$ = 0.32,

$\frac{z}{H}$ = 0.9.

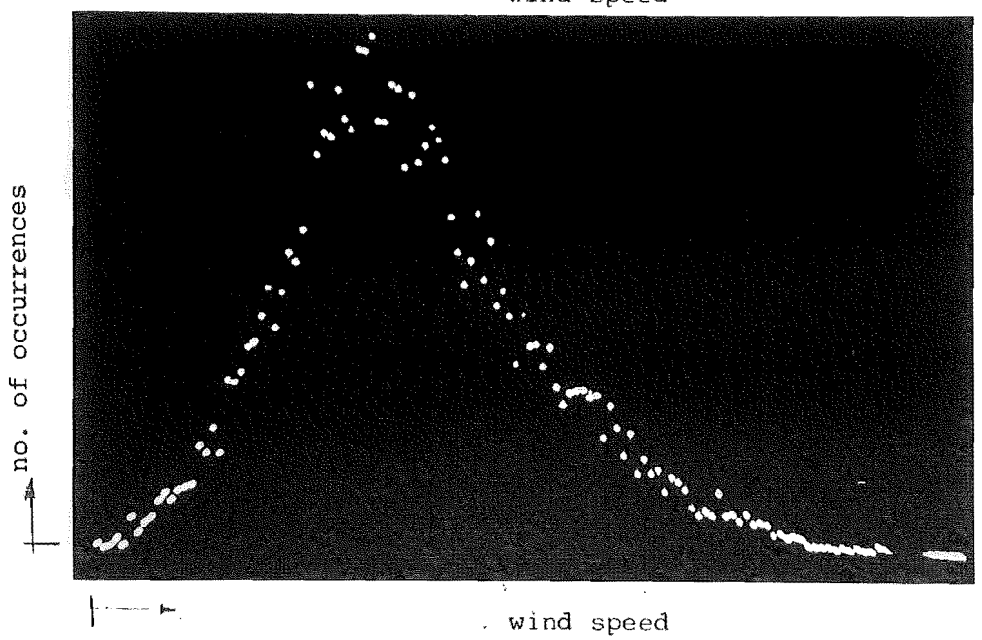

Photograph

Pattern Z

x = +3H

$\frac{S}{H}$ = 0.61

$\frac{z}{H}$ = 0.95.

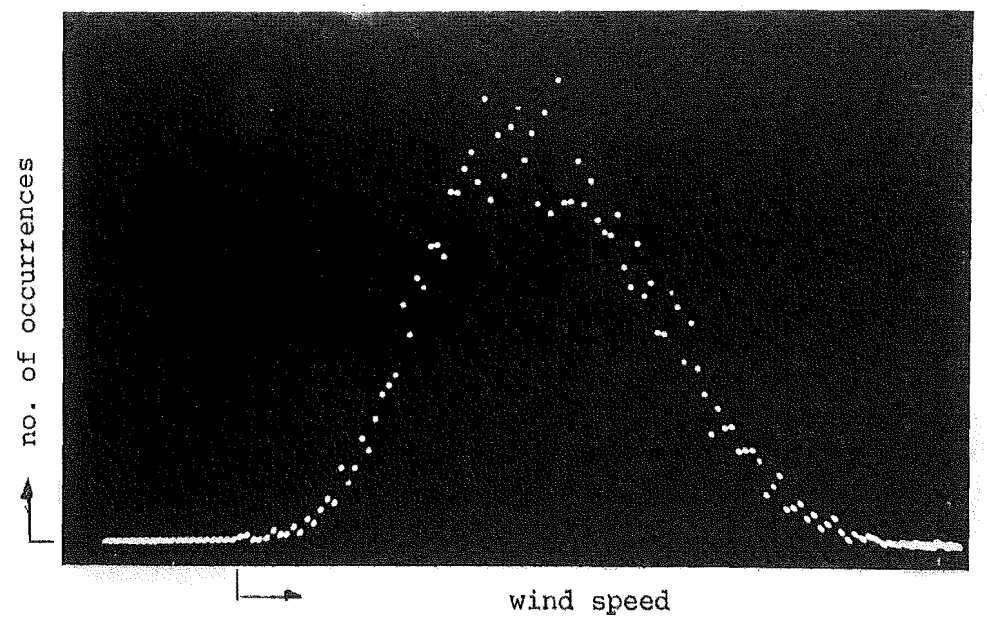

Photograph

Pattern Z

x = +7H,

$\frac{S}{H}$ = 0.61,

$\frac{z}{H}$ = 1.1.

FIGURE : 6.19(a) r.m.s. Turbulent Velocity Distribution (Oxford).

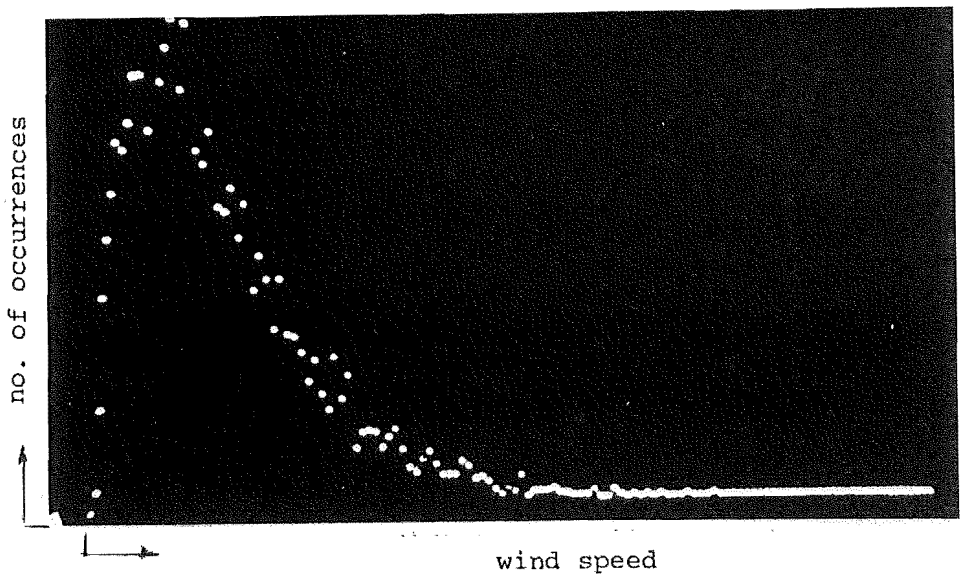

Photograph

Pattern S

x = +10H,

$\frac{S}{\bar{H}}$ = 0.32,

$\frac{z}{\bar{H}}$ = 0.9.

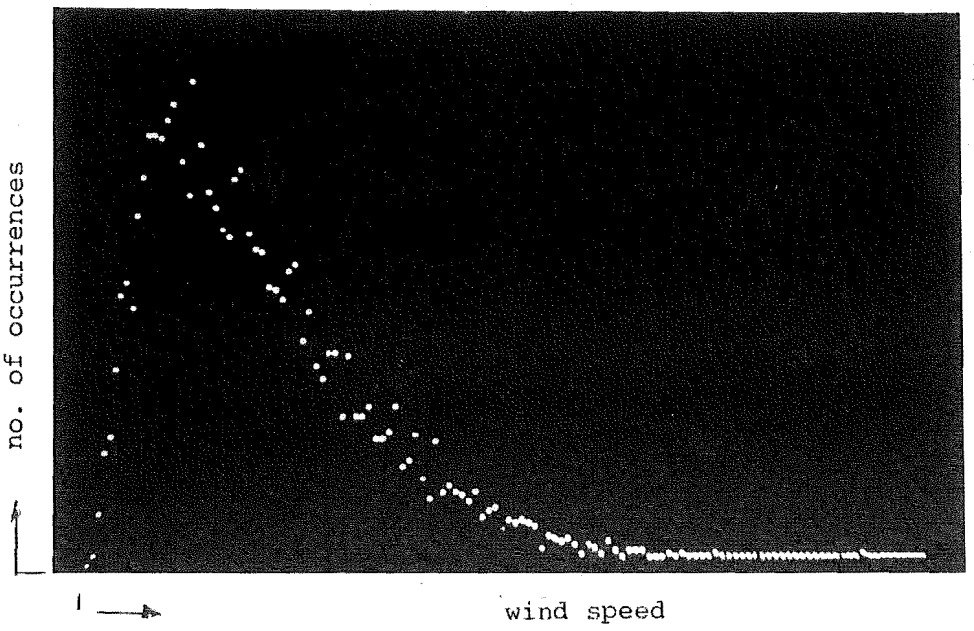

Photograph

Pattern S

x = +10H,

$\frac{S}{\bar{H}}$ = 0.32,

$\frac{z}{\bar{H}}$ = 0.95.

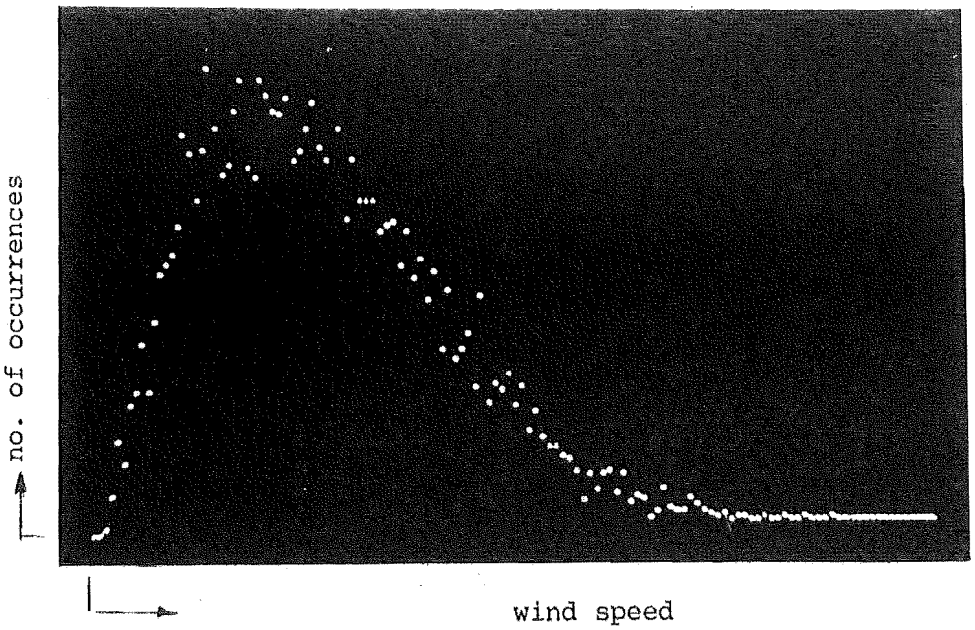

Photograph

Pattern S

x = +10H,

$\frac{S}{\bar{H}}$ = 0.32,

$\frac{z}{\bar{H}}$ = 1.1.

FIGURE : 6.19(b) r.m.s. Turbulent Velocity Distribution (Oxford).

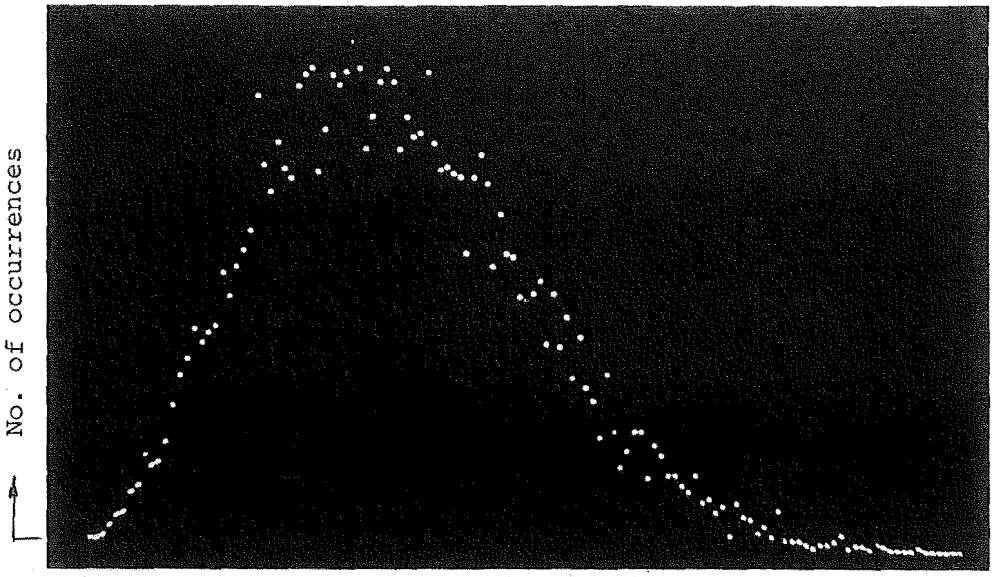

Photograph

Pattern S

x = +10H,

$\frac{S}{H}$ = 0.32,

$\frac{z}{H}$ = 1.3.

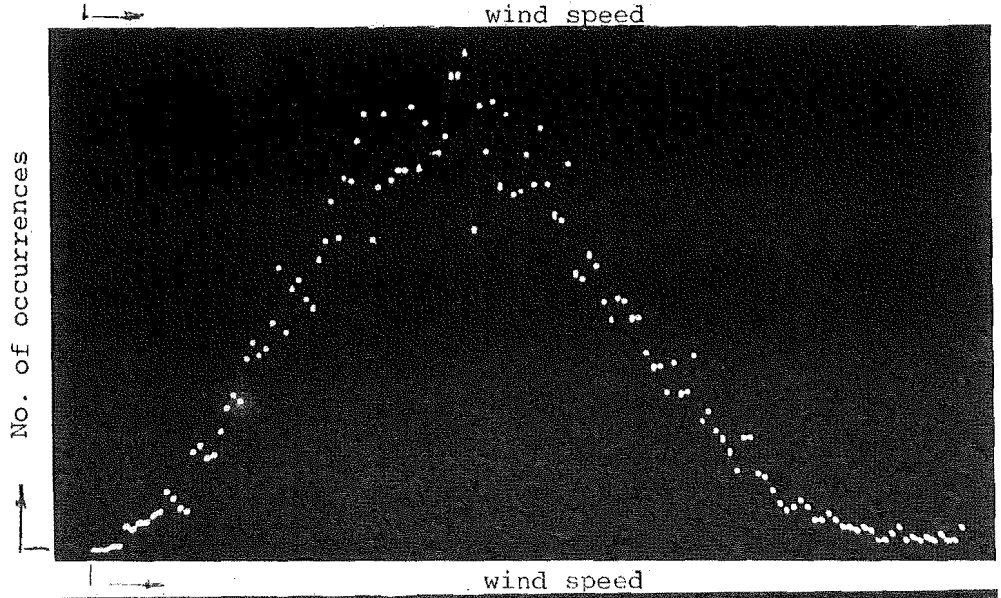

Photograph

Pattern S

x = +10H,

$\frac{S}{H}$ = 0.32,

$\frac{z}{H}$ = 1.5

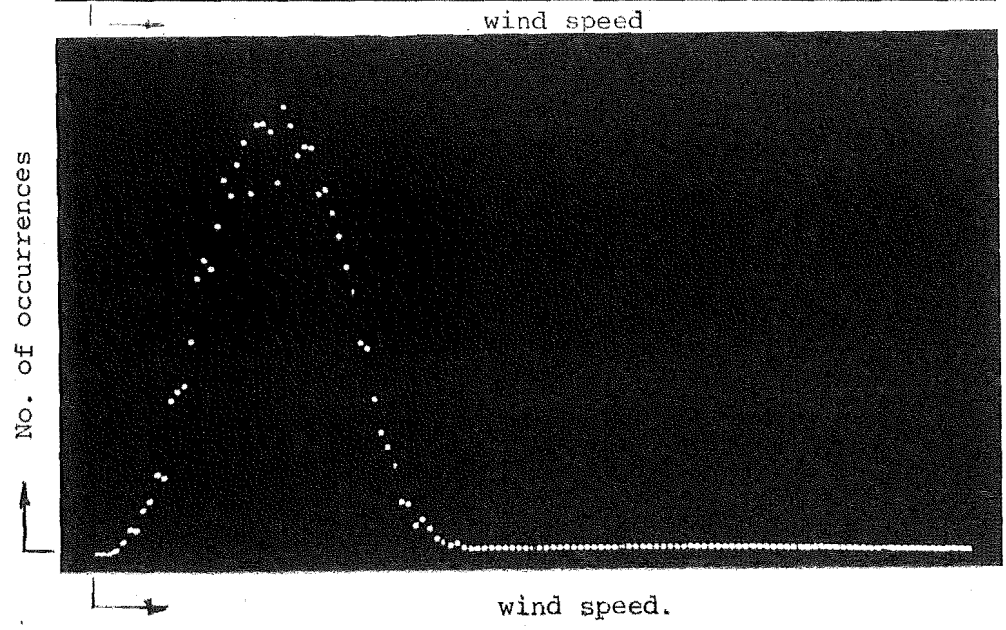

Photograph

Pattern S

x = +10H,

$\frac{S}{H}$ = 0.32,

$\frac{z}{H}$ = 1.75

FIGURE: 6.19(c)

r.m.s. Turbulent Velocity Distribution (Oxford)

6.8.2 Mean wind velocity and turbulence intensity along-wind distribution versus spacing

Mean velocity and turbulence intensity profiles (Figs 6.20 - 6.24) are compared for each pattern by plotting mean velocity and turbulence intensity along-wind distributions (Figs 6.25(a)-(k) and 6.26(a)-(k)). The vertical scale is twice the horizontal scale. From the mean velocity distributions several important points emerge:-

(a) maximum shear occurs at z_T, 0.3 H above mean tree-top height (4.4);

(b) maximum shear occurs at 3 H - 5 H behind the leading edge for close spacings, but diffuse along-wind over the canopy for wide spacings;

(c) right at the front the constant mean velocity lines diverge (suggesting a rise in surface static pressure) before the flow acceleration. The static pressure appears to fall below atmospheric pressure. (Fig.4.15).

(d) away from the leading edge the constant mean velocity lines are parallel with the canopy at 10 H and range between 50% and 60% of the upstream velocity at the equivalent full scale reference height of 10 m (Reifsnyder, 3.2);

(e) Pattern P had little tree-top motion (because of crown contact), but it has the highest vertical velocity components and appears to possess a separation 'bubble' between 3 H and 5 H.

z_o'' and $\bar{U}_{*_\ell}$ were obtained from each mean velocity profile. These values are compared with the Canterbury (Table 6.7) and full scale (Table 5.12) results. At 10 H, $\frac{z_o''}{H}$ is 0.147 H, which is close to the Rivox average result (0.15 H); shear stress coefficients vary, but are still of the right order of magnitude to suggest a return to equilibrium conditions. Also, at this fetch, the mean windspeed profiles appear logarithmic (Patterns U* and P have minor 'kinks'), and local aerodynamic roughnesses return to constant values. The mean velocity and turbulence intensity profiles for Patterns P, U*, S and V are required when model and full scale spectra are standardized before comparison.

The turbulence intensity distributions (Figs 6.26(a)-(k)), suggest the following points.

(a) At 10 H, turbulence intensities appear to have a logarithmic variation with height (ESDU). At mean tree-top height, turbulence intensities

To p.246

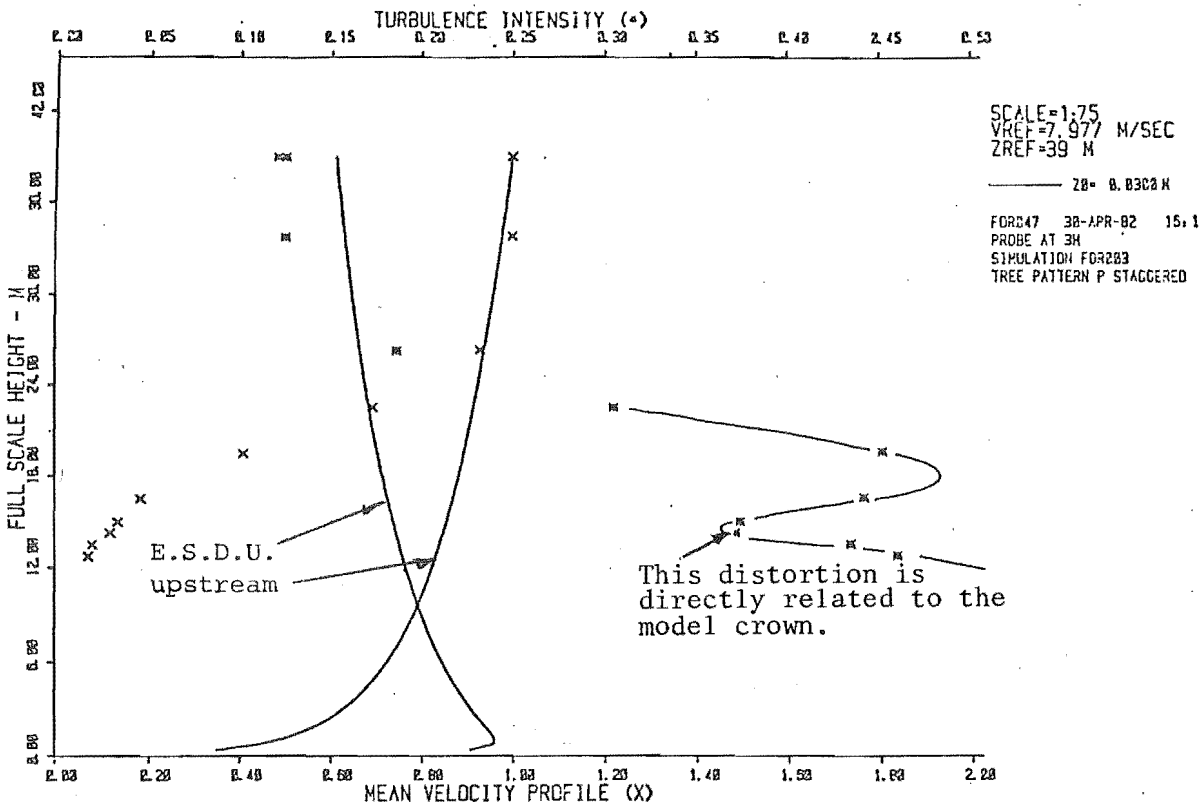

DATA FILE FOR047

30-4 -82
PROBE AT +3H
SIMULATION FOR003
TREE PATTERN P STAGGERED

SAMPLING INTERVAL MILLISECS	SAMPLING DURATION SECONDS	TUNNEL HEIGHT METRES	VELOCITY METRES/SEC	TURBULENCE INTENSITY	DEVIATION METRES/SEC
10.0	95.480	0.520	7.974	0.121	0.962
10.0	92.130	0.450	7.976	0.125	0.997
10.0	89.340	0.350	7.415	0.186	1.382
10.0	94.240	0.300	5.539	0.305	1.687
10.0	63.220	0.260	3.271	0.450	1.471
10.0	38.280	0.220	1.468	0.440	0.646
10.0	34.360	0.200	1.074	0.373	0.401
10.0	33.660	0.190	0.948	0.371	0.352
10.0	75.870	0.180	0.649	0.433	0.281
10.0	67.170	0.170	0.580	0.458	0.266
10.0	73.180	0.520	7.983	0.125	0.997

FIGURE 6.20: Mean wind velocity and turbulence intensity profiles (Pattern P, +3H), Oxford.

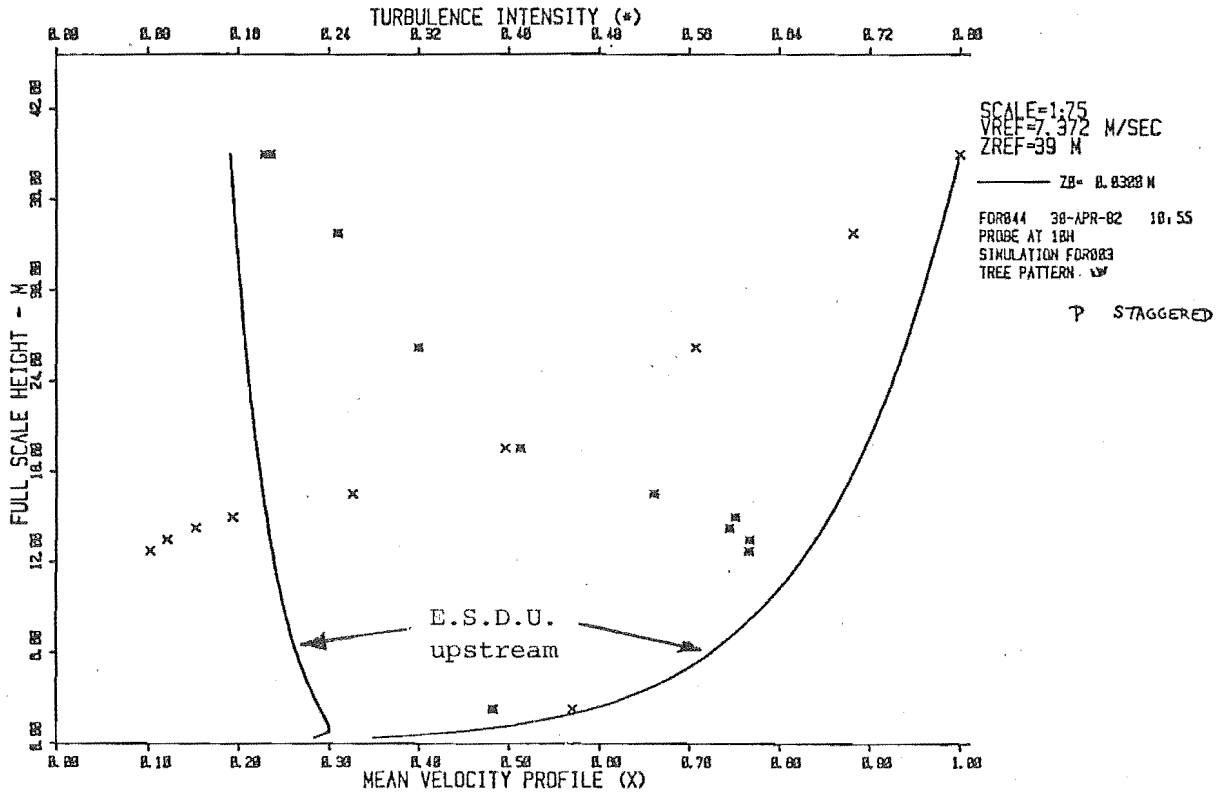

DATA FILE FOR044
****

30-APR-82 10:55
PROBE AT 10H
SIMULATION FOR003
TREE PATTERNP10H

SAMPLING INTERVAL MILLISECS	SAMPLING DURATION SECONDS	TUNNEL HEIGHT METRES	VELOCITY METRES/SEC	TURBULENCE INTENSITY	DEVIATION METRES/SEC
10.0	61.170	0.520	7.372	0.188	1.388
10.0	76.360	0.450	6.499	0.248	1.609
10.0	86.900	0.350	5.216	0.320	1.669
10.0	54.610	0.0300	4.205	0.386	1.622
10.0	58.980	0.260	3.660	0.410	1.502
10.0	44.840	0.220	2.408	0.529	1.273
10.0	26.350	0.200	1.429	0.602	0.859
10.0	46.990	0.190	1.124	0.596	0.670
10.0	34.770	0.180	0.088	0.614	0.545
10.0	46.100	0.170	0.754	0.614	0.463
10.0	56.870	0.520	7.371	0.183	1.351

FIGURE 6.21: Mean wind velocity and turbulence intensity profiles (Pattern P, +10H).

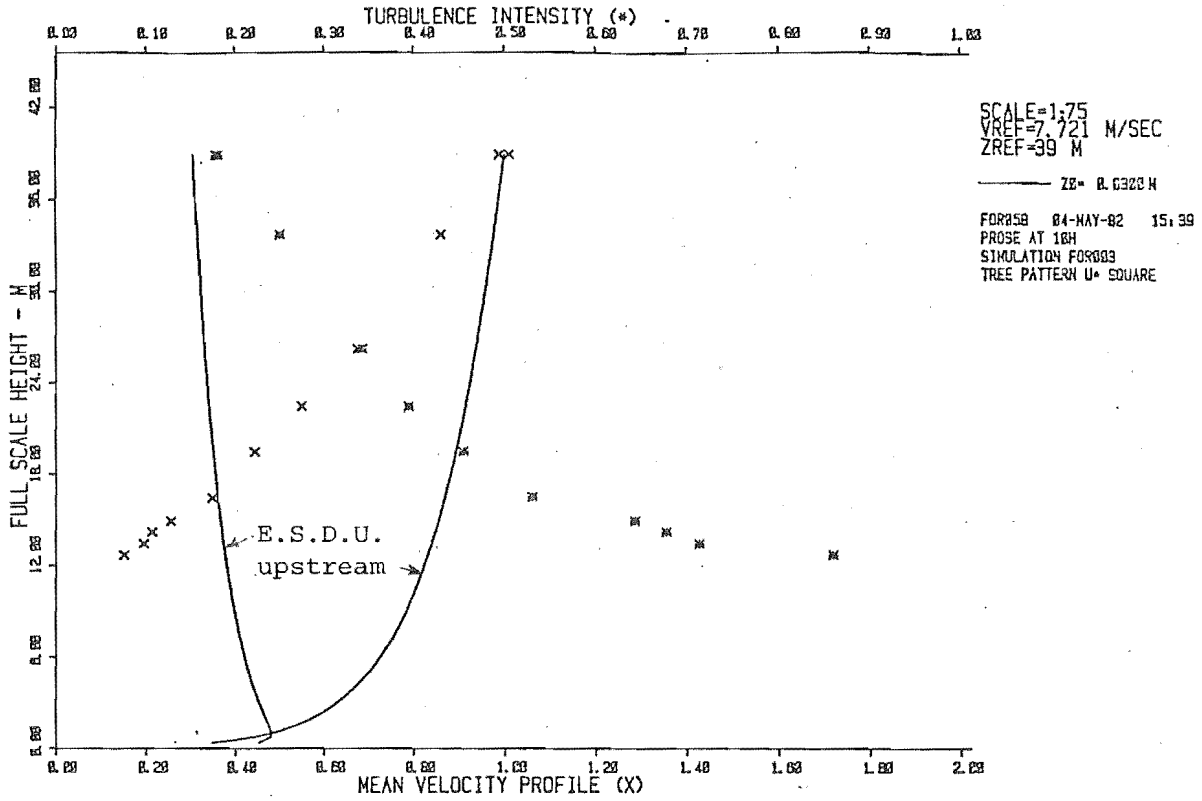

DATA FILE FOR058
****

04-MAY-82 15:39
PROBE AT 10H
SIMULATION FOR003
TREE PATTERN U* SQUARE

SAMPLING INTERVAL MILLISECS	SAMPLING DURATION SECONDS	TUNNEL HEIGHT METRES	VELOCITY METRES/SEC	TURBULENCE INTENSITY	DEVIATION METRES/SEC
10.0	59.110	0.520	7.637	0.179	1.365
10.0	72.950	0.450	6.652	0.250	1.666
10.0	96.370	0.350	5.230	0.343	1.796
10.0	74.150	0.300	4.251	0.395	1.679
10.0	69.530	0.260	3.444	0.455	1.568
10.0	61.190	0.220	2.709	0.530	1.437
10.0	45.260	0.200	1.976	0.643	1.270
10.0	42.610	0.190	1.653	0.677	1.120
10.0	46.030	0.180	1.523	0.714	1.087
10.0	36.900	0.170	1.176	0.859	1.010
10.0	60.880	0.520	7.805	0.182	1.417

FIGURE 6.22: Mean wind velocity and turbulence intensity profiles (Pattern U*, +10H).

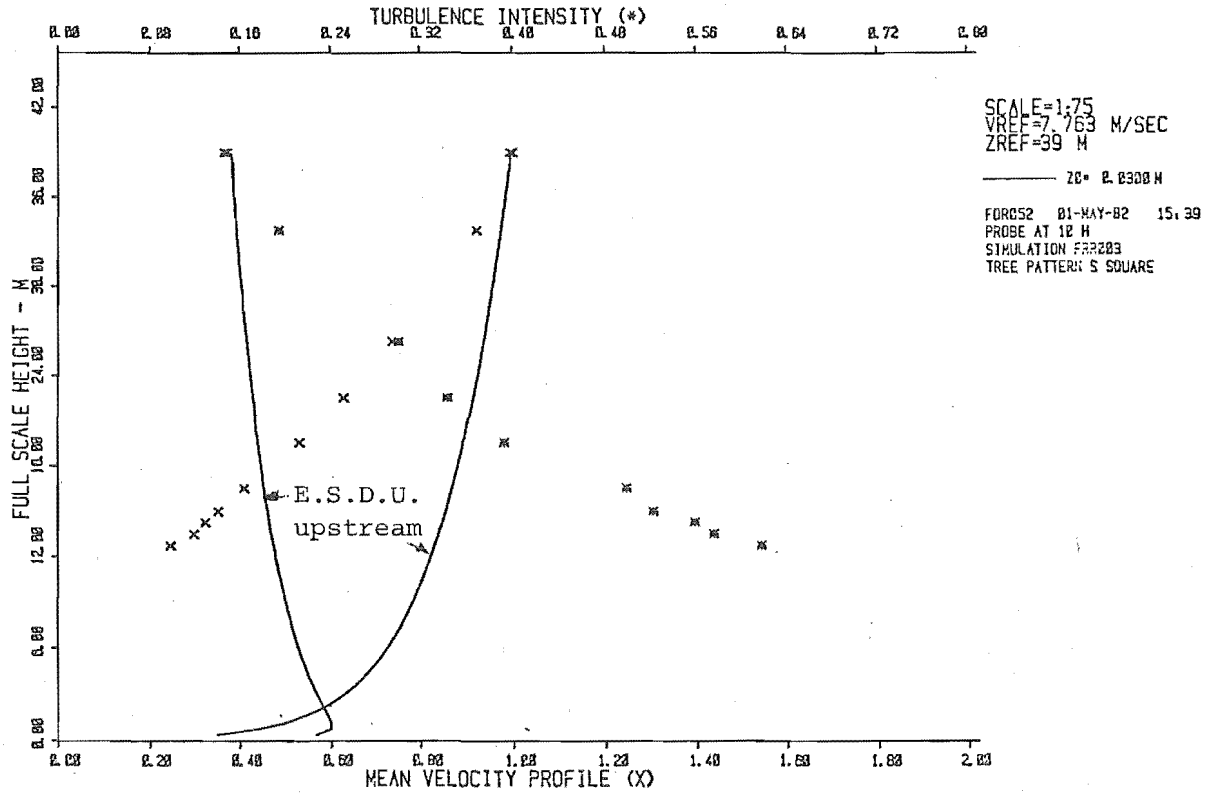

DATA FILE FOR052
****

01-MAY-82 15:39
PROBE AT 10 H
SIMULATION FRR003
TREE PATTERN S SQUARE

SAMPLING INTERVAL MILLISECS	SAMPLING DURATION SECONDS	TUNNEL HEIGHT METRES	VELOCITY METRES/SEC	TURBULENCE INTENSITY	DEVIATION METRES/SEC
10.0	24.210	0.520	7.740	0.147	1.136
10.0	23.210	0.170	1.917	0.617	1.183
10.0	26.760	0.180	2.314	0.575	1.330
10.0	29.950	0.190	2.517	0.558	1.404
10.0	30.870	0.200	2.728	0.521	1.422
10.0	37.310	0.220	3.179	0.498	1.583
10.0	43.540	0.260	4.125	0.393	1.622
10.0	38.200	0.300	4.877	0.343	1.675
10.0	41.470	0.350	5.731	0.301	1.723
10.0	30.650	0.450	7.174	0.195	1.400
10.0	24.050	0.520	7.785	0.149	1.162

FIGURE 6.23: Mean wind velocity and turbulence intensity profiles (Pattern S, +10H).

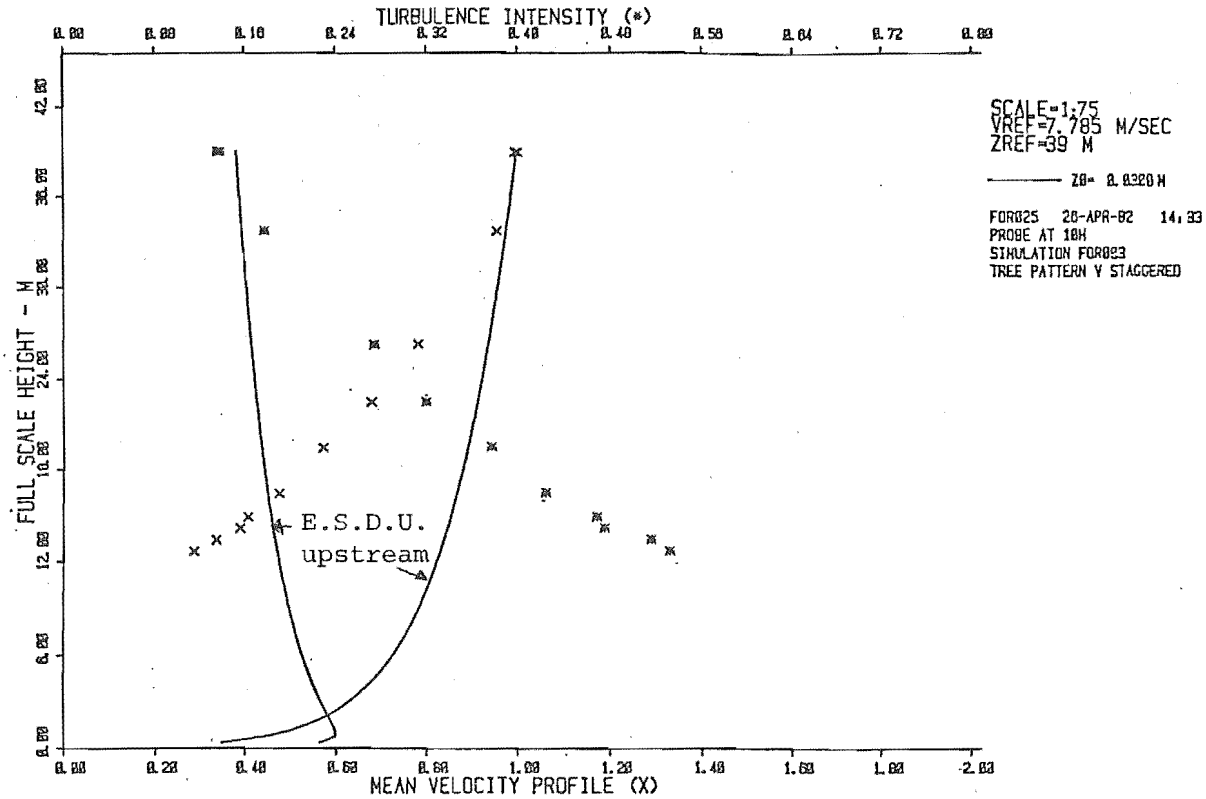

DATA FILE FOR025
****

26-APR-82 14:33
PROBE AT 10H
SIMULATION FOR003
TREE PATTERN V STAGGERED

SAMPLING INTERVAL MILLISECS	SAMPLING DURATION SECONDS	TUNNEL HEIGHT METRES	VELOCITY METRES/SEC	TURBULENCE INTENSITY	DEVIATION METRES/SEC
10.0	51.140	0.520	7.808	0.139	1.084
10.0	58.750	0.450	7.449	0.178	1.327
10.0	86.800	0.350	6.087	0.274	1.668
10.0	78.420	0.300	5.293	0.320	1.693
10.0	79.900	0.260	4.475	0.378	1.691
10.0	68.800	0.220	3.730	0.425	1.585
10.0	54.140	0.200	3.195	0.469	1.499
10.0	50.060	0.190	3.058	0.476	1.455
10.0	49.970	0.180	2.638	0.517	1.363
10.0	41.380	0.170	2.246	0.532	1.196
10.0	48.930	0.520	7.762	0.136	1.055

FIGURE 6.24: Mean wind velocity and turbulence intensity profiles (Pattern V, +10H).

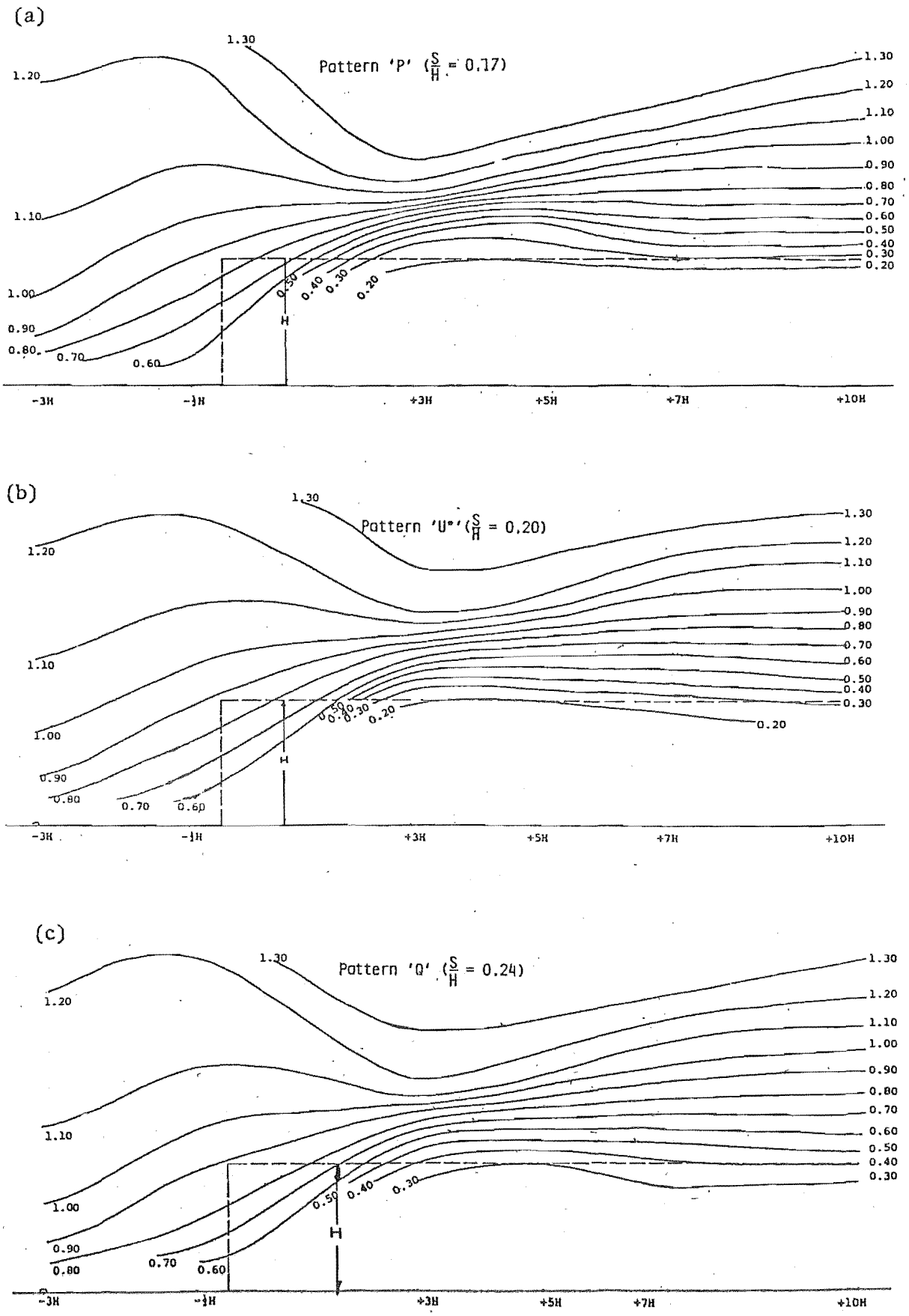

FIGURE 6.25: Mean wind velocity distribution in the x and z directions.

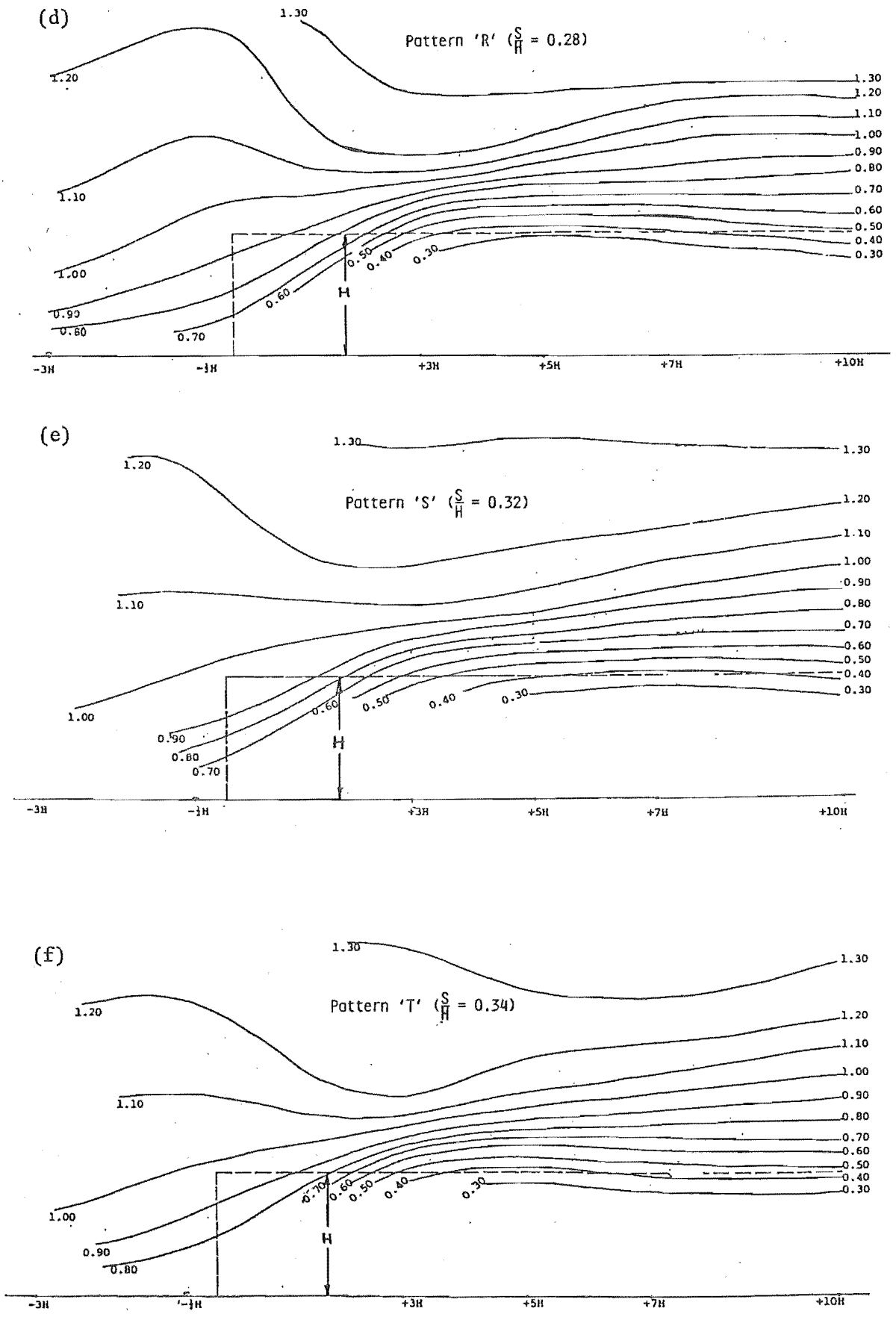

FIGURE 6.25 (cont'd): Mean wind velocity distribution in the x and z directions.

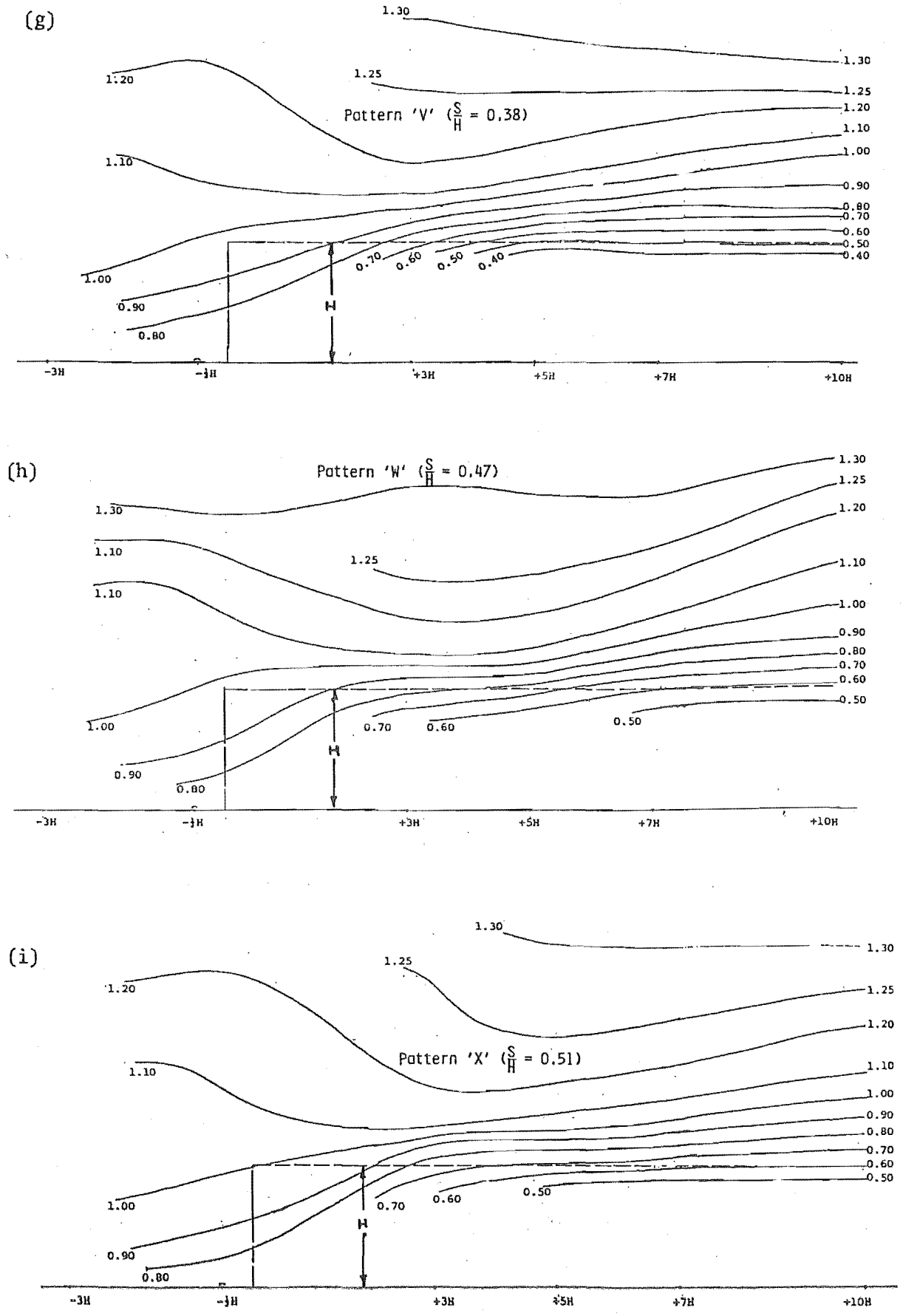

FIGURE 6.25 (Cont'd): Mean wind velocity distribution in the x and z directions.

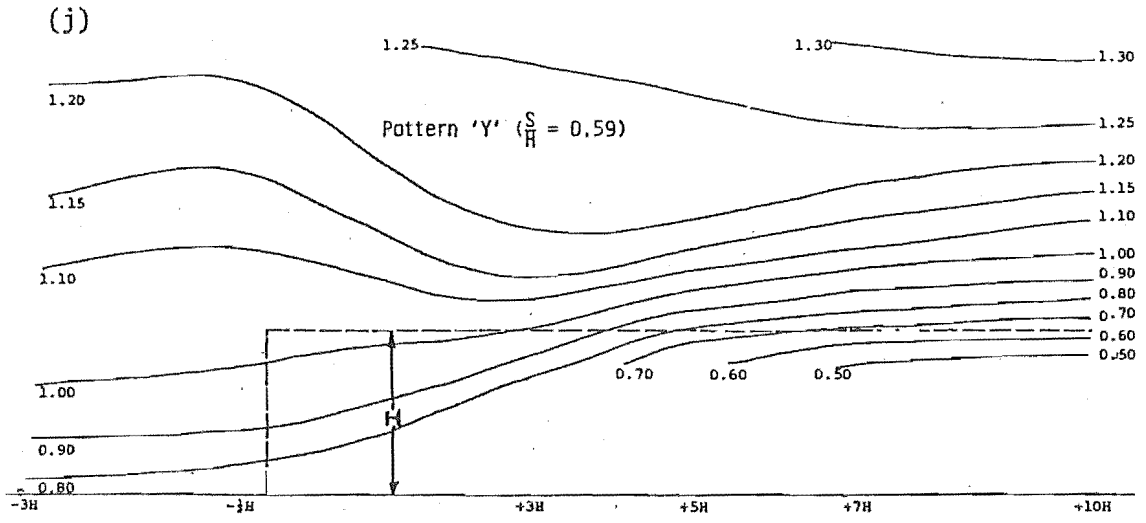

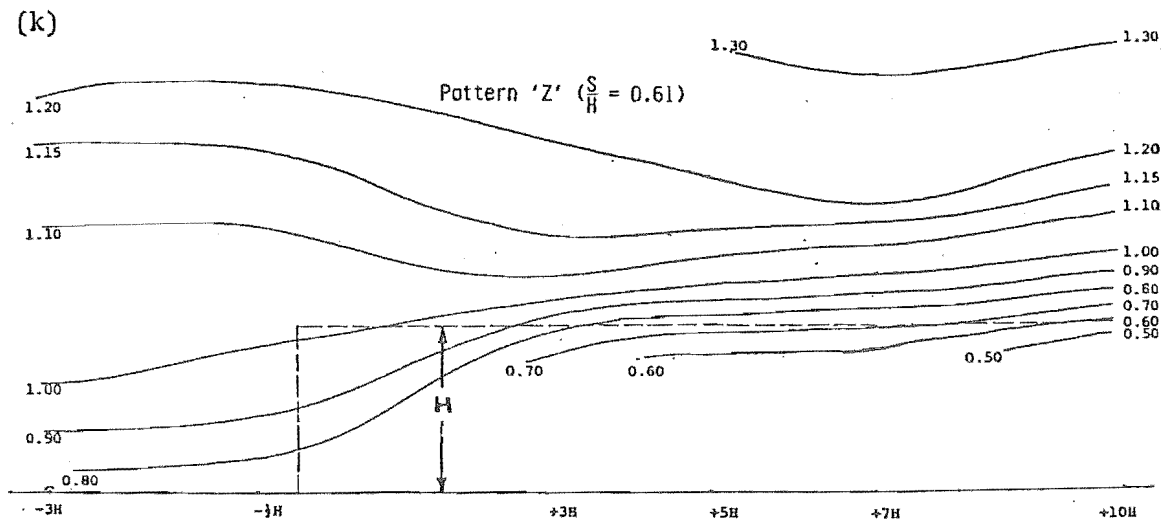

FIGURE 6.25 (Cont'd): Mean wind velocity distribution in x and z directions.

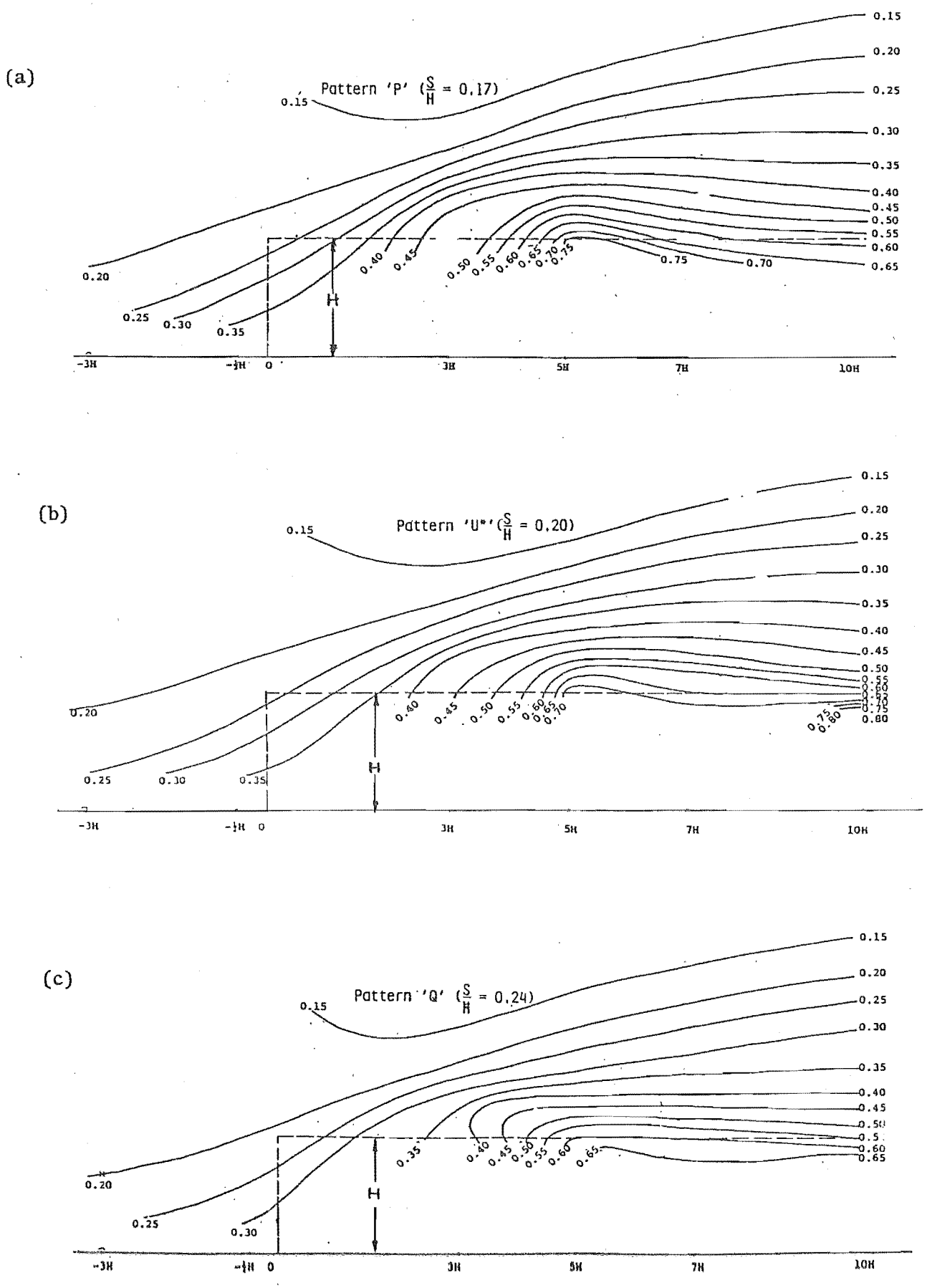

FIGURE 6.26: Turbulence intensity distribution in the x and z directions.

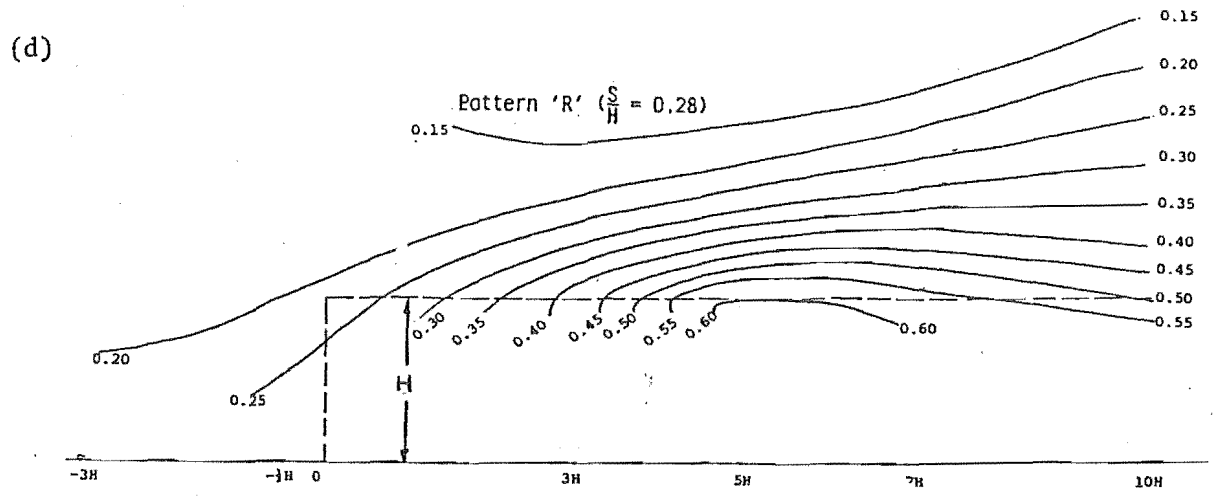

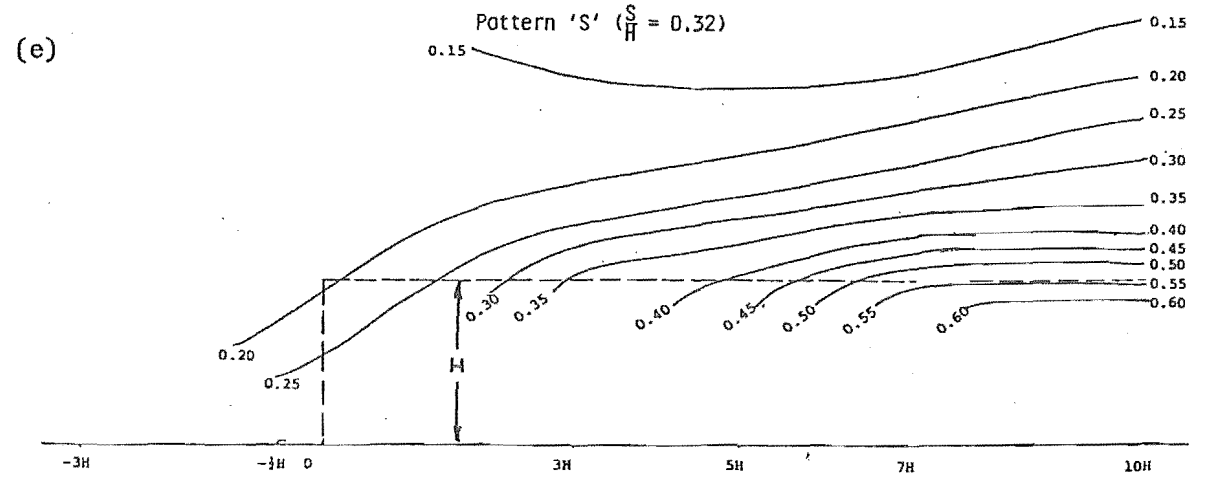

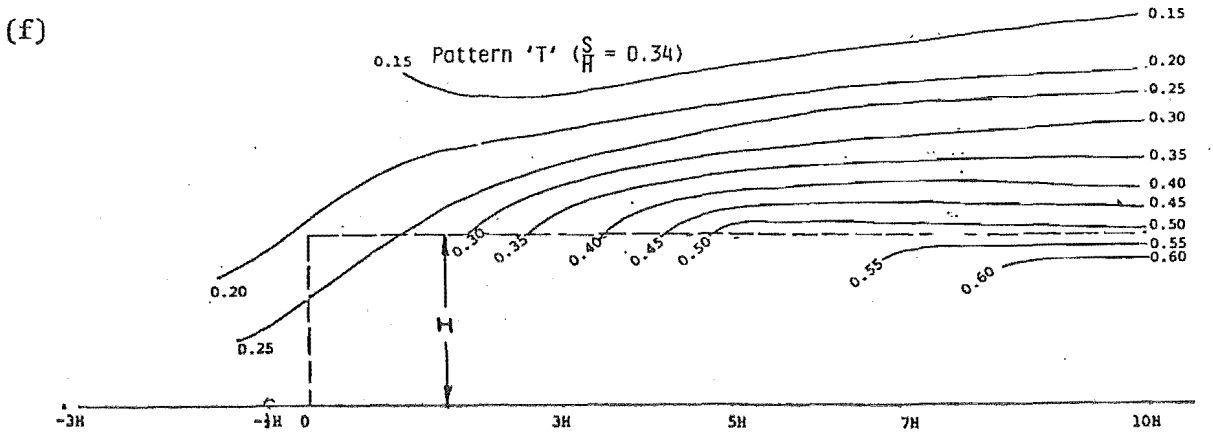

FIGURE 6.26 (Cont'd): Turbulence intensity distribution in the x and z directions.

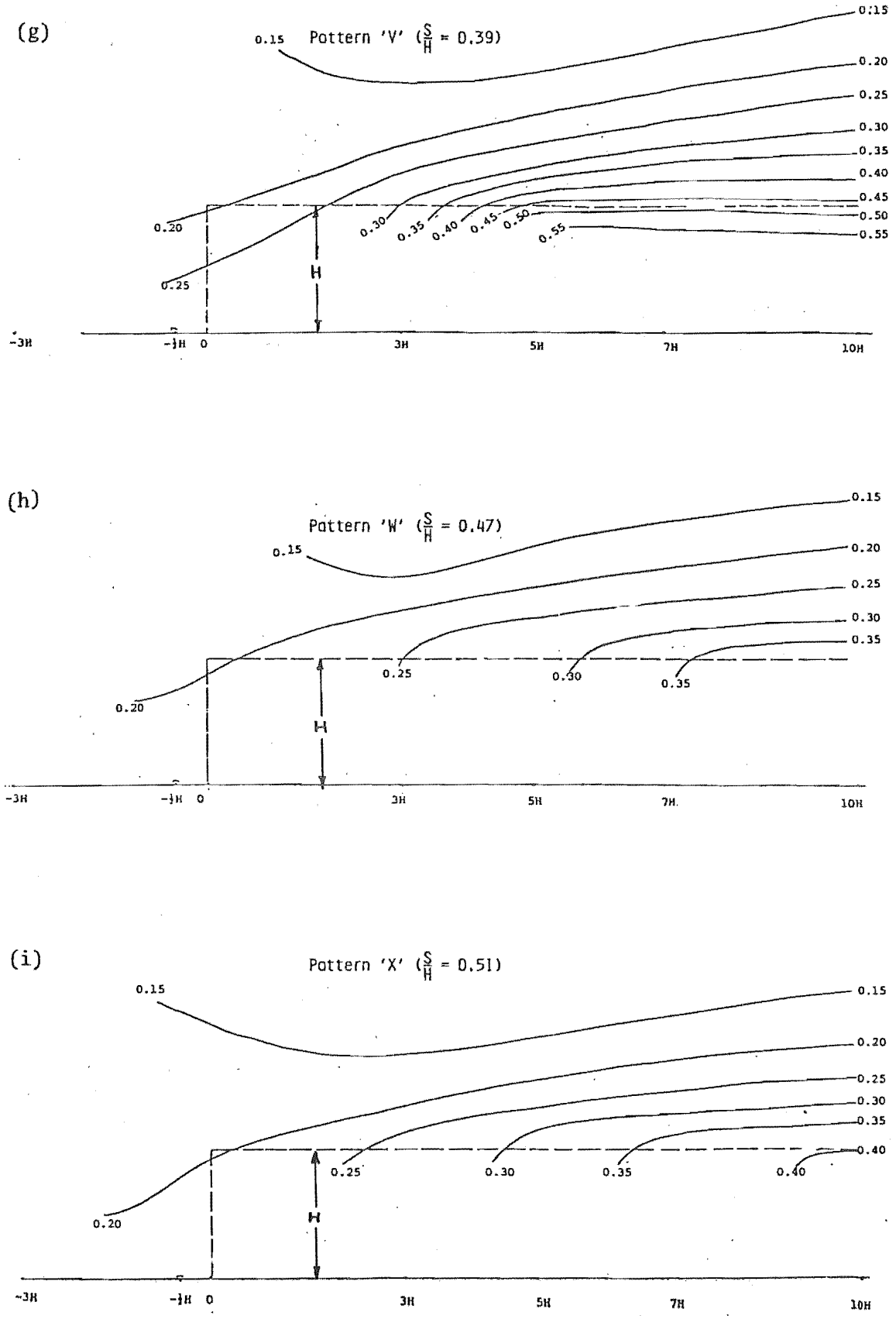

FIGURE 6.26 (Cont'd): Turbulence intensity distribution in the x and z directions.

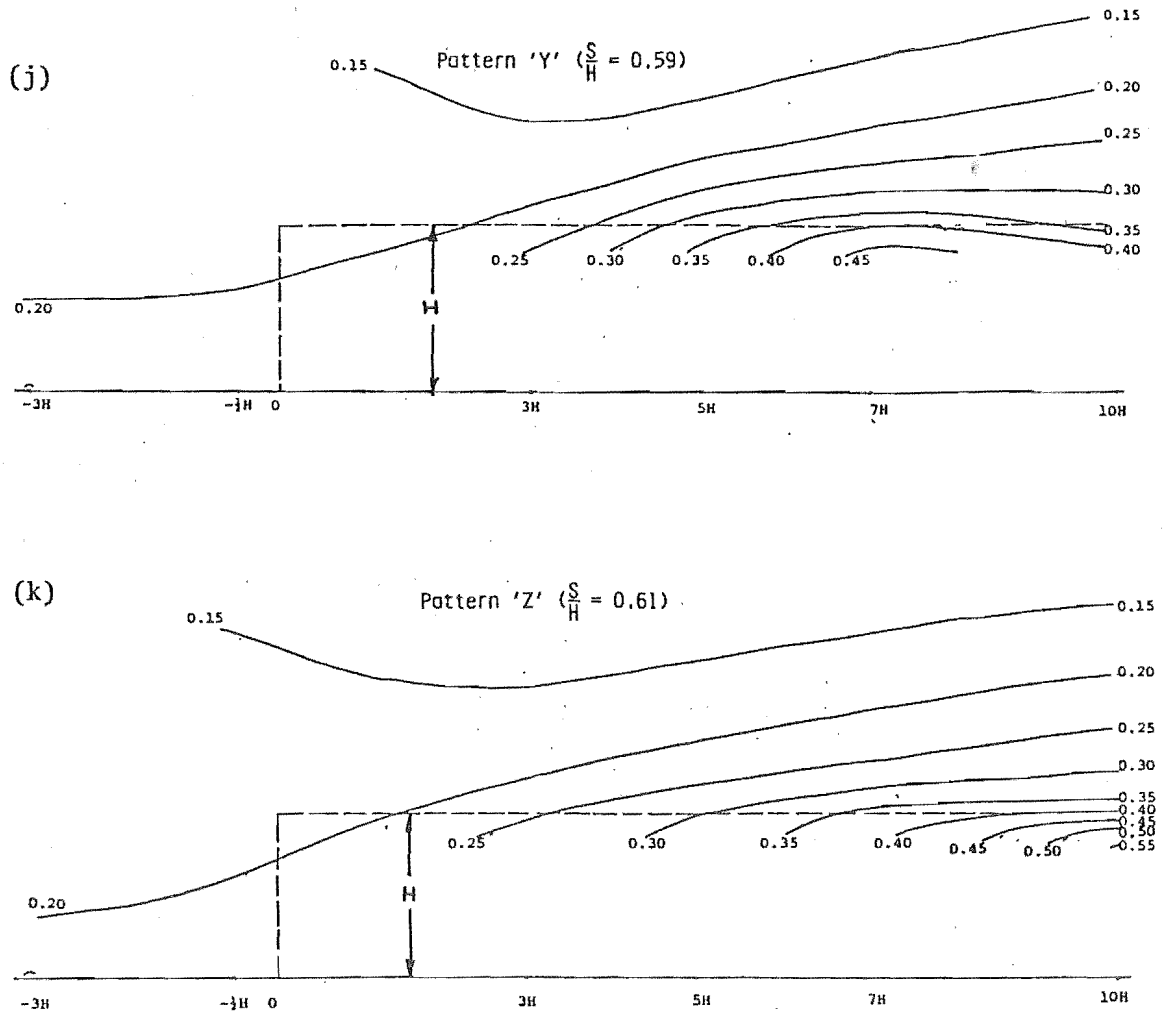

FIGURE 6.26 (Cont'd): Turbulence intensity distribution in the x and z directions.

gradually reduce from about 50% for close spacings to 40% at wider spacings.

(b) Along-wind turbulence intensities for close spacings at mean tree-top height increase from 25% at leading edges to 75% at 5 H, before reducing to between 50% and 60% at 10 H.

(c) Along-wind changes for wider spacings are more gradual. Turbulence intensities rise from 20% at leading edges to reach about 45% at 10 H in from the leading edge.

(d) For the widest spacings, turbulence intensities at tree height are twice upstream levels. Upstream, at -3 H, turbulence intensities remain constant at 20% when measured at a height above the floor equivalent to 10 m full scale.

6.8.3 Total along-wind turbulent kinetic energy changes with spacing

Beyond $\frac{S}{H}$ of 0.35, the kinetic energy, or variance $(\overline{u'^2})$, is consistently high just above mean tree-top height. Just below mean tree-top height it rises from very low levels at close spacings to the higher levels existing just above mean tree-top height at wide spacings (Figs 6.27(a)-(h)).

6.8.4 Shear stress coefficients and aerodynamic roughness

Measurements of local Reynolds stresses $(-\overline{\rho w'v'})$ were obtained for Pattern W (and Z) (Table 6.6).

These were referenced to the mean velocity at mean tree-top height $(\bar{U}_H)$, and to the upstream velocity $(\bar{U}_o)$, to obtain the shear stress coefficients, C_{f_H} and C_{f_o}. These coefficients are similar to those obtained from the mean velocity profiles (Table 6.7).

At -3 H, mean vertical component winds $(\bar{W})$ are very low. Just upwind of the forest leading edge they rapidly increase; then, as the wind traverses the leading edge inwards, these components gradually reduce back to zero at 7 H. This means that the hot-wire probes are operative (6.7.3), and that equilibrium is restored to the flow at 7 H. At 10 H equilibrium flow continues in the inner layer, since $\bar{W}$ components remain near zero.

In Table 6.7 these coefficients and aerodynamic roughness changes from the model forest tests are compared with other artificial roughness tests by Kawatani and Meroney and by Cook and Heppel. Calculations of C_{f_o} using the relationship of Koloseus (3.6.) complete the comparison table (cf. Table 3.2).

To p.254

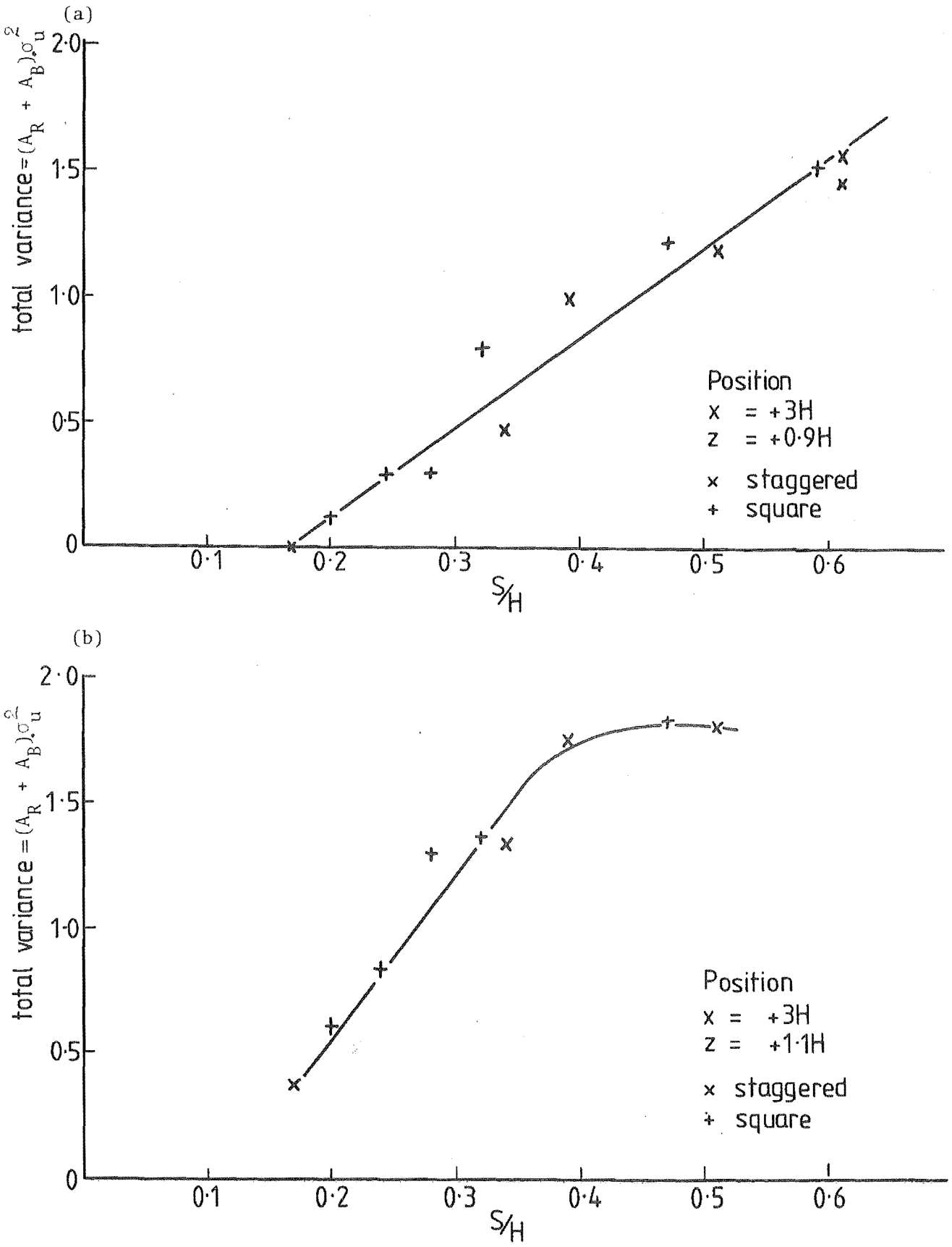

FIGURE 6.27(a) & (b): Total turbulent kinetic energy v spacing density.

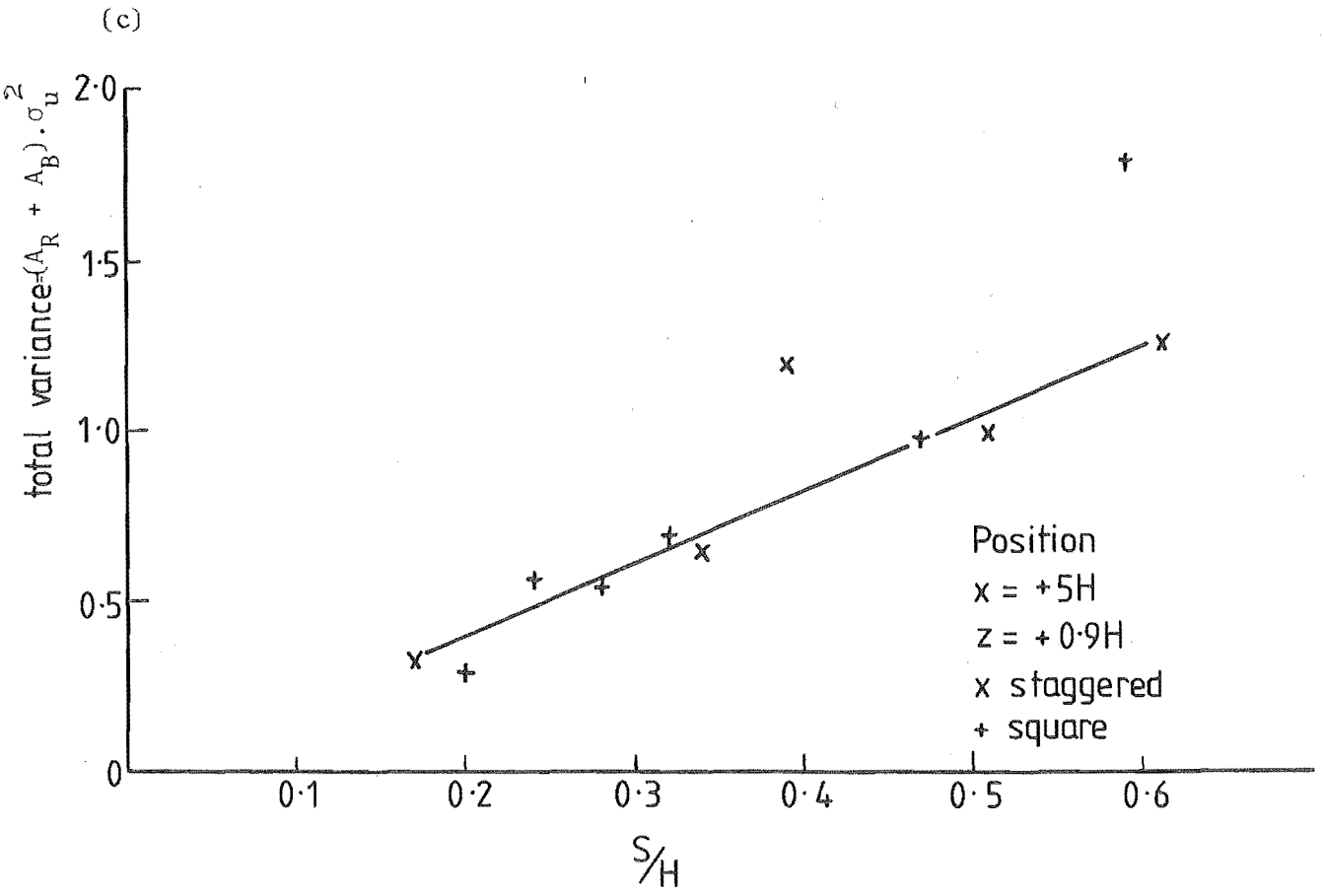

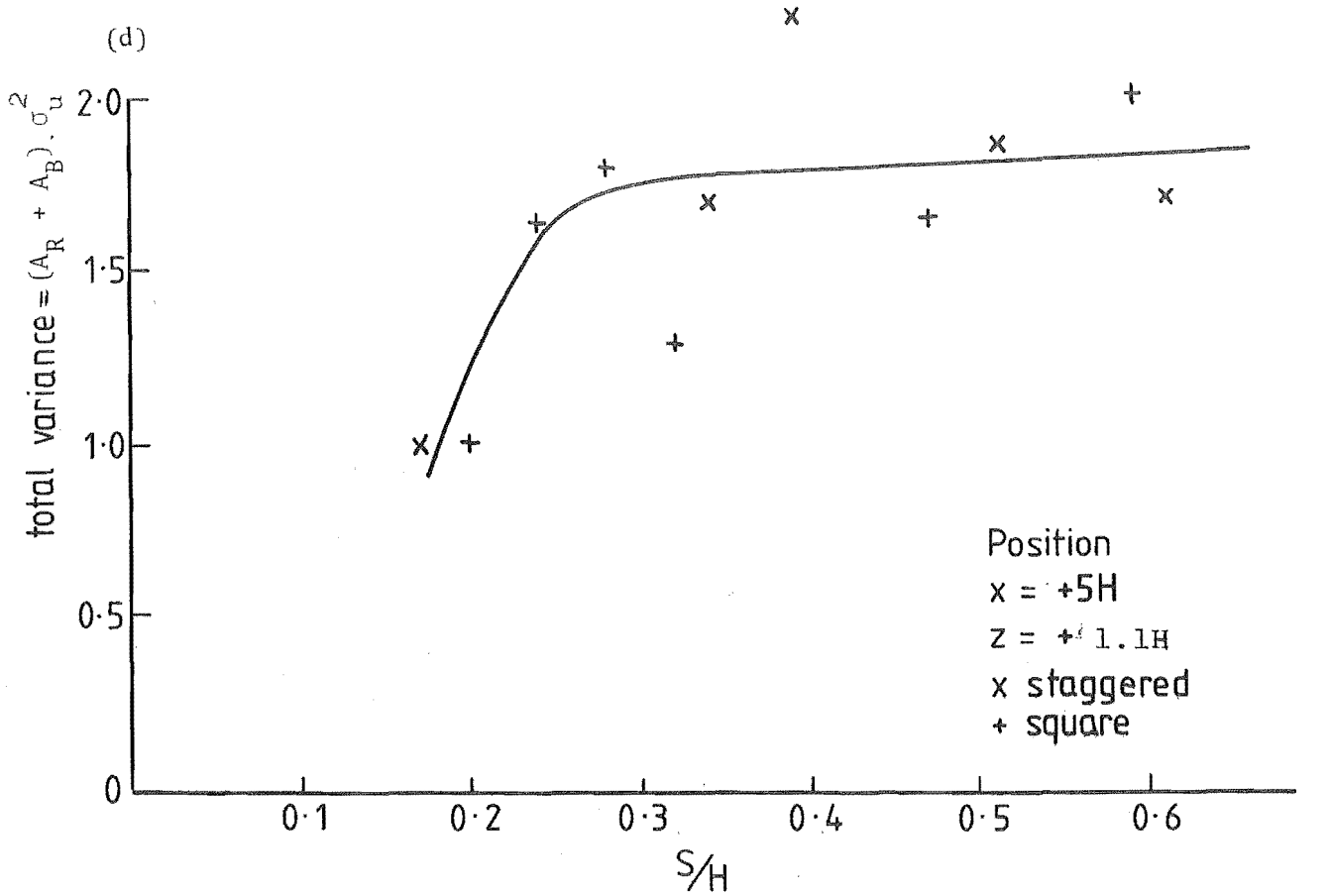

FIGURE 6.27(c) & (d): Total turbulent kinetic energy v spacing density,

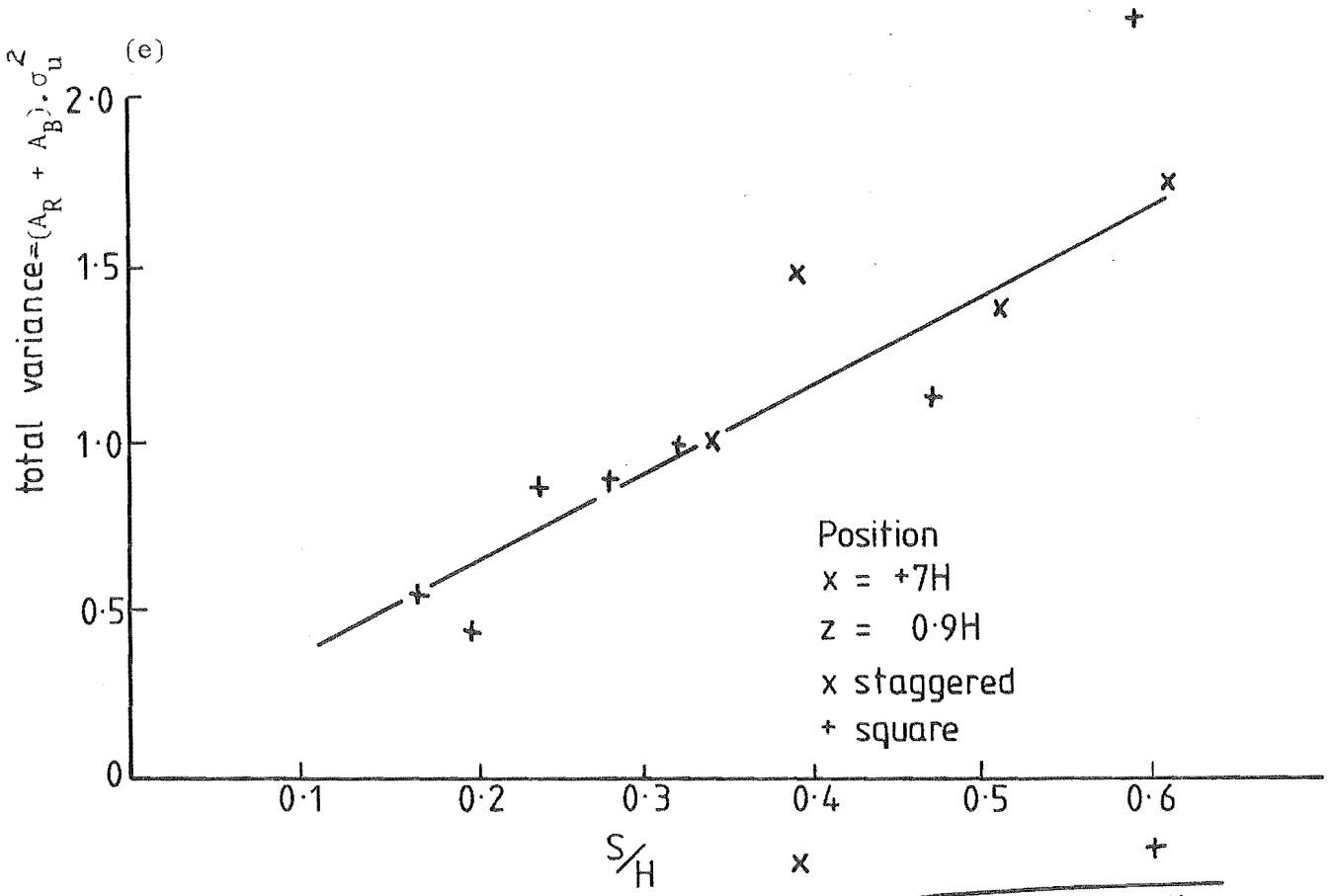

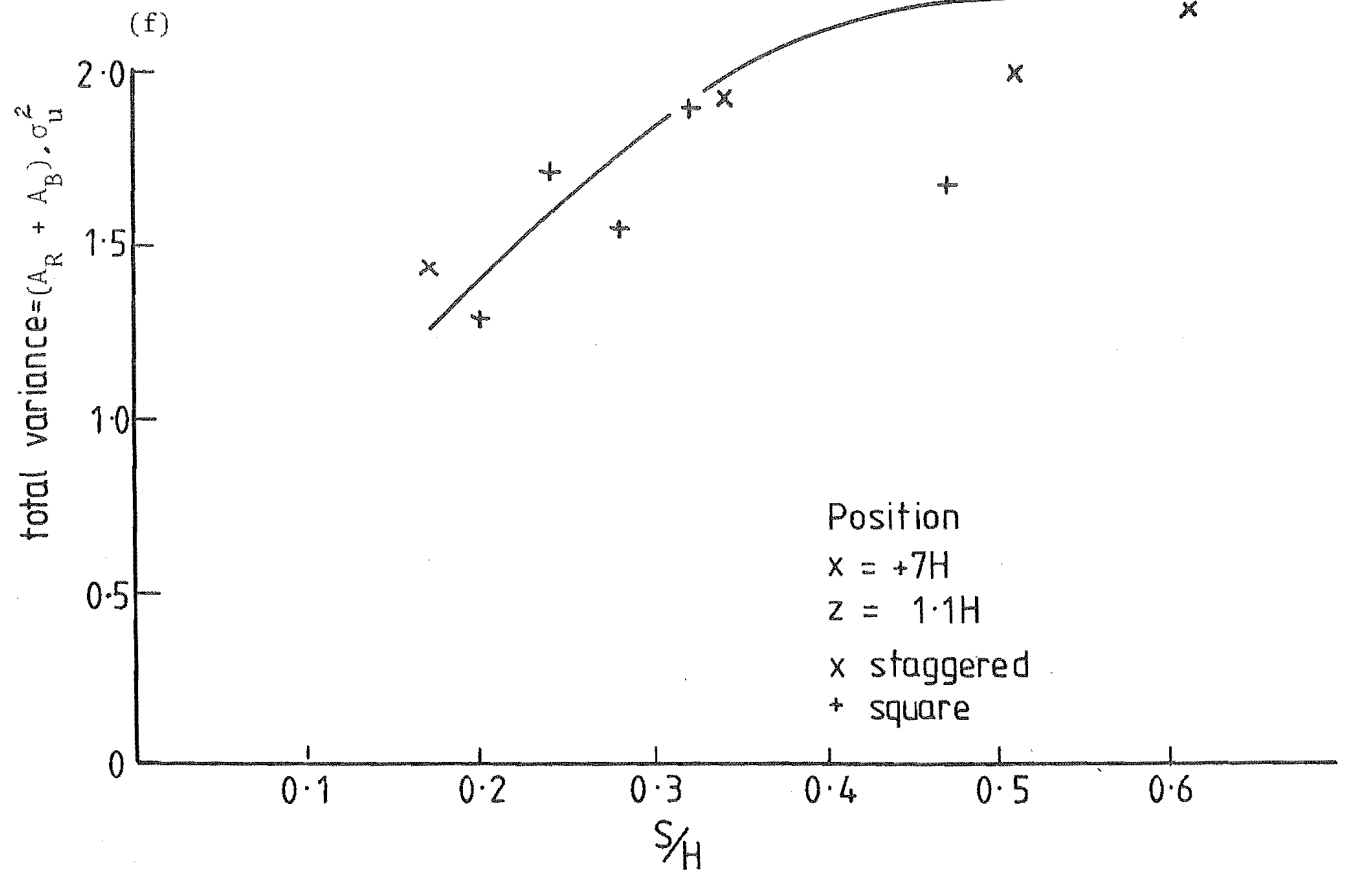

FIGURE 6.27(e) & (f): Total turbulent kinetic energy v spacing density.

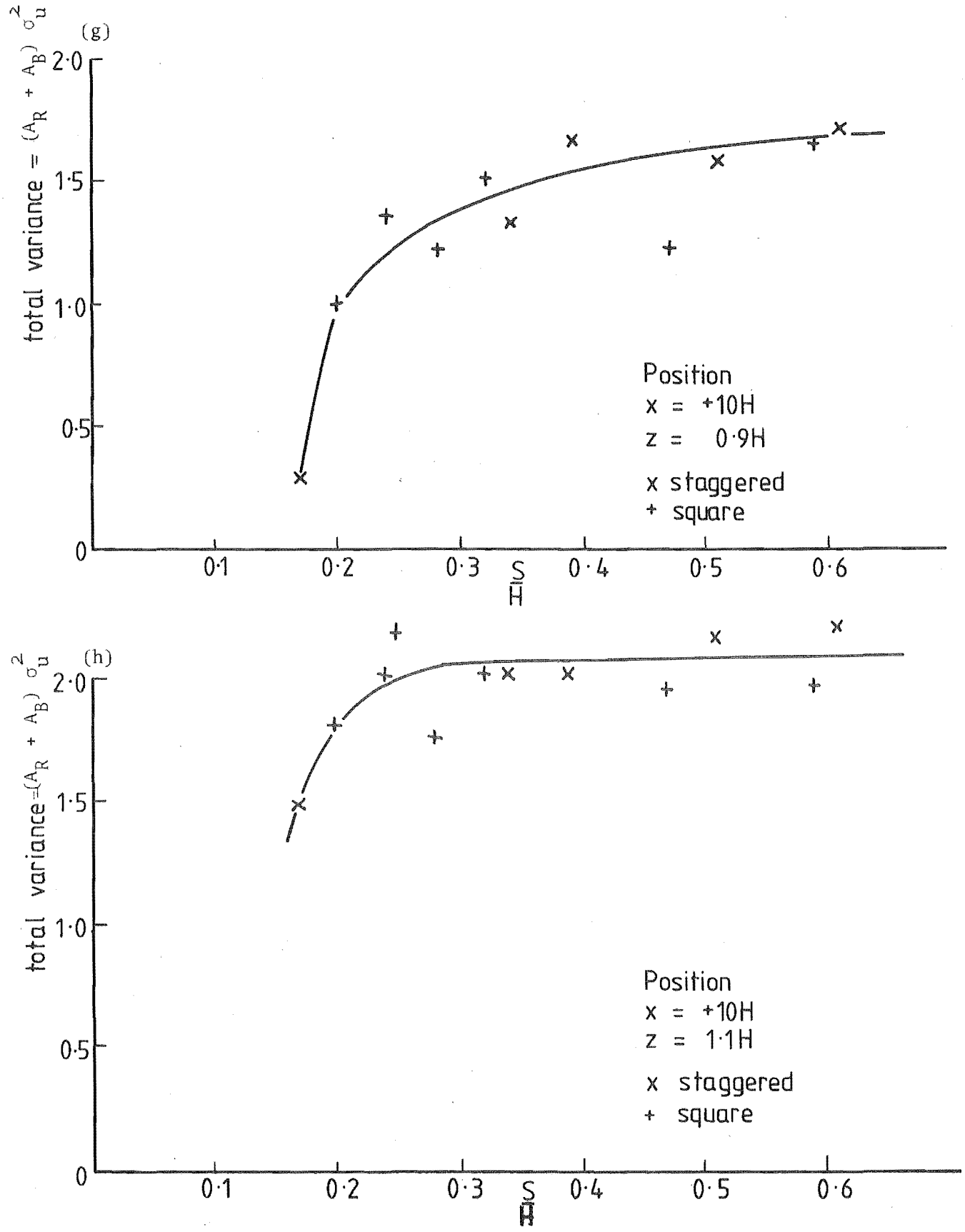

FIGURE 6.27(g) & (h): Total turbulent kinetic energy v spacing density.

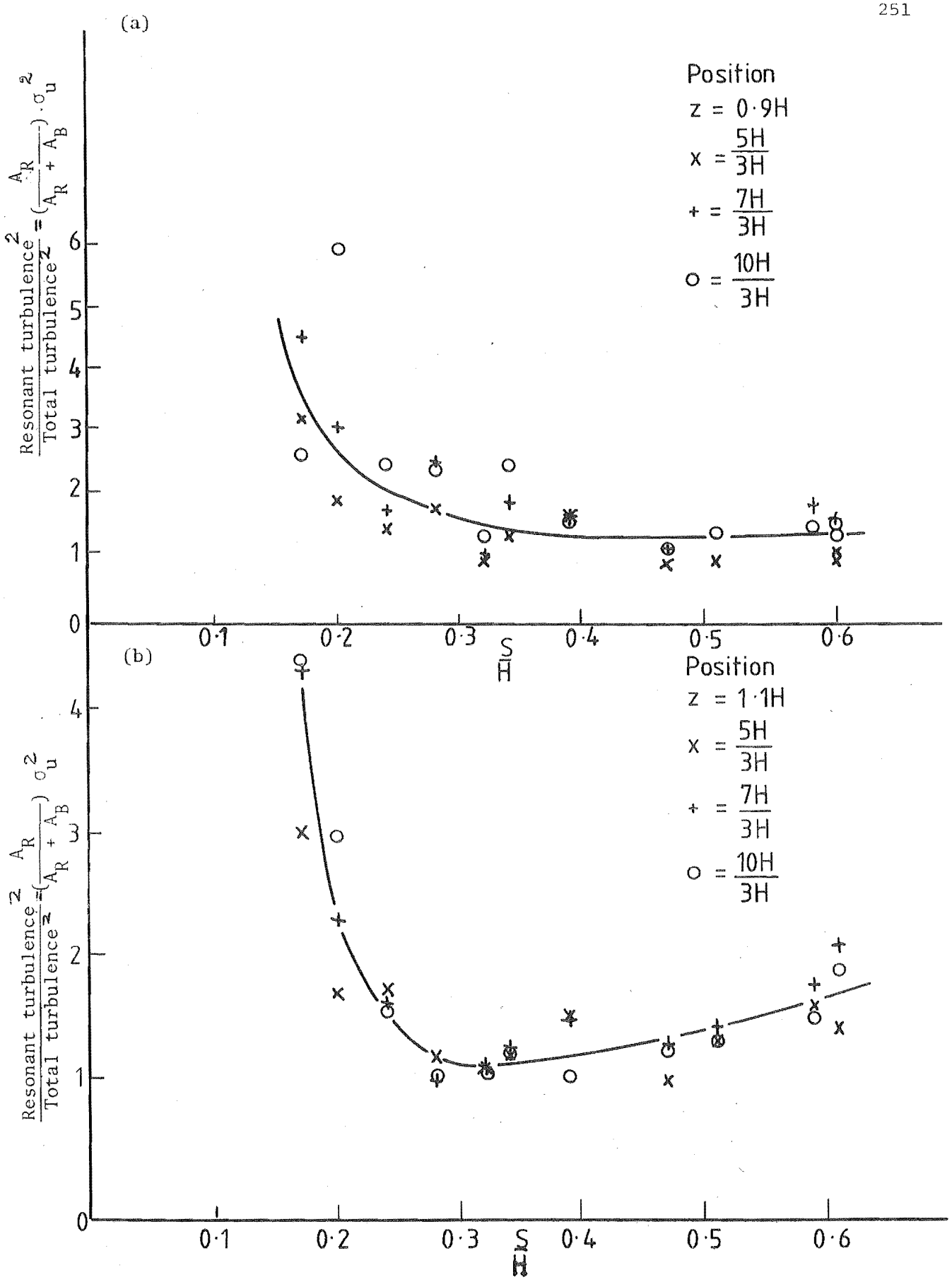

FIGURE 6.28(a) & (b): $\frac{\text{Resonant turbulence}}{\text{Total turbulence}}$ v spacing density.

TABLE 6.6: Reynolds stress measurements (Pattern W).

x-position (Tree heights)	Height z (mm)	$\bar{U}_z$ (m/s)	$\frac{u_z'}{\bar{U}_z}$	$\bar{W}_z$ (m/s)	$\frac{w'}{\bar{W}_z}$	$\frac{-\overline{u'w'}}{\bar{U}_*^2}$ or	$C_{f_{z,o}} = 2 \times \frac{-\overline{u'w'}}{\bar{U}_*^2}_{z,o}$
-3H	133	6.263	0.182	0.040	0.102	0.211	
-3H	133	6.264	0.193	0.063	0.098	0.202	
-3H	133	6.286	0.174	0.078	0.101	0.166	
-3H	133	6.373	0.187	0.059	0.099	0.212	
		$\bar{U}_{o_{av}} = 6.297$				Av. = 0.198	$C_{f_o} = 0.010$
$-\frac{1}{2}$H	180	6.346	0.166	0.375	0.116	0.099	
$-\frac{1}{2}$H	180	6.324	0.177	0.369	0.118	0.155	
$-\frac{1}{2}$H	180	6.383	0.171	0.353	0.112	0.101	
$-\frac{1}{2}$H	180	6.542	0.174	0.350	0.113	0.118	
		$\bar{U}_{z_{av}} = 6.399$				Av. = 0.118	$C_{f_o} = 0.006$
$-\frac{1}{2}$H	220	6.531	0.162	0.397	0.121	0.086	
$-\frac{1}{2}$H	220	6.574	0.169	0.419	0.122	0.147	
$-\frac{1}{2}$H	220	6.649	0.164	0.418	0.118	0.130	
$-\frac{1}{2}$H	220	6.547	0.166	0.457	0.124	0.141	
		$\bar{U}_{z_{av}} = 6.575$				Av. = 0.126	$C_{f_o} = 0.006$
3H	180	4.433	0.280	0.238	0.173	0.181	
3H	180	4.492	0.289	0.246	0.170	0.175	
3H	180	4.586	0.391	0.235	0.174	0.182	
		$\bar{U}_{z_{av}} = 4.504$				Av. = 0.179	$C_{f_z} = 0.018$ $C_{f_o} = 0.009$
3H	220	5.080	0.279	0.298	0.149	0.303	
3H	220	5.153	0.277	0.268	0.143	0.351	
3H	220	5.140	0.263	0.273	0.144	0.302	
		$\bar{U}_{z_{av}} = 5.158$				Av. = 0.319	$C_{f_z} = 0.024$ $C_{f_o} = 0.018$
5H	180	3.948	0.250	0.079	0.165	0.181	
5H	180	3.882	0.258	0.119	0.164	0.168	
5H	180	3.867	0.259	0.106	0.164	0.160	
		$\bar{U}_{z_{av}} = 3.916$				Av. = 0.170	$C_{f_z} = 0.022$ $C_{f_o} = 0.009$
5H	220	4.777	0.307	0.076	0.128	0.358	
5H	220	4.678	0.300	0.080	0.131	0.331	
5H	220	4.714	0.302	0.071	0.129	0.363	
		$\bar{U}_{z_{av}} = 4.723$				Av.= 0.351	$C_{f_z} = 0.031$ $C_{f_o} = 0.018$
7H	180	3.595	0.328	-0.012	0.199	0.328	
7H	180	3.525	0.335	-0.006	0.201	0.328	
		$\bar{U}_{z_{av}} = 3.560$				Av. = 0.328	$C_{f_z} = 0.052$ $C_{f_o} = 0.017$
7H	220	4.215	9,347	0.017	0.163	0.466	
7H	220	4.289	0.343	0.020	0.156	0.423	
7H	220	4.333	0.347	0.018	0.166	0.444	
		$\bar{U}_{z_{av}} = 4.279$				Av. = 0.431	$C_{f_z} = 0.047$ $C_{f_o} = 0.022$
10H	180	3.210	0.372	-0.005	0.244	0.369	
10H	180	3.275	0.380	-0.019	0.240	0.440	
10H	180	3.136	0.372	0.016	0.235	0.327	
10H	180	3.134	0.377	0.045	0.241	0.325	
		$\bar{U}_{z_{av}} = 3.180$				Av. = 0.365	$C_{f_z} = 0.072$ $C_{f_o} = 0.018$
10H	220	4.068	0.360	-0.002	0.197	0.522	
10H	220	4.099	0.358	-0.011	0.193	0.532	
10H	220	4.292	0.359	-0.043	0.197	0.616	
		$\bar{U}_{z_{av}} = 4.153$				Av. = 0.557	$C_{f_z} = 0.065$ $C_{f_o} = 0.028$

TABLE 6.7: Friction velocity and aerodynamic roughness of model tests compared.

Experiment	CANTERBURY (d ≈ 0.70 H)						OXFORD (d ≈ 0.75 H)						KAWATANI & MERONEY (d = H)				COOK & HEPPEL			
Pattern	B	C_1	C_2	E	F	I	P	U_*	Q	S	V	X								
$\frac{S}{H}$	0.27	0.32	0.32	0.39	0.39	0.59	0.17	0.20	0.24	0.32	0.38	0.51	0.20	0.28	0.40	0.56				0.30
A_r/A_t	0.38	0.27	0.27	0.18	0.16	0.08											0.10	0.15	0.20	0.25
$\bar{U}_o$ (m/s)	17.80	12.55	12.55	12.28	14.00	12.80	5.70	5.67	5.93	6.20	6.11									
α	0.17	0.20	0.20	0.23	0.18	0.19	Logarithmic ($z_o \equiv 0.03$ m) ($\alpha \equiv 0.17$)													
x-position	← ≈ 4.5 H →						← 3H →						← 5.5 H →				← 4 H →			
$\frac{z_o''}{H}$	0.24	-	0.25	-	0.10	-	0.33	0.28	0.21	0.09	0.05	0.04	0.34	0.18	0.30	0.12	0.03	0.05	0.10	0.07
$\bar{U}_{*\ell}$ (m/s)	1.78			2.40			0.397	0.473	0.474	0.540	0.617	0.592								
C_{f_ℓ}	0.11		0.04	0.10	0.11	0.07	0.010	0.014	0.013	0.015	0.021	0.019					0.016	0.021	0.020	0.018
$\frac{z_o'}{H}$	0.09			0.05	0.10	0.003														
C_{f_o}	0.08	0.02		0.08	0.12								0.05	0.03	0.04	0.03				
x-position	← ≈11 H →						← 10 H →						← 45 H →							
$\frac{z_o'}{H}$	0.12	0.17	0.13	0.08	0.03	0.02	0.15	0.22	0.16	0.16	0.12	0.07	0.41	0.47	0.24	0.17				
$\bar{U}_{*prof}$	2.92	2.72	2.86	2.50	1.88	1.61	1.14	1.43	1.25	1.30	1.18	1.03								
C_{f_o}	0.05	0.09	0.10	0.08	0.04	0.03	0.07	0.12	0.08	0.08	0.07	0.05	0.04	0.05	0.03	0.03				
C_{f_o}(Koloseus)	0.07	0.08	-	0.03	0.02	0.02														

The Oxford model forest gives the most consistent aerodynamic roughness estimates (Table 6.7). For the longest fetch tested,

$\frac{z''_o}{H}$ (Oxford) = 0.147 (Table 6.9)

$\frac{z''_o}{H}$ (Canterbury) = 0.10 (Table 6.7)

$\frac{z''_o}{H}$ (Rivox) = 0.15 } Table 5.12

$\frac{z''_o}{H}$ (Kielder) = 0.10 }

Notice how $\frac{z''_o}{H}$ reduces to $\frac{z'_o}{H}$ at 10 H (Kondo; Counihan; Shaw and Pereira). Also, it is evident that z''_o decreases as mean wind speeds at tree-top height increase from 1 m/s to 6 m/s (Table 6.10; Bache and Unsworth).

6.8.5 Spectra measurements along-wind versus spacing

At 10 H, a vertical traverse (Fig. 6.19) down towards the canopy of Pattern S, gave spectra where the apex of the probability distribution (Fig. 6.32) increased and moved sideways to higher frequencies. Below mean tree-top height this apex reduces rapidly in peak spectral density, especially for the closest spacings, while maintaining the same shape, or 'Q' factor. Spectra with high skew (4.6), near mean tree-top height, become less distorted towards the rear of the model forest. It appears that the wind peak frequency remains constant down into the canopy. Finnigan noted that the wind peak frequency (wavelength), resulting from frequency shifts, remains constant down into the canopy; the decelerating air moving downwards and the accelerating air moving upwards appear to cause the height dependence of the spectrum peak.

The total wind variance was compared with the wind variance near the natural frequencies of the model forest ε(5.3, 18.2 Hz) for all patterns. Changes in the ratio of these wind components near resonance and the total variance (kinetic energy), at each x-position were similar for all 11 spacing patterns (Fig. 6.28). It became a minimum near $\frac{S}{H}$ of 0.35. Beyond this spacing density the tree swaying motion also increases (Fig. 6.38). Power spectra for Patterns P, U*, S and V (Figs 6.29 - 6.33) have a high 'Q' factor just near the canopy top (cf Finnigan, Maitani, 3.8.2). Just above the canopy, the slope of the log-log plots of wind spectra in the dissipative region is $-\frac{5}{3}$ (Kolomogorov Laws). There is an added component (7.1; 7.2.4) in the

To p.260

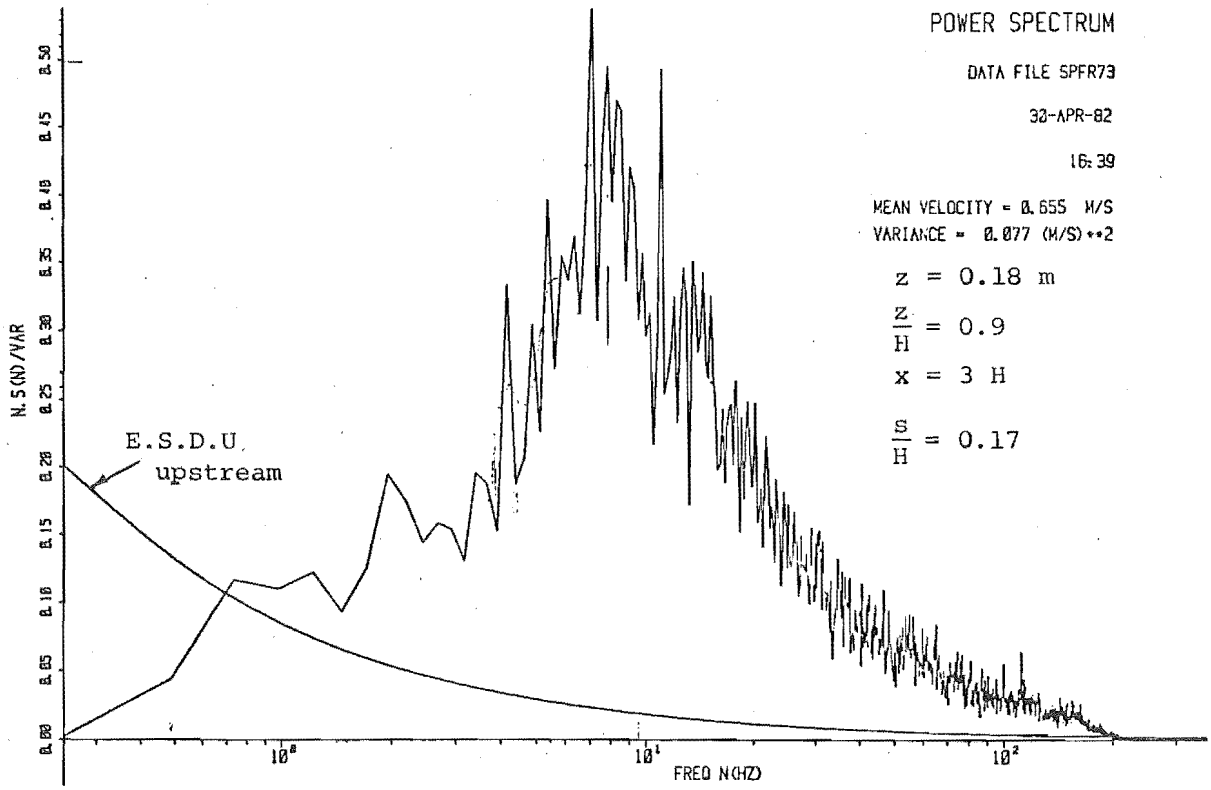

POWER SPECTRUM
****

SPECTRUM PARAMETERS

SPECTRUM PLOTTING FILE SPFR73
RAW DATA FILE RWFR73

NO. OF HANN SMOOTHING = 0
NO. OF POINTS IN F.F.T. = 2048
NO. OF SPECTRA AVERAGED = 38
LOWEST FREQUENCY = 0.244 HZ
HIGHEST FREQUENCY = 250.000 HZ
LOW PASS FILTER SETTING = 200.000 (HZ)
HIGH PASS FILTER SETTING = 0.488 (HZ)
SAMPLING TIME FOR VARIANCE = 62.960 SECS

MEAN VELOCITY = 0.655 M/S

VARIANCE = 0.077 (M/S)**2

VELOCITY SPECTRUM

DATE: 30-APR-82 TIME: 16:39

COMMENT: PROBE AT +3H, TREE PATTERN P STAGGERED

PROBE AMPLIFIER

CALIBRATION FACTOR = 10.392 (M/S PER V)
PROBE POSITION: X = 0.000 Y = 0.000 Z = 0.000
3.000 H 0.180m

FIGURE 6.29: Power spectral density distribution (Pattern P, +3H), Oxford.

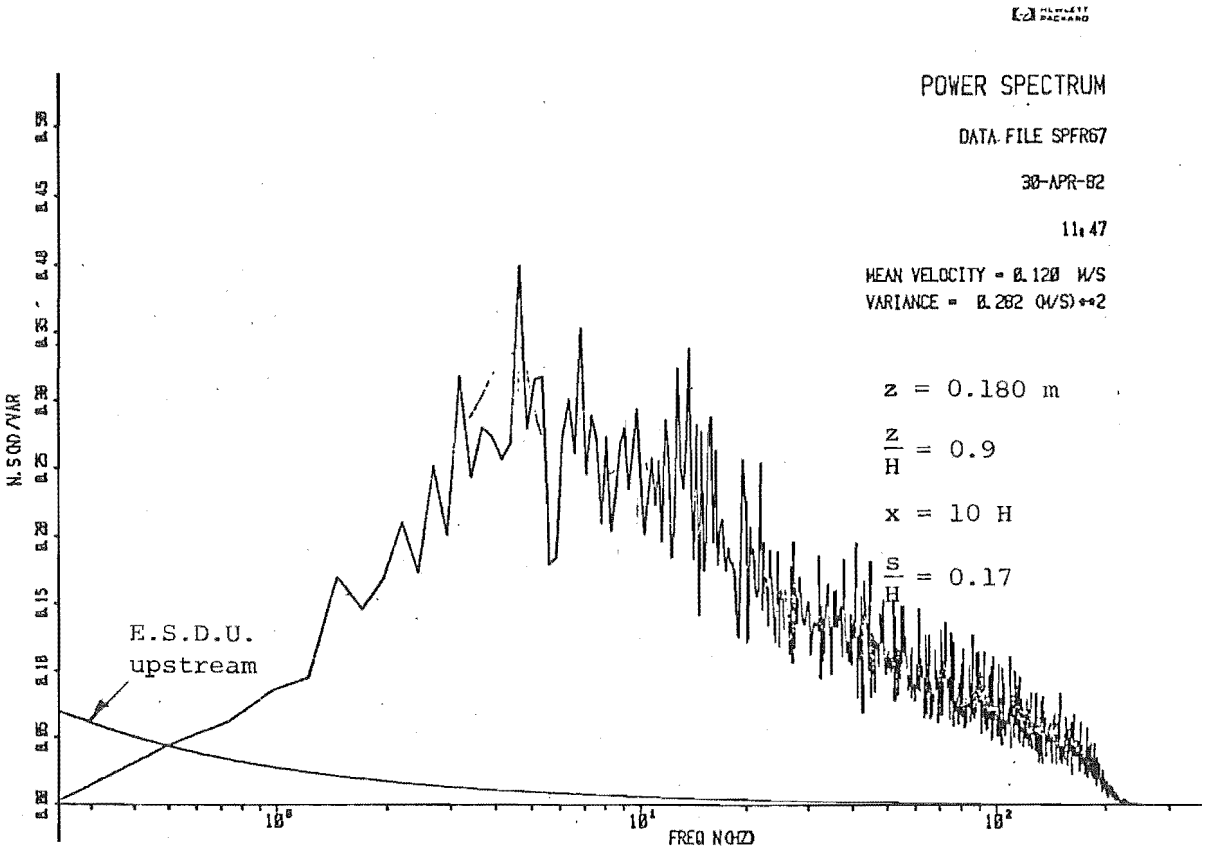

POWER SPECTRUM
****

SPECTRUM PARAMETERS

SPECTRUM PLOTTING FILE SPFR67
RAW DATA FILE RWFR67

NO. OF HANN SMOOTHING = 0
NO. OF POINTS IN F.F.T. = 2048
NO. OF SPECTRA AVERAGED = 28
LOWEST FREQUENCY = 0.244 HZ
HIGHEST FREQUENCY = 250.000 HZ
LOW PASS FILTER SETTING = 200.000 (HZ)
HIGH PASS FILTER SETTING = 0.488 (HZ)
SAMPLING TIME FOR VARIANCE = 113.130 SECS

MEAN VELOCITY = 0.120 M/S

VARIANCE = 0.282 (M/S)**2

VELOCITY SPECTRUM

DATE: 30-APR-82 TIME: 11:47

COMMENT: PROBE AT 10H, TREE PATTERN P STAGGERED

PROBE Y AMPLIFIER 0

CALIBRATION FACTOR = 10.400 (M/S PER V)
PROBE POSITION, X = 10.000 M Y = 0.000 Z = 0.180 m

FIGURE 6.30: Power spectral density distribution (Pattern P, +10H).

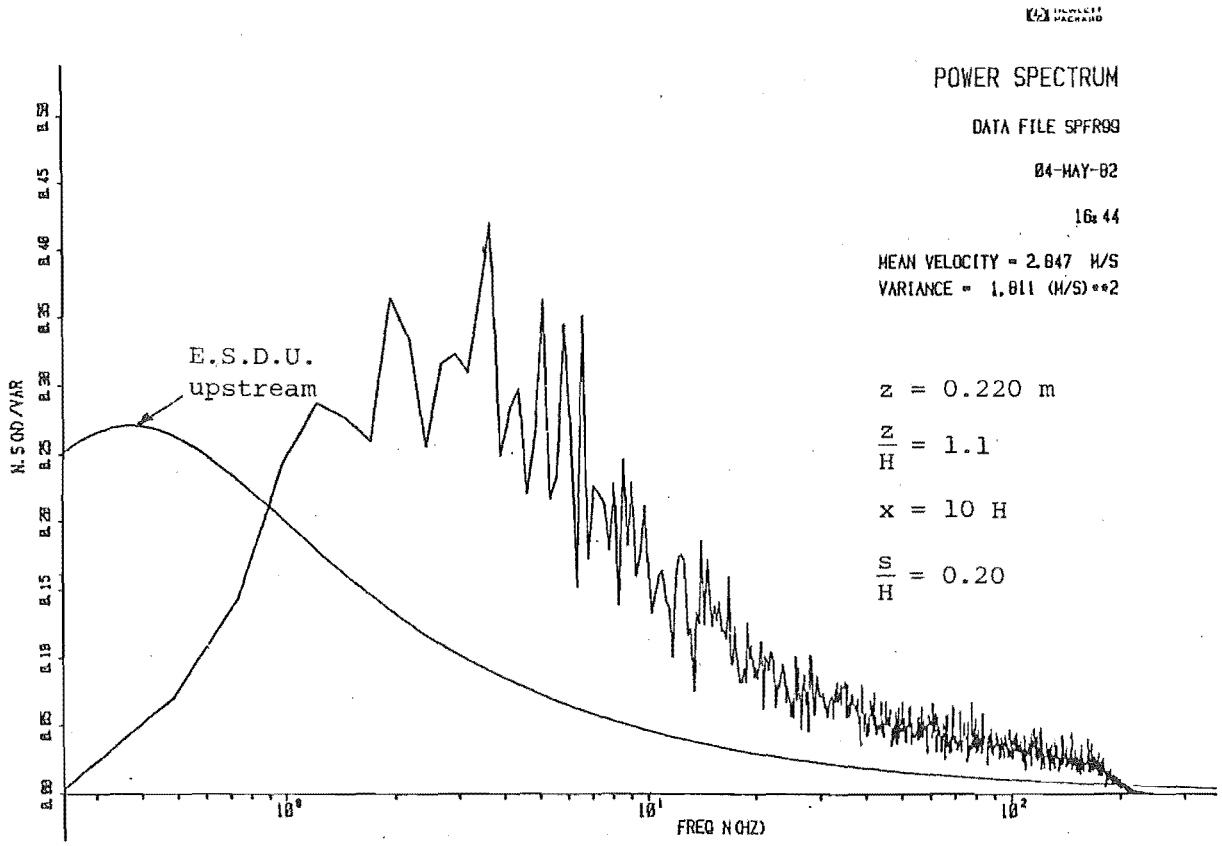

POWER SPECTRUM
****

SPECTRUM PARAMETERS

SPECTRUM PLOTTING FILE SPFR99
RAW DATA FILE RWFR99

NO. OF HANN SMOOTHING = 0
NO. OF POINTS IN F.F.T. = 2048
NO. OF SPECTRA AVERAGED = 28
LOWEST FREQUENCY = 0.244 HZ
HIGHEST FREQUENCY = 250.000 HZ
LOW PASS FILTER SETTING = 200.000 (HZ)
HIGH PASS FILTER SETTING = 0.488 (HZ)
SAMPLING TIME FOR VARIANCE = 110.600 SECS

MEAN VELOCITY = 2.847 M/S

VARIANCE = 1.811 (M/S)**2

VELOCITY SPECTRUM

DATE: 04-MAY-82 TIME: 16:44

COMMENT: PROBE AT 10H, TREE PATTERN U

PROBE Y AMPLIFIER 0

CALIBRATION FACTOR = 10.240 (M/S PER V)
PROBE POSITION, X = 10.000 H Y = 0.000 Z = 0.220 m

FIGURE 6,31: Power spectral density distribution (Pattern U*, +10H).

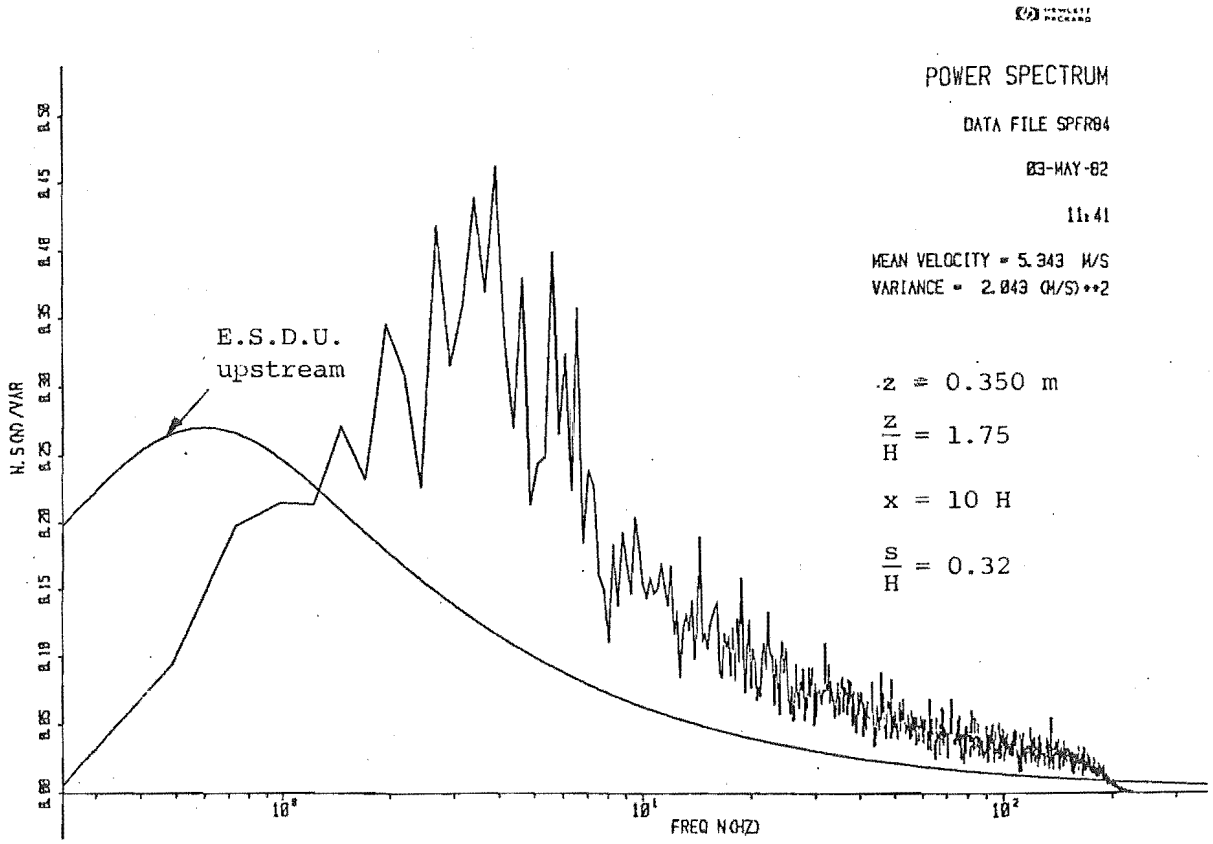

POWER SPECTRUM
****

SPECTRUM PARAMETERS

SPECTRUM PLOTTING FILE SPFR84
RAW DATA FILE RWFR84

NO. OF HANN SMOOTHING = 0
NO. OF POINTS IN F.F.T. = 2048
NO. OF SPECTRA AVERAGED = 28
LOWEST FREQUENCY = 0.244 HZ
HIGHEST FREQUENCY = 250.000 HZ
LOW PASS FILTER SETTING = 200.000 (HZ)
HIGH PASS FILTER SETTING = 0.488 (HZ)
SAMPLING TIME FOR VARIANCE = 62.340 SECS

MEAN VELOCITY = 5.343 M/S

VARIANCE = 2.043 (M/S)**2

VELOCITY SPECTRUM

DATE: 03-MAY-82 TIME: 11:41

COMMENT: BIDH, 350mm S-Squeg.

PROBE AMPLIFIER

CALIBRATION FACTOR = 10.233 (M/S PER V)
PROBE POSITION, X = 0.000 Y = 0.000 Z = 0.000

FIGURE 6.32: Power spectral density distribution (Pattern S, +10H).

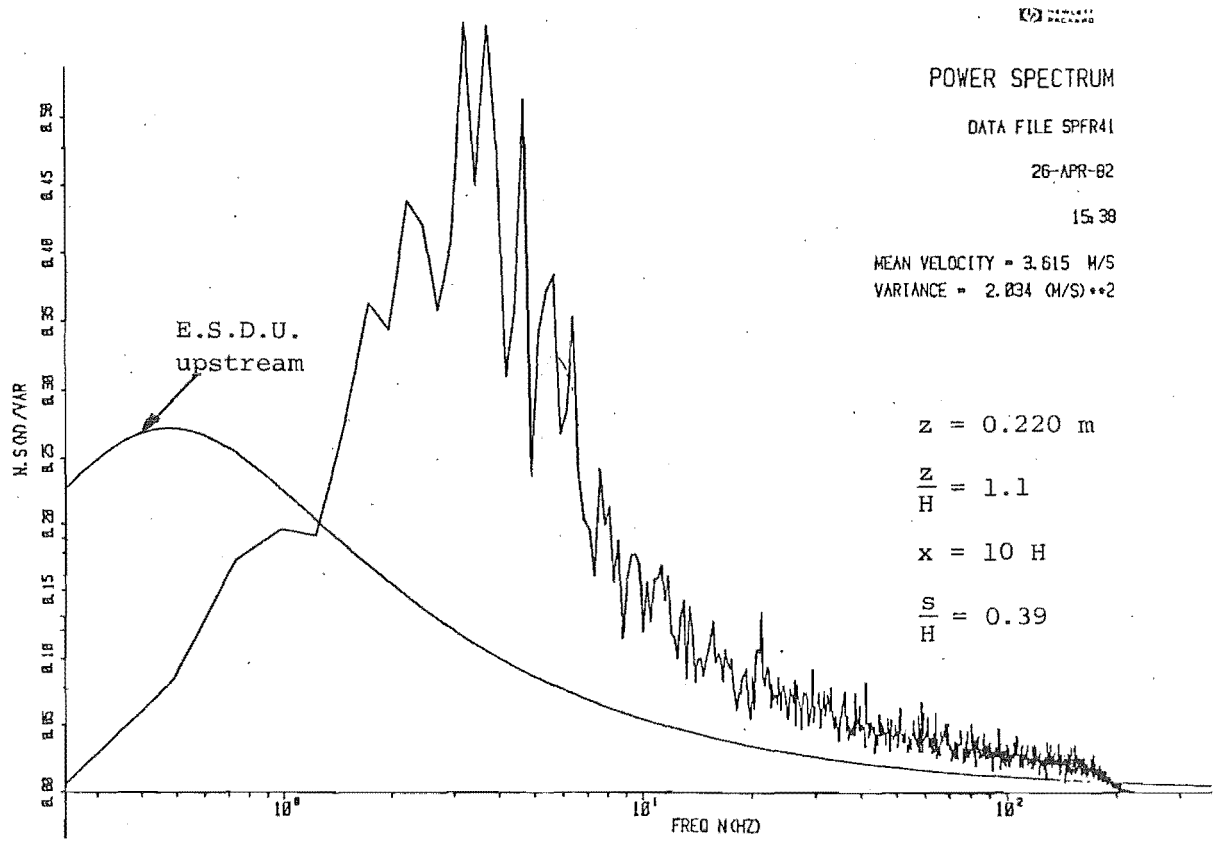

POWER SPECTRUM
****

SPECTRUM PARAMETERS

SPECTRUM PLOTTING FILE SPFR41
RAW DATA FILE RWFR41

NO. OF HANN SMOOTHING = 0
NO. OF POINTS IN F.F.T. = 2048
NO. OF SPECTRA AVERAGED = 28
LOWEST FREQUENCY = 0.244 HZ
HIGHEST FREQUENCY = 250.000 HZ
LOW PASS FILTER SETTING = 200.000 (HZ)
HIGH PASS FILTER SETTING = 0.488 (HZ)
SAMPLING TIME FOR VARIANCE = 130.090 SECS

MEAN VELOCITY = 3.615 M/S

VARIANCE = 2.034 (M/S)**2

VELOCITY SPECTRUM

DATE: 26-APR-82 TIME: 15:38

COMMENT: PROBE AT 10H, TREE PATTERN V STAGGERED

PROBE Y AMPLIFIER 0

CALIBRATION FACTOR = 10.000 (M/S PER V)
PROBE POSITION, X = 10.000 H Y = 0.000 Z = 0.220m

FIGURE 6.33: Power spectral density distribution (Pattern V, +10H).

spectra as spacing increases and the slope appears greater than $-\frac{5}{3}$ (Figs 6.31 - 6.33; Fig. 7.6).

The peak frequencies for all spectra (Tables 6.8(a)-(d)) were used to calculate the resonant and background components of model tree response using the simple second order solution (3.9.1). The areas of all spectra were measured using images of the spectra projected onto a calibrated screen. The resonant areas, (A_R), ε(5.3, 18.2 Hz) and background areas A_B (Table 6.8(a) -(d)) were used to calculate the along-wind tree-top response from the complex closed-form solution (3.10.2).

6.9 ALONG-WIND TREE RESPONSE ESTIMATES

6.9.1 Simple calculation

The magnification $M_R\left(\simeq \sqrt{\frac{R}{B}}\right)$ and phase angle, ϕ_R, are calculated for the simple, second order, dynamic response (3.9.1; Appendix I) and shown in Figs 6.34(a)-(d). At 3 H (near the forest front) this method does not compare well with the complex calculations of $\sqrt{\frac{R}{B}}$. The phase angle is almost at 180°, which suggests that the dynamic response of the model trees is in anti-phase with the wind, and that the two effects may almost cancel each other out. Towards the rear, at 7 H and 10 H, there is better agreement and, because ϕ_R is lower, aerodynamic damping may be less, so that the cancelling modes may not be present. Beyond $\frac{S}{H}$ of 0.35, increases in ϕ_R do not appear to reduce the dynamic components (Fig. 6.38).

Although this hypothesis has not been tested, the phase shift is a likely reason for the reduced dynamic tree-sway motion that occurs at close spacings (up to $\frac{S}{H}$ of 0.35). The shape of the remainder of the response curves follows the expected second order sinusoidal response shapes.

6.9.2 Complex calculation

The closed-form solution to along-wind tree-top response (3.10, Appendix I.2) for the mean static deflections (D), and the background and resonant components for the dynamic deflections are plotted separately (Figs 6.36, 6.37) and together (Fig. 6.38). The ratio $\frac{A}{D}$ obtained by the calculation procedure (Appendix I.2) is compared with that obtained by photographic analysis (6.6.4, Fig. 6.7) in Figs 6.39(a)-(c).

To p.267

TABLE 6.8(a): Spectra areas and n_{p_k} measurement (summary).

Pattern & Spacing	Computer File Number	Height (mm)	Position (H = 0.2m)	A_R $(mm)^2$	$A_R\sigma_u^2$	$A_R + A_B$ $(mm)^2$	$\frac{A_R}{A_R + A_B}$	n_{pk} (Hz)	σ_u^2 $(m/s)^2$	$\bar{U}_z$ (m/s)
Upstream No Forest	SP 09 FR			21.88		ESDU 99.17 Actual 101.78		1.4	1.139	
P	SP FR 66	180	5H	22.33	25.880	106.92	0.209	3.9	1.159	
	SP FR 67	180	10H	30.86	8.703	102.25	0.302	4.3	0.282	
$\frac{S}{H}$ = 0.17	SP FR 68	220	10H	25.00	37.150	106.78	0.234	3.1	1.486	
	SP FR 69	180	7H	27.56	15.158	100.98	0.273	3.2	0.550	
ST	SP FR 70	220	7H	24.99	36.585	109.99	0.227	2.3	1.464	
	SP FR 71	180	5H	31.51	10.619	117.45	0.268	5.0	0.337	
	SP FR 72	220	5H	27.93	25.511	115.90	0.241	4.1	0.985	
	SP FR 73	180	3H	43.52	3.351	100.21	0.434	6.9	0.077	0.655
	SP FR 74	220	3H	22.70	8.490	110.93	0.205	5.1	0.374	
U*	SP FR 92	180	3H	40.63	4.876	111.18	0.365	6.7	0.120	0.662
	SP FR 93	220	3H	22.88	14.048	101.53	0.225	4.3	0.614	
$\frac{S}{H}$ = 0.20	SP FR 94	180	5H	30.97	9.230	101.56	0.305	5.2	0.298	
	SP FR 95	220	5H	22.31	23.671	110.05	0.203	4.4	1.061	
SQ	SP FR 96	180	7H	33.14	14.814	113.39	0.292	4.1	0.447	
	SP FR 97	220	7H	24.79	32.029	109.64	0.226	4.7	1.292	
	SP FR 98	180	10H	27.93	29.103	106.40	0.262	2.7	1.042	
	SP FR 99	220	10H	22.85	41.381	103.57	0.221	3.4	1.811	
Q	SP FR 58	108	3H	39.45	11.598	110.05	0.358	7.4	0.294	1.859
	SP FR 59	220	3H	28.93	23.893	105.87	0.273	2.6	0.829	
$\frac{S}{H}$ = 0.24	SP FR 60	180	5H	28.97	16.600	101.73	0.285	5.0	0.573	
	SP FR 61	220	5H	25.16	41.212	104.71	0.240	4.9	1.638	
SQ	SP FR 62	180	7H	22.77	19.673	105.19	0.216	2.1	0.864	
	SP FR 63	220	7H	22.56	38.578	105.75	0.213	2.8	1.710	
	SP FR 64	180	10H	20.88	28.334	108.76	0.192	2.5	1.357	
	SP FR 65	220	10H	18.00	36.396	99.60	0.181	2.6	2.022	

TABLE 6.8(b): Spectra areas and n_{pk} measurement (summary).

Pattern & Spacing	Computer File Number	Height (mm)	Position (H = 0.2m)	A_R $(mm)^2$	$A_R\sigma_u^2$	$A_R + A_B$ $(mm)^2$	$\frac{A_R}{A_R + A_B}$	n_{pk} (Hz)	σ_u^2 $(m/s)^2$	$\bar{U}_z$ (m/s)
R	SP 01 FR	180	3H	32.24	9.543	110.14	0.293	4.4	0.296	1.378
	SP 02 FR	220	3H	28.37	36.626	99.59	0.285	5.4	1.291	
$\frac{S}{H}$ = 0.28	SP 03 FR	180	5H	30.39	16.806	107.61	0.282	5.0	0.553	
	SP 04 FR	220	5H	24.86	43.505	99.86	0.249	5.5	1.785	
SQ	SP 05 FR	180	7H	27.31	24.033	109.30	0.250	5.1	0.880	
	SP 06 FR	220	7H	23.04	35.505	108.29	0.213	4.0	1.541	
	SP 07 FR	180	10H	18.53	22.607	97.86	0.189	2.4	1.220	
	SP 08 FR	220	10H	21.80	38.128	106.99	0.204	2.7	1.749	
S	SP FR 75	180	3H	32.88	26.271	102.84	0.320	11.0	0.799	2.967
	SP FR 76	220	3H	28.33	38.472	114.27	0.248	4.0	1.358	
$\frac{S}{H}$ = 0.32	SP FR 77	180	5H	33.83	23.410	102.58	0.330	6.0	0.692	
	SP FR 78	220	5H	33.99	42.539	119.89	0.284	5.4	1.274	
SQ	SP FR 70	180	7H	26.49	26.146	95.92	0.276	4.9	0.987	
	SP FR 80	220	7H	23.59	44.774	106.02	0.223	3.9	1.898	
	SP FR 81	180	10H	22.45	33.990	105.49	0.213	3.8	1.514	
	SP FR 82	220	10H	19.76	39.639	100.53	0.197	3.5	2.006	
	SP FR 83	260	10H	19.83	41.286	101.48	0.195	2.7	2.082	
	SP FR 84	350	10H	22.84	46.662	107.59	0.212	3.7	2.043	
	SP FR 85	520	10H	20.84	38.320	98.56	0.212	3.5	1.830	
	SP FR 86	133	10H	26.06	16.235	108.58	0.240	4.4	0.623	
	SP FR 87	520	5H	24.34	22.612	106.66	0.228	3.2	0.929	
	SP FR 88	350	5H	24.07	50.836	101.45	0.237	4.4	2.112	
	SP FR 89	133	5H	40.44	14.640	102.36	0.395	7.2	0.362	
	SP FR 90	150	5H	39.29	13.752	108.24	0.363	9.7	0.350	
Upstream	SP FR 91	180	-3H	21.68	24.694	114.66	0.189	1.4	1.139	

TABLE 6.8(c). Spectra areas and n_{p_k} measurement (summary).

Pattern & Spacing	Computer File Number	Height (mm)	Position (H = 0.2m)	A_R $(mm)^2$	$A_R\sigma_u^2$	$A_R + A_B$ $(mm)^2$	$\frac{A_R}{A_R + A_B}$	n_{pk} (Hz)	σ_u^2 $(m/s)^2$	$\bar{U}_z$(m/s)
T	SP FR 50	180	3H	32.34	15.459	102.92	0.314	9.6	0.478	2.336
	SP FR 51	220	3H	27.62	37.204	108.75	0.254	4.1	1.347	
$\frac{S}{H}$ = 0.34	SP FR 52	180	5H	30.44	20.151	103.64	0.294	4.9	0.662	
	SP FR 53	220	5H	26.15	44.063	97.67	0.268	5.2	1.685	
ST	SP FR 54	180	7H	27.14	28.633	109.44	0.248	3.4	1.055	
	SP FR 55	220	7H	24.22	46.527	105.28	0.230	5.0	1.921	
	SP FR 56	180	10H	28.30	37.706	103.07	0.275	5.3	1.332	
	SP FR 57	220	10H	22.09	45.307	112.57	0.196	2.9	2.051	
V	SP FR 33	180	3H	25.15	26.030	103.05	0.244	2.9	1.035	3.583
	SP FR 34	220	3H	24.42	42.955	112.59	0.217	3.7	1.759	
$\frac{S}{H}$ = 0.39	SP FR 35	180	5H	36.05	43.476	109.00	0.331	7.0	1.206	
	SP FR 36	220	5H	28.97	64.922	112.98	0.256	6.0	2.241	
ST	SP FR 37	180	7H	28.91	43.018	104.71	0.276	5.7	1.488	
	SP FR 38	220	7H	27.37	63.143	105.94	0.258	5.9	2.307	
	SP FR 40	180	10H	24.16	40.130	109.68	0.220	4.2	1.661	
	SP FR 41	220	10H	21.88	44.504	111.28	0.197	3.4	2.034	
W	SP FR 42	180	3H	26.08	32.078	102.37	0.255	4.7	1.230	4.537
	SP FR 43	220	3H	21.77	39.534	95.66	0.228	4.8	1.816	
$\frac{S}{H}$ = 0.47	SP FR 44	180	5H	28.00	27.356	103.18	0.271	7.4	0.977	
	SP FR 45	220	5H	23.67	38.890	99.64	0.238	4.6	1.643	
	SP FR 46	180	7H	31.43	35.422	106.12	0.296	5.3	1.127	
	SP FR 47	220	7H	30.10	50.267	111.25	0.271	5.5	1.670	
	SP FR 48	180	10H	27.91	34.190	106.45	0.262	5.7	1.225	
	SP FR 49	220	10H	25.24	48.738	104.55	0.241	3.2	1.931	

TABLE 6.8(d). Spectra areas and n_{p_k} measurement (summary).

Pattern & Spacing	Computer File Number	Height (mm)	Position (H = 0.2m)	A_R $(mm)^2$	$A_R\sigma_u^2$	$A_R + A_B$ $(mm)^2$	$\frac{A_R}{A_R + A_B}$	n_{pk} (Hz)	σ_u^2 $(m/s)^2$	$\bar{U}_z$ (m/s)
X	SP FR 23	180	$-\frac{1}{2}$H	21.79	24.100	107.77	0.202	1.2	1.106	
	SP FR 24	220	$-\frac{1}{2}$H	22.00	22.638	107.97	0.204	2.2	1.029	
$\frac{S}{H}$ = 0.51	SP FR 25	180	3H	27.96	33.748	104.99	0.266	5.7	1.207	4.124
	SP FR 26	220	3H	22.49	40.684	99.30	0.226	3.4	1.809	
ST	SP FR 27	180	5H	30.16	30.673	106.41	0.283	6.8	1.017	
	SP FR 28	220	5H	28.39	52.919	105.23	0.270	4.4	1.864	
	SP FR 29	180	7H	31.84	44.003	105.54	0.302	6.1	1.382	
	SP FR 30	220	7H	28.60	57.686	108.33	0.264	5.3	2.017	
	SP FR 31	180	10H	29.35	46.226	103.37	0.284	6.0	1.575	
	SP FR 32	220	10H	25.46	55.095	106.99	0.238	3.1	2.164	
Y	SP FR 14	133	-3H	20.65	23.376	108.98	0.190	1.5	1.132	
	SP FR 15	180	3H	22.64	34.594	102.50	0.221	6.9	1.528	5.325
$\frac{S}{H}$ = 0.59	SP FR 16	220	3H	22.14	32.214	105.14	0.211	4.1	1.455	
	SP FR 17	180	5H	27.22	48.860	110.41	0.247	7.4	1.795	
SQ	SP FR 18	220	5H	24.26	50.655	107.47	0.225	1.5	2.088	
	SP FR 19	180	7H	28.31	63.386	99.75	0.284	6.7	2.239	
	SP FR 20	220	7H	23.81	56.430	102.07	0.233	2.0	2.370	
	SP FR 21	180	10H	30.21	49.937	103.59	0.292	5.8	1.653	
	SP FR 22	220	10H	24.45	47.604	98.12	0.249	4.9	1.947	
Z	SP FR 10	180	7H	30.13	53.119	103.18	0.292	6.5	1.763	
	SP FR 11	220	7H	27.25	59.351	83.89	0.325	5.9	2.178	
$\frac{S}{H}$ = 0.61	SP FR 12	180	10H	31.06	53.237	104.38	0.298	7.3	1.714	
	SP FR 13	220	10H	24.41	53.360	105.25	0.232	5.1	2.186	
ST	SP FR 09	220	5H	23.38	39.956	106.78	0.219	1.4	1.709	
	SP FR 08	180	5H	28.75	36.426	107.59	0.267	7.9	1.267	
	SP FR 07	220	3H	27.26	28.459	105.43	0.259	2.1	1.044	
	SP FR 06	180	3H	24.41	38.739	103.83	0.235	2.0	1.587	3.983
	SP FR 05	180	3H	23.45	34.307	101.45	0.231		1.463	3.993
	SP FR 04	220	$-\frac{1}{2}$H	29.39	32.259	99.57	0.295	2.0	1.098	
	SP FR 03	180	$-\frac{1}{2}$H	32.14	38.086	98.85	0.325	1.6	1.185	
	SP FR 02	133	$-\frac{1}{2}$H	38.70	35.445	97.67	0.294	2.7	1.235	
	SP FR 01	133	-3H	33.57	36.390	95.07	0.353	1.9	1.084	

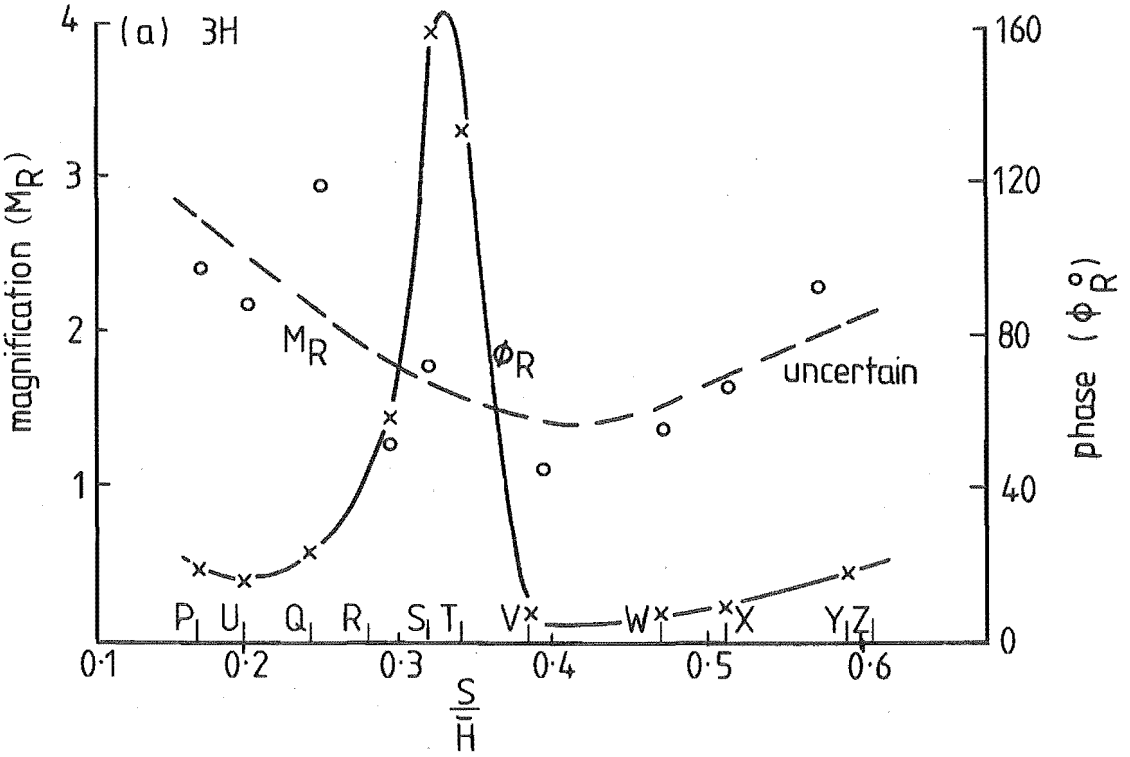

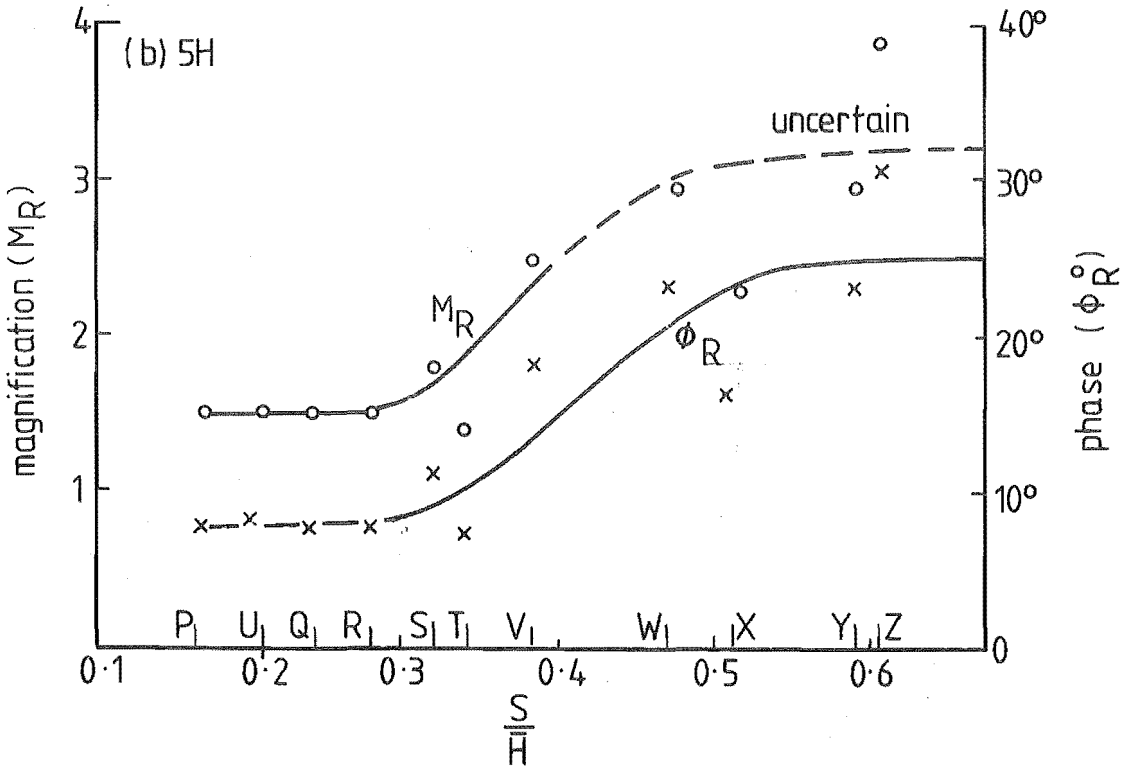

FIGURES 6.34 (a) & (b): Ideal response (M_R), ϕ_R v $\frac{S}{H}$

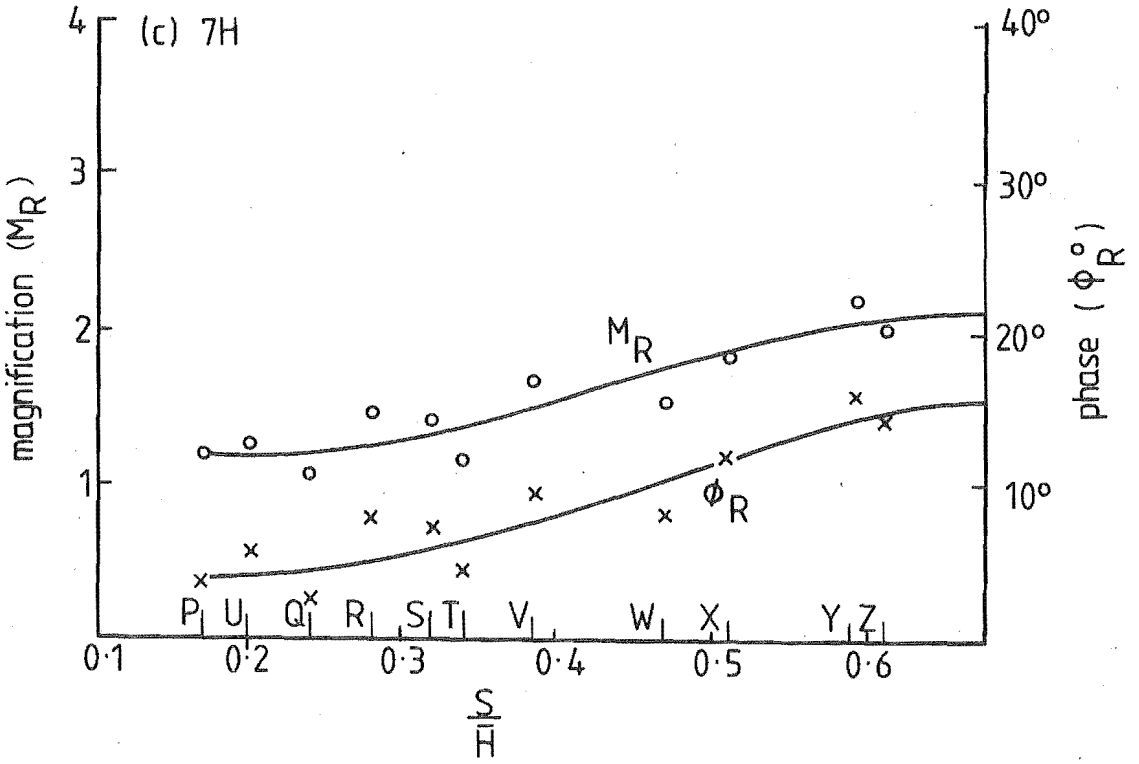

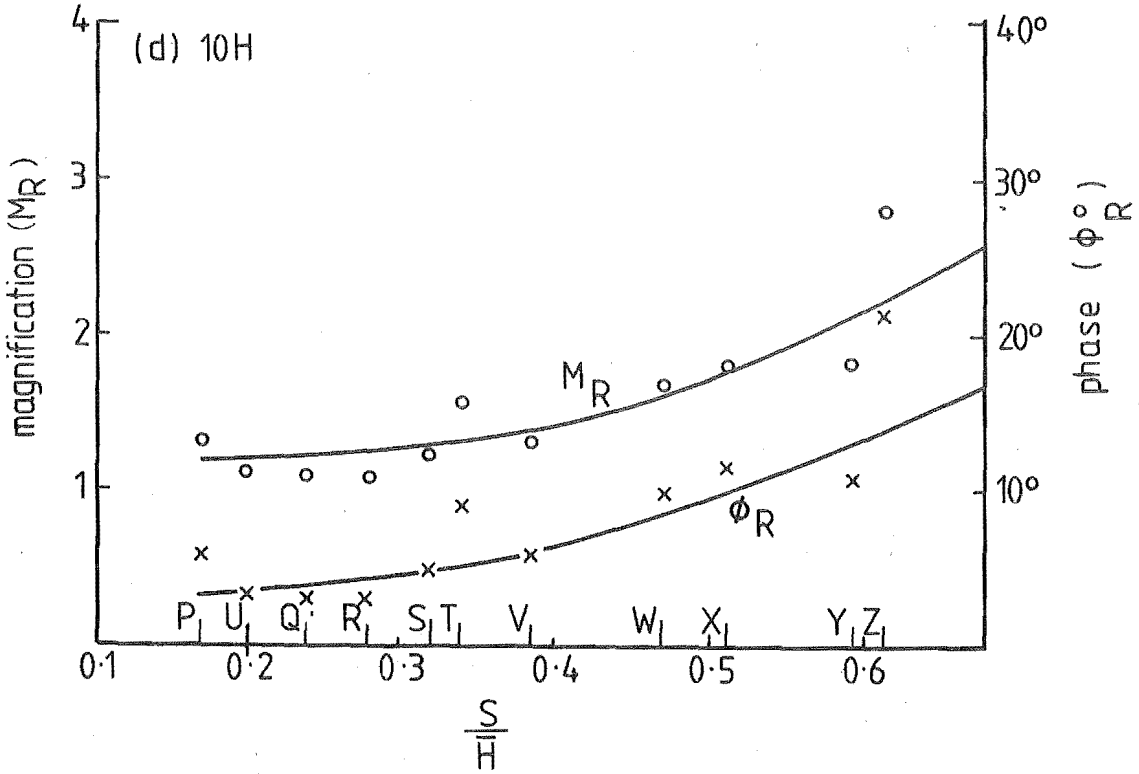

FIGURES 6.34 (c) & (d): Ideal response (M_R), ϕ_R v $\frac{S}{H}$

Direct application of Solari's closed-form solution failed because the integrals I_1, I_2, I_3 (3.10), calculated from assumed profiles, were lower than the same integrals computed numerically from the actual measured profiles. The actual mean velocity profiles extend into the transition region above the crop (where the logarithmic shape has 'kinks') and down into the crop where the mean wind speed is never actually zero. Spectra in the non-equilibrium regions cannot be fitted to the model spectra proposed by Högström et al and used by Solari because of the high skew and 'Q' factor present (6.8.5). Solari suggests that his profile assumptions can be modified to accommodate large values of zero-plane displacement when errors are above 12%.

No calculations from the direct method were compared with Solari's Method except that, at 10 H, there appears to be some correspondence. This is where the flow conditions return to equilibrium and the profiles have extended logarithmic shapes with only small inflexions. Plots B, R, $\sqrt{\frac{R}{B}}$, $A.M_T^1$, $D.M_T$. and $(A+D)M_T$. from Tables 6.9 to 6.12 allowed estimates of $\frac{A}{H}$ by complex calculation and by photography to be compared both with each other and with one full scale measurement of $\frac{A}{H}$ (Fig. 5.29).

The plots of $\frac{A}{D}$, AM_T, DM_T and $(A+D)M_T$ (Figs 6.36 and 6.38) clearly indicate that:-

(a) amplitudes are higher than mean deflections for all spacings;

(b) both amplitudes and deflections increase with increasing spacing density (6.6.4);

(c) amplitudes are much the same for any x-position at any particular spacing;

(d) up to $\frac{S}{H}$ of 0.35 tree response is dominated by the mean deflections caused by high mean wind speeds near the forest leading edge;

(e) above $\frac{S}{H}$ of 0.35 tree response near the front is dominated by the amplitude deflections caused by the background and resonant turbulent wind components ($\sqrt{B+R}$).

---

1. The mean model tree mass (M_T) of $\frac{0.00663 \text{ Kg}}{9.81}$ has only recently been obtained.

To p.278

TABLE 6.9(a): Deflection due to background turbulence (B) by complex calculation (Oxford)

Pattern	S/H	$\frac{z_o''}{H}$	U_*profile	K_1	σ_u^2	$A_R + A_B$	$\frac{A_R}{A_R + A_B}$	A_B	I_2	F_1	$B(\times 10^{-3})$
+3H	$\hat{n}_o$=5.6Hz; I_3 = 0.138 for all positions; H = 0.202m; n_o = 8.9 H_z;							$C_{z_o} \approx 0.012$m; $\frac{z}{H}$ = 0.9;		H_{z_o} =	0.0404m;
P	.17	0.33	2.86	0.0396	0.077	1.002	0.434	0.567	0.0418	0.889	0.434
U_*	.20	0.28	2.29	0.0641	0.120	1.112	0.365	0.706	0.052	0.890	1.10
Q	.24	0.205	1.99	0.0410	0.294	1.101	0.358	0.706	0.0632	0.878	0.858
R	.28	0.163	1.67	0.0436	0.296	1.101	0.293	0.779	0.043	0.890	0.511
S	.32	0.0885	1.22	0.051	0.799	1.028	0.320	0.700	0.057	0.874	0.940
T	.34	0.180	1.93	0.0415	0.478	1.029	0.314	0.706	0.054	0.876	0.673
V	.38	0.047	1.03	0.0432	1.035	1.031	0.244	0.779	0.0559	0.876	0.747
W	.47	0.03	0.902	0.0414	1.230	1.024	0.255	0.763	0.0745	0.869	1.13
X	.51	0.035	0.958	0.0410	1.207	1.050	0.266	0.770	0.0683	0.871	0.967
Y	.59	0.002	0.507	0.0339	1.528	1.205	0.221	0.799	0.0704	0.870	0.815
Z	.61	0.0112	0.680	0.0466	1.587	1.039	0.235	0.794	0.0585	0.872	0.876
+5H											
P	.17	0.36	2.47	0.215	0.337	1.1745	0.268	0.859	0.053	0.884	5.94
U	.20	0.340	2.36	0.134	0.298	1.0156	0.305	0.706	0.050	0.889	2,78
Q	.24	0.210	1.71	0.175	0.573	1.0173	0.285	0.728	0.0543	0.885	2.73
R	.28	0.205	1.72	0.1312	0.553	1.0761	0.282	0.772	0.0558	0.886	3.05
S	.32	0.163	1.59	0.075	0.692	1.0258	0.330	0.688	0.062	0.879	1.73
T	.34	0.173	1.59	0.100	0.662	1.0364	0.294	0.732	0.057	0.882	2.19
V	.38	0.104	1.31	0.099	1.206	1.0900	0.331	0.730	0.0539	0.881	2.00
W	.47	0.046	1.106	0.038	0.977	1.0318	0.271	0.752	0.0670	0.871	0.855
X	.51	0.054	1.07	0.044	1.017	o.0641	0.283	0.763	0.0614	0.873	0.874
Y	.59	0.023	0.838	0.061	1.795	1.1041	0.247	0.832	0.0614	0.872	1.31
Z	.61	0.0255	0.794	0.054	1.267	1.0759	0.267	0.788	0.0617	0.872	1.13

TABLE 6.9(b) : Deflection due to background turbulence (B) by complex calculation (Oxford) (Continued)

Pattern	S/H	$\frac{z_o''}{H}$	U_*profile	K_1	σ_u^2	$A_R + A_B$	$\frac{A_R}{A_R + A_B}$	A_B	I_2	F_1	$B(\times 10^{-3})$
+7H											
P	.17	0.32	1.98	0.164	0.550	1.010	0.273	0.734	0.046	0.886	3.19
U_*	.20	0.275	1.79	0.171	0.447	1.134	0.292	0.803	0.053	0.887	4.02
Q	.24	0.193	1.44	0.174	0.864	1.052	0.216	0.824	0.053	0.883	4.13
R	.28	0.185	1.50	0.146	0.880	1.095	0.250	0.820	0.055	0.880	3.43
S	.32	0.183	1.51	0.135	0.987	0.959	0.276	0.694	0.060	0.881	3.48
T	.34	0.158	1.39	0.139	1.055	1.094	0.248	0.823	0.061	0.876	3.66
V	.38	0.113	1.25	0.122	1.488	1.047	0.276	0.758	0.0605	0.876	3.06
W	.47	0.069	1.07	0.0595	1.127	1.061	0.296	0.747	0.0628	0.871	1.32
X	.51	0.059	1.05	0.0713	1.382	1.055	0.302	0.737	0.0572	0.874	1.43
Y	.59	0.042	0.925	0.0889	2.239	0.998	0.284	0.714	0.0592	0.874	1.98
Z	.61	0.0345	0.864	0.0696	1.763	1.032	0.292	0.731	0.0659	0.871	1.71
+10H											
P	.17	0.15	1.14	0.0985	0.282	1.023	0.302	0.714	0.044	0.894	1.49
U_*	.20	0.218	1.43	0.215	1.042	1.064	0.262	0.782	0.052	0.884	5.33
Q	.24	0.16	1.25	0.185	1.357	1.088	0.192	0.879	0.046	0.878	3.72
R	.28	0.20	1.43	0.131	1.220	0.979	0.189	0.794	0.061	0.876	3.39
S	.32	0.16	1.30	0.166	1.514	1.055	0.213	0.850	0.058	0.873	4.30
T	.34	0.135	1.205	0.136	1.332	1.031	0.275	0.743	0.056	0.880	3.20
V	.38	0.119	1.18	0.141	1.661	1.097	0.220	0.856	0.058	0.875	3.43
W	.47	0.071	0.985	0.0773	1.225	1.065	0.262	0.786	0.056	0.871	1.51
X	.51	0.071	1.03	0.0816	1.575	1.033	0.284	0,742	0.062	0.871	1.91
Y	.59	0.036	0.827	0.0687	1.653	1.036	0.292	0.733	9.059	0.875	1.41
Z	.61	0.0585	0.947	0.1037	1.714	1.044	0.298	0.734	0.056	0.873	2.19

TABLE 6.10(a) Deflection due to resonant turbulence (R); and $\sqrt{\frac{R}{B}}$ by complex calculation.

Pattern	S/H	$\bar{U}_o$	$\bar{U}_H$	I_2	A_R	N_f	$\frac{C_{D_{prof}}^2}{C_{D_\ell}}$	$\lvert J_{y_R} \rvert^2$	$\lvert J_{z_R} \rvert^2$	F_2	$R(\times 10^{-3})$	$\frac{R}{B}$	$\sqrt{\frac{R}{B}}$
+3H													
P	.17	5.70	1.05	0.042	0.435	0.444	0.753	0.681	0.488	0.25	1.89	4.35	2.09
U_*	.20	5.67	1.15	0.052	0.406	0.469	0.764	0.702	0.513	0.28	3.47	3.15	1.77
Q	.24	5.93	2.25	0.063	0.394	0.649	0.844	0.827	0.687	0.48	3.96	4.61	2.15
R	.28	5.76	2.30	0.043	0.323	0.655	0.846	0.830	0.692	0.49	1.79	3.50	1.87
S	.32	6.20	3.31	0.057	0.329	0.737	0.883	0.877	0.768	0.59	4.59	4.88	2.21
T	.34	5.89	2.85	0.054	0.323	0.705	0.869	0.859	0.739	0.55	2.89	4.30	2.07
V	.38	6.03	4.32	0.056	0.251	0.788	0.906	0.906	0.815	0.67	2.42	3.24	1.80
W	.47	5.96	4.76	0.074	0.261	0.805	0.913	0.912	0.829	0.69	3.86	3.42	1.85
X	.51	6.11	4.76	0.068	0.279	0.805	0.913	0.912	0.829	0.69	3.62	3.74	1.93
Y	.59	6.05	6.00	0.070	0.227	0.840	0.929	0.929	0.860	0.74	2.35	2.88	1.70
Z	.61	5.93	5.20	0.059	0.244	0.819	0.919	0.919	0.842	0.71	2.85	3.25	1.80
+5H													
P	.17		1.16	0.056	0.315	0.471	0.765	0.704	0.515	0.277	11.70	1.97	1.40
U_*	.20		1.24	0.050	0.310	0.490	0.773	0.718	0.539	0.299	7.48	2.69	1.64
Q	.24		1.83	0.054	0.290	0.596	0.821	0.794	0.637	0.415	8.48	3.10	1.76
R	.28		1.80	0.056	0.304	0.592	0.819	0.791	0.633	0.410	9.19	3.01	1.73
S	.32		2.52	0.062	0.339	0.677	0.856	0.843	0.713	0.515	7.98	4.63	2.15
T	.34		2.20	0.057	0.305	0.644	0.842	0.824	0.682	0.473	7.92	3.61	1.90
V	.38		2.98	0.054	0.361	0.715	0.873	0.865	0.748	0.565	11.26	5.63	2.37
W	.47		4.40	0.067	0.280	0.791	0.907	0.905	0.817	0.671	3.19	3.73	1.93
X	.51		4.22	0.061	0.301	0.784	0.904	0.902	0.811	0.661	3.59	4.11	2.03
Y	.59		4.95	0.061	0.273	0.811	0.916	0.915	0.835	0.699	4.64	3.55	1.88
Z	.61		4.31	0.062	0.287	0.788	0.906	0.908	0.822	0.676	4.39	3.89	1.97

TABLE6.10(b):Deflection due to resonant turbulence (R); and $\sqrt{\frac{R}{B}}$ by complex calculation. (Continued)

Pattern	S/H	$\bar{U}_o$	$\bar{U}_H$	I_2	A_R	N_f	$\frac{C_{D_{prof}}^2}{C_{D_\ell}}$	$\lvert J_{y_R} \rvert^2$	$\lvert J_{z_R} \rvert^2$	F_2	$R(\times 10^{-3})$	$\frac{R}{B}$	$\sqrt{\frac{R}{B}}$
+7H													
P	.17		1.57	0.046	0.276	0.555	0.802	0.766	0.598	0.368	8.84	2.77	1.66
U_*	.20		1.45	0.053	0.331	0.553	0.793	0.751	0.577	0.343	11.56	2.87	1.69
Q	.24		2.02	0.053	0.227	0.622	0.832	0.810	0.662	0.446	8.50	2.06	1.44
R	.28		2.22	0.055	0.273	0.646	0.843	0.825	0.684	0.476	9.66	2.81	1.68
S	.32		2.25	0.060	0.265	0.649	0.844	0.827	0.687	0.479	11.57	3.33	1.82
T	.34		2.50	0.061	0.271	0.675	0.855	0.842	0.711	0.512	10.60	2.90	1.70
V	.38		3.04	0.061	0.289	0.719	0.875	0.867	0.752	0.571	11.97	3.91	1.98
W	.47		3.76	0.063	0.314	0.762	0.894	0.891	0.791	0.630	5.83	4.43	2.10
X	.51		3.78	0.058	0.319	0.763	0.895	0.894	0.799	0.639	7.00	4.92	2.22
Y	.59		4.24	0.059	0.283	0.785	0.904	0.902	0.812	0.662	9.14	4.62	2.15
Z	.61		4.31	0.066	0.301	0.788	0.906	0.903	0.814	0.666	7.84	4.59	2.14
+10H													
P	.17		1.43	0.044	0.309	0.529	0.791	0.748	0.573	0.339	4.40	2.95	1.72
U_*	.20		1.95	0.052	0.279	0.613	0.828	0.805	0.653	0.435	16.22	3.04	1.74
Q	.24		2.54	0.046	0.209	0.678	0.857	0.844	0.714	0.517	7.43	2.00	1.44
R	.28		2.72	0.061	0.185	0.694	0.864	0.856	0.729	0.538	6.28	1.85	1.36
S	.32		2.75	0.058	0.225	0.697	0.865	0.855	0.732	0.542	10.32	2.40	1.55
T	.34		2.70	0.056	0.283	0.693	0.863	0.853	0.728	0.536	12.09	3.78	1.94
V	.38		3.18	0.058	0.241	0.729	0.879	0.873	0.761	0.584	9.21	2.69	1.64
W	.47		3.53	0.056	0.279	0.750	0.889	0.884	0.783	0.615	5.56	3.67	1.92
X	.51		3.78	0.062	0.294	0.763	0.895	0.891	0.792	0.632	8.20	4.30	2.07
Y	.59		4.20	0.059	0.303	0.783	0.904	0.901	0.810	0.659	6.61	4.69	2.17
Z	.61		3.48	0.056	0.311	0.747	0.888	0.883	0.778	0.610	10.75	4.90	2.21

TABLE6.11(a): Mean deflection ($D.M_T$); and $\frac{A}{D}$ by complex calculation.

Pattern	S/H	$\bar{U}_o$	$\bar{U}_H$	$\bar{U}_*$profile	$(U_*\phi_m)^2$	C_{D_ℓ}	U_z	$\frac{z_o''}{H}$	$D.M_T$	I_1	$\sqrt{B+R}$	$\frac{A}{D}=\frac{\sqrt{B+R}}{I_1}$
+3H												
P	.17	5.70	1.05	2.86	0.188	0.93	0.66	0.30	8.26	0.019	0.049	2.61
U	.20	5.67	1.15	2.29	0.290	1.12	0.83	0.32	15.40	0.240	0.068	2.82
Q	.24	5.93	2.25	1.99	0.210	1.42	1.85	0.13	13.8	0.035	0.069	1.99
R	.28	5.76	2.30	1.67	0.321	1.71	1.93	0.32	6.69	0.017	0.048	2.82
S	.32	6.20	3.31	1.22	0.145	1.41	2.89	0.07	24.70	0.029	0.070	2.57
T	.34	5.89	2.85	1.93	0.255	1.31	2.29	0.07	16.60	0.028	0.060	2.13
V	.38	6.03	4.32	1.03	0.260	1.33	3.90	0.10	37.30	0.027	0.056	2.08
W	.47	5.96	4.76	0.90	0.218	1.10	4.44	0.06	71.40	0.048	0.071	1.46
X	.51	6.11	4.76	0.96	0.154	1.16	4.16	0.08	63.60	0.041	0.068	1.66
Y	.59	6.05	6.00	0.51	0.241	0.78	5.93	0.06	69.30	0.041	0.056	1.36
Z	.61	5.93	5.20	0.68	0.482	1.05	4.34	0.04	49.10	0.029	0.061	2.10
+5H												
P	.17		1.16	2.47	0.122	0.95	0.84	0.23	1.73	0.026	0.133	4.66
U	.20		1.24	2.36	0.180	1.10	0.86	0.30	1.70	0.023	0.101	4.39
Q	.24		1.83	1.71	0.265	1.48	1.29	0.24	6.45	0.027	0.106	3.88
R	.28		1.80	1.72	0.310	1.68	1.29	0.26	5.93	0.025	0.111	4.43
S	.32		2.52	1.59	0.279	1.53	2.02	0.16	14.90	0.032	0.089	3.05
T	.34		2.20	1.59	0.316	1.48	1.67	0.20	16.20	0.027	0.101	3.73
V	.38		2.98	1.31	0.622	1.42	2.18	0.18	16.40	0.025	0.115	4.57
W	.47		4.40	1.11	0.462	1.19	3.89	0.05	44.40	0.038	0.064	1.70
X	.51		4.22	1.07	0.382	1.24	3.50	0.11	42.00	0.032	0.067	2.08
Y	.59		4.95	0.84	0.348	0.95	4.16	0.08	44.00	0.032	0.077	2.41
Z	.61		4.31	0.79	0.337	1.09	3.79	0.09	40.40	0.034	0.074	2.22

TABLE 6.11(b): Mean deflection ($D.M_T$); and $\frac{A}{D}$ by complex calculation (Continued)

Pattern	S/H	$\bar{U}_o$	$\bar{U}_H$	$\bar{U}_*$profile	$(U_*\phi_m)^2$	C_{D_ℓ}	U_z	$\frac{z_o''}{H}$	$D.M_T$	I_1	$\sqrt{B+R}$	$\frac{A}{D} = \frac{\sqrt{B+R}}{I_1}$
+7H P	.17		1.57	1.98	0.246	1.00	1.07	0.26	2.31	0.022	0.110	5.12
U_*	.20		1.45	1.71	0.150	1.13	1.12	0.28	2.59	0.025	0.125	4.99
Q	.24		2.02	1.44	0.078	1.48	1.99	0.21	7.85	0.027	0.112	4.12
R	.28		2.22	1.50	0.255	1.60	1.67	0.17	8.91	0.026	0.114	4.40
S	.32		2.25	1.51	0.260	1.53	1.78	0.15	11.30	0.031	0.123	4.01
T	.34		2.50	1.39	0.227	1.37	2.03	0.11	15.10	0.032	0.119	3.73
V	.38		3.04	1.25	0.305	1.40	2.44	0.11	22.60	0.032	0.123	3.88
W	.47		3.76	1.07	0.185	1.20	3.27	0.05	37.10	0.037	0.085	2.30
X	.51		3.78	1.05	0.382	1.31	3.16	0.07	31.00	0.030	0.092	3.07
Y	.59		4.24	0.93	0.326	1.25	3.55	0.07	39.60	0.032	0.106	3.31
Z	.61		4.31	0.86	0.236	1.00	3.73	0.02	40.40	0.037	0.098	2.66
+10H P	.17		1.43	1.14	0.348	1.42	0.88	0.37	1.86	0.018	0.077	4.26
U_*	.20		1.95	1.42	0.270	1.24	1.40	0.23	5.17	0.023	0.147	6.38
Q	.24		2.54	1.25	0.275	1.44	1.97	0.13	9.70	0.022	0.106	4.80
R	.28		2.72	1.43	0.193	1.53	2.23	0.11	17.30	0.032	0.098	3.08
S	.32		2.75	1.30	0.193	1.33	2.26	0.07	12.80	0.029	0.121	4.14
T	.34		2.70	1.21	0.437	1.55	1.97	0.17	15.70	0.027	0.124	4.57
V	.38		3.18	1.18	0.246	1.37	2.53	0.09	23.30	0.030	0.112	3.70
W	.47		3.53	0.99	0.165	1.24	3.10	0.06	25.20	0.028	0.084	3.06
X	.51		3.78	1.03	0.181	1.40	3.21	0.03	41.20	0.035	0.101	2.40
Y	.59		4.20	0.83	0.201	1.01	3.46	0.09	30.50	0.031	0.090	2.89
Z	.61		3.48	0.95	0.388	1.19	2.76	0.07	22.80	0.027	0.114	4.74

TABLE 6.12(a): Deflection due to total turbulence ($A.M_t$); and total movement ($(A + D)M_T$).

Pattern	S/H	$\frac{z_o''}{H}$	U_H	σ_u^2	C_{z_o}	$\frac{A_R}{A_R + A_B}$	A_R	K_2	I_2	$A.M_T$	$(A + D)M_T$
	$\hat{n} = 5.6$; $I_3 = 0.138$; $H = 0.202$ m; $n_o = 8.9$ Hz; (AM_T & $(A+D)M$ x 10^{-8}) m; $\frac{z}{H} = 0.9$.										
+3H											
P	.17	0.33	1.05	0.077	0.011	0.434	0.435	0.298	0.042	2.15	2.98
U_*	.20	0.28	1.15	0.120	0.011	0.365	0.406	0.362	0.052	4.36	5.90
Q	.24	0.21	2.25	0.294	0.014	0.358	0.394	0.225	0.063	27.60	41.40
R	.28	0.16	2.30	0.296	0.011	0.293	0.323	0.177	0.043	18.90	25.60
S	.32	0.09	3.31	0.799	0.014	0.320	0.329	0.236	0.057	63.60	88.30
T	.34	0.02	2.85	0.478	0.014	0.314	0.328	0.186	0.054	35.30	51.90
V	.38	0.05	4.32	1.035	0.014	0.244	0.251	0.137	0.056	77.60	115.00
W	.47	0.03	4.76	1.230	0.015	0.255	0.261	0.139	0.075	104.00	175.50
X	.51	0.04	4.76	1.207	0.015	0.266	0.279	0.146	0.068	106.00	169.50
Y	.59	0.002	6.00	1.528	0.015	0.221	0.227	0.094	0.071	94.30	163.60
Z	.61	0.01	5.20	1.587	0.015	0.235	0.244	0.141	0.059	103.00	152.40
+5H											
P	.17	0.36	1.16	0.337	0.012	0.268	0.315	0.774	0.056	8.08	9.81
U_*	.20	0.34	1.24	0.298	0.011	0.305	0.310	0.590	0.050	7.45	9.15
Q	.24	0.21	1.83	0.573	0.012	0.585	0.290	0.487	0.054	25.00	31.48
R	.28	0.21	1.80	0.553	0.011	0.282	0.304	0.509	0.056	26.30	32.21
S	.32	0.16	2.52	0.692	0.012	0.330	0.339	0.362	0.062	45.40	60.30
T	.34	0.17	2.20	0.662	0.012	0.294	0.305	0.409	0.057	69.10	85.32
V	.38	0.10	2.98	1.203	0.013	0.331	0.361	0.481	0.054	74.90	91.26
W	.47	0.05	4.40	0.977	0.013	0.271	0.280	0.139	0.067	75.40	119.80
X	.51	0.06	4.22	1.017	0.015	0.283	0.301	0.169	0.061	87.50	129.40
Y	.59	0.02	4.95	1.795	0.015	0.247	0.273	0.196	0.061	106.00	150.40
Z	.61	0.03	4.31	1.262	0.015	0.267	0.287	0.192	0.066	89.60	130.00

TABLE 6.12(b): Deflection due to total turbulence ($A.M_T$); and total movement ($(A + D)M_T$) (Continued).

Pattern	S/H	$\frac{z_o''}{H}$	U_H	$\sigma_u{}^z$	C_{z_o}	$\frac{A_R}{A_R + A_B}$	A_R	K_2	I_2	$A.M_T$	$(A + D)M_T$
+7H											
P	.17	0.32	1.57	0.550	0.011	0.273	0.276	0.604	0.046	11.80	14.10
U_*	.20	0.27	1.45	0.447	0.011	0.292	0.331	0.691	0.053	12.90	15.50
Q	.24	0.19	2.02	0.864	0.012	0.216	0.227	0.472	0.053	32.30	40.20
R	.28	0.18	2.22	0.880	0.011	0.250	0.273	0.479	0.055	39.20	48.10
S	.32	0.18	2.25	0.987	0.012	0.276	0.265	0.507	0.060	45.10	56.40
T	.34	0.16	2.50	1.055	0.014	0.248	0.272	0.450	0.061	56.50	71.60
V	.38	0.11	3.04	1.488	0.014	0.276	0.289	0.457	0.061	87.70	110.40
W	.47	0.07	3.76	1.927	0.015	0.296	0.314	0.246	0.063	85.40	122.40
X	.51	0.06	3.78	1.382	0.014	0.302	0.319	0.303	0.058	95.10	126.10
Y	.59	0.04	4.24	2.239	0.014	0.284	0.283	0.283	0.059	131.00	170.90
Z	.61	0.03	4.31	1.763	0.015	0.292	0.301	0.281	0.066	107.00	147.90
+10H											
P	.17	0.15	1.43	0.282	0.009	0.302	0.309	0.418	0.044	7.95	9.81
U_*	.20	0.22	1.95	1.042	0.012	0.262	0.279	0.750	0.052	33.00	38.20
Q	.24	0.16	2.54	1.356	0.012	0.192	0.209	0.431	0.046	46.60	56.30
R	.28	0.20	2.72	1.220	0.012	0.189	0.185	0.300	0.061	53.10	70.30
S	.32	0.16	2.75	1.514	0.011	0.213	0.225	0.442	0.058	53.00	65.80
T	.34	0.14	2.70	1.332	0.013	0.275	0.283	0.508	0.056	71.90	87.70
V	.38	0.12	3.18	1.661	0.014	0.220	0.261	0.389	0.058	86.20	109.50
W	.47	0.07	3.53	1.225	0.015	0.262	0.278	0.269	0.056	77.00	102.20
X	.51	0.07	3.78	1.575	0.015	0.286	0.294	0.318	0.062	119.00	160.60
Y	.59	0.04	4.20	1.653	0.014	0.292	0.303	0.378	0.059	88.10	118.60
Z	.61	0.06	3.48	1.714	0.015	0.298	0.311	0.432	0.056	97.00	119.80

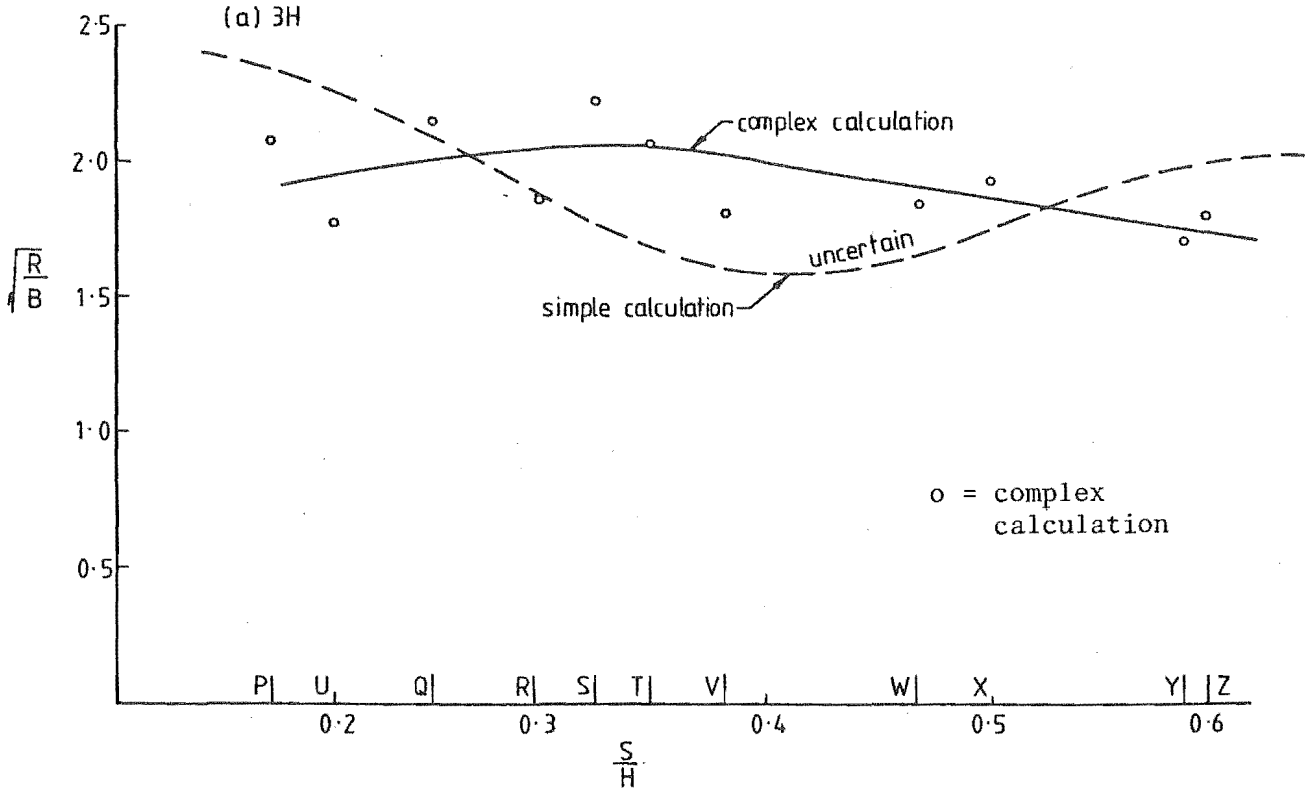

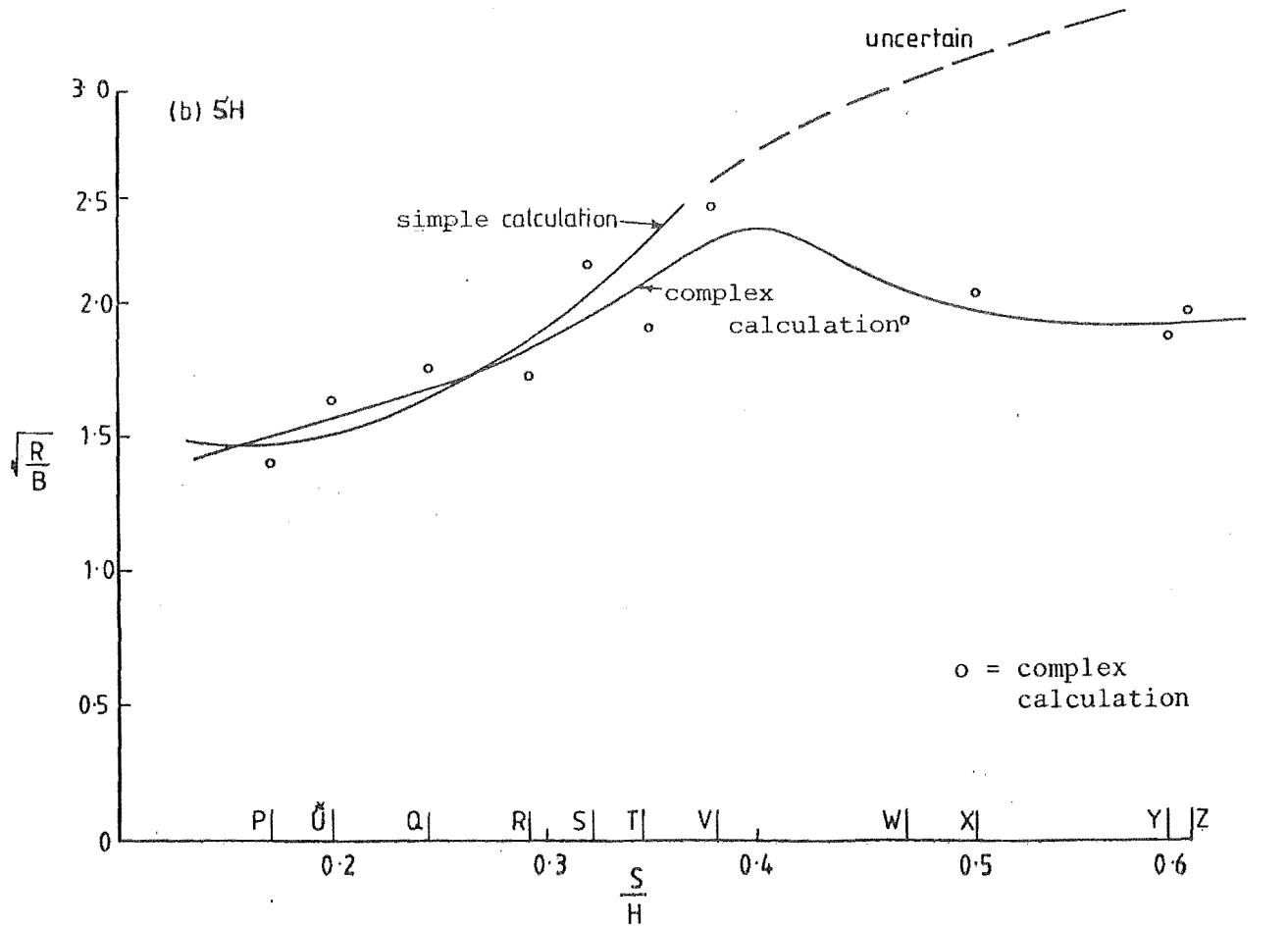

FIGURES 6.35(a) & (b): Simple and complex calculations compared, Oxford.

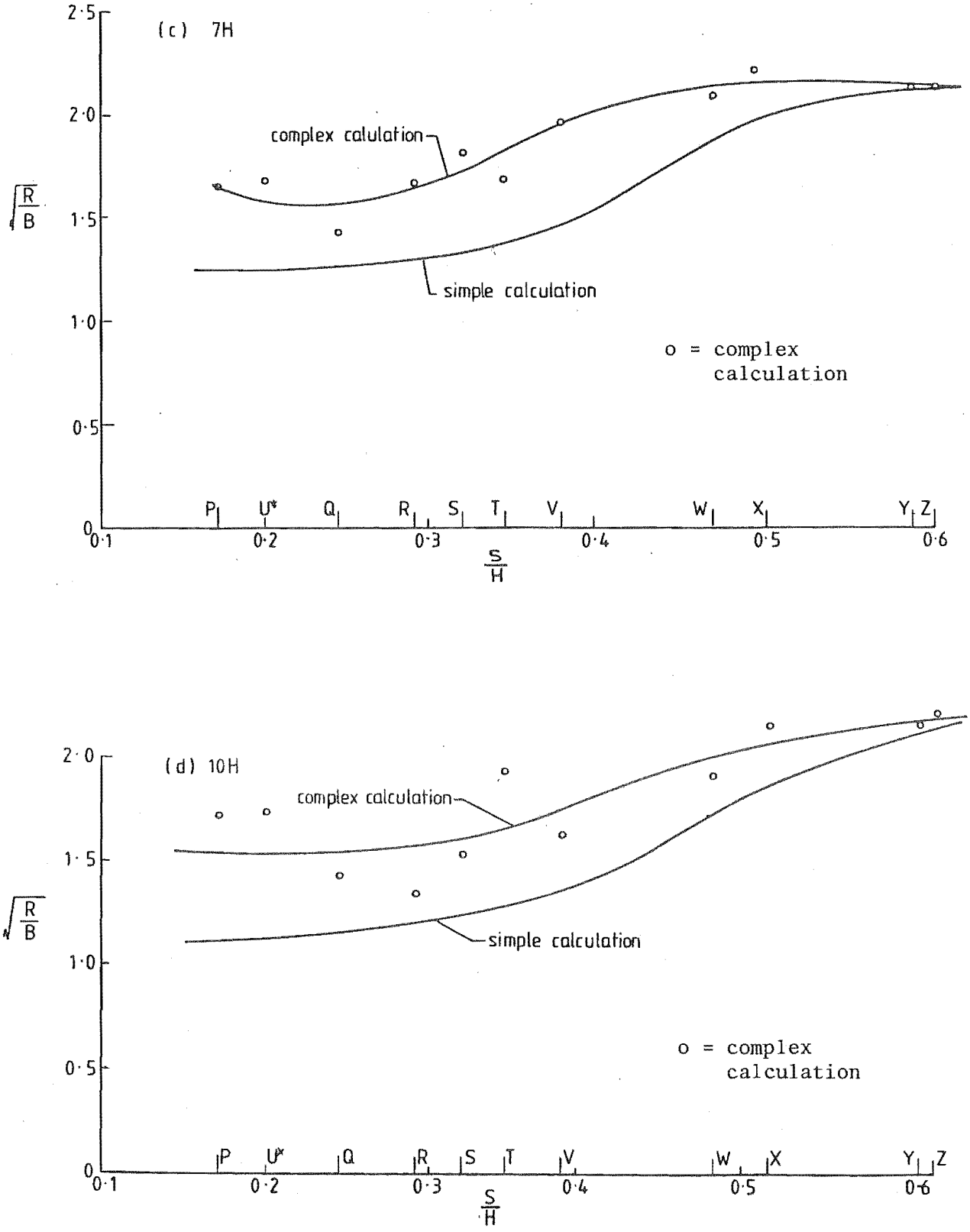

FIGURES 6.35(c) & (d): Simple and complex calculations compared, Oxford.

The simple second order solution for $\sqrt{\frac{R}{B}}$ (Figs 6.35(a)-(c)) provides a quick and simple method of estimating dynamic tree response away from the forest leading edge. This solution is used to estimate the shape of the spectra for waving crops in the inertial region where wind loading on the trees occurs. This spectra shape is based on Högström et al's spectra curve for high roughness (3.8.1).

6.10 CANTERBURY AND OXFORD MODEL FOREST ALONG-WIND TREE-TOP RESPONSE

6.10.1 Tree-top response by calculation and by photography compared

These two separate estimates of $\frac{A}{D}$ along-wind produced similarly-shaped curves (Fig. 6.39(a)-(c)). $\frac{A}{D}$ estimates by photographic analysis of the Oxford cine films have been added to the data.

Since the dynamic response is proportional to the mean velocity[1], $\bar{U}_o$, and the static response is proportional to $\bar{U}_o^2$, then $\frac{A}{D}$ is proportional to $\frac{1}{\bar{U}_o}$.

The average value of $\bar{U}_o$ for 4 patterns traversed at Canterbury was 13.66 m/s (Table 6.7), while for the 11 patterns tested at Oxford it was 5.93 m/s (Table 6.10).

So, on average, where turbulence intensities are not too high[1], $\frac{A}{D}$ r.m.s. estimates for the Oxford tests should be up to $\frac{13.66}{5.93}$, or 2.30 times greater than the $\frac{A}{D}$ r.m.s. estimates for Canterbury. The Canterbury $\frac{A}{D}$ ratios were found by averaging the amplitudes of the largest swings to obtain A in any row. These A_{max} amplitudes are assumed smaller than $A_{r.m.s.}$ amplitudes down to the limiting value of 0.707. So, the conversion ratio for the data where turbulence intensities are not too high is up to 2.3 x .707 or 1.63.

From averages of $\frac{A}{D}$ (Fig. 6.39(a)-(c)),

(a) 0 - 3 H

$\frac{A}{D}$ (Canterbury)	=	1.46
$\frac{A}{D}$ (Oxford)	=	2.12
1.46 x 1.63	=	2.38

---

1. In regions of high turbulence the complex solution (3.10) adds a further component which suggests that dynamic response is proportional to $\bar{U}_o$ + constant.

To p.282

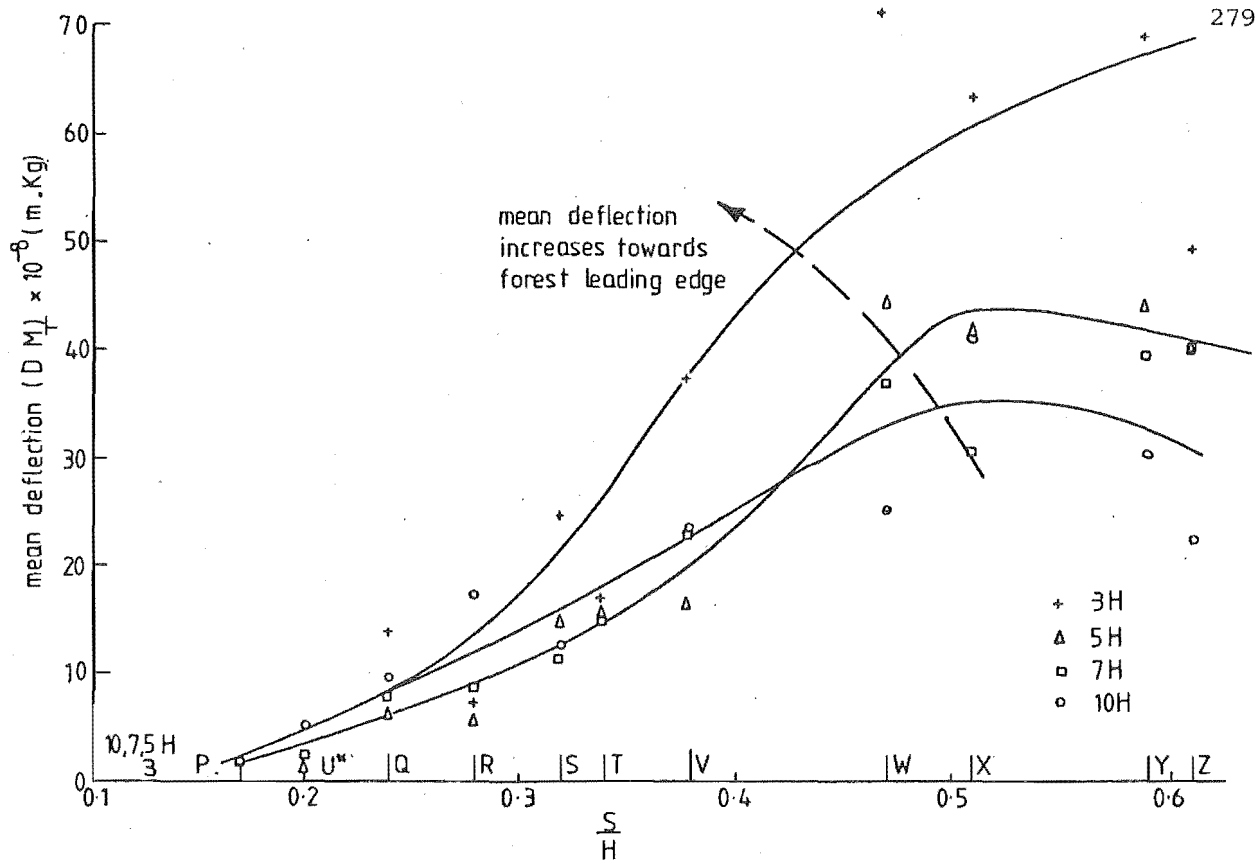

FIGURE 6.36: Mean deflection ($D.M_T$) by complex calculation.

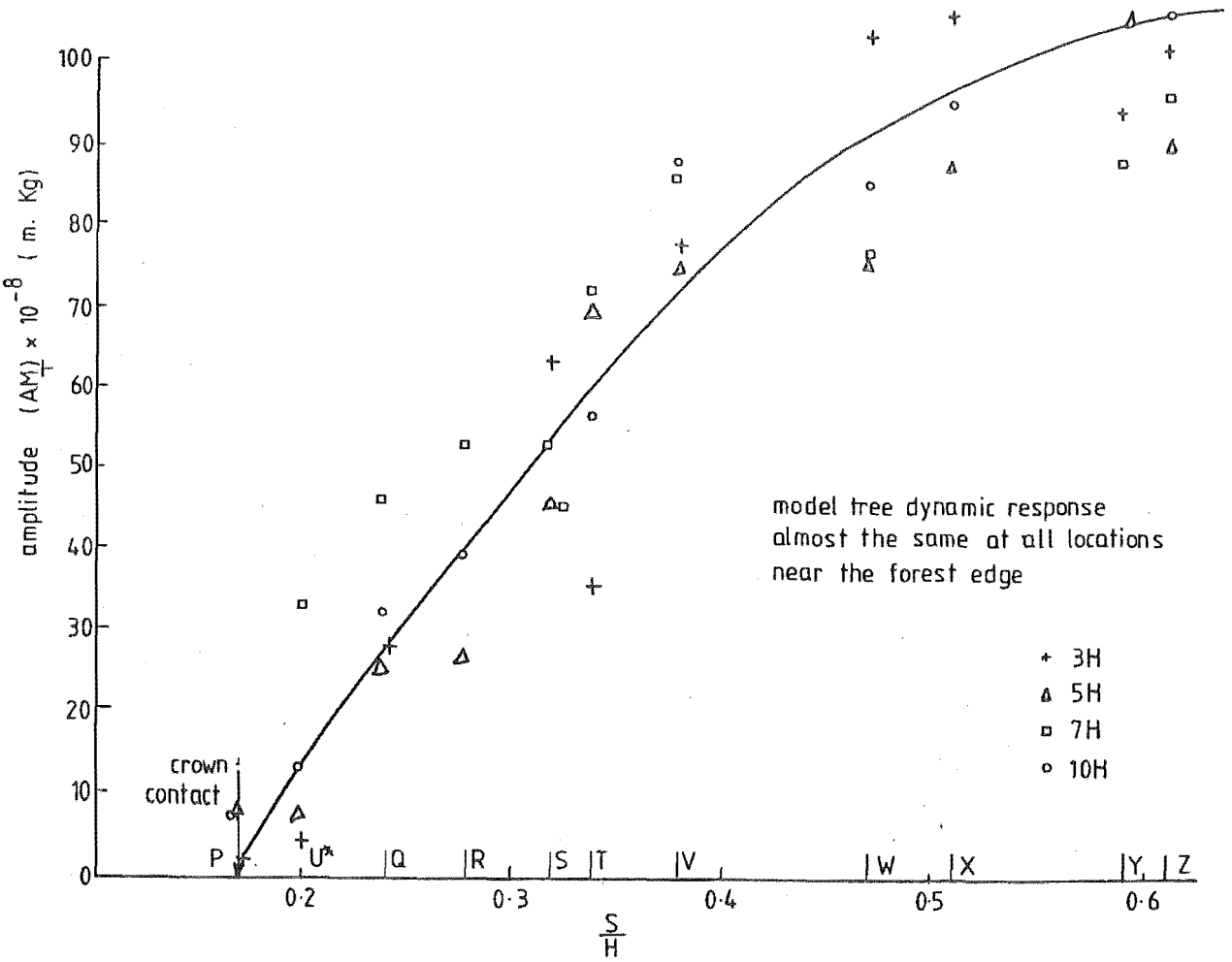

FIGURE 6.37: Amplitude ($A.M_T$) by complex calculation.

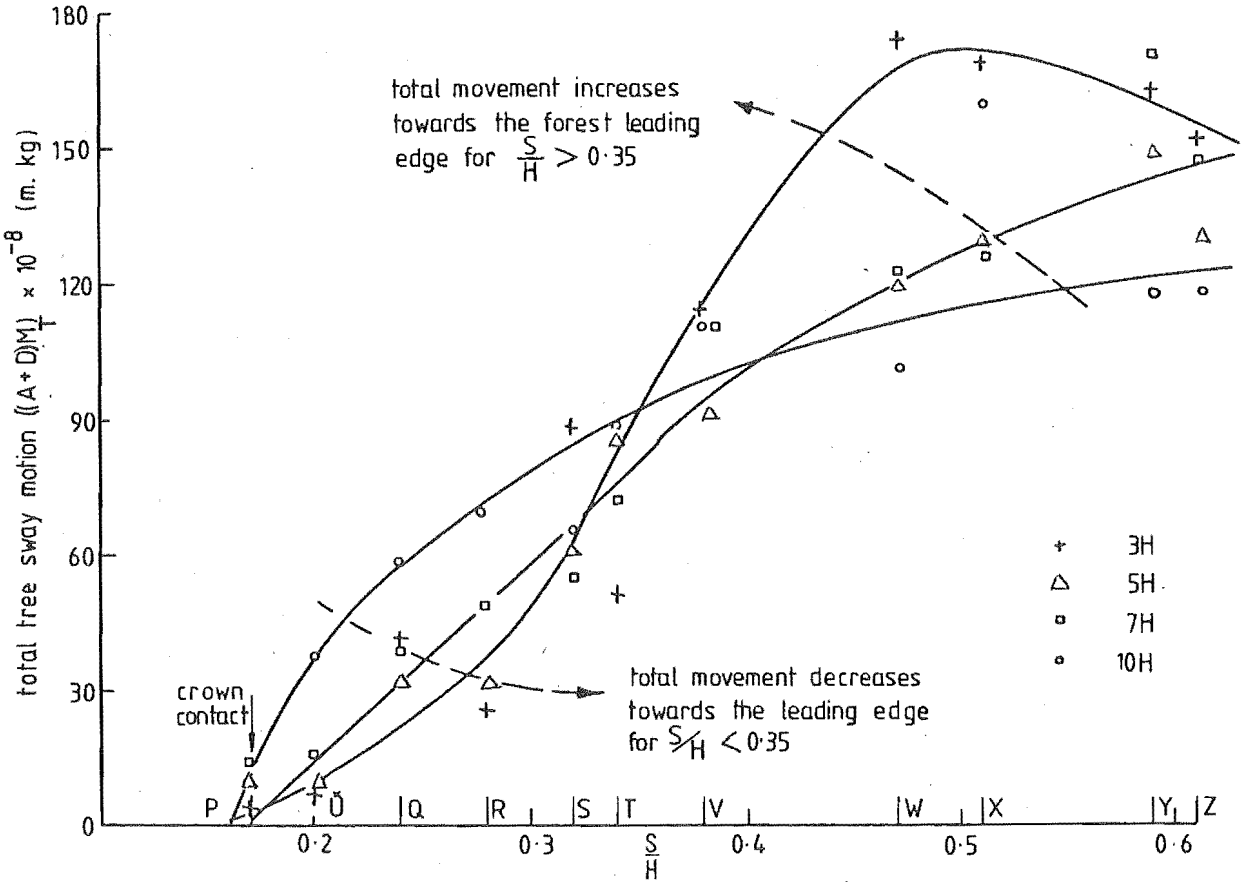

FIGURE 6.38: Total tree top swaying motion ((A+D), M_T) by complex calculation.

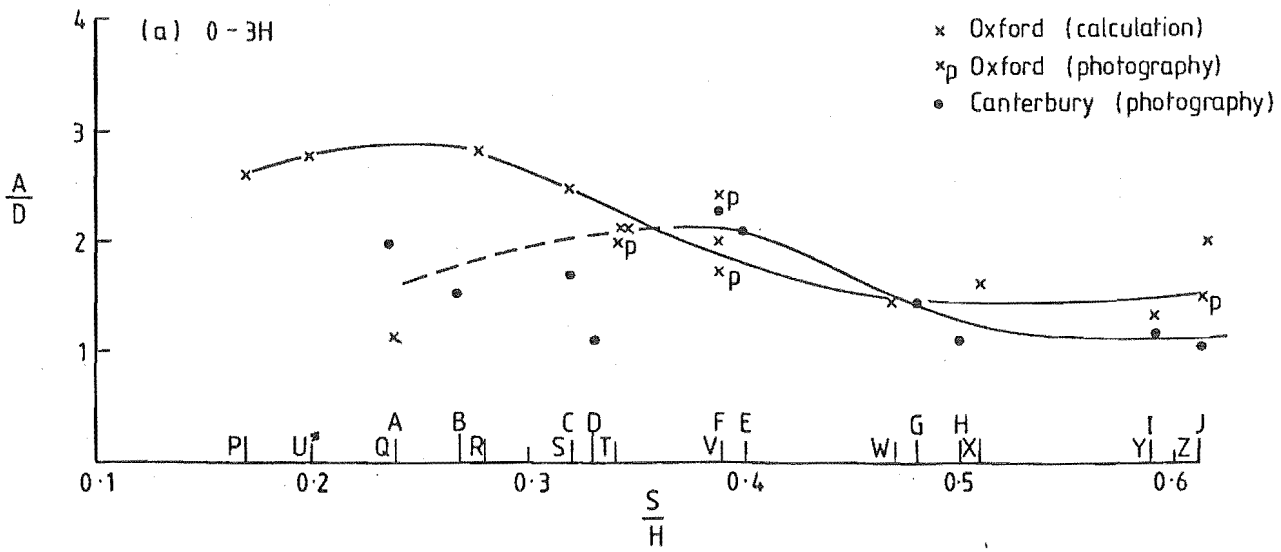

FIGURE 6.39(a): $\frac{A}{D}$ by complex calculation and photography compared.

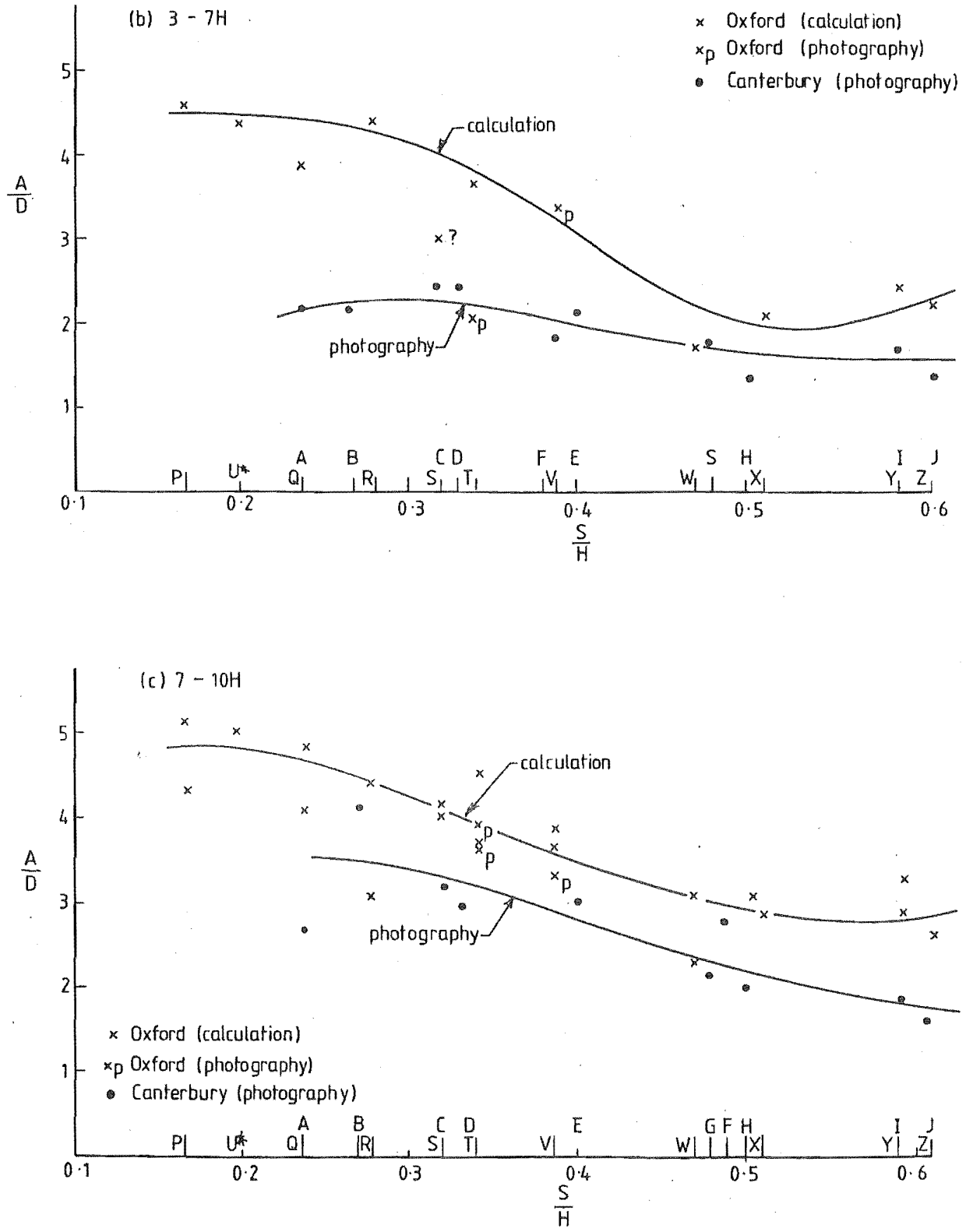

FIGURE 6.39(b) & (c): $\frac{A}{D}$ by complex calculation and photography compared.

(b) 3 - 5 H

$\frac{A}{D}$ (Canterbury) = 1.97

$\frac{A}{D}$ (Oxford) = 3.28

1.97 x 1.63 = 3.21,

(c) 5 - 7 H

$\frac{A}{D}$ (Canterbury) = 2.64

$\frac{A}{D}$ (Oxford) = 3.76

2.64 x 1.63 = 4.29.

Since these estimates are close, and the shapes of the curves are similar, the two experiments are compatible.

6.10.2 Absolute values of amplitudes and mean deflections compared

Pattern B was the closest spacing for which wind structure was measured in the Canterbury tests ($\frac{S}{H}$ = 0.28). Pattern R was its equivalent in the Oxford tests. (These pattern letters are not related to resonant or background effects.)

At 10 H,

$\bar{U}_{O_{Canterbury_{(B)}}}$ = 17.8 m/s

$\bar{U}_{O_{Oxford_{(R)}}}$ = 5.76 m/s

M_T = $\frac{0.00663}{9.8}$ kg.[1]

So for,

(a) Oxford (Fig. 6.37),

$AM_{T(R)} = 40.\ 10^{-8}$ kg.m.

$A_{(R)} = \frac{9.81\ 40.\ 10^{-8}}{.00663}$

= 5.92 mm

---

1. Data on the mean model tree mass of 100 samples was only received on 19. 1.84

$$\frac{A}{H}(R) = 0.029 \ ;$$

similarly, $$\frac{D}{H}(R) = 0.011 \ ;$$

(b) Canterbury (Fig. 6.3(b); Fig. 6.5(c)),

$$\frac{A}{H}(B) = 0.09$$

$$\frac{D}{H}(B) = 0.03 \ .$$

Now, amplitudes appear to be proportional to $\bar{U}_o$, and mean deflections proportional to $\bar{U}_o^2$, so,

(a) $$\frac{A}{H}(R) = 0.029 \times \frac{17.8}{5.76} = 0.09$$

$$\equiv \frac{A}{H}(B) \ ;$$

(b) $$\frac{D}{H}(R) = 0.011 \times \left(\frac{17.8}{5.76}\right)^2 = .11$$

$$\neq \frac{D}{H}(B) \ .$$

Dynamic response, therefore, appears to be proportional to upstream reference mean wind speeds. These results are complemented by data in one component acceleration spectrum (Fig. 5.29) which are used to compute a full scale estimate of dynamic r.m.s. amplitude (r.m.s. length scale). Maitani (Fig. 7.7) uses a similar approach when studying wheat-top response.

Mean deflections are normally proportional to the mean profile drag which is proportional to $\bar{U}_o^2$. In these tests the wind speed at mean tree-top height for Pattern R is much lower than $\bar{U}_o$; $\bar{U}_H$ is 2.72 m/s at 10 H (Fig. 6.11(b)). For Pattern B, $\bar{U}_H$ is 0.42 $\bar{U}_o$;

so, $$\frac{D}{H}(R) = 0.011 \times \left(\frac{17.8 \times 0.42}{2.72}\right)^2$$

$$= 0.08$$

$$\neq \frac{D}{H}(B) \ .$$

But, if $$\frac{D}{H}(R) = 0.011 \times \left(\frac{17.8 \times 0.42}{2.72}\right)$$

$$= 0.03 \ ,$$

$$\equiv \frac{D}{H}(B) \ .$$

To p.285

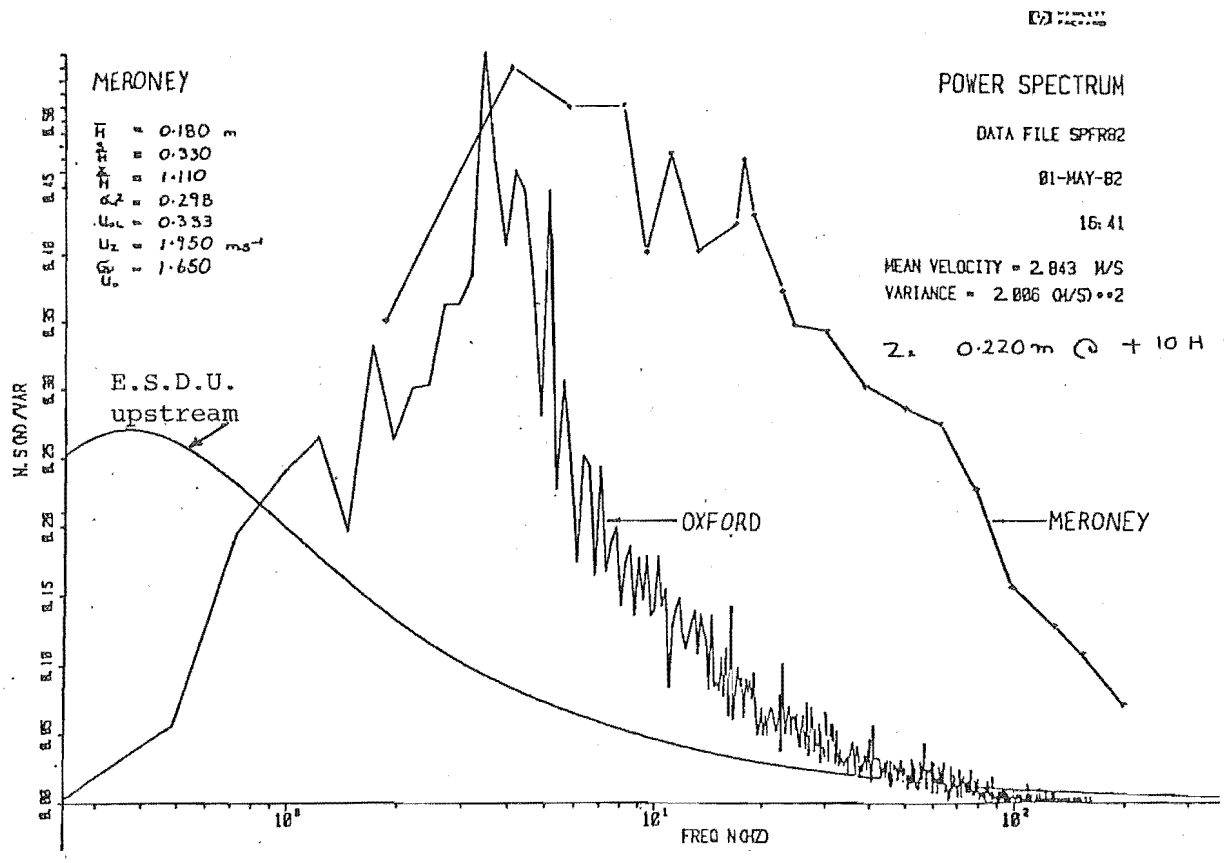

POWER SPECTRUM
****

SPECTRUM PARAMETERS

SPECTRUM PLOTTING FILE SPFR82
RAW DATA FILE RWFR82

NO. OF HANN SMOOTHING = 0
NO. OF POINTS IN F.F.T. = 2048
NO. OF SPECTRA AVERAGED = 28
LOWEST FREQUENCY = 0.244 HZ
HIGHEST FREQUENCY = 250.000 HZ
LOW PASS FILTER SETTING = 200.000 (HZ)
HIGH PASS FILTER SETTING = 0.488 (HZ)
SAMPLING TIME FOR VARIANCE = 93.950 SECS

MEAN VELOCITY = 2.843 M/S

VARIANCE = 2.006 (M/S)**2

VELOCITY SPECTRUM

DATE: 01-MAY-82 TIME: 16:41

COMMENT: TREE PATTERN S SQUARE

PROBE AMPLIFIER

CALIBRATION FACTOR = 10.441 (M/S PER V)
PROBE POSITION, X = 10.000 Y = 0.000 Z = 0.220

FIGURE 6.40: Spectra of pattern S +10H, and by Meroney +20H, compared.

So, mean static deflections do not seem to be proportional to $\bar{U}_o^2$ of $\bar{U}_H^2$, but proportional to $\bar{U}_o$ or $\bar{U}_H$. This needs further investigation.

6.11 DISCUSSION

The results from both the model forest experiments and the two full scale experiments fulfil the objectives of the thesis (1.4.1) and are summarised in Chapter 7.

Published spectra (Meroney 1968) from model forest tests by Kawatani and Meroney do not compare with spectra from the Oxford model forest tests (Fig. 6.40). Therefore, if their wind frequencies are reduced by a factor of 10, their spectra then look similar to the Oxford spectra and both are also similar to other full scale spectra (Fig. 7.5).

Walshe and Fraser (1963) produced diagrams of bending moment contours (Fig. 6.41) over a model forest in an aeronautical wind tunnel. The localised regions of high bending moment that occur just behind the front are probably greater because of turbulence created by increased shear at the model forest leading edge. These localised high bending moment regions would have been greater if the same model were subject to winds simulated in a natural boundary layer wind tunnel.

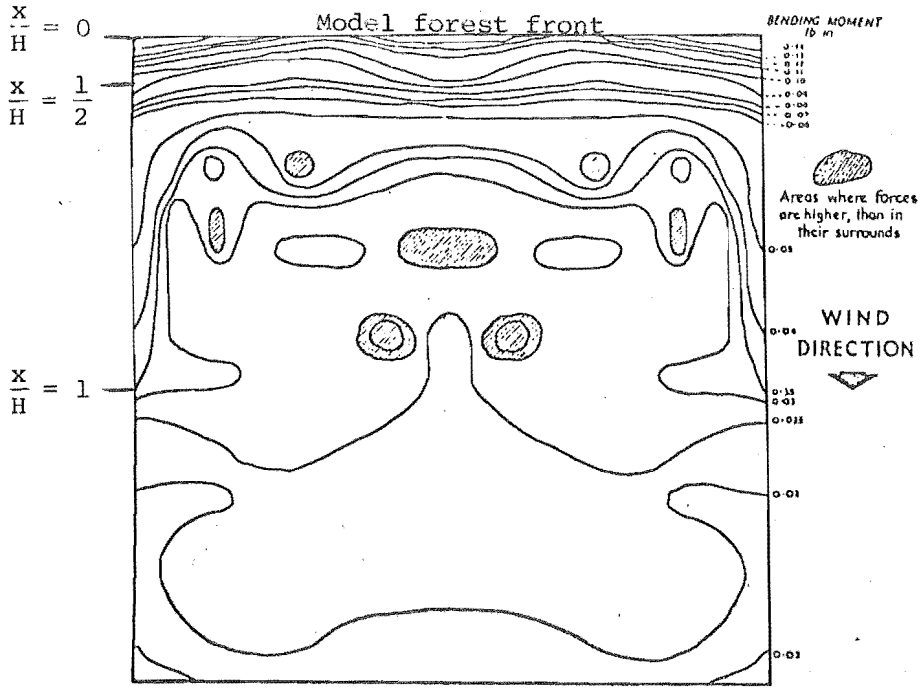

FIGURE 6.41: Contours of bending moment over a regular model forest (after Walshe & Fraser).

Walshe and Fraser ignored model tree flexure. Finnigan, however, considers that crop flexibility cannot be ignored in any formal analysis of crop response to wind forces. He considers that the drag of waving plants is dependent on the mean and fluctuating wind speed components. Also, the phenomenon of Honami waves (Inoue 1955) complicates the momentum transfer process. His power spectra measured at crop height are dominated by two peaks (Fig. 3.19) which show a consistent variation with height. In Run 2 of his full scale experiments the first peak in the power spectral density occurs at 0.35 Hz. This is related to the frequency disturbances associated with the wind and crop natural frequency, rather than to the normal wind spectrum peak at about 0.05 - 0.1 Hz. The second peak could be a frequency shift: once the canopy is set in motion by the wind gusts, the waving plants create wake turbulence which interacts with the wind.

These findings of Finnigan's suggest that the frequency shift can result from groups of trees swaying in unison (Honami), and that turbulence at these frequencies propagates over the forest with the bulk air flow. (The wind damage shown in Photographs 7 and 8, Appendix III, may be due to Honami waves.)

The maximum frequency shift is likely to occur near the leading edge of the forest where the shear turbulence intensity and dynamic tree response are greatest in the model experiments. This frequency shift will be more pronounced for wider spacings, beyond $\frac{S}{H}$ 0.35, where tree response is greatest near the forest front (Fig. 6.38). The effect should also become apparent in full scale measurements of wind and tree response at Rivox as the test sector (5.6.2) is thinned.

Finnigan obtained high vertical velocity components in the wind throughout the inner layer up to the transition region above his wheat crop. Measured values of w' were above normal in the Rivox and Oxford experiments (Table 5.10(a)-(c); Table 6.6), but unfortunately, in the model tests, these wind components were not measured accurately for any spacings except Pattern W ($\frac{S}{H}$ of 0.47).

Sadeh and Fox (1982), studying canopy turbulence, mentioned downbursts but not Honami effects. Honami effects in forest have recently been noted by Cremer et al (1982).

6.12 CHAPTER SUMMARY

The structure of the wind flow in and above forests can be studied in boundary layer wind tunnels because:-

(a) the wind structure over full scale forests can be successfully modelled in meteorological wind tunnels with neutrally stable atmospheres;

(b) atmospheric simulations can produce 2-dimensional flow patterns and 3 dimensional edge effects;

(c) problems such as instrument calibration, serviceability, and failure are eliminated;

(d) data collection is simple. There are no delays in data collection from lack of strong winds in the correct sector.

The wind structure:-

(a) is completely modified by the presence of

(i) the forest leading edge,

(ii) the gaps between tree crowns,

(iii) the tree swaying motion,

(iv) Honami waves ;

(b) produces non-linear plant responses similar to linear responses (Finnigan and Mulhearn);

(c) causes damage zones in full scale forests (Sommerville) which can be studied successfully in boundary layer wind tunnels large enough for the right model tree stiffness;

(d) over more complex terrain with mature forest stands can be analysed to pinpoint areas of high local turbulence intensity and spectral distortions, where there is an increased risk of wind damage.

The response of model trees within a model forest stand can be studied in boundary layer wind tunnels because:-

(a) model trees can be made to respond dynamically to the turbulent wind distributions;

(b) the response of model trees can be estimated by calculation or by photography;

(c) the tree response equations are third order or greater, and along-wind aero-elastic instabilities can develop.

(d) model tree response appears to relate to full scale tree response (7.2.5).

CHAPTER 7

COMPARISONS OF RESULTS, FINDINGS, AND CONCLUSIONS

7.1 INTRODUCTION

In engineering structures for which wind loading is significant, the estimation of the amplitudes in the lowest modes alone is adequate for many design purposes. Trees within a forest are no exception to this principle, when made to oscillate in response to gust loading in the natural wind. A forest exposed to the wind will experience a steady wind load caused by the mean winds, and a fluctuating wind load caused by the associated turbulence. The fluctuating loads range from low frequency gusts which envelop the tree crowns, to medium and small wind gusts, some of which are in phase with the natural frequencies of the trees. Smaller gusts may affect the natural frequency of only larger branches of the trees and these may add or subtract sway motion components to tree fundamental frequencies and produce harmonic frequency components. Higher wind frequencies in the energy spectrum do not affect tree response and are dissipated within the canopy.

So, in a forest, the energy input from the wind gusts (after allowing for aerodynamic and mechanical admittance terms) can be related to the tree swaying motion. This occurs at amplitudes an order of magnitude smaller than the wind amplitudes, and at tree fundamental frequencies normally an order of magnitude above the main bulk of wind frequencies.

By adding the dynamic response produced by the turbulent wind components to the mean deflection from the drag produced by the mean winds, zones of high wind loads on forests can be found. These zones occur particularly just behind the forest leading edge, and also in localised areas over complex forested terrain. Mathematical and wind tunnel modelling of forests combine to permit comparison of wind structure and tree response with full scale forests. The wind tunnel tests show that zones of high wind loading are just behind the leading edge and increase beyond $\frac{S}{H}$ of 0.35 (Fig. 6.38). The changes in wind and tree disturbances seem to be caused by the Doppler shift. The spectral frequency distribution probably arises from at least four different spectral components:-

(a) the normal spectra formed by the flow over high roughness;

(b) adjustment of wind spectra by the turbulence from high shear flow, which has in turn been generated by the abrupt change in height process;

(c) redistributions caused by wind frequency inputs close to tree-top sway-motion amplitudes;

(d) the advance with the spectra of pairs of discrete gusts close to each other (Fig. 7.1).

This mixture produces resultant peak wind energy distributions at higher frequencies which differ from normal wind spectral distributions (6.11). The high tree amplitudes that result (Holbo, Mayer) appear to cause an unusual type of wind damage (Photographs 7 and 8). Wind damage to forests in local pockets can be caused by the same wind frequency redistributions without the effects of shear distortions (Photograph 1). More general wind damage is shown in Photograph 2 (§ App.III for photographs 1-11).

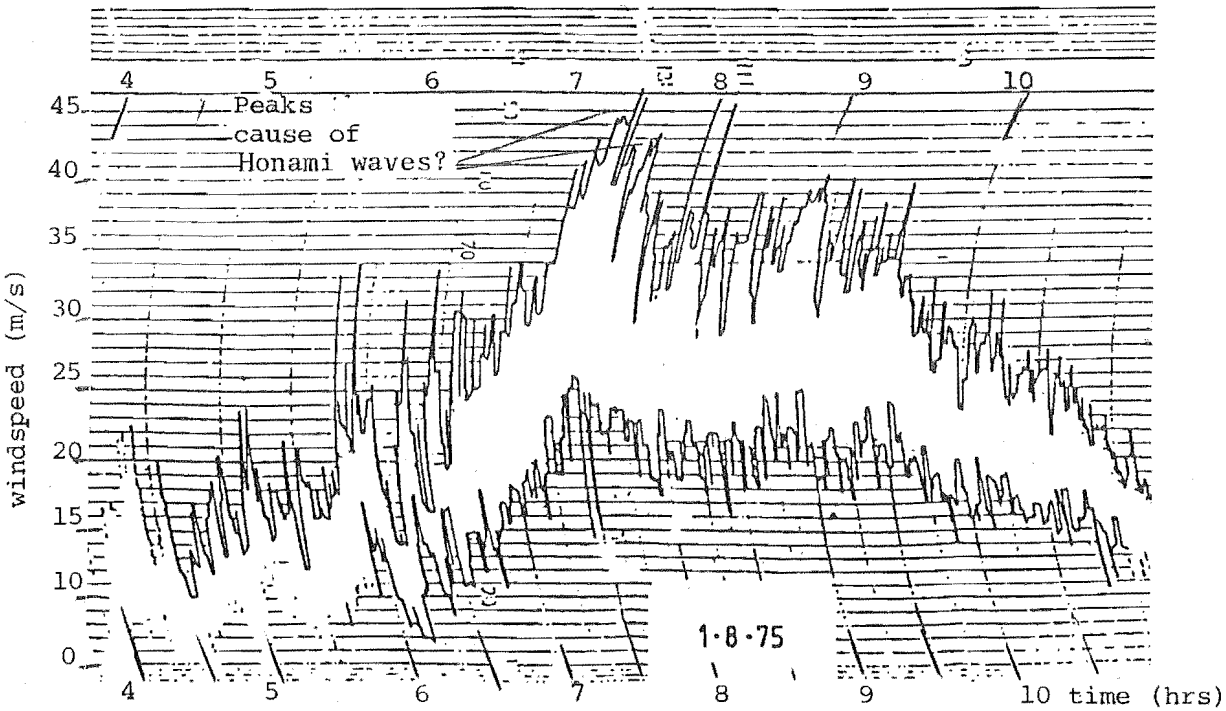

FIGURE 7.1: Wind structure in the August 1975 storms in Canterbury.

Wind conditions (a) to (d) cause tree responses which have tree fundamental and first harmonic frequencies (Fig. 5.29). The likely response equations governing the tree swaying motion may therefore be third order, or higher, oscillatory systems. From nyquist plots, these systems may have

positive real roots which inevitably produce unstable exponential response terms (Routh Criteria). These higher order instabilities can be reduced: either by making the trees stiffer and thus increasing their fundamental frequency, or by increasing their above-ground mass and damping.

Within a forest stand, however, individual tree sway properties appear to be controlled by the canopy architecture. Tree spacing has the greatest influence on canopy architecture. Model forest studies confirm that, provided an optimum spacing of $\frac{S}{H}$ of 0.35 is maintained, the combined forest and tree geometry at the leading edge and internally helps keep tree response to a minimum.

7.2 COMPARISONS OF WIND STRUCTURE, FULL SCALE AND MODEL

7.2.1 Mean wind speed profiles

In open country, wind profiles near the ground are shaped by the 'average' eddy size; this changes with height. In turn, these eddies are affected by convective turbulence from the sun's radiation. At Rivox, no open country boundary layer exists. At Kielder, the open country profile has a power exponent of 0.22 (Fig. 5.3). For the Canterbury model tests this exponent was near 0.19, and for Oxford it was 0.17.

Over the forests, the wind profiles at maximum fetch (Table 7.1, Fig. 7.2) are reasonably consistent with profiles from other complex canopies (Fig. 3.3). So, the flow is near equilibrium by 6 H in the Kielder experiment, and by 10 H in the model forests (6.8.4).

TABLE 7.1: Mean wind speed profiles compared (model and full scale).

	FULL SCALE												MODEL				
Experiment	RIVOX						KIELDER						OXFORD			CANTERBURY	
x-position	>10H						6H						10H			11H	
$\frac{S}{H}$	← 0.176 →			← 0.186 →			← ≈0.38 →						0.17	0.20	0.32	0.27	0.32
Run or Pattern	5	9	BT14	BT15	25 27.12.83	27 31.12.83	Set 3/5	Set 4/5	Set 2/5	Set 3/3	Set 4/3	Set 2/3	P	U*	S	B	C
$\bar{U}_{(\frac{z-d}{H})=1}$	1.57	6.30	7.83	7.11	12.21	11.51	9.25	9.96	8.71	7.64	8.60	10.17	5.18	5.21	6.54		
$\frac{z-d}{H}$	0.10	0.10					0.16	0.11	0.11	0.11	0.11	0.16	0.14	0.14	0.15	0.10	0.08
$\bar{U}_z/\bar{U}_{(z-d)}$	0.19	0.16					0.30.	0.06	0	0.20	0	0.06	0.17	0.27	0.25	0.38	0.31
$\frac{z-d}{H}$	0.25	0.25							0.29	0.29					0.25	0.29	0.29
$\bar{U}_z/\bar{U}_{(z-d)}$	0.43	0.36							0.18	0.54					0.35	0.54	0.54
$\frac{z-d}{H}$	0.41	0.41	0.41	0.41	0.36	0.36	0.35	0.35	0.50	0.50	0.35	0.35	0.34	0.34	0.35	0.45	0.49
$\bar{U}_z/\bar{U}_{(z-d)}$	0 66	0.54	0.57	0.43	0.41	0.43	0.54	0.37	0.38	0.63	0.28	0.29	0.41	0.48	0.45	0.63	0.68
$\frac{z-d}{H}$	0.64	0.64	0.64	0.64	0.53	0.53	0.58	0.68	0.76	0.76	0.67	0.58	0.44	0.44	0.55	0.68	0.74
$\bar{U}_z/\bar{U}_{(z-d)}$	0.79	0.78	0.75	0.67	0.63	0.65	0.70	0.72	0.75	0.82	0.66	0.54	0.53	0.58	0.65	0.78	0.82
$\frac{z-d}{H}$	1.00	1.00	1.00	1.00	0.86	0.86	0.85	1.00			1.00	0.85	0.98	0.98	1.00	1.05	1.00
$\bar{U}_z/\bar{U}_{(z-d)}$	1.00	1.00	1.00	1.00	0.96	0.95	0.86	1.00			1.00	0.78	1.00	1.00	1.00	1.02	1.00
$\frac{z-d}{H}$	1.44	1.44	1.44	1.44	1.28	1.28	1.23	1.25	1.12	1.12	1.32	1.23	1.48	1.48	1.50	1.69	
$\bar{U}_z/\bar{U}_{(z-d)}$	1.15	1.20	1.15	1.35	1.09	1.10	1.21	1.25	1.13	1.08	1.28	1.34	1.26	1.27	1.16	1.24	

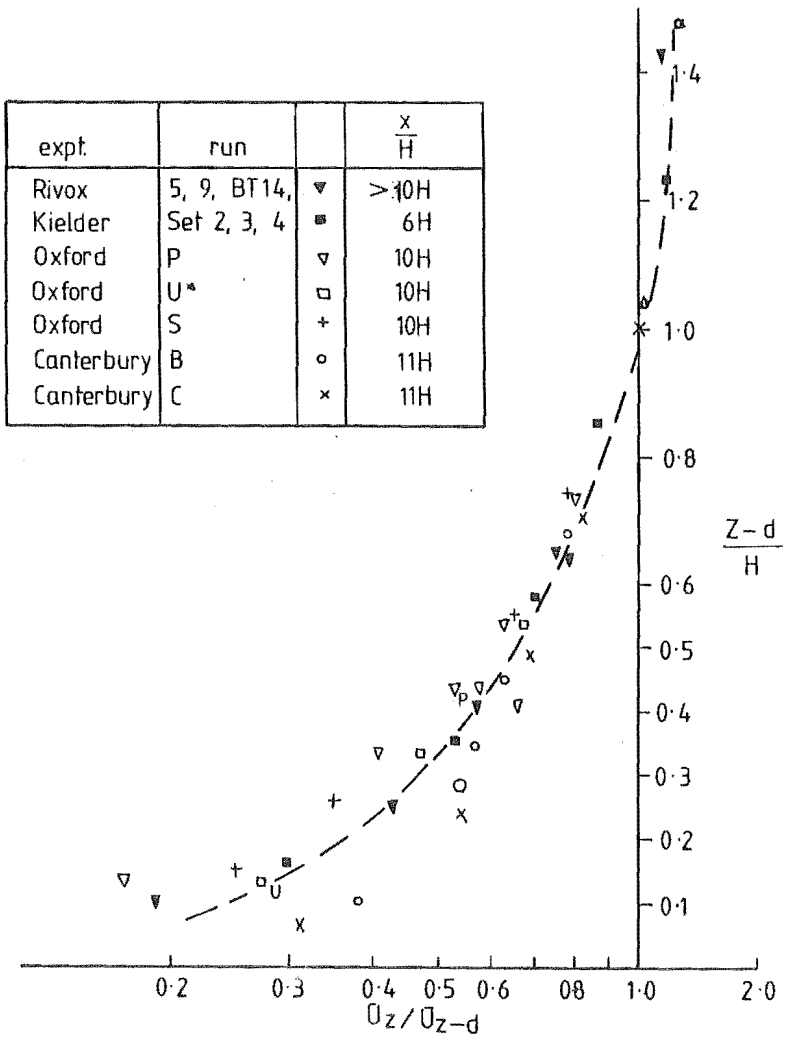

FIGURE 7.2: Mean wind speed profiles compared (model and full scale).

Cionco (1983) measures the changes in mean wind speed profiles over complex canopies for different stocking densities by defining a coupling ratio. Coupling is the ratio of the slope of the power law mean wind speed profile down in the crop to the logarithmic profile slope above the crop at transition. Coupling was low and near constant for dense arrays, but increased rapidly as densities increased above $\frac{S}{H}$ of 0.35. At the leading edge of the arrays, coupling reduced down to that of more established flows after 10 H. The amount of coupling was similar for short crops and a model forest (Meroney). In this thesis the model and full scale experiments exhibit similar mean wind profile shape changes (Figs 5.2; 6.2; 6.20, 6.21). Coupling ratios have not been calculated. Instead, local and profile shear stress coefficients and their aerodynamic roughnesses, z_o'' and z_o' are compared (7.2.3).

7.2.2 Turbulence intensity profiles

Model and full scale turbulence intensity profiles (Tables 5.10, 5.11; Figs 5.11, 5.16, 5.18, 6.20), are drawn alongside other profiles in Figure 7.3. For close spacings the shapes of the profiles are similar. However, those from the Oxford tests are displaced downwards relative to the Rivox full scale profiles. The curves match when the zero-plane displacement of the model forest profiles is changed from 0.75 H to 0.60 H (Fig. 7.4). Maximum turbulence intensities ε(70%, 90%) are similar to those measured in other equivalent experiments. In the model tests I_{σ_u} reduced down ε(50%, 60%) as spacings increased from $\frac{S}{H}$ of 0.17 to $\frac{S}{H}$ of 0.4. The ESDU turbulence intensity profile shape (2.3.1) for large aerodynamic roughness (z_o > 1 m) is different from the model and full scale profile shapes. It matches the full scale profile at 2½ mean tree-top heights above the ground. Nearer the trees, the ESDU profile is similar to the profiles obtained from wind measured over Patterns P and U*.

In Figure 7.4 the mean curve for 17 profiles has the form:

$$I_{\sigma_u} = 0.385 - 0.319 \ln. \left(\frac{z-d}{H}\right) ,$$

which probably applies to near neutral conditions. The curve appears to be simpler than the ESDU equation (2.3.1). The difference that apparently exists in zero-plane displacements is probably due to the difference in horizontal pressure distribution which arises from changes in atmospheric pressure and/or understorey density. At Rivox the spruce plantation is unpruned, while the model forest 'understorey' is open to about $\frac{1}{3}$ tree-height. The reduction in turbulence intensity near tree-top height from Pattern U* to Pattern P is probably caused by crown contact in Pattern P which prevents tree sway motion and therefore wind/tree interaction (Fig. 6.21)(also § 6.7.3).

As spacing increased in the model forest, the turbulence intensity diminished ε(50%, 60%) at 10 H. Tree response increased with an increase in both local mean wind speeds and turbulence intensity at tree-top height. This feature will probably occur at Rivox also. So far, the average of the measurements of a number of individual wind structures does not significantly alter as $\frac{S}{H}$ is changed from 0.176 to 0.186 (Table 5.10). The mean values of the wind properties are much the same, even though atmospheric stability alters the individual wind structure parameters (Fig. 3.9).

At the FC mast, Rivox, the turbulence structure above the forest reaches turbulence intensities similar to the open country structures (15%)

To p.297

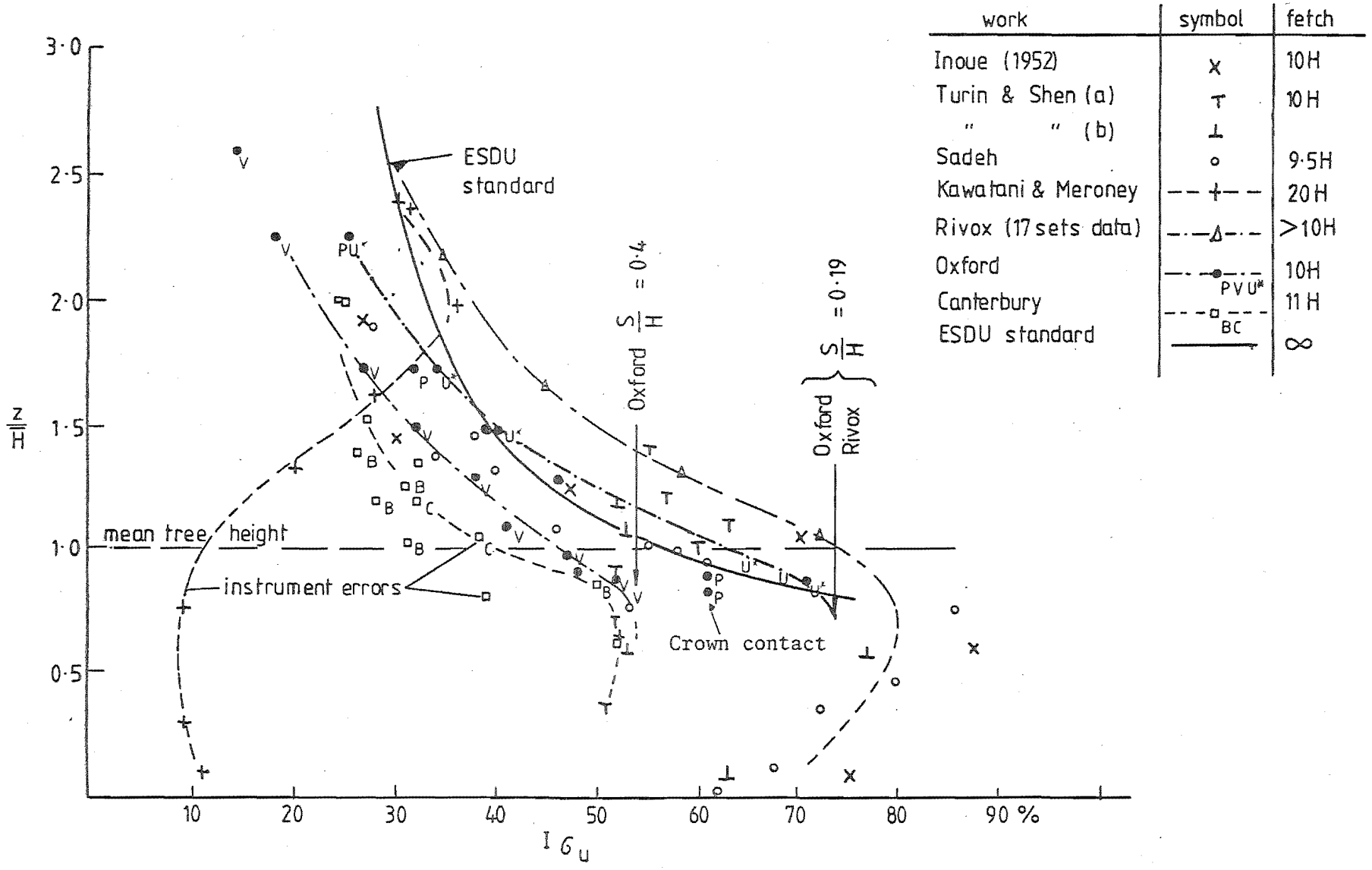

FIGURE 7.3: Turbulence intensity profiles compared (model and full scale).

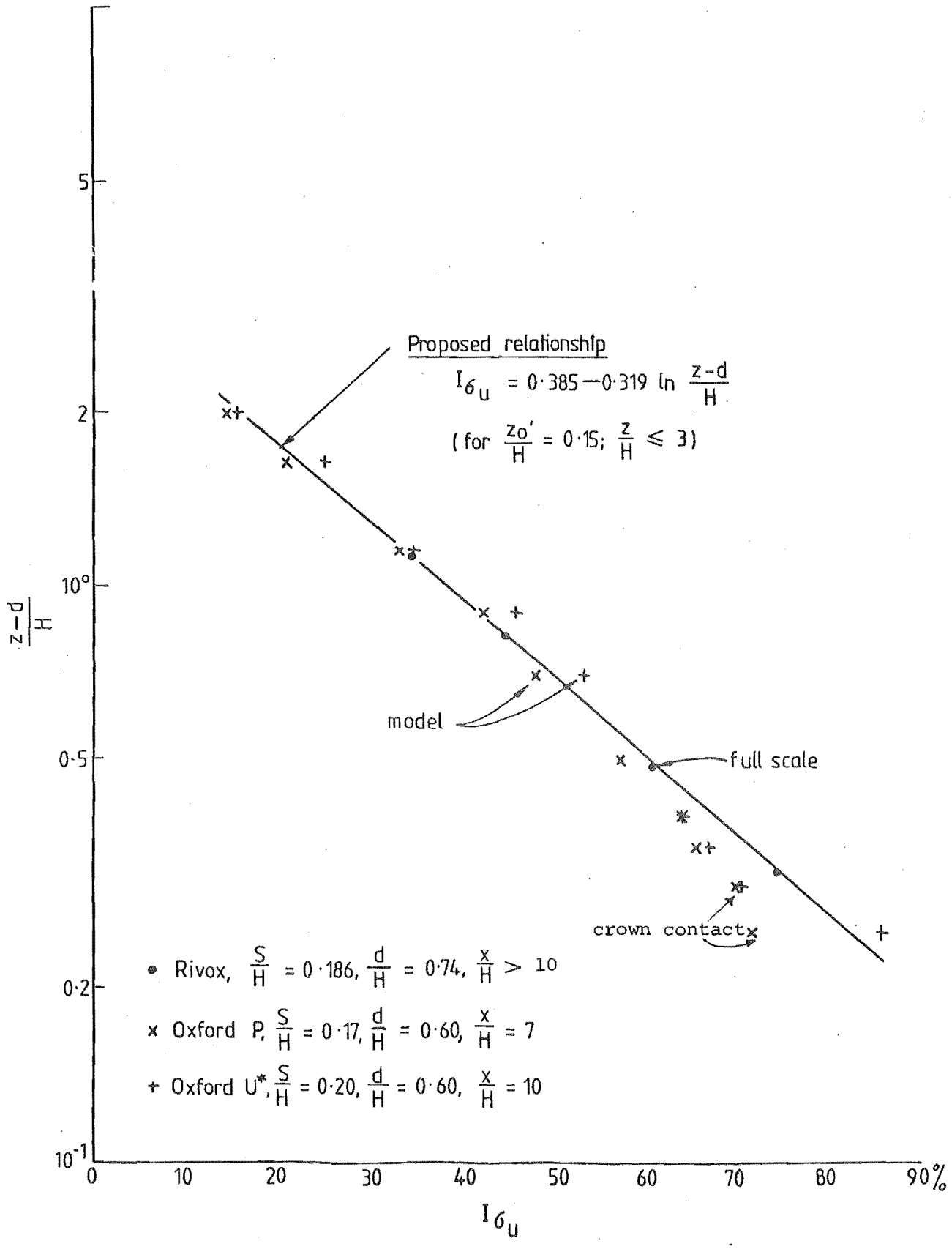

FIGURE 7.4: Turbulence intensity profile relationship (model and full scale)

at $\frac{z-d}{H}$ of 2.07, or almost 3 tree heights above ground level. This agrees with other research work (3.5).

7.2.3 Aerodynamic roughness and shear stress coefficients

From the model and full scale mean wind velocity profiles, model and full scale values of z_o'' and C_{f_o} have been compared (6.8.2). At 7 H, the values of z_o'' and z_o' are much the same, indicating return to equilibrium (cf Table 3.2). C_{f_o} values are compatible with C_{f_o} obtained in equilibrium conditions (Tables 2.2, 5.11(a)-(b) and 6.10). For Rivox, the average value of C_{f_H} was 1.05 (Table 5.11(a)-(b)). In the Oxford tests, the mean wind speed at 10 H for Patterns P and U* gives $\frac{\bar{U}_H}{\bar{U}_o}$ of 0.30 (Figs 6.25(a) and (b)). So, C_{f_o} is estimated to be 0.095, or K_{10} is close to 0.048. This agrees with Davenport's average result (Table 2.1) and corresponds with Counihan's summary for urban roughness (Table 2.2).

In the Oxford tests, Reynolds stresses were measured for Pattern W (Table 6.6). These agreed with stress coefficients calculated from the friction velocities which were measured from the mean wind speed profiles (Table 6.7). Because of this agreement it appears that, in the inner layer at least, equilibrium exists, turbulent mixing is logarithmic with height, and so k_a is constant (4.3).

7.2.4 Wind spectra

Measurements of the wind structure over high roughness (2.5, 3.8.2, 3.8.3, 4.6) were analysed and collated for Rivox (5.10.6) and Oxford (6.8.5). Comparisons were then made with these spectral measurements over forests and other smaller crops (Table 7.2; Figs 7.5 and 7.6). Meroney provides a model forest spectrum (Fig. 6.40) which has an absiccae scale 10 times the Oxford scale for the wind frequency (n). This model spectrum was similar to other spectra when the frequency scale was changed to $\frac{n}{10}$. All the compared spectra lay below the spectral curve for waving crops (7.2.6). This curve was obtained from the spectral shape for high roughness (Högström et al) adapted from Kaimal's open country spectral shape (3.8.2). (Kaimal's spectral measurements are considered to be an accurate measure of spectral distributions over open country because he used sonic anemometers.)

The spectra results show that:-

(a) model and full scale spectra slopes, in the inertial range, are comparable at tree-top height (5.3.9);

To p.301

TABLE 7.2: Spectral distributions compared (model and full scale).

Rivox BT14		Rivox BT15		Rivox BT770		Holbo		Finnigan		Maitani (Rush)		Meroney ($\frac{n}{10}$)		Oxford S 0.22(10H)		Oxford U* 0.22(10H)		Oxford V 0.22(10H)	
$\frac{nH}{U_{*\ell}}$	$\frac{Sn}{U_{*\ell}^2}$	$\frac{nH}{U_{*\ell}}$	$\frac{Sn}{U_{*\ell}^2}$	$\frac{nH}{U_{*\ell}}$	$\frac{Sn}{U_{*\ell}^2}$	$\frac{nH}{U_{*\ell}}$	$\frac{Sn}{U_{*\ell}^2}$	$\frac{nH}{U_{*\ell}}$	$\frac{Sn}{U_{*\ell}^2}$	$\frac{nH}{U_{*\ell}}$	$\frac{Sn}{U_{*\ell}^2}$	$\frac{nH}{U_{*\ell}}$	$\frac{Sn}{U_{*\ell}^2}$	$\frac{nH}{U_{*\ell}}$	$\frac{Sn}{U_{*\ell}^2}$	$\frac{nH}{U_{*\ell}}$	$\frac{Sn}{U_{*\ell}^2}$	$\frac{nH}{U_{*\ell}}$	$\frac{Sn}{U_{*\ell}^2}$
0.26	4.76	0.16	2.41	0.36	3.95	0.22	1.37	0.68	2.28	0.87	4.61	0.11	0.96	0.14	0.76	0.14	0.40	0.18	0.92
0.52	3.58	0.31	2.76	0.72	2.83	0.31	1.33	0.90	2.98	1.09	3.07	0.22	1.46	0.20	0.95	0.20	0.69		
0.78	2.59	0.47	2.67	1.08	1.74	0.93	0.85	1.22	1.49	1.33	2.30	0.33	1.39	0.28	0.80	0.28	0.85	0.26	0.89
1.05	1.95	0.63	2.14	1.45	1.03	1.24	0.76	1.41	1.23	1.50	1.46	0.45	1.39	0.55	0.56	0.55	0.61	0.44	0.87
1.31	1.41	0.79	1.53	1.81	0.78	1.60	0.52	1.70	0.96	1.69	1.04	0.54	1.09	0.83	0.48	0.83	0.36	0.58	0.80
1.57	0.95	0.94	1.12	2.17	0.70	1.90	0.57	1.94	2.01	1.88	1.04	0.67	1.30						
1.83	0.68	1.09	0.91	2.53	0.55	2.20	0.33	2.43	1.06	2.12	0.69	0.75	1.10						
2.09	0.56	1.26	0.79	2.89	0.44	3.10	0.19	4.86	0.79	2.45	0.46	0.88	1.15						
2.35	0.52	1.41	0.71	3.25	0.39	9.30	0.05	8.27	0.53	2.72	0.58	0.99	1.29						
2.62	0.45	1.57	0.60	3.61	0.32	15.60	0.02	9.24	0.49	5.44	0.12	1.10	1.17					0.87	0.68
2.88	0.39	1.72	0.47	3.98	0.27	18.70	0.005	12.16	0.42	8.16	0.05	1.21	1.02	0.97	0.58	0.97	0.41	1.02	0.79
3.14	0.42	1.88	0.40	4.34	0.25			18.00	0.31	10.87	0.04	2.18	0.82	1.11	0.45	1.11	0.25	1.17	0.66
3.66	0.51	2.05	0.38	4.70	0.22							3.45	0.75	1.38	0.29	1.38	0.19	1.37	0.47
4.18	0.41	2.21	0.35	5.42	0.18							5.45	0.42	1.51	0.31			1.55	0.31
4.71	0.29	2.65	0.41	6.16	0.20							8.74	0.29	1.66	0.16	1.66	0.15	1.72	0.19
5.23	0.22	2.97	0.33	6.85	0.17							11.09	0.20	1.94	0.12	1.94	0.10	2.07	0.10
5.95	0.35	3.13	0.28	7.59	0.22							13.80	0.13	2.19	0.10	2.16	0.08	2.32	0.10
7.06	0.36	3.60	0.30	8.33	0.26							17.70	0.10	2.49	0.07	2.49	0.06	2.39	0.10
7.58	0.30	4.21	0.30	9.03	0.39							22.00	0.06	2.77	0.06	2.77	0.06	2.77	0.08
8.63	0.34	4.85	0.30	9.40	0.44							34.00	0.08	5.48	0.02	4.15	0.03	2.92	0.05
9.68	0.33	5.17	0.38	10.14	0.36							54.00	0.02					4.37	0.03
10.72	0.44	6.90	0.31	11.20	0.39											8.30	0.01	5.83	0.02
11.24	0.60	7.38	0.26	12.32	0.45														

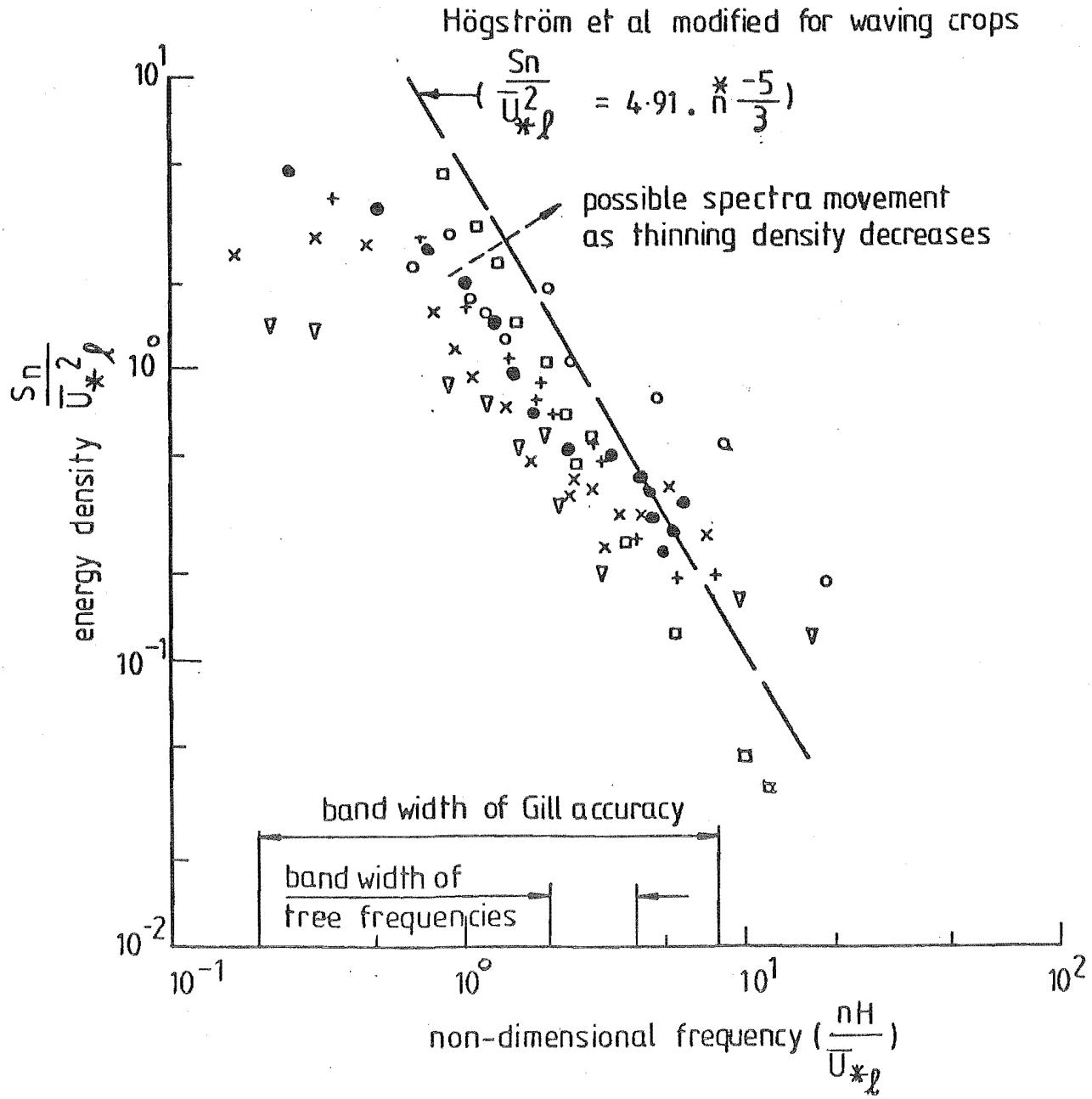

Work	Crop Type	Symbol	H (m)	$\frac{z}{H}$	$\frac{S}{H}$	σ_u^2	$\bar{U}_*$ (m/s)	$\bar{U}_z$ (m/s)	$(\sigma_u/\bar{U}_{*\ell})^2$
Rivox BT14	Spruce Unthinned	●	10.1	1.1	.183	4.67	2.52	3.80	0.74
Rivox BT15	Spruce Unthinned	X	10.1	1.1	.183	3.42	1.93	3.04	0.92
Rivox BT770	Spruce Thinned	+	10.83	1.06	.197	6.20	2.34	4.23	1.12
Holbo	Fir	▽	28.0	1.0	.21	3.84	0.90	6.75	4.75
Finnigan	Wheat	o	1.25	1.2	.16	2.28	0.54	3.36	7.72
Maitani	Rush	□	1.3	1.3	-	0.87	0.48	3.83	3.83

FIGURE 7.5: Wind spectral distributions compared (full scale).

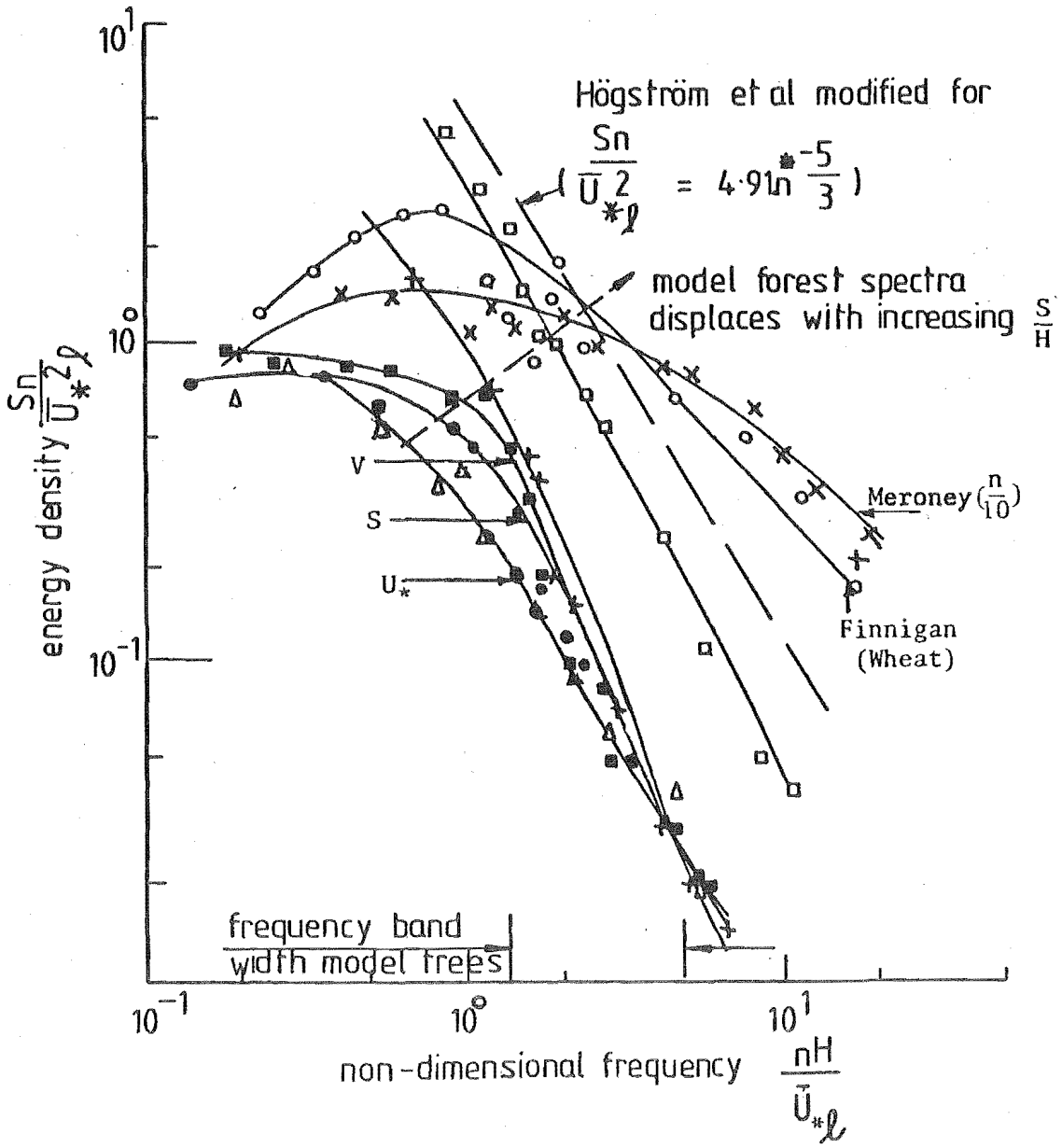

Work	Crop Type	Symbol	H (m)	$\frac{z}{H}$	$\frac{S}{H}$	σ_u^2	$U_{*\ell}$	$\bar{U}_z$	$(\sigma_u/U_{*\ell})^2$
Oxford (S)	Model Trees	●	0.20	1.1	0.32	2.00	0.730	2.80	3.80
Finnigan	Wheat R2	⊖	1.25	1.2	0.16	2.28	0.544	3.36	7.72
Maitani	Rush R5	□	1.30	1.0	-	0.87	0.478	1.70	3.83
Maitani	Wheat R3	+	1.0	1.3	-	≈0.80	0.467	1.60	3.67
Meroney	Model Trees	×	0.18	1.1	0.30	0.30	0.330	1.95	2.73
Oxford (U_*)	Model Trees	△	0.20	1.1	0.20	1.81	0.730	2.85	3.40
Oxford (V)	Model Trees	▣	0.20	1.1	0.39	2.03	0.693	3.62	4.23

FIGURE 7.6: Wind spectral distributions compared (model and full scale).

(b) there is a small frequency shift in the peak energy when stocking density decreases up to $\frac{S}{H}$ of 0.35;

(c) the normalised peak energy levels of the full scale spectra are higher than the normalised energy levels of the model forest spectra. (This is due, in part, to the reduced sampling times used in data analysis with the Apple II; 5.3.8);

(d) the mean natural frequency of 10 m Sitka spruce trees (0.52 Hz) in a full scale forest lies in a band width which is likely to be influenced by wind gusts passing over the forest once stocking density goes beyond $\frac{S}{H}$ of 0.35;

(e) the peak power of the spectra shifts to its highest frequencies and highest energy levels just above mean tree-top height. (This shift is more a function of tree spacing than of vertical height (Fig. 7.5);

(f) waving crops shift wind energy to wind frequencies which are near the natural frequency of the individual elements (Finnigan, Maitani, Holbo).

From these spectra results it appears that:-

(a) the spectral distribution of Högström et al and others is similar to the spectral distribution over forests and other crops at $\frac{z}{H} \simeq 2.0$, and at densities of $\frac{S}{H} < 0.35$;

(b) the same spectral distribution does not appear to account for the higher energy levels at the high frequency end of the spectra for $\frac{S}{H} > 0.35$.

Spectra over waving crops can exhibit:-

(a) wind frequencies caused by atmospheric instabilities, mean wind velocity changes, high shear flow, canopy architecture, Honami waves, and random crop sway.

(b) skew, which varies with a combination of mean wind speed and turbulence;

(c) a high 'Q' factor (or peakiness) at mean tree-top height.

Crop amplitude response may be studied in greater depth if changes in skew and 'Q' factor of spectra are related to the background and resonant response (Högström et al, 3.2).

Most wind spectra measurements over high roughness lose accuracy because of:-

(a) inadequate instrumentation and recording systems (cf. Kielder);

(b) insufficient data capture points;

(c) insufficient data collection periods and data averaging because of lack of strong winds;

(d) changes in atmospheric conditions from one measurement to another;

(e) changes in 'mean' wind speeds and directions;

(f) aliasing, instrument errors and incorrect filtering.

7.2.5 Tree response

The response of a matrix of model trees within a model forest of fetch up to 11 H, has been compared by calculation and by photography (6.10). To date, only one data set of full scale tree response spectra from one accelerometer on Tree 81 has been received (Fig. 5.29). In the full scale measurements, with $\bar{U}_H$ of 2.6 m/s, $\frac{A}{H}$ was found to be 0.032 for $\frac{S}{H}$ of 0.186 (5.11).

At this spacing, the difference between $\frac{A}{H}$ (model) and $\frac{A}{H}$ (full scale) is small (6.10.2). This difference could be due to the short sampling times (350 s) that are a feature of the Apple II system (5.3.8).

At the time of writing, these comparisons are tentative; but as more tree acceleration spectra and wind measurements become available from the Rivox experiment, these comparisons will be verified.

Uchijima and Wright measured corn-top dynamic response spectra. More recently, Finnigan and Maitani each studied both wheat-top and rush-top sway motion. With Uchijima and Wright they show that crop-tops produce a

response spectrum in the inertial region with a slope of $-\frac{7}{3}$. This was predicted by Inoue (1955) when he discussed Honami waves (6.11).

Although it is not yet possible to make any conclusive statements on tree-top spectra slopes in the inertial region at Rivox, the first response spectrum does follow a slope of $-\frac{7}{3}$ (Fig. 5.29).

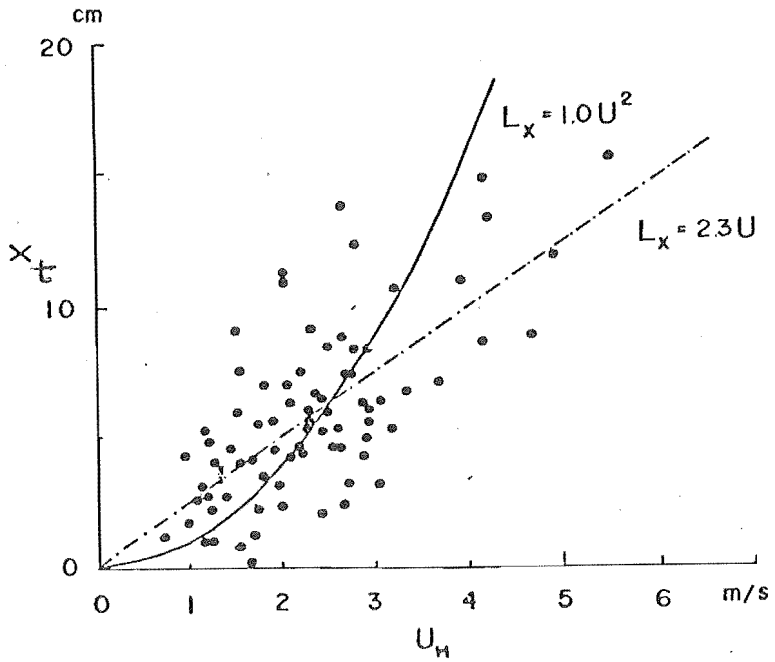

FIGURE 7.7: Relation between horizontal wind velocity and the displacement of a rush plant along the mean wind for 40 s (after Maitani). (note: x_t = A+D)

Maitani produced results which compare rush-top amplitude response in the wind to mean horizontal wind velocity $\bar{U}_H$. He could not decide whether the response results were proportional to $\bar{U}_H$ or $\bar{U}_H^2$ (Fig. 7.7), but he indicates that the crop response may be proportional to $\bar{U}_H^2$. On the other hand, the Rivox and Oxford tree amplitude response results suggest that the dynamic background and resonant components (A) are proportional to $\bar{U}_H$. The mean deflection component (D) is also proportional to $\bar{U}_H$ and not $\bar{U}_H^2$ (6.10.2). The available full scale results of $\frac{A}{H}$ at Rivox also suggest that A is proportional to $\bar{U}_H$ and not $\bar{U}_H^2$.

The response equations (3.10.2) assume that the dynamic response is proportional to $\bar{U}_H.u'$ plus $u_H'^2$. The Canterbury results are a direct measurement of model tree response. Fig. 7.7 shows that the data can also be represented by a straight-line relationship between (A+D) and $\bar{U}_H$.

The damping ratio ($\zeta = 0.08$) used in this research is affected by branch, stem, root and soil mechanical strength properties and by the way in which these properties change with moisture content. Dominance of any one component of these combinations of properties will alter the damping ratio and hence the proportions of dynamic to static response.

At Rivox, at $\frac{S}{H}$ of 0.176, about 30% of the tree crowns can touch each other in strong winds. This reduces average tree response and turbulence intensity (of. Pattern P and U*, Fig. 7.3). During the sway tests in the thinned sector (Fig. 5.9), tree frequencies and their settling times (related to damping) were much the same along or across the plough lines.

With *Pinus radiata*, sway measurements produced along-wind and across-wind characteristics similar to spruce. As *Pinus radiata* are taller and have more mass, settling times and natural frequencies are correspondingly altered.

These studies appear to suggest that tree damping is controlled by the tree's above-ground stem weight, crown size and top height more than by changes in the root/soil interface moisture content and strength (Mayhead, Loo, Finnigan and Mulhearn, 1978).

7.2.6 The modified wind spectra curve over waving crops

For wind-loading purposes, the simple and complex tree response calculations (Figs 6.35(a)-(d)) suggest that in the close-spaced model tests, the ratio of resonant response to background response at 10 H is the same $\left(M_R = \sqrt{\frac{R}{B}}\right)$.

Because the model and full scale experiments are comparable,

$$M_R = \frac{1}{\sqrt{\left(\frac{2\ \zeta\ n_{pk_w}}{n_o}\right)^2 + \left(1 - \left(\frac{n_{pk_w}}{n_o}\right)^2\right)^2}}$$

and,

$$\sqrt{\frac{R}{B}} \simeq \frac{1 - \left(\frac{n_{pk_w}}{n_o}\right)^2}{\frac{2\ \zeta\ n_{pk_w}}{n_o}}$$

so,

$$n_{pk} \simeq \frac{n_o \cdot 1}{2\zeta \cdot \sqrt{\frac{R}{B}}} \cdot \left(1 - \left(\frac{n_{pk_w}}{n_o}\right)^2\right) .$$

Now, from Högström et al,

$$\frac{nS(n)}{\bar{U}^2_{*\ell}} = 0.64\, n^{*-\frac{2}{3}} \quad . \ . \ . \quad (3.8.2)$$

or,

$$\frac{S(n)}{\bar{U}^2_{*\ell}} = 0.64 \cdot \frac{H}{\bar{U}_{*\ell}} \cdot n_{pk_w} \cdot n^{*-\frac{5}{3}}$$

where $\frac{n_{pk_w} H}{\bar{U}_{*\ell}}$ appears to be close to unity for most spectra compared.

So,

$$\frac{S(n)}{\bar{U}^2_{*\ell}} = 0.64 \cdot \frac{H}{\bar{U}_{*\ell}} \cdot \frac{n_o}{2\zeta} \cdot \frac{1}{\sqrt{\frac{R}{B}}} \left(1 - \left(\frac{n_{pk_w}}{n_o}\right)^2\right) \cdot n^{*-\frac{5}{3}} .$$

In the Oxford Model forest experiment, Pattern S appears to divide the spectra form between waving and non-waving crops. So, at 10 H, and at 0.22 m ($\frac{Z}{H} = 1.1$) it gives;

$$n_o = 8.9 \text{ Hz}, \quad \zeta = 0.08, \quad n_{pk} = 4.4 \text{ Hz}, \quad n^*_{pk} = 1.2,$$

$$\bar{U}_{*\ell} = 0.730, \text{ and } \sqrt{\frac{R}{B}} = 1.5, \quad \text{(Table 6.10, Fig. 6.34)}$$

and so,

$$\frac{S(n)}{\bar{U}^2_{*\ell}} = 4.91\, n^{*-\frac{5}{3}} \quad , \text{ (Fig. 7.5; 7.6).}$$

This spectral curve shape passes just above most of the spectra plotted in Figures 7.5 and 7.6. Waving crops appear to produce spectra beyond this curve (Finnigan).

7.2.7 Summary of experimental measurements

Table 7.3 summarises measurements of the mean wind speed and turbulence intensity profiles, aerodynamic roughness and shear stress coefficients, and the wind and tree response spectra. These comparisons have all appeared acceptable, and in most cases the compatibility is within the limits of the assumptions and the experimental errors. This compatibility between model and full scale results should improve as more data become available from the Rivox experiment.[1] As the test sector is thinned further, the risk of premature windthrow is always present. This could cut short the experiment.

7.3 SUMMARY OF FINDINGS

The location and types of measurements made in Zones A, B, C, (Fig. 1.1) are summarised in Fig. 7.8.

For each zone comparisons were made (7.2.1; 7.2.5) for:-

(1) mean wind speed profiles;

(2) turbulence intensity profiles;

(3) wind spectra;

and (4) tree response.

Where these properties are comparable in each zone, the experiments, along with ESDU standards, are named. These findings imply that wind and tree response characteristics over full scale forests can be duplicated in boundary layer wind tunnels. Model trees must be designed so that their stiffnesses duplicate full scale tree stem stiffnesses.

Table 7.3 also implies that, if stocking density exceeds $\frac{S}{H}$ of 0.35, trees just in from the forest front may be the first to blow down in a man-managed conifer forest.

Planting patterns are probably unimportant inside the forest, but tree and canopy architecture, along with tree spacing, are critical near the forest leading edge. For these reasons, a heterogeneous forest canopy surface (3.1.3) may be more acceptable if the forest front is to have a correct aerodynamic design.

---

1. The Forestry Commission hopes to complete two more thinnings by July 1984 and conclude wind recordings soon after. Data analysis from the main frame computer will continue for a number of months after that.

To p.309

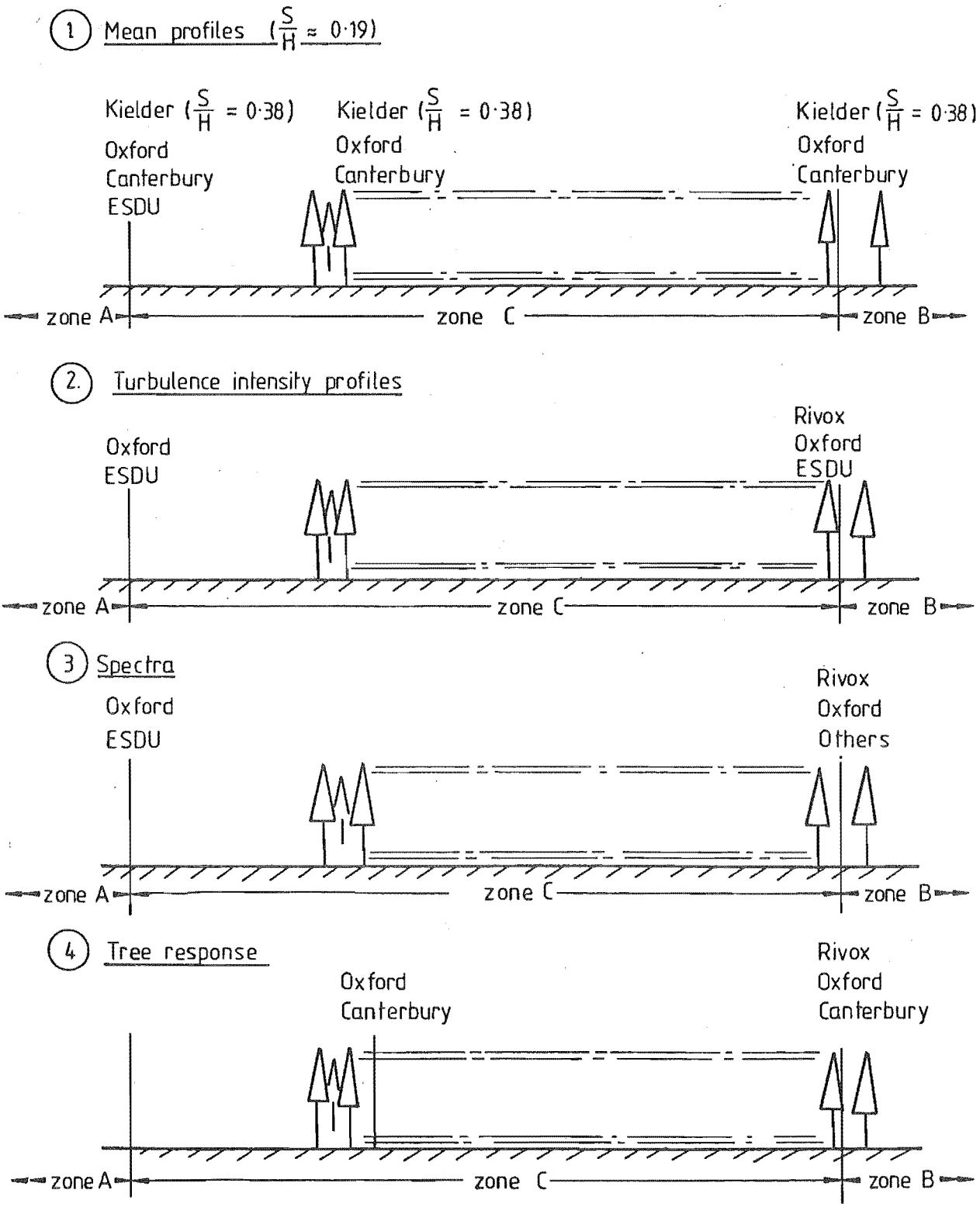

FIGURE 7.8: Positions of measurements of model and full scale experiments.

TABLE 7.3: Summary of Measurements

✓ = Significant	X = Not Signifcant
✓X = Partial Significance	- = Not Tested

	Fullscale			Model					
	Kielder		Rivox	Canterbury			Oxford		
Amount of Thinning	Slight		1 Step	8 Steps			11 Steps		
Zone	A	B	C	A	B	C	A	B	C
Mean wind speed profiles	✓	✓	✓	✓X	✓	✓	✓	✓	✓
Turbulence Intensity profiles	X	X	✓	X	✓X	✓X	✓	✓	✓
Shear Stress Co-efficient and roughness	X ✓	✓X ✓	✓X ✓	✓X ✓	✓ ✓	✓ ✓	✓ ✓	✓ ✓	✓ ✓
Wind Spectra Changes	-	X	✓	-	-	-	✓	✓	✓
Tree sway motion by a) Photography b) Simple Calculation c) Complex Calculations		- - -	X ✓X ✓X		✓ ✓X X	✓ ✓X X		✓X ✓ ✓	X ✓ ✓
Useful Comparisons	✓	✓	✓	✓	✓	✓	✓	✓	✓

The strip system used in the full scale Eyrewell and Balmoral forests on the Canterbury Plains appears to have these characteristics.

7.4 APPLICATION OF THESIS FINDINGS TO FOREST MANAGEMENT

7.4.1 A proposed optimum thinning practice

Current thinning practices in Canterbury forests have been outlined (Table 3.1). Thinning practices in current use have been devised to maintain volume increment within stands.

The following adjustment to current thinning practices for Canterbury forests is proposed: maintain $\frac{S}{H}$ at near 0.3 (6.6.2; 6.9.2) with two thinnings; the second thinning needs to be delayed until tree height reaches 16.4 m (age 15 years). Spacing would then increase from 3.5 m to 5.2 m, or $\frac{S}{H}$ would increase from 0.21 to 0.32.

This does not differ significantly from the current thinning practices in Canterbury. $\frac{S}{H}$ of 0.3 can be used in any forest with different crop rotation times and stocking densities, provided it is modified to account for local terrains, soil changes[1] and moisture levels.

These proposals for thinning forests on flat open terrain are depicted in Fig. 7.9.

---

1. Measured in tree-pulling tests at Eyrewell (unpublished).

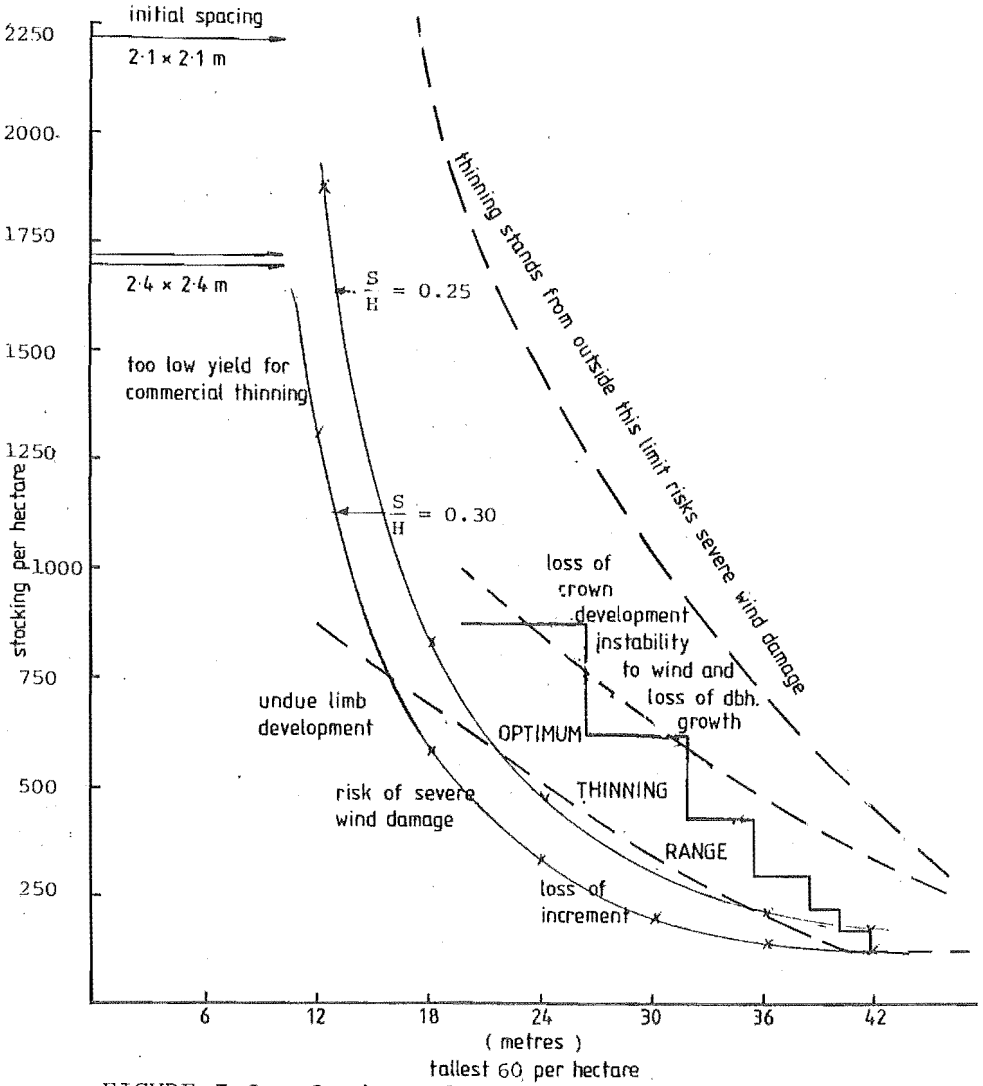

FIGURE 7.9: Optimum forest thinning for wind stability (after Lewis (1963), South Australia Forestry Commission)

7.4.2 Measurement of forest stability

There are several ways of predicting the onset of wind-instability in forests approaching maturity. Just in from the leading edge:-

(a) conduct annual measurements of wind-thrown trees and relate tree position to tree stem height and diameter (Fig.4.2);

(b) monitor the amplitude response of two or three trees using sensors and compare the changes that occur from year to year;

(c) measure the mean natural frequencies and settling times of samples of trees within each stand, and compare these frequencies with a known spectrum measurement of the local wind structure;

(d) conduct wind tunnel topographical tests for existing and proposed forests and map spectra skew and turbulence intensity contours in the horizontal plane;

(e) analyse the contour maps from (d) with known forest wind damage records for the full scale forested topography.

7.4.3 Measurement of forest storm damage

When forests have been damaged by high winds it is essential to:-

(a) measure variations in damage in from forest leading edges;

(b) measure the ratio of blowdown to breakage occurring from the forest front inwards to at least 10 H;

(c) take low-level aerial photographs of the damaged forests before they are cleared for replanting.

7.4.4 Forest and tree design

The model forest investigations indicate additional proposals for increasing stability.

(a) The forest borders at leading edges and up to 5 H inwards should:-

(i) gradually increase in mean tree height and mean spacing, so that $\frac{S}{H}$ remains below 0.35;

(ii) gradually increase in understorey density by reducing pruning height (zero-plane displacement rise);

(iii) be orientated at right angles to the most damaging wind;

(iv) in complex terrain, be located at positions where mean wind accelerations and turbulence intensities are low;

(v) be thinned and pruned as in (i) and (ii) so that the crown forms that grow give a gradual transition from a heterogeneous surface to a homogeneous surface.

(b) A forest tree should have:-

(i) a branch, crown and stem mass distribution which produces a high fundamental natural frequency;

(ii) high stem stiffness;

(iii) a balance between damping at the soil/root interface and fixity of the roots in the soil;

(iv) a branch distribution which filters out the stem harmonic frequencies before they affect tree stem frequency response.

Some of these findings have already been implemented in Canterbury forests (Swale, 1983).

7.5 SUGGESTIONS FOR FURTHER RESEARCH

Some future research proposals are listed below.

(a) Extend the Rivox experiment, using more masts and more thinning steps to reduce dependence on wind direction.

(b) Conduct a full scale experiment over a forest leading edge (the Kielder or Thetford sites are suitable) to allow turbulence intensity, wind spectra and tree dynamic response spectra comparisons with Canterbury and Oxford model forest leading edge results.

(c) Conduct topographical wind tunnel studies before forests are planted to identify regions at risk from high winds. Thinning treatments can be adjusted accordingly.

(d) Study the effects of Honami waves on a correctly-designed model forest in a natural boundary layer wind tunnel.

(e) Measure the stiffness, mass, damping, crown form, tree-top height and breast height diameter of several groups of trees of:-

(i) differing height,
(ii) differing species,
(iii) differing soils and moisture content.

(f) Conduct model forest studies by adjusting the forest design at the leading edge (Zone C) keeping $\frac{S}{H}$ constant in Zones B and C at several different spacings.

(g) Develop mathematical models for the behaviour of tall crops within plantations using the complex solution for crop-top swaying motion. Compare these with the Oxford and Canterbury swaying motion estimates.

(h) Apply some of the techniques used in the Canterbury and Oxford experiments to the study of shelterbelt design in natural boundary layer wind tunnels.

7.6 CONCLUDING REMARKS

Windthrow of trees within man-managed forests is a continuing cause of economic loss. The need to minimise windthrow, and at the same time explain some of the unusual phenomena associated with it, have led to the research described in this thesis.

The research shows that the properties of the wind and the response of the trees at the leading edges of forests differ significantly from these properties in from the edge. Optimum thinning densities are found which should improve forest stability in medium and strong winds.

This is a first attempt to measure and calculate the along-wind total response of trees within forests.

New Zealand often experiences very high wind speeds. In particular, the Canterbury Plains are prone to gusty, damaging, north-west föhn winds, especially in spring and autumn. It is hoped that this study will complement current protective measures, and thus improve the wind stability of forests.

ACKNOWLEDGEMENTS

Firstly, my thanks are due to Professor D. C. Stevenson and Dr. A. J. Bowen for supervising this work and for their encouragement.

The substantial research grants from the New Zealand Forest Research Institute and the Canterbury University enabled much of the initial work for this thesis to be undertaken. I am also grateful for financial assistance from the New Zealand Forest Service and from the Selwyn Plantation Board.

I would like to thank the British Forestry Commission for inviting me to work at their research stations in 1972 and in 1981-82. I express my appreciation to the following people who were involved in the experiments: J. Gardiner, D. Seal, K. Miller, B. Reynard, J. Whyatt, Professor J. Schaeffer and Dr. C. Wood.

The technical assistance in both the laboratory and the field of H. J. Anink, H. J. Bright, L. M. Cheeseman, Jill Shelton and R. E. Tinker of the Mechanical Engineering Department at Canterbury University was greatly appreciated; as was the dedicated student help.

Advice from Professor H. A. Panofsky was welcome.

Finally I would like to thank Lesley Tuffley for her untiring help during the preparation of this thesis and Beryl Nottingham for typing it.

REFERENCES

ANNAND, W.J.D. (1966). The mechanics of machines. Heinemann Educational Books Ltd, London. 353 p.

ANTONIA, R.A. and LUXTON, R.E. (1971). The response of a turbulent boundary layer to a step change in a surface roughness. Part I: Smooth to rough. Journal of Fluid Mechanics, 48:721-761.

ARIE, M. and ROUSE, H. (1956). Experiments on two dimensional flow over a normal wall. Journal of Fluid Mechanics, 1:129-141.

BACHE, D.H. and UNSWORTH, M.H. (1977). Some aerodynamic features of a cotton canopy. Quarterly Journal of the Royal Meteorological Society. 103: 121-134.

BAINES, G.B.K. (1972) Turbulence in a wheat crop. Agricultural Meteorology, 10:93-105.

BATZR, H.O. (1960) Two cases of wind damage to Balsam Fir after cutting. No. 590, Technical Notes. Lake States Forest Experiment Station, U.S. Department of Agriculture.

BEARMAN, P.W. (1972). Some recent measurements of the flow around bluff bodies in smooth and turbulent streams. Symposium on External Flows, University of Bristol, p. B1-B15.

BERGEN, J.D. (1971). Vertical profiles of windspeed in a pine stand. Forest Science, 17: 314-321.

BILL, K.R.G., ALLEN, L.H., AUDUNSON, T., GEBHART, B. and LEMON, E. (1976). Turbulent transport within and above a Maine canopy. Boundary Layer Meteorology, 10:199-220 .

BOE, K.H. (1965). Windfall after experimental cuttings in Old-growth Redwood. Proc. Soc. Amer. For. 59-63.

BOOTH, T.C. et al (1976). Wind conditions over the forest Ae in South Scotland. Report No. TVL/7620, University of Bristol (unpublished). 12 p.

BOWEN, A.J. (1979). Some effects of escarpments on the atmospheric boundary-layer. Ph.D. Thesis, University of Canterbury, Christchurch, N.Z. 322 p.

BRADLEY, E.F. (1968). A micrometeorological study of velocity profiles and surface drag in the region modified by a change in surface roughness. Quarterly Journal of the Royal Meteorological Society, 94: 361-379.

BRADLEY, E.F. (1980). An experimental study of the profiles of wind speed, shearing stress and turbulence of the crest of a large hill. Quarterly Journal of the Royal Meteorological Society, 106: 101-123.

BULL, G.A.D. and REYNOLDS, E.R.C. (1968). Wind turbulence generated by vegetation and its implications. Supplement to Forestry. Oxford Univ. Press: 28:37.

CIONCO, R.M. (1978). Analysis of canopy index values for various canopy densities. Boundary-Layer Meteorology, 15:81-93.

CIONCO, R.M. (1983). On the coupling of canopy flow to ambient flow for a variety of vegetation types and densities. Boundary-Layer Meteorology 26: 325-335.

COOK, N.J. (1972). Wind tunnel simulation of the atmospheric boundary layer: methods in current use at Bristol. Symposium on External Flows, University of Bristol. p. f1-f3.

COOK, N.J. and HEPPEL, F.J. (1976). Data for the wind tunnel simulation of the adiabatic atmospheric boundary layer. Part A; Flow over 100 mm x 50 mm x 50 mm blocks., BRE. Note N96/76. 12 p.

COOPER, R.W. (1965). Wind movement in pine stands. Georgia Forest Research Paper No. 33, Georgia Forest Research Council. 4 pp.

COUNIHAN, J. (1971). Wind tunnel determination of the roughness length as a function of the fetch and the roughness density of three dimensional roughness elements. Atmospheric Environment, 5:637-642.

COUNIHAN, J. (1972). The structure and the wind tunnel simulation of rural and urban adiabatic boundary layers. Symposium on External Flows, University of Bristol, p. E1-E15.

COUNIHAN, J. (1975). Adiabatic atmospheric boundary layers: a review and analysis of data from the period 1880-1972. Atmospheric Environment, 9: 871-905.

CREMER, K.W. (1975). 1974 wind damage in A.C.T. plantations. Pers. Com. Letter KWC/HF.

CREMER, K.W. et al (1977). Silvicultural lessons from the 1974 windthrow in radiata pine plantations near Canberra, Australian Forestry, 40:274-292.

CREMER, K.W., BOROUGH, C.J., McKINNELL, F.H., CARTER, P.R., (1982). N.Z. Journal of Forestry Science, 12:244-268.

DAVENPORT, A.G. (1967). Gust loading factors. Journal of the Structural Division, ASCE, ST3. p.11-34.

DAVENPORT, A.G., VICKEY, B.J. and MELBOURNE, W.H. (1975). The structural and environmental effects of wind on buildings and structures. 16 lectures (unpublished).

DAVIS, F.K. and NEWSTEIN, H. (1968). The variation of gust factors with mean wind speed and with height. Journal of Applied Meteorology, 7:372-278.

DORAN, J.C. and POWELL, D.C. (1982). Gust structure in the neutral surface boundary layer. Journal of Applied Meteorology, 21:14-17.

ENGINEERING SCIENCES DATA UNIT, (1974). Characteristics of atmospheric turbulence near the ground, Part II, ESDU Item 74031, Regent St., London, 29 p.

ENGINEERING SCIENCES DATA UNIT, (1975). Characteristics of atmospheric turbulence near the ground, Part III, ESDU Item 75001, Regent St., London, 27 p.

FLAY, R.G.J. (1978). Structure of a rural atmospheric boundary layer near the ground. University of Canterbury, Christchurch. Thesis for degree of Ph.D. in Mechanical Engineering. 400p.

FABER, P.J. (1975). Stability of stands to wind: a theoretical approach. Translated by M. Goosens (1978). Nederlands Bosbouw Tijdschirift, 47:179-193.

FERNOW, B.E. (1909). A brief history of forestry in Europe, the United States and other countries. University Press, Toronto. 438 p.

FINNIGAN, J.J. (1979). Turbulence in waving wheat. I. Mean Statistics and Honami. Boundary-Layer Meteorology, 16:181-211.

FINNIGAN, J.J. (1979). Turbulence in waving wheat. II. Structure of Momentum Transfer. Boundary-Layer Meteorol. (following paper).

FINNIGAN, J.J. and MULHEARN, P.J. (1978a). Modelling waving crops in a wind tunnel. Boundary Layer Meteorol. 14:253-277.

FINNIGAN, J.J. and MULHEARN, P.J. (1978b). A simple mathematical model of airflow in waving plant canopies. Boundary-Layer Meteorology, 14:415-431.

FRASER, A.I. (1962)a. The soil and roots as factors in tree stability. Forestry, 35:117-127.

FRASER, A.I. (1962)b. Wind tunnel studies of the forces acting on the crowns of small trees. Report on Forest Research, British Forestry Commission. p.178-183.

FRASER, A.I. (1963). Wind tunnel and other related studies on coniferous trees and tree crops. Scottish Forestry, 18:84-92.

FRASER, A.I. (1968). Recording some aspects of a forest environment. Blackwell Scientific Publications. Oxford and Edinburgh: 235-242.

FRASER, A.I. and GARDINER, J.B.H. (1967). Rooting and stability in Sitka spruce. Bulletin Forestry Commission, H.M.S.O., No.40. 28 p.

FREESTON, D.H. (1974). Atmospheric shear flows over ramps and escarpments. Paper presented at the Fifth Australasian Conference on Hydraulics and Fluid Mechanics, University of Canterbury, Christchurch, New Zealand. 7 p.

FROST, W. (1974). Wind fields over terrain irregularities. Aspects of NASA's Wind Energy Program. p.80-106.

GARRATT, J.R. (1978a). Flux profile relations above tall vegetation. Quarterly Journal of the Royal Meteorological Society, 104:199-211.

GARRATT, J.R. (1978b). Transfer characteristics for a heterogeneous surface of large aerodynamic roughness. Quarterly Journal of the Royal Meteorological Society, 104:491-502.

GARTSHORE, I.S. (1973). A relationship between roughness geometry and velocity profile shape for turbulent boundary layers. LTR-LA-140 National Aeronautical Establishment, Ottawa, Canada, 27 p.

GILL, G.C. (1975). Development and use of the UVW anemometer. Boundary-Layer Meteorology, 8:475-495.

GILL, G.C., OLSSON, L.E., SELA, J. and SUDA, M. (1967). Accuracy of wind measurements on towers or stacks. Bulletin of the American Meteorological Society, 48:665-674.

HARRIS, R.I. (1970). The nature of the wind. Modern design of wind sensitive structures. Summary of proceedings of CIRIA Seminar 18.6.70, Institute of Engineers, England. Paper 3, p.29.

HARRIS, R.I. (1972). Measurements of wind structure. Symposium on external flows, Bristol University. p.H1-H31.

HICKS, B.B. (1973). Eddy fluxes over a vineyard. Agricultural Meteorology, 12:203-215.

HIRATA, T. (1951)a. Fundamental studies on the formation of cutting series (I). On the protection of a stand against storm damages. Bulletin of the Tokyo University Forests, 39:1-12.

HIRATA, T. (1951)b. Fundamental studies of the formation of cutting series (II). On the centre pressure, the drag coefficient of a tree and one effect of shelter belts. Bulletin of the Tokyo University Forests. 45:67-87.

HOAG, D.L. et al (1971). Experimental measurement of internal and external damping properties of tree limbs. Transactions of the American Society of Agricultural Engineers, p.20-28.

HOERNER, S.F. (1965). Fluid-dynamic drag. The Otterbein Press, Dayton, Ohio, U.S.A., 259 p.

HÖGSTRÖM, U., BERGSTRÖM, H. and ALEXANDERSSON, H. (1983). Turbulence characteristics in a near neutrally stratified urban atmosphere. Boundary-Layer Meteorology, 23:449-472.

HØJSTRUP, J. (1981). A simple model for the adjustment of velocity spectra in unstable conditions downstream of an abrupt change in roughness and heat flux. Boundary-Layer Meteorology, 21:341-356.

HOLBO, M.R., CORBETT, I.C. and HORTON, P.J. (1980). Aeromechanical behaviour of selected Douglas fir. Agricultural Meteorology, 21:81-91.

HORST, T.W. (1973). A computer algorithm for correcting non-cosine response in the Gill anemometer. Battelle North West Laboratories report. BNWL-1651, PT1.

HSI, G. and NATH, J.H. (1970). Wind drag within simulated forest canopies. Journal of Applied Meteorology, 9:592-602.

HUNT, J.C.R. (1972). Some theories for the mean and turbulent velocity distributions in flows around bluff bodies. Symposium on External Flows, University of Bristol, p.C1-C10.

HUNT, J.C.R. (1980). Wind over hills. American Meteorological Society. pp 107-144.

HUTCHINSON, J.R. et al (1970). Tree vibrations. Symposium on Structural Dynamics, Paper No. D.I., University of California, Davis. 21 p.

HÜTTE, P. (1968)a. Experiments on windflow and wind damage in Germany; site and susceptibility of spruce forests to storm damage. Supplement to Forestry. O.U.P., 1968, p.20-27.

HÜTTE, P. (1968)b. The site conditions that conduce to wind damage. Translated by E.W. Jones. Forst. Wiss., 86:276-297.

INOUE, E. (1955). Studies of the phenomena of waving plants ("HONAMI") caused by wind, Part 1. Mechanism and characteristics of waving plants phenomena. J. Agric. Meteorol. (Japan), 11:18-22.

JACKSON, D.S. (1974). Extreme weather events - problems of definition for forest management. Symposium on Meteorology and Forestry, N.Z. Meteorological Service, p.17-29.

JACKSON, P.S. and HUNT, J.C.R. (1975). Turbulent wind flow over a low hill. Quarterly Journal of the Royal Meteorological Society, 101: 929-955.

JACOBS, M.R. (1936). The effect of wind on trees. Australian Forestry 1(2), 25-32.

JENSEN, N.O. and PETERSON, E.W. (1978). On escarpment wind profile. Quarterly Journal of the Royal Meteorological Society, 104: 719-728.

JOHNSON, R.C., RAMEY, G.E. and O'HAGAN, D.S. (1982). Wind induced forces on trees. Journal of Fluids Engineering, 104: 25-30.

KAIMAL, J.C., WYNGAARD, J.C., HAUGEN, D.A., COTÉ, O.R. and IZUMI, Y. (1976). Turbulence structure in the convective boundary-layer, J. Atmos. Sci, 33:2152-2169.

KALMA, J.D. and STANHILL, G. (1972). The climate of an orange orchard: physical characteristics and micro climate relationships. Agricultural Meteorology, 10:185-201.

KAWATANI, T. and MERONEY, R.N. (1968). The structure of canopy flow field. Colorado State University, TR CER67-68TK66. 125 p.

KHALSA, S.J.S. and BUSINGER, J.A. (1977). The drag coefficient as determined by the dissipation method and its relation to intermittent convection in the surface layer. Boundary-Layer Meteorology, 12: 273-297.

KNIGHT, D.W. and MACDONALD, J.A. (1979). Hydraulic resistance of artificial strip roughness. Proceedings of the American Society of Civil Engineers, Vol.105, No.HY6. pp 675-690.

KOLMOGOROV, A.N. (1941). The local structure of turbulence in incompressible viscous fluid for very large Reynolds Numbers. Doklady, ANSSSR, 30, 301-305, (in Russian).

LANDSBERG, J.J. and JAMES, G.B. (1971). Wind profiles in plant canopies: studies on an analytical model. Journal of Applied Ecology, 8:729-741.

LANDSBERG, J.J. and POWELL, D.B.B. (1973). Surface exchange characteristics of leaves subject to mutual interference. Agricultural Meteorology, 12:169-184.

LANDSBERG, J.J. and THOM, A. S. (1971). Aerodynamic properties of a plant of complex structure. Quarterly Journal of the Royal Meteorological Society, 97:(414) 565-570.

LEGG, B.J. (1975). Turbulent diffusion within a wheat canopy: I measurement using nitrous oxide. Quarterly Journal of the Royal Meteorological Society, 101:597-610.

LEGG, B.J. and LONG, I.F. (1975). Turbulent diffusion within a wheat canopy: II results and interpretation. Quarterly Journal of the Royal Meteorological Society, 101:611-628.

LEWIS, N.B. (1963). Optimum thinning range of *Pinus radiata* in South Australia. Australian Forestry, 27: 113-120.

LO, A.K. (1977). Boundary-layer flow over gentle curvilinear topography with a sudden change in surface roughness. Quarterly Journal of the Royal Meteorological Society, 103:199-209.

LOO, S.P. (1975). The aerodynamic characteristic of a flexure structure (tree). University of Canterbury, N.Z. (Thesis: M.E.) 208 p.

LOUIS, J.F., WEILL, A. and VIDAL-MADJAR, D. (1983). Dissipation length in stable layers. Boundary-Layer Meteorology, 25:229-243.

MACDONALD, A.J. and MORGAN, J. (1967). A method for calculating the vibration amplitudes of slender structures in turbulent winds. ASCE Environmental Conference, University of Edinburgh, 11 p.

MAITANI, T. (1978). On the downward transport of turbulent kinetic energy in the surface layer over plant canopies. Boundary-Layer Meteorology, 14:571-584.

MAITANI, T. (1979). An observational study of wind-induced waving of plants. Boundary-Layer Meteorology, 16:49-65.

MARTIN, H.C. (1971). Average winds above and within a forest. Journal of Applied Meteorology, 10:1132-1137.

MASON, P.J. and SYKES, R.I. (1979). Separation effects in Ekman Layer flow over ridges. Quarterly Journal of the Royal Meteorological Society, 105:129-146.

MASSEY, B.J. (1971). Mechanics of fluids, 2nd edition. Van Nostrand, Reinhold, London, 508 pp p.290-296.

MAYER, H. (1981). Wind gustiness at the tree top in a spruce forest. Translated by W. Linnard. Archives for Meteorology, Geophysics and Bioclimatology, 29:181-190.

MAYHEAD, G.J. (1973)a. Sway periods of forest trees. Scottish Forestry, 27:19-23.

MAYHEAD, G.J. (1973)b. Some drag coefficients for British forest trees derived from wind tunnel studies. Agricultural Meteorology, 12:123-130.

MERONEY, R.N. (1968). Characteristics of wind and turbulence in and above model forests. Journal of Applied Meteorology, 7:780-788.

MERONEY, R.N. (1970). Wind tunnel studies of the air flow and gaseous plume diffusion in the leading edge and downstream regions of a model forest. Atmospheric Environment, Pergamon Press, 4:597-614.

MING, Z., PANOFSKY, H.A., BALL, R. (1983). Wind profiles over complex terrain. Boundary-Layer Meteorology 25:221-228.

MULHEARN, P.J. (1977). Relations between surface fluxes and mean profiles of velocity, temperature and concentration, downwind of a change in surface roughness. Quarterly Journal of the Royal Meteorological Society, 103:785-802.

MULHEARN, P.J. (1978). A wind-tunnel boundary layer study of the effects of a surface roughness change: rough to smooth. Boundary-Layer Meteorology, 15:3-30.

MUNRO, D.S. and OKE, T.R. (1973). Estimating wind profile parameters for tall dense crops. Agricultural Meteorology, 11:223-228.

NARASIMHA, R. and SREENIVASAN, K.R. (1973). Relaminarization in highly accelerated turbulent boundary layers. Journal of Fluid Mechanics, 61:417-447.

NEAL, D. (1979). Wind flow and structure over Gebbies Pass, New Zealand. A comparison between a wind tunnel simulation and field measurements. Ph.D. Thesis. University of Canterbury. 486 p.

OLIPHANT, J.E. (1964). Growth of the internal boundary layer following large changes in surface roughness. Thesis presented in partial fulfilment of the requirements for the degree of Master of Science in Meteorology. The Pennsylvania State University, 45 pp.

OKE, T.R. (1970). Turbulent transport near the ground in stable conditions. Journal of Applied Meteorology, 9:778-785.

OLIVER, H.R. (1971). Wind profiles in and above a forest canopy. Quart. J.R. Met. Soc. 97:548-553.

PANCHEV, S., DONEV, E. and GODEV, N. (1971). Wind profile and vertical motions above an abrupt change in surface roughness and temperature. Boundary-Layer Meteorology, 2:52-63.

PANOFSKY, H.A., LARKO, D., LIPSCHUTZ, R., STRONG, G., BRADLEY, E.F., BOWEN, A.J. and HØJSTRUP, J. (1982). Spectra of velocity components over complex terrain. Quarterly Journal of the Royal Meteorological Society, 108:215-230.

PANOFSKY, H.A., MAZZOLA, C.A., WOODS, J. and EIDSVIK, K. (1970). Turbulence characteristics over heteorogeneous terrain. Research and Development Technical Report Ecom-0079-F. The Pennsylvania State University, University Park, Pennsylvania, 77 p.

PANOFSKY, H.A. and TOWNSEND, A.A. (1964). Change of terrain roughness and the wind profile. Quart. J.R. Met. Soc., 90:147-155.

PAPESCH, A.J.G. (1970). Researchers seek ways to reduce forest windthrow losses. Forest Industries Review, [illegible] Vol 1 no 11 pg 2-4

PAPESCH, A.J.G. (1971). The problem of wind damage in Canterbury forests. N.Z. Engineering, 26:293-297.

PAPESCH, A.J.G. (1974). A simplified theoretical analysis of the factors that influence windthrow of trees. Fifth Australasian Conference on Hydraulics and Fluid Mechanics, University of Canterbury, Christchurch. p.235-242.

PAPESCH, A.J.G. (1977). A field study to determine the drag coefficient and the associated centre of pressure of a forest front. Sixth Australasian Conference on Hydraulics and Fluid Mechanics, Adelaide, p.451-454.

PEARSE, J.R., LINDLEY, D. and STEVENSON, D.C. (1981). Wind flow over ridges in simulated atmospheric boundary layers. Boundary-Layer Meteorology, 21:77-92.

PETERSON, E.W. (1969). Modification of mean flow and turbulent energy by a change in surface roughness under conditions of neutral stability. Quarterly Journal of the Royal Meteorological Society, 95:561-575.

PETERSON, E.W. (1975). The Risø Profiles: a study of wind and temperature data from the 123 m tower at Risø, Denmark. Quarterly Journal of the Royal Meteorological Society, 101:107-117.

PETERSON, E.W., KRISTENSEN, L. and CHANG-CHUN SU. (1976). Some observations and analysis of wind over non-uniform terrain. Quarterly Journal of the Royal Meteorological Society, 102:857-869.

PIELKE, R.A. and PANOFSKY, H.A. (1970). Turbulence characteristics along several towers. Boundary-Layer Meteorology, 1:115-130.

PLATE, E.J. and QURAISHI, A.A. (1965). Modelling of velocity distributions inside and above tall crops. Journal of Applied Meteorology, 4:400-408.

POPE, A. and HARPER, J.J. (1966). Low speed wind tunnel testing. John Wiley and Son Inc., New York, 457 p.

POPPENDIEK, H.F. (1949). Investigation of velocity and temperature profiles in air layer and within and above trees and bushes. University of California Department of Engineering. NR-082-036. 45 p.

PRESTON, A.P. (1969). The wind factor in orchard tree spacing. Scientific Horticulture, 17:17-74.

RAINE, J.K. (1974). Modelling the natural wind: wind protection by fences. University of Canterbury, N.Z. 2 Vol. 559 p. (Thesis: Ph.D. Engineering).

RAO, K.S., WYNGAARD, J.C. and COTÉ, O.R. (1974). The structure of the two-dimensional internal boundary layer over a sudden change of surface roughness. Journal of the Atmospheric Sciences, 31:738-746.

RAYMER, W.G. (1962). Wind resistance of conifers. National Physical Laboratory, England. Aero Report No.1008. 14 p.

RAYNOR, G.S. (1971). Wind and temperature structure in a coniferous forest and a contiguous field. Forest Science, 17(3):351-363.

RAYNOR, G.S., HAYES, J.V. and OGDEN, E.C. (1974). Particulate dispersion into and within a forest. Boundary-Layer Meteorology, 7:429-456.

RAYNOR, G.S., HAYES, J.V. and OGDEN, E.C. (1975). Particulate dispersion from sources within a forest. Boundary-Layer Meteorology, 9:257-277.

RAYNOR, G.S., OGDEN, E.C. and HAYES, J.V. (1974). Enhancement of particulate concentrations downwind of vegetative barriers. Agricultural Meteorology, 13:181-188.

RAYNOR, G.S., OGDEN, E.C. and HAYES, J.V. (1976). Dispersion of fern spores into and within a forest. Rhodora, 78(815):473-487.

REDFORD, T.G., VERMA, S.B., ROSENBORG, N.J., (1981). Drag anemometer measurements of turbulence over vegetated surfaces. Journal of Applied Meteorology, 20: 1222-1230.

REIFSNYDER, W.E. (1955). Wind profiles in a small isolated forest stand. Forest Science, 1:289-297.

ROBINSON, S.M. (1962). Computing wind profile parameters. Journ. Atmos. Sci., 19:189-190.

SADEH, W.Z., CERMAK, J.E. and KAWATANI, T. (1971). Flow over high roughness elements. Boundary-Layer Meteorology, 1:321-344.

SADEH, W.Z. and FOX, D.G. (1982). Canopy effects on turbulence and diffusion. Proceedings of the Workshop on the Parameterization of mixed layer diffusion, 217-234 p.

SAUER, et al (1951). Experimental investigation of aerodynamic drag in tree crowns exposed to steady wind - conifers. U.S. Department of Agriculture Forest Service, Rep. Div. Forest Fire Res.

SAUGIER, B. and RIPLEY I.A. (1978). Evaluation of the aerodynamic method of determining fluxes over natural grassland. Quart. J. Royal Met. Soc., 194:257-270.

SEGINER, I. (1972). Windbreak drag calculated from the horizontal velocity field. Boundary-Layer Meteorology, 3:87-97.

SHAW, R.H. and PEREIRA, A.R. (1982). Aerodynamic roughness of a plant canopy: A numerical experiment. Agricultural Meteorology, 26:51-65.

SHINN, J.H. (1969). Analysis of wind data from a South Carolina coastal forest. U.S. Army Electronics Command, Atmos. Sci. Lab., Arizona. R & DTR, ECOM-6036. 23 p.

SILBERT, M.N. (1970). A structured fluids approach to canopy flow. New York University Contract No. NR 285 (57). 27 p.

SIMUI, E. (1980). Revised procedure for estimating along-wind response. Journal of the Structural Division, ASCE, ST1, 106:1-10.

SMITH, D.M. (1946). Storm damage in New England forests. University of Yale. (Thesis). 173 p.

SMITH, F.B., CARSON, D.J. and OLIVER, H.R. (1972). Mean wind direction shear through a forest canopy. Boundary-Layer Meteorology, 3:178-190.

SOLARI, G. (1982). Along-wind response estimation: Closed form solution. Journal of the Structural Division, ASCE, ST1, 108:225-244.

SOMERVILLE, A. (1978). Patterns of wind damage in the Canterbury Plain forests. N.Z. Forest Service Forest Research Institute, Report No.111. 12 p. (unpublished).

SREENIVASAN, K.R. (1973). Rapid distortion of axisymmetric turbulence. Curr. Sci., 42:632-634.

SREENIVASAN, K.R. and NARASIMHA, R. (1974). Rapid distortion of shear flows. From Aero Society of India Silver Jubilee Technical Conference, Bangalore. Paper 2:11-13.

STEVENSON, D.C. and NEAL, D. (1983). Fullscale measurements of velocity, Reynolds stress, spectra and cospectra upwind and at the crest of a large hill in complex terrain. Eighth Australian Fluid Mechanics Conference, University of Newcastle, N.S.W., A14-17.

STEWART, J.B. and THOM, A.S. (1973). Energy budgets in a pine forest. Quarterly Journal of the Royal Meteorological Society, 99: 154-170.

SWALE, B.J. (1983). Wind and forests - A review, with special reference to the choice of silvicultural systems for the state pine forests of the Canterbury Plains. Paper prepared for a review of the management of Canterbury Plains State Forests, Christchurch, 19 p.

TEUNISSEN, H.W. (1970). Characteristics of the mean wind and turbulence in the planetary boundary layer. Institute for aerospace studies, University of Toronto, UTIAS review No. 32:221 pp.

TEUNISSEN, N.W. (1980). Structure of mean winds and turbulence in the planetary boundary layer over rural terrain. Boundary-Layer Meteorology, 19:187-221.

THOM, A.S. (1971). Momentum absorption by vegetation. Quart. J. R. Met. Soc., 97:414-428.

THOM, A. S. (1972). Momentum, mass and heat exchange of vegetation. Quart. J. R. Met. Soc., 98:124-134.

THOM, A.S., STEWART, J.B., OLIVER, N.R. and GASH, J.A.C. (1975). Comparison of aerodynamic and energy budget estimates of fluxes over a pine forest. Quarterly Journal of the Royal Meteorological Society, 101:93-105.

UCHIJIMA, Z. and WRIGHT, J.L. (1964). An experimental study of air flow in a corn-plant-air layer. Japan. Bull. Nat. Inst. Agri. Sci. Ser. A, No.11:19-65.

VALENDIK, E.N. (1964). The penetration and transformation of wind in pine forests. Moscow, Izdatelstvo "Nauka". p.61-82.

VELLOZI, J. and COHEN, E. (1968). Gust response factors. Journal of the Structural Division, ASCE, ST6.94:1295-1313.

WALSHE, D.E. (1972). Wind-excited oscillations of structures. London, H.M.S.O. 71 p.

WALSHE, D.E. and FRASER, A.I. (1963). Wind tunnel tests on a model forest. NPL Aero Report 1078. 20 p.

WARDLAW, R.L. and COOPER, K.R. (1974). The aeroelastic instability of slender cylinders and wakes. The Fifth Australasian Conference on Hydraulics and Fluid Mechanics, Christchurch, N.Z. (unpublished), 8 p.

WENDELKEN, W.J. (1966). Eyrewell Forest: a search for stable management. N.Z. Journal of Forestry, 11:43-65.

WHITE, R.G., WHITE, M.F., MAYHEAD, G.S. et al (1975). Measurement of the motion of trees in two dimensions. Institute of Sound and Vibration Research, University of Southampton, Technical Report No.86, 22 p.

WHITESIDE, I.D. (1978). The quality of Radiata pine framing timber from Eyrewell Forest. Workshop on Canterbury Forests. (unpublished). 225 p.

WOOD, D.M. (1978). Calculations of the neutral wind profile following a large step change in surface roughness. Quarterly Journal of the Royal Meteorological Society, 104:383-392.

WOODING, R.A., BRADLEY, E.F. and MARSHALL, J.K. (1973). Drag due to regular arrays of roughness elements of varying geometry. Boundary-Layer Meteorology, 5:285-308.

APPENDIX I

Sample calculation of along-wind response

(a) Simple solution

(b) Complex solution

APPENDIX I

SAMPLE CALCULATION OF ALONG-WIND RESPONSE

AI.1 SIMPLE SOLUTION

AI.1.1 Relationships

Suppose the initial conditions are always zero (D = 0) and the fluctuating motion is due only to a harmonic sinusoidal wind force. The motion takes place at the wind forcing frequency ($w = 2\pi n_{pk_w}$) but lags behind the applied wind force by angle ϕ_R. The amplitude of the motion is,

$$X_R = \frac{n_o^2 \frac{F_w}{k_s}}{\left[(n_o - n_{pk_w}^2)^2 + (2\zeta\, n_o\, n_{pk_w})^2\right]^{\frac{1}{2}}}$$

Now, the value $\frac{F_w}{k_s}$ is wind force due to turbulence divided by the stiffness of the tree, and is the deflection which the tree would produce if the turbulence force was applied statically. It is therefore equivalent to the background turbulence. The ratio of the resonant deflection X_R to the background deflection X_B is M_R.

Since the admittances are all unity,

$$X_B = \frac{F_w}{k_s} \times 1,$$

and

$$M_R = \frac{X_R}{\frac{F_w}{k_s}} = \frac{X_R}{X_B}$$

So,

$$M_R = \left[\left(1 - \left(\frac{n_{pk_w}}{n_o}\right)^2\right)^2 + \left(\frac{2\zeta n_{pk_w}}{n_o}\right)^2\right]^{-\frac{1}{2}}.$$

The phase angle between the two components of deflection and the wind sinusoidal input is

$$\phi_R = \tan^{-1} \frac{\frac{2\zeta n_{pk_w}}{n_o}}{1 - \left(\frac{n_{pk_w}}{n_o}\right)^2}$$

If the damping is small ($\zeta << 1$), M_R is very high when n_{pk_w} and n_o are close together and the phase angle is also small.

M_R is the ratio at resonant sinusoidal input, to the background effect from the same input and so M_R is equivalent to $\sqrt{\frac{R}{B}}$ for random signal inputs.

AI.1.2 Calculation of M_R and ϕ_R

(a) Pattern P + 3 H (see Fig. 6.34(a)-(d))

ζ = 0.08 = constant ,

n_o = 8.9 Hz = constant ,

n_{pk_w} = 6.9 Hz = frequency at spectrum peak (Table 6.8).

so,

$$M_R = \left[\left(1 - \left(\frac{6.9}{8.9}\right)^2\right)^2 + (2 \times 0.08)^2 \left(\frac{6.9}{8.9}\right)^2\right]^{-\frac{1}{2}}$$

$$= \left[(1 - (0.775)^2)^2 + 0.16^2 (0.775)^2\right]^{-\frac{1}{2}}$$

$$= \left[(1 - 0.601)^2 + 0.0256 \times 0.601\right]^{-\frac{1}{2}}$$

$$= \left[0.159 + 0.015\right]^{-\frac{1}{2}}$$

$$\underline{M_R = 2.39}$$

$$\text{Tan}\phi_R = \frac{2 \times 0.08 \times \frac{6.9}{8.9}}{\left[1 - \left(\frac{6.9}{8.9}\right)^2\right]} ,$$

$$\text{Tan}\phi_R = \frac{0.16 \times 0.775}{(1 - (0.775)^2)} ,$$

$$\phi_R = \tan^{-1} \frac{0.124}{0.399} ,$$

$$\underline{\phi_R = 17.23^{\circ}} .$$

(b) Tree 81 (Rivox) $\zeta = 0.08$, $n_o = 0.42$ Hz, $n_{pk_W} = 0.05$ Hz

$$M_R = \left[\left[1 - \left(\frac{0.1}{0.42}\right)^2\right]^2 + \left[2 \times 0.08 \times \frac{0.1}{0.42}\right]^2\right]^{-\frac{1}{2}} ,$$

$$= \left[0.890 + 0.002\right]^{-\frac{1}{2}}$$

or $M_R = 1.06$ for $\frac{S}{H} = 0.186$,

and $\phi_R = 1.2^{\circ}$.

Note: This implies that tree response is shared equally between the background and resonant components of sway motion.

AI.1 COMPLEX SOLUTION

AI.2.1 Calculation Methods

AI.2.1.1 Tree as a point-like structure

(The general relationships are presented in 3.10. Model tree dimensions are given in Figure 6.15).

Theoretically the wind forces are zero at $d + z_o''$. The smallest value of the local aerodynamic roughness in the inner layer is the height for the largest crown width ($C_{z_o''}$) so,

$$z_o'' = 0.05\ H = 10 \text{ mm} ,$$

$$\frac{C_{z_o''}}{40} = \frac{200 - (d + z_o'')}{130} ,$$

$$C_{z_o''} = 12.3 \text{ mm} ,$$

$$\frac{C_{z_o''}}{H} = 0.06 .$$

The height of the crown at this crown width is

$$\frac{H_{z_o}''}{130} = \frac{12.3}{40}$$

$$\text{or,} \quad \frac{H_{z_o}''}{H} = 0.20 \ .$$

Both these values for the width and height of the tree crown, influenced by the wind, are within the limit of 0.5 suggested by Solari, for point-like treatment for the along-wind response estimation.

AI.2.1.2 Resonant aerodynamic admittance, F_2

$$|J_{y_R}|^2 = G\left(\frac{2.56\ \hat{n}_o\ C_{z_o}''}{H \quad P}\right) \qquad \text{. . . . . Solari}$$

$$|J_{y_R}|^2 = G\left(2.56\ \frac{n_o H}{\bar{U}_{*\ell}} \cdot \frac{C_{z_o}''}{H} \cdot \frac{\bar{U}_{*\ell}}{\bar{U}_H k_a}\right)$$

$$= G\left(\frac{2.56\ n_o\ C_{z_o}''}{0.41 \quad \bar{U}_H}\right)$$

$$= G(f_1)$$

So, for $|J_{y_R}|^2$,

$$G(f) = \frac{1}{f} - \frac{1}{2f^2}\left(1 - e^{-2f}\right) \qquad \text{. . . . . Solari}$$

Similarly, $|J_{z_R}|^2 = G\left(\frac{1.60\ .\ n_o\ H_{z_o}''}{0.41 \quad \bar{U}_H}\right) = G(f_2)$

Also, $N_f = G\left(\frac{15.4\ x\ n_o\ x\ C_{z_o}''}{0.41 \quad \bar{U}_H}\right) = G(f_3)$.

Now, $C_{D_f}^2 = C_{D_F}^2 + 2\ C_{D_F}\ C_{D_W}\ .\ N_f\ .\ + C_{D_W}^2$.

Also, $C_{D_F} = \frac{2}{3}\ C_{D_\ell}$ and $C_{D_W} = \frac{1}{3}\ C_{D_\ell}$ . . . . . Solari

so, $$\left(\frac{C_{D_f}}{C_{D_\ell}}\right)^2 = \frac{5}{9} + \frac{4}{9} G(f_3)$$

Hence $$F_2 = \left(\frac{C_{D_f}}{C_{D_\ell}}\right)^2 \cdot |J_{z_R}|^2 \cdot |J_{H_R}|^2 \quad .$$

AI.2.1.3 Background total admittance term (F_1)

Because the aerodynamic joint acceptance functions are constant and the mechanical admittance is unity,

$$F_1 = \frac{1}{1.06 + 0.4 \frac{C_{z_o}''}{H} + 0.25 \frac{H_{z_o}''}{H} - 0.23 \frac{C_{z_o}''}{H} \cdot \frac{H_{z_o}''}{H}} \quad \text{. . . Solari}$$

AI.2.1.4 Integrals for numerical solutions

The Integrals I_1, I_2, and I_3, are first, second, and third moments of area integrals, which define the location of the centre of pressure and its 'line of action' on the tree crown area $\left(\frac{H_{z_o}'' \times C_{z_o}''}{2}\right)$. Since the wind profile has been measured, the deflection modal shape of the stem is $(\frac{z}{H})^{1.5}$ (Walshe) and the crown width is defined as triangular, by normalising using H,

$$I_1 = \int_o^1 \hat{U}^2 . \hat{z}^{1.5} . \left(\frac{H-z}{H-70}\right) . d\hat{z} \quad ,$$

$$I_2 = \int_o^1 \hat{U} . \hat{z}^{1.5} . \left(\frac{H-z}{H-70}\right) . d\hat{z} \quad ,$$

$$I_3 = \int_o^1 1 . \hat{z}^{1.5} . \left(\frac{H-z}{H-70}\right) . d\hat{z} \quad ,$$

and I_3 = constant (0.138) .

Inspection of the mean windspeed profiles shows that the value H_{z_o} and I_3 (=70 mm) is below d.

AI.2.1.5 Spectra areas

The area of the non-dimensionalised power spectral density distribution represents the turbulent kinetic energy at the frequency bondwidth considered. The model trees have a frequency range of 5.3 Hz to 18.2 Hz, with an average of 8.9 Hz.

A_R = Area of the power spectrum curve between 5.3 Hz and 18.2 Hz.

$\simeq$ turbulent kinetic energy for resonant response.

A_B = Total Area $(A_B + A_R) - A_R$

= Total Variance $(\sigma_u^2) - A_R$

$\simeq$ turbulent kinetic energy for background response.

AI.2.1.6 Calculation of $\frac{A}{D}$, $A.M_T$, $D.M_T$.

To calculate these deflections (Figs 6.36, 6.37, 6.38),

(a) obtain values of σ_{u_H}, $\bar{U}_H$ from the wind profile data. Calculate B and R (see AI.2.2.7), and then $\frac{A}{D}$

(b) find C_{D_ℓ}, ρ, ζ, H, C_{z_o}'', n_o and $\bar{U}_H$ from tables and calculate K_T, and hence $A.M_T$ and $D.M_T$.

AI.2.1.7 Flowchart for B and R calculation

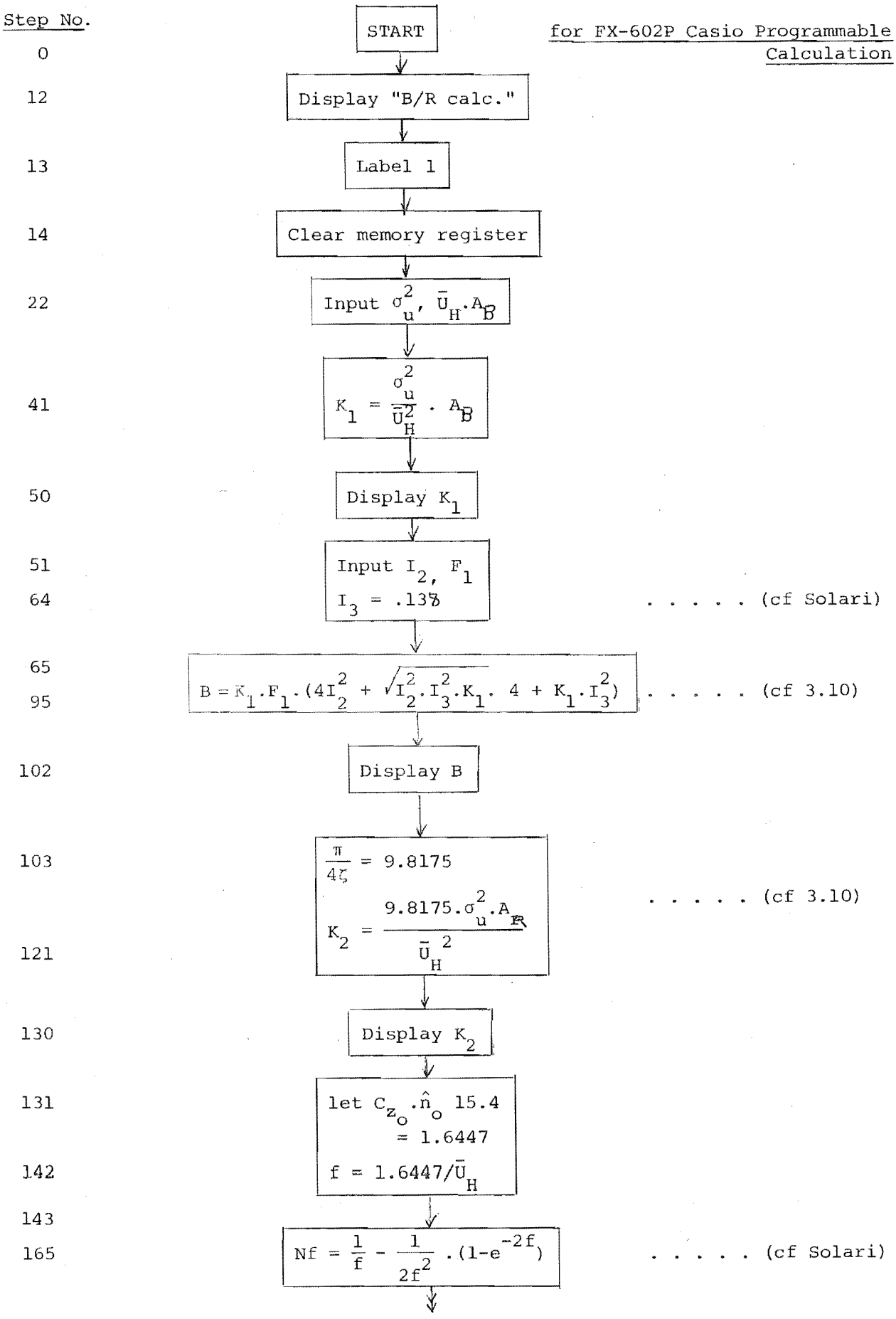

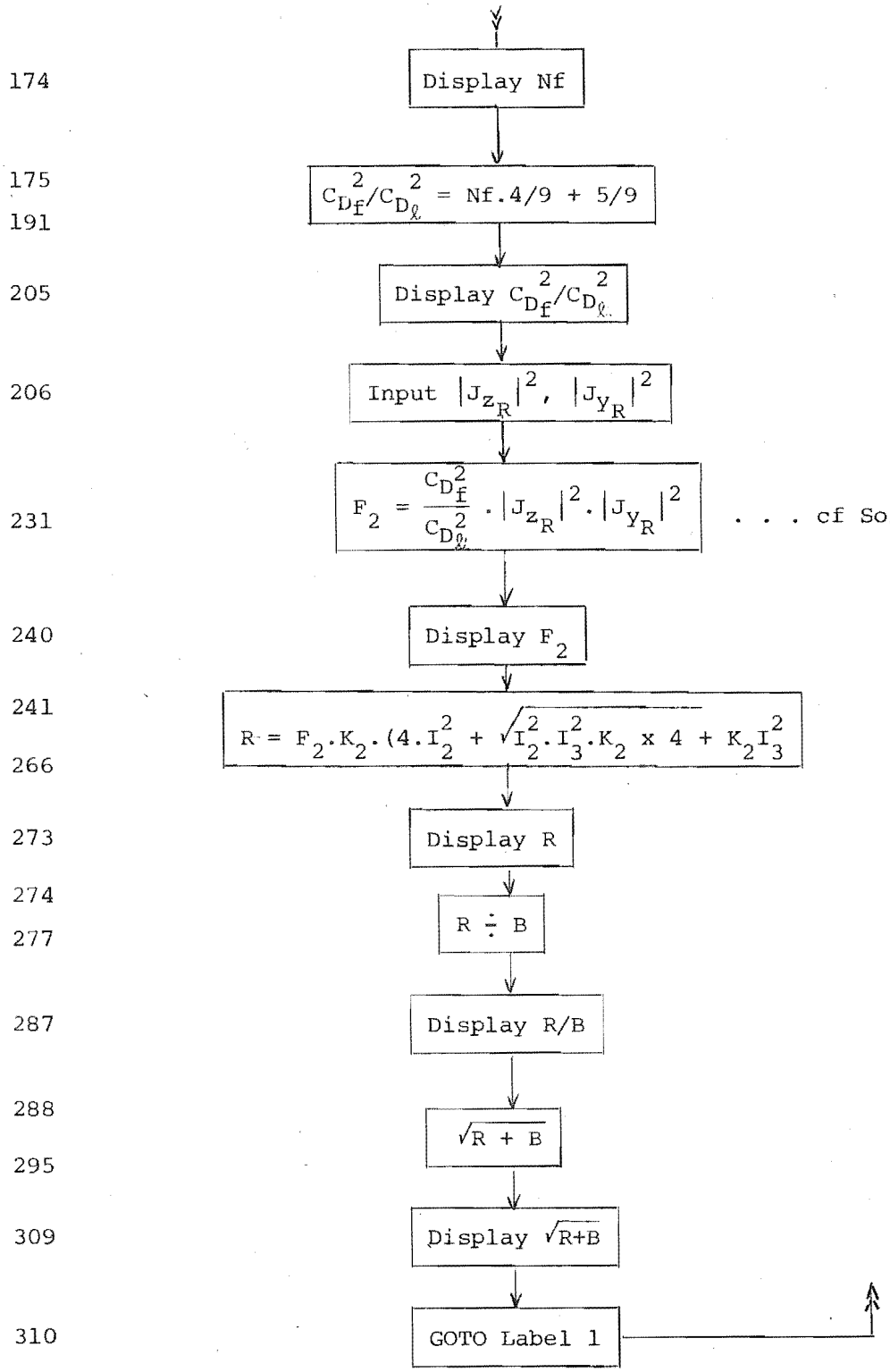
174
Display Nf
175
191
$C_{D_f}^2/C_{D_\ell}^2 = Nf.4/9 + 5/9$
205
Display $C_{D_f}^2/C_{D_\ell}^2$
206
Input $|J_{z_R}|^2$, $|J_{y_R}|^2$
231
$F_2 = \frac{C_{D_f}^2}{C_{D_\ell}^2} . |J_{z_R}|^2 . |J_{y_R}|^2$
. . . cf Solari.
240
Display F_2
241
$R = F_2.K_2.(4.I_2^2 + \sqrt{I_2^2.I_3^2.K_2 \times 4} + K_2 I_3^2$
266
273
Display R
274
R ÷ B
277
287
Display R/B
288
$\sqrt{R + B}$
295
309
Display $\sqrt{R+B}$
310
GOTO Label 1

APPENDIX II

Some definitions.

APPENDIX II

SOME DEFINITIONS

Definitions of some of the terms used in this thesis are listed below:

Aerodynamic admittance

The translation of the wind velocity fluctuations into aerodynamic forces on a tree depends on the aerodynamic admittance. This quantity takes into account the spatial characteristics of the turbulence and their organisation over the tree crown, and also a factor which might be termed the aerodynamic efficiency of the tree in generating forces. Aerodynamic admittance is low and mechanical admittance is high at resonance. Aerodynamic and mechanical admittances are both unity for background response.

Aerodynamic roughness height

Aerodynamic roughness height enters as a constant of integration into the form of the logarithmic velocity profile appropriate to fully rough flow near a surface. It is proportional to the average height of the elements responsible for the roughness of the surface. Over rough surfaces when the wind forces are in equilibrium it is about 10% of the height of the elements producing the rough surfaces (viz; 10% of the tree crown depth).

Aliasing

Due to the finite intervals between observations, energy with fluctuations of frequency greater than half the sampling frequency is distributed in the spectrum, into frequencies below this value. The half-sampling frequency is called the Nyquist, or folding frequency, and represents the absolute maximum usable frequency in the analysis of wind spectra.

Auto correlation

Auto correlation signifies correlation within a series of observations at a single point in space, at equal intervals of time. The measure of the auto correlation coefficient (= 1.0 at zero time lag) is frequently employed as a measure of the degree of persistence within a time series. Evaluated for lags of a range of intervals, the curves can be used to find the 'average' size of the eddies in a boundary layer.

Coherence

This is also called the cross-spectral density distribution and is a cross-coupling which quantifies the interdependence of two or more modes of fluctuations, whether aero-mechanical or purely mechanical. It includes correlation factors which vary with frequency and describe the statistical relationship between the modes. At a point in space coherence is unity, and so for point-like structures coherence is small for resonant conditions, and unity for non-resonant conditions.

Friction velocity

This is a surface roughness reference velocity used to relate wind speed profiles to the shear stresses exerted on a surface by the wind. So, it is directly related to the standard deviation of the turbulent (r.m.s.) component of the wind. It is normally ¼ of the turbulent windspeed.

Kolmogorov constants

Von Karman's constant is strongly related to the Kolmogorov constant. In the Kolmogorov range of heights the values of u' and v' do not differ from place to place. The Kolmogorov law has universal constants in the expression for wind spectra. The Kolmogorov cascade appears to be the dominant mechanism for the distribution of turbulent energy through the inertial sub-range. Reynolds number must be sufficiently high for the creation of such a sub-range. For along-wind spectra, the constant is $\frac{-5}{3}$ or $\frac{-2}{3}$, depending on axes chosen and whether or not spectral energy or spectral power is plotted against frequency.

Modal shape

This defines the deflected shape of a structure under loading in a non-dimensional form. The response of the structure is not sensitive to the exact form of the modal shape.

Monin-Obukhov length, and Richardson's number

The Monin-Obukhov relationship (as for the Ri_f) shows the relative importance of mechanical turbulence and heat convection.

Honami Waves

Patches of coherent waving in crops and forests caused by intermittent downward motion of vortex formations from the upper regions of the surface boundary layer to the earth's surface which superimpose on the normal surface winds.

$$Ri_f = \frac{g}{T}\frac{(\gamma d-\gamma)}{(\frac{\partial v}{\partial z})^2} \quad \text{and,} \quad \frac{z}{L} = -\frac{K_g H z}{\bar{U}_*^3 c_p \rho T} \quad ,$$

so, $$Ri_f \frac{K_H}{K_M} = \frac{k^*}{k_a}\frac{z}{L} \quad \text{or} \quad Ri_f \alpha \frac{z}{L} \quad .$$

where, K_H = eddy diffusivity for heat

K_M = eddy diffusivity for momentum

k^* = a dimensionless mixing coefficient similar to Von-Karman constant

k^* = k_a in neutral atmosphere near ground.

Power Law and Logarithmic Law

The boundary layer can be represented by either the Power Law or the Logarithmic Law. Most engineers use the Power Law, $(\frac{\bar{U}_z}{\bar{U}_g})^{\alpha}$, where α is the exponent. This exponent provides a ready way of defining the shape of the velocity profile for different surfaces; for instance $\alpha = 0.28$ for urban areas (Harris, 1972). The Logarithmic Law is suited for wind flow profiles over high roughness. The Power Law and the Logarithmic Law are related.

Power spectral density

The power spectral density is the variance and is the same as the turbulent wind component kinetic energy, at a specific frequency bandwidth, Δ_n. The energy contained in each frequency bandwidth can be compared to the whole frequency range in the natural wind by producing a spectrum of the distribution. The total spectrum area is unity when it is divided by the total variance $(\sigma_u)^2$. Fourier transforms relate power spectral densities to Auto-correlation functions.

Surface stress and surface stress coefficient

These are also referred to as the shear stress, Reynolds stress, or eddy shearing stress, and operate within a turbulent fluid to transport momentum. Horizontal stress is measured by the time average of the vertical and horizontal components of instantaneous velocities; that is, $\overline{\rho u'w'}$ where u' is the turbulent velocity component along the horizontal plane and w' is the turbulent velocity component in the vertical direction. The surface stress (or drag) per unit area gives a measure of the shearing forces at the top of a rough surface so that loading on the surface can be found.

The surface stress coefficient is a non-dimensionalised form of the surface stress so that experimental results can be compared. The coefficient C_{f_o} is found by dividing the surface stress by $\frac{1}{2}\rho(\bar{U}_o)^2$; this quantity is the mean pressure of the wind in the horizontal direction. $\bar{U}_o$ is the mean velocity of the wind at an upstream reference position and a height normally 10 m above the ground.

Turbulence

While there is no precise mathematical definition of turbulence, it is generally taken to comprise the complex spectrum of fluctuating motion which is superimposed on the mean flow. Turbulent motion is defined as motion which contains random oscillations of finite sizes, leading to irregularities in the path of a particle of scale comparable with lengths which determine the kinematics of the mean motion, such as the shape of the boundary layer. Small scale atmospheric turbulence is evident in the fluctuations of wind speed and direction recorded by any anemograph. These fluctuations, often termed eddies, have high angular velocities and are smaller in scale near the surface over which they flow.

The turbulence is comprised of velocity components of the turbulence in three directions which are above or below the mean wind speed. The turbulence intensity, I_{σ_u} is a measure of the magnitude of the turbulent velocity in the horizontal direction compared with the mean wind speed, and is expressed as a percentage.

Zero-plane displacement

Wind speeds over forests which have high roughness do not reduce to zero at ground level, but at an effective height above the ground called the zero-plane displacement. The horizontal mean wind is "nearly zero' at this height, which is within the tree crowns. The eddy sizes near this height are measured by the aerodynamic roughness. This is found from wind profiles to be a small distance interval added on to the zero-plane displacement height.

Yield Class

Tree stem volume yields allow classification of growth rates in man-managed forests. The volume figure is the mean annual tree stem volume increment in cubic metres per hectare of forest per year.

APPENDIX III

Some wind damage photographs

(Photographs 1-11)

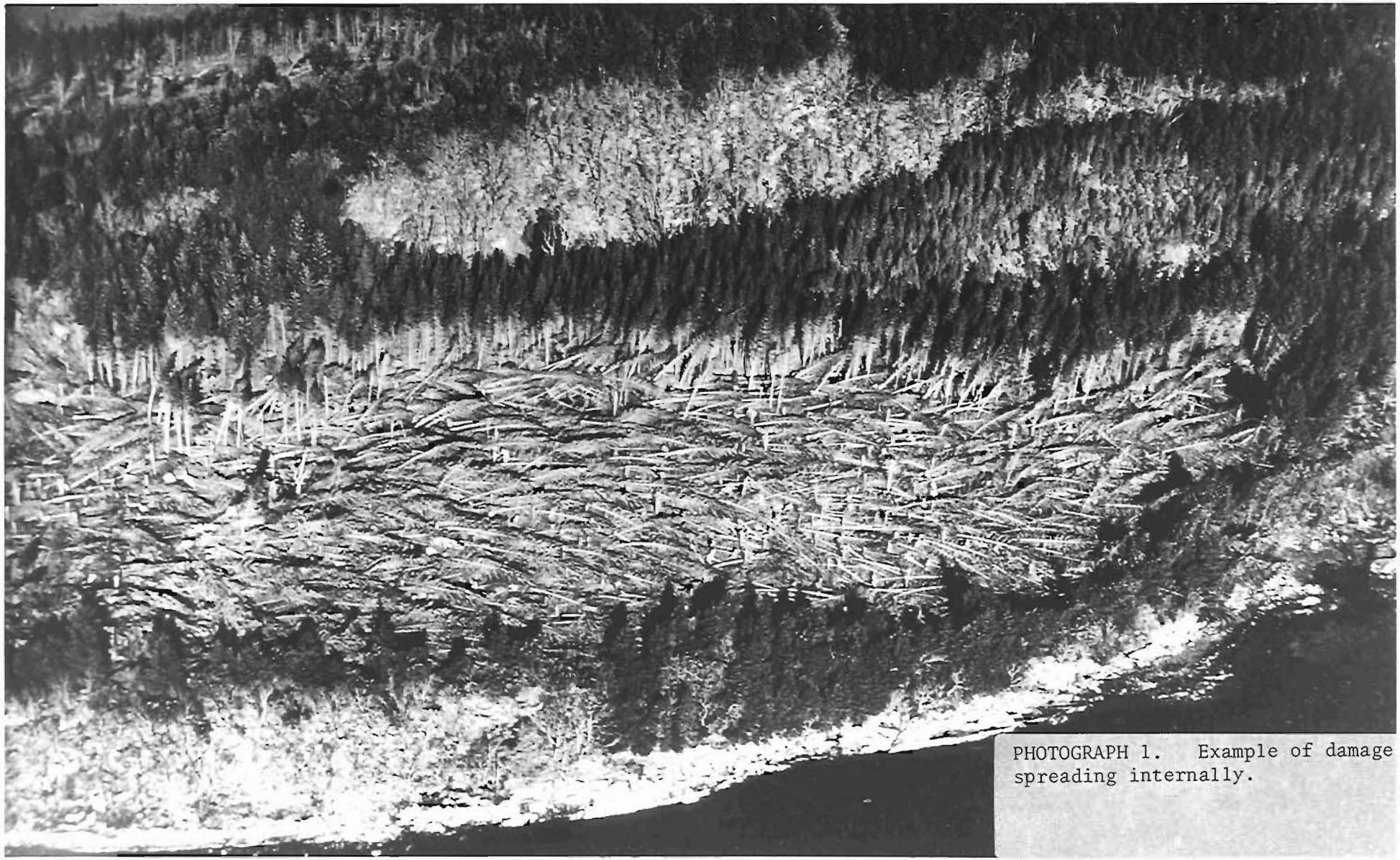

PHOTOGRAPH 1. Example of damage spreading internally.

PHOTOGRAPH 2. Burnham Forest - blowdown and breakage. (August 1975).

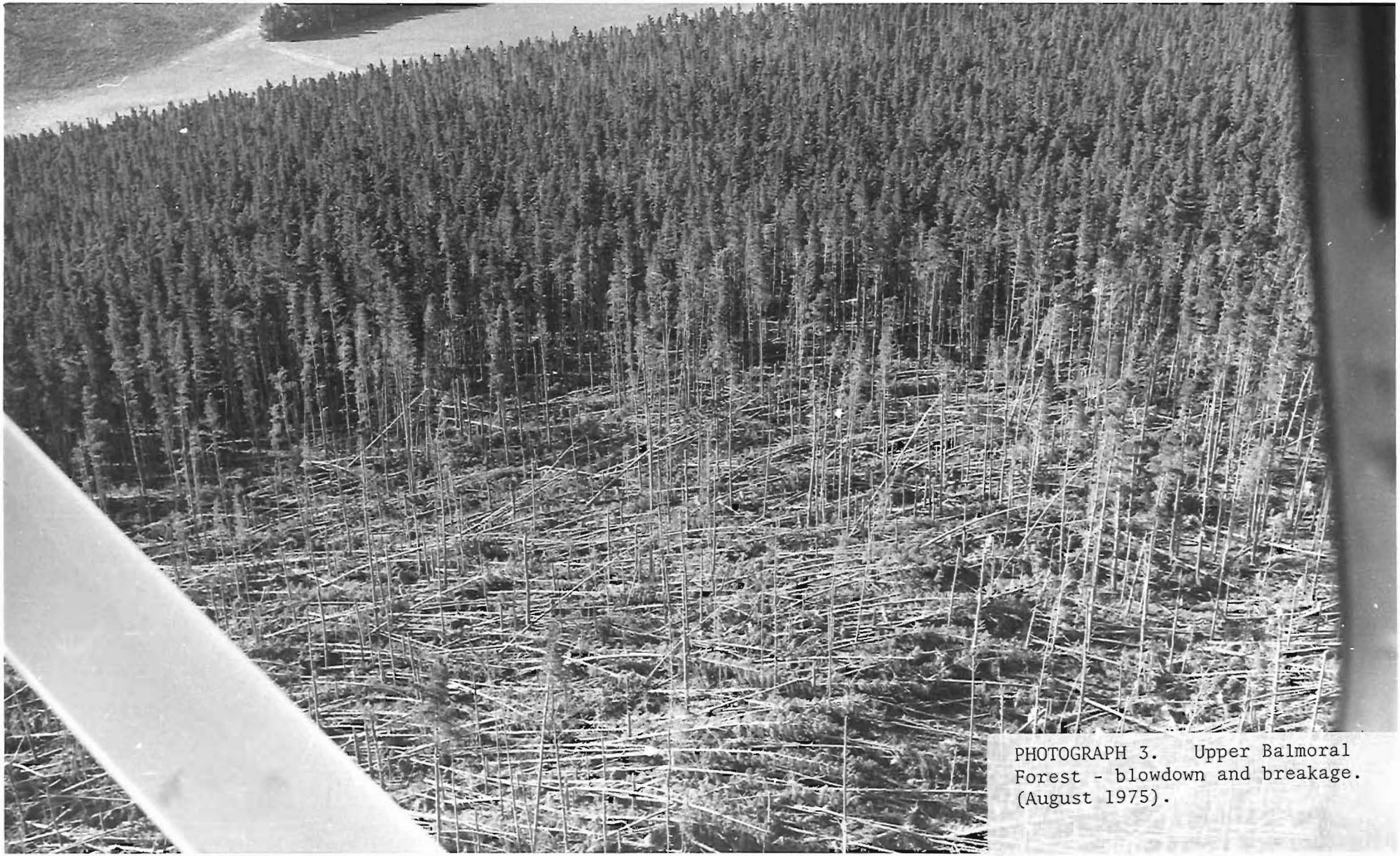

PHOTOGRAPH 3. Upper Balmoral Forest - blowdown and breakage. (August 1975).

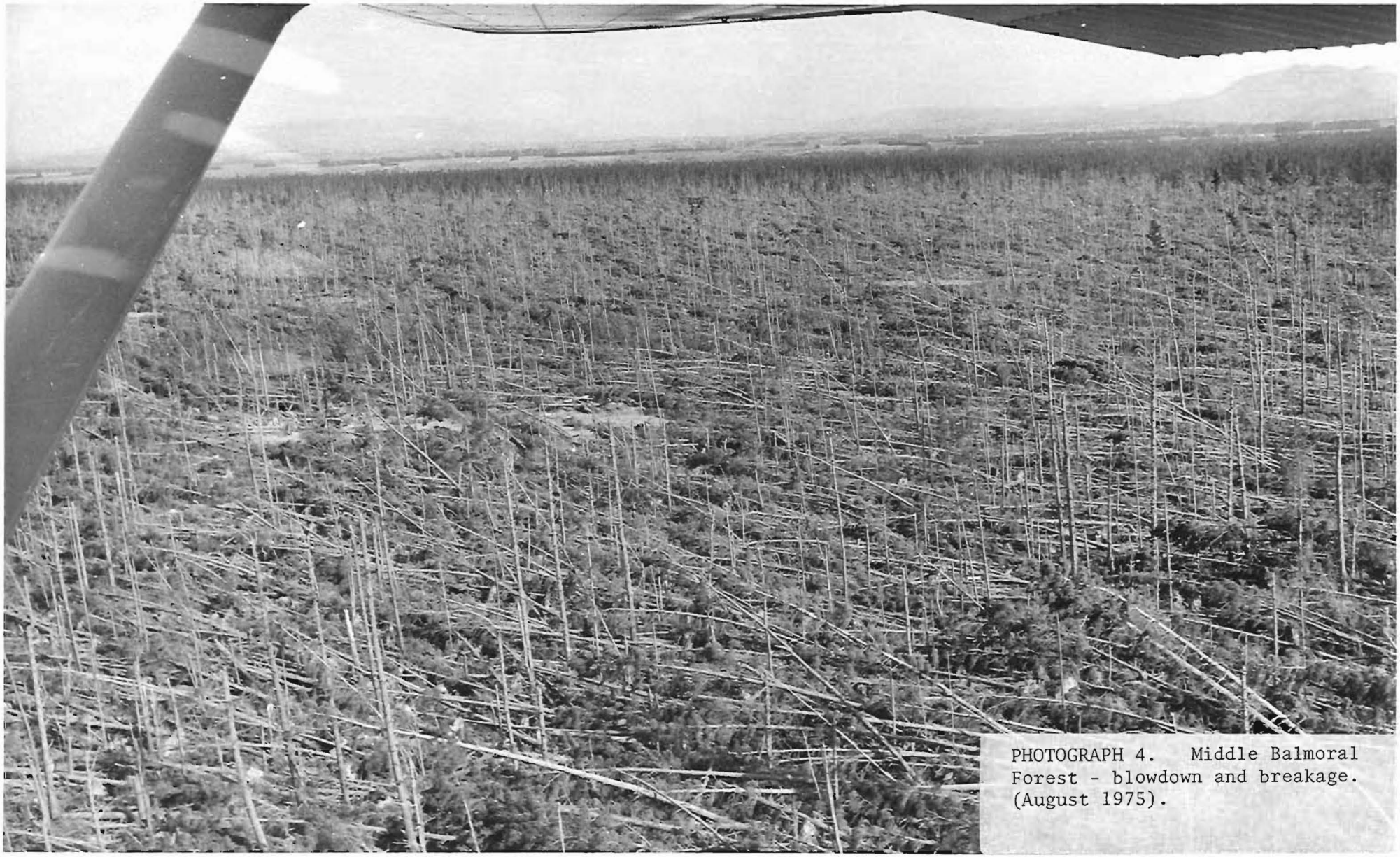

PHOTOGRAPH 4. Middle Balmoral Forest - blowdown and breakage. (August 1975).

PHOTOGRAPH 5. Ashley Forest foothills - blowdown and breakage concentrations. (August 1975).

PHOTOGRAPH 6. Ashley Forest foothills - blowdown and breakage concentrations. (August 1975).

PHOTOGRAPH 7. Burnham Forest (Southwest) bands of blowdown and breakage. (August 1975).

PHOTOGRAPH 8. Burnham Forest (Southwest) bands of blowdown and breakage. (August 1975).

PHOTOGRAPH 9. Storm damage in the eastern Balmoral Forest - showing breakage prevalent in the older plantation but almost non-existent in the younger plantation. (August 1975).

PHOTOGRAPH 10. Storm damage in the south-eastern Balmoral Forest shows the difference in tolerance to winds between pinus radiata (windthrow) and pinus ponderosa (standing). (August 1975).

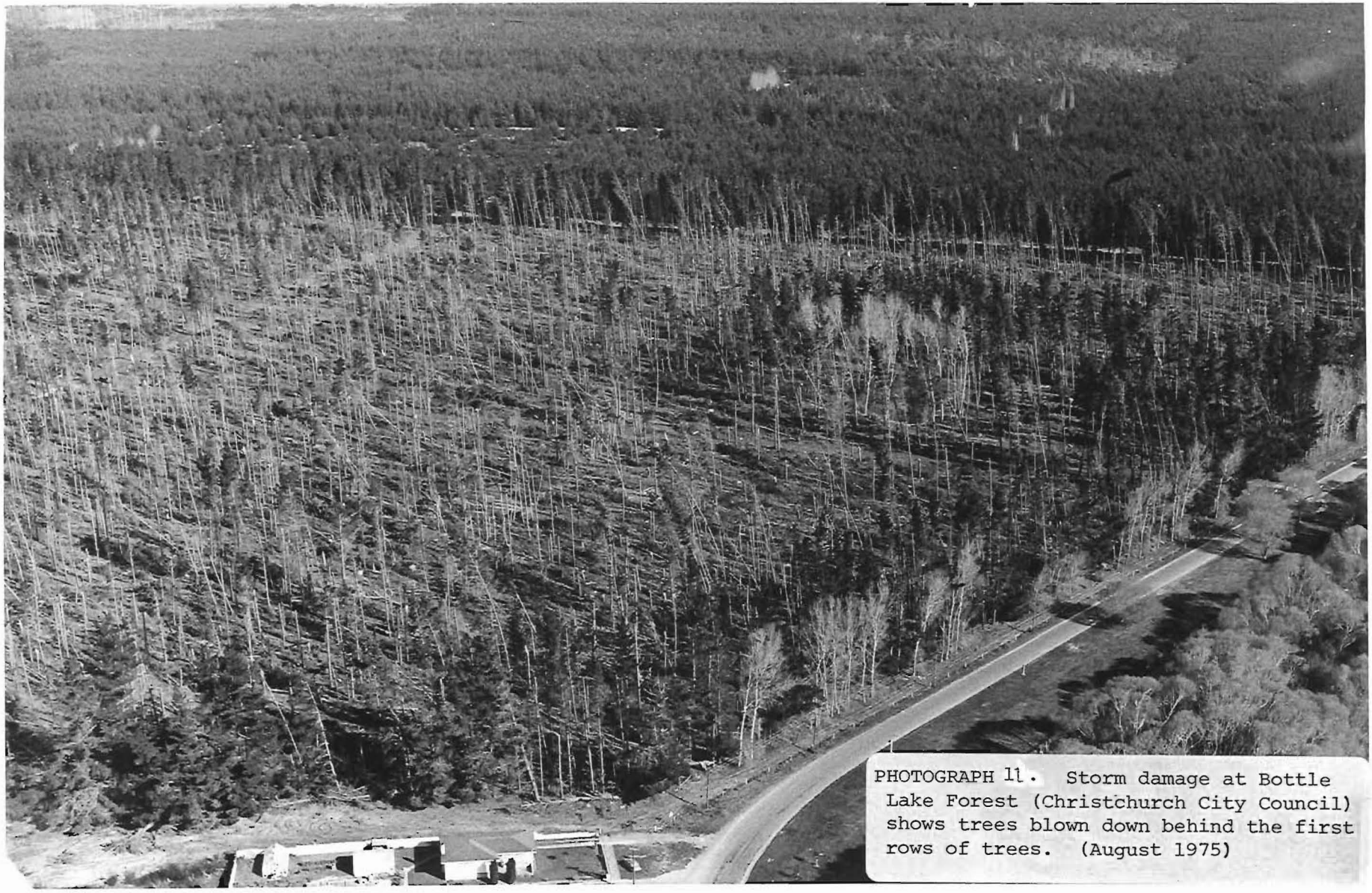

PHOTOGRAPH 11. Storm damage at Bottle Lake Forest (Christchurch City Council) shows trees blown down behind the first rows of trees. (August 1975)